NEW TOOLS FOR CHEMICAL BIOLOGY FROM MAIN GROUP ELEMENTS

By

Matthew Ronald Aronoff

A dissertation submitted in partial fulfillment of
the requirements for the degree of

Doctor of Philosophy
(Chemistry)

at the
UNIVERSITY OF WISCONSIN–MADISON
2015

Date of final oral examination: October 21, 2015

The dissertation is approved by the following members of the Final Oral Committee:
Ronald T. Raines, Professor of Biochemistry and Chemistry
Sam Gellman, Professor of Chemistry
Sandro Mecozzi, Associate Professor of Pharmacy
M. Thomas Record, Professor of Biochemistry and Chemistry
Eric Strieter, Assistant Professor of Chemistry

ProQuest Number: 10187591

All rights reserved

INFORMATION TO ALL USERS
The quality of this reproduction is dependent upon the quality of the copy submitted.

In the unlikely event that the author did not send a complete manuscript
and there are missing pages, these will be noted. Also, if material had to be removed,
a note will indicate the deletion.

ProQuest 10187591

Published by ProQuest LLC (2018). Copyright of the Dissertation is held by the Author.

All rights reserved.
This work is protected against unauthorized copying under Title 17, United States Code
Microform Edition © ProQuest LLC.

ProQuest LLC.
789 East Eisenhower Parkway
P.O. Box 1346
Ann Arbor, MI 48106 – 1346

ABSTRACT

NEW TOOLS FOR CHEMICAL BIOLOGY FROM MAIN GROUP ELEMENTS

Matthew Ronald Aronoff
Under the supervision of Professor Ronald T. Raines
at the University of Wisconsin–Madison

A tremendous amount of knowledge of biological processes has been gained from our grasp of the central dogma of molecular biology. Comprehending the information flow in a biological process allows us to administer the appropriately intervene in order to implement change. However, in many components of biology the flow of information is not clearly understood. Additionally, many lesser-understood processes in biology do not follow the central dogma. These types of biological processes often include post-translational modifications, lipidations, and glycosylations. The study of such events in biology is further complicated as they often occur transiently and are very difficult if not impossible to study using traditional methods. Accordingly, new approaches and new disciplines such as Chemical Biology answer the challenge to elaborate on these more challenging biological events. This thesis will focus on novel chemical methods that have been designed to serve multiple roles in the study of biology.

The contents of this thesis are divided into three major parts. PART 1 focuses on chemical advancements that are orthogonal to processes in biology. In CHAPTER 2 of PART 1 I

utilize a stabilized diazo group as a chemical reporter to probe the mammalian cellular glycocalyx. In CHAPTER 3 I explore the unique characteristics of the diazo group to uncover 1,3-dipolar cycloadditions that occur orthogonally to an azido group. In CHAPTER 4, I then employ the azido group to react with novel phosphinothioesters in the traceless-Staudinger reaction. In combination with protein engineering these reagents will generate ubiquitin chains of precise length and connectivity.

PART 2 focuses on new chemical technologies that facilitate the advancement of boronic acids in biological study. Benzoxaborole is the most promising boronic acid for biological application, and in CHAPTER 2 I describe a novel protecting group for benzoxoaborole that greatly expands the synthetic scope of these valuable compounds. In CHAPTER 3 I demonstrate a new method for the selective detection of boronic acids that facilitates handling and identification of these compounds during synthetic transformations and purifications.

Finally, PART 3 provides details regarding possible future directions for the novel technologies explored within this thesis.

ACKNOWLEDGEMENTS

This work would not have been possible without the help of very many individuals. I will do my best to be as comprehensive as possible but please excuse me if I leave anyone out as you have all played a role in the events leading up to this point in my career.

I must first thank Professor Ron Raines. He offered me a place as a member of his research group during my second rotation as a graduate student, and for this I will always be grateful. The incredible research diversity in the Raines laboratory, and the enthusiasm of the graduate students and post docs made me immediately realize I wanted to be a part of his research group. Working for Professor Raines I was trusted to pursue some of my own research interests that resulted in a varied group of projects comprising many different facets of chemical biology. Additionally, in the Raines laboratory I have been exposed to research areas not found within many single groups including structural biology, physical organic chemistry, biochemistry, biofuels, cellular and molecular biology, and medicinal chemistry. This exposure was a direct result of the many varied projects regularly pursued in the Raines group, and the diverse backgrounds of the researchers. Professor Raines cultivates this environment, and it has provided his lab members a rich knowledge base that extends far beyond our own research projects.

The environment of the Raines laboratory is maintained by a fantastic group of graduate students and post-docs. I thank Christine Bradford, Nick McGrath, and Mike Palte for providing a great first impression that motivated me to eventually join the group. Joelle Lomax, Chelcie Eller, and John Lukesh all provided wisdom and experience when we overlapped in the group.

Sean Johnson was always happy to chat and help with any lab computer issues. Jim Vasta was always willing to talk about research and teach me how to run the HPLC and UPLC, as well as decompress with me on road-bike rides through the country outside of Madison. Trish Hoang always answered my biological questions, and asked how things were going whenever we would cross paths in the hall. I have to thank Robert Newberry for always pushing me to be a better researcher and scientist. Robert made all of us in the lab perform at a higher level, whether this was by always offering to edit and review writings or manuscripts or by challenging our ideas and experimental plans. Robert sets a great example for any aspiring student of science, and he always pushed me to be my best. Other lab members such as Caglar Tanrikulu, Aubrey Ellison, Wen Chyan, Kalie Mix, Emily Garnett, Val Ressler, Thom Smith, and Ian Windsor have all been important peers throughout graduate school and I have learned something from all of you. Promising new students including Jesus Dones Monroig, Brian Graham, and Leland Hyman will continue great work in the Raines group.

I have been able to work with several talented collaborators in the Raines group, without whom my projects would have had a much different focus. Early in my graduate career I learned many valuable lessons from Brett VanVeller. Brett sincerely loves research and is always truly excited to discuss new ideas. I hope to continue our conversations long into the future. I was fortunate to work with Kristen Andersen for two projects. I am indebted to her for all of the biological knowledge and techniques I was able to gain while working together. Kristen humbles all of us with her ability to multi-task more projects and undertakings than should be possible for one individual. Lastly, as a relatively recent post-doc addition to the Raines group, Brian Gold has been fantastic to work with on cycloaddition chemistry. To the chagrin of the other lab members, it has been great to discuss all of the aspects of this interesting reaction. I think at one point we were coming up with a new research idea nearly every day. I am sorry there was not time to work on all of the ideas we have come up with, but if Brian had come a few months earlier I may have stayed for another year in the graduate program. I will miss all of you.

I was also able to work with a talented undergraduate student, Kevin Walters. By always questioning what we were doing, and why we were doing something Kevin managed to keep me aware of the context of my research. This was especially important in the early years of graduate school. Working with Kevin helped me to maintain a broader perspective about being in graduate school, and I am grateful for his years of help. Congratulations on your new adventure, and I look forward to hearing your stories sometime in the future.

The faculty of the UW–Madison chemistry department greatly influenced my decision to attend for graduate school, and I must acknowledge several in particular. I thank my committee for devoting their time to aid my completion of this process. Professor Sandro Mecozzi and Professor M. Thomas Record have provided feedback since my preliminary exam. Professor Eric Strieter met with me as a prospective student and cemented my decision to accept the offer to attend the graduate school. Prof. Strieter also challenged me in on of the hardest parts of Phys. Org. class with his section on reaction kinetics. I first became interested in UW–Madison because of the research of Professor Sam Gellman. When I was an undergrad Prof. Gellman kindly and promptly answered my emails about foldamers while I was preparing a literature seminar on the topic. I know for certain that I would not have attended this program without his involvement and for that I will always be grateful. Prof. Gellman also mentored me as one of his discussion TAs for his Chem 343 Organic Chemistry course during my second year and served on my RP committee during the oral examination for my third year research proposal. Most importantly, Professor Gellman told me that having a family in graduate school shouldn't be seen as a limitation on my time, but rather I should view having a family as a benefit as it could provide me with a perspective that would make me a better researcher. Additionally, Professors Kiessling, McMahon, Raines, Reich, Burke, and Shomaker all played an important role in my graduate coursework and development. I am indebted to all of you.

Many other individuals have been invaluable to my experience at the graduate program at UW–Madison. This includes Stephanie Nagle, the former graduate coordinator, who helped me in the early days of the graduate program even before I was a student here. Nick Hill, Matt Bowman, and Brian Esselman all aided in my education when I was a teaching assistant in the organic chemistry lab program. Martha Vestling has analyzed every mass spec sample I have brought, and has always spent the extra time with more difficult samples. Martha was always excited to talk about science while also sharing her vast wisdom regarding mass spec. Mark Anderson has helped me with technical issues at the NMRFAM for the duration of graduate school, while always sharing many interesting stories as well as delicious chocolate treats. I want to thank Robin Davies from the IPIB Media Lab for his help with photography for the Org. Lett. images, in addition to our regular chats in the hallway. Laura Vanderploeg worked with me many times preparing my posters for printing while also teaching me so many things about Adobe Illustrator. Tracy Drier has taught me so much about the craft of glassblowing, and I will never look at chemical glassware in the same way every again. Tracy is an invaluable resource to the department, and our conversations in the glass shop always managed to help keep things in perspective. Kristi Heming has helped me many times over the last several years as the Chem. Bio. division coordinator, and Arrietta Clauss has been incredibly helpful in the planning and organization of finalizing the graduation process.

I first discovered my love for chemistry at Fort Lewis College in Durango, Colorado. Professor Ted Bartlett had me hooked on organic chemistry by the end of my first semester in his lecture, and I continued to take three more organic-related courses from him. It was always interesting to hear Ted tell stories about his research while working for Bill Johnson and Gilbert Stork. I did not at all appreciate the significance of these stories until years later. Steve Ottersberg shared Ted's enthusiasm for chemistry and I credit both of you for cultivating my own interest and showing me how to relate organic chemistry back to the natural world and everyday life. Professor Ron Estler taught me P-chem while also demonstrating absolute dedication to improving the lives of his students while also championing undergraduate research at Fort Lewis. Professor Rob Milofsky taught me how to respect work/life balance as well as the importance of significant figures. Professor Shere Byrd convinced me to attend Fort Lewis, and later taught me both cellular physiology and the techniques of cell culture. Professor Les Sommerville taught me how to connect the biological world with organic chemistry, and this understanding will forever influence my perspective as a scientist. Professor Kenny Miller exposed me to my first experience with teaching, as well as my first significant opportunity for research. In his first semester as a professor, Kenny taught my Synthesis and Spectroscopy class with classmates Earl and Kevin. This class provided us with the experience of what is involved in research, and ultimately influenced the decisions of all three of us to pursue graduate school. I use knowledge I learned from Kenny every day in my own research, and I am very grateful for his continual guidance and mentorship. I am sure Kenny would be proud to see how my column chromatography skills have continually improved since those early days in the synthesis lab.

I would like to thank my parents for their continual support for me to pursue my dreams in my own way. My parents always instilled in their children the immeasurable value of knowledge and education. I hope to continue this value to my own children, and hopefully to my students one day. I may not have become the type of "doctor" that was originally envisioned for me, but my parents still provided their support and encouragement.

Lastly, but most importantly, I have to thank my family. My wife, Gretchen Tracy, supported my decision to pursue a doctorate in chemistry, and fully supported our decision to move to Madison so I could attend this program. The last four years have been challenging, but Gretchen kept our family strong throughout this experience. I know that after accomplishing this we can do anything including moving overseas for my post-doc. The enormous time demands of graduate school frequently put the entire burden of responsibility on her to care for our three sons in addition to her own work. The hardest part of being in graduate school was balancing school life with family life. However, by the end of my graduate career I was able to see my family as a huge benefit. The motivation to make it home to see my boys kept me focused and efficient in my own research. My sons were a source of my own strength and determination and always reminded me to maintain a "normal" perspective. I love all of you, and cannot imagine going through this journey without you. I know I am now prepared for the next step in my career, and the next big move in our lives.

TABLE OF CONTENTS

ABSTRACT i
ACKNOWLEDGEMENTS iii
TABLE OF CONTENTS ix
LIST OF FIGURES AND TABLES xi
LIST OF ABBREVIATIONS xiv
PART 1 1
CHAPTER 1 Introduction: Variations of the Staudinger Reaction Generate New Tools for Chemical Biology 1
- 1.1.1 Introduction to the Staudinger Reaction and its Variations 2
- 1.1.2. Diazo Compounds 3
- 1.1.3. 1,3-Dipolar Cycloadditions with Diazo Groups 4
- 1.1.4. Diazo Groups as Chemical Reporters 6
- 1.1.5. Diazo Group Selective Cycloadditions 7
- 1.1.6. The Traceless Staudinger Ligation 8
- 1.1.7. Protein and Peptide Synthesis with the Staudinger Ligation 9

CHAPTER 2 Diazo Groups Endure Metabolism and Enable Chemoselectivity *in Cellulo** 24
- 1.2.1 Introduction 26
- 1.2.2 Results & Discussion 27
- 1.2.3 Materials & Methods 31
- 1.2.4 NMR Spectra 76

CHAPTER 3 Preferential 1,3-Dipolar Cycloadditions of Diazoacetamides with Unstrained Dipolarophiles in the Presence of Azides 84
- 1.3.1 Introduction 86
- 1.3.2 Results and Discussion 88
- 1.3.3 Conclusions 103
- 1.3.4 Materials and Methods 104
- 1.3.5 Acknowledgements 107
- 1.3.6 Synthesis 178

CHAPTER 4 Uncharged Phosphinothiols for the Traceless Staudinger-Ligation in Aqueous Conditions 218
- 1.4.1 Introduction 220
- 1.4.2 Results and Discussion 224
- 1.4.4 Materials & Methods 229
- 1.4.5 NMR 258

PART 2 276

CHAPTER 1 Introduction: Protection and Detection of Boronic Acids 276
2.1.1 Introduction to Boronic Acids 277
2.1.2 Synthetic Transformations of Boronic Acid Derivatives 278
2.1.3 Protection of Boronic Acids with the Pinacol Group 279
2.1.4 Organotrifluoroborates as Surrogates for Boronic Acids 279
2.1.5 Diaminonaphthalene-Enabled Iterative Cross-Couplings of Boronic Acids 281
2.1.6 Multistep Transformations with MIDA Boronic Acids 282
2.1.7 Benzoxaborole 283
2.1.8 A Protecting Group for Benzoxaborole 284
2.1.9 Boron-Specific Sensing and Recognition 286
2.1.10 Boron-Based Fluorophores 286
2.1.11 Boron-Sensing Chromophores 287
2.1.12 Boron-Sensing Fluorophores 287
2.1.13 Determination of Boron with ESIPT Fluorescence 288
2.1.14 Conclusions 289

CHAPTER 2 A Divalent Protecting Group for Benzoxaboroles 302
2.2.1 Introduction 304
2.2.2 Results and Discussion 306
2.2.3 Future Directions and Conclusions 308
2.2.4 Acknowledgements 309
2.2.5 Materials & Methods 320
2.2.6 Evaluation of Other Protecting Groups 321
2.2.7 Deprotection Analyses 322
2.2.8 Synthesis 324
2.2.9 NMR Spectra 339

CHAPTER 3 Detection of Boronic Acids through Excited-State Intramolecular Proton-Transfer Fluorescence 360
2.3.1 Introduction 362
2.3.2 Results and Discussion 363
2.3.3 Conclusions 365
2.3.4 Acknowledgements 365
2.3.5 Materials & Methods 366

PART 3 388

FUTURE DIRECTIONS 388
Part 1 Chapter 3: Diazo Specific Dipolar Cycloadditions 390
Part 1 Chapter 4: Uncharged Water-Soluble Phosphinothioesters for the Traceless Staudinger Ligation 391
Part 2 Chapter 2: A Divalent Protecting Group for Benzoxaboroles 392
Part 2 Chapter 3: Detection of Boronic Acids through ESIPT 392

APPENDIX 398
Investigations toward diazo-selective reactions 398

LIST OF FIGURES AND TABLES

Figure 1.1.1 Progression of the Staudinger reaction ... 12
Figure 1.1.2 Cycloaddition reactions commonly applied for chemical biology... 14
Figure 1.1.3 Categories of cycloaddition reactions ... 16
Figure 1.1.4 Overall scheme for the internalization and incorporation of diazo-group appended nonnatural mannosamine derivatives as chemical reporters... 18
Figure 1.1.5 Competition reactions between diazo and azido groups... 20
Figure 1.1.6 Traceless Staudinger ligation for peptide couplings ... 22
Table 1.2.S1 Rate constants ($M^{-1}s^{-1}$) for the reaction of Diazo 1 and Azide 2 with strained cyclooctynes ... 51
Figure 1.2.1 Space-filling models of diazo and azido derivatives of acetamide... 52
Figure 1.2.2 Variations of *N*-acetylmannosamine used in this study that are trafficked into sialic acid ... 54
Figure 1.2.3 ^{1}H NMR spectra... 56
Figure 1.2.4 Chemoselectivity of diazo and azido groups ... 58
Figure 1.2.5 Trafficking of diazo and azido sugars in mammalian cells ... 60
Figure 1.2.6 Metabolic incorporation of Ac_4ManDiaz into sialic acid... 62
Figure 1.2.7 Detection of sialic acid derivatives generated *in cellulo* from Ac_4ManDiaz and Ac_4ManNAz... 64
Figure 1.2.8 Histogram of CHO K1 cells grown in medium containing Ac_4ManDiaz. 66
Figure 1.2.9 Histogram of CHO K1 cells grown in medium containing Ac_4ManDiaz. 68
Figure 1.2.10 Graph of the cytotoxicity of Ac_4ManDiaz and Ac_4ManNAz (10 µM–10 mM) for CHO K1 cells ... 70
Figure 1.2.11 Dual labeling of mammalian cells with diazo and alkynyl sugars ... 72
Figure 1.2.12 Dual labeling of mammalian cells grown with derivatives of *N*-acetylmannosamine and *N*-acetylgalactosamine... 74
Scheme 1.3.1 1,3-dipolar cycloadditions of diazoacetamides... 108
Scheme 1.3.2 A competition reaction between 1 eq. each of diazo (R=Bn), azide (R=Bn), and DIBAC ... 110
Figure 1.3.1 Comparison of activation via strain or electron-withdrawing substituents for 1,3-dipolar cycloadditions of carbamoyl azide and diazoacetamide – R = Me ... 112
Scheme 1.3.3 Competition of diazoacetamide (1, 1 eq.) and azide (2, 1 eq). with unstrained dipolarophiles... 114
Table 1.3.1 Calculated activation energies and experimentally determined pseudo-first order rate constants ... 116
Scheme 1.3.4 Synthesis and intramolecular competition reaction ... 118
Figure 1.3.2 Transition state geometries, activation energies, and distortion-interactions energies ... 120
Figure 1.3.3 Substituent effects on activation energies of azido and diazo group cycloadditions ... 122
Figure 1.3.4 Exemplary transition-state geometries of azide and diazo group cycloadditions ... 124
Figure 1.3.5 Activation energies vs. FMO gap and distortion energies ... 126
Figure 1.3.6 Distortion-interaction analysis for selected cycloadditions ... 128

Figure 1.3.7 Comparison of the strategies of predistortion acceleration and electronic tuning 130
Figure 1.3.8 Comparison of bending in diazopropanone and acetyl azide 132
Figure 1.3.9 Activation energies vs. reaction energies 134
Table 1.3.2 NBO charge on dipole in the TS 136
Figure 1.3.10 Electrostatic potential maps 138
Figure 1.3.11 Pseudo-first order rate constant measured in 50:50 $CH_3CN:H_2O$ at r.t. in $M^{-1}s^{-1}$ 140
Figure 1.3.S1 Absorbance maximum (388 nm) of the diazo-acetamide 142
Figure 1.3.S2 Representative kinetic plot for the absorbance assay 144
Figure 1.3.S3 Rate enhancement observed in aqueous cosolvent conditions 146
Figure 1.3.S4 Comparison of activation via strain or electon-withdrawing substituents 148
Figure 1.3.S5 Substituent effects on activation energies of azido and diazo group cycloadditions 150
Table 1.3.S1 Gas phase activation energies of azide and diazo group cycloadditions 152
Table 1.3.S2 Gas phase reaction energies of azide and diazo group cycloadditions... 154
Table 1.3.S3 Activation energies of azide and diazo group cycloadditions 156
Table 1.3.S4 Reaction energies of azide and diazo group cycloadditions 158
Figure 1.3.S6 Transition geometries of azide and diazo group cycloadditions 160
Figure 1.3.S7 Orbitals calculated at the HF/6-31G(d) level of theory 162
Figure 1.3.S8 Activation energies vs. FMO gap for cycloadditions 164
Figure 1.3.S9 Distortion–interaction analysis for cycloadditions 166
Figure 1.3.S10 Distortion–interaction analysis for experimentally investigated carbonyl series 168
Figure 1.3.S11 Activation energies vs. reaction energies and separated by dipoles ... 170
Table 1.3.S5 Intrinsic reaction bariers of azide and diazo group cycloadditions 172
Figure 1.3.S12 Implicit and explicit solvation for azide and diazo group cycloadditions with methyl vinyl ketone 174
Figure 1.3.S13 Electrostatic potential maps 176
Table 1.4.1 Small-molecule Staudinger ligation testing 245
Figure 1.4.1 Phosphinothiols compared directly in the aqueous Staudinger ligation. 246
Figure 1.4.2 Retrosynthetic scheme for the production of ubiquitin chains. 248
Figure 1.4.3 Preparation of the proximal ubiquitin 250
Figure 1.4.4 Preparation of the distal ubiquitin. 252
Figure 1.4.6 Ubiquitin-ubiquitin dimer formation via the Staudinger ligation. 256
Figure 2.1.1 Boron-variations utilized in organic chemistry are sorted by oxidation state 290
2.1.2 Protection of a boronic acid with pinacol generates a boronic ester 292
Figure 2.1.3 Common protecting group strategies for boronic acids 294
Figure 2.1.4 Applications of benzoxaborole in medicinal chemistry and chemical biology. 296
Figure 2.1.5 The protecting group derived from Proton Sponge® facilitates synthetic manipulation of compounds containing the benzoxaborole moiety. 298
Figure 2.1.6 The boron-interrupted emission of HBQ is ~200 nm shorter than the typically predominating ESIPT emission. 300

Figure 2.2.2 Structure of free benzoxaborole (1), its complexation with a polyol (2), 310
and other general structures of protected boronic acids (3–6) and their unsuitable.. 310
complexes (7–9) with 1. 310
Figure 2.2.3 Protection of benzoxaborole derivatives 312
Figure 2.2.4 Characterization of complex 11a 314
Table 2.2.5 Screening of the stability of 11a under various conditions 316
Figure 2.2.6 Synthetic evaluation of protected benzoxaborole derivatives 318
Figure 2.3.1 Excited-State Intramolecular Proton Transfer (ESIPT) cycle of 10-hydroxybenzo[*h*]quinoline (HBQ). 370
Figure 2.3.2 Comparison of the sensitivity of HBQ and ARS for the detection of a boronic acid. 372
Figure 2.3.3 Detection of boronic acids and other boron-containing compounds with HBQ. 374
Figure 2.3.4 Selectivity of HBQ for functional groups. 376
Figure 2.3.5 Detection of a boronic acid on a solid support. 378
Figure 2.3.6 Agarose beads viewed “in vial” by illuminating at ~365 nm using a handheld UV lamp without (left image) supplemental lights, and with (right image) overhead lighting. 380
Figure 2.3.7 Relationship between phenylboronic acid concentration and emitted fluorescence following staining with HBQ. 382
Figure 2.3.8 Comparison of 10-hydroxybenzo[*h*]quinolone (HBQ) to 2-(2′-hydroxyphenyl)benzimidazole. 384
Figure 2.3.9 Absorption and emission spectra of HBQ and its complex with benzoxaborole. 386
Figure 3.1.2 Phosphinothioesters investigated for efficiency during the traceless Staudinger ligation 394
Figure 3.1.3 Water soluble HBQ-S for the ESIPT detection of boronic acids 396

LIST OF ABBREVIATIONS

ε	extinction coefficient
Ac	acetyl
ACN	acetonitrile
ATCC	American Type Culture Collection
Benzoboroxole	2-hydroxymethylphenylboronic acid
Bn	benzyl
BCN	bicyclo[6.1.0]non-4-yne
BSA	bovine serum albumin
CBD	chitin binding domain
CHO	Chinese hamster ovary
CuAAC	copper(I)-catalyzed azide–alkyne cycloaddition
Da	dalton
ddH2O	distilled, deionized water
DCM	dichloromethane
DIBAC	dibenzyl-aza-bicyclooctyne
DMAD	dimethyl acetylenedicarboxylate
DMEM	Dulbecco's modified Eagle's medium
DMSO	dimethylsulfoxide
DNA	deoxyribonucleic acid
DPBS	Dulbecco's phosphate-buffered saline
DTNB	5,5’-dithiobis(2-nitrobenzoic acid)

DTT	dithiothreitol
E. coli	*Escherichia coli*
EDTA	ethylenediaminetetraacetic acid
ESI	electron spray ionization
ESIPT	excited state intramolecular proton transfer
ETOH	ethanol
FBS	fetal bovine serum
FMO	frontier molecular orbital
Fmoc	fluorenylmethyloxycarbonyl
FPLC	fast performance liquid chromatography
FRET	Förster resonance energy transfer
GSH	reduced glutathione
GSSH	oxidized glutathione
h	hour
HBQ	10-Hydroxybenzo[*h*]quinoline
HBQ-S	10-Hydroxybenzo[*h*]quinoline sulfonate
HCl	hydrochloric acid
HEPES	2[4-(2-hydroxyethyl)-l-piperazinyl]ethanesulfonic acid
HOMO	highest occupied molecular orbital
HPLC	high-performance liquid chromatography
IC50	half maximal inhibitory concentration
IED	inverse electron demand
IPTG	isopropyl-1-thio-ß-$_{\text{D}}$-galactopyranoside

k_{cat}	first-order enzymatic rate constant
k_{d}	kinetic dissociation rate constant
K_{d}	equilibrium dissociation constant
kDa	kilodalton
λ_{em}	emission wavelength
λ_{ex}	excitation wavelength
LB	Luria–Bertani medium
logP	partition coefficient
LUMO	lowest unoccupied molecular orbital
MALDI-TOF	matrix-assisted laser desorption/ionization time-of-flight
MEM	2-methoxyethoxymethyl ether
MeOH	methanol
MES	2-(*N*-morpholino)ethanesulfonic acid
MESNA	2-mercaptoethanesulfonic acid, sodium salt
min	minute
MW	molecular weight
MWCO	molecular weight cutoff
NaCl	sodium chloride
NaOH	sodium hydroxide
NCL	native chemical ligation
NED	normal electron demand
NHS	*N*-hydroxysuccinimide
NMR	nuclear magnetic resonance

OD	optical density
PCR	polymerase chain reaction
PBS	phosphate-buffered saline
PDB	protein data bank
PEG	polyethylene glycol
pI	isoelectric point
pK_a	log of the acid dissociation constant
RNA	ribonucleic acid
rt	room temperature
s	second
S. cerevisiae	*Saccharomyces cerevisiae*
SDS–PAGE	sodium dodecyl sulfate–polyacrylamide gel electrophoresis
SPAAC	strain-promoted azide–alkyne cycloaddition
t	time
TB	terrific broth medium
TCA	trichloroacetic acid
TFA	trifluoroacetic acid
Tris	2-amino-2-(hydroxymethyl)-1,3–propanediol
Ub	Ubiquitin
UW	University of Wisconsin
UWCCC	University of Wisconsin Carbone Cancer Center

PART 1

CHAPTER 1

Introduction:
Variations of the Staudinger Reaction Generate New Tools for Chemical Biology

1.1.1 Introduction to the Staudinger Reaction and its Variations

The Staudinger reaction between an azide and a phosphine has provided one of the greatest chemical tools for the field of chemical biology. This reaction—also referred to as the Staudinger reduction—has found widespread application in organic synthesis since its initial report by Staudinger and Meyer in 1919.[1] There are examples of Staudinger reductions employed for biological investigations,[2] but the true value of Staudinger chemistry lies with key intermediates generated during this seemingly simple process and the versatile transformations that can be accomplished through the modulation of key substituents on the phosphine reagent.

Insight into the mechanism of the Staudinger reaction has generated the opportunity to perform several new transformations, each operating through the interception of key intermediates.[3,4] The overall reaction sequence and subsequent variations are outlined in Figure 1.1.1. The phosphine and azide undergo an imination reaction to form a phosphazide, the first important intermediate. From the phosphazide the reaction can be diverted along pathway **B** to ultimately generate a diazo group (*vide infra*). Unperturbed, the phosphazide will decompose through a loss of $N_2(g)$ in pathway **A**, and generate an iminophosphorane, another important intermediate. The iminophosphorane is a nucleophilic aza-ylide; however, in aqueous conditions absent of electrophiles the iminophosphorane can protonate and hydrolyze to the resulting amine and phosphine oxide, which is an overall reduction of the azide. If an electrophile is present, especially an intramolecular carbonyl electrophile, the iminophosphorane nitrogen attacks this group through an aza-Wittig process that initiates the Staudinger Ligation (pathway **C**). This is the first example of diverting reactivity to produce an amide bond.

If the intramolecular trapping moiety is sufficiently electrophilic, reactivity is diverted earlier. Here, the phosphazide nitrogen can deviate the Staudinger reaction to another transformation as outlined with pathway **B**. In this pathway, the electrophilic trap substituted on the phosphine prevents N_2(g) extrusion and phosphazide decomposition. Instead, an acyl triazenophosphonium salt is created. In aqueous conditions, this intermediate is hydrolyzed quickly to an isolable acyl triazene with a pendant phosphine oxide. With the addition of heat or aqueous base, the acyl triazene can be decomposed to generate a diazo group, and this overall process is named azide deimidogenation (loss of NH).

These two alternate pathways of the Staudinger reaction and the accompanying chemical transformations form the foundation for the first part of this thesis. Chapters 1 and 2 focus on the diazo group as an emerging tool for the field of chemical biology. In Chapter 3, the Staudinger ligation—an amide-forming tool for the conjugation of biomolecules containing an azide and a phosphinothioester—is investigated with the goal of applying novel uncharged phosphines that are water-soluble.

1.1.2. Diazo Compounds

Diazo compounds represent some of the most versatile reagents in synthetic organic chemistry, but their application in chemical biology has been investigated only recently. The diazo group provides a useful alternative to the widely utilized azide functional group, as it possesses unique reactivity in addition to some useful redundancy with the azide. Protonation of a diazo group generates a diazonium salt, which is effective for alkylation chemistry.[5] The diazo group is capable of generating carbenes either through photochemical, thermal, or mechanical processes, in addition to carbenoids formed from transition metal interactions.[6] Furthermore, the diazo group can mediate alkene and alkyne additions as well as C–H, O–H, and N–H insertions.[7-9] Diazo groups are also capable of rapid 1,3-dipolar cycloadditions with a broad range of dipolarophiles.[10,11] This reactivity is most applicable for chemical biology and is the focus within this thesis.

The diazo group first appeared in the late 19th century,[12-15] yet relatively few methods exist for the preparation of these compounds. These methods include a Regitz diazo-transfer to an activated C–H,[16,17] diazotization of an amine,[18] hydrazine decomposition,[19] and oxidation.[20,21] Diazo groups can also be prepared from the fragmentation of triazenes,[22,23] which is the process utilized in the method developed by the Raines group.[24] This mild preparation of diazo groups has enabled the development of the diazo compound as a reagent for chemical biology. It can be performed in aqueous buffer,[25] and has excellent functional group tolerance as a result of the excellent specificity between azides and phosphines.

1.1.3. 1,3-Dipolar Cycloadditions with Diazo Groups

Whereas the Staudinger ligation initiated the field of bioorthogonal chemistry by utilizing abiotic functional groups, the cycloaddition reaction has become the primary tool for chemical biology. The success of the cycloaddition reaction is a result of two related transformations—the Cu(I) catalyzed azide–alkyne cycloaddition (CuAAC),[26,27] or "copper-click" reaction,[28] and the strain-promoted azide–alkyne cycloaddition (SPAAC), or "Cu-free click" reaction (Figure 1.1.2).[29-31] These two reactions nearly comprise the field of bioorthogonal chemistry, and they have enabled an enormous number of biological investigations and synthetic pursuits.[32,33] It is significant that all three reactions—the Staudinger ligation, the copper-click, and the strain-promoted click—all require an azide reactant. The azido group is nearly ideal for chemical biology. It is synthetically accessible, small, abiotic, and inert to biological functional groups with few exceptions. Nevertheless, the dominance of this functional group is also a downside, as the azido group is not amenable to multiple reactions in a single assay. There is a growing need for alternative transformations that can occur orthogonally to reactions of an azide.

The diazo group represents a useful alternative to the azido group within the field of chemical biology. The diazo group is capable of alkylations and esterifications of biomolecules including nucleic acids, peptides, and proteins; these reactions occur with[34-41] and without the addition of a catalyst.[42-44] Additionally, the reactivity of the diazo group in the 1,3-dipolar cycloaddition reaction has been utilized since the discovery of this functional group, starting with von Pechmann's synthesis of pyrazole from acetylene and diazomethane in 1894.[14]

In a 1,3-dipolar cycloaddition reaction, the diazo group has several benefits that surpass the azido group as a dipole. These benefits include faster reaction rates with commonly applied reactants, as well as a "tunability" of the diazo group that is not possible with most azides.[45] The diazo group reacts with a dipolarophile, such as an alkene or alkyne, by a concerted pericyclic reaction that involves 4 electrons of the diazo-dipole and 2 π electrons from the dipolarophile to produce a cyclic 5-membered product. 1,3-Dipolar cycloadditions can be examined with frontier molecular orbital (FMO) theory (Figure 1.1.3). The mode and efficiency of the reaction is determined by (relative) orbital energies. This analysis typically includes the highest occupied molecular orbital of one reactant (HOMO) and the lowest unoccupied molecular orbital (LUMO) of the other. The Huisgen cyclization[46] is applied in the field of chemical biology with the SPAAC reaction. Diazo groups are typically electron-rich with a high energy HOMO, and so, unlike the azido group, the diazo group reacts predominantly with electron-poor dipolarophiles with a low-energy LUMO in a Type I dipolar cycloaddition (Figure 1.1.3). As the azido group is somewhat ambiphilic—and can react by either Type I or Type 2 cycloadditions—this ambiphilicity provides a mode of selectivity for the diazo group.

There are only a few examples in which diazo groups have been applied as dipoles in SPAAC reactions with octynes,[47-50] yet this reactivity creates tremendous opportunity for the diazo group in the field of chemical biology. Because the diazo group can be generated directly from a parent azide and will react with substrates already used in bioorthogonal applications, the diazo group fits almost seamlessly within current chemical biology technology.

1.1.4. Diazo Groups as Chemical Reporters

The chemical reporter strategy employs the reaction between two unique functional groups not commonly found in nature to provide enzyme-like specificity within a biological context for the purpose of studying transient or post-translational events. Many of the diazo-containing molecules prepared in the Raines laboratory through azide-deimidogenation possess an inherent stability not found with alkyl-diazo compounds. Additionally, these stabilized diazo groups react more rapidly with cyclooctynes than do their parent azido groups. We were curious to know whether the diazo group would be tolerated in a biological setting, as the diazo group can confer another degree of chemoselectivity with current bioorthogonal reactions. In Chapter 1, I describe the application of a diazo-appended *N*-acetyl mannosamine derivative as a chemical reporter for sialic acid metabolism, a demanding metabolic process that consists of several enzymatic transformations (Figure 1.1.4). The diazo-derivative is prepared easily from the parent azide using the Raines method;[24] compared to the azide, the diazo compound allows for more rapid cycloadditions with a dibenzyl-aza-bicyclooctyne (DIBAC) in water. I also demonstrate that the diazo compound allows for multicomponent imaging alongside another chemical reporter—a terminal alkyne—while overlapping reactivity with the azide leads to detrimental cross-reactions. This insight makes it feasible to conduct future investigations that rely on multicomponent imaging, as the diazo group is the simplest functional group for use alongside alkyne chemical reporters.

1.1.5. Diazo Group Selective Cycloadditions

Selective cycloadditions highlight the chemical differences between azido and diazo groups. It has been shown that the reaction between dimethyl acetylenedicarboxylate (DMAD) and diazoacetyl azide undergoes a cycloaddition only with the diazo group[51] (Figure 1.1.5A). Although these reactants cannot be applied in a biological context, this chemoselectivity illustrates the significance of the differing electronics of the diazo group and the carbonyl-azide. For SPAAC reactions in chemical biology, most of the efforts to improve reactivity focus on tuning the dipolarophile (cyclooctynes). The dipoles can be tuned to an even greater extent, although, for the azide, it is only possible with aryl derivatives. In one example, removing electron density from the azide with an *ortho*-nitro substitution improves the inverse electron demand (IED) reaction with an electron-rich cyclooctyne (bicyclo[6.1.0]non-4-yne, BCN), whereas on the same molecule, an ambiphilic alkyl azide reacts predominately with an electron-poor cyclooctyne (DIBAC) through a normal electron demand (NED) cycloaddition[52] (Figure 1.1.5B). Although this example is not completely selective, it does demonstrate how dipole tuning can persuade selectivity in a cycloaddition process.

In Chapter 2, I explore selective reactivity by cycloaddition between the diazo group and the azide. I demonstrate that by removing strain from the dipolarophile and focusing on electronic tuning, alkenes and alkynes react preferentially with the diazo group instead of an alkyl azido group. These reactions can be performed at ambient temperature and in aqueous cosolvent with complete selectivity, and the reaction rates meet or exceed the fastest SPAAC reactions. I evaluate the involved reactants, which provides insight into the observed rate enhancement of the diazo group in water as well as its selectivity. I also consider the implications of this type of diazo-selective cycloaddition reaction for biological investigations.

1.1.6. The Traceless Staudinger Ligation

The Staudinger ligation has enabled a new era for bioconjugation and protein synthesis. The key deviation from the standard Staudinger reaction is the *O*→*N* acyl transfer that traps the iminophosphorane. Staudinger first observed this aza-Wittig reaction 100 years ago, when imines were formed by the nucleophilic addition of an iminophosphorane to ketones and aldehydes.[53] Much more recently, the first application of the Staudinger ligation installed an electrophilic intramolecular ester as a trap for the aza-ylide in a biologically relevant context to label azide-bearing glycans on a cell surface.[54]

The first modification to the original Staudinger ligation addresses the tri-aryl phosphine oxide that remains on the ligation product. While the residual phosphine oxide does not limit the utility of the ligation for many applications,[55,56] it does prohibit use of this ligation reaction when a native amide bond is desired. To address this, both the Raines group and the Bertozzi group developed traceless variations that cleave away the phosphine oxide during the hydrolysis of the amidophosphonium salt.[57,58]

The Raines group has explored the traceless variation further by elaborating on the reaction mechanism and kinetics of the ligation as well as some steric and electronic effects.[57,59-61] One notable observation is that electron-donating substituents on the diphenyl phosphine, such as *para*-methoxy groups, lead to improved ligations at non-glycyl residues.[62] The traceless Staudinger ligation reaction has enabled numerous applications including the site-specific immobilization of azide-bearing peptides and proteins,[63] stereoselective *N*-glycoslyation of amino acids,[64] and peptide coupling on solid supports for the orthogonal assembly of a functional RNase.[65]

Major obstacles complicate performing the Raines traceless Staudinger ligation in water, including solubility of the reagent, the competing hydrolysis, and the oxidation of the iminophosphorane (Figure 1.1.1). First, as the original diphenylphosphine reagent is not soluble outside of organic conditions, a more-soluble derivative is needed to perform the ligation in aqueous conditions. Second, hydrolysis of the iminophosphorane halts the ligation reaction and generates an amine, and in water this reduction represents a substantial side reaction. Lastly, diphenyl phosphines are more sensitive to oxidation and deactivation than the triphenylphosphine derivatives.

1.1.7. Protein and Peptide Synthesis with the Staudinger Ligation

The chemical total synthesis of proteins represents a substantial effort for the fields of chemistry and biochemistry.[66] It is possible to prepare a functional protein from two synthesized pieces with native chemical ligation (NCL).[67] Solid-phase peptide synthesis is limited by peptide length (≤40 residues) and ligations such as NCL facilitate a greater range of targets. Still, the residual cysteine required for the NCL reaction prevents some applications; and as cysteine is one of the least abundant residues, this process often requires the introduction of at least one substitution in the wild-type sequence. Following ligation, an additional desulfurization step is often required to remove the thiol moiety. Although NCL is a powerful tool, the chemical tools for peptide ligation and protein synthesis are constantly improving and evolving. The traceless Staudinger reaction represents one alternative to NCL for protein synthesis.

In order to ligate two proteins chemoselectively with an isopeptide bond, I have pursued yet another improvement to the traceless Staudinger ligation. Previous water-soluble derivatives possess a carboxylate moiety or pendant dimethyl-amino substituents.[68] These substitutions install either positive or negative charges on each aryl ring of the reagents. Although the introduction of charge likely contributes to the water solubility, it can interact detrimentally with protein side chains. Coulombic effects can facilitate the reaction, as a negatively charged water-soluble derivative does not perform as well as one that is positively charged.[68] Electronic effects ($\sigma_p = +0.36$) resulting from the amide-substituent of the anionic phosphinothiol can hinder the reaction,[62,69] which confounds this result. Ultimately, due to solubility limitations for the diphenylphosphinothiols, the effects of charge and electronics in aqueous conditions have not been investigated previously.

In Chapter 3 of Part 1 I describe *uncharged* water-soluble phosphinothiols that will be applied to form isopeptide linked ubiquitin–ubiquitin dimers. These phosphinothiols utilize polyethylene glycol-like (PEG-like) side chains for water-solubility (Figure 1.1.6), and these substituents also facilitate their preparation. Intramolecular non-covalent interactions from the ether oxygens may also contribute to their stability and efficiency. Lastly, structural isomers are used to compare the electronic effects of substituents on the reactivity of the phosphine in aqueous conditions.

Figure 1.1.1 Progression of the Staudinger reaction

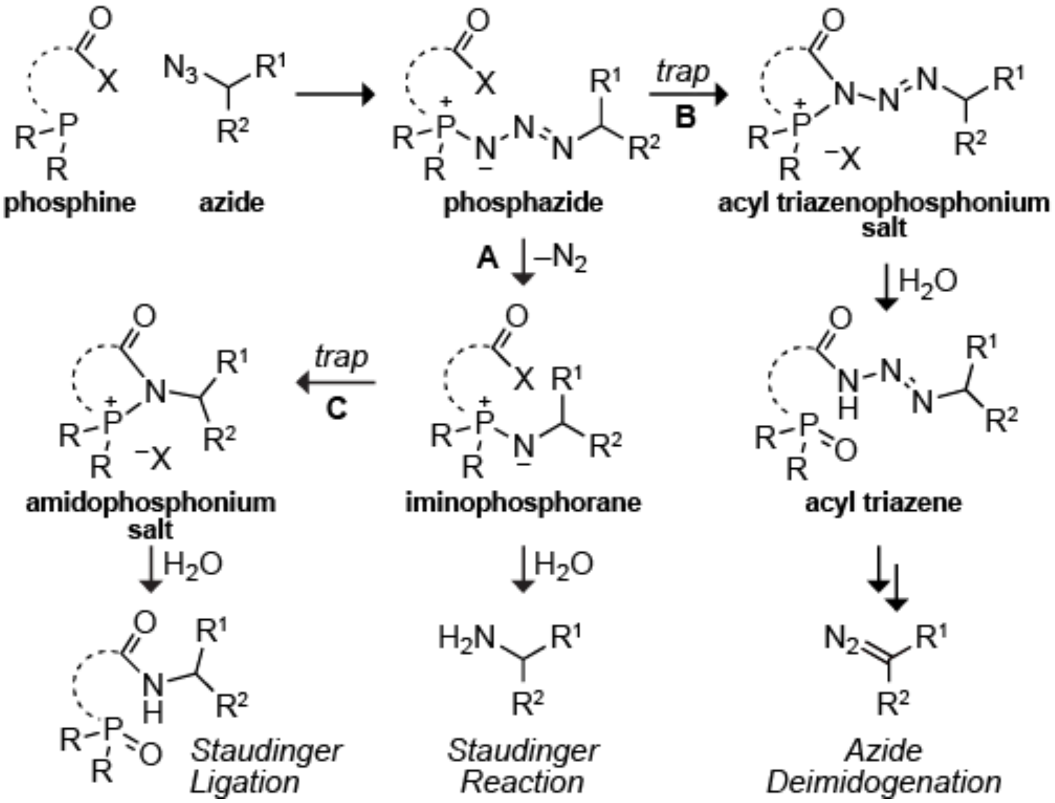
phosphine
azide
phosphazide
trap
B
acyl triazenophosphonium salt
A
–N₂
H₂O
trap
C
amidophosphonium salt
iminophosphorane
acyl triazene
H₂O
H₂O
Staudinger Ligation
Staudinger Reaction
Azide Deimidogenation

Figure 1.1.1 Progression of the Staudinger reaction generates two key intermediates that are individually utilized to generate a diazo group (pathway **A**) and to perform a ligation (pathway **B**). **A**. The phosphine and azide react to generate an iminophosphorane that is trapped to make an acyltriazenophosphonium salt. Hydrolysis of the salt creates a stable acyl triazene that can be fragmented to the diazo group. **B.** Trapping the Staudinger reaction at the iminophosphorane intermediate—following the decomposition and release of $N_2(g)$— generates an amidophosphonium salt that is hydrolyzed to form an amide-containing ligation product.

Figure 1.1.2 Cycloaddition reactions commonly applied for chemical biology

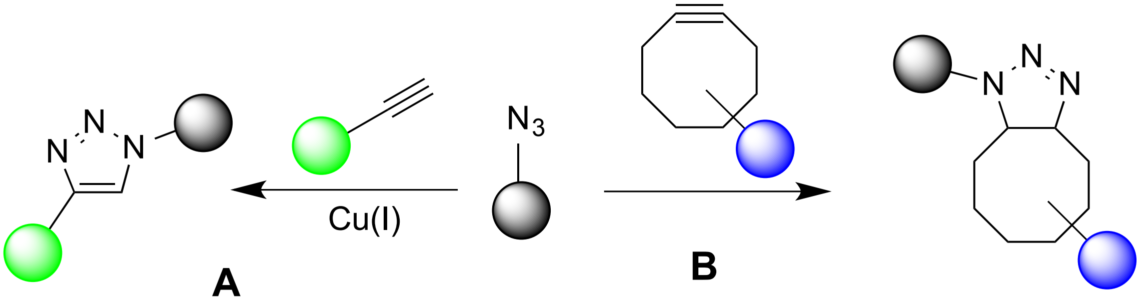
N
N
N
N3
Cu(I)
A
B
N
N
N

Figure 1.1.2 Cycloaddition reactions commonly applied for chemical biology: (**A)** the Cu(I) catalyzed azide–alkyne cycloaddition (CuAAC), and (**B**) the strain-promoted azide–alkyne cycloaddition (SPAAC).

Figure 1.1.3 Categories of cycloaddition reactions

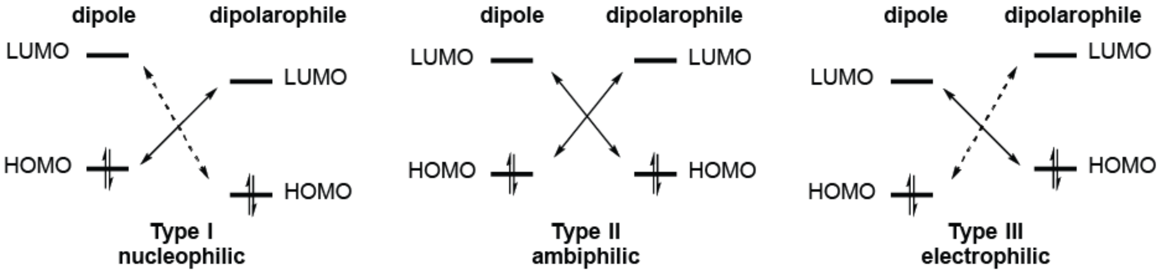
dipole
dipolarophile
LUMO
LUMO
HOMO
HOMO
Type I
nucleophilic
dipole
dipolarophile
LUMO
LUMO
HOMO
HOMO
Type II
ambiphilic
dipole
dipolarophile
LUMO
LUMO
HOMO
HOMO
Type III
electrophilic

Figure 1.1.3 Categories of cycloaddition reactions: **Type I** nucleophilic reactions are considered normal electron demand (NED) cycloadditions and favor interactions between the HOMO of the dipole to the LUMO of the dipolarophile. **Type II** amiphilic dipolar cycloadditions involve similar energy gaps between HOMO and LUMOs for both dipole and dipolarophile resulting in two-way interactions as observed with azido groups. **Type III** reactions proceed through inverse electron demand (IED) and orbital overlap involves a low energy LUMO of the dipole interacting with the HOMO of the dipolarophile.

Figure 1.1.4 Overall scheme for the internalization and incorporation of diazo-group appended nonnatural mannosamine derivatives as chemical reporters

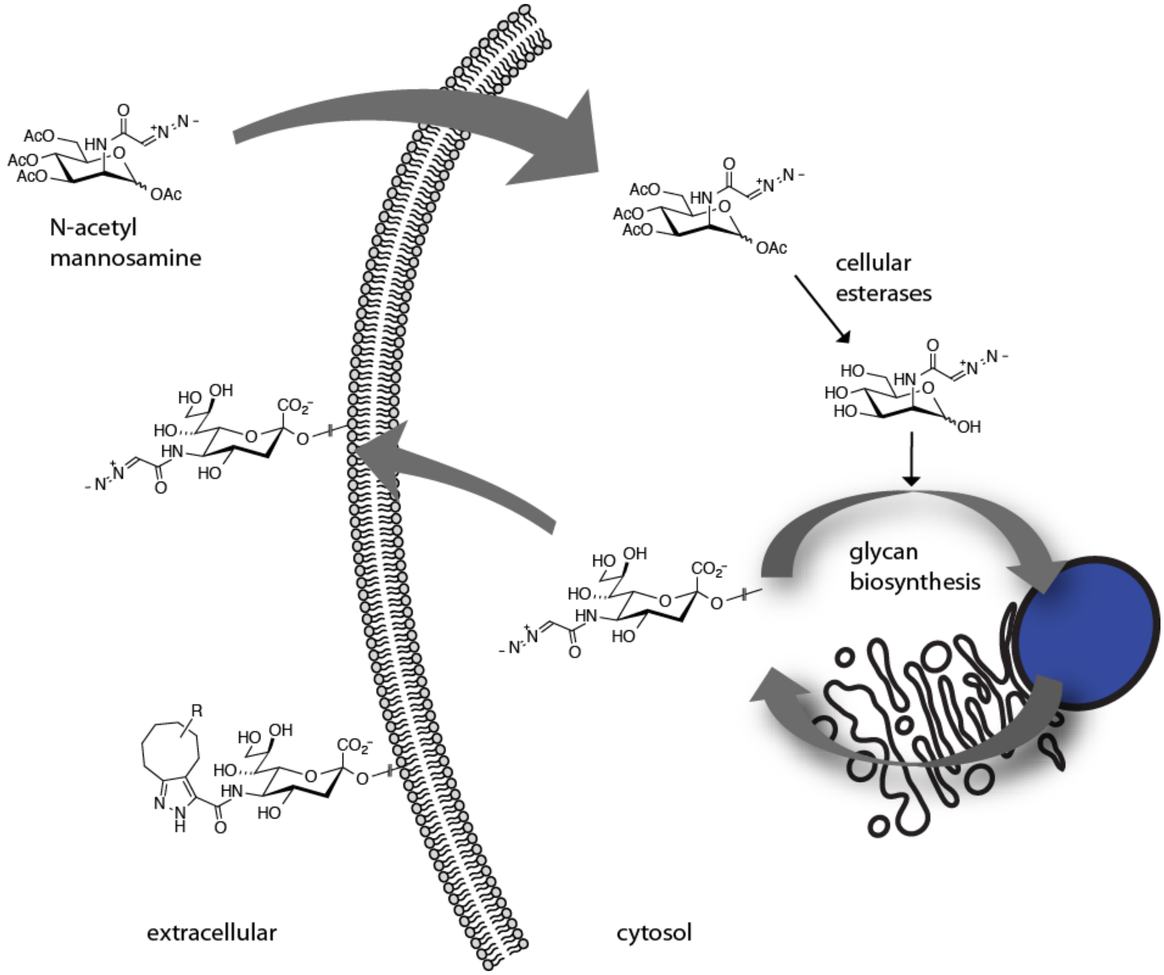
N-acetyl
mannosamine
cellular
esterases
glycan
biosynthesis
extracellular
cytosol

Figure 1.1.4 Overall scheme for the internalization and incorporation of diazo-group appended nonnatural mannosamine derivatives as chemical reporters.

Figure 1.1.5 Competition reactions between diazo and azido groups

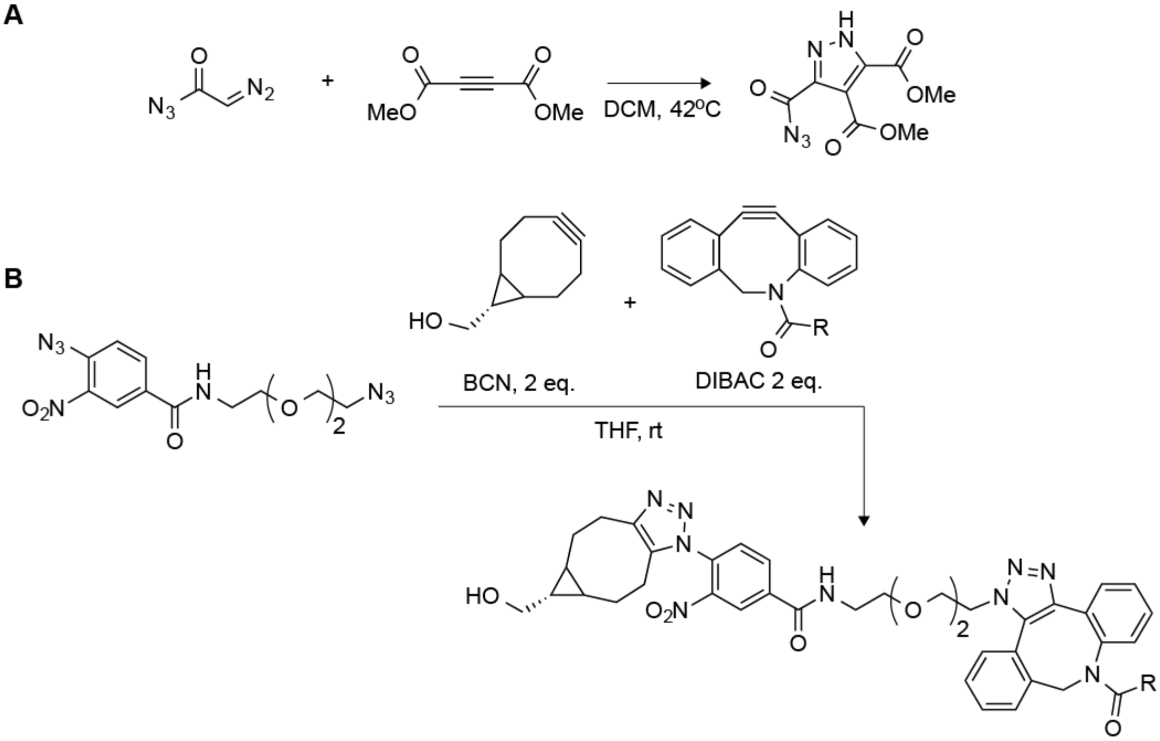
A
N3
N2
O
+
MeO
OMe
DCM, 42oC
N
H
N
OMe
N3
B
HO
BCN, 2 eq.
DIBAC 2 eq.
R
O2N
THF, rt
2
N3

Figure 1.1.5 Competition reactions between diazo and azido groups. **A**. Reaction of an α-diazo carbonyl azide with dimethylacetylene dicarboxylate preferentially undergoes a cycloaddition with the electron-rich diazo group and not the electronically deactivated azido group.[51] **B**. Preferential reactivity based on electron demand is observed when the azide is tuned for electron-deficiency to perform IED cycloadditions.[52]

Figure 1.1.6 Traceless Staudinger ligation for peptide couplings

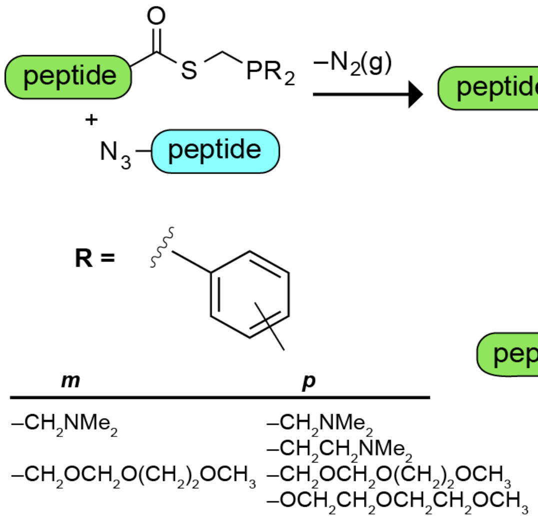
peptide
O
S
PR2
+
N3
peptide
−N2(g)
peptide
O
S
+
PR2
−
N
peptide
H2O
R =
peptide
O
N
H
peptide
+
HS
O
PR2
m
p
–CH2NMe2
–CH2OCH2O(CH2)2OCH3
–CH2NMe2
–CH2CH2NMe2
–CH2OCH2O(CH2)2OCH3
–OCH2CH2OCH2CH2OCH3

Figure 1.1.6 Traceless Staudinger ligation for peptide couplings and the various water-soluble derivatives including substitutions at the *meta* (*m*) and *para* (*p*) positions of the aryl groups.

PART 1

CHAPTER 2

Diazo Groups Endure Metabolism and Enable Chemoselectivity *in Cellulo**

*This chapter has been published in part, under the same title. Reference: Andersen, K.A.#, Aronoff, M.R.#, McGrath, N.A., Raines, R.T. Diazo Groups Endure Metabolism and Enable Chemoselectivity *in Cellulo*. *J. Am. Chem. Soc.* **137**, 2412–2415 (2015).

(#these authors contributed equally)

Contributions: I performed all chemical synthesis and analysis. K.A.A. completed cell culture and analysis. I co-conceived the experiments and wrote the manuscript together with K.A.A. N.A.M. originally prepared Ac_4ManDiaz.

Abstract

We introduce a stabilized diazo group as a reporter for chemical biology. ManDiaz, which is a diazo derivative of *N*-acetylmannosamine, is found to endure cellular metabolism and label the surface of a mammalian cell. There its diazo group can undergo a 1,3-dipolar cycloaddition with a strained alkyne, providing a signal comparable to that from the azido congener, ManNAz. The chemoselectivity of diazo and alkynyl groups enables dual labeling of cells that is not possible with azido and alkynyl groups. Thus, the diazo group, which is approximately half the size of an azido group, provides unique opportunities for orthogonal labeling of cellular components.

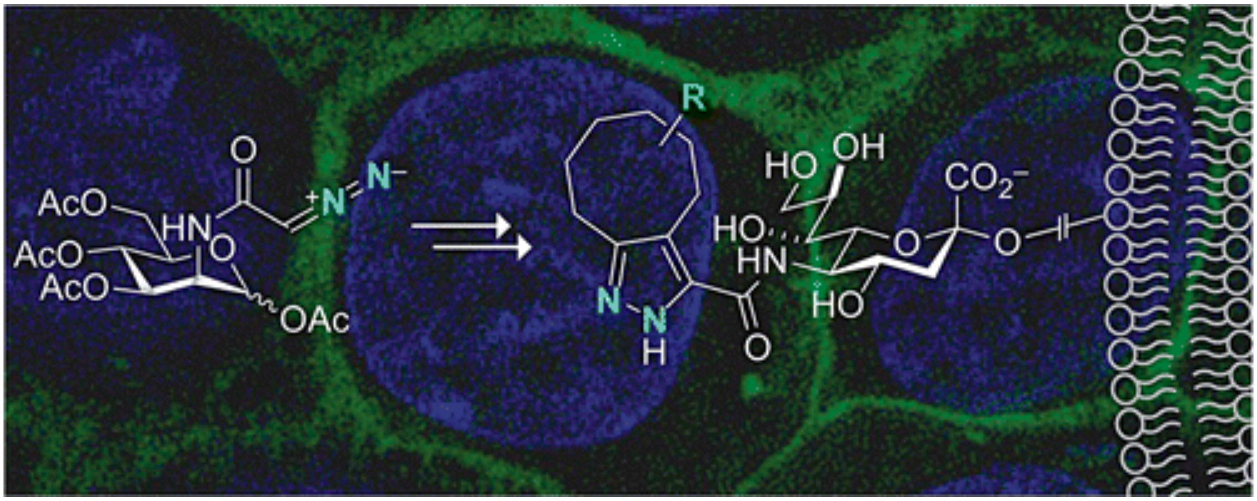

1.2.1 Introduction

Appreciation[70-72] of the broad utility of the Huisgen azide−alkyne 1,3-dipolar cycloaddition[73] has had a profound impact on chemical biology.[74-77] The diazo group shares this reactivity with the azido group while conferring additional versatility. For example, cycloaddition with a diazo compound can be tuned to be much faster or much slower than that with its azide analogue.[50,78] Diazo compounds offer other useful modes of reactivity, including the *O*-alkylation of carboxylic acids in water to form esters.[79] Indeed, the utility of diazo compounds in chemical synthesis was established long ago[80-83] and likely exceeds that of azides.[84-89] Nevertheless, rightful concern about their toxicity and high, even explosive, reactivity[90-92] has deterred the application of diazo compounds in chemical biology. While recent work has demonstrated their utility in biomolecular transformations *in vitro*,[50,78] we are unaware of any application of diazo compounds *in cellulo* or *in vivo*.

A diazo group has attributes of an ideal reporter for chemical biologists. Smaller than an azido group (Figure 1.1.1A), a diazo group has the same number of atoms as a methyl group (RCH_3 versus $RCHN_2$) or a methylene group ($R_1R_2CH_2$ versus $R_1R_2CN_2$). Moreover, a diazo compound can be prepared readily from its parent azide by simple deimidogenation, that is, loss of “NH” (Figure 1.1.1B).[24,94] This deimidogenation reaction allows access to diazo compounds in aqueous solution via abstraction of an α-proton from an incipient acyl triazene with a mild base such as bicarbonate. The requisite acidity of that α-proton requires conjugation of the anion with, for example, an amidic carbonyl group.* We hypothesized that such mitigation of reactivity could allow diazo compounds to endure physiological conditions.

We sought to assess the resilience of a diazo group in a meaningful context. To do so, we chose metabolic trafficking, which is more demanding than the mere demonstration of chemoselective reactivity in a biomolecular milieu. The labeling of cell-surface glycans is an ideal theater for this test because of the high tolerance demanded by cellular biosynthetic machinery,[95-98] the rigid constraint on size,[99] and the precedent for this labeling established by Reutter, Bertozzi, and others with derivatives of *N*-acetylmannosamine (ManNAc) (Figure 1.1.2).[54,100,101]

1.2.2 Results & Discussion

We began by examining the *in vitro* reactivity of a relevant diazo compound with strained functionalizable alkynes. Three cyclooctynes were reacted with a representative azide (**1**, R = Bn) and diazo compound (**2**, R = Bn). In acetonitrile, the reactions with the diazo compound were as fast or faster than those with the azide (Figure 1.1.1C). Notably, the addition of water augmented both the rates and their differential, likely as a result of stabilization of the especially polar transition state for cycloaddition with the diazo compound.[78,102,103] On the basis of these data, we chose DIBAC as an optimal functionalizable alkyne for our experiments.

Next, we sought to confirm the chemoselectivity of the diazo group in a biological context. First, we stirred a solution of *N*-benzyl-2-diazoacetamide (**2**, R = Bn) and glutathione for 24 h and did not observe a reaction (Figure 1.1.3). Then we linked a diazoacetamide to biotin to probe for nonspecific labeling *in cellulo*. CHO K1 cells treated with the diazo−biotin conjugate or its parent azide showed no labeling on an immunoblot, in contrast to an analogous acrylate (Figure 1.1.4A). Likewise, nonspecific labeling with the diazo group was not detectable with flow cytometry or confocal microscopy at 24 h (Figure 1.1.4B,C).

Next, we asked whether a diazo compound would be accepted by an endogenous biosynthetic pathway alongside extant biomolecules. To answer this question, we synthesized the stabilized diazo compound $Ac_4ManDiaz$ (Figure 1.1.2) by deimidogenation of $Ac_4ManNAz$. The four acetyl groups enhance cell permeability and are hydrolyzed by intracellular esterases.[104] We added $Ac_4ManDiaz$ or $Ac_4ManNAz$ to medium containing live CHO K1 cells. After 2 days, any extracellular diazo or azido groups were reacted with a DIBAC−biotin conjugate and labeled with avidin−Alexa Fluor 488, which is green. Super-resolution images of cells exposed to $Ac_4ManDiaz$ and $Ac_4ManNAz$ were indistinguishable (Figure 1.1.5A). Quantification with flow cytometry revealed that labeling with $Ac_4ManDiaz$ was slightly less efficient (Figure 1.1.5B), despite its higher reaction rate (Figure 1.1.1C). The differential labeling is likely related to the instability of a diazo group at low pH. Most peracylated sugars are taken up by passive diffusion across the outer membrane, but some are taken up by endocytosis.[104] The low pH of endosomes[105] likely leads to C-protonation and hydrolysis of the ensuing diazonium salt.[79] Finally, we showed that $Ac_4ManDiaz$ is metabolized and displayed on the surface of three other cell types, though at different rates (Figure 1.1.5C).

To confirm that $Ac_4ManDiaz$ was trafficked into sialic acid in the same manner as $Ac_4ManNAz$, we grew CHO K1 cells in each peracylated sugar at 250 μM for 3 days and labeled them with DIBAC−biotin as described above. We then treated the cells with either neuraminidase (sialidase) or peptide-N glycosidase F (PNGase F). Both the azido and diazo sugars showed high levels of labeling with DIBAC−biotin in the absence of enzyme, with diazo labeling being (86 ± 3)% of the azido labeling. Exogenous addition of either enzyme decreased the labeling levels sharply (Figure 1.1.6), indicating that labeling was due to incorporation of the sugars.[106] In addition, using the pendant biotin of the DIBAC conjugate, we isolated the cellular metabolites generated from the azido and diazo precursors and observed the expected sialic acid conjugates by mass spectrometry (Figure 1.1.7).

To ascertain the optimal conditions for labeling of CHO K1 cells that had metabolized Ac_4ManDiaz, we exposed these cells to 0−20 μM DIBAC−biotin for 60 min or 10 μM DIBAC−biotin for 0−120 min. Although labeling continued to increase with increasing levels of DIBAC−biotin, concentrations in excess of 10 μM or times beyond 60 min began to elicit cytotoxicity (Figures 1.1.8 and 1.1.9). Accordingly, we chose labeling at 10 μM for 60 min as a compromise between high labeling efficiency and cell viability. Notably, the cytotoxic activities of Ac_4ManDiaz and Ac_4ManNAz were similar (LD_{50} ~ 1 mM; Figure 1.1.10).

Next, we sought to perform chemoselective dual labeling on the cell surface.[107-110] Unlike azide **1** (R = Bn), diazo compound **2** (R = Bn) is a poor substrate for Cu(I)-catalyzed cycloaddition with a terminal alkyne in aqueous solution (data not shown). Hence, we reasoned that a cell surface displaying both diazo and terminal alkynyl groups could provide opportunities for orthogonal reactivity. To test this hypothesis, we allowed cells to metabolize Ac_4ManDiaz, Ac_4ManKyne, or both. We then probed for diazo groups by using strain-promoted cycloaddition with DIBAC−biotin and labeling with avidin−Alexa Fluor 594 (microscopy) or avidin−Alexa Fluor 647 (flow cytometry), which are red; we probed for alkynyl groups by using Cu(I)-catalyzed cycloaddition with picolyl azide−Alexa Fluor 488,[111,112] which is green. Both microscopy and flow cytometry indicated that the two cycloaddition reactions could be performed in either order without interfering cross-reactivity (Figure 1.1.11). In marked contrast, performing the same experiment with Ac_4ManNAz and Ac_4ManKyne resulted in diminished cell-surface labeling, especially when Cu(I)-catalyzed cycloaddition was performed first. We suspect that the labeling was diminished by the crosslinking of cell-surface azido and alkynyl groups, as these two functional groups are not orthogonal in the presence of Cu(I). The evident clumping of cells displaying both azido and alkynyl groups also suggests that the glycocalyx of two cells can be in such close proximity that their sialic acid residues react to form covalent cross-links. The data in Figure 1.1.11 indicate that diazo compounds, unlike azides, are orthogonal to terminal alkynes in a cellular context, and this orthogonality enables novel dual labeling experiments.

To provide another example of the chemoselectivity of the diazo group, we performed dual labeling with Ac_4ManDiaz and Ac_4GalKyne, which is a peracetylated galactosamine functionalized with an alkyne. Metabolism positions the galactosamine moiety in the core of mucin-type *O*-linked glycoproteins.[113] Again, we probed for diazo groups by using strain-promoted cycloaddition with DIBAC− biotin and subsequent labeling with avidin−Alexa Fluor 594 (microscopy) or avidin−Alexa Fluor 647 (flow cytometry), and we probed for alkynyl groups by using Cu(I)-catalyzed cycloaddition with picolyl azide−Alexa Fluor 488.[111,112] Both microscopy and flow cytometry data showed an orthogonal labeling pattern that colocalized at the cell surface (Figure 1.1.12A,C). Because of the lower abundance of the alkynyl sugar (Figure 1.1.12B), the deleterious cross-reactivity with the Ac_4ManNAz metabolite was even more apparent in this experiment. Labeling of the alkyne was diminished substantially in the presence of the azido sugar (Figure 1.1.12D). In contrast, labeling of the alkyne was not affected by the presence of the diazo group. These data highlight the importance of orthogonal labeling methods for the simultaneous analysis of more than one metabolite and how diazo and alkynyl groups can provide the requisite chemoselectivity.

We conclude that stabilized diazo groups can rival azido groups as probes in chemical biology. The diazo group is smaller than an azido group and has overlapping but distinct reactivity. Remarkably, an α-diazo amide is able to survive complex metabolic transformations in a mammalian cell. Although other systems exist for dual labeling,[107-109] we conclude that none provide the small size, metabolic stability, and chemoselective reactivity of the diazo group. Our findings encourage the development of new biocompatible reactions for stabilized diazo compounds that could further manifest their potential.

1.2.3 Materials & Methods

1.2.3.1 Materials

Silica gel (40 μm) was from SiliCycle (Québec City, Canada). All reagent-grade materials were from Sigma–Aldrich (St. Louis, MO) and were used without further purification, except for D-mannosamine·HCl, which was from CarboSynth (San Diego, CA). Alexa Fluor® reagents, and cell culture medium and supplements were from Invitrogen (Carlsbad, CA). Instrumentation. ^{1}H, ^{13}C NMR spectra for all compounds were acquired at ambient temperature on Bruker Spectrometers in the National Magnetic Resonance Facility at Madison (NMRFAM) at the University of Wisconsin–Madison operating at 400, 500, or 750 MHz for ^{1}H and 126 or 189 MHz for ^{13}C. Chemical shift data are reported in units of δ (ppm) relative to residual solvent or TMS. Electrospray ionization (ESI) mass spectrometry was performed with a Micromass LCT at the Mass Spectrometry Facility in the Department of Chemistry at the University of Wisconsin–Madison. Super-resolution structured illumination microscopy (SR-SIM) was performed with an Elyra PS.1 super-resolution system from Zeiss (Oberkochen, Germany). Confocal microscopy was carried out with an Eclipse TE2000-U laser scanning confocal microscope from Nikon (Tokyo, Japan), equipped with an AxioCam digital camera from Zeiss. Flow cytometry was performed at the University of Wisconsin–Madison Carbone Cancer Center Flow Cytometry Facility with a FACS Calibur instrument from BD Biosciences (San Jose, CA). Cytometry data were analyzed by using the program FlowJo 8.7 from Treestar (Ashland, Oregon). Absorbance measurements were made with an infinite M1000 plate reader from Tecan (Männedorf, Switzerland). Immunoblots were imaged on an ImageQuant LAS4000 from GE Healthcare Bio-Sciences (Pittsburgh, PA). Image quantification was performed with the program ImageJ.

1.2.3.2 Statistics

Calculations were performed with GraphPad Prism version 6 software from GraphPad Software (La Jolla, CA).

1.2.3.3 Computational Methods

Calculations were performed using Gaussian software (Wallingford, CT). Structures were first constructed and calculated for geometry optimization at routine HF/6-31G basis set. Optimized structures were then subjected to full natural bond order (NBO) computations. Output files were exported to PyMOL Molecular Graphics System, Version 1.5.0.4 Schrödinger, LLC. Solvent-accessible surface areas were discretely approximated using the "get_area" selection command of PyMOL for each of the NBO output for the acetamide, diazoacetamide, and the azidoacetamide model compounds.

Solvent-Accessible Surface Area

acetamide	85.698 Å^2
diazoacetamide	101.109 Å^2
azidoacetamide	117.310 Å^2

1.2.3.4 Caution

***Caution!** The deimidogenation procedure cannot be used to produce an unstabilized diazo compound (e.g., a primary diazoalkane). Such unstabilized diazo compounds are dangerous, and their use should never be attempted in the context of chemical biology.

Diazo compounds can be unstable and thus dangerous. The diazo-containing compounds in our work are, however, stabilized by their conjugation with an acetamido group and do not pose the same dangers as do primary diazoalkanes such as diazomethane. Milligram quantities of diazo compound 2 (R=Bn) were subjected to (1) impact tests, (2) vigorous grinding with a mortar and pestle, and (3) heating to >150 °C, as described previously.[114] None of these procedures led to an explosion. Moreover, diazoacetamide compounds used in this work have been stored as solids at –20 °C for >1 year with no apparent decomposition or deterioration. Nevertheless, caution should be invoked upon handling any diazo compound.

1.2.3.5 Synthesis

The phrase "concentrated under reduced pressure" refers to the removal of solvents and other volatile materials using a rotary evaporator at water aspirator pressure (<20 torr) while maintaining the water-bath temperature below 40 °C. Residual solvent was removed from samples at high vacuum (<0.1 torr).

Ac_4ManAc and $Ac_4ManNAz$ were synthesized as reported previously,[115] as was $Ac_4ManKyne$.[116] *N*-Benzyl-2-azidoacetamide (**1**, R=Bn) and *N*-benzyl-2-diazoacetamide (**2**, R=Bn) were prepared as reported previously.[24,78,93] The ^{1}H and ^{13}C NMR spectra of diazo compound **2** (R=Bn) were recorded in acetonitrile. ^{1}H NMR (400 MHz, CD_3CN) δ 7.38–7.21 (m, 6H), 6.53 (s, 1H), 5.02 (s, 1H), 4.37 (d, *J* = 6.1 Hz, 2H). ^{13}C NMR (101 MHz, CD_3CN) δ 166.48, 140.63, 129.50, 128.31, 128.04, 47.47, 43.96. Starting materials for the synthesis of biotinylated compounds (2-(acryloyloxy)ethanaminium trifluoroacetate[117] and diazoacetamide–NHS ester[118,119] were also prepared as reported previously. NMR spectroscopy and mass spectrometry data matched those in the literature.

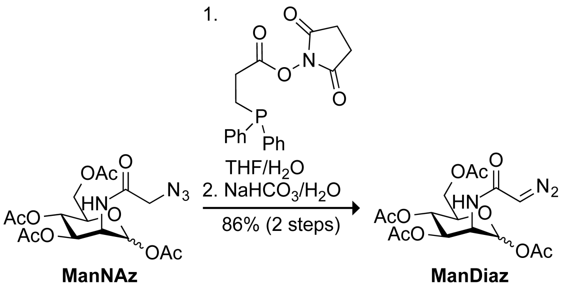

Tetra-*O*-acetyl-*N*-2-diazoacetyl mannosamine (ManDiaz). Tetra-*O*-acetyl-*N*-2-azidoacetyl mannosamine (Ac_4ManNAz)[2] (285 mg, 0.662 mmol) was dissolved in 90:10 THF/H_2O (5 mL). *N*-Succinimidyl 3-(diphenylphosphino)propionate[3] (247 mg, 0.695 mmol) was added, and the resulting solution was stirred for 5 h. A saturated solution of $NaHCO_3$(aq) (4 mL) was added, and the resulting solution was stirred for an additional 6 h. The reaction mixture was diluted with brine (20 mL) and extracted with dichloromethane (4 × 30 mL), dried over Na_2SO_4(s), and concentrated under reduced pressure to a yellowish solid. The residue was purified by chromatography on silica gel (30:70 EtOAc/hexanes) to provide ManDiaz as a yellow solid (236 mg, 86%) (~1:1 mixture of α/β anomers). ^{1}H NMR (750 MHz, CD_3Cl) δ 6.03 (s, 1H), 5.98 (d, J = 9.3 Hz, 1H), 5.86 (s, 1H), 5.73 (d, J = 9.1 Hz, 1H), 5.33 (dd, J = 10.3, 4.5 Hz, 1H), 5.17 (t, J = 10.3 Hz, 1H), 5.11 (t, J = 9.8 Hz, 1H), 5.06 (dd, J = 10.0, 3.9 Hz, 1H), 5.00 (s, 1H), 4.96 (s, 1H), 4.88–4.81 (m, 1H), 4.71 (s, 1H), 4.29 (td, J = 12.1, 5.5 Hz, 2H), 4.09–4.01 (m, 3H), 3.81 (ddd, J = 8.4, 5.3, 2.3 Hz, 1H), 2.18 (s, 3H), 2.12 (s, 3H), 2.09 (s, 6H), 2.06 (s, 6H), 2.03 (s, 6H). ^{13}C NMR (189 MHz, $CDCl_3$) δ 170.64, 170.60, 170.18, 170.10, 169.77, 169.75, 168.45, 168.22, 91.93, 90.82, 73.45, 71.47, 70.16, 69.02, 65.71, 65.44, 62.34, 62.11, 49.77, 47.58, 45.78, 42.22, 20.87, 20.80, 20.77, 20.75, 20.73, 20.66, 20.64. HRMS (ESI) calc'd. for $C_{16}H_{21}N_3O_{10}$ $[M + H]^+$ 416.1300, found 416.1310.

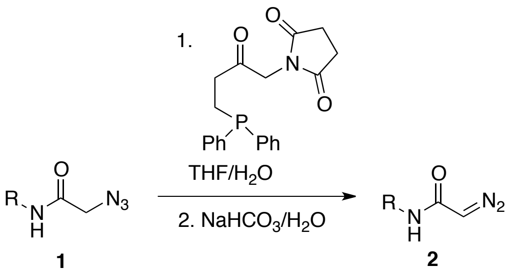
1.
O
N
O
O
P
Ph
Ph
THF/H$_2$O
2. NaHCO$_3$/H$_2$O
R
N
H
O
N$_3$
1
R
N
H
O
N$_2$
2

N-Benzyl-2-diazoacetamide (2). N-Benzyl-2-azidoacetamide (**1**) and N-benzyl-2-diazoacetamide (**2**) were prepared as reported previously.[4]

^{1}H NMR (400 MHz, CD_3CN) δ 7.38–7.21 (m, 6H), 6.53 (s, 1H), 5.02 (s, 1H), 4.37 (d, J = 6.1 Hz, 2H). ^{13}C NMR (101 MHz, CD_3CN) δ 166.48, 140.63, 129.50, 128.31, 128.04, 47.47, 43.96.

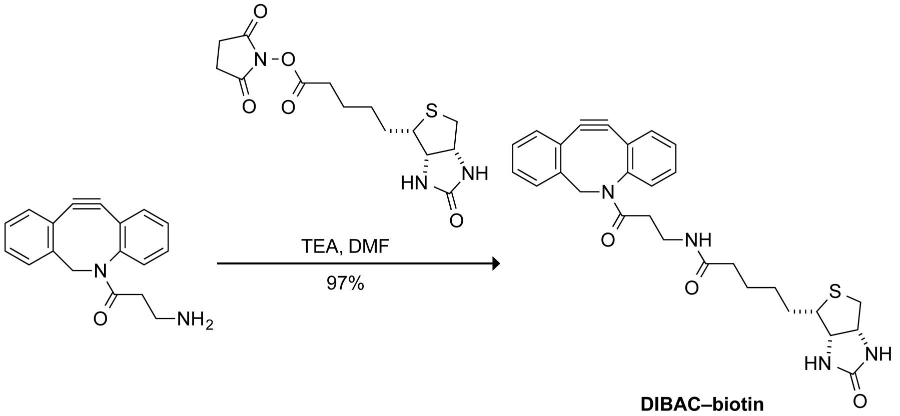
TEA, DMF
97%
NH$_2$
N
O
N-O
O
O
O
S
HN
NH
O
NH
DIBAC–biotin

DIBAC–biotin. DIBAC (0.022 g, 0.078 mmol) was dissolved in 1 mL of anhydrous DMF. Triethylamine (0.022 mL, 0.159 mmol) and biotin–NHS (0.03 g, 0.084 mmol) were added, and the resulting solution was stirred for 7 h. The reaction mixture was then concentrated under reduced pressure. The residue was dissolved in dichloromethane (5 mL), washed with brine (2 × 5 mL), dried over Na_2SO_4(s), and concentrated under reduced pressure. The residue was purified by chromatography on silica gel (90:10, DCM/MeOH) to give the DIBAC–biotin conjugate. (0.039 g, 97%). ^{1}H NMR (750 MHz, DMSO-d_6) δ 7.63 (d, J = 7.6 Hz, 1H), 7.59 (td, J = 7.8, 6.1, 3.8 Hz, 2H), 7.51–7.49 (m, 1H), 7.48–7.44 (m, 2H), 7.39 (td, J = 7.5, 1.4 Hz, 1H), 7.35 (t, J = 7.5 Hz, 1H), 7.30 (d, J = 7.5 Hz, 1H), 6.40–6.38 (s, 1H), 6.35 (s, 1H), 5.04 (d, J = 14.2 Hz, 1H), 4.30 (t, J = 6.4 Hz, 1H), 4.10 (dt, J = 5.2, 2.4 Hz, 1H), 3.63 (d, J = 14.2 Hz, 1H), 3.1 –3.02 (m, 2H), 2.94–2.88 (m, 1H), 2.81 (dd, J = 12.5, 5.2 Hz, 1H), 2.57 (d, J = 12.5 Hz, 1H), 2.44–2.38 (m, 1H), 1.91 (t, J = 7.6 Hz, 2H), 1.85–1.79 (m, 1H), 1.55 (m, 1H), 1.44–1.33 (m, 3H), 1.26–1.15 (m, 2H).^{13}C NMR (126 MHz, DMSO) δ 171.91, 170.22, 162.75, 151.45, 148.44, 132.45, 129.59, 129.00, 128.28, 128.13, 127.80, 126.88, 125.27, 122.50, 121.44, 114.34, 108.12, 61.03, 59.21, 55.44, 54.87, 35.03, 34.94, 34.31, 28.19, 28.02, 27.99, 25.16. HRMS (ESI) calc'd. for $C_{28}H_{30}N_4O_3S$ $[M + H]^+$ 503.2112, found 503.2105.

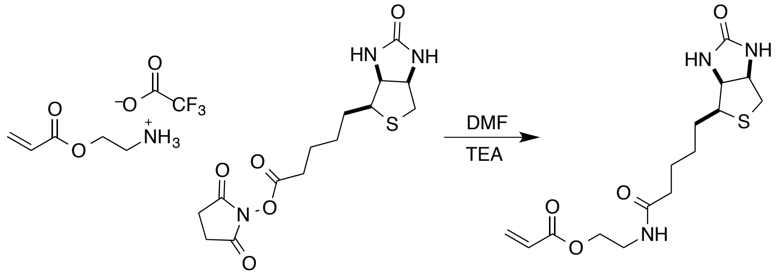

2-Aminoethyl Acrylate–biotin Conjugate (AEB). 2-(Acryloyloxy)ethanaminium trifluoroacetate[6] (0.041 g, 0.176 mmol) was dissolved in 1.5 mL of anhydrous DMF and followed by the addition triethylamine (0.051 mL, 0.44 mmol). Biotin–NHS was added (0.05 g, 0.146 mmol), and the resulting solution was stirred at overnight. The reaction mixture was concentrated by rotary evaporation, and the residue was purified by chromatography on silica gel (DCM/MeOH 9:1) to give the acrylate–biotin conjugate. (0.049 g, 98%). ^{1}H NMR (500 MHz, MeOD) δ 6.37 (dd, J = 17.3, 1.5 Hz, 1H), 6.14 (dd, J = 17.3, 10.5 Hz, 1H), 5.86 (dd, J = 10.5, 1.5 Hz, 1H), 4.45 (dd, J = 7.8, 4.9 Hz, 1H), 4.26 (dd, J = 7.9, 4.5 Hz, 1H), 4.17 (t, J = 5.4 Hz, 2H), 3.43 (tt, J = 5.5, 3.1 Hz, 2H), 3.14 (d, J = 6.9 Hz, 1H), 2.88 (dd, J = 12.8, 5.0 Hz, 1H), 2.69–2.62 (m, 2H), 2.17 (t, J = 8.1 Hz, 1H), 1.74–1.50 (m, 4H), 1.43–1.35 (m, 2H). ^{13}C NMR (126 MHz, MeOD) δ 177.62, 168.82, 167.38, 133.11, 130.65, 65.41, 64.61, 62.88, 58.26, 42.31, 40.69, 37.94, 30.98, 30.74, 28.10. HRMS (ESI) calc'd. for $C_{15}H_{23}N_3O_4S$ $[M + H]^+$ 342.1483, found 342.1486.

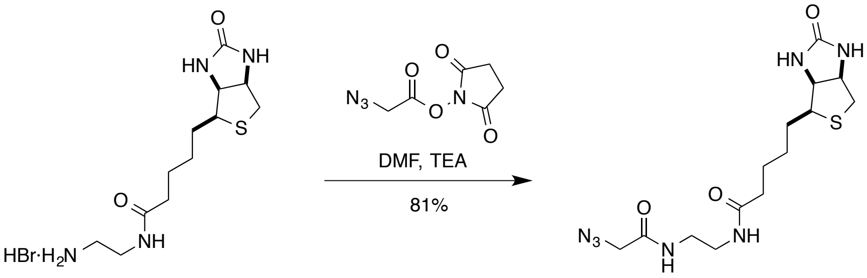

Azidoacetamide–biotin Conjugate (AB). Biotin ethylenediamine hydrobromide (0.040 g, 0.109 mmol) was dissolved in 1 mL of anhydrous DMF followed by triethylamine (0.030 mL, 0.22 mmol). The azidoacetamide–NHS ester (0.023 g, 0.114 mmol) was added, and the resulting solution was stirred overnight. The reaction mixture was concentrated under reduced pressure, and the residue was purified by chromatography on silica gel (DCM/MeOH 9:1) to give the azide–biotin conjugate. (0.033 g, 81%). ^{1}H NMR (500 MHz, MeOD) δ 4.46 (dd, J = 7.8, 4.8 Hz,

1H), 4.28 (dd, *J* = 7.9, 4.5 Hz, 1H), 3.87 (s, 2H), 3.28 (m, 5H), 2.90 (dd, *J* = 12.7, 5.0 Hz, 1H), 2.67 (d, *J* = 12.7 Hz, 1H), 2.17 (td, *J* = 7.3, 2.3 Hz, 2H), 1.77–1.49 (m, 4H), 1.41 (m, 2H). ^{13}C NMR (126 MHz, MeOD) δ 177.78, 171.78, 167.41, 64.61, 62.90, 58.25, 54.29, 42.31, 41.54, 41.06, 38.05, 31.03, 30.74, 28.02. HRMS (ESI) calc'd. for $C_{14}H_{23}N_7O_3S$ $[M + H]^+$ 370.1656, found 370.1658.

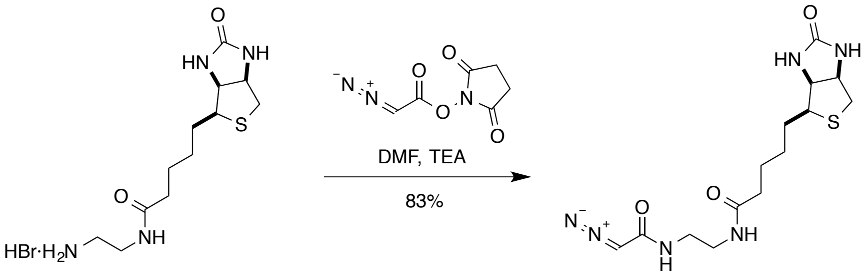

Diazoacetamide–biotin Conjugate (DB). Biotin ethylenediamine hydrobromide (0.025 g, 0.068 mmol) was dissolved in 0.7 mL of anhydrous DMF. The resulting solution was cooled to 0 °C and stirred for 15 min before the addition of triethylamine (0.020 mL, 0.143 mmol). After stirring at 0 °C for 15 min, the diazo–NHS ester[6] (0.014 g, 0.0715 mmol) was added, and the resulting mixture was stirred at 0 °C for 30 min before warming to room temperature and stirring for an additional 16 h. The reaction mixture was then concentrated under reduced pressure, and the residue was purified by chromatography on silice gel (DCM/MeOH 9:1) to give the diazo–biotin conjugate (0.020 g, 83%). ^{1}H NMR (500 MHz, MeOD) δ 5.10 (s, 1H), 4.46 (dd, *J* = 7.8, 4.9 Hz, 1H), 4.27 (dd, *J* = 7.8, 4.4 Hz, 1H), 3.33–3.28 (m, 1H), 3.24 (m 1H), 2.89 (dd, *J* = 12.7, 5.0 Hz, 1H), 2.81 (d, *J* = 16.4 Hz, 1H), 2.70–2.64 (d, *J* = 12.7 Hz 1H), 2.63 (s, 2H), 2.17 (td, *J* = 7.3, 1.7 Hz, 2H), 1.75–1.50 (m, 4H), 1.45–1.35 (m, 2H). ^{13}C NMR (126 MHz, MeOD) δ

177.66, 170.20, 167.40, 64.61, 62.90, 58.25, 42.33, 41.65, 38.05, 31.00, 30.74, 28.04, 27.69, 27.54. HRMS (ESI) calc'd. for $C_{14}H_{22}N_6O_3S$ [M + Na]$^+$ 377.1367, found 377.1370.

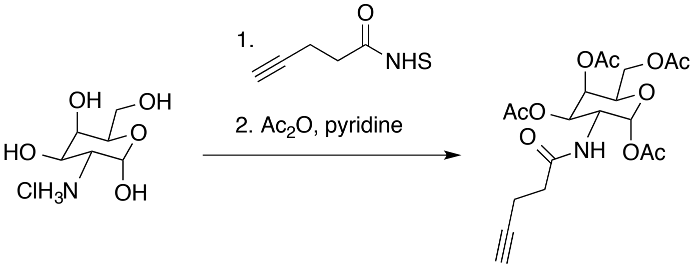

1,3,4,6-Tetra-*O*-acetyl-*N*-4-pentynoylgalactosamine (GalKyne) was prepared from 2-amino-2-deoxy-D-galactopyranose·HCl by using the procedure reported for 1,3,4,6-tetra-*O*-acetyl-*N*-4-pentynoylmannosamine (ManKyne).[3] α/β Anomers ~10:1, α anomer: ^{1}H NMR (500 MHz, $CDCl_3$) δ 6.23 (d, J = 3.5 Hz, 1H), 5.75–5.66 (d, J = 8.5 Hz 1H), 5.43 (dd, J = 3.4, 1.3 Hz, 1H), 5.23 (dd, J = 11.6, 3.2 Hz, 1H), 4.82–4.71 (m, 1H), 4.29–4.21 (m, 1H), 4.15–4.04 (m, 2H), 2.50 (td, J = 7.2, 6.4, 2.6 Hz, 2H), 2.36 (tt, J = 7.2, 3.0 Hz, 2H), 2.18 (s, 6H), 2.04 (s, 3H), 2.03 (s, 3H).^{13}C NMR (126 MHz, $CDCl_3$) δ 171.23, 171.21, 170.53, 170.36, 168.94, 91.37, 82.68, 69.69, 68.64, 67.91, 66.75, 61.38, 46.88, 35.31, 21.12, 20.94, 20.83, 20.79, 14.87. HRMS (ESI) calc'd. for $C_{19}H_{25}NO_{10}$ [M+H]$^+$ 428.1552, found 428.1541.

1.2.3.6 Reaction Rate Constants

NMR spectroscopy was used to determine rate constants for cycloaddition reactions, as described previously.[78] Briefly, an equimolar solution of reactants in CD_3CN were mixed in an NMR tube (final concentration: 0.02 M). The tube was inverted once and inserted into a spectrometer, and scanning was initiated 60 s after the initial mixing. A 16-scan NMR spectrum was acquired every 77 s, and integrations were used to calculate concentrations from the known initial concentrations. The second-order rate constant was then determined from the slope of a plot of $[\text{octyne}]^{-1}$ *vs* time. All NMR kinetics experiments were conducted in triplicate, and the reported rate constants are the mean (± SE) in Table 4.S1.

1.2.3.7 Assay for the Reactivity of a Diazo Compound with Glutathione

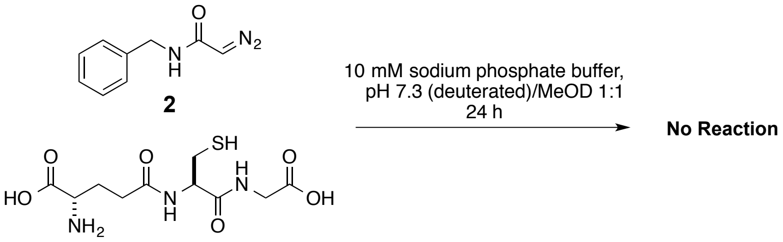

N-Benzyl-2-diazoacetamide (**2**) (1 equiv, 0.066 mmol, 1.16 mg) and reduced glutathione (1 equiv, 0.066 mmol, 2.0 mg) were dissolved in 10 mM sodium phosphate buffer, pH 7.3 (deuterated)/MeOD 1:1 (0.33 mL, pH 7.3). The resulting solution was stirred for 24 h, then analyzed by ^{1}H NMR spectroscopy.

Diazo compound 2: ^{1}H NMR (500 MHz, 10 mM sodium phosphate buffer, pH 7.3 (deuterated)/MeOD 1:1) δ 7.37–7.26 (m, 5H), 4.39 (s, 2H).

GSH: ^{1}H NMR (500 MHz, 10 mM sodium phosphate buffer, pH 7.3 (deuterated)/MeOD 1:1) δ

4.53 (dd, $J = 7.2, 5.1$ Hz, 1H), 3.79 (s, 2H), 3.71 (t, $J = 6.3$ Hz, 1H), 2.91 (qd, $J = 14.1, 6.2$ Hz, 2H), 2.54 (t, $J = 7.5$ Hz, 2H), 2.14 (q, $J = 7.6$ Hz, 2H).

1.2.3.8 General Cell Culture

Cell lines were obtained from American Type Culture Collection (Manassas, VA) and were maintained according to the recommended procedures. Cells were grown in a cell-culture incubator at 37 °C under CO_2(g) (5% v/v) in flat-bottomed culture flasks. Cell medium was supplemented with GIBCO fetal bovine serum (FBS) (10% v/v), penicillin (100 units/mL), and streptomycin (100 μg/mL) in an appropriate cellular medium: Chinese hamster ovary (CHO K1), F12K nutrient medium; HeLa, DMEM; HEK293T, DMEM; and Jurkat, RPMI 1640. Cells were counted with a hemocytometer to determine their seeding density in 12-well plates from Corning Costar (Lowell, MA) or 8-well chambered glass slides from Ibidi (Madison, WI).

1.2.3.9 Biotin Conjugates to Probe Chemoselectivity

Microscopy. CHO K1 cells were seeded at a density of 50,000 cells/dish in 35-mm μ-dish microscopy imaging dishes from Ibidi. Cells were incubated with 1 mM acrylic ester–biotin, 25 μM biotin–diazo, 25 μM biotin–azide, or DMSO in standard medium for 24–48 h. On the day of an experiment, cells were rinsed twice with wash buffer (DPBS containing 1% v/v FBS) and incubated with avidin–Alexa Fluor488® (20 μg/mL) for 20 min at 4 °C. After treatments, cell nuclei were stained with Hoechst 33342 (2 μg/mL) for 5 min at 37 °C. Cells were then washed twice with wash buffer, and examined using a scanning confocal microscope.

Flow Cytometry. CHO K1 cells were seeded at a density of 50,000 cells/well in 12-well plates. Cells were incubated with 1 mM acrylic ester–biotin, 25 μM biotin–diazo, or 25 μM biotin–azide for 24–48 h. The medium was then removed, and the cells were washed twice with wash buffer (DPBS containing 1% v/v FBS) and incubated with avidin–Alexa Fluor488® (20 μg/mL) for 20 min at 4 °C. After these treatments, cells were rinsed twice with wash buffer and released from the plate with 250 μL of trypsin/EDTA (0.25% w/v). Cells were resuspended in an additional 500 μL of medium and incubated on ice until analyzed by flow cytometry. The fluorescence intensity of at least 20,000 events was then measured by flow cytometry. Alexa Fluor488® was excited with a 488 nm solid- state laser, and the emission was measured through a 530/30 bandpass filter.

Immunoblotting. CHO K1 cells were seeded at a density of 50,000 cells/well in 12-well plates. Cells were incubated in 1 mM acrylic ester–biotin, 25 μM biotin–diazo, 25 μM biotin–azide, or DMSO for 24–48 h. After these treatments, cells were rinsed twice with DPBS and released from the plate with 250 μL of trypsin/EDTA (0.25% w/v). Cells were washed twice, pelleted by centrifugation, and resuspended in DPBS. SDS–PAGE sample buffer was added to cell suspensions, and samples were boiled for 5 min, subjected to brief centrifugation, and analyzed by SDS–PAGE on a 12% w/v gel before being transferred to a PVDF membrane. Membranes were analyzed for the presence of azido or diazo sugars by immunoblotting with α-biotin (1:1000) from Cell Signaling Technology (Danvers, MA). To control for loading levels, membranes were analyzed for β-actin by immunoblotting with α–β-actin (1:1000) from Cell Signaling Technology.

1.2.3.10 Metabolism of Ac_4ManDiaz and Ac_4ManNAz by CHO K1 Cells

Microscopy. CHO K1 cells were seeded at a density of 100,000 cells/dish in 35-mm μ-dish microscopy imaging dishes from Ibidi, and grown in the presence of Ac_4ManDiaz or Ac_4ManNAz (25 μM) in standard medium for 2 d. On the day of the experiment, the cells were rinsed twice with wash buffer (DPBS containing 1% v/v FBS) and treated with DIBAC–biotin

(10 µM) in standard medium for 1 h at 37 °C. Cells were again washed twice, and incubated with avidin–Alexa Fluor488® (20 µg/mL) for 20 min at 4 °C. Cell nuclei were stained with Hoechst 33342 (2 µg/mL) from Invitrogen for 5 min at 37 °C. Cells were again washed twice, and incubated on ice in standard medium until ready to be imaged by super-resolution microscopy.

Cytometry. CHO K1 cells were seeded at a density of 50,000 cells/well in 12-well plates, and grown in the presence of Ac_4ManDiaz (0–50 µM) for 2 days in standard medium. The cells were then rinsed twice with wash buffer (DPBS containing 1% v/v FBS) and treated with DIBAC–biotin (10 µM) in standard medium for 1 h at 37 °C. Cells were again washed twice, and incubated with avidin–Alexa Fluor488® (20 µg/mL) for 20 min at 4 °C. Cells were again washed twice and released from the dish by treatment with trypsin/EDTA (0.25% w/v) for 5 min at 37 °C. Cells were resuspended in standard medium, and incubated on ice. The fluorescence intensity of 20,000 events was then measured by flow cytometry. Alexa Fluor488® was excited with a 488 nm solid-state laser, and the emission was measured through a 530/30 bandpass filter.

1.2.3.11 Metabolism of Ac_4ManDiaz by Multiple Cell Types

CHO K1, HeLa, HEK293T, and Jurkat cells were seeded at a density of 50,000 cells/well in 12-well plates, and grown in the presence of Ac_4ManDiaz (0–50 µM) for 2 days in standard medium. Cells were then rinsed twice with wash buffer (DPBS containing 1% v/v FBS) and treated with DIBAC–biotin (10 µM) in standard medium for 1 h at 37 °C. Jurkat cells were washed by centrifugation at 1000*g* for 5 min; all other cell types are adherent. Cells were again washed twice, and incubated with avidin–Alexa Fluor488® (20 µg/mL) for 20 min at 4 °C. Cells were washed twice with wash buffer, and adherent cells were released from the dish by incubation with trypsin/EDTA (0.25% w/v) for 5 min at 37 °C. Cells were resuspended in standard medium, and incubated on ice until analysis. The fluorescence intensity of 20,000 events was then measured by flow cytometry. Alexa Fluor488® was excited with a 488 nm solid-state laser, and the emission was measured through a 530/30 bandpass filter.

1.2.3.12 Neuraminidase and Peptide-N-Glycosidase F treatment of CHO K1 cells

CHO K1 cells were treated with $Ac_4ManNAc$, $Ac_4ManNAz$, or $Ac_4ManDiaz$ (250 μM) for 3 d. Cells were lifted from the plate with trypsin/EDTA (0.25% w/v), collected by centrifugation, and washed twice with DPBS. Cells were treated with DIBAC–biotin (20 μM) for 2 h at 37 °C. G7 reaction buffer (New England Biolabs) was added, and the suspension was divided into three samples. Neuraminidase (acetyl-neuraminyl hydrolase) from New England Biolabs (Ipswich, MA) was added to one sample; peptide-*N*-glycosidase F (PNGase F) from New England Biolabs was added to another sample, and PBS was added to the remaining sample. Samples were incubated at 37 °C overnight. SDS–PAGE sample buffer was added, and samples were boiled for 5 min, subjected to brief centrifugation, and analyzed by SDS–PAGE on a 12% w/v gel before being transferrred to a PVDF membrane. Membranes were analyzed for the presence of azido or diazo sugars by immunoblotting with α-biotin (1:1000) from Cell Signaling Technology. To control for loading levels, membranes were analyzed for β-actin by immunoblotting with α–β-actin (1:1000) from Cell Signaling Technology.

1.2.3.13 Mass Analysis of Sialic acids from Biological Samples

Sialic acids were isolated for analysis by using a method reported by Hackenberger and coworkers.[106] CHO K1 cells were seeded into 6-well plates and treated with $Ac_4ManDiaz$ or $Ac_4ManNAz$ (250 μM) for 3 d. Cells were released from the dish by incubation with trypsin/EDTA (0.25% w/v) for 5 min at 37 °C. Cells were washed twice in DPBS. The cells were resuspended in 200 μL of H_2O, and 500 μL of 3 M acetic acid was added. The resulting suspension was incubated at 90 °C for 90 min before being cooled to 0 °C for 15 min and neutralized by the addition of 650 μL of 3% v/v NH_3 for 30 min at room temperature. Samples were lyophilized, and resuspended in 500 μL of EtOH/H_2O 4:1. Samples were mixed with a vortex mixer and subjected to centrifugation at 10,000*g* for 2 min. The supernatant was lyophilized. The residue was suspended in 300 μL of EtOH/MeOH 2:1, and the resulting suspension was mixed with a vortex mixer and subjected to centrifugation at 10,000*g* for 2 min. The supernatant was lyophilized. The residue was dissolved in PBS, and enriched for biotin–linked sugars by purification over SoftLink^{TM} Soft Release Avidin Resin from Promega. The biotin–linked sugars were eluted from the resin with 3 M acetic acid, and the eluent was concentrated by lyophilization. Enriched isolates were dissolved in 100 μL of MeOH, and 25 μL was injected directly onto a Shimadzu 2010A single quadrupole mass analyzer LCMS in single-ion monitoring mode with a scanning width of 0.9 *m*/*z* so as to observe the sialic acid conjugates in the presence of excess DIBAC–biotin.

1.2.3.14 Optimal Labeling of CHO K1 Cells with Ac_4ManDiaz

1.2.3.14.1 Increasing Amounts of DIBAC–Biotin. CHO K1 cells were seeded at a density of 50,000 cells/well in 12-well plates, and grown in the presence of Ac_4ManDiaz (25 μM) for 2 days in standard medium. The cells were then rinsed twice with wash buffer (DPBS containing 1% v/v FBS) and treated with DIBAC–biotin (0–20 μM) in standard medium for 1 h at 37 °C. Cells were again washed twice, and incubated with avidin–Alexa Fluor488$^{®}$ (20 μg/mL) for 20 min at 4 °C. Cells were washed twice with wash buffer, and released from the dish by incubation with trypsin/EDTA (0.25% w/v) for 5 min at 37 °C. Cells were resuspended in standard medium, and incubated on ice. The fluorescence intensity of 20,000 events was then measured by flow cytometry. The fluorescence intensity of 20,000 events was then measured by flow cytometry. Alexa Fluor488® was excited with a 488 nm solid-state laser, and the emission was measured through a 530/30 bandpass filter.

1.2.3.14.2 Increasing Incubation Times with DIBAC–Biotin. CHO K1 cells were seeded at a density of 50,000 cells/well in 12-well plates, and grown in the presence of Ac_4ManDiaz (25 µM) for 2 days in standard medium. The cells were then rinsed twice with wash buffer (DPBS containing 1% v/v FBS) and treated with DIBAC–biotin (10 µM) in standard medium for 0–120 min at 37 °C. Cells were again washed twice, and incubated with avidin–Alexa Fluor488® (20 µg/mL) for 20 min at 4 °C. Cells were washed twice with wash buffer, and released from the dish by incubation with trypsin/EDTA (0.25% w/v) for 5 min at 37 °C. Cells were resuspended in standard medium, and incubated on ice. The fluorescence intensity of 20,000 events was then measured by flow cytometry. The fluorescence intensity of 20,000 events was then measured by flow cytometry. Alexa Fluor488® was excited with a 488 nm solid-state laser, and the emission was measured through a 530/30 bandpass filter.

1.2.3.15 Cytotoxicity of Ac4ManDiaz and Ac4ManNAz for CHO K1 Cells.

The cytotoxicity of the $Ac_4ManDiaz$ and $Ac_4ManNAz$ was determined using the CellTiter 96® AQueous One Solution Cell Proliferation Assay (MTS) from Promega (Madison, WI). Briefly, CHO K1 cells were plated at a concentration of 5000 cells/well in a clear 96-well plate. Cells were allowed to adhere for 4 h. The medium was removed, and varying concentrations of either $Ac_4ManDiaz$ or $Ac_4ManNAz$ in medium was added. Cells were incubated at 37 °C for 24 h. The medium was removed, and cells were washed with DPBS. The MTS reagent was added at a ratio of 1:5, and cells were incubated at 37 °C for 2 h before measuring the absorbance at 490 nm. Reported data are the average of three measurements for each concentration, and the entire experiment was repeated in triplicate. The percentage of viable cells was determined by normalizing to a PBS control (100% viable), and a H_2O_2 control (0% viable). Values for LD_{50} were calculated by fitting the curves by nonlinear regression analysis.

1.2.3.16 Dual-Color Labeling of Mannosamine in the Glycocalyx.

Microscopy. CHO K1 cells were seeded at a density of 100,000 cells/dish in 35-mm μ-dish microscopy imaging dishes from Ibidi, and grown in the presence of a peracetylated sugar (25 μM) in standard medium for 2 d. On the day of an experiment, cells were rinsed twice with wash buffer (DPBS containing 1% v/v FBS).

Alkyne treatment. Cells were treated with medium containing DIBAC–biotin (10 μM) for 1 h at 37 °C. Cells were rinsed twice with wash buffer (DPBS containing 1% v/v FBS), and incubated with avidin–Alexa Fluor594® (20 μg/mL) for 20 min at 4 °C.

Azide treatment. Cells were treated with medium containing picolyl azide–Alexa Fluor647® (5 μM), $CuSO_4$ (50 μM), THPTA (250 μM), and sodium ascorbate (2.5 mM) for 5 min at room temperature.[6]

In one experiment, cells were treated with azide and then alkyne; in another experiment, cells were treated with alkyne and then azide. After treatments, cell nuclei were stained with Hoechst 33342 (2 μg/mL) for 5 min at 37 °C. Cells were then washed twice with wash buffer, and examined using a scanning confocal microscope.

Cytometry. Two days prior to an experiment, CHO K1 cells were seeded in 12-well plates at 1×10^5 cells/well, and a sugar was added to a final concentration of 25 μM. On the day of an experiment, cells were rinsed twice with wash buffer (DPBS containing 1% v/v FBS).

Alkyne treatment. Cells were treated with medium containing DIBAC–biotin (10 μM) for 1 h at 37 °C. Cells were rinsed twice with wash buffer (DPBS containing 1% v/v FBS), and incubated with avidin–Alexa Fluor647® (20 μg/mL) for 20 min at 4 °C.

Azide treatment. Cells were treated with medium containing picolyl azide–Alexa Fluor647® (5 μM), $CuSO_4$ (50 μM), THPTA (250 μM), and sodium ascorbate (2.5 mM) for 5 min at room temperature.[112]

In one experiment, cells were treated with azide and then alkyne; in another experiment, cells were treated with alkyne and then azide. After these treatments, cells were rinsed twice with wash buffer (DPBS containing 1% v/v FBS) and released from the plate with 250 μL of trypsin/EDTA (0.25% w/v). Cells were resuspended in an additional 500 μL of medium and incubated on ice until analyzed by flow cytometry. The fluorescence intensity of at least 20,000 events was measured by flow cytometry. Alexa Fluor488® was excited with a 488 nm solid-state laser, and the emission was measured through a 530/30 bandpass filter. Alexa Fluor647® was excited with a 633 nm solid-state laser and the emission was collected with a 661/16 bandpass filter.

1.2.3.17 Dual-Color Labeling of Mannosamine and Galactosamine in the Glycocalyx. *Microscopy*. CHO K1 cells were seeded at a density of 100,000 cells/dish in 35-mm μ-dish microscopy imaging dishes from Ibidi, and grown in the presence of a peracetylated sugar (25 μM) in standard medium for 2 d. On the day of an experiment, cells were rinsed twice with wash buffer (DPBS containing 1% v/v FBS).

Alkyne treatment. Cells were treated with medium containing DIBAC–biotin (10 μM) for 1 h at 37 °C. Cells were rinsed twice with wash buffer (DPBS containing 1% v/v FBS), and incubated with avidin–Alexa Fluor594® (20 μg/mL) for 20 min at 4 °C.

Azide treatment. Cells were treated with medium containing picolyl azide–Alexa Fluor647® (5 μM), $CuSO_4$ (50 μM), THPTA (250 μM), and sodium ascorbate (2.5 mM) for 5 min at room temperature.[112]

After treatments, cell nuclei were stained with Hoechst 33342 (2 μg/mL) for 5 min at 37 °C. Cells were then washed twice with wash buffer, and examined using a scanning confocal microscope.

Cytometry. Two days prior to an experiment, CHO K1 cells were seeded in 12-well plates at 1×10^5 cells/well, and a sugar was added to a final concentration of 25 μM. On the day of an experiment, cells were rinsed twice with wash buffer (DPBS containing 1% v/v FBS).

Alkyne treatment. Cells were treated with medium containing DIBAC–biotin (10 μM) for 1 h at 37 °C. Cells were rinsed twice with wash buffer (DPBS containing 1% v/v FBS), and incubated with avidin–Alexa Fluor647® (20 μg/mL) for 20 min at 4 °C.

Azide treatment. Cells were treated with medium containing picolyl azide–Alexa Fluor647® (5 μM), $CuSO_4$ (50 μM), THPTA (250 μM), and sodium ascorbate (2.5 mM) for 5 min at room temperature.[112]

Cells were treated with alkyne for 60 min and then azide for 5 min. After these treatments, cells were rinsed twice with wash buffer (DPBS containing 1% v/v FBS) and released from the plate with 250 μL of trypsin/EDTA (0.25% w/v). Cells were resuspended in an additional 500 μL of medium and incubated on ice until analyzed by flow cytometry. The fluorescence intensity of at least 20,000 events was measured by flow cytometry. Alexa Fluor488® was excited with a 488 nm solid-state laser, and the emission was measured through a 530/30 bandpass filter. Alexa Fluor647® was excited with a 633 nm solid-state laser, and the emission was collected with a 661/16 bandpass filter.

Table 1.2.S1 Rate constants ($M^{-1}s^{-1}$) for the reaction of Diazo 1 and Azide 2 with strained cyclooctynes

Table 1.2.S1. Rate constants ($M^{-1}s^{-1}$) for the reaction of Diazo 1 and Azide 2 with strained cyclooctynes

	BCN[a]	DIBONE[a]	DIBAC[a]	DIBAC[b]
Diazo **1**	0.08 ± 0.02	0.34 ± 0.01	0.45 ± 0.09	2.6 ± 0.2
Azide **2**	0.11 ± 0.02	0.14 ± 0.04	0.23 ±0.06	0.40 ± 0.09

[a] In CD_3CN. [b] In 1:1 CD_3CN/H_2O.

Figure 1.2.1 Space-filling models of diazo and azido derivatives of acetamide

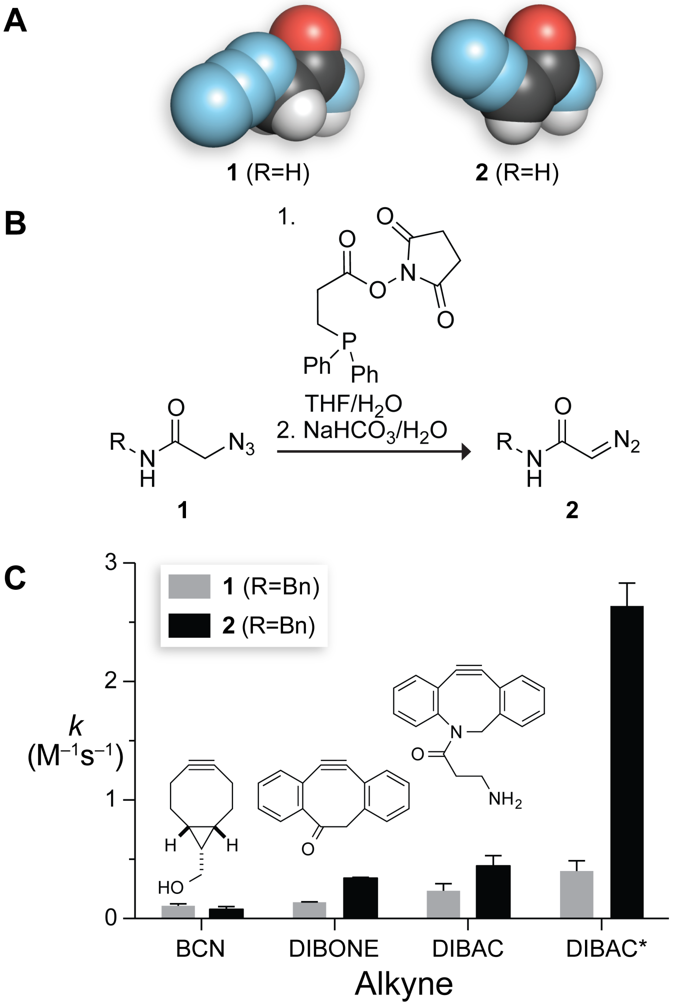
A
1 (R=H)
2 (R=H)
B
1.
O
O
N
O
O
P
Ph
Ph
THF/H$_2$O
2. NaHCO$_3$/H$_2$O
R
N
H
O
N$_3$
1
R
N
H
O
N$_2$
2
C
1 (R=Bn)
2 (R=Bn)
k
(M^{-1}s^{-1})
3
2
1
0
H
H
HO
O
N
O
NH$_2$
BCN
DIBONE
DIBAC
DIBAC*
Alkyne

Figure 1.2.1 (A) Space-filling models of diazo and azido derivatives of acetamide. A diazo group and azido group add 15.4 and 31.6 Å of solvent-accessible surface area, respectively (Table 4.S1). (B) Scheme for the deimidogenation of an azide to form a diazo compound. (C) Bar graph of the rate constants for the reaction of an azide (1) and diazo compound (2) with strained cyclooctynes in CD_3CN or $*CD_3CN/H_2O$ 1:1 as determined by ^1H NMR spectroscopy.

Figure 1.2.2 Variations of *N*-acetylmannosamine used in this study that are trafficked into sialic acid

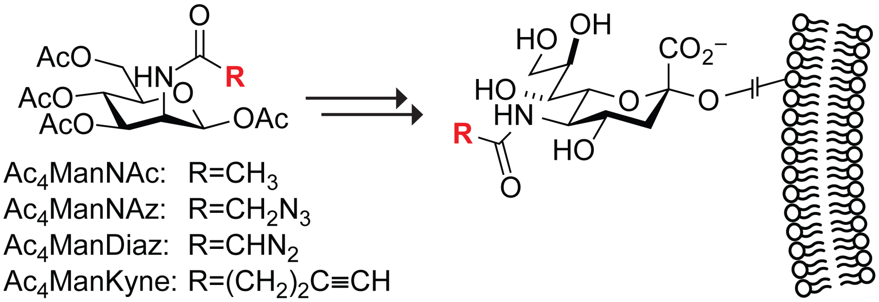
AcO
AcO
AcO
HN
O
R
O
OAc
HO
OH
HO
HN
R
O
O
HO
CO_2^-
O

Ac$_4$ManNAc: R=CH_3
Ac$_4$ManNAz: R=CH_2N_3
Ac$_4$ManDiaz: R=CHN_2
Ac$_4$ManKyne: R=$(CH_2)_2C{\equiv}CH$

Figure 1.2.2 Variations of *N*-acetylmannosamine used in this study that are trafficked into sialic acid.

Figure 1.2.3 ^{1}H NMR spectra

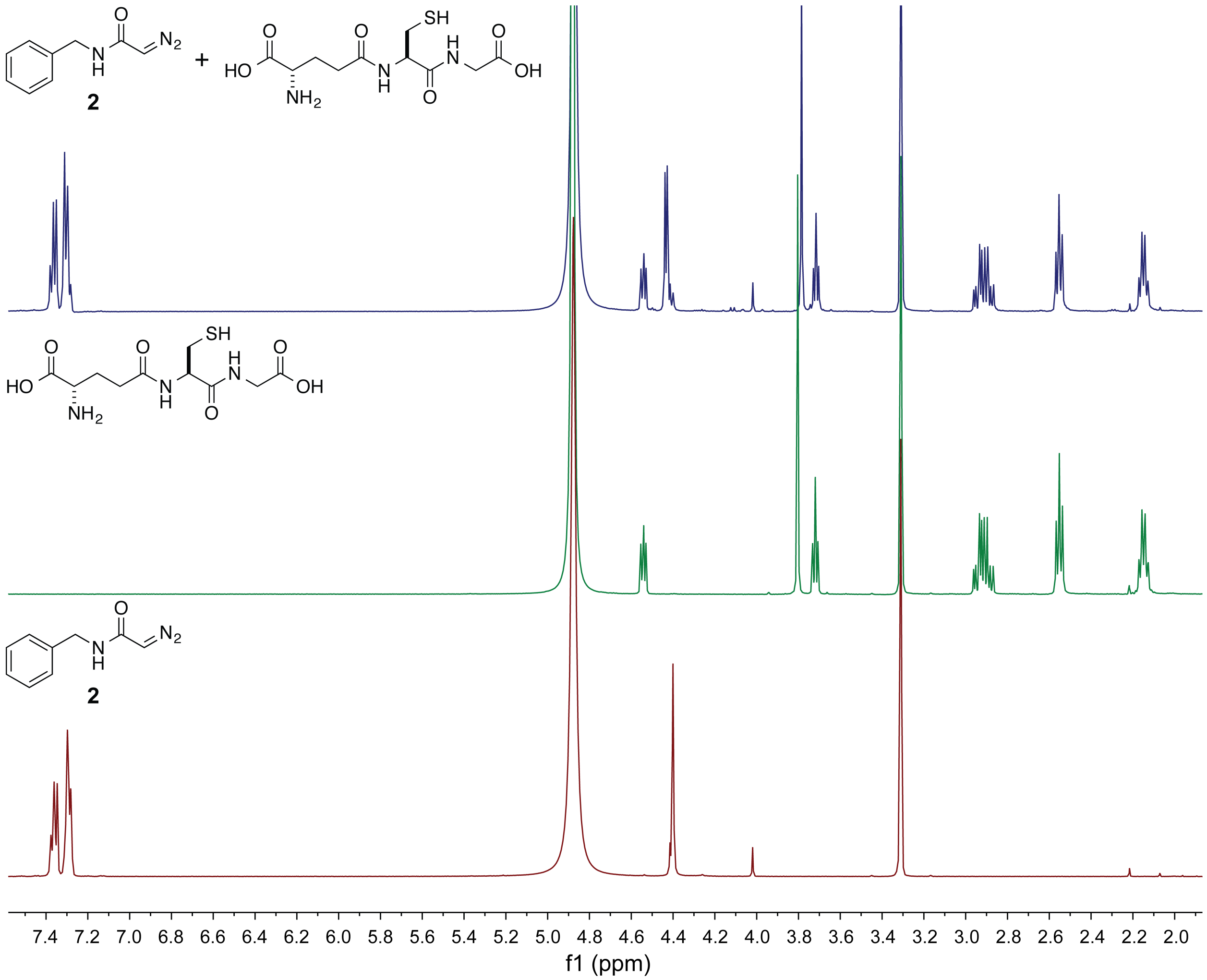

Figure 1.2.3 ^{1}H NMR spectra (500 MHz, 10 mM sodium phosphate buffer, pH 7.3 (deuterated)/MeOD 1:1) of *N*-benzyl-2-diazoacetamide (**2**) (bottom, red), reduced glutathione (middle, green), and an equimolar mixture (0.20 M each) after a 24-h incubation in 10 mM sodium phosphate buffer, pH 7.3 (deuterated)/MeOD 1:1 (top, blue). There was no apparent reaction between the glutathione and diazo compound **2**.

Figure 1.2.4 Chemoselectivity of diazo and azido groups

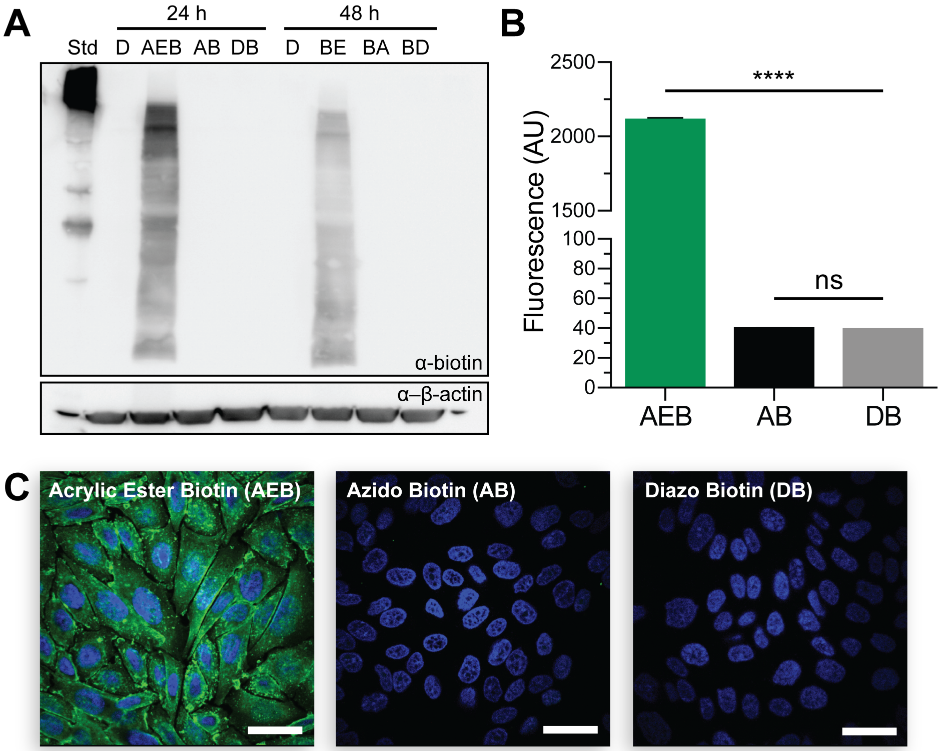

Figure 1.2.4 Chemoselectivity of diazo and azido groups. (A) Immunoblot of biotin signal of cell lysates grown in either DMSO (D), acrylic ester–biotin (AEB; 1 mM), azido–biotin (AB; 25 μM), or diazo–biotin (DB; 25 μM) for 24 or 48 h. (B) Flow cytometry analysis of cells grown as in panel A for 24 h, $p < 0.0001$. (C) Microscopy of fixed and permeabilized cells grown as in panel A for 24 h. Cells were stained with avidin–Alexa Fluor488® and Hoechst 33342. Scale bars correspond to 25 μm.

Figure 1.2.5 Trafficking of diazo and azido sugars in mammalian cells

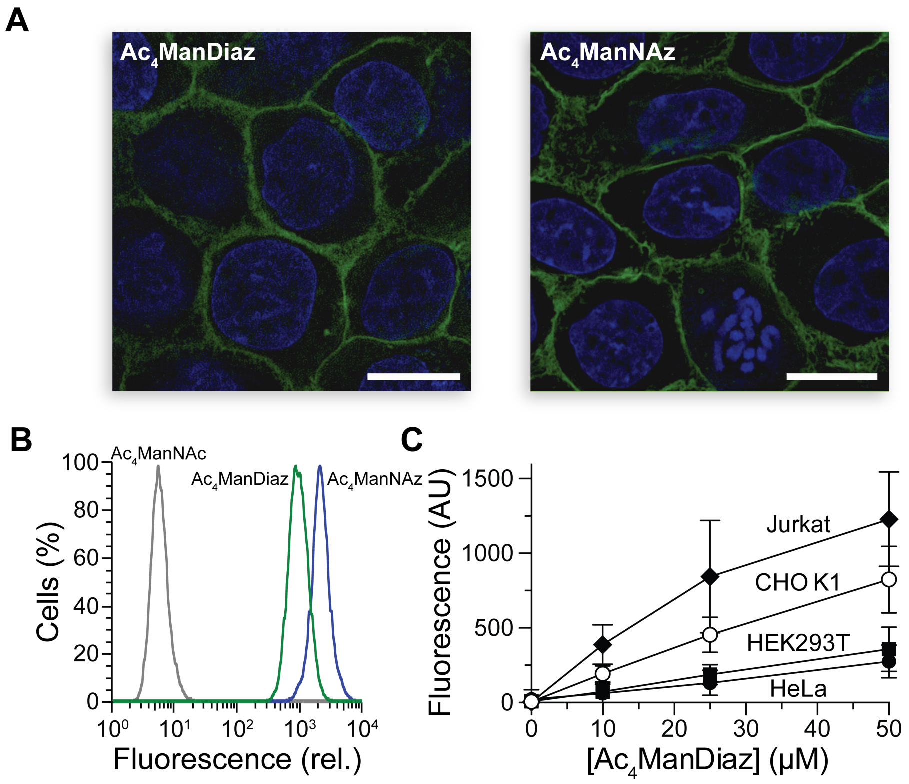

Figure 1.2.5 Trafficking of diazo and azido sugars in mammalian cells. (A) Super-resolution images of CHO K1 cells grown in medium containing $Ac_4ManDiaz$ or $Ac_4ManNAz$ (25 μM) for 2 d, washed, treated with DIBAC–biotin (10 μM) for 60 min and then avidin–Alexa Fluor488® and Hoechst 33342, and fixed. Scale bars: 10 μm. (B) Histogram of CHO K1 cells grown in medium containing $Ac_4ManNAc$, $Ac_4ManDiaz$, or $Ac_4ManNAz$ (25 μM) as in panel A. (C) Graph of the concentration-dependent fluorescence of Jurkat, CHO K1, HEK293T, and HeLa cells grown in medium containing $Ac_4ManDiaz$ (0–50 μM) as in panel A. Data in panels B and C were acquired by flow cytometry.

Figure 1.2.6 Metabolic incorporation of $Ac_4ManDiaz$ into sialic acid

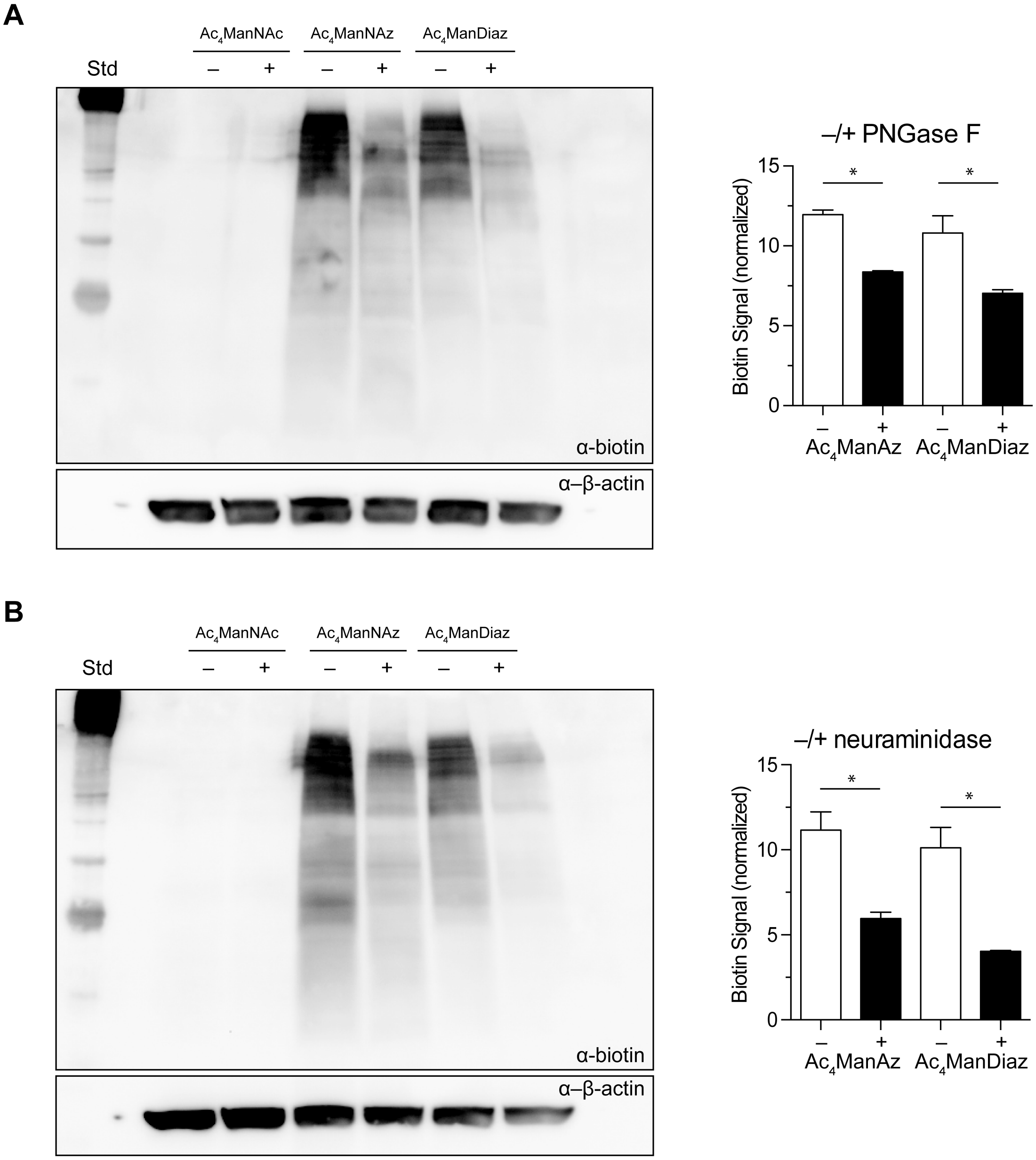

Figure 1.2.6 Metabolic incorporation of Ac_4ManDiaz into sialic acid. Immunoblot analysis of cell lysates treated with DIBAC–biotin, after growth in the presence of Ac_4ManNAc, Ac_4ManNAz, or Ac_4ManDiaz (250 μM) for 3 d, and (A) incubation in either PNGase F or buffer, and (B) incubation in either neuraminidase or buffer. Quantification was normalized to actin to control for loading, $p < 0.05$. Quantification of the azido and diazo untreated lanes from all experiments showed that expression of a diazo group from Ac_4ManDiaz is (86 ± 3)% of the azido group from Ac_4ManNAz.

Figure 1.2.7 Detection of sialic acid derivatives generated *in cellulo* from Ac_4ManDiaz and Ac_4ManNAz

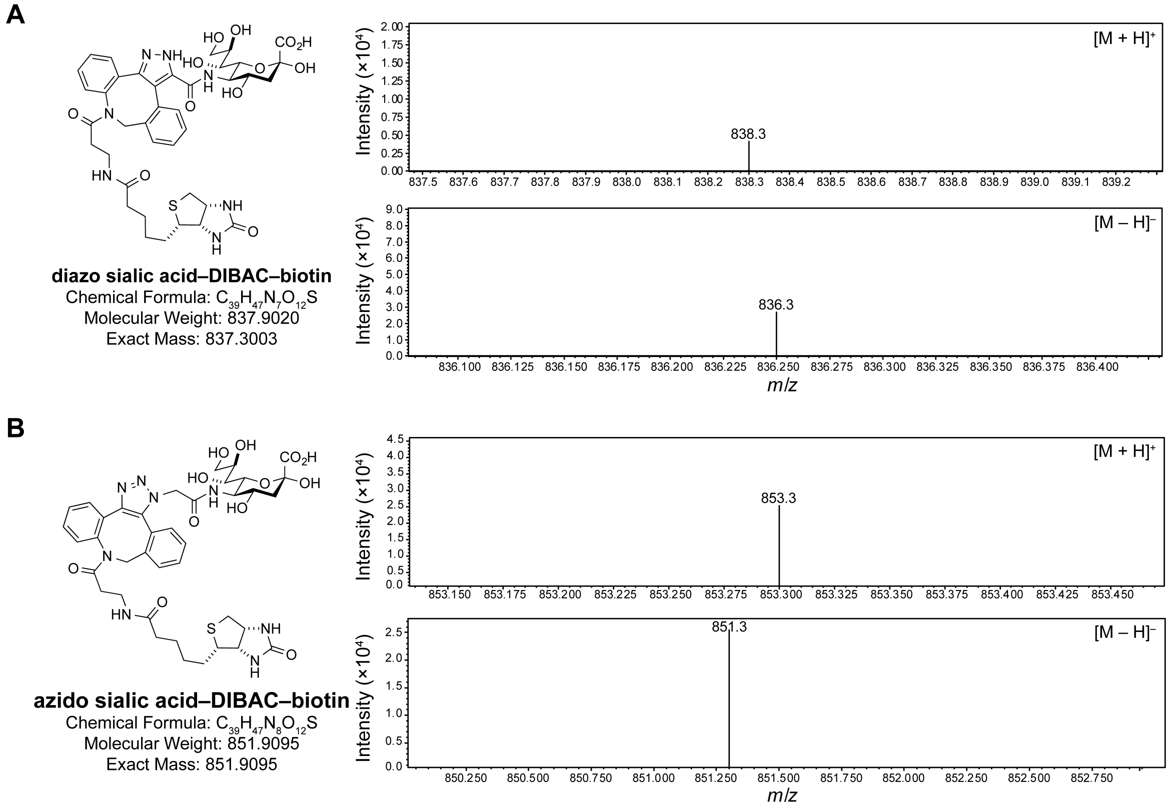

Figure 1.2.7 Detection of sialic acid derivatives generated *in cellulo* from Ac_4ManDiaz and Ac_4ManNAz. Positive and negative ions were observed in independent LC-LRMS (ESI) analyses after cycloaddition with DIBAC–biotin and product isolation.

Figure 1.2.8 Histogram of CHO K1 cells grown in medium containing Ac$_4$ManDiaz

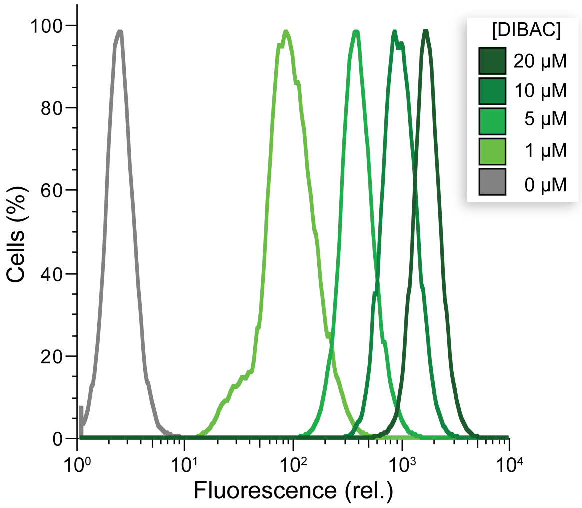

Figure 1.2.8 Histogram of CHO K1 cells grown in medium containing Ac_4ManDiaz (25 μM) and treated with increasing amounts of DIBAC–biotin and avidin–Alexa Fluor488®. Data were acquired by flow cytometry. At 20 μM, DIBAC–biotin begins to cause cytotoxicity.

Figure 1.2.9 Histogram of CHO K1 cells grown in medium containing Ac$_4$ManDiaz

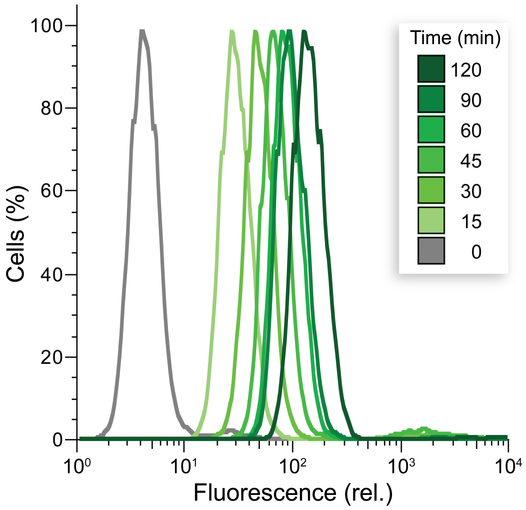

Figure 1.2.9 Histogram of CHO K1 cells grown in medium containing Ac_4ManDiaz (25 μM) and treated with 10 μM DIBAC–biotin for increasing time, then avidin–Alexa Fluor488®. Data were acquired by flow cytometry. At times >60 min, DIBAC–biotin begins to cause cytotoxicity.

Figure 1.2.10 Graph of the cytotoxicity of Ac_4ManDiaz and Ac_4ManNAz (10 µM–10 mM) for CHO K1 cells

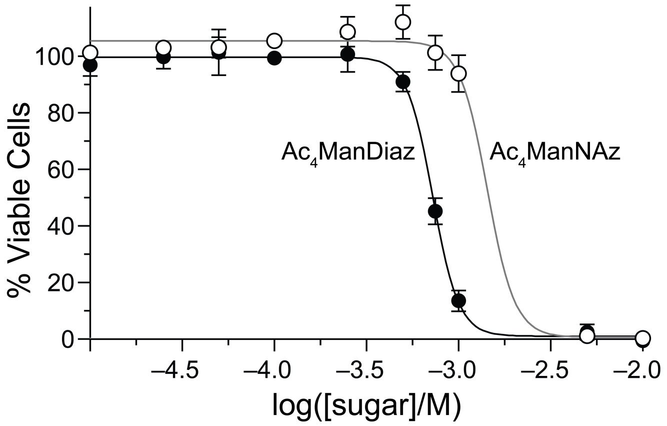

Figure 1.2.10 Graph of the cytotoxicity of Ac_4ManDiaz and Ac_4ManNAz (10 µM–10 mM) for CHO K1 cells. LD_{50} values are (0.7 ± 0.1) mM for Ac_4ManDiaz and (1.4 ± 0.1) mM for Ac_4ManNAz.

Figure 1.2.11 Dual labeling of mammalian cells with diazo and alkynyl sugars

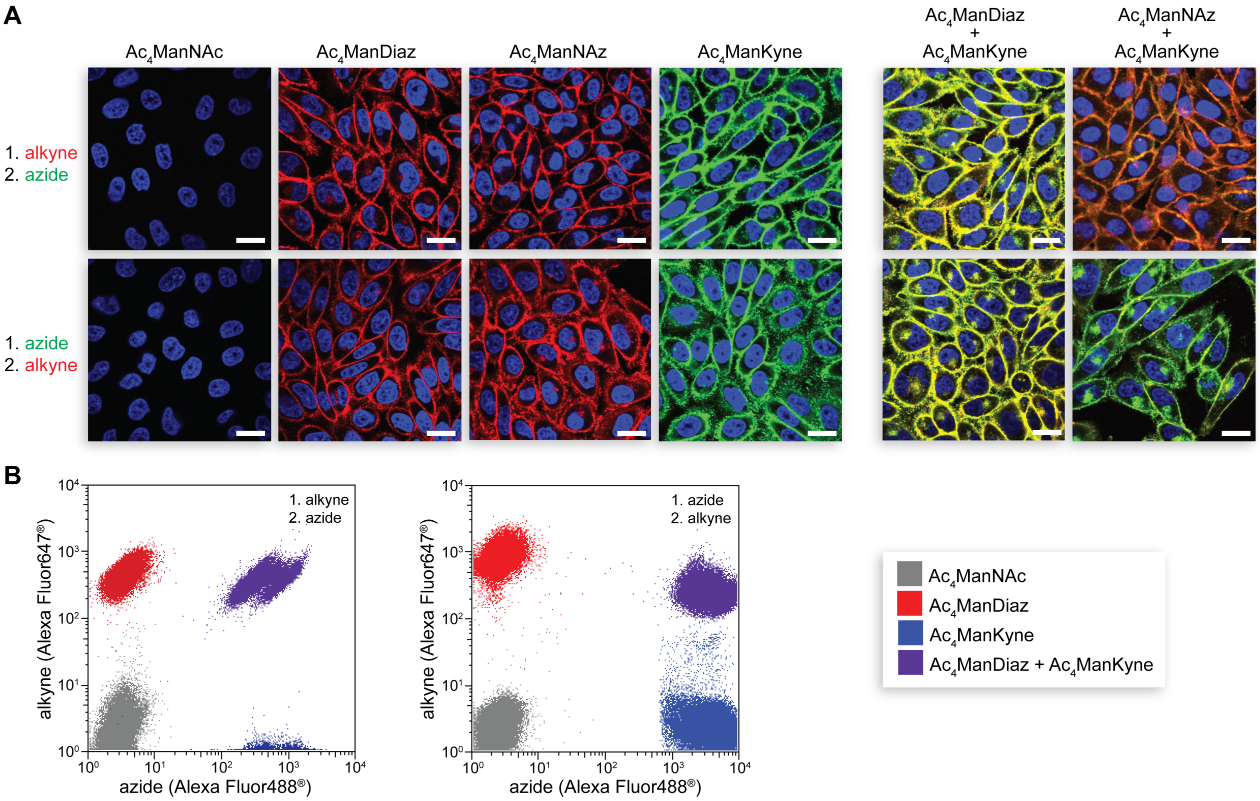
A
Ac$_4$ManNAc
Ac$_4$ManDiaz
Ac$_4$ManNAz
Ac$_4$ManKyne
Ac$_4$ManDiaz + Ac$_4$ManKyne
Ac$_4$ManNAz + Ac$_4$ManKyne
1. alkyne
2. azide
1. azide
2. alkyne
B
alkyne (Alexa Fluor647®)
azide (Alexa Fluor488®)
10^0
10^1
10^2
10^3
10^4
1. alkyne
2. azide
1. azide
2. alkyne
Ac$_4$ManNAc
Ac$_4$ManDiaz
Ac$_4$ManKyne
Ac$_4$ManDiaz + Ac$_4$ManKyne

Figure 1.2.11 Dual labeling of mammalian cells with diazo and alkynyl sugars. (A) Images of CHO K1 cells grown in medium containing derivatives of *N*-acetylmannosamine for 2 d, then labeled by cycloaddition with an alkyne (red) and azide (green), and visualized with confocal microscopy. Scale bars: 10 μm. (B) Plots demonstrating the dual labeling of cells that had metabolized Ac_4ManDiaz and Ac_4ManKyne. Data were acquired by flow cytometry.

Figure 1.2.12 Dual labeling of mammalian cells grown with derivatives of *N*-acetylmannosamine and *N*-acetylgalactosamine

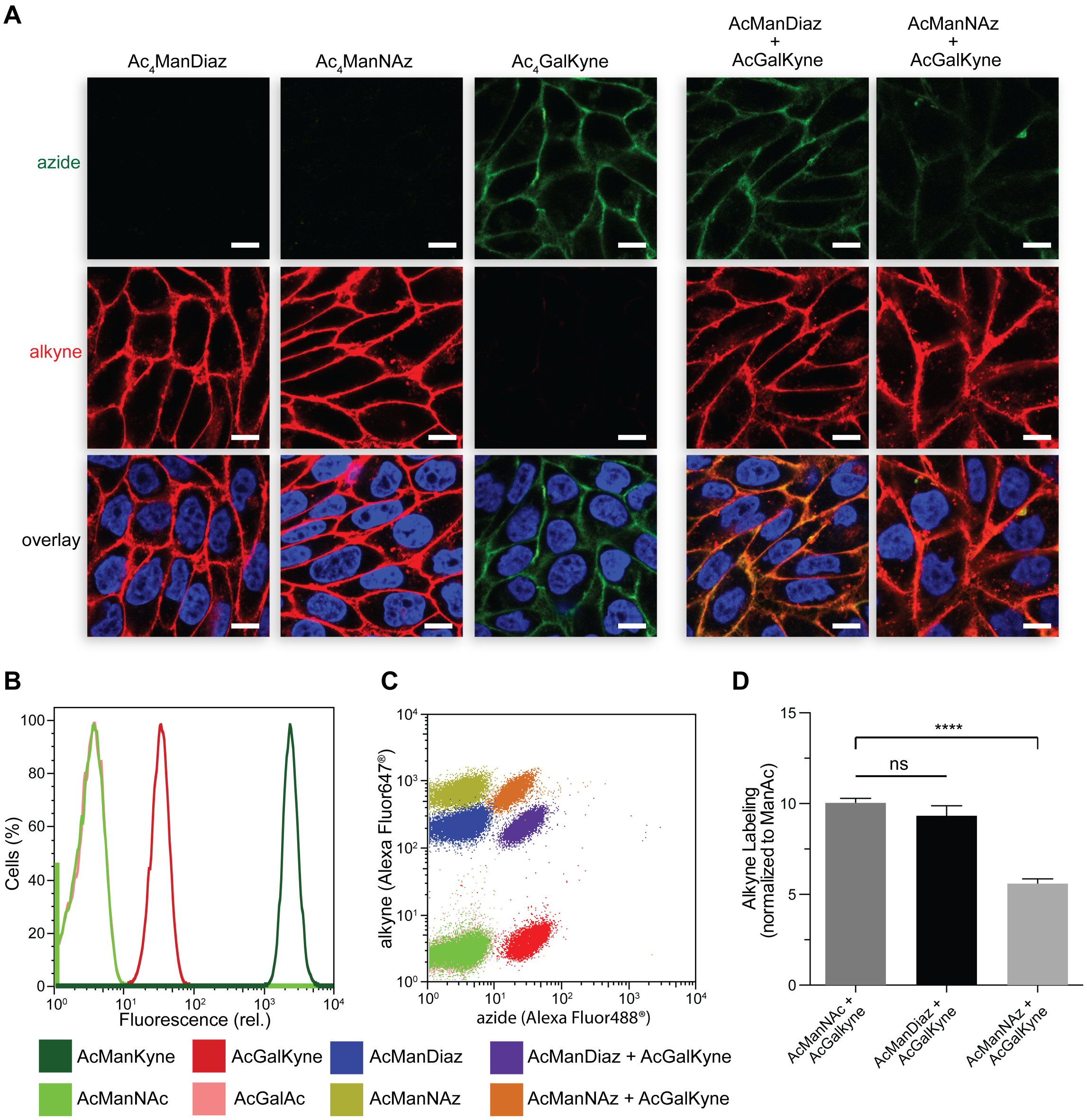
A
Ac4ManDiaz
Ac4ManNAz
Ac4GalKyne
AcManDiaz + AcGalKyne
AcManNAz + AcGalKyne
azide
alkyne
overlay
B
Cells (%)
100
80
60
40
20
0
10⁰
10¹
10²
10³
10⁴
Fluorescence (rel.)
C
alkyne (Alexa Fluor647®)
azide (Alexa Fluor488®)
10⁰
10¹
10²
10³
10⁴
D
Alkyne Labeling (normalized to ManAc)
15
10
5
0
****
ns
AcManNAc + AcGalkyne
AcManDiaz + AcGalkyne
AcManNAz + AcGalkyne
AcManKyne
AcGalKyne
AcManDiaz
AcManDiaz + AcGalKyne
AcManNAc
AcGalAc
AcManNAz
AcManNAz + AcGalKyne

Figure 1.2.12 Dual labeling of mammalian cells grown with derivatives of *N*-acetylmannosamine and *N*-acetylgalactosamine. (A) Images of CHO K1 cells grown in medium containing *N*-acetylmannosamine or *N*-acetylgalactosamine derivatives (25 μM) for 2 d, then labeled by cycloaddition with an alkyne (red) and azide (green), and visualized with confocal microscopy. Scale bars: 5 μm. (B) Histogram showing the lesser labeling of cells exposed to Ac_4GalKyne than Ac_4ManKyne as measured by flow cytometry. (C) Plot demonstrating the dual labeling of cells that had metabolized Ac_4GalKyne and either Ac_4ManDiaz or Ac_4ManNAz as measured by flow cytometry. (D) Quantification of the level of Ac_4GalKyne labeling obtained in cells grown with derivatives of *N*-acetylmannosamine, $p < 0.0001$.

1.2.4 NMR Spectra

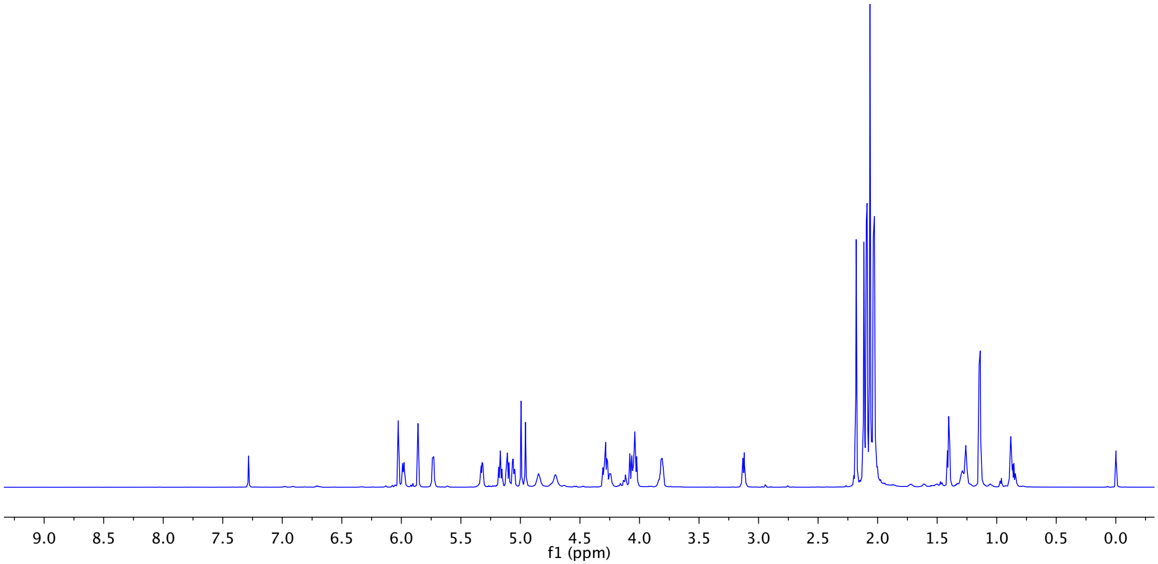

Spectra 1a. ^{1}H NMR spectrum of **tetra-*O*-acetyl ManNDiaz** (mixed anomers) in $CDCl_3$ (750 MHz)

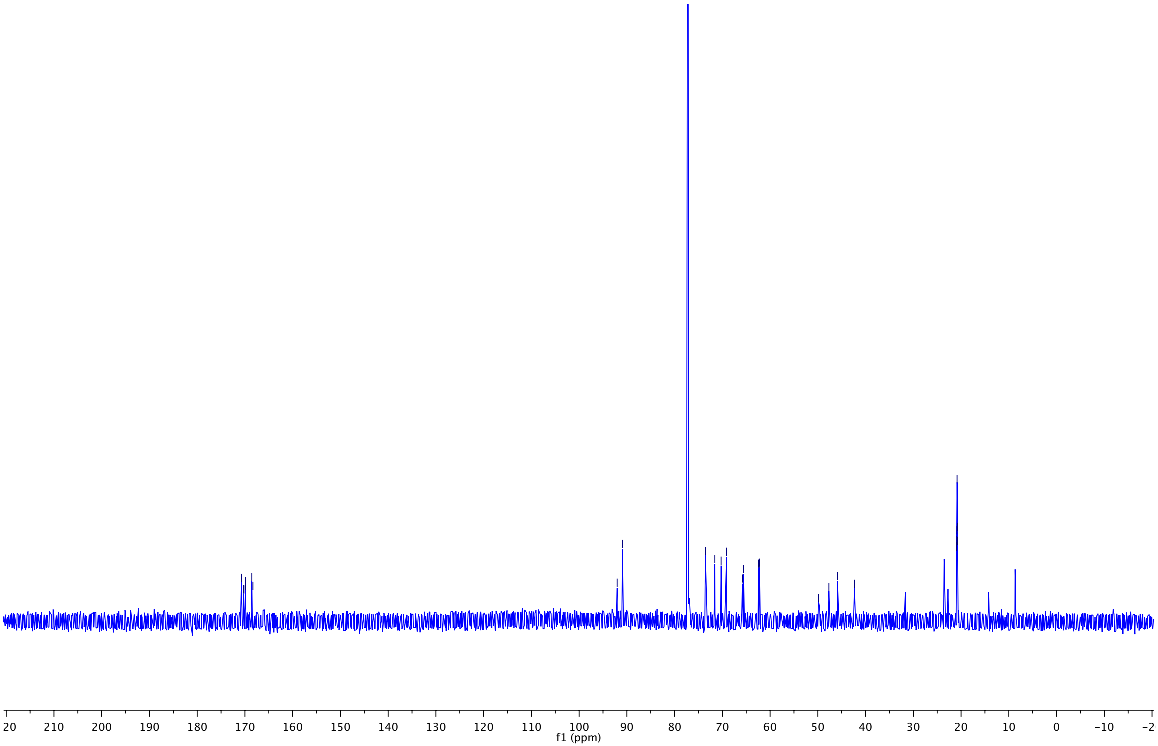

Spectra 1b. ^{13}C NMR spectrum of **tetra-*O*-acetyl ManNDiaz** (mixed anomers) in $CDCl_3$ (189 MHz)

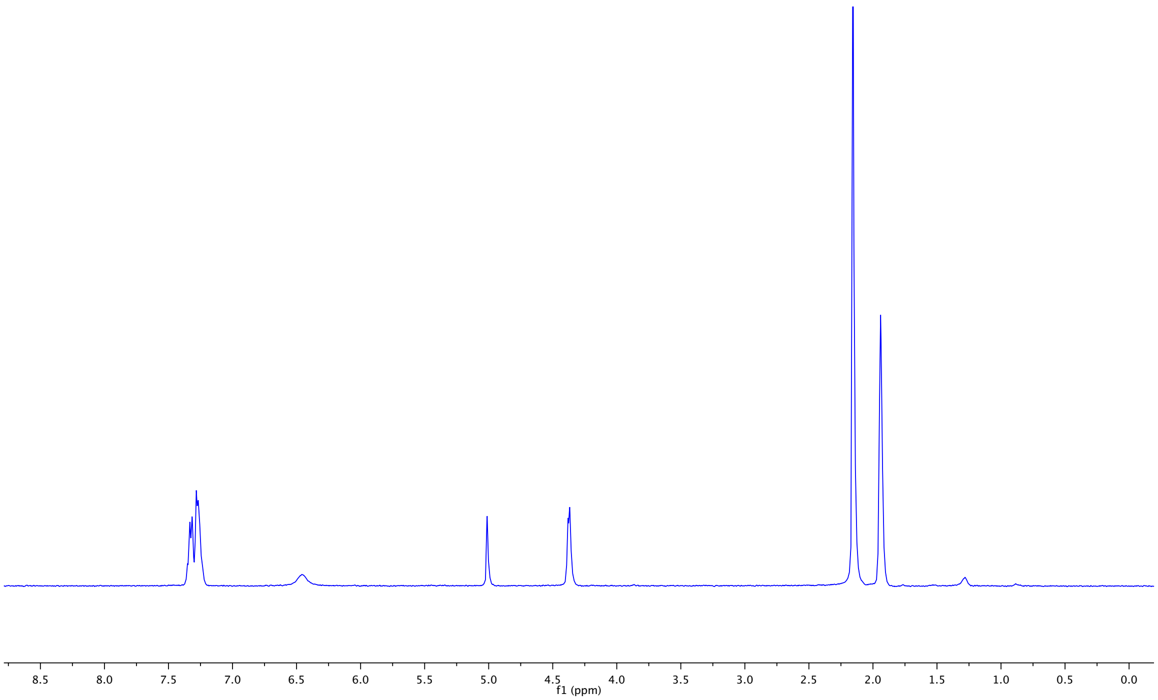

Spectra 2a. ^{1}H NMR spectrum of ***N*-diazoacetamide benzylamine** in CD_3CN (400 MHz).

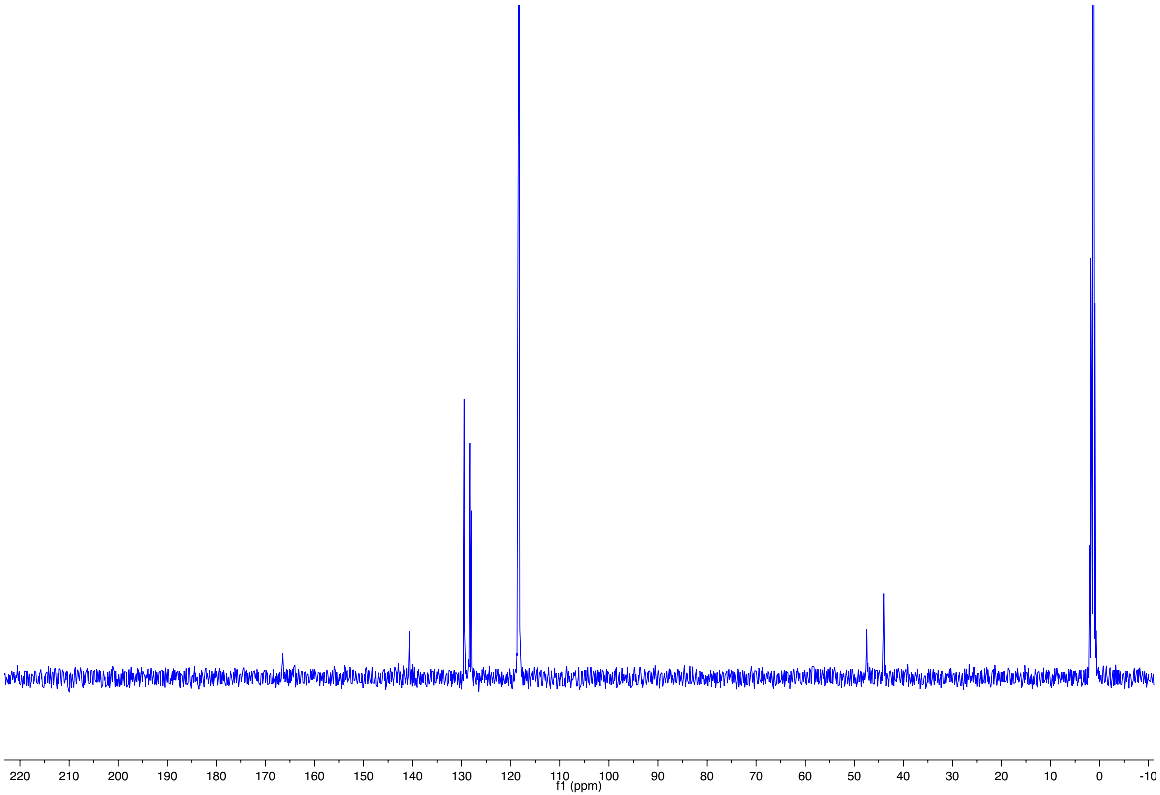

Spectra 2b. ^{13}C NMR spectrum of ***N*-diazoacetamide benzylamine** in CD_3CN (101 MHz).

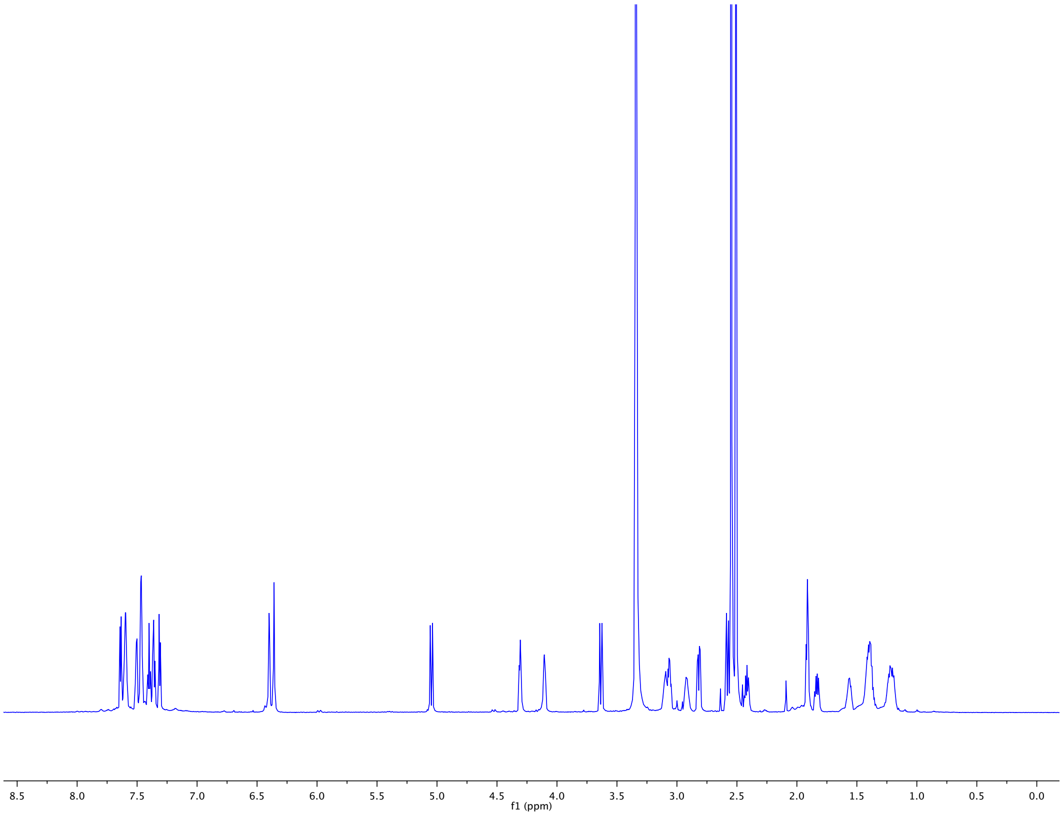

Spectra 3a. ^{1}H NMR spectrum of **DIBAC–biotin** in DMSO (750 MHz).

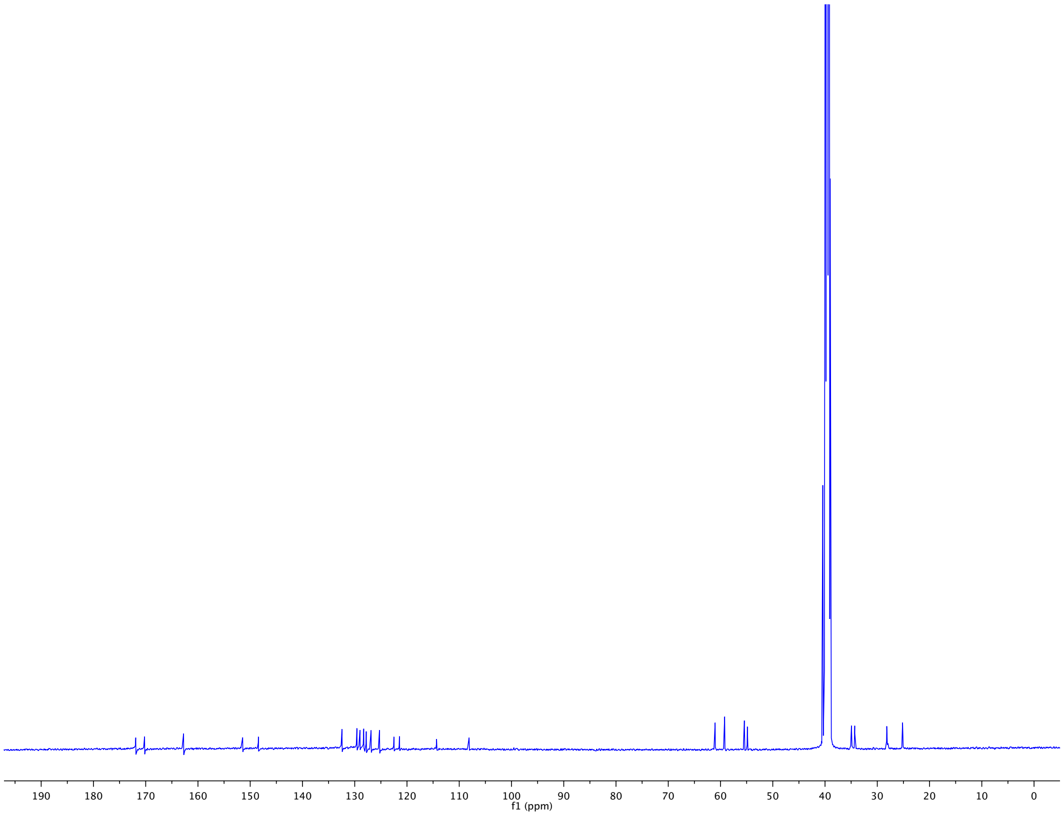

Spectra 3b. ^{13}C NMR spectrum of **DIBAC–biotin** in DMSO (126 MHz).

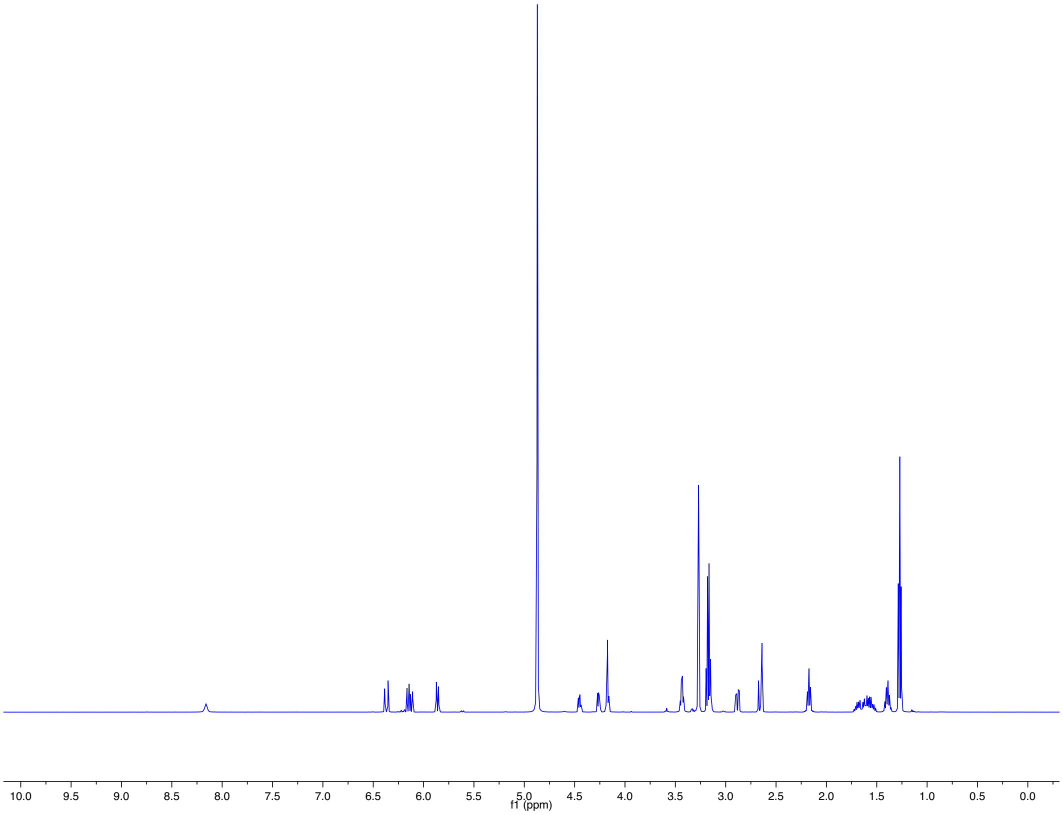

Spectra 4a. ^{1}H NMR spectrum of **2-aminoethyl acrylate-biotin** in MeOD (500 MHz).

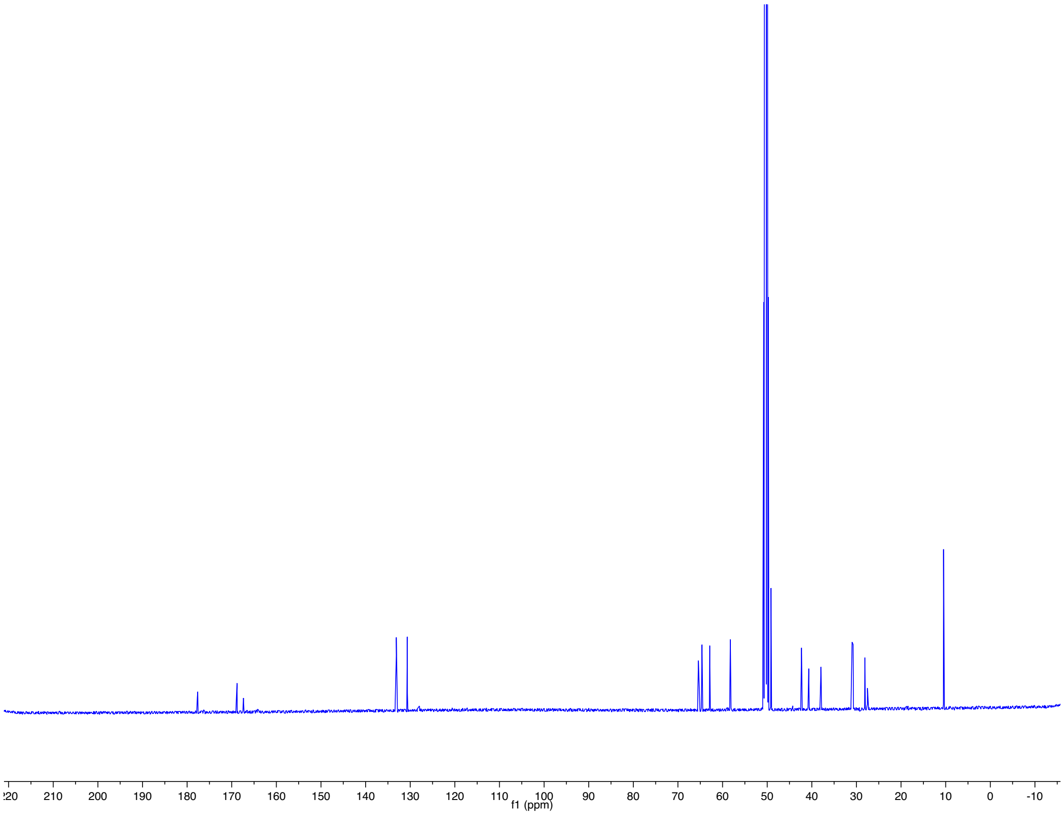

Spectra 4b. ^{13}C NMR spectrum of **2-aminoethyl acrylate-biotin** in MeOD (126 MHz).

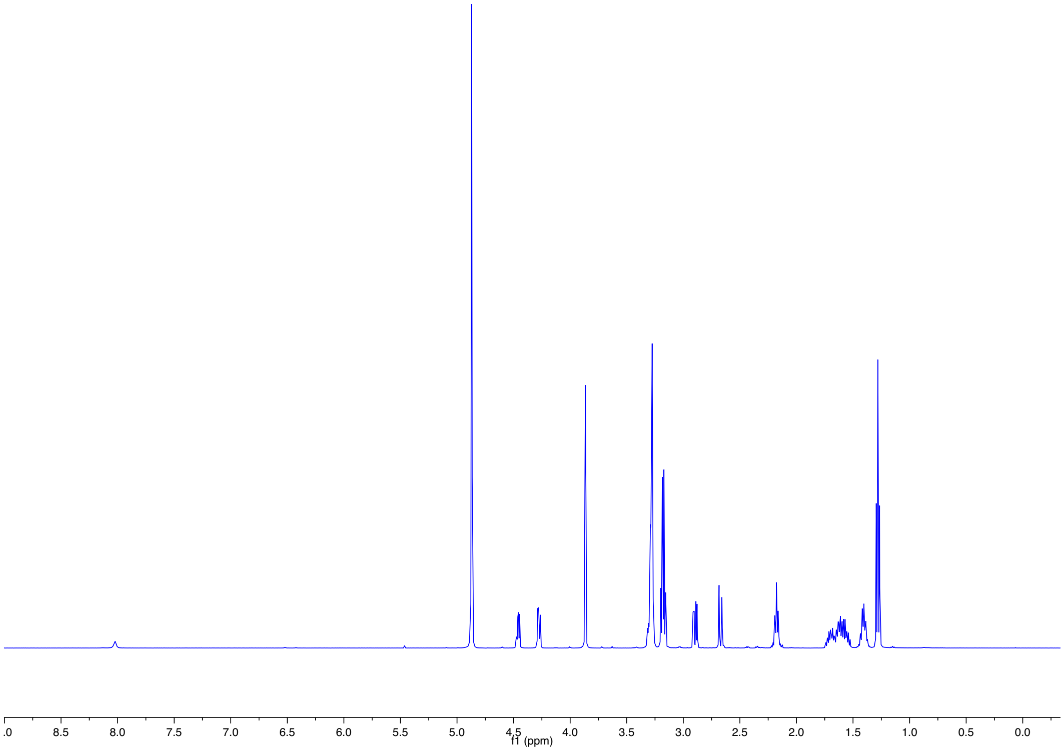

Spectra 5a. ^{1}H NMR spectrum of **azide–ethylenediamine–biotin conjugate** (500 MHz).

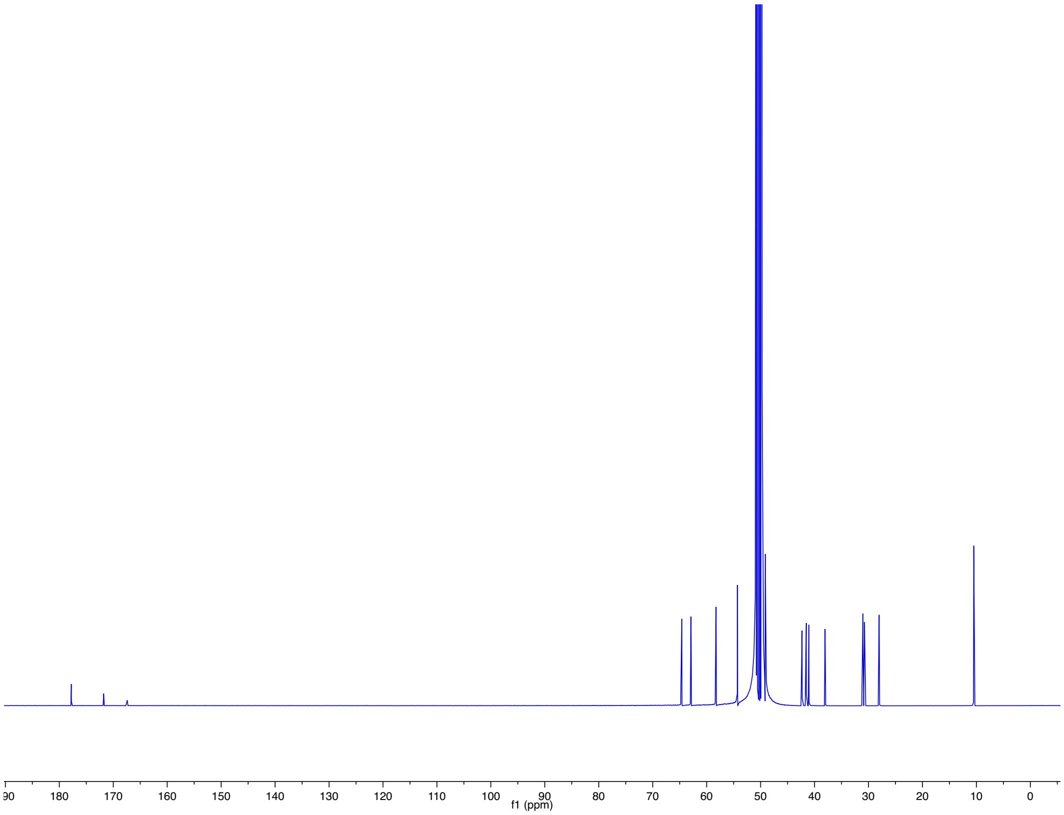

Spectra 5b.^{13}C NMR spectrum of **azide–ethylenediamine–biotin conjugate** in MeOD (126 MHz).

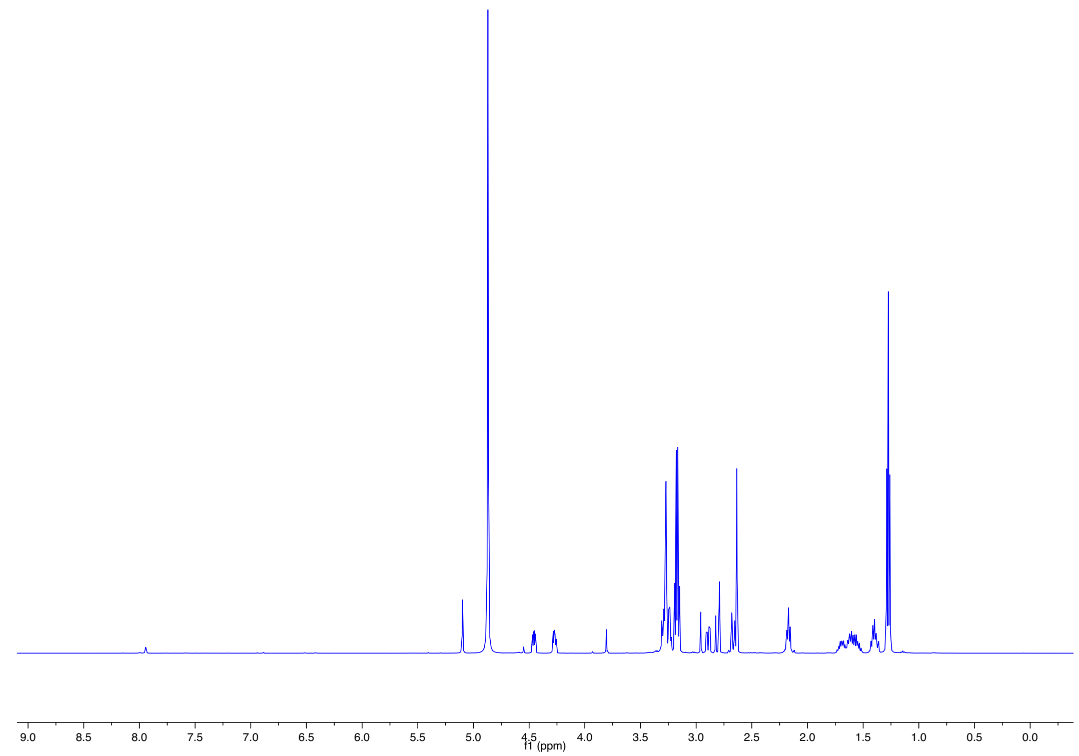

Spectra 6a. ^{1}H NMR spectrum of **Diazo-ethylenediamine-biotin conjugate** in MeOD (500 MHz).

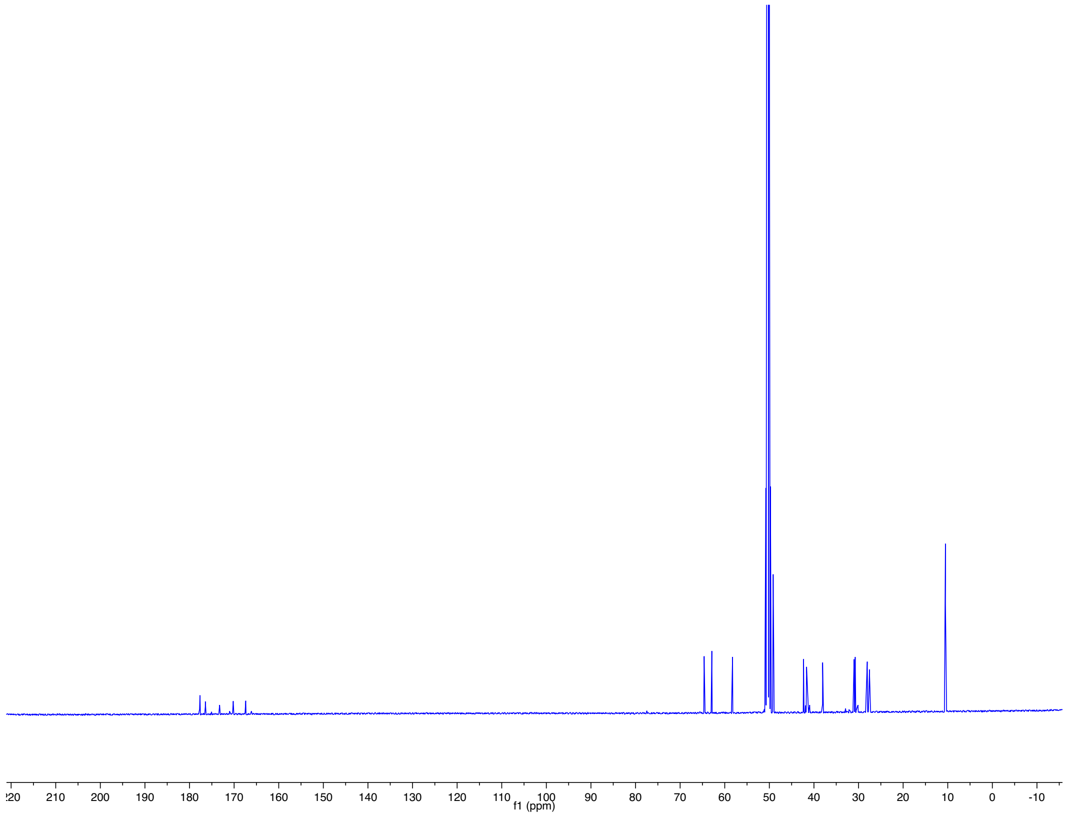

Spectra 6b. ^{13}C NMR spectrum of **Azide-ethylenediamine-biotin conjugate** in MeOD (126 MHz).

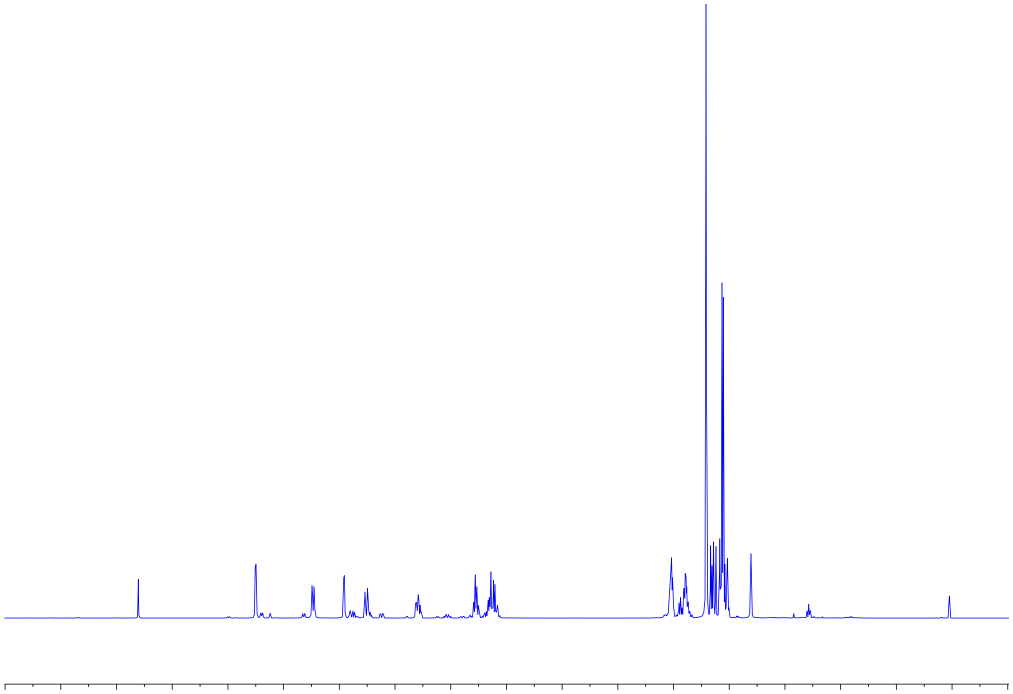

Spectra 7a. ^{1}H NMR spectrum of **1,3,4,6-tetra-*O*-acetyl-*N*-4-pentynoylgalactosamine (GalKyne)** mixed anomers in $CDCl_3$ (500 MHz).

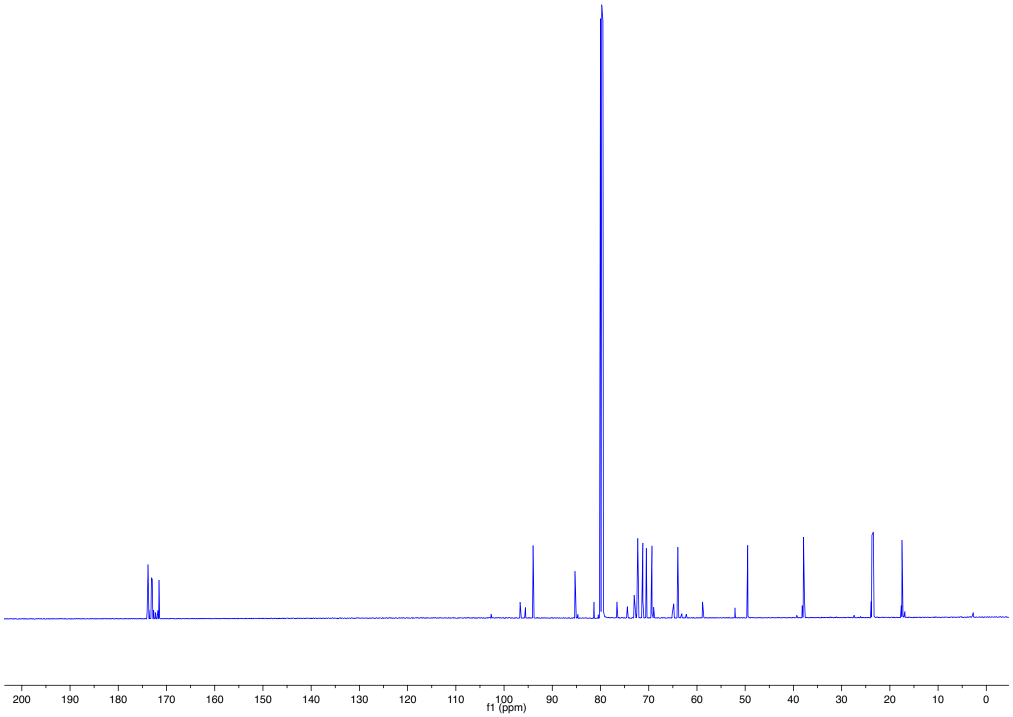

Spectra 7b. ^{13}C NMR spectrum of **1,3,4,6-tetra-*O*-acetyl-*N*-4-pentynoylgalactosamine (GalKyne)** mixed anomers in $CDCl_3$ (126 MHz).

PART 1

CHAPTER 3

Preferential 1,3-Dipolar Cycloadditions of Diazoacetamides with Unstrained Dipolarophiles in the Presence of Azides

This chapter was originally prepared as: Aronoff, M.R.,* Gold, B.A.,* Raines, R.T. Preferential 1,3-dipolar cycloadditions of diazoacetamides with unstrained dipolarophiles in the presence of azides

Contributions: I performed experiments and Brian Gold performed calculations. Both M.A. and B.G. designed experiments and wrote the manuscript.

Abstract

Recent advances illustrate the potential for the diazo-group as an attractive tool for chemical biology. In particular, the ability to survive cellular metabolism and provide unique reactivity makes the diazo-group an attractive alternative to the azido-moiety. However, as both the azide and diazo group undergo rapid 1,3-dipolar cycloadditions with strained alkynes, selective reactivity between these two dipoles has been elusive. Herein we explore strategies of strain and electronic tuning to develop diazo-selective 1,3-dipolar cycloadditions that can be carried out in the presence of an azide under ambient aqueous conditions without catalysis. Findings provide the ability to selectively react a diazoacetamide with the naturally occurring amino acid residue, dehydroalanine, a functional moiety with significant biological relevance.

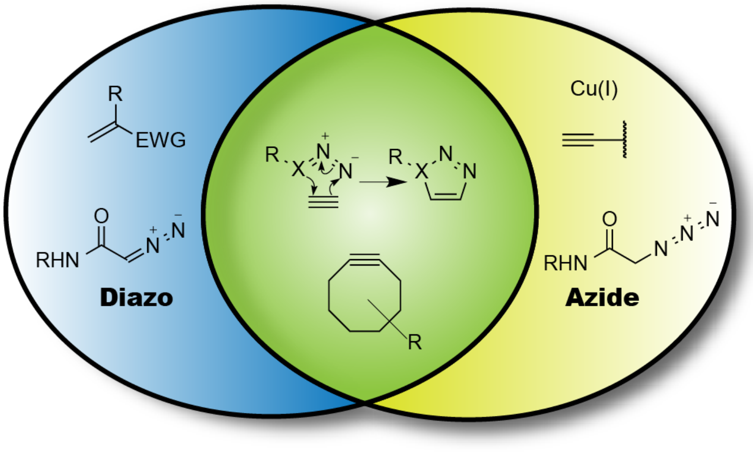

1,3-Dipolar Cycloadditions

1.3.1 Introduction

"If one regards reactions as new only if they have no forerunners, not even singular examples buried in the literature, then 1,3-dipolar additions cannot claim novelty. But if one defines reactions as novel which are for the first time recognized for their generality, scope, and mechanism, the judgement must be different."[120]

—Rolf Huisgen, 1961

The Huisgen azide–alkyne 1,3-dipolar has created a modern age of the azide, yet this azidophilia has caused a bottleneck where the most frequently applied chemoselective reactions for chemical biology all involve participation of the azide as one component.[31,121-129] The similar but unique reactivity of the diazo group makes it an attractive alternative, especially when multicomponent selectivity is a concern.

The diazo functional group has provided tremendous utility to the field of organic chemistry for over a century.[130-133] The diazo group is capable of an extensive list of valuable and varied reactivity including alkylation, carbene generation, nucleophilic addition, homologation, and ring expansions.[131] More recently, the versatile reactivity of the stabilized diazo group permits its use as a reporter for chemical biology—it is a potent 1,3-dipole for cycloadditions with cyclooctynes commonly applied used in the strain-promoted azide-alkyne cycloaddition (SPAAC) (Scheme 1.3.1).[134]

Owing to its facile preparation, compact size, and stability in aqueous environments, the pendant diazoacetamide group became our first choice for these investigations. It is apparent that the diazo group is capable of faster cycloadditions with commonly applied cyclooctynes—in comparison to the equivalent precursor azide.[45] However, the redundant reactivity shared between these two valuable groups necessitates a simple cycloaddition that can be selective for the diazo group. Such a reaction can greatly broaden the utility for the diazo group in chemical biology, as multiple selective transformations exist that are widely used for the azide.

We required a reaction that differentiated the reactivity between the diazo group and the azide but was also compatible with aqueous biological conditions. Known strategies exist for diazo-specific reactions in aqueous conditions such as metal-carbenoid additions/insertions,[34,35,39-41,135] esterifications,[44,136] and carbonyl additions,[137] but each of these have drawbacks that prevent application in a general context. Frustrated by the lack of selectivity produced from SPAAC-type reactions with the diazo group or the azide, we sought out other means to generate a simple cycloaddition reaction that would favor the chemical characteristics of the diazo-group. Although not immediately apparent, the 1,3-dipolar cycloaddition reaction itself was an ideal arena to highlight the unique and distinctive reactivity of the diazo group separate from the azide.

While much effort has focused on the development of activated alkynes that are suited for many applications,[31,121-129,138-142] less effort has focused on the fabrication of activated dipoles.[52,143-147,148] The preexisting lack of focus on dipole tuning is especially surprising, as it has been shown in many theoretical studies that the bulk of the activation barrier (~80%) comes from the energy required to distort the dipole to the TS geometry (see later discussion).[149] Owing to the inherent conjugation to its attached carbon atom, the stabilized diazo group represents an excellent substrate for dipole-tuning.

It has been previously demonstrated that orthogonal cycloadditions can be generated through modulation of the electronic demand of the two sets of reacting partners—in this instance one performs a normal electron demand (NED) cycloaddition, while the other reacts by inverse electron demand (IED). Selectivity by electronic demand has been accomplished applying electronically diverse azides[52] as well as deactivated nitrones.[150]

In the work of Floris and Bickelhaupt, chemoselective NED and IED 1,3-dipolar cycloadditions were achieved with two unique azides.[52] It was noted that an apparent ceiling of reactivity for strain-promoted azide-alkyne cycloadditions (SPAAC) had been reached. Modification of aryl azides to promote IED reactivity allowed this limit to be overcome, yet the ceiling for NED cycloadditions with alkyl azide remains. Thus, exploration into diazo group reactivity provides a new means to access more rapid NED 1,3-dipolar cycloaddition rates with dipoles that can undergo cellular metabolism.[151] Herein we report a strategy to differentiate the diazo group and alkyl azides through chemoselective normal demand dipolar cycloadditions and provide theoretical groundwork towards optimized NED 1,3-dipolar cycloadditions to compliment the rapid IED cycloadditions earlier reported.[52] We also report the utility of diazo group cycloadditions, selectively accelerated in aqueous conditions, towards modification of naturally occurring peptides without prior modification.

1.3.2 Results and Discussion

Computational Details

Optimizations were performed using Gaussian 09 software[152] at M06-2X level of theory[153,154] using the 6-31+G(2d,p) basis set. M06-2X has been shown to accurately describe trends in reactivity in a number of cycloadditions.[155] Optimizations were performed in the gas-phase followed by single point solvation corrections. An IEFPCM dielectric continuum solvent model for water with UFF radii was employed. Frequency calculations were performed to confirm each stationary point as minima or first-order saddle points. All ΔE values include zero-point corrections. *N*-methyl acetamide was used for *N*-benzyl acetamide dipoles computationally. **Selectivity:** Diazo groups are primed for more rapid NED cycloadditions due to higher polarity and increased nucleophilicity. We hypothesized that by matching reciprocally tuned dipolarophiles, the diazo group would be a more suitable reaction partner than the azide. Diazo groups are capable of uncatalyzed cycloadditions with numerous dipolarophiles in addition to commonly employed strained alkynes,[45,130,134,156] yet the decreased HOMO-LUMO gap imparted by strain also enables efficient reactions with azides. As it has been shown that diazo groups often react more rapidly than azides,[134] we wished to examine the possibility of chemoselective transformations in the presence of both diazo and azido dipoles.

Electron-rich azides have been shown to react more rapidly than electron-deficient azides in the cycloaddition with DIBAC.[52,144] Additionally, DIBAC was the most rapid cyclooctyne to react with the diazoacetamide functionality.[134] Thus, we wanted to see if this could be extended to the more electron-rich diazo group over the azide in the context of azide-diazo-competition reactions. One equivalent each of the diazoacetamide (**1**) and its azide precursor (**2**) were combined with a single equivalent of DIBAC and allowed to react until the octyne was consumed (Scheme 1.3.2). Despite the pronounced rate of the diazo group, a significant percentage of the azide had also reacted.

The lack of selectivity presumably results from the electronic character of the employed diazo and azide groups. The stabilization necessary to render the diazo group practically useful also slows down the rate of the desired cycloaddition. The azide applied here was not conjugated to the deactivating carbonyl π-system, and the two dipoles are poised to display competitive reactivity. As DIBAC did not give a highly selective reaction (Scheme 1.3.2), we foresaw selectivity by removing strain.

As strain generally gives faster reaction kinetics, but does not provide desired selectivity, we wished to examine the utility of both strain and electronic tuning as means to increase reactivity and selectivity. As can be seen in Figure 1, a general decrease in barriers for both the diazo **1** and azide **2** are observed with increasing strain (top) or with increased electron-withdrawing capabilities (bottom). The slopes of both dipoles when activated by strain are much steeper, illustrating the rapid reactivity afforded by strained precursors. However, the $\Delta\Delta E^{\ddagger}$ between the azide and diazo are within ~0.6 kcal/mol for the reactions with 2-butyne, cyclononyne, and cyclooctyne (**a-c**), suggesting little selectivity. It is not until large amounts of strain are imparted, that any selectivity should be expected. This evidence, along with previous experimental results, shows that strain-activation alone is not likely to create selective reactivity for the diazo independent of the azide.

Noteworthy, is the steeper slope of diazo group cycloadditions accelerated by electronic tuning relative to the analogous azide cycloadditions. This reveals the opportunity to obtain both faster reaction kinetics and increased selectivity as electron-withdrawing capabilities are increased. Examining $\Delta\Delta E^{\ddagger}$ using the Arrhenius equation suggests we can take a reaction that is ~7 times faster for the diazo group than the azide **f** and generate a reaction that is >1000 fold faster **k**. This is surprising as the diazo group is deactivated for NED via conjugation to the carbonyl, but the azide is not. Despite the deactivating effects of conjugation, the diazo group HOMO remains higher in energy than the azide (see SI).

Additionally, the calculated barrier for the cycloaddition of diazo acetamide **1** with MVK **j** of ~12 kcal/mol is lower than the barrier of ~14 kcal/mol for the cycloaddition of azide **2** with cyclooctyne **c**. This led us to believe that the increased reactivity of these diazo groups over alkyl azides may allow for reactions with unstrained alkenes that are able to surpass first generation SPAAC.[31]

Kinetics: From this inference, we reevaluated the need for strain altogether for 1,3-dipolar cycloadditions with the diazo acetamide **1**. We reasoned that by first removing strain from the reaction partner, the more nucleophilic diazo group should make a more suitable dipole for dipolarophiles that possessed a lower energy LUMO generated from bond polarization of adjacent electron-withdrawing groups.

We first examined ethyl propiolate **n**, a compound with a terminal triple bond, but activated by a conjugated electron withdrawing ester moiety. Here, selective reactivity for the diazo group dipole was observed even in the presence of excess propiolate (Scheme 1.3.3). It should be noted that in this competition reaction both dipoles (**1&2**) are capable of performing NED cycloadditions, yet the increased nucleophilic character of the diazo group and greater acceleration in aqueous conditions (*vide infra*) allow it to outcompete the NED azide (**2**).

The alkene congener of propiolate, ethyl acrylate **i**, was next evaluated as it has been postulated that alkenes react more rapidly in cycloaddition reactions.[157] The alkene indeed reacted more quickly with the diazoacetamide **1** in aqueous co-solvent. As the reaction with propiolate proved to be more sluggish, we focused our attention on ethyl acrylate and related alkenyl compounds. Upon examining the reaction kinetics of a carbonyl series of electron-deficient alkenes, we found the rate of the reaction was dependent upon the electron-withdrawing capabilities of the substituent. The reactions with even the least reactive (**h**-**m**) of these unstrained, yet electronically tuned cycloadditions, produced rate constants similar to those of early generation SPAAC (Table 1.3.1).

The faster reaction kinetics of ethyl acrylate **i** over propiolate **n** was initially surprising, as previous reports suggest similar reaction kinetics between alkenes and alkynes, despite different FMO energies.[149] Differences are due, however, to a smaller distortion energy of the dipolarophile and slightly larger interaction energy (Figure 1.3.2). It has previously been shown that while alkynes are easier to bend than alkenes, the alkyne must be bent to a larger degree to reach TS geometries.[157,158] The difference in dipolarophile distortion energy of 1.7 kcal/mol is similar to the value of 2.1 kcal/mol previously reported for the cycloadditions of diazomethane with ethylene and acetylene calculated at the B3LYP/6-31G(d) level of theory.[149] These results are consistent with the smaller HOMO-LUMO gap of alkenes relative to alkynes.

Applications: We next wanted to demonstrate a simple example of this reactivity in a useful context, while also further verifying the selectivity of this type of cycloaddition. In order to accomplish this task we prepared a compact linker molecule simultaneously containing both pendant functional groups. Compound **3** was prepared from 3-bromoproplyamine as shown in Scheme 1.3.4. This dual-linker molecule was then reacted with an excess of ethyl acrylate **i** at room temperature in H_2O:CH_3CN cosolvent. The results were further inspiring—the diazo group was completely reacted to form the pyrazoline product **3-i** whereas the azide remained completely unchanged and free for subsequent functionalization or derivation (Scheme 1.3.4, also SI).

Substituent Effects of 1,3-Dipolar Cycloadditions of Diazo- and Azido-compounds: In order to better understand observed reactivity, we examined the effects of substituents on cycloadditions between alkenes and both diazo and azide dipoles. We started with simple dipoles (see SI) but focus on the stabilizing substituents that allow for practically accessible diazo group dipoles (Figure 1.3.3&1.3.4).

An advantage of diazo group dipoles is the larger tunability relative to analogous azides, as illustrated from the larger range of activation barriers. The total range of azide cycloadditions is ~9 kcal/mol, while the range of diazo group cycloadditions is ~21 kcal/mol (see SI). Even when focusing on only practically accessible diazoacetamide **1**, a range of ~13 kcal/mol is observed.

As expected by the preference of diazo groups to undergo NED cycloadditions, electron-withdrawing substituents are predicted to provide substantial activation (Figure 1.3.3 & SI). Interestingly, azides show ambiphilic character—benefitting from both donors and acceptors—however, donor-substituents on the alkene (e.g., -OMe **q**) are not productive towards increased reactivity until sufficient acceptor substituents are present on the azide. This correlates well with that found by both Houk[143] and Bickelhaupt and van Delft.[52]

The lower calculated barriers for the cycloaddition of diazo compounds with electron-deficient alkenes than with cyclooctyne are in accord with the fact that cycloadditions of electronically-tuned reacting partners are able to compete with early generation SPAAC (Table 1.3.1). In addition to much less tunability, azides display the lowest predicted barriers in the cycloadditions with cyclooctyne. This illustrates the potential advantages of diazo group cycloadditions over those of azides, where careful electronic tuning can become the primary design principle. On the contrary, it has been claimed that the "primary importance in the design and synthesis of reactive cycloalkynes for copper-free click chemistry is ring strain, followed by electronic activation and steric effects."[159,160] A strategy based on pairing of electronics in reacting partners is a much more elegant approach when the end goal is selective reactivity.[161]

Predictive Tools–FMO vs Distortion-Interaction Energies: In the study of Huisgen cycloadditions, the classically utilized predictive tool of FMO gaps[162-166] has recently been shown to be less valuable than the distortion-interaction analysis developed by Ess and Houk.[167] This approach is analogous to the strain-activation analysis developed by Bickelhaupt.[168] We wished to analyze the relative utility of each approach to understanding the reactivity of electronically "tamed" diazo groups and azides.

As is readily apparent from Figure 1.3.5, distortion energies are much more reliable as predictors of relative reactivity. The plot of activation energies vs. total distortion energies displays an R^2 value of 0.75 compared to the value 0.47 for the plot of activation energies vs FMO gap (smaller HOMO/LUMO pair).

Upon examination of calculated FMOs (see SI) and TS geometries (Figure 1.3.4 & S1.3.5), it becomes apparent that the dominant interactions in the TS may not necessarily be between HOMO of the dipole and LUMO of the dipolarophile or vice versa. In nearly every dipole examined, the HOMO and LUMO orbitals reside within orthogonal π-systems. The sterically unencumbered azide can rotate to allow interactions of both π-systems with dipolarophile FMOs. Calculated diazo group transition states, however, display a geometry where the HOMO can directly interact with unoccupied orbitals of the dipolarophile, but this leaves the LUMO orthogonal to the forming bonds.

As this is the case, we reexamined the correlation of activation energies with FMO gaps, but instead used diazo group LUMO+1 energies for IED gaps in relevant cases (see SI). The R^2 increased only slightly to 0.53, confirming that distortion energies are a much better descriptor of reactivity.

SPAAC – distortion acceleration: The approach of strain activation has also been termed distortion acceleration when viewed through distortion-interaction analysis.[140,169,170] Alkynes contained within a cycle are constrained to a non-optimal, bent geometry, much closer to the TS geometry than their unstrained counterparts. As the geometries for each calculated cycloaddition involve significant distortion (Figure 1.3.4), pre-distortion is accelerating in both azide and diazo group cycloadditions (Figure 1.3.1).

The concept of distortion acceleration is interesting from both a theoretical viewpoint and when designing reactants for chemical biology. Although it has been established that cycloaddition reactivities cannot be explained via a strict Bell-Evans-Polanyi, or Marcus treatment[149,161] (cycloadditions of vastly different reaction energies often have comparable rates), pre-distortion of the dipolarophile enforces a more reactant-like TS in regards to the dipolarophile.[171] Based on the Hammond-Leffler postulate, this should have a negative effect on selectivity.[161]

The selectivity seen in many competing cycloadditions then comes from the alternative strategy of FMO matching between reactants.[52,150] More specifically, this effect arises from the smaller distortion energy required by dipoles with better matched FMOs.[149]

There are inherent drawbacks to both approaches, especially when the end goal is to carry out selective reactions in living systems. Pre-distortion towards cycloaddition geometries cannot be accomplished without also pre-distorting towards geometries of other TSs, such as nucleophilic addition. Tuning MOs suffers from the same problem, where FMO energies primed for dipolar cycloadditions can overlap with optimal energies for unwanted side reactions. While we have shown that selective 1,3-dipolar cycloadditions can be attained via FMO tuning, the optimal balance of strain and substituent effects is required in order to maximize reaction efficiency. Finding this balance for a series of dipoles will provide a myriad of possibilities for chemical biology.

Distortion-Interaction Analysis: In earlier studies, it was found that the distortion energy of simple diazo compounds are essentially always lower than the distortion energies of simple azides.[149] Electron-withdrawing substituents on the diazo were shown to increase distortion energies, but analogous azides were not examined.[172]

Our first goal was to determine if lower distortion energies of diazo group cycloadditions was the factor favoring diazo group cycloadditions over azido compounds when substituents are added to the 1,3-dipole. While this was our initial hypothesis, it could not be ruled out that interaction energies became the dominant factor as dipole-stabilizing substituents were added.[173] We mainly focus on the diazoacetamide **1**, as this substitution provides practically accessible compounds and still displays attractive substituent effects (Figure 1.3.3).

Diazo group cycloadditions benefit from both decreased distortion energies and increased interaction energies (Figure 1.3.6 and Figure S1.3.8). The total distortion energies for the electronically tuned diazo-MVK cycloaddition **1-f-TS** are less than the total distortion energies of the distortion accelerated azide-OCT cycloaddition **4-c-TS** (23.8 vs 24.1 kcal/mol). In addition, the diazo-MVK cycloaddition **1-f-TS** also benefits from increased interaction energies (-11.4 vs. -7.1 kcal/mol, respectively).

The $\Delta\Delta E^{\ddagger}$ between diazo and azido groups was 4.3 kcal/mol for the parent ethylene TSs (**1-f-TS** & **4-f-TS**). Electronic activation increases this difference ($\Delta\Delta E^{\ddagger}$ = 8.5 kcal/mol for **1-j-TS** & **4-j-TS**), while strain decreases the difference (3.0 kcal/mol for **1-c-TS** & **4-c-TS**), in agreement with Figure 1.3.1 and S1.3.3.

Electron-withdrawing substituents on the diazo group increase the dipole distortion energies relative to diazomethane and diazoethane (see SI), however, little effect is seen on the interaction energies. In comparison, electron-withdrawing substituents on azides have the same effect on distortion energies, but also decrease interaction energies. In these cases of electron-deficient dipoles, interaction energies remain largest for the electron-deficient methyl vinyl ketone **j** in reactions with diazos **1** & **5** (-11.4 kcal/mol, **1-j-TS**), but the azides **4** & **6** show larger interaction energies in the reaction with electron-rich methyl vinyl ether (-10.6 kcal/mol, **4-j-TS**). This can be attributed to the nature of each cycloaddition. Even with electron-withdrawing substituents the diazo group favors Type I interactions, where the azide cycloadditions are truly Type II, benefitting from both $\text{HOMO}_{\text{dipole}} \rightarrow \text{LUMO}_{\text{dipolarophile}}$ interactions as well as $\text{HOMO}_{\text{dipolarophile}} \rightarrow \text{LUMO}_{\text{dipole}}$. This is in agreement with calculated NBO charges (Figure 1.3.4). When strong electron-withdrawing groups are incorporated to the 1,3-dipole, such as in the case of 1-diazopropan-2-one (**5**), the total distortion energies are similar to those of the analogous azido group (**6**), and interaction energies begin to determine relative reactivities (see SI). This is expected from the distortion-interaction analysis, as strong interactions in stabilized starting materials are often lost in the transition state, simultaneously increasing both distortion and interaction energies (Figure 1.3.8).

In this case, delocalization of the carbon lone pair of the diazo group (**5**) into the carbonyl π* (78.1 kcal/mol) is traded for delocalization into the forming C-C bond. While a large energy must be paid to turn off interactions in the starting material (distortion energy), stabilization is gained via bond formation (interaction energy). The distortion energy of acetyl azide **6** is similar to that of diazopropanone, despite a higher degree of bending (~139° vs ~145°) in the reaction with methyl vinyl ketone. This stems from the weaker $n_N \rightarrow \sigma^*_{C=O}$ hyperconjugative interaction (9.1 kcal/mol) that must be sacrificed in the TS, while the π-conjugation is maintained.

Decreased distortion energies without pre-distortion: As stated above, ~80% of the distortion energy comes from the 1,3-dipole.[149] As the approach of SPAAC focuses on decreased distortion energies of the dipolarophile (the reacting partner that only contributes ~20% of the overall barrier),[174] diazo group cycloadditions provide the opportunity of directly decreasing dipole distortion energies without pre-distortion of our starting compounds.

While it has been shown that distortion-interaction analysis is a better descriptor of reactivity than ground state FMO gaps, it does not provide the “back of the envelope” predicting power provided by the well-established FMO approach.[162-166] Additionally, the two are intricately tied, thus one cannot be evaluated without the other. For simplicity, our subsequent discussion will focus on the differences of ground state FMO energies of the diazo and azides dipoles, as well as the two approaches of strain and electronic activation.

The decreased distortion energies result from the higher HOMO of diazo compounds relative to analogous azides.[175] This leads to an earlier transition state, where less bending is required to allow for sufficient interactions towards bond formation. Despite an earlier, less synchronous TS, larger interaction energies are also observed relative to azide dipoles.

As the diazoacetamide **1** has been shown to endure cellular metabolism, this alternate approach can provide increased reaction rates without compromising selectivity. This is in stark contrast to the high amount of strain (~20 kcal/mol for **c**) associated with the LUMO lowering strategy of distortion acceleration.

In all cases, the HOMO is raised substantially upon diazotization (Figure 1.3.7). For the transformation from the carbamoyl azide **4** to the diazoacetamide **1**, an increase of ~25 kcal/mol is observed. Even from the nonconjugated methyl azide **10** to diazoacetamide **1**, an increase of almost 20 kcal/mol is observed.

In contrast, increasing strain by almost 20 kcal/mol from 2-butyne **a** to cyclooctyne **c** leads to only ~5 kcal/mol decrease in the LUMO energy of the alkyne. The strategy of electronic activation provides much larger effects, where the LUMO of methyl vinyl ketone **j** is ~35 kcal/mol lower than propene **p**.

Marcus Analysis: Also explored was the potential Dimroth-Bronsted-Marcus relationship, correlating kinetic reactivity to thermochemistry.[176-179] An adaptation of the Marcus equation, utilizing electronic energies rather than free energies (Equation 1), has proven useful in exploring electronic effects governing chemical transformations.[180-182] The last term can be neglected in most cases, unless the reaction is sufficiently exothermic or the barrier is relatively small. The intrinsic barrier ($\Delta E^{\ddagger}{}_0$) is the reaction barrier of a hypothetical thermoneutral reaction.

$$\Delta E^{\ddagger} = \Delta E^{\ddagger}_{0} + \frac{1}{2}\Delta E_{rxn} + \frac{\Delta E^{2}_{rxn}}{16\Delta E^{\ddagger}_{0}} \qquad (1)$$

In a set of reactions with similar intrinsic barriers, equation 1 reduces to $\Delta\Delta E^{\ddagger}$=1/2$\Delta\Delta E_{\mathrm{rxn}}$—the assumption made in the empirically derived Bell-Evans-Polyani relationship.[183,184] It was previously shown that for 1,3-dipolar cycloadditions there was a general decrease in the activation barrier for more exothermic reactions, but the $\Delta\Delta E^{\ddagger}$=1/2$\Delta\Delta E_{\mathrm{rxn}}$ relationship was not general amongst all cycloadditions examined.[149]

Interestingly, for diazonium betaine dipolar cycloadditions with ethylene, this relationship was observed.[149] However, the same dipoles did not display the linear correlation in the cycloaddition with acetylene, as the diazomethane cycloadditions do not lead to aromatic products. This results in similar barrier heights, despite largely different reaction energies. In addition to the complications arising from formation of aromatic and non-aromatic products, it is well documented that alkyne π-bonds benefit from kinetic stability, yet form stronger bonds and are often more exothermic than their alkene analogues.[185,186] As a result, alkene and alkyne reactions—despite striking similarity—have largely different intrinsic barriers.

As our focus is on the difference in reactivity between diazo groups and azides in the cyloadditions with different alkene dipolarophiles (here we omit cyclooctyne from the discussion to avoid complications discussed above), a case where a general Dimroth-Bronsted-Marcus relationship was previously observed for ethylene as a dipolarophile, we wished to examine the effects of substitution.

When all cycloadditions from Figure 1.3.3 and Tables S1.3.1&1.3.3 (minus OCT) are plotted, no correlation is observed (R^2=0.27, see SI). Separating the diazo and azide dipoles gives even worse correlation (R^2=0.23 and 0.0003, respectively). Interestingly, plotting the electron-deficient alkenes **j** & **o** and electron-neutral/rich alkenes **f**, **p**, **q** separately gives much better correlation (Figure 1.3.9), especially for diazo cycloadditions (R^2=0.98 and 0.92, respectively). The lowered barriers of electron-deficient alkenes displaying similar reaction energies and the steeper slope suggest that the intrinsic reaction barriers are much lower for these electronically matched cycloadditions, a result of selective TS stabilization[128,138,139,181] This also illustrates the dangers of making the assumption that intrinsic reaction barriers are similar, thus simplifying the Marcus relationship to $\Delta\Delta E^{\ddagger}=1/2\Delta\Delta E_{\mathrm{rxn}}$.[187]

Despite forming similar bonds, substituent effects render intrinsic barriers drastically different (see SI) as a result of strengthened stereoelectronic interactions with high-energy incipient bonds. Notably, the differences in intrinsic barriers between the two sets of reactions for diazo group cyloadditions are much larger (≥10 kcal/mol) than for azido group cycloadditions (~4-5 kcal/mol), as a result of the larger effects of substituents in the former.

Solvent Effects: Reactions insensitive to—and even accelerated by—water are of particular interest for green chemistries[188] and is a tenet of click chemistry.[28] While insensitivity to water is a requirement for chemical biology, selective rate-acceleration in aqueous environments can be used to obtain greater selectivities.

The notion of little to no solvent effects on cycloaddition rate[189,190] has long since been abandoned.[103] Experimental[191,192] and theoretical[102,193,194] reports show that not only aggregation, but also TS state stabilization via H-bonding are responsible for enhanced rates in water.

In addition to previous reports by our lab, we have observed larger solvent effects and rate increases in aqueous conditions for the diazo group than for the azide (see SI). It was previously speculated this is due to greater charge transfer in the TS as a result of the nature of diazo group cycloadditions,[45] but a thorough computational investigation was not performed.

Solvation corrections using both acetonitrile and water gave similar values (see SI). As the IEFPCM solvation model does not explicitly include nonelectrostatic contributions such as H-bonding, it should be considered as the first approximation of solvation effects.[195-197] This is especially important when explicit H-bonding can lead to large stabilization of the TS.[193] Effects of explicit H-bonding on reaction barriers were examined (see SI). To simplify calculations, we focused our attention on the extent of charge transfer in the transition state.

We calculated NBO charges on reacting fragments in the TS and found a much larger degree of charge transfer in the diazo cycloadditions (Table 1.3.2).[163] This indicates a more polar TS, and thus larger rate enhancements due to polar solvents. This is noteworthy, as the diazo group is conjugated to the amide, while the azide is not.

The charge transfer in cycloadditions with aliphatic strained systems is much less than electron-deficient alkenes (Figure 1.3.10). Cycloadditions with DIBAC, however, display a transfer of 0.14 e^- from the diazo group, while only a transfer of 0.08 e^- from the azido group (Figure 1.3.2). Recently reported inverse demand cycloadditions of azides with BCN show similar magnitude of charge transfer in the TS, but from BCN to electron-poor azides (0.22-0.26 e^-).[52] These findings can be used to one's advantage when designing reactions in aqueous environments.

Lastly, we considered applications of this interesting reactivity within the arena of chemical biology. The ethyl acrylate moiety is too reactive for any biological application,[134] however the reduced reactivity of the acrylamide has allowed its metabolic incorporation as an unnatural amino acid into proteins such as GFP.[198] While the cycloaddition between the diazo group and the acrylamide is much slower kinetically than the more reactive nitrile-imine,[199] within a biological context the diazo group can serve as a more selective reaction partner. Ultimately further inspired, we considered other similar groups including those found in nature that would provide good substrates for cycloaddition specifically with the diazo group.

An obvious choice was dehydroalanine (Dha), a naturally occurring amino acid found primarily in microbial peptides including Class I bacteriocin antibiotics. In mammalian tissues dehydroalanine exists only transiently as an enzymatic intermediate, but this interesting residue can artificially be generated from a cysteine providing a means for vastly useful site-selective protein modifications following the addition of functionalized thiolates.[200-202]

Dehydroalanine possesses two electronically modulating groups bonded to the alkene. We hypothesized this functionality might create a better substrate for the diazo group to undergo cycloaddition with. Reactivity was tested using an *O*-acyl Dha fragment, and the kinetics indeed exceeded that of previously tested alkenes (Figure 1.3.11). The additional electronic modulation induced by the second substituted group did make Dha an excellent substrate. This was corroborated with computational investigations (SI)—the $\Delta E^{\ddagger}$ was found to be 13.8 kcal/mol with 0.217 e^- transfer in the TS.

Inspired by this reactivity, with additional consideration of the biological endurance of the diazo group, we wished to investigate Dha-containing substrates found to persist in nature. Dehydroalanine is common in many lantibiotics including the preeminent member of the class, nisin.[203-206] Nisin is well suited for testing the biological compatibility for cycloaddition with the diazo group as it contains three potentially reactive residues. This includes two dehydroalanine (Dha) and one dehydrodrobutyrine (Dhb), but nisin also displays a myriad of other more common peptidic functional groups (see SI). We combined a crude mixture of denatured protein solids containing 2.5% mass of nisin with a novel compound containing a diazoacetamide moiety installed pendant to a pegylated biotin. We observed a change in mass by MALDI that corresponded to labeling of the peptide by cycloaddition with the biotinylated diazo compound (see SI). Installation of the biotin molecule—which has a high affinity for streptavidin—facilitates purification and could be used for isolation and discovery of novel Dha-containing peptides with potential antibacterial activity.

1.3.3 Conclusions

Here we report a new means to differentiate reactivity between very similar 1,3-dipoles. While strain is necessary to obtain sufficient reaction kinetics for cycloadditions of azides, a decrease in the energy required to distort the diazo group to its TS geometry allows for relatively rapid reactivity without destabilization associated with pre-distortion.

Diazo group cycloadditions with electronically activated alkenes display reaction kinetics competitive with first generation SPAAC. The extent of charge transfer in the TS allows for large rate enhancements in aqueous conditions. As a result, highly selective reactivity is observed via electronic tuning that cannot be accomplished via strain activation.

These insights paved the way for cycloadditions to the naturally occurring amino acid, dehydroalanine. Functionalization of nisin was possible without prior modification or incorporation of a chemical reporter functional group. To our knowledge, this is the only example of synthetic modification of a naturally occurring amino acid via a direct cycloaddition reaction.

We have additionally provided a means to selective reactivity between compact diazo groups and alkyl azides at rates comparable to strain-promoted diazo-alkyne cycloadditions. These insights can provide the theoretical groundwork for further optimization to allow for rapid reactivity and selectivity between diazo compounds and the more-commonly utilized azide.

1.3.4 Materials and Methods

Silica gel (40 μm) was from SiliCycle. All reagent-grade materials were from Sigma–Aldrich (St. Louis, MO) and were used without further purification, Nisin from *Lactococcus lactis* was also from Sigma–Aldrich and used directly. Slide-A-Lyzer Dialysis cassettes (2K MWCO) were purchased from Life Technologies (Grand Island, NY).

General Experimental

Solvent removal. The phrase “concentrated under reduced pressure” refers to the removal of solvents and other volatile materials using a rotary evaporator at water aspirator pressure (<20 torr) while maintaining the water-bath temperature below 40 °C. Residual solvent was removed from samples at high vacuum (<0.1 torr). The term “high vacuum” refers to vacuum achieved by mechanical belt-drive oil pump.

Instrumentation. ^{1}H, ^{13}C NMR spectra for all compounds were acquired on Bruker Spectrometers in the NMRFAM at the University of Wisconsin–Madison operating at operating at 400, 500, or 750 MHz for ^{1}H and 126 or 189 MHz for ^{13}C. The chemical shift data are reported in units of δ (ppm) relative to residual solvent or TMS. Electrospray ionization (ESI) mass spectrometry was performed with a Micromass LCT at the Mass Spectrometry Facility in the Department of Chemistry at the University of Wisconsin–Madison. Absorbance measurements were made with an Infinite M1000 plate reader from Tecan (Männedorf, Switzerland).

General Procedures. All reactions were performed at ambient temperature and air conditions unless specified otherwise.

Kinetics

General procedure for all kinetic experiments:

The diazo-acetamide was dissolved in the appropriate organic or organic/aqueous solvent at a concentration of 40mM. In a clear 96-well plate 50mL the diazo-acetamide stock solution was combined with 50mL of a stock solution of the dipolarophile (5eq) to produce a final concentration of 20mM for the diazo. Absorbance was measured using an infinite M1000 plate reader from Tecan, monitoring at the absorbance maximum for the diazo-acetamide of 388nm (Figure S1). Multiple readings were taken from each well (circle (filled) 3x3) every 60s at ambient temperature, followed by an orbital mixing of 10s. All assays were performed in triplicate with simlilar results and an average of these values was applied for rate determinations. The formation of final products was confirmed by mass spectroscopy and NMR-spectroscopy from identical assays. A graphical plot of the decrease in absorbance of the diazo-acetamide group was converted to a plot of concentration as a function over time (Figure S2). Pseudo-first order kinetics were determined from the slope, converted to M^{-1}/s^{-1}.

Competition reactions

N-benzyl-2-diazoacetamide[24] (**1**)(3.5 mg, 0.02 mmol), and *N*-benzyl-2-azidoacetamide[24] (**2**) (3.8 mg, 0.02 mmol) were dissolved in CH_3CN (0.5 mL) with stirring, and ddH_2O was added (0.5 mL). To the solution, ethyl acrylate (**i**) (0.011 mL, 0.1 mmol) was added and the reaction mixture was stirred 24 h. The reaction mixture was then concentrated to dryness under high vacuum, and analyzed by ^{1}H-NMR. Spectral data was identical when the procedure was replicated with the reaction time extended to 72 h.

N-benzyl-2-diazoacetamide (**1**) (3.5 mg, 0.02 mmol), and *N*-benzyl-2-azidoacetamide (**2**) (3.8 mg, 0.02 mmol) were dissolved in CH_3CN (0.5mL), and ddH_2O was added (0.5mL). To the resulting solution, DIBAC-amine (0.055 mg, 0.02 mmol) was added and stirred 24 h at r.t. The reaction mixture was then concentrated to dryness under high vacuum, and analyzed by ^{1}H-NMR.

1.3.5 Acknowledgements

This work was supported by Grant R01 GM044783 (NIH) and made use of the National Magnetic Resonance Facility at Madison, which is supported by Grant P41 GM103399 (NIH). We are grateful to Kristen A. Andersen and I. Caglar Tanrikulu (University of Wisconsin–Madison) for contributive discussions.

Scheme 1.3.1 1,3-dipolar cycloadditions of diazoacetamides

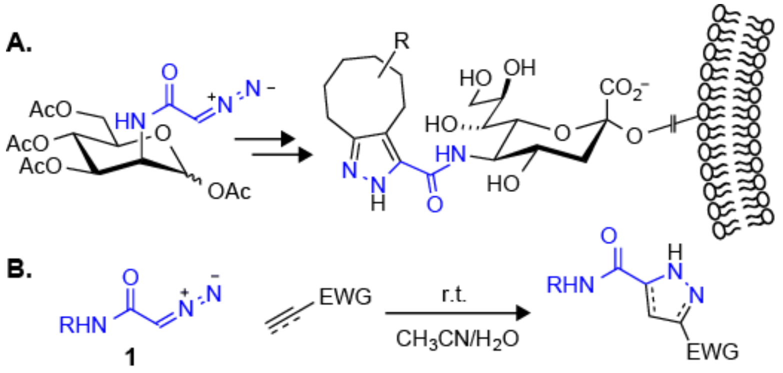
A.
AcO
AcO
AcO
HN
O
OAc
R
HO
OH
HO
CO$_2^-$
O
HN
HO
N
N
H
O
B.
RHN
1
EWG
r.t.
CH$_3$CN/H$_2$O
RHN
H
N
N
EWG

Scheme 1.3.1. (A) Metabolic incorporation of the diazoacetamide and labeling by cycloaddition on a cell when appended to an *N*-acetylmannosamine. (B) General reaction for 1,3-dipolar cycloadditions of diazoacetamides with electronically activated alkenes and alkynes to produce the 3,5 disubstituted pyrazoline or pyrazole.

Scheme 1.3.2 A competition reaction between 1 eq. each of diazo (R=Bn), azide (R=Bn), and DIBAC

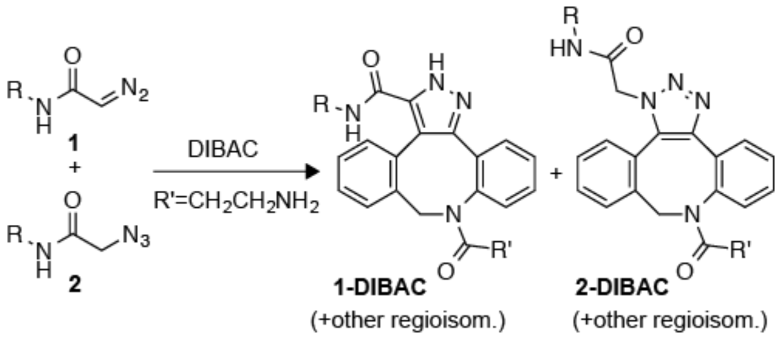
1
+
2
DIBAC
R'=CH2CH2NH2
1-DIBAC
(+other regioisom.)
2-DIBAC
(+other regioisom.)

Scheme 1.3.2. A competition reaction between 1 eq. each of the diazo group (R=Bn), the azide (R=Bn), and DIBAC performed in 50:50 $CH_3CN:H_2O$ failed to afford adequate selectivity for the faster diazo group reactant.

Figure 1.3.1 Comparison of activation via strain or electron-withdrawing substituents for 1,3-dipolar cycloadditions of carbamoyl azide and diazoacetamide – R = Me

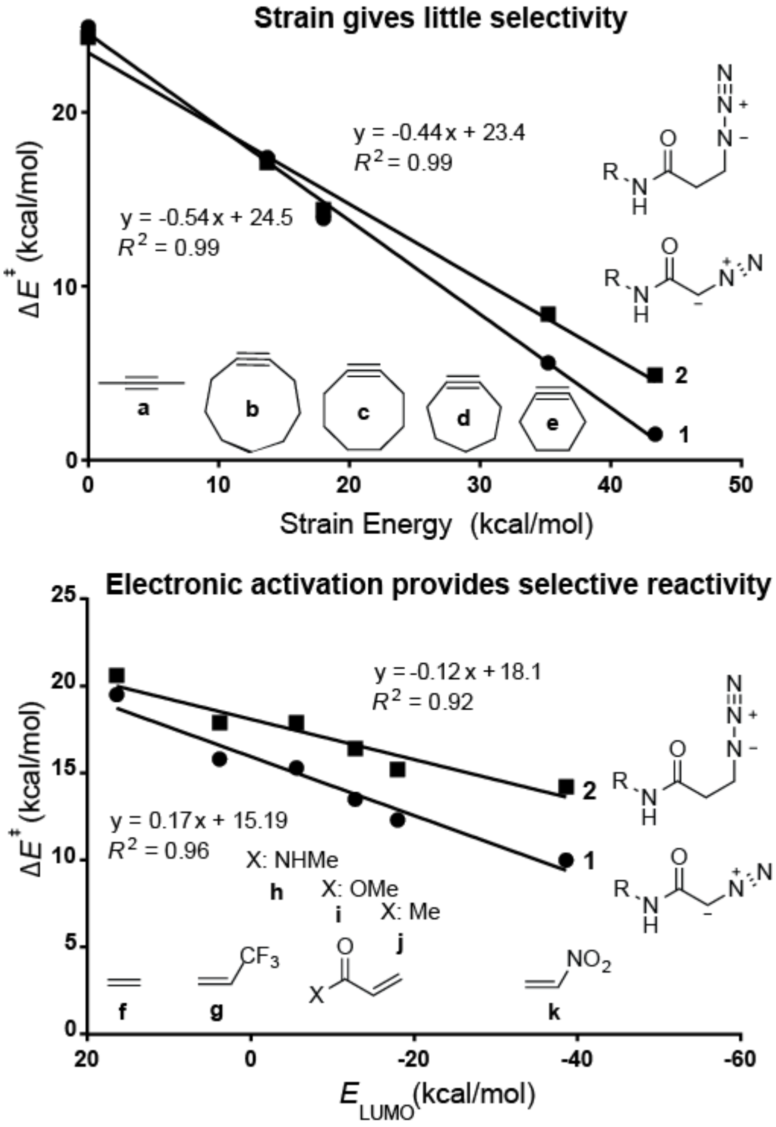

Figure 1.3.1. Comparison of activation via strain (above) or electron-withdrawing substituents (below) for 1,3-dipolar cycloadditions of carbamoyl azide (squares) and diazoacetamide (circles) – R = Me. Strain energy calculated from the isodesmic equation found in reference [207]. Activation energies calculated at the M06-2X/6-31+G(2d,p) level of theory. Energies include solvation corrections (water) on gas-phase geometries using IEFPCM model (radii=UFF). All energies in kcal/mol.

Scheme 1.3.3 Competition of diazoacetamide (1, 1 eq.) and azide (2, 1 eq). with unstrained dipolarophiles

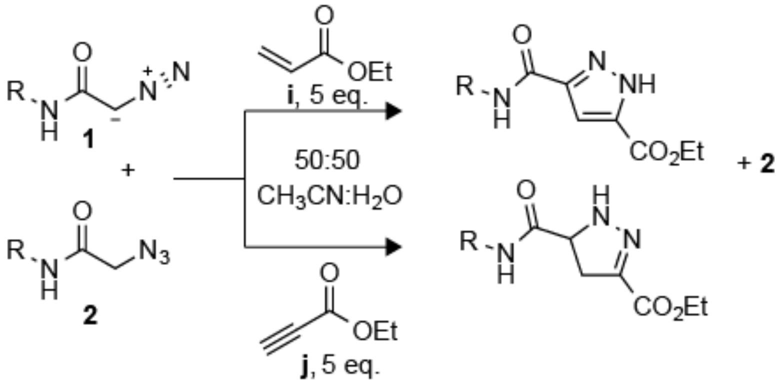
1
2
+
i, 5 eq.
j, 5 eq.
50:50
CH3CN:H2O
+ 2

Scheme 1.3.3. Competition of diazoacetamide (**1**, 1 eq.) and azide (**2**, 1 eq). with unstrained dipolarophiles (5 eq.) provides selectivity for the diazo group. Conditions: 50:50 CH_3CN:H_2O, r.t., 24h. (SI-16)

Table 1.3.1 Calculated activation energies and experimentally determined pseudo-first order rate constants

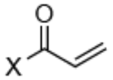

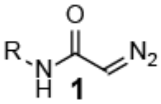

1

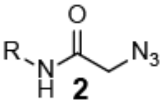

2

	X	$\Delta E^{\ddagger}$	$\Delta G^{\ddagger}$	k_{exp}^{a} (x10^{3})	$\Delta E^{\ddagger}$	$\Delta G^{\ddagger}$	k_{exp}^{b} (x10^{3})
		R = Me		R = Bn	R = Me		R = Bu
j	**Me**	**12.3**	**26.0**	**5.4**	**15.2**	**28.6**	**—**
i	**OEt**[c]	**13.5**	**26.6**	**1.1**	**16.4**	**30.3**	**—**
h	**NH_2**	**14.5**	**27.6**	**0.42**	**17.3**	**30.8**	**—**
l	**NH*i*Pr**[c]	**15.2**	**29.0**	**0.17**	**17.9**	**31.9**	**—**
m	**NMe_2**	**14.5**	**27.0**	**0.17**	**16.5**	**30.5**	**—**
c	**OCT**[c]	**13.9**	**26.1**	**0.93**	**14.4**	**28.1**	**0.95**

Table 1.3.1. Calculated activation energies and experimentally determined pseudo-first order rate constants for 1,3-dipolar cycloadditions of in 50:50 H_2O:CH_3CN at room temperature. [a]Rate constants measured 50:50 CH_3CN:H_2O in $M^{-1}s^{-1}$. [b]Rate determined in CD_3CN.[31] [c]Me used for Et or *i*Pr and cyclooctyne used for the derivatized OCT computationally.

Scheme 1.3.4 Synthesis and intramolecular competition reaction

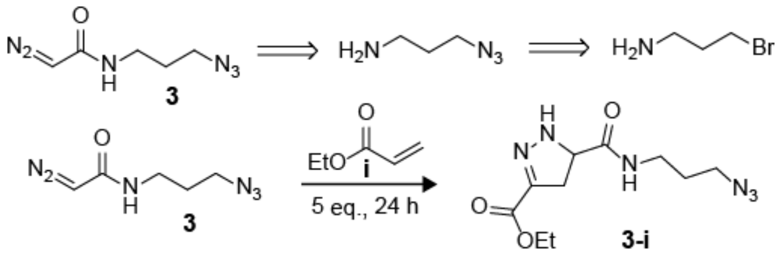
N_2
O
N
H
N_3
3
H_2N
N_3
H_2N
Br
EtO
O
i
5 eq., 24 h
H
N
N
O
N
H
N_3
O
OEt
3-i

Scheme 1.3.4: Synthesis and intramolecular competition reaction using a dual-linker molecule containing pendant diazo group and azido functionalities.

Figure 1.3.2 Transition state geometries, activation energies, and distortion-interactions energies

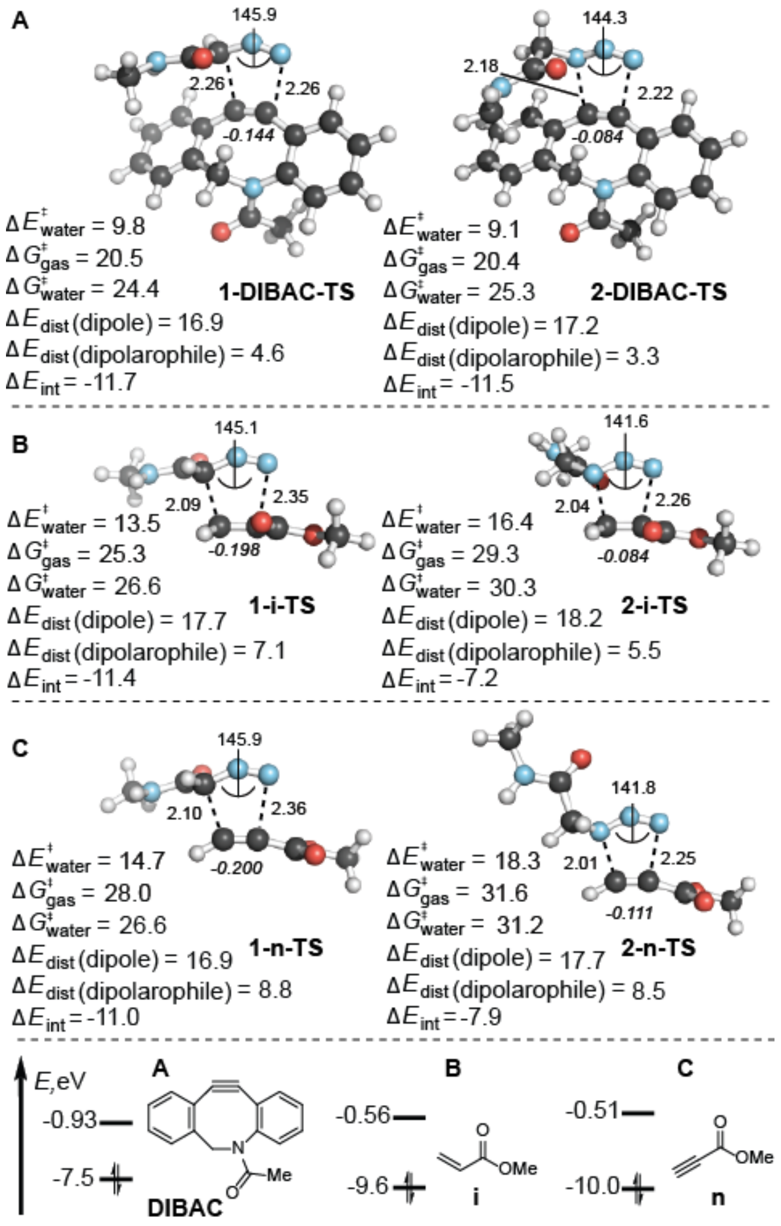
A
145.9
2.26
2.26
-0.144
$\Delta E^{\ddagger}_{water}$ = 9.8
$\Delta G^{\ddagger}_{gas}$ = 20.5
$\Delta G^{\ddagger}_{water}$ = 24.4
1-DIBAC-TS
ΔE_{dist}(dipole) = 16.9
ΔE_{dist}(dipolarophile) = 4.6
ΔE_{int} = -11.7
144.3
2.18
2.22
-0.084
$\Delta E^{\ddagger}_{water}$ = 9.1
$\Delta G^{\ddagger}_{gas}$ = 20.4
$\Delta G^{\ddagger}_{water}$ = 25.3
2-DIBAC-TS
ΔE_{dist}(dipole) = 17.2
ΔE_{dist}(dipolarophile) = 3.3
ΔE_{int} = -11.5
B
145.1
2.09
2.35
-0.198
$\Delta E^{\ddagger}_{water}$ = 13.5
$\Delta G^{\ddagger}_{gas}$ = 25.3
$\Delta G^{\ddagger}_{water}$ = 26.6
1-i-TS
ΔE_{dist}(dipole) = 17.7
ΔE_{dist}(dipolarophile) = 7.1
ΔE_{int} = -11.4
141.6
2.04
2.26
-0.084
$\Delta E^{\ddagger}_{water}$ = 16.4
$\Delta G^{\ddagger}_{gas}$ = 29.3
$\Delta G^{\ddagger}_{water}$ = 30.3
2-i-TS
ΔE_{dist}(dipole) = 18.2
ΔE_{dist}(dipolarophile) = 5.5
ΔE_{int} = -7.2
C
145.9
2.10
2.36
-0.200
$\Delta E^{\ddagger}_{water}$ = 14.7
$\Delta G^{\ddagger}_{gas}$ = 28.0
$\Delta G^{\ddagger}_{water}$ = 26.6
1-n-TS
ΔE_{dist}(dipole) = 16.9
ΔE_{dist}(dipolarophile) = 8.8
ΔE_{int} = -11.0
141.8
2.01
2.25
-0.111
$\Delta E^{\ddagger}_{water}$ = 18.3
$\Delta G^{\ddagger}_{gas}$ = 31.6
$\Delta G^{\ddagger}_{water}$ = 31.2
2-n-TS
ΔE_{dist}(dipole) = 17.7
ΔE_{dist}(dipolarophile) = 8.5
ΔE_{int} = -7.9
E, eV
A
-0.93
-7.5
N
O
Me
DIBAC
B
-0.56
-9.6
O
OMe
i
C
-0.51
-10.0
O
OMe
n

Figure 1.3.2. Transition state geometries, activation energies, and distortion-interactions energies calculated at the M06-2X/6-31+G(2d,p) level of theory. Energies and NBO charges on dipolarophiles (*italics*) include solvation corrections (water) on gas-phase geometries using IEFPCM model (radii=UFF). All energies in kcal/mol.

Figure 1.3.3 Substituent effects on activation energies of azido and diazo group cycloadditions

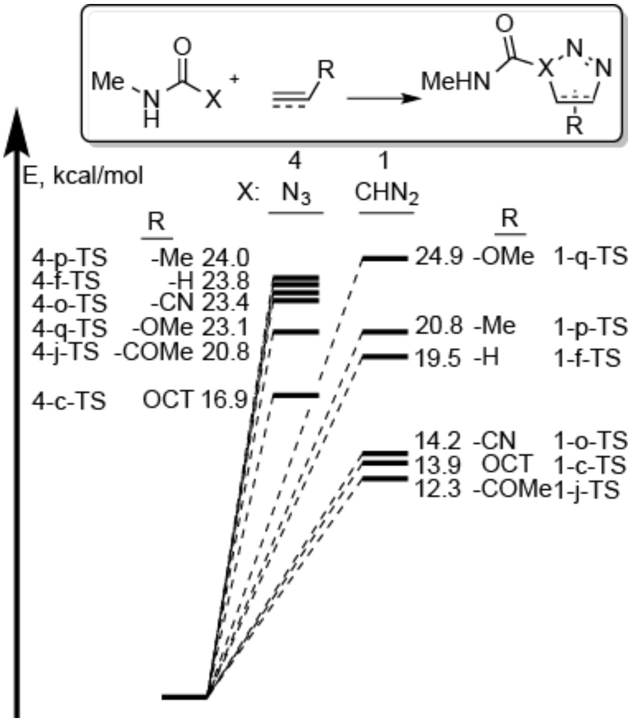

Figure 1.3.3. Substituent effects on activation energies of azido and diazo group cycloadditions calculated at the M06-2X/6-31+G(2d,p) level of theory. Energies include solvation corrections (water) on gas-phase geometires using IEFPCM model (radii=UFF). All energies in kcal/mol. See SI for substituent effects on cycloadditions with other dipoles.

Figure 1.3.4 Exemplary transition-state geometries of azide and diazo group cycloadditions

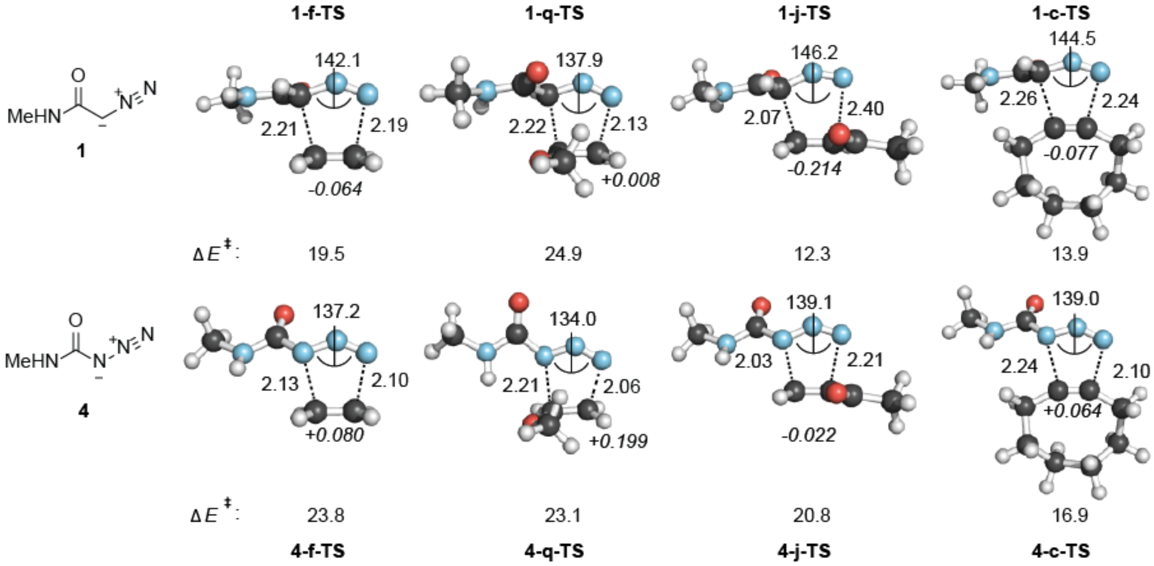
1-f-TS
1-q-TS
1-j-TS
1-c-TS
MeHN
O
N
N
1
142.1
2.21
2.19
-0.064
137.9
2.22
2.13
+0.008
146.2
2.07
2.40
-0.214
144.5
2.26
2.24
-0.077
ΔE‡:
19.5
24.9
12.3
13.9
MeHN
O
N
N
N
4
137.2
2.13
2.10
+0.080
134.0
2.21
2.06
+0.199
139.1
2.03
2.21
-0.022
139.0
2.24
2.10
+0.064
ΔE‡:
23.8
23.1
20.8
16.9
4-f-TS
4-q-TS
4-j-TS
4-c-TS

Figure 1.3.4. Exemplary transition-state geometries of azide and diazo group cycloadditions calculated at the M06-2X/6-31+G(2d,p) level of theory. Energies and NBO charges on dipolarophiles (*italics*) include solvation corrections (water) on gas-phase geometries using IEFPCM model (radii=UFF). All energies in kcal/mol.

Figure 1.3.5 Activation energies vs. FMO gap and distortion energies

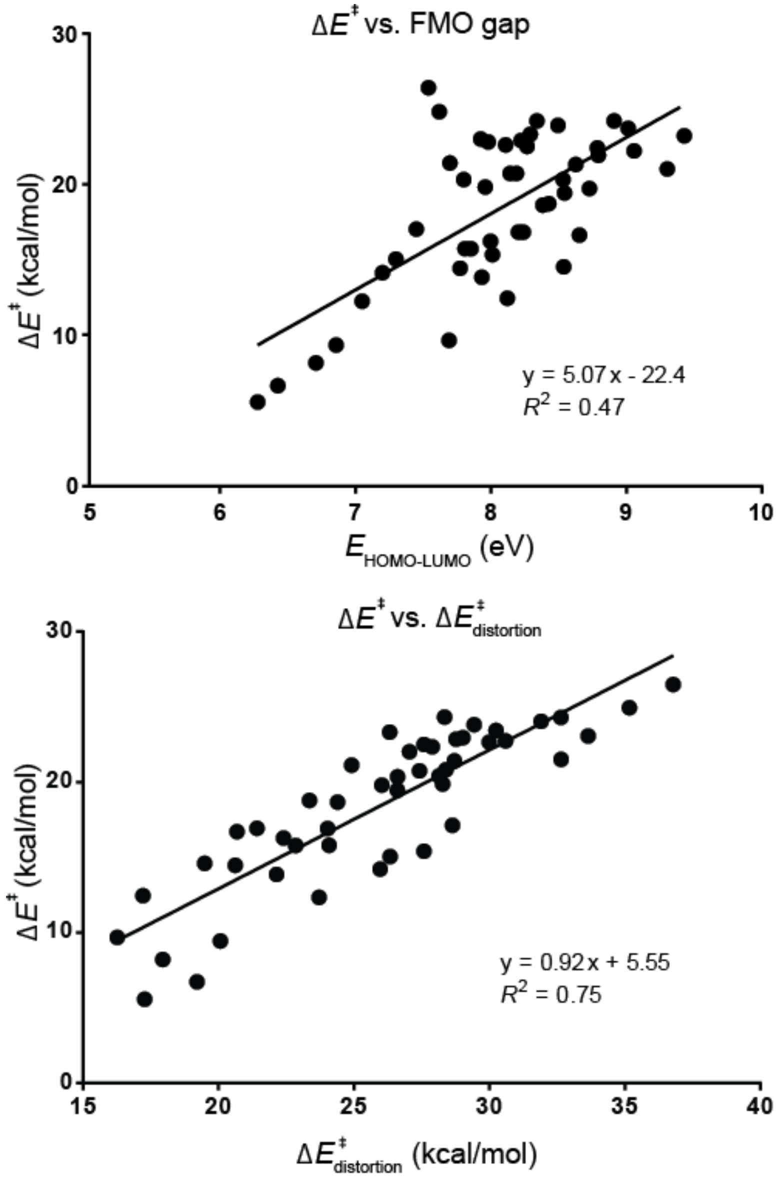

Figure 1.3.5. Activation energies vs. FMO gap (top) and distortion energies (bottom) for cycloadditions from Fig 1.3.4 and Table S1.3.3 (see SI). FMO gap is defined by the smaller of the NED/IED HOMO-LUMO energy difference.

Figure 1.3.6 Distortion-interaction analysis for selected cycloadditions

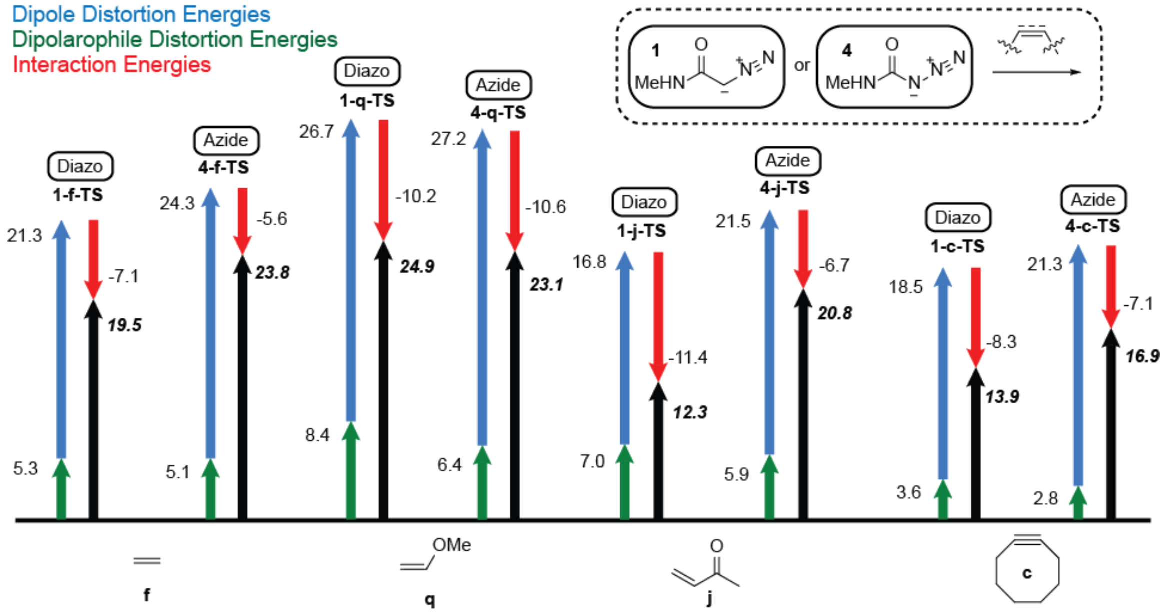

Figure 1.3.6. Distortion-interaction analysis for selected cycloadditions calculated at the M06-2X/6-31+G(2d,p) level of theory. Energies include solvation corrections (water) on gas-phase geometries using IEFPCM model (radii=UFF). All energies in kcal/mol.

Figure 1.3.7 Comparison of the strategies of predistortion acceleration and electronic tuning

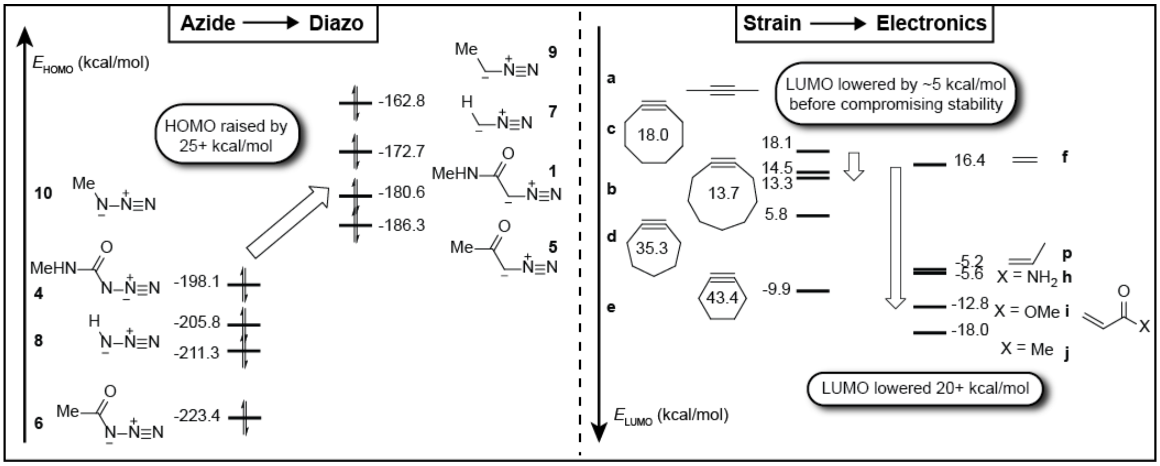
Azide ⟶ Diazo
E_{HOMO} (kcal/mol)
HOMO raised by 25+ kcal/mol
10
4
8
6
-162.8
-172.7
-180.6
-186.3
-198.1
-205.8
-211.3
-223.4
9
7
1
5
Strain ⟶ Electronics
LUMO lowered by ~5 kcal/mol before compromising stability
a
c
b
d
e
18.0
13.7
35.3
43.4
18.1
14.5
13.3
5.8
-9.9
16.4
f
-5.2
-5.6
-12.8
-18.0
p
X = NH₂ h
X = OMe i
X = Me j
LUMO lowered 20+ kcal/mol
E_{LUMO} (kcal/mol)

Figure 1.3.7. Comparison of the strategies of predistortion acceleration and electronic tuning. All orbital energies calculated at the M06-2X/6-31+G(2d,p) level of theory, including solvation corrections (water) on gas-phase geometries using IEFPCM model (radii=UFF). Contained within cycloalkynes are strain energies (kcal/mol) calculated as in Figure 1.3.2.

Figure 1.3.8 Comparison of bending in diazopropanone and acetyl azide

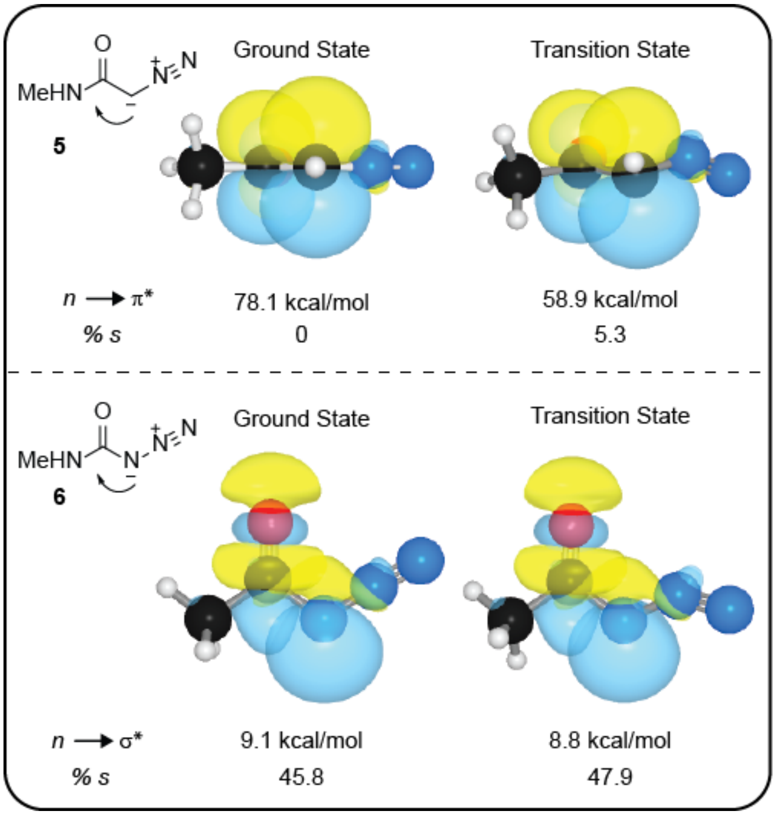
O
MeHN
N≡N
5
Ground State
Transition State
$n \rightarrow \pi^*$
% s
78.1 kcal/mol
0
58.9 kcal/mol
5.3
O
MeHN
N
N≡N
6
Ground State
Transition State
$n \rightarrow \sigma^*$
% s
9.1 kcal/mol
45.8
8.8 kcal/mol
47.9

Figure 1.3.8. Comparison of bending in diazopropanone (top) and acetyl azide (bottom) and effects on (hyper)conjugation. The larger decrease in conjugation in diazopropanone leads to similar distortion energies despite less bending. Geometries for **5-j-TS** and **6-j-TS**.

Figure 1.3.9 Activation energies vs. reaction energies

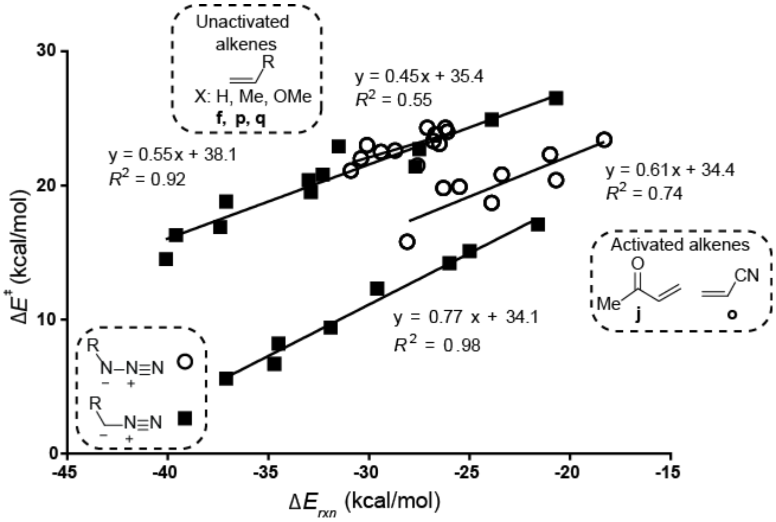

Figure 1.3.9. Activation energies vs. reaction energies separated by dipoles and activated and non-activated dipolarophiles for cycloadditions from Fig 1.3.5. and Table S1.3.3. Cyclooctyne is excluded for reasons discussed in the text. For alternate fitting, see SI.

Table 1.3.2 NBO charge on dipole in the TS

	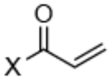	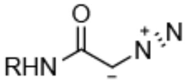	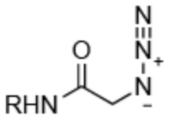
	X	**1**	**2**
j	Me	0.214	0.087
i	OMe	0.198	0.084
h	NH_2	0.177	0.068
l	NHMe	0.163	0.059
m	NMe_2	0.177	0.062

Table 1.3.2. NBO charge on dipole in the TS.

Figure 1.3.10 Electrostatic potential maps

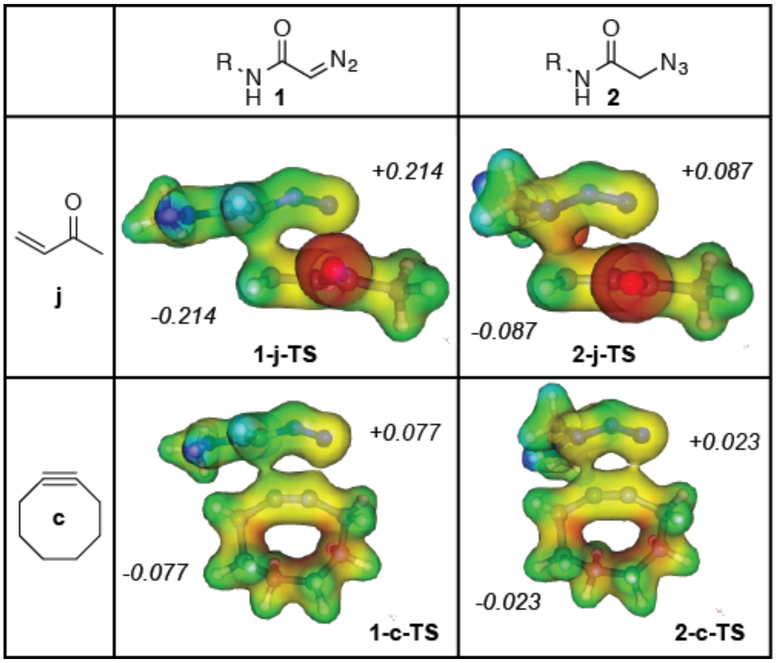
O
R
N
H
N2
1
O
R
N
H
N3
2
O
j
+0.214
-0.214
1-j-TS
+0.087
-0.087
2-j-TS
c
+0.077
-0.077
1-c-TS
+0.023
-0.023
2-c-TS

Figure 1.3.10. Electrostatic potential maps calculated at the B3LYP/6-31G(d) level of theory on M06-2X/6-31+G(2d,p) geometries. NBO charges (italics) calculated at the M06-2X/6-31+G(2d,p) level of theory, including solvation corrections (water) on gas-phase geometries using IEFPCM model (radii=UFF).

Figure 1.3.11 Pseudo-first order rate constant measured in 50:50 $CH_3CN:H_2O$ at r.t. in $M^{-1}s^{-1}$

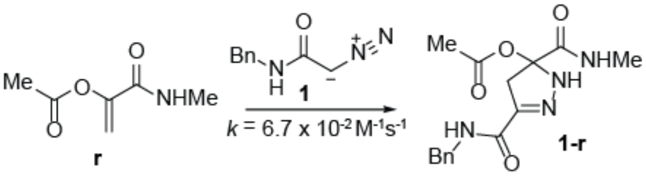
Me
O
O
NHMe
r
Bn
N
H
O
N
N
1
k = 6.7 x 10-2 M-1s-1
Me
O
O
O
NHMe
NH
N
HN
Bn
O
1-r

Figure 1.3.11. Pseudo-first order rate constant measured in 50:50 CH_3CN:H_2O at r.t. in $M^{-1}s^{-1}$.

Figure 1.3.S1 Absorbance maximum (388 nm) of the diazo-acetamide

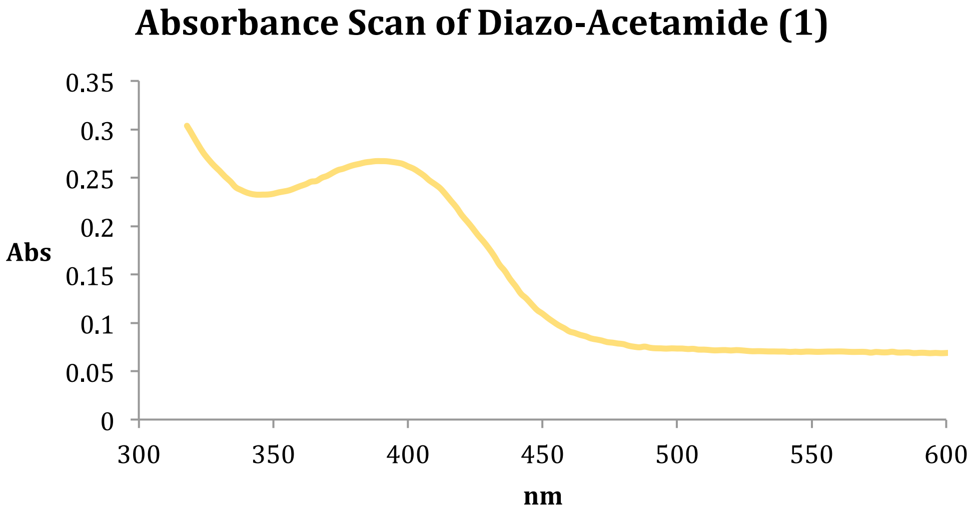

Figure 1.3.S1. Absorbance maximum (388 nm) of the diazo-acetamide (**1**).

Figure 1.3.S2 Representative kinetic plot for the absorbance assay

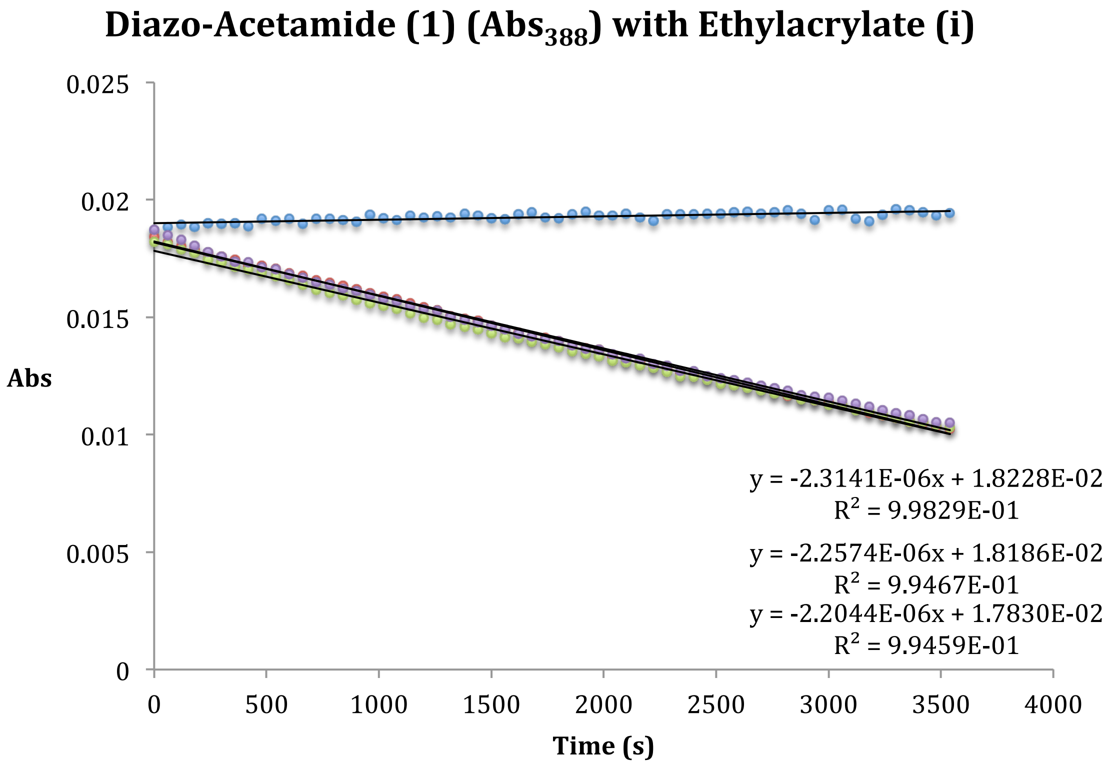

Figure 1.3.S2. Representative kinetic plot for the absorbance assay.

Figure 1.3.S3 Rate enhancement observed in aqueous cosolvent conditions

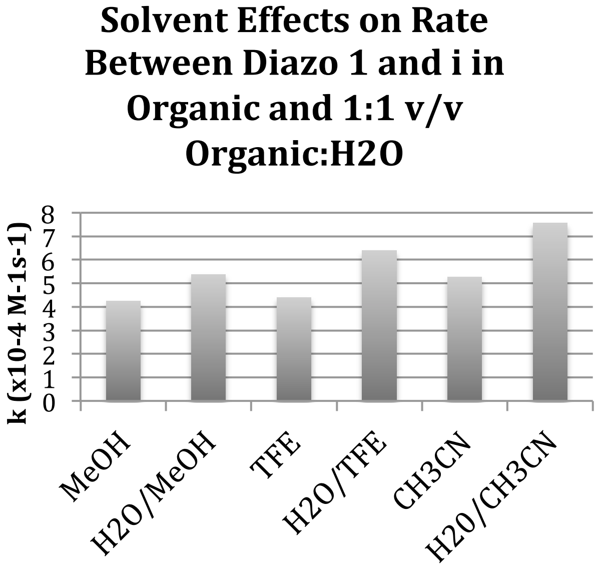

Figure 1.3.S3. Reaction rates determined for 1:1 v/v of organic solvent:ddH_2O where enhancement was observed in all aqueous cosolvent conditions relative to the reaction rates only in organic solvent. Acetonitrile produced the fastest rates without cosolvent, and was chosen for subsequent assays. The addition of water generated an average increase of 39% in rates with the conditions tested above.

Figure 1.3.S4 Comparison of activation via strain or electon-withdrawing substituents

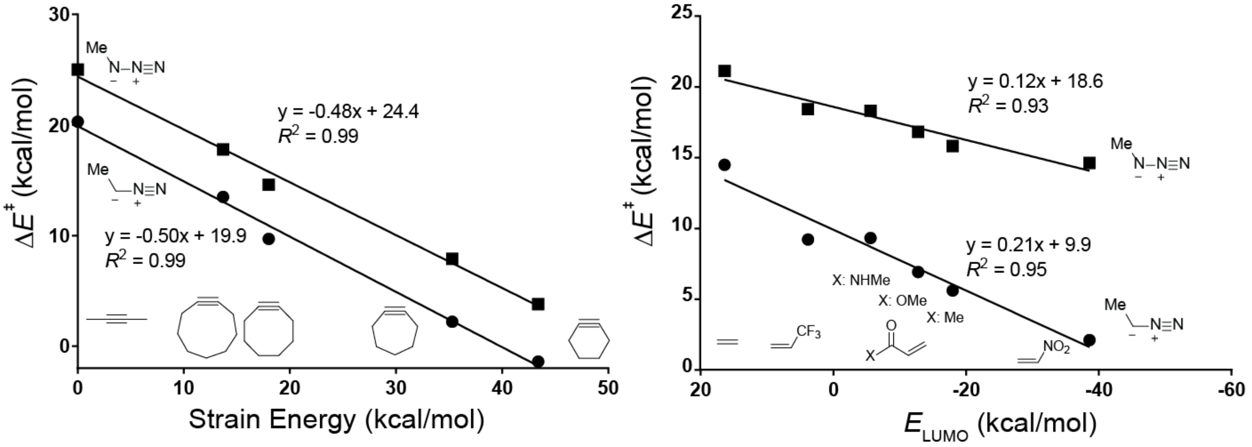

Figure 1.3.S4. Comparison of activation via strain (left) or electon-withdrawing substituents (right) for 1,3-dipolar cycloadditions of methyl azide (squares) and diazoethane (circles). Strain energy calculated from the isodesmic equation described by Bach.[207] Activation energies calculated at the M06-2X/6-31+G(2d,p) level of theory. Energies include solvation corrections (water) on gas phase geometries using IEFPCM model (radii=UFF). All energies in kcal/mol.

Figure 1.3.S5 Substituent effects on activation energies of azido and diazo group cycloadditions

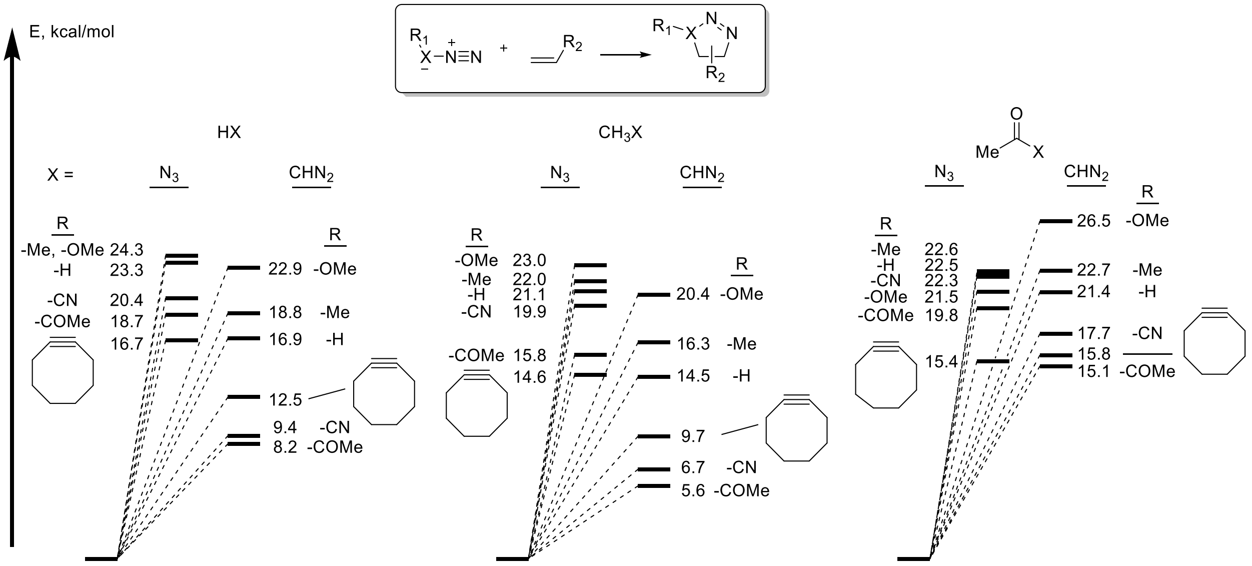

Figure 1.3.S5. Substituent effects on activation energies of azido and diazo group cycloadditions calculated at the M06-2X/6-31+G(2d,p) level of theory. Energies include solvation corrections (water) on gas phase geometries using IEFPCM model (radii=UFF). All energies in kcal/mol.

Table 1.3.S1 Gas phase activation energies of azide and diazo group cycloadditions

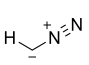
7

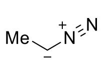
9

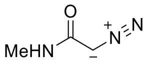
1

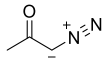
5

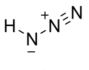
8

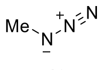
10

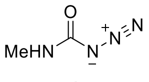
4

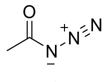
6

	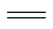		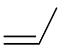		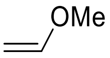		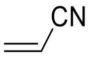		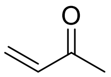		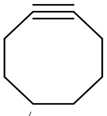	
	$\Delta E^{\neq}$	$\Delta G^{\neq}$	$\Delta E^{\neq}$	$\Delta G^{\neq}$	$\Delta E^{\neq}$	$\Delta G^{\neq}$	$\Delta E^{\neq}$	$\Delta G^{\neq}$	$\Delta E^{\neq}$	$\Delta G^{\neq}$	$\Delta E^{\neq}$	$\Delta G^{\neq}$
7	16.5	27.7	18.1	29.6	22.1	33.5	11.6	23.0	8.5	20.6	11.0	22.6
8	22.1	33.0	23.1	34.3	22.9	34.0	21.0	32.4	18.4	30.0	14.8	26.0
9	14.2	26.3	15.7	28.2	19.5	32.3	8.8	21.3	6.0	18.7	8.3	20.6
10	20.3	31.9	21.2	33.2	21.7	33.8	17.8	30.3	15.9	28.1	13.1	24.8
1	19.2	30.9	20.2	32.8	23.0	35.9	15.0	27.2	11.4	23.7	12.8	25.3
4	24.1	34.9	24.4	35.9	23.5	34.6	24.1	35.7	20.6	32.3	16.4	28.4
5	20.7	31.9	21.9	33.5	24.7	36.9	17.6	29.2	13.8	25.8	14.5	26.7
6	23.2	34.9	23.6	36.3	22.6	35.0	23.7	36.9	19.6	32.7	15.3	27.8

Table 1.3.S1. Gas phase activation energies of azide and diazo group cycloadditions calculated at the M06-2X/6-31+G(2d,p) level of theory. All energies in kcal/mol.

Table 1.3.S2 Gas phase reaction energies of azide and diazo group cycloadditions

	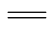		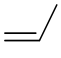		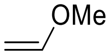		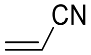		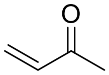		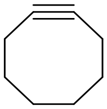	
	ΔE	*ΔG*	*ΔE*	*ΔG*	*ΔE*	*ΔG*	*ΔE*	*ΔG*	*ΔE*	*ΔG*	*ΔE*	*ΔG*
7	-35.8	-23.7	-35.5	-23.5	-30.0	-17.3	-31.0	-19.0	-34.8	-22.5	-61.2	-48.3
8	-25.2	-13.7	-25.7	-13.6	-25.8	-13.4	-19.5	-7.5	-24.1	-12.0	-75.4	-62.6
9	-38.6	-25.9	-38.1	-24.8	-37.1	-18.1	-34.1	-20.9	-37.6	-24.1	-63.5	-49.3
10	-29.3	-16.9	-28.7	-15.6	-29.3	-16.0	-25.3	-12.5	-28.4	-15.2	-81.1	-67.3
1	-33.8	-21.5	-33.8	-20.5	-22.1	-9.2	-28.3	-15.6	-32.3	-19.1	-59.2	-45.5
4	-21.4	-9.8	-21.2	-8.6	-23.8	-11.0	-14.5	-2.3	-20.9	-8.2	-66.3	-53.0
5	-28.3	-16.8	-28.2	-16.0	-19.2	-6.5	-23.1	-10.9	-27.2	-16.2	-52.9	-39.8
6	-23.7	-11.1	-23.2	-9.7	-24.2	-10.1	-16.8	-4.2	-23.2	-9.9	-64.8	-49.9

Table 1.3.S2. Gas phase reaction energies of azide and diazo group cycloadditions calculated at the M06-2X/6-31+G(2d,p) level of theory. All energies in kcal/mol.

Table 1.3.S3 Activation energies of azide and diazo group cycloadditions

	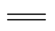		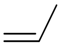		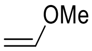		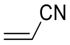		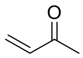		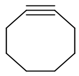	
	$\Delta E^{\neq}$	$\Delta G^{\neq}$	$\Delta E^{\neq}$	$\Delta G^{\neq}$	$\Delta E^{\neq}$	$\Delta G^{\neq}$	$\Delta E^{\neq}$	$\Delta G^{\neq}$	$\Delta E^{\neq}$	$\Delta G^{\neq}$	$\Delta E^{\neq}$	$\Delta G^{\neq}$
7	16.9	28.0	18.8	30.2	22.9	34.2	9.4	20.9	8.2	20.3	12.5	24.1
8	23.3	34.2	24.3	35.6	24.3	35.2	20.4	31.6	18.7	30.1	16.7	27.8
9	14.5	26.4	16.3	28.6	20.4	33.1	6.7	19.1	5.6	18.3	9.7	21.9
10	21.1	32.7	22.0	34.1	23.0	35.0	19.9	32.3	15.8	27.9	14.6	26.3
1	19.5	31.1	20.8	32.4	24.9	37.6	14.2	25.9	12.3	26.0	13.9	26.1
4	23.8	35.6	24.0	34.5	23.1	35.3	23.4	34.4	20.8	33.5	16.9	29.2
5	21.4	32.5	22.7	34.1	26.5	38.7	17.1	28.5	15.1	26.7	15.8	27.9
6	22.5	33.0	22.6	36.1	21.5	34.6	22.3	34.2	19.8	32.2	15.4	28.6

Table 1.3.S3. Activation energies of azide and diazo group cycloadditions calculated at the M06-2X/6-31+G(2d,p) level of theory. Energies include solvation corrections (water) on gas phase geometries using IEFPCM model (radii=UFF). All energies in kcal/mol.

Table 1.3.S4 Reaction energies of azide and diazo group cycloadditions

	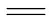		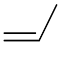		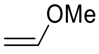		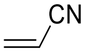		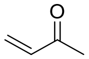		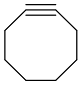	
	ΔE	ΔG	ΔE	ΔG	ΔE	ΔG	ΔE	ΔG	ΔE	ΔG	ΔE	ΔG
7	-37.4	-25.4	-37.1	-25.1	-31.5	-18.8	-31.9	-19.8	-34.5	-22.3	-62.5	-49.5
8	-26.8	-15.3	-27.1	-15.0	-26.2	-13.8	-20.7	-8.8	-23.9	-12.0	-77.8	-64.9
9	-40.1	-27.5	-39.6	-26.5	-33.0	-19.5	-34.7	-21.7	-37.1	23.7	-64.5	-50.4
10	-30.9	-18.5	-30.4	-17.2	-30.1	-16.7	-25.5	-12.6	-28.1	-15.1	-83.5	-69.7
1	-32.9	-20.6	-32.3	-20.5	-23.9	-10.8	-26.0	-12.3	-29.6	-17.2	-56.3	-42.6
4	-26.7	-15.0	-26.1	-13.5	-26.5	-13.6	-18.3	-6.3	-23.4	-11.1	-70.3	-57.0
5	-27.7	-16.5	-27.5	-15.4	-20.7	-8.0	-21.6	-9.7	-25.0	-12.4	-51.4	-38.3
6	-29.4	-17.1	-28.7	-15.4	-27.6	-13.8	-21.0	-8.2	-26.3	-11.9	-68.7	-54.3

Table 1.3.S4. Reaction energies of azide and diazo group cycloadditions calculated at the M06-2X/6-31+G(2d,p) level of theory. Energies include solvation corrections (water) on gas phase geometries using IEFPCM model (radii=UFF). All energies in kcal/mol.

Figure 1.3.S6 Transition geometries of azide and diazo group cycloadditions

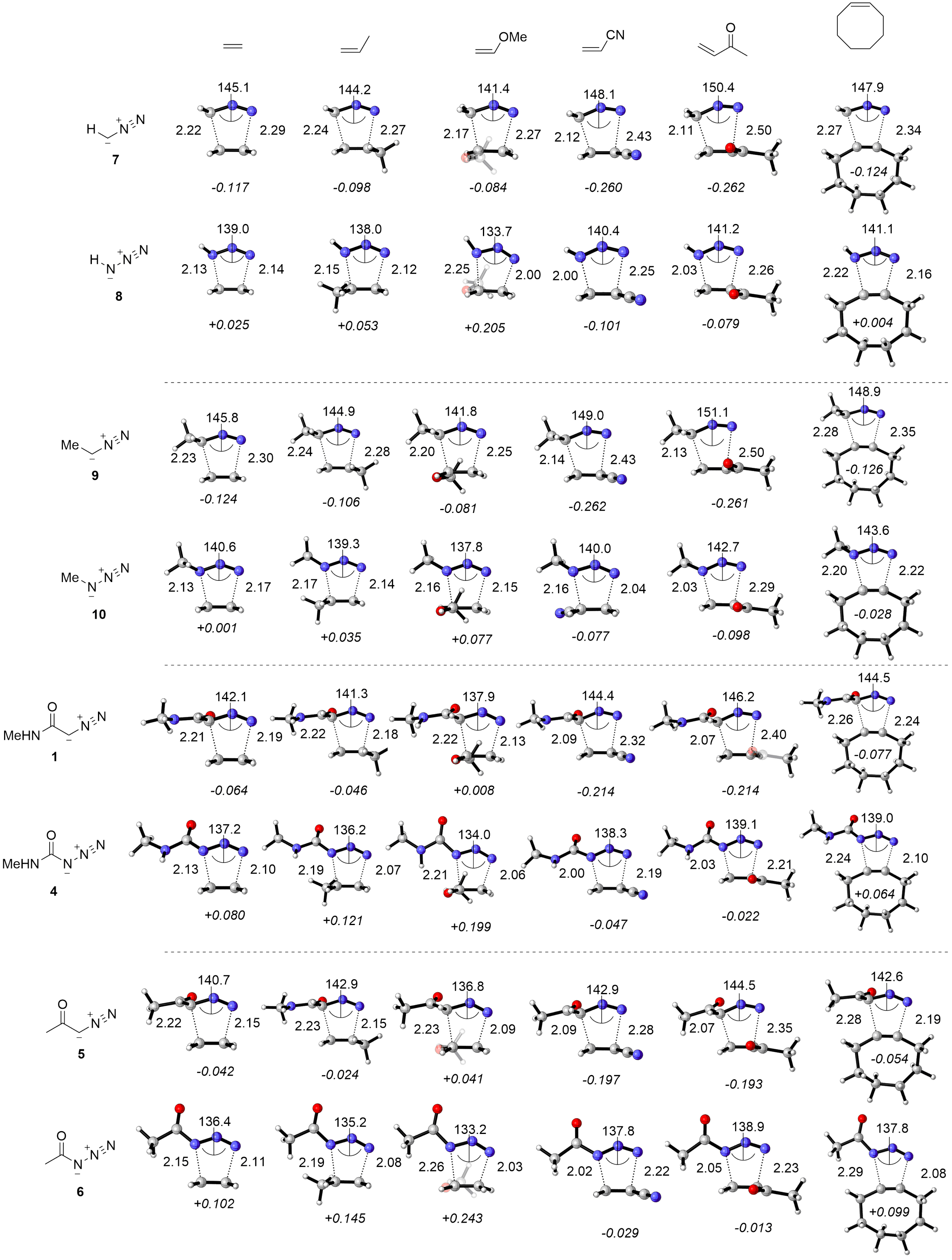
OMe
CN
O
7
145.1 2.22 2.29 -0.117
144.2 2.24 2.27 -0.098
141.4 2.17 2.27 -0.084
148.1 2.12 2.43 -0.260
150.4 2.11 2.50 -0.262
147.9 2.27 2.34 -0.124
8
139.0 2.13 2.14 +0.025
138.0 2.15 2.12 +0.053
133.7 2.25 2.00 +0.205
140.4 2.00 2.25 -0.101
141.2 2.03 2.26 -0.079
141.1 2.22 2.16 +0.004
Me
9
145.8 2.23 2.30 -0.124
144.9 2.24 2.28 -0.106
141.8 2.20 2.25 -0.081
149.0 2.14 2.43 -0.262
151.1 2.13 2.50 -0.261
148.9 2.28 2.35 -0.126
Me
10
140.6 2.13 2.17 +0.001
139.3 2.17 2.14 +0.035
137.8 2.16 2.15 +0.077
140.0 2.16 2.04 -0.077
142.7 2.03 2.29 -0.098
143.6 2.20 2.22 -0.028
MeHN
1
142.1 2.21 2.19 -0.064
141.3 2.22 2.18 -0.046
137.9 2.22 2.13 +0.008
144.4 2.09 2.32 -0.214
146.2 2.07 2.40 -0.214
144.5 2.26 2.24 -0.077
MeHN
4
137.2 2.13 2.10 +0.080
136.2 2.19 2.07 +0.121
134.0 2.21 2.06 +0.199
138.3 2.00 2.19 -0.047
139.1 2.03 2.21 -0.022
139.0 2.24 2.10 +0.064
5
140.7 2.22 2.15 -0.042
142.9 2.23 2.15 -0.024
136.8 2.23 2.09 +0.041
142.9 2.09 2.28 -0.197
144.5 2.07 2.35 -0.193
142.6 2.28 2.19 -0.054
6
136.4 2.15 2.11 +0.102
135.2 2.19 2.08 +0.145
133.2 2.26 2.03 +0.243
137.8 2.02 2.22 -0.029
138.9 2.05 2.23 -0.013
137.8 2.29 2.08 +0.099

Figure 1.3.S6. Transition geometries of azide and diazo group cycloadditions calculated at the M06-2X/6-31+G(2d,p) level of theory. NBO charges on dipolarophiles (*italics*) include solvation corrections (water) on gas phase geometries using IEFPCM model (radii=UFF). All energies in kcal/mol given in Tables 1.3.S1 & 1.3.S3.

Figure 1.3.S7 Orbitals calculated at the HF/6-31G(d) level of theory

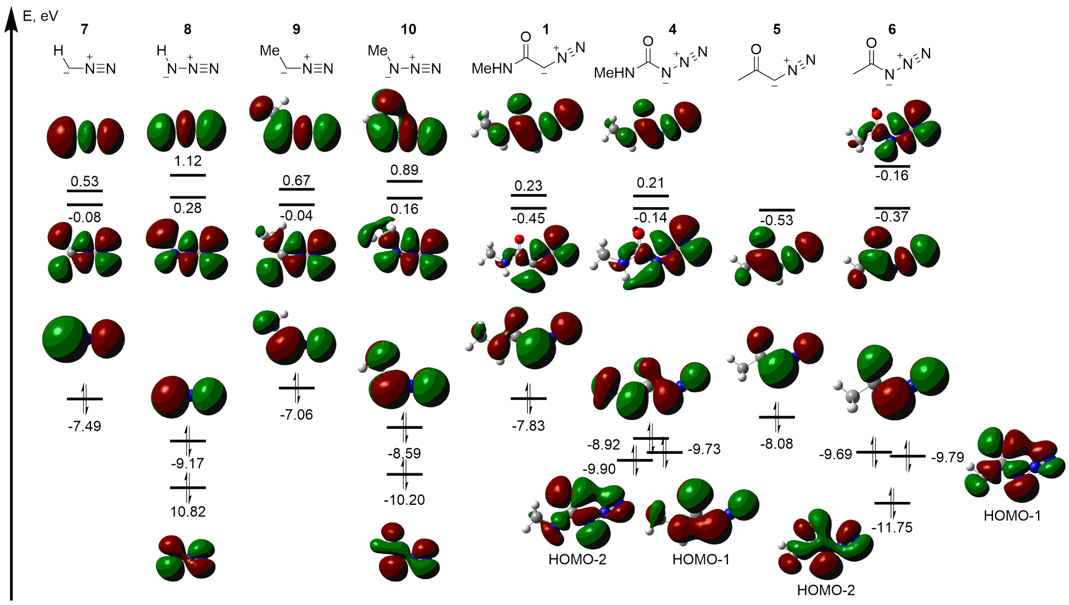
E, eV
7
8
9
10
1
4
5
6
H
N≡N
H
N–N≡N
Me
N≡N
Me
N–N≡N
MeHN
O
N≡N
MeHN
O
N
N≡N
O
N≡N
O
N
N≡N
0.53
-0.08
1.12
0.28
0.67
-0.04
0.89
0.16
0.23
-0.45
0.21
-0.14
-0.53
-0.16
-0.37
-7.49
-9.17
10.82
-7.06
-8.59
-10.20
-7.83
-8.92
-9.90
-9.73
-8.08
-9.69
-9.79
-11.75
HOMO-2
HOMO-1
HOMO-2
HOMO-1

Figure 1.3.S7. Orbitals calculated at the HF/6-31G(d) level of theory. Energies obtained at the M06-2X/6-31+G(2d,p) level of theory, including single point solvation corrections (water) using IEFPCM.

Figure 1.3.S8 Activation energies vs. FMO gap for cycloadditions

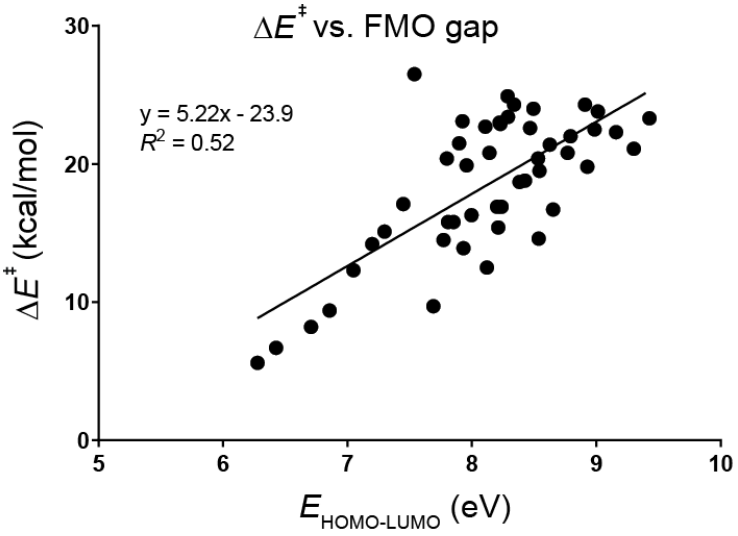

Figure 1.3.S8. Activation energies vs. FMO gap for cycloadditions from Fig 1.3.5 and Tables 1.3.S1&1.3.3. FMO gap is defined by the smaller of the NED/IED HOMO-LUMO energy difference using HOMO+1 for IED diazo group cycloadditions when relevant.

Figure 1.3.S9 Distortion–interaction analysis for cycloadditions

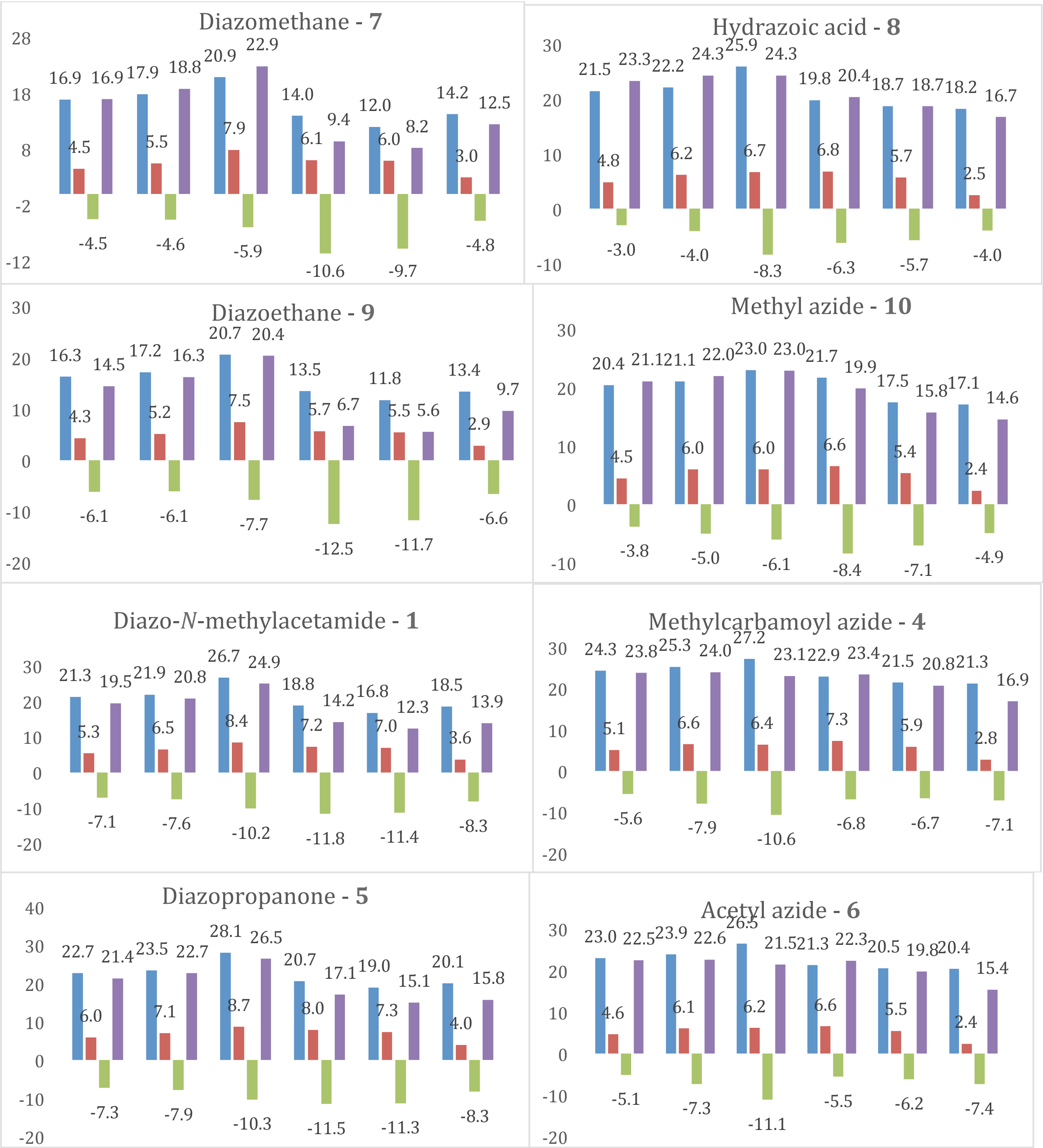

Figure 1.3.S9. Distortion–interaction analysis for cycloadditions calculated at the M06-2X/6-31+G(2d,p) level of theory. Energies include solvation corrections (water) on gas phase geometries using IEFPCM model (radii=UFF). All energies in kcal/mol. From left to right in each plot, the values are for ethylene, propene, methyl vinyl ether, acrylonitrile, methyl vinyl ketone, and cyclooctyne. Color coding is as follows: Blue=dipole distortion, red=dipolarophile distortion, green=interaction, purple=activation energy.

Figure 1.3.S10 Distortion–interaction analysis for experimentally investigated carbonyl series

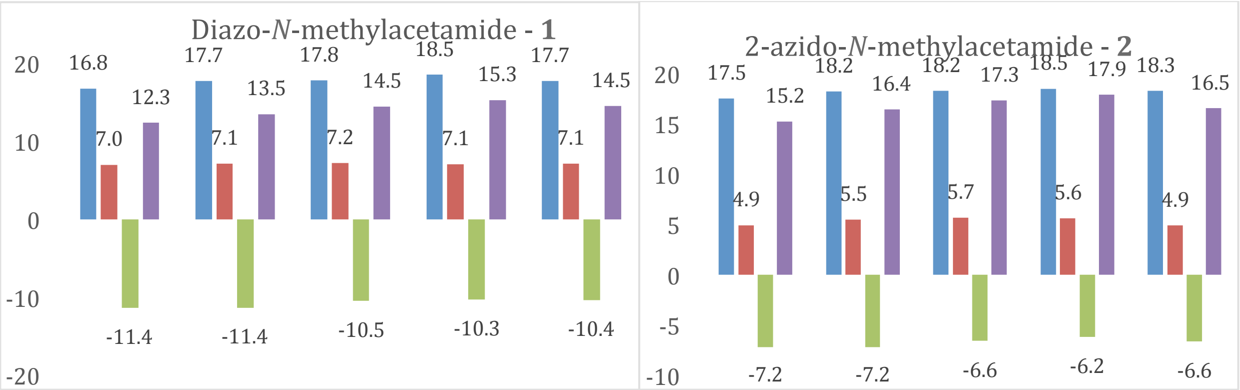

Figure 1.3.S10. Distortion–interaction analysis for experimentally investigated carbonyl series calculated at the M06-2X/6-31+G(2d,p) level of theory. Energies include solvation corrections (water) on gas phase geometries using IEFPCM model (radii=UFF). All energies in kcal/mol. From left to right in each plot, the values are for methyl vinyl ketone, methyl acrylate, acrylamide, *N*-methylacrylamide, and *N,N*-dimethylacrylamide. Blue=dipole distortion, red=dipolarophile distortion, green=interaction, purple=activation energy.

Figure 1.3.S11 Activation energies vs. reaction energies and separated by dipoles

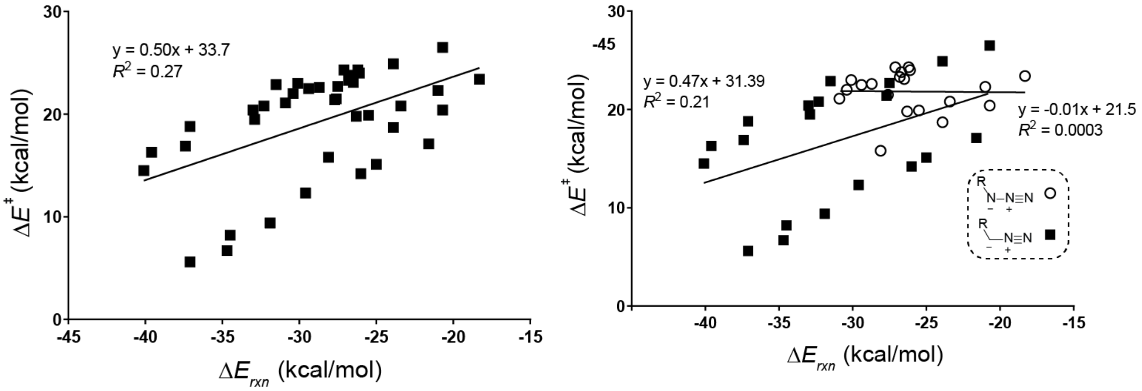

Figure 1.3.S11. Activation energies vs. reaction energies (left) and separated by dipoles (right) for cycloadditions from Tables 1.3.S1 & 1.3.3. Cyclooctyne is excluded for reasons discussed in the main manuscript.

Table 1.3.S5 Intrinsic reaction bariers of azide and diazo group cycloadditions

	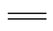	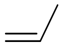	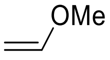	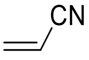	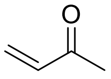	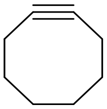
	$\Delta E^{\ddagger}_0$	$\Delta E^{\ddagger}_0$	$\Delta E^{\ddagger}_0$	$\Delta E^{\ddagger}_0$	$\Delta E^{\ddagger}_0$	$\Delta E^{\ddagger}_0$
7	32.9	34.9	37.0	22.5	22.1	37.2
8	35.4	36.6	36.2	29.9	29.4	47.7
9	31.3	33.1	35.0	20.4	19.8	34.4
10	34.8	35.6	36.5	31.4	28.1	47.1
1	34.0	35.1	35.9	25.5	24.9	36.6
4	35.9	35.9	35.1	31.9	31.4	45.2
5	33.8	35.1	36.1	26.8	26.1	37.0
6	35.7	35.5	33.9	31.9	31.6	42.9

Table 1.3.S5. Intrinsic reaction bariers of azide and diazo group cycloadditions calculated at the M06-2X/6-31+G(2d,p) level of theory. Energies include solvation corrections (water) on gas phase geometries using IEFPCM model (radii=UFF). All energies in kcal/mol.

Figure 1.3.S12 Implicit and explicit solvation for azide and diazo group cycloadditions with methyl vinyl ketone

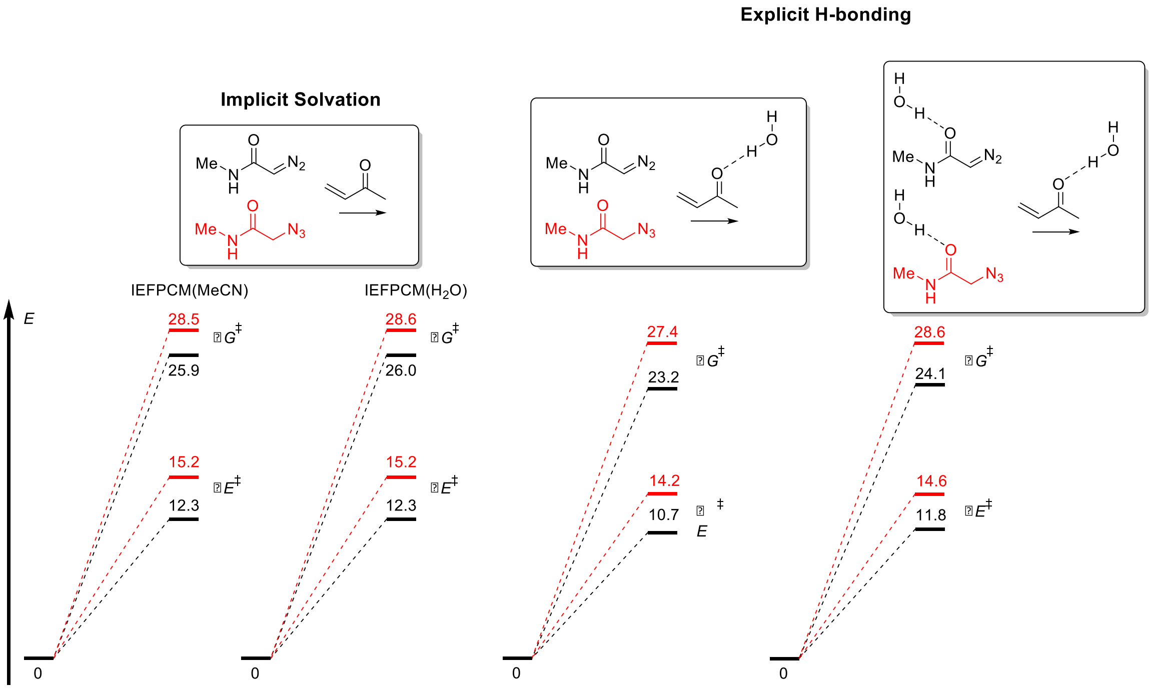
Explicit H-bonding
Implicit Solvation
IEFPCM(MeCN)
IEFPCM(H2O)
E
28.5
25.9
15.2
12.3
28.6
26.0
15.2
12.3
27.4
23.2
14.2
10.7
28.6
24.1
14.6
11.8
ΔG‡
ΔE‡
0
Me
N
H
O
N2
N3
H
O

Figure 1.3.S12. Implicit and explicit solvation for azide and diazo group cycloadditions with methyl vinyl ketone calculated at the M06-2X/6-31+G(2d,p) level of theory. Energies on the left include solvation corrections (acetonitrile or water) on gas phase geometries using IEFPCM model (radii=UFF). All energies in kcal/mol.

Figure 1.3.S13 Electrostatic potential maps

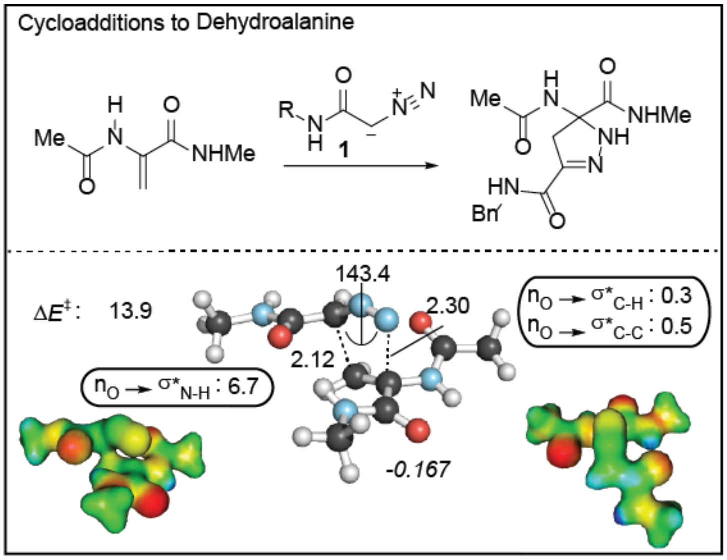
Cycloadditions to Dehydroalanine
Me
H
N
O
O
NHMe
R
N
H
O
N
N
1
Me
H
N
O
O
NHMe
NH
N
HN
Bn
O
ΔE‡: 13.9
143.4
2.30
2.12
n_O → σ*_N-H : 6.7
n_O → σ*_C-H : 0.3
n_O → σ*_C-C : 0.5
-0.167

Figure 1.3.S13. Electrostatic potential maps calculated at the B3LYP/6-31G(d) level of theory on M06-2X/6-31+G(2d,p) geometries. Activation energies and NBO interaction energies calculated at the M06-2X/6-31+G(2d,p) level of theory. Energies include solvation corrections (water) on gas phase geometries using IEFPCM model (radii=UFF). All energies in kcal/mol.

1.3.6 Synthesis

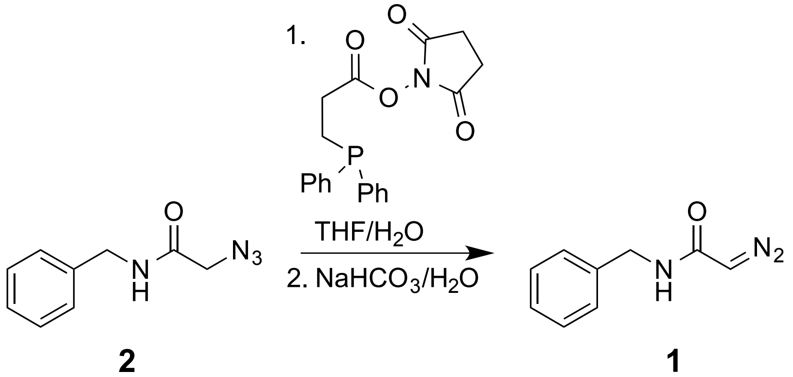

***N*-benzyl-2-diazoacetamide (1)** was prepared from ***N*-benzyl-2-azidoacetamide (2)** according to a previously reported method and was confirmed with identical spectroscopic data.[24]

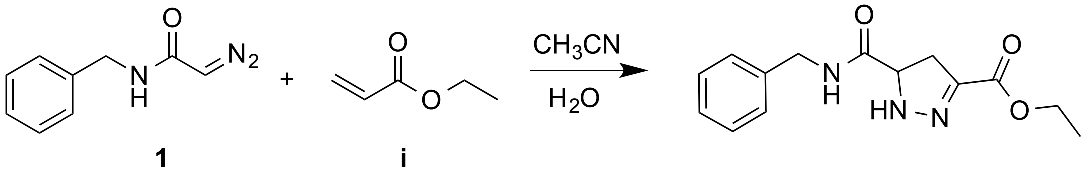

Synthesis of **ethyl 5-(benzylcarbamoyl)-4,5-dihydro-1*H*-pyrazole-3-carboxylate**: *N*-benzyl-2-diazoacetamide (**1**) (3.5 mg, 0.02 mmol) was dissolved in CH_3CN (0.5 mL) with stirring, and ddH_2O was added (0.5 mL). Ethyl acrylate (**i**) (0.011 mL, 0.1 mmol) was added and the reaction mixture was stirred O/N. The resulting solution was concentrated to dryness under high vacuum to provide the desired pyrazoline product as a mixture of isomers (5.5 mg, quant.) Spectral characterization is provided for the major isomer as observed (see HSQC and HMBC for isomer determination): ^{1}H NMR (500 MHz, CD_3CN) δ 7.37 – 7.25 (m, 6H), 7.12 (d, J = 3.0 Hz, 1H),

4.42 (dd, *J* = 9.7, 3.0 Hz, 1H), 4.38 (d, *J* = 6.2 Hz, 2H), 4.23 (q, *J* = 7.1 Hz, 2H), 3.25 (dd, *J* = 17.4, 12.9 Hz, 1H), 2.95 (ddd, *J* = 17.4, 9.5, 1.2 Hz, 1H), 1.29 (t, *J* = 7.1 Hz, 3H). ^{13}C NMR (126 MHz, CD_3CN) *δ* 172.42, 163.07, 143.40, 140.05, 129.43, 128.28, 128.02, 63.79, 61.67, 43.49, 37.03, 14.49. HRMS (ESI) calcd. for $C_{14}H_{17}N_3O_3$ $[M+H]^+$ 276.1343, found 276.1348.

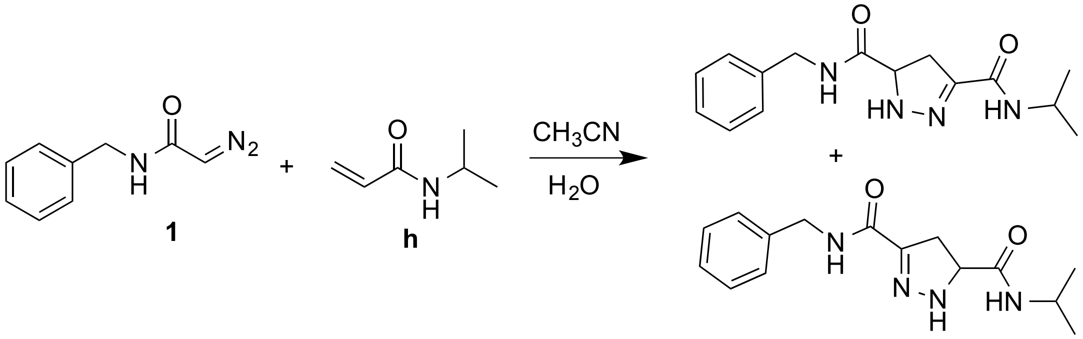

Synthesis of ***N*^5^-benzyl-*N*^3^-isopropyl-pyrazoline-3,5-dicarboxamide**: *N*-benzyl-2-diazoacetamide (**1**) (3.5 mg, 0.02 mmol) was dissolved in CH_3CN (0.5 mL) with stirring, and ddH_2O was added (0.5 mL). N-isopropyl acrylamide (**h**) (0.011 mL, 0.1 mmol) was added and the reaction mixture was stirred 4 h. The resulting solution was concentrated to dryness, and purified by preparatory chromatography on silica gel (50% v/v EtOAc in hexanes) and concentrated to provide the desired product as a mixture of isomers 1:0.72 (5.5 mg, 96%). ^{1}H NMR (500 MHz, CD_3CN) *δ* 7.66 (ddd, *J* = 49.6, 5.7, 3.3 Hz, 0.7H), 7.48 – 7.40 (m, 1H), 7.36 – 7.22 (m, 8.5H), 6.76 – 6.66 (m, 2H), 6.59 (s, 1H), 4.41 (d, *J* = 6.4 Hz, 2H), 4.36 (d, *J* = 6.1 Hz, 1.4H), 4.31 (ddd, *J* = 12.8, 9.4, 3.6 Hz, 0.7H), 4.22 (ddd, *J* = 12.5, 9.2, 3.4 Hz, 1H), 4.18 (m, 0.7H), 4.01 (ddt, *J* = 13.2, 8.3, 6.6 Hz, 0.7 H), 4.01 (ddt, *J* = 13.2, 8., 6.6 Hz, 1H), 3.24 (dt, *J* =

17.6, 12.2 Hz, 1.7H), 2.89 (dddd, *J* = 17.7, 9.1, 3.4, 1.3 Hz, 1.7H), 1.14 (dd, *J* = 6.7, 1.1 Hz, 4.2H), 1.10 (dd, *J* = 6.6, 2.1 Hz, 6H). ^{13}C NMR (126 MHz, CD_3CN) *δ* 172.56, 171.43, 168.38,162.54, 161.53, 148.45, 147.93, 140.43, 140.10, 133.18, 132.17, 129.62, 129.34, 129.31, 128.18, 128.16, 127.90, 127.85, 68.60, 63.36, 43.32, 43.06, 42.00, 41.80, 39.51, 37.01, 36.91, 31.04, 29.57, 24.44, 23.59 22.58, 22.51, 22.47, 14.26, 11.25. HRMS (ESI) *m/z* calc'd for $C_{14}H_{17}N_3O_3$ [M+H]$^+$ 289.1660, found 289.1656.

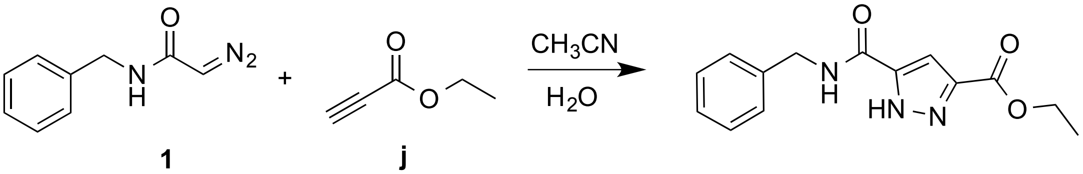

Synthesis of **ethyl 5-(benzylcarbamoyl)-1*H*-pyrazole-3-carboxylate**: *N*-benzyl-2-diazoacetamide (**1**) (3.5 mg, 0.02 mmol) was dissolved in CH_3CN (0.5 mL) with stirring, and ddH_2O was added (0.5 mL). Ethyl propiolate (**j**) (0.011 mL, 0.1 mmol) was added and the reaction mixture was stirred O/N. The resulting solution was concentrated to dryness under high vacuum to provide the product as a white solid (5.5 mg, quant.). ^{1}H NMR (500 MHz, MeOD) *δ* 7.38 – 7.19 (m, 6H), 4.56 (s, 2H), 4.38 (q, *J* = 7.1 Hz, 2H), 1.38 (t, *J* = 7.1 Hz, 3H). ^{13}C NMR (126 MHz, MeOD) *δ* 139.97, 129.54, 128.53, 128.24, 109.35, 62.40, 43.84, 14.54. HRMS (ESI) *m/z* calc'd for $C_{14}H_{15}N_3O_3$ [M+H]$^+$ 274.1187, found 274.1193.

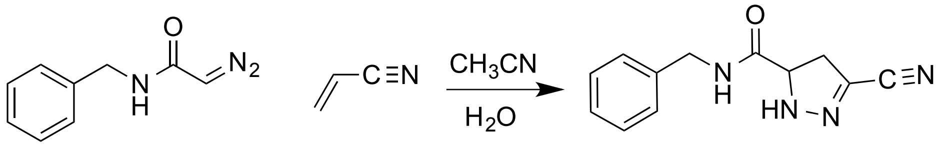

1

Synthesis of ***N*-benzyl-3-cyano-4,5-dihydro-1*H*-pyrazole-5-carboxamide**: *N*-benzyl-2-diazoacetamide (**1**) (3.5 mg, 0.02 mmol) was dissolved in CH_3CN (0.5 mL) with stirring, and ddH_2O was added (0.5 mL). Acrylonitrile (0.010 mL, 0.1 mmol) was added and the reaction mixture was stirred O/N. The reaction was concentrated to dryness under high vacuum to provide the product as a white solid (0.005 g, quant.). ^{1}H NMR (500 MHz, CD_3CN) δ 7.15 – 7.02 (m, 6H), 6.96 (s, 1H), 4.25 – 4.18 (m, 1H), 4.14 (d, J = 6.1 Hz, 2H), 3.03 (dd, J = 17.1, 13.1 Hz, 1H), 2.81 (ddd, J = 17.1, 9.4, 1.0 Hz, 1H). ^{13}C NMR (126 MHz, CD_3CN) δ 172.86, 141.59, 131.14, 130.01, 129.77, 126.07, 117.21, 65.07, 45.28, 40.26. HRMS (ESI) *m/z* calc'd for $C_{12}H_{12}N_4O$ $[M+H]^+$ 229.1084, found 229.1079.

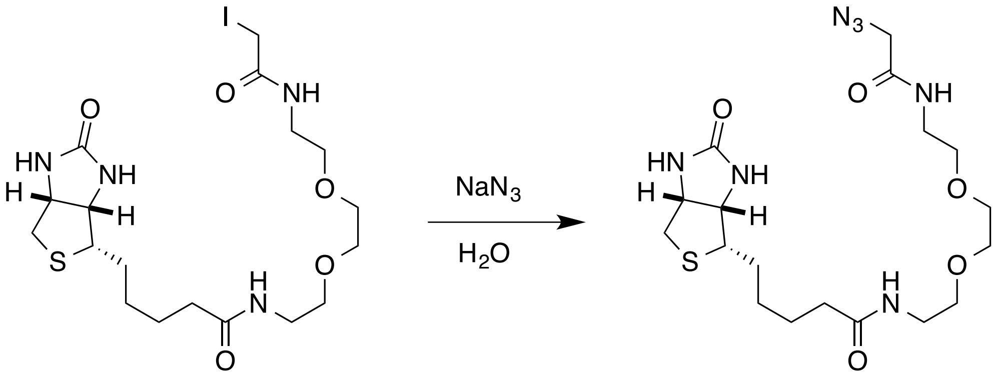

Biotin-PEG$_2$-azidoacetamide: Biotin-PEG$_2$-iodoacetamide (0.010 g, 0.001 mmol) was dissolved in ddH$_2$O (0.25 mL) with stirring and the solution was cooled to 0^0 C. Sodium azide (0.03g, 0.0836 mmol) was added, and the reaction mixture was allowed to warm to r.t. O/N. The reaction mixture was then concentrated to dryness. The resulting residue was triturated into DCM (5 mL) and filtered, and the filtrate was washed with DCM (5 mL). The combined organics were concentrated under reduced pressure to provide the biotin-PEG$_2$-azidoacetamide conjugate as a high purity white solid (0.014 g, 98%) that was used without further purification. ^{1}H NMR (750 MHz, CDCl$_3$) δ 7.16 (t, *J* = 5.8 Hz, 1H), 6.91 (s, 1H), 6.77 (t, *J* = 5.7 Hz, 1H), 5.87 (s, 1H), 4.50 (dd, *J* = 7.8, 4.8 Hz, 1H), 4.30 (dd, *J* = 8.0, 4.7 Hz, 1H), 3.97 (s, 2H), 3.61 (s, 3H), 3.57 (q, *J* = 5.2 Hz, 4H), 3.48 (q, *J* = 5.4 Hz, 2H), 3.46 – 3.38 (m, 1H), 3.13 (td, *J* = 7.3, 4.5 Hz, 1H), 2.89 (dd, *J* = 12.9, 4.8 Hz, 1H), 2.74 (d, *J* = 12.8 Hz, 1H), 2.22 (t, *J* = 7.6 Hz, 2H), 1.75 – 1.62 (m, 3H), 1.47 – 1.37 (m, 2H). ^{13}C NMR (126 MHz, CDCl$_3$) δ 173.51, 167.26, 164.35, 70.23, 70.08, 70.02, 69.67, 61.85, 60.34, 55.78, 52.59, 40.63, 39.33, 39.22, 36.13, 28.33, 28.19, 25.72. HRMS (ESI) *m/z* calc'd for $C_{18}H_{31}N_7O_5S$ $[M+H]^+$ 458.2181, found 458.2185.

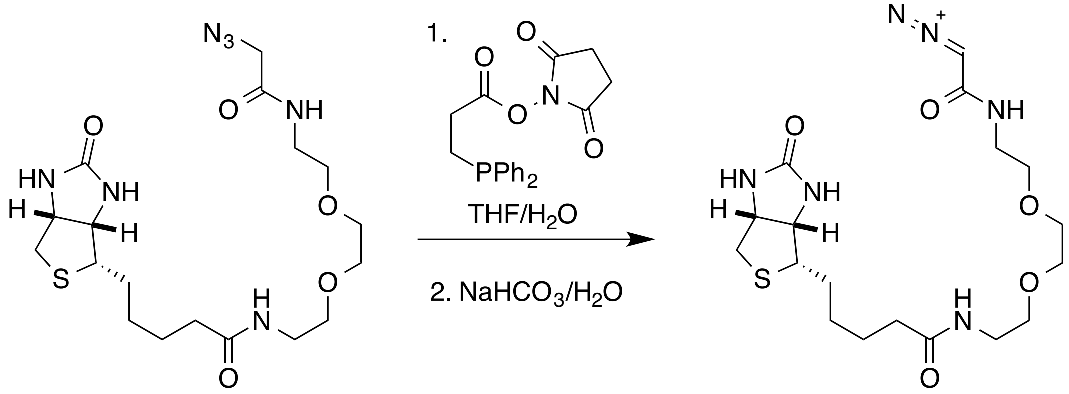

Biotin-PEG$_2$-diazoacetamide: Biotin-PEG$_2$-azidoacetamide (0.037 g, 0.08 mmol) was dissolved in an aqueous solution of THF (10% H_2O v/v in THF) (0.75 mL) with stirring. To the solution, *N*-succinimidyl 3-(diphenylphosphino)propionate[24] (0.03 g, 0.086 mmol) was added and the reaction mixture was stirred O/N. A saturated aqueous solution of $NaHCO_3$ (1 mL) was added and the reaction mixture was stirred vigorously for 6 h. The reaction mixture was salted with NaCl (0.05 g) and extracted into DCM (6x 5 mL), and the combined organics were dried over $NaSO_4$, and concentrated to a pale yellow solid. The residue was purified by chromatography over silica gel (10% v/v MeOH in DCM) to give the **biotin-PEG$_2$-diazoacetamide** conjugate as a pale yellow solid (0.023 g, 62%). ^{1}H NMR (500 MHz, $CDCl_3$) δ 6.56 (s, 2H), 6.41 (s, 1H), 5.29 (s, 1H), 4.52 (dd, *J* = 7.8, 4.9 Hz, 1H), 4.33 (td, *J* = 5.1, 2.4 Hz, 1H), 3.69 – 3.35 (m, 10H), 3.17 (td, *J* = 7.4, 4.7 Hz, 1H), 2.92 (dd, *J* = 12.8, 4.9 Hz, 1H), 2.74 (d, *J* = 12.9 Hz, 1H), 2.24 (t, *J* = 7.2 Hz, 2H), 1.80 – 1.60 (m, 6H), 1.54 – 1.37 (m, 2H). ^{13}C NMR (126 MHz, $CDCl_3$) δ 173.56, 164.01, 70.42, 70.28, 70.00, 69.84, 61.78, 60.29, 55.46, 47.17, 40.67, 39.62, 39.31, 36.10, 28.05, 28.03, 25.49. HRMS (ESI) *m/z* calc'd for $C_{18}H_{30}N_6O_5S$ $[M+Na]^+$ 465.1891, found 465.1905.

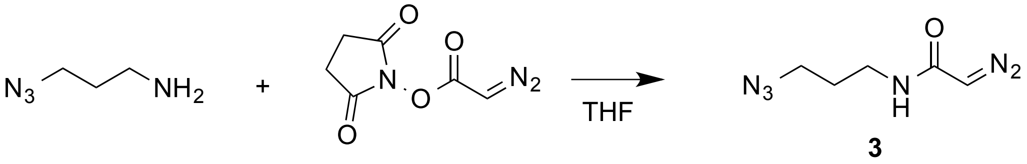

Synthesis of ***N*-(3-azidopropyl)-2-diazoacetamide**: *NHS*-diazoacetamide[117] (0.094 g, 0.5 mmol) was dissolved in THF (1 mL) with stirring, and the solution was cooled to 0° C. 3-azidopropanamine (0.1 g, 0.5 mmol) was added as a 28% w/v solution in Et_2O (0.2 mL) and the reaction mixture was allowed to warm to r.t. O/N. The reaction mixture was then concentrated by rotary evaporation, and purified by chromatography on silica gel (50:50 EtOAc:Hexanes) to provide the ***N*-(3-azidopropyl)-2-diazoacetamide** as a yellow oil (0.05 g, 60%). ^1H NMR (500 MHz, CD_3CN) δ 6.18 (s, 1H), 4.95 (s, 1H), 3.33 (t, $J = 6.8$ Hz, 2H), 3.24 (q, $J = 6.5$ Hz, 1H), 1.70 (p, $J = 6.7$ Hz, 1H). ^{13}C NMR (126 MHz, CD_3CN) δ 168.16, 51.41, 49.03, 39.29, 31.50. HRMS (ESI) *m/z* calc'd for $C_{14}H_{17}N_3O_3$ $[M+H]^+$ 169.0833, found 169.0832.

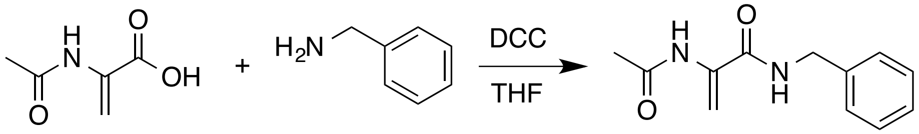

Synthesis of **2-acetamido-*N*-benzylacrylamide**: 2-acetamidoacrylic acid (0.260 g, 2 mmol) and DCC (0.413 g, 2 mmol) was suspended in THF (5 mL) and the solution was cooled to -5° C. Benzylamine (0.214 g, 2 mmol) was added, and the reaction mixture was allowed to gradually warm to r.t. O/N. The reaction mixture was then concentrated by rotary evaporation, and purified by chromatography on silica gel (50% v/v EtOAc in hexanes) to provide **2-acetamido-*N*-benzylacrylamide** as a white solid (0.18 g, 41%). ^{1}H NMR (500 MHz, $CDCl_3$) δ 8.13 (s, 1H), 7.39 – 7.27 (m, 5H), 6.49 (s, 1H), 6.46 (d, J = 1.8 Hz, 1H), 5.20 (d, J = 1.7 Hz, 1H), 4.53 (d, J = 5.8 Hz, 2H), 2.13 (s, 3H). ^{13}C NMR (126 MHz, $CDCl_3$) δ 171.88, 166.59, 139.98, 136.88, 131.59, 130.60, 130.49, 103.57, 46.90, 27.50. HRMS (ESI) *m/z* calc'd for $C_{12}H_{14}N_2O_2$ $[M+H]^+$ 219.1129, found 219.1125.

Labeling of Nisin peptide

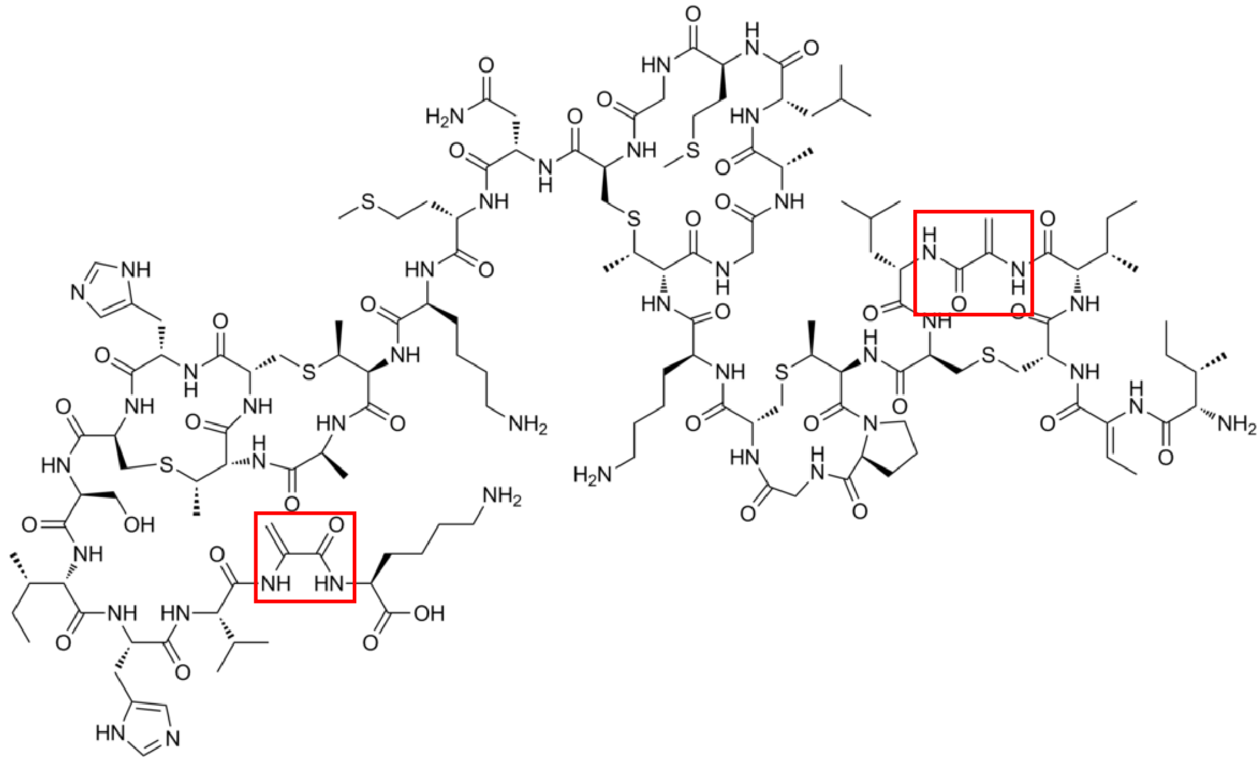

Figure 1.3.S13. Nisin peptide (full sequence) with 2 probable Dha sites for conjugation (red boxes).

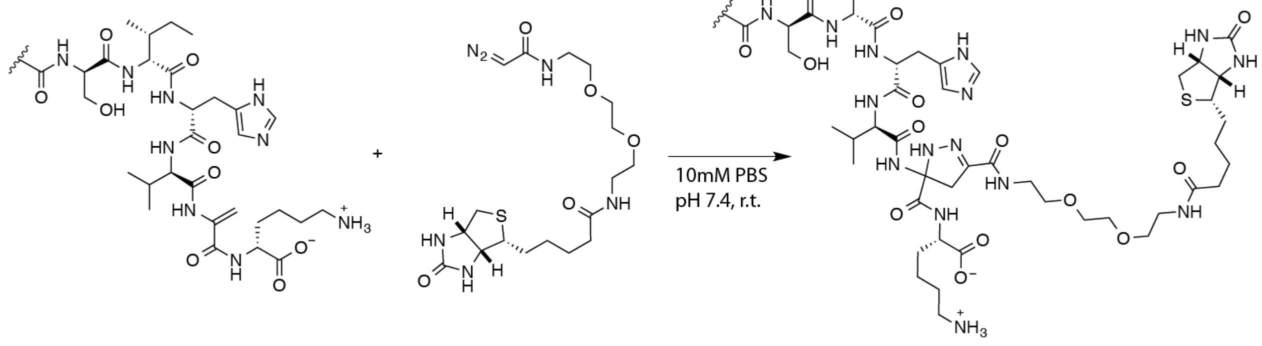
10mM PBS
pH 7.4, r.t.

Nisin from *Lactococcus lactis* (2.5% by mass, balance sodium chloride and denatured milk solids) (0.01 g, 7.5x10^{-4} mmol) was dissolved in sodium phosphate buffer (1 mL, 10 mM, pH 7.4) with stirring. To the resulting solution, biotin-PEG$_2$-diazoacetamide (0.002 g, 4.5x10^{-3} mmol) was added as a solution in sodium phosphate buffer (0.5 mL, 10 mM, pH 7.4), and the reaction mixture was nutated for 16 h. The resulting solution was purified by dialysis (2K MWCO) into the same buffered solution, and analyzed directly by MALDI-TOF using sinapic acid as matrix and unlabeled Nisin for internal calibration. Caluculated mass for Nisin + biotin-PEG$_2$-diazoacetamide, 3796.6, meas. m/z 3795.12.

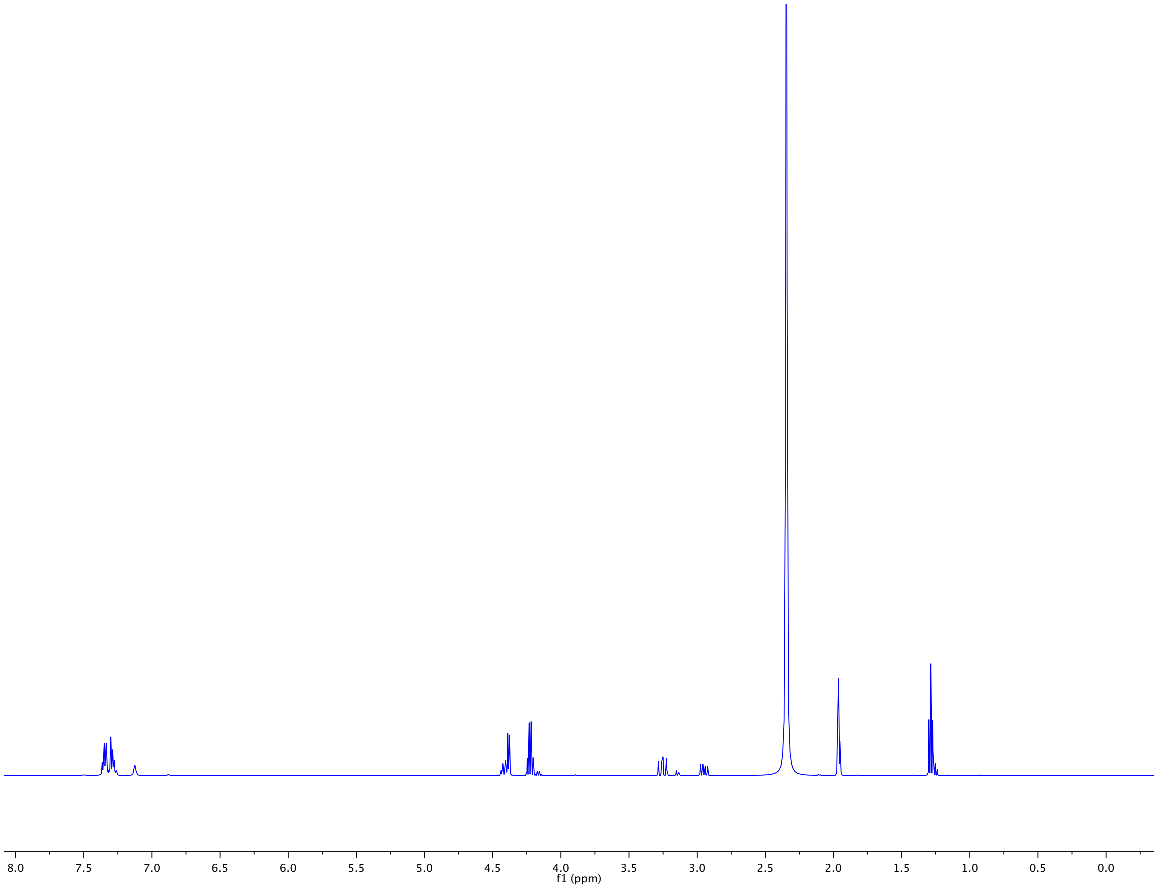

Fig. 1.3.S14. ^{1}H NMR spectrum of **ethyl 5-(benzylcarbamoyl)-4,5-dihydro-1*H*-pyrazole-3-carboxylate** in CD_3CN (500 MHz).

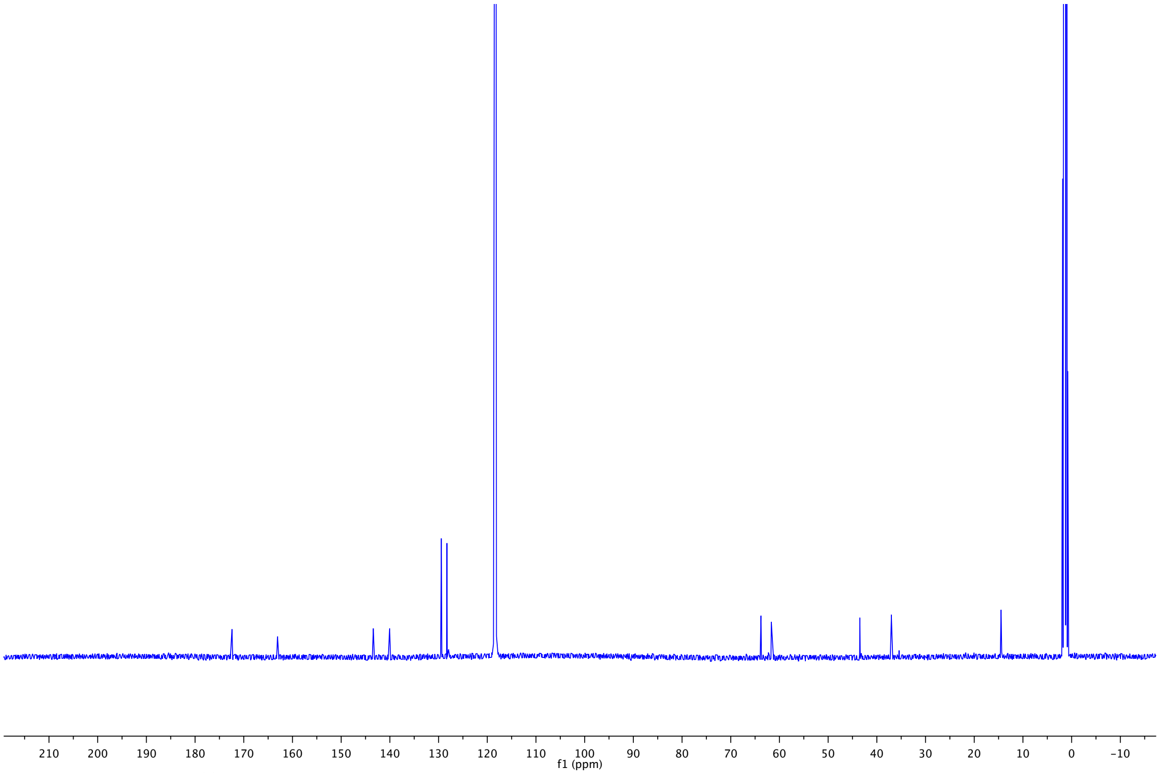

Fig. 1.3.S15. ^{13}C NMR spectrum of **ethyl 5-(benzylcarbamoyl)-4,5-dihydro-1*H*-pyrazole-3-carboxylate** in CD_3CN (126 MHz).

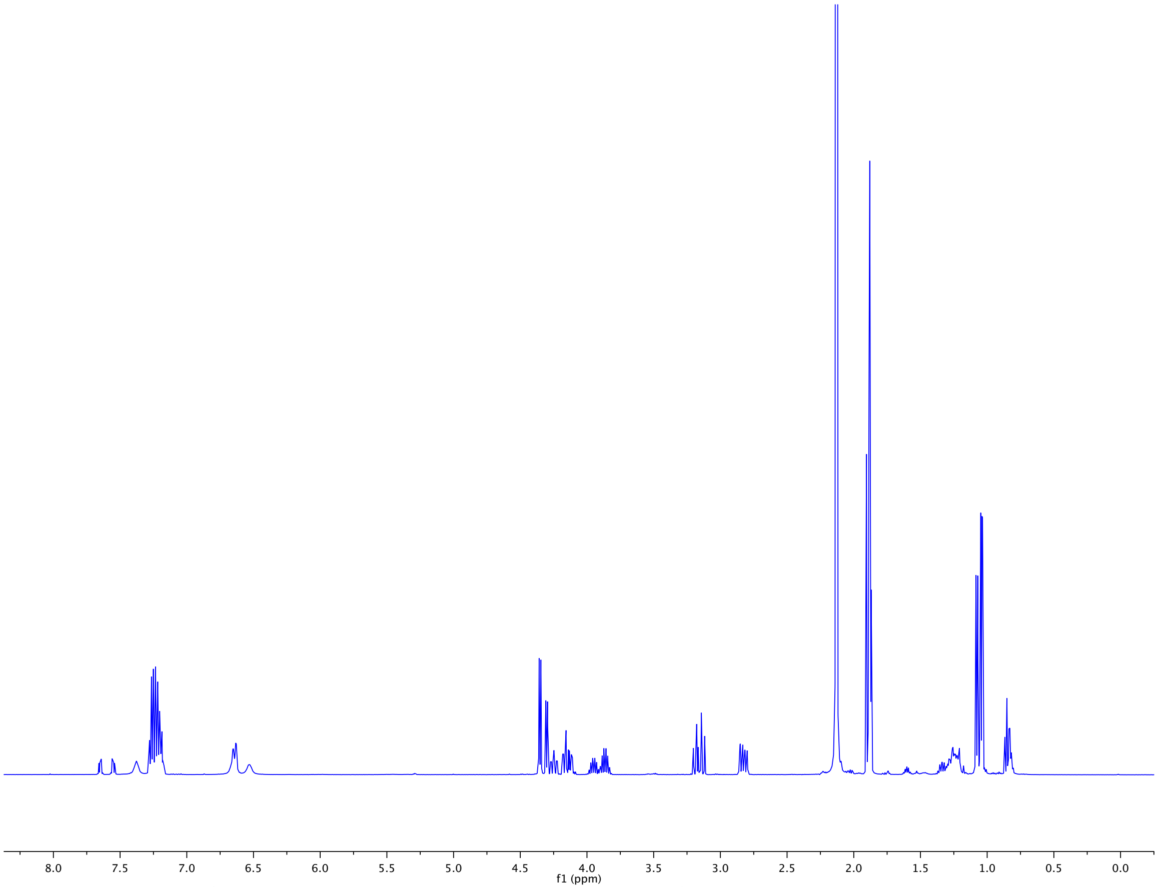

Fig. 1.3.S16. ^{1}H NMR spectrum of ***N*^{5}-benzyl-*N*^{3}-isopropyl-pyrazoline-3,5-dicarboxamide** (mixed isomers) in CD_3CN (500 MHz).

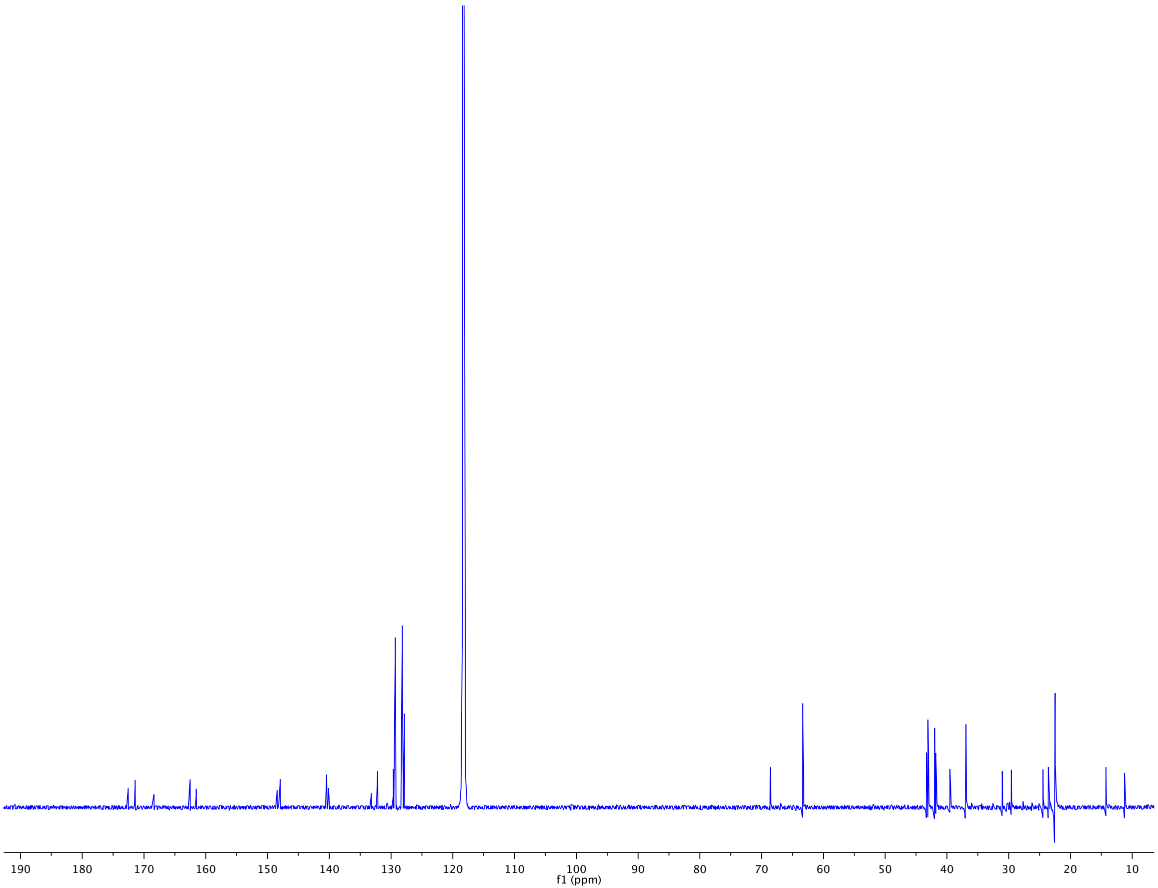

Fig. 1.3.S17. ^{13}C NMR spectrum of ***N*^{5}-benzyl-*N*^{3}-isopropyl-pyrazoline-3,5-dicarboxamide** (mixed isomers in CD_3CN (126 MHz).

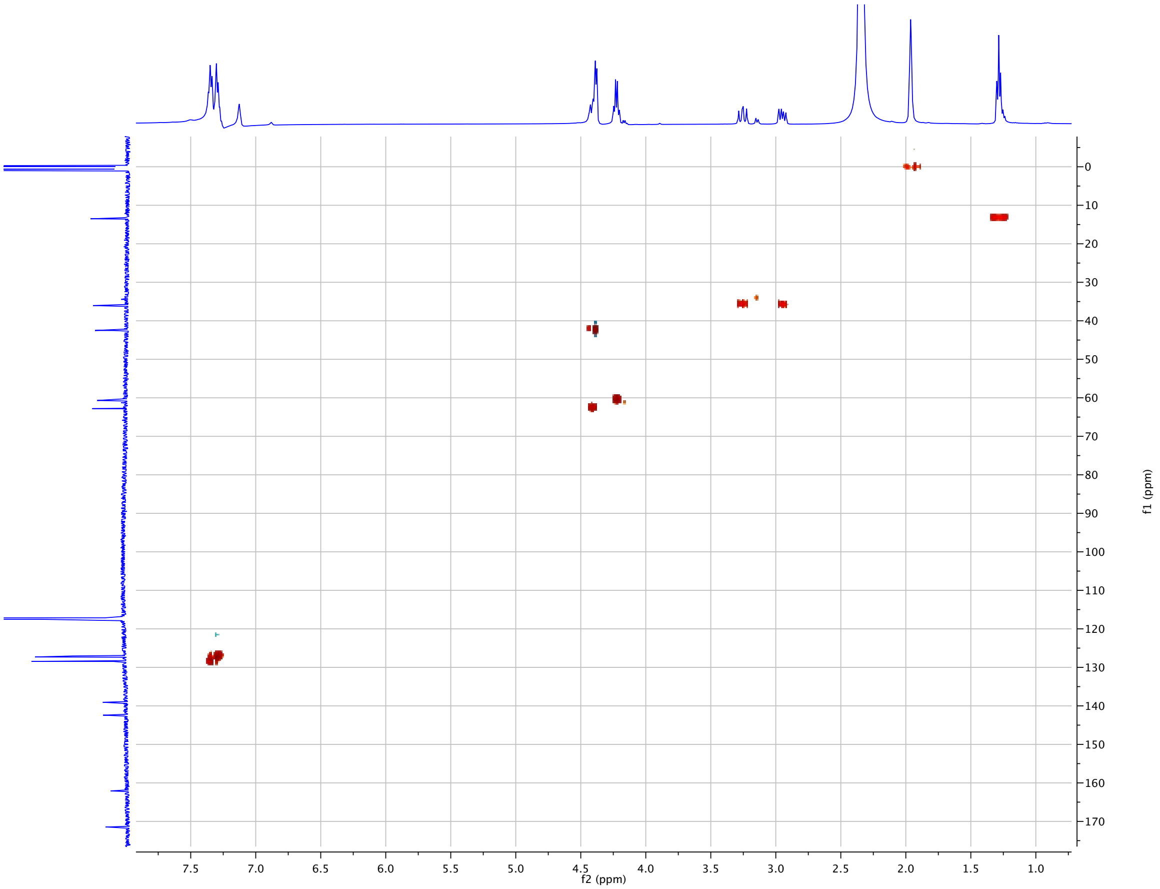

Fig. 1.3.S18. HSQC 2D spectrum of **ethyl 5-(benzylcarbamoyl)-4,5-dihydro-1*H*-pyrazole-3-carboxylate** in CD_3CN (500, 126 MHz).

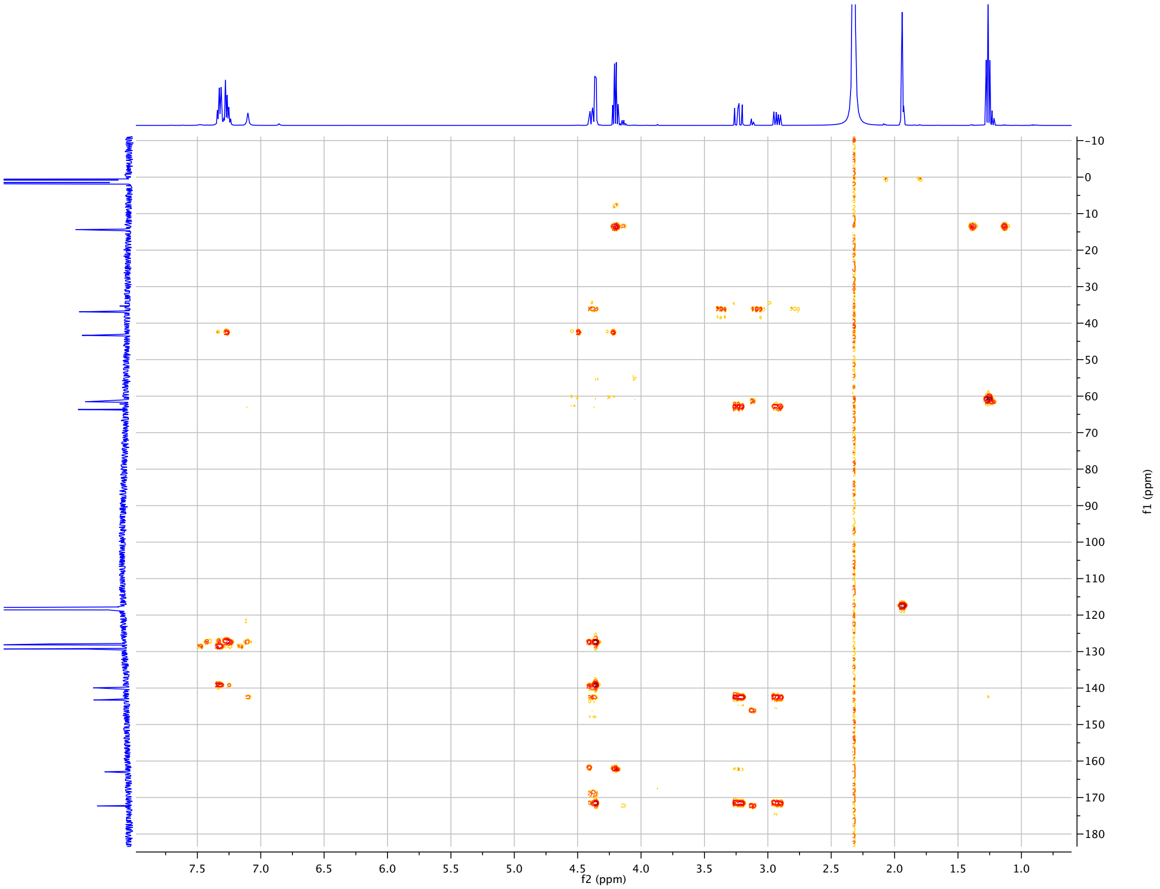

Fig. 1.3.S19. HMBC 2D spectrum of **ethyl 5-(benzylcarbamoyl)-4,5-dihydro-1*H*-pyrazole-3-carboxylate** in CD_3CN (500, 126 MHz).

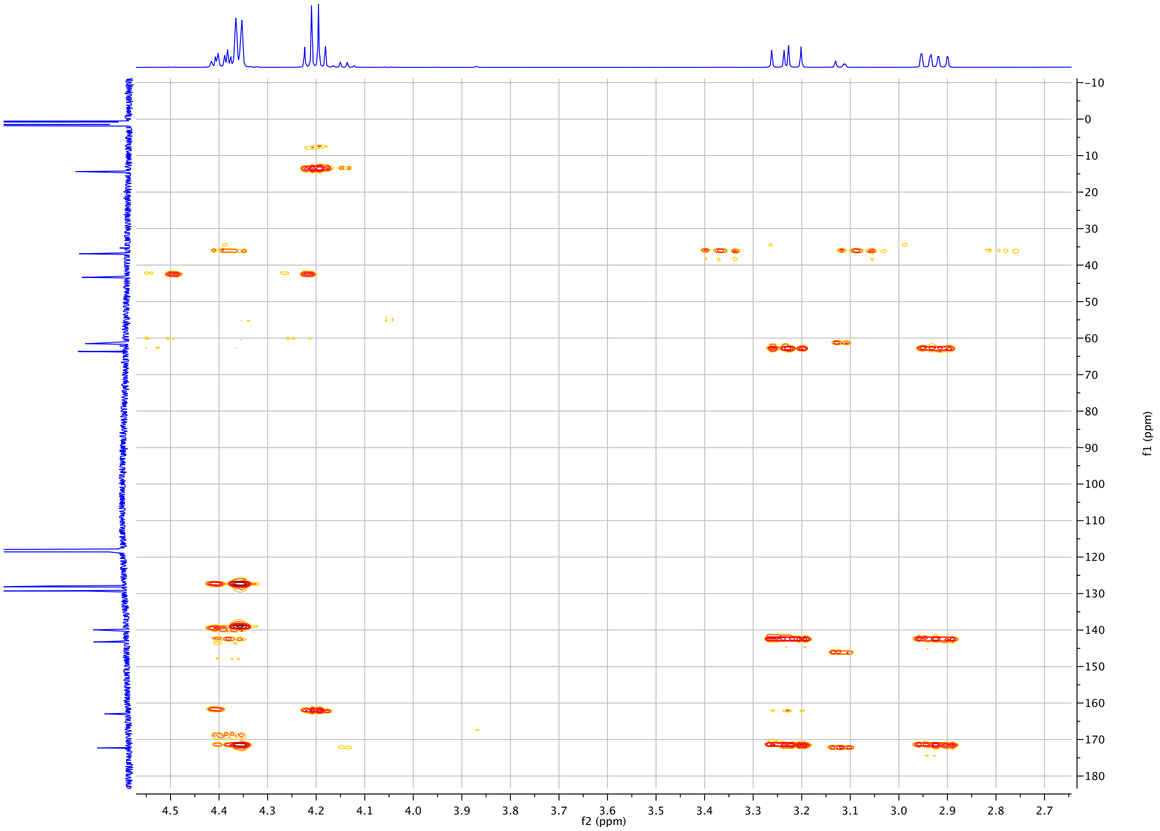

Fig. 1.3.S20: HMBC 2D spectrum of **ethyl 5-(benzylcarbamoyl)-4,5-dihydro-1*H*-pyrazole-3-carboxylate** in CD_3CN (500, 126 MHz).

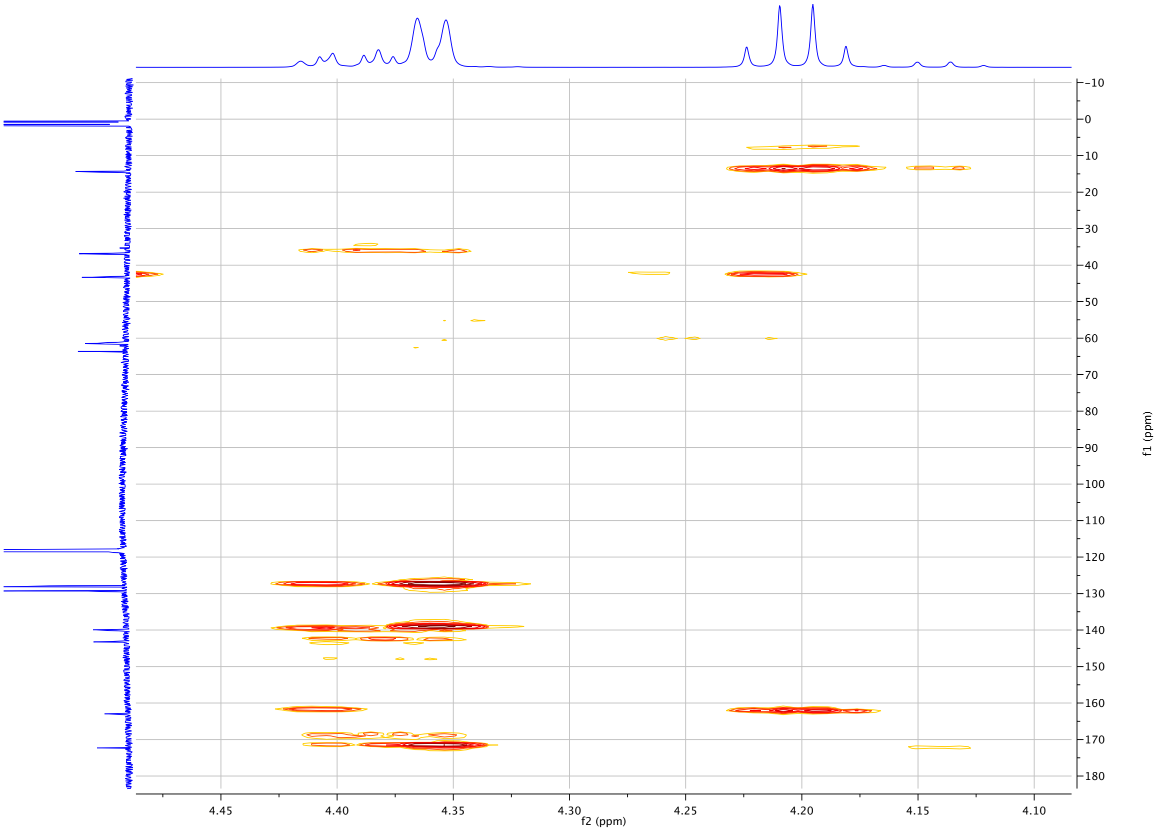

Fig. 1.3.S21: HMBC 2D spectrum ZOOM of **S20 ethyl 5-(benzylcarbamoyl)-4,5-dihydro-1*H*-pyrazole-3-carboxylate** in CD_3CN (500, 126 MHz).

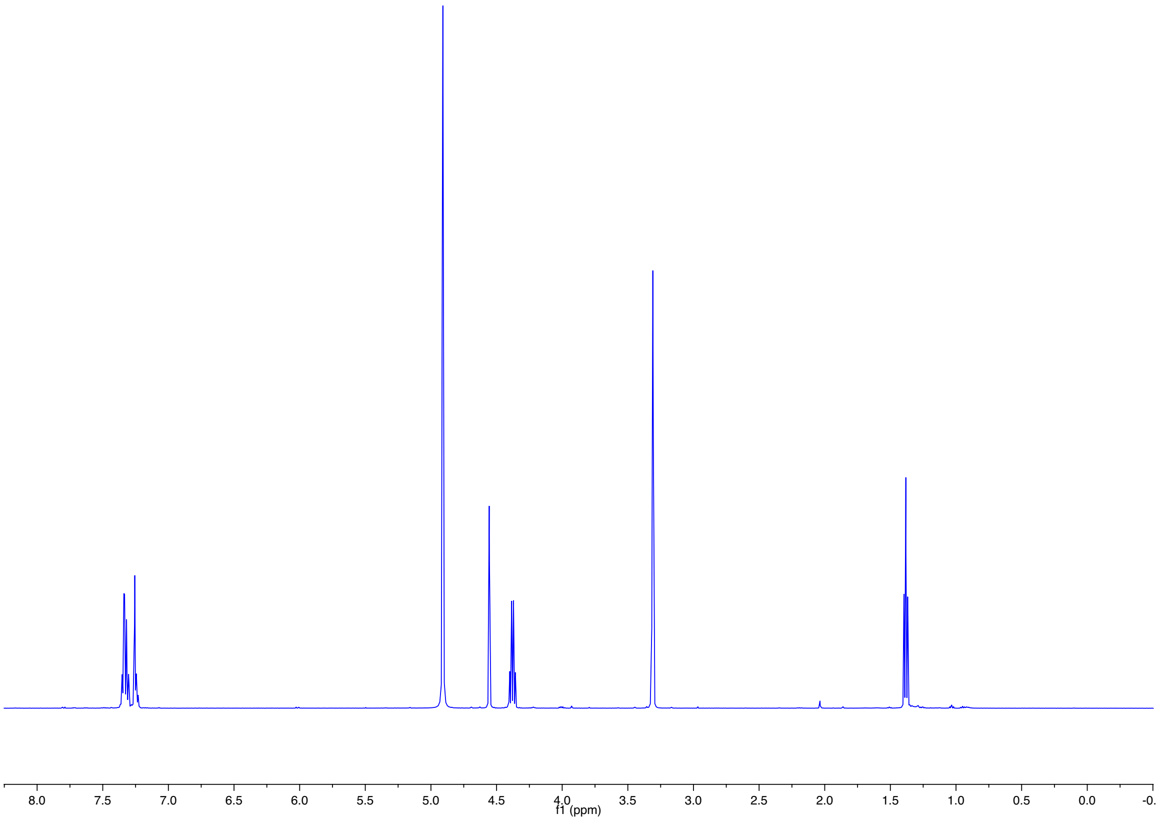

Fig. 1.3.S22. ^{1}H NMR spectrum of **ethyl 5-(benzylcarbamoyl)-1*H*-pyrazole-3-carboxylate** in MeOD (500 MHz).

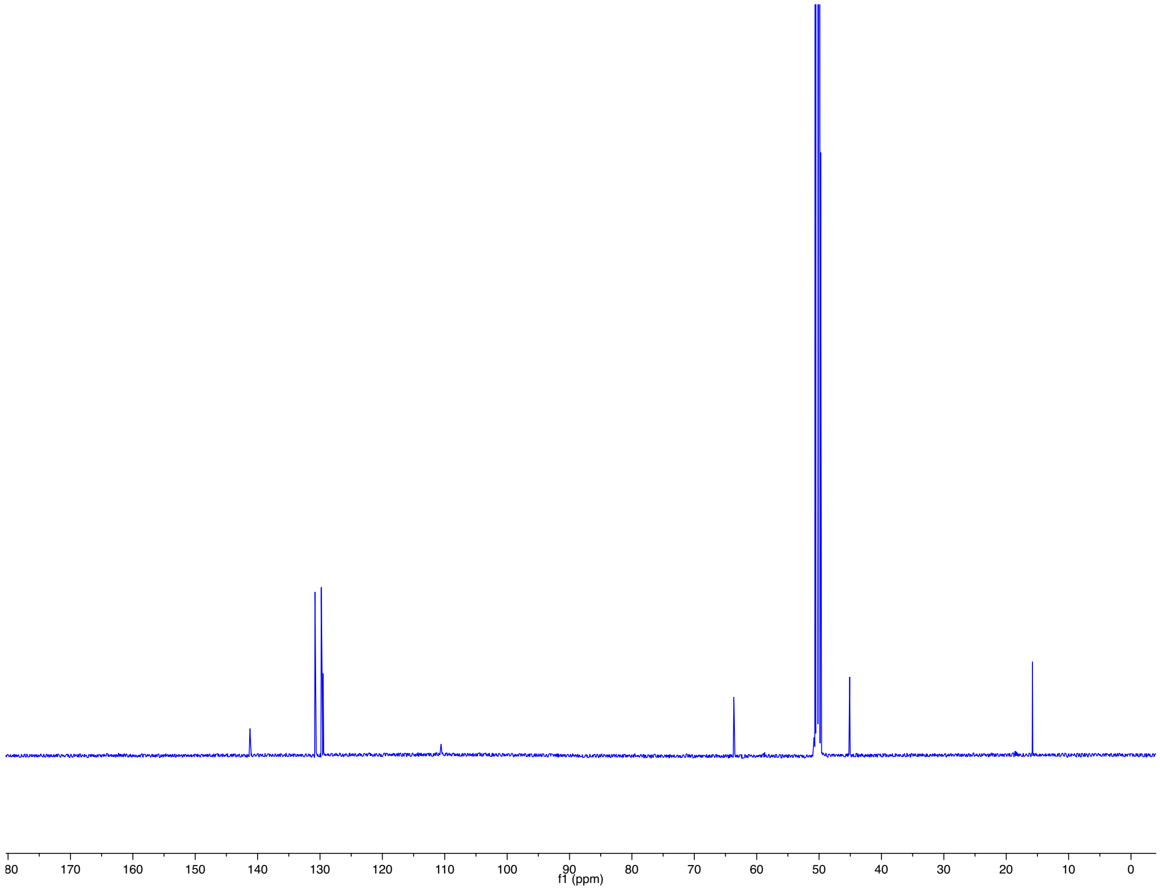

Fig. 1.3.S23. ^{13}C NMR spectrum of **ethyl 5-(benzylcarbamoyl)-1*H*-pyrazole-3-carboxylate** in MeOD (126 MHz).

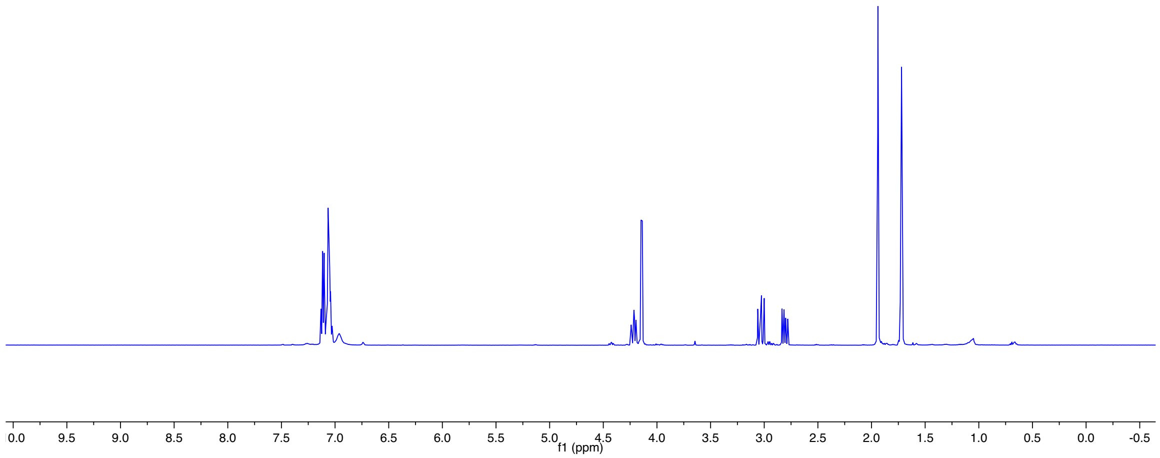

Fig. 1.3.S24. ^{1}H NMR spectrum of ***N*-benzyl-3-cyano-4,5-dihydro-1*H*-pyrazole-5-carboxamide** in CD_3CN (500 MHz).

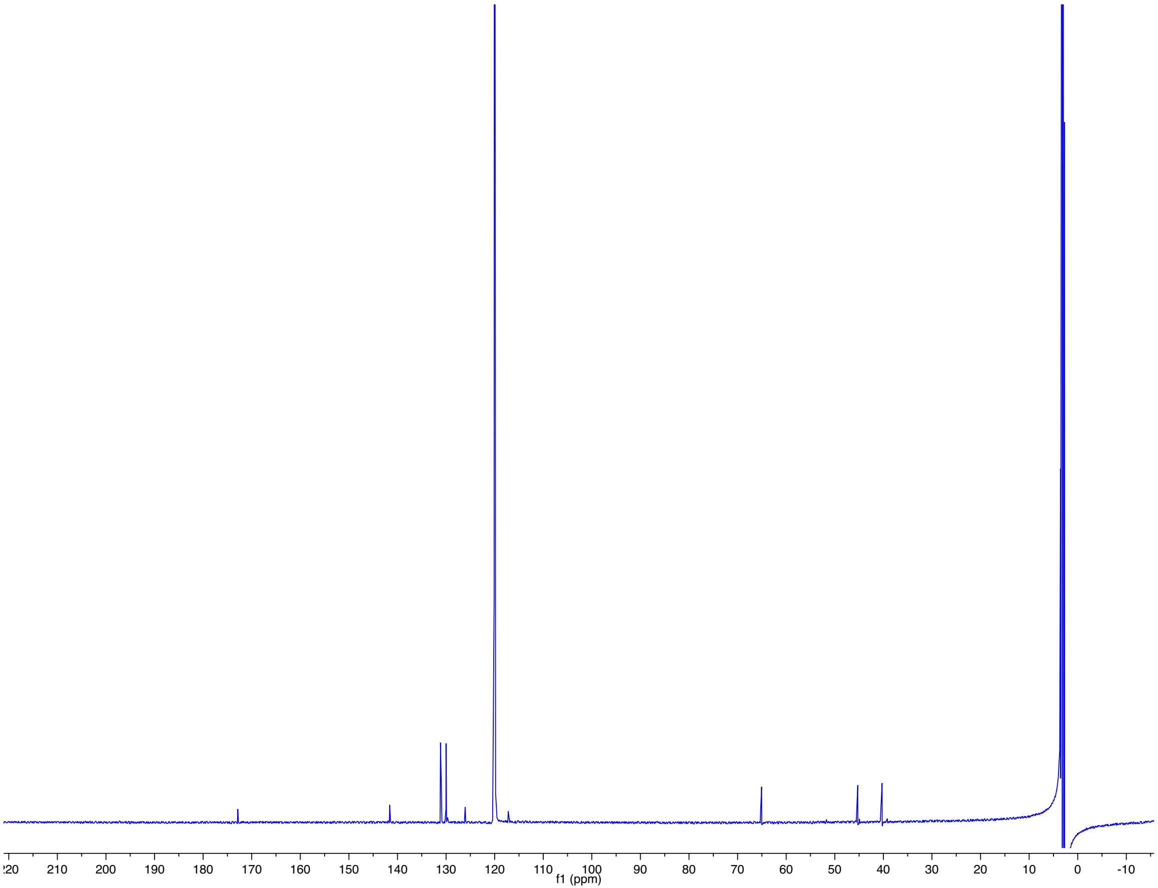

Fig. 1.3.S25. ^{13}C NMR spectrum of ***N*-benzyl-3-cyano-4,5-dihydro-1*H*-pyrazole-5-carboxamide** in CD_3CN (126 MHz).

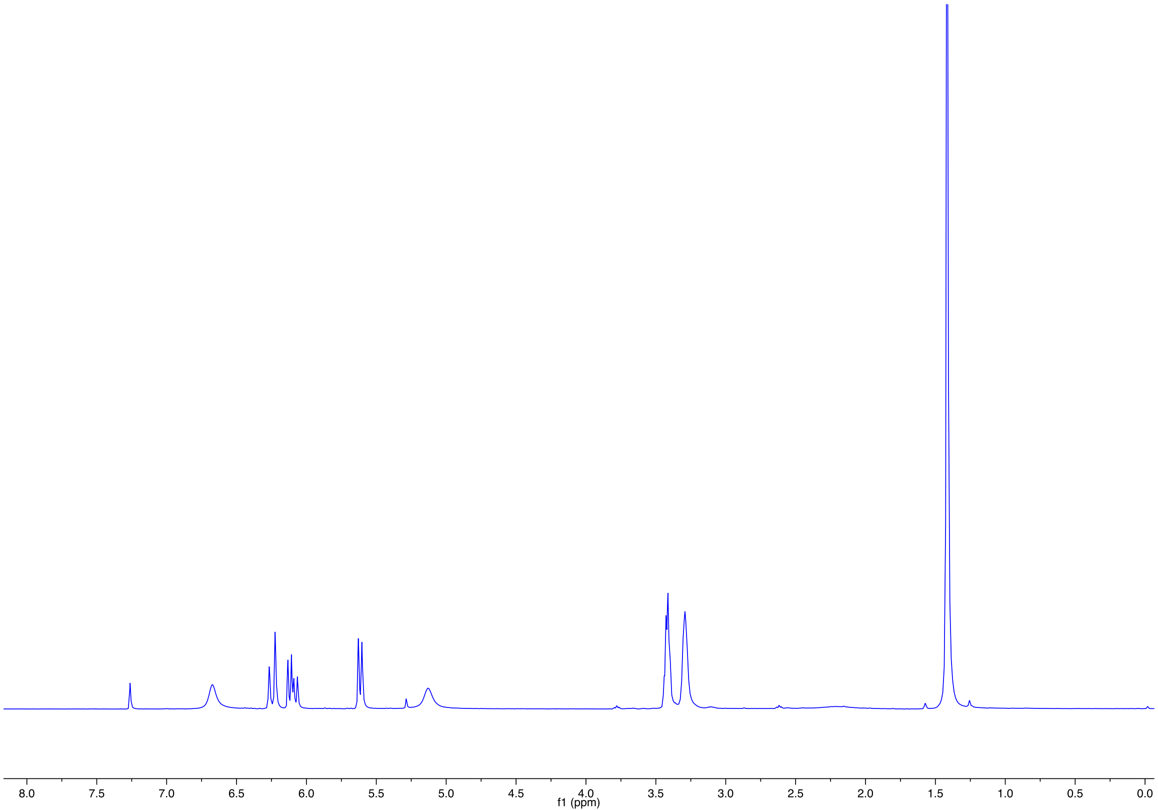

Fig. 1.3.S26. ^{1}H NMR spectrum of ***isopropyl*-2-acrylamidoethylcarbamate** in $CDCl_3$ (400 MHz).

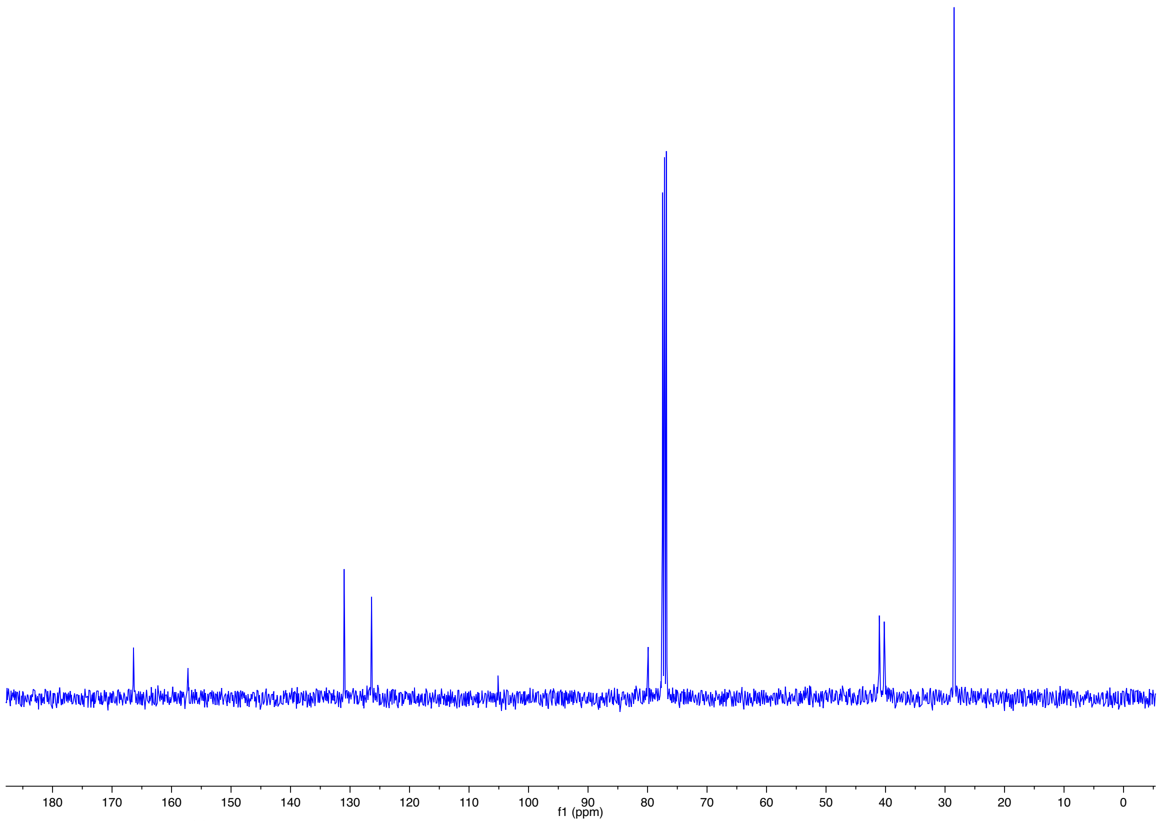

Fig. 1.3.S27. ^{13}C NMR spectrum of ***isopropyl*-2-acrylamidoethylcarbamate** in $CDCl_3$ (101 MHz).

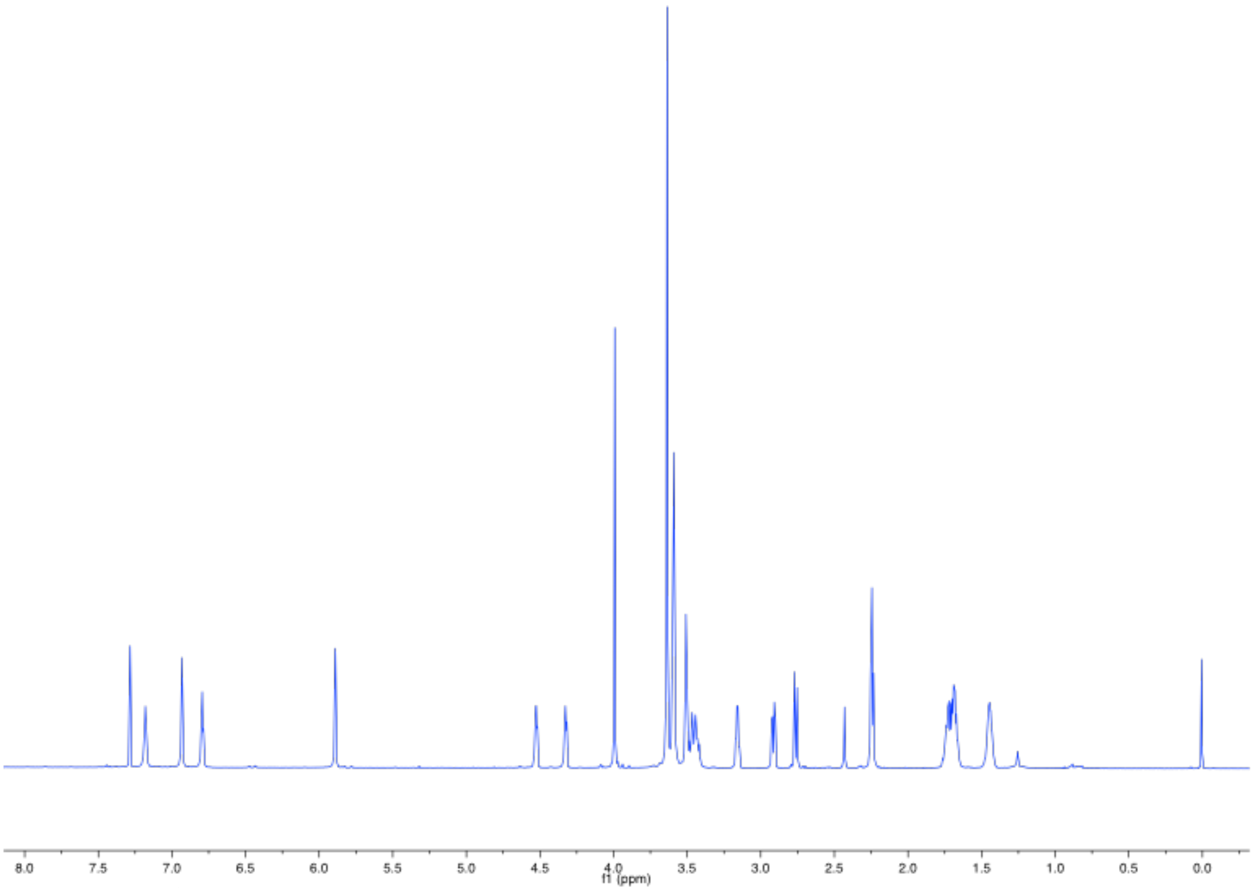

Fig. 1.3.S28. ^{1}H NMR spectrum of **biotin-PEG$_2$-azidoacetamide** in $CDCl_3$ (750 MHz).

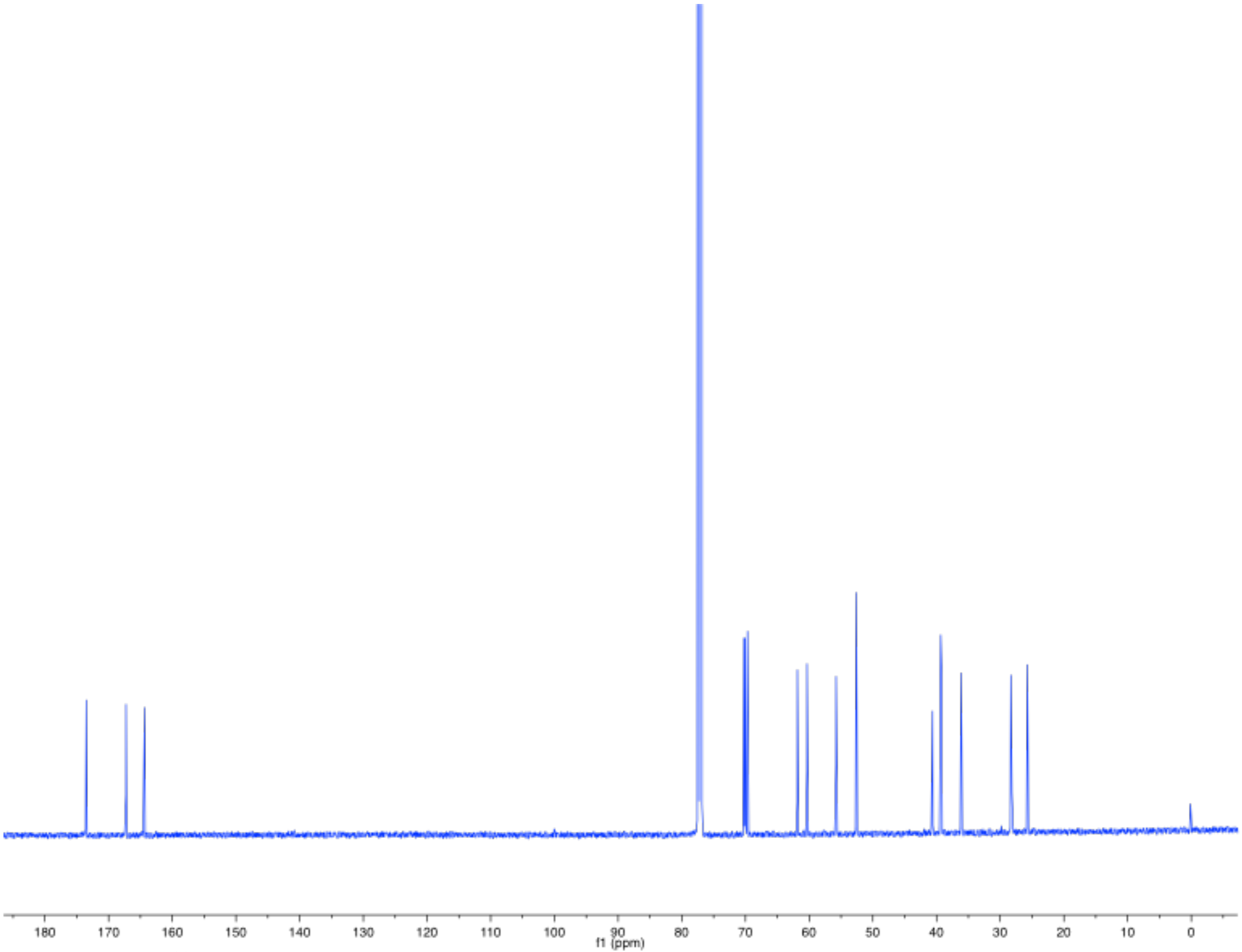

Fig. 1.3.S29. ^{13}C NMR spectrum of **biotin-PEG$_2$-azidoacetamide** in $CDCl_3$ (126 MHz).

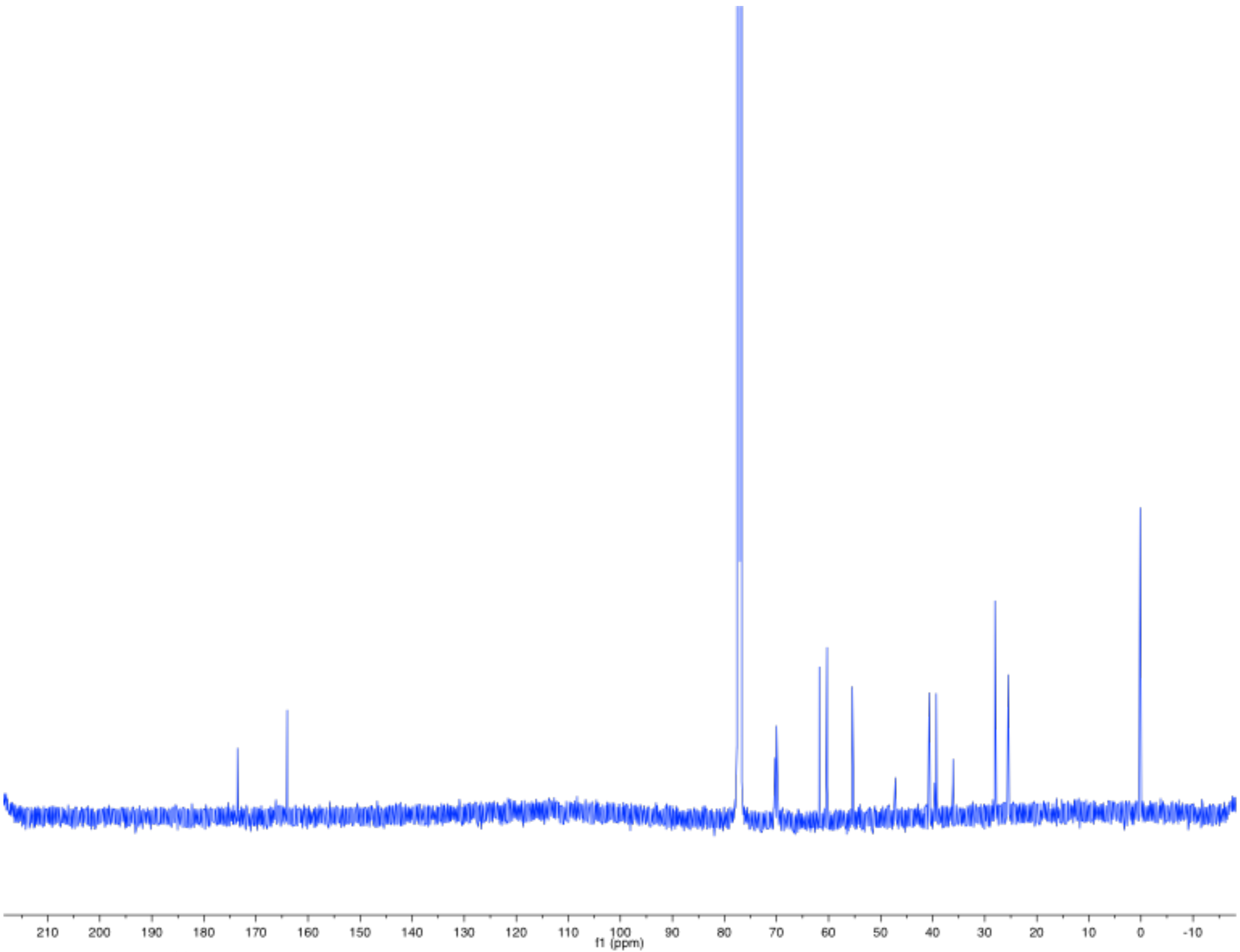

Fig. 1.3.S30. ^{13}C NMR spectrum of **biotin-PEG$_2$-diazoacetamide** in $CDCl_3$ (126 MHz).

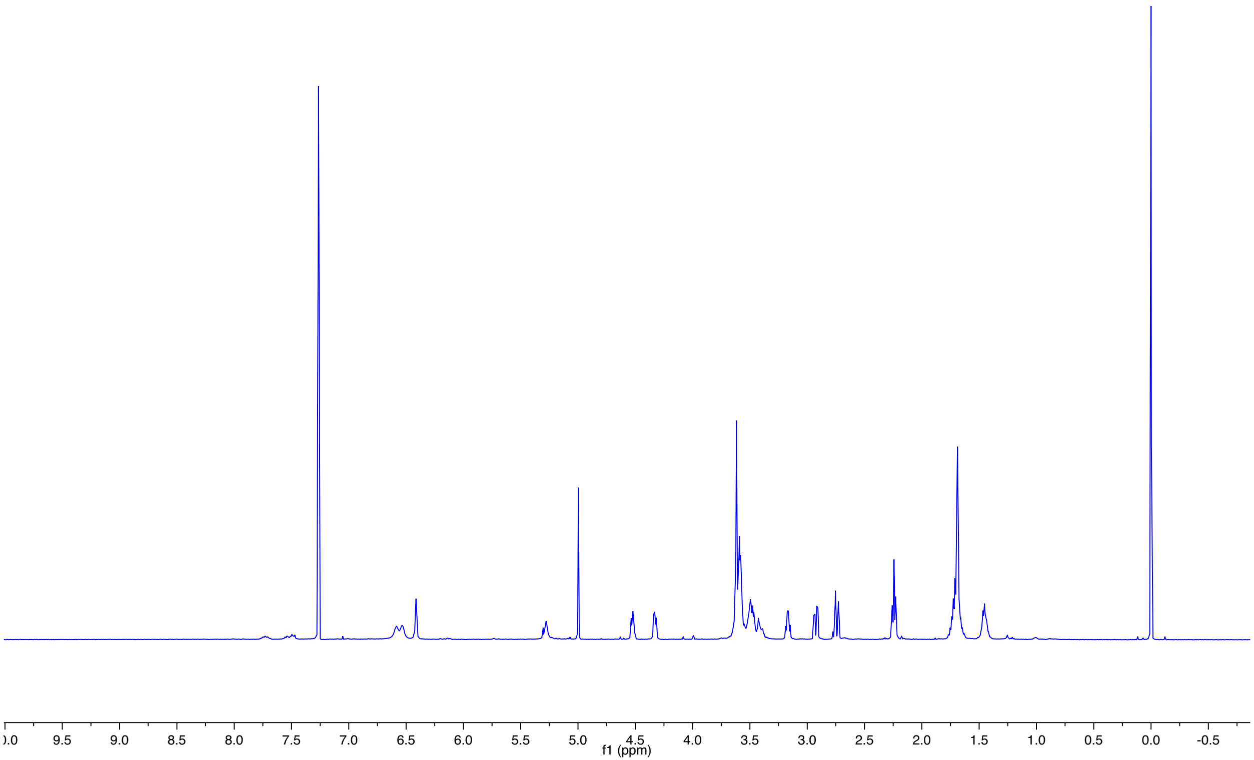

Fig. 1.3.S31. ^{1}H NMR spectrum of **biotin-PEG$_2$-diazoacetamide** in CD_3CN (500 MHz).

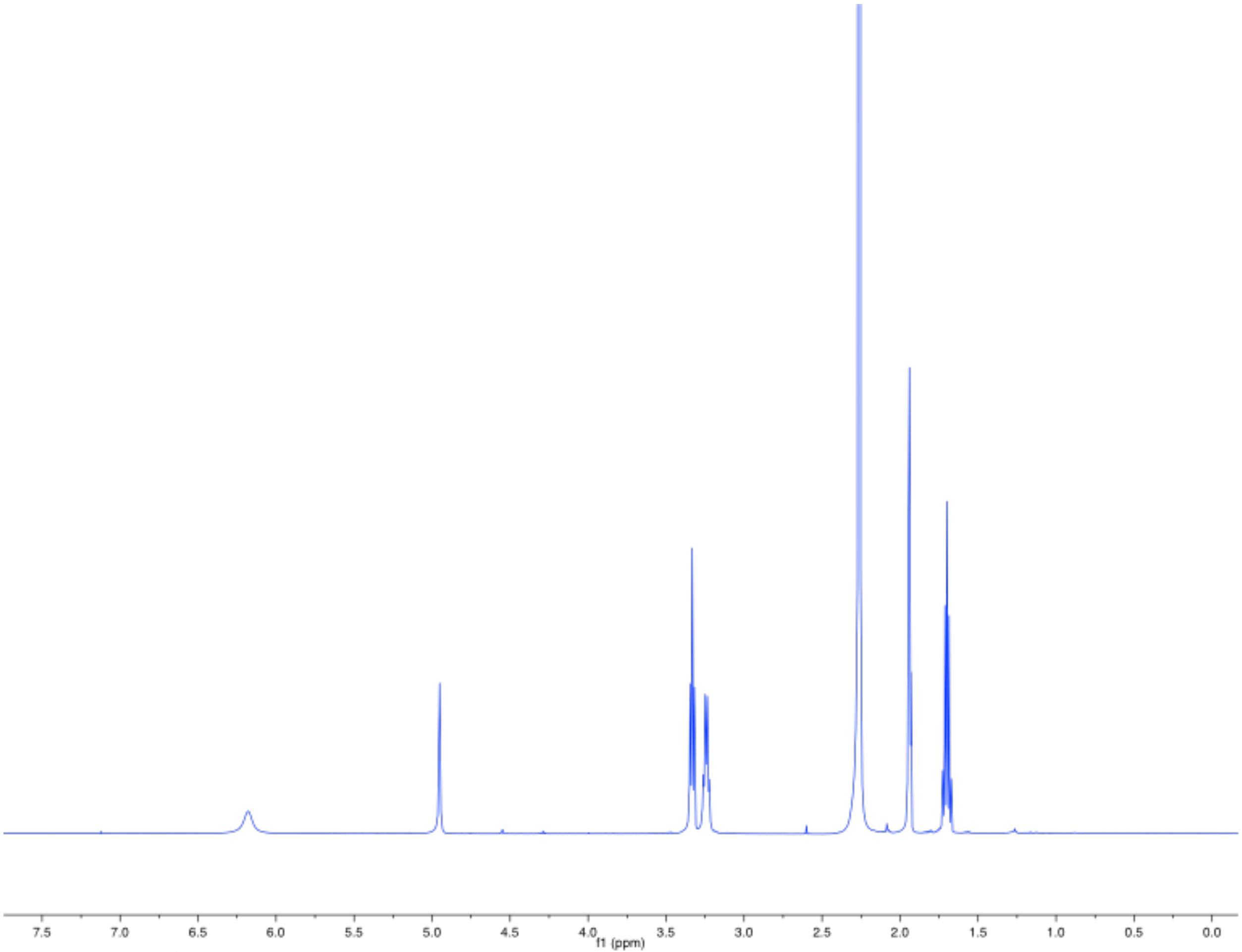

Fig. 1.3.S32. ^{1}H NMR spectrum of ***N*-(3-azidopropyl)-2-diazoacetamide** in CD_3CN (500 MHz).

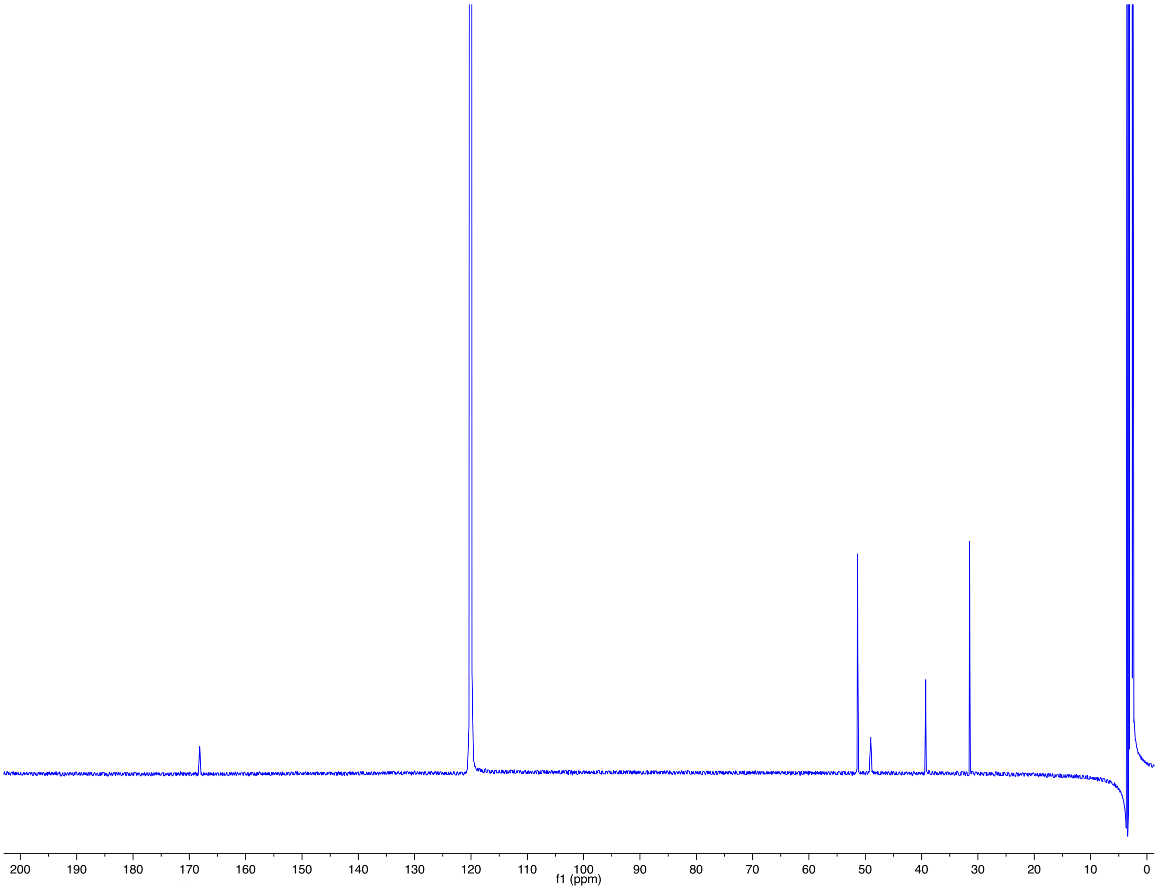

Fig. 1.3.S33. ^{13}C NMR spectrum of ***N*-(3-azidopropyl)-2-diazoacetamide** in CD_3CN (126 MHz).

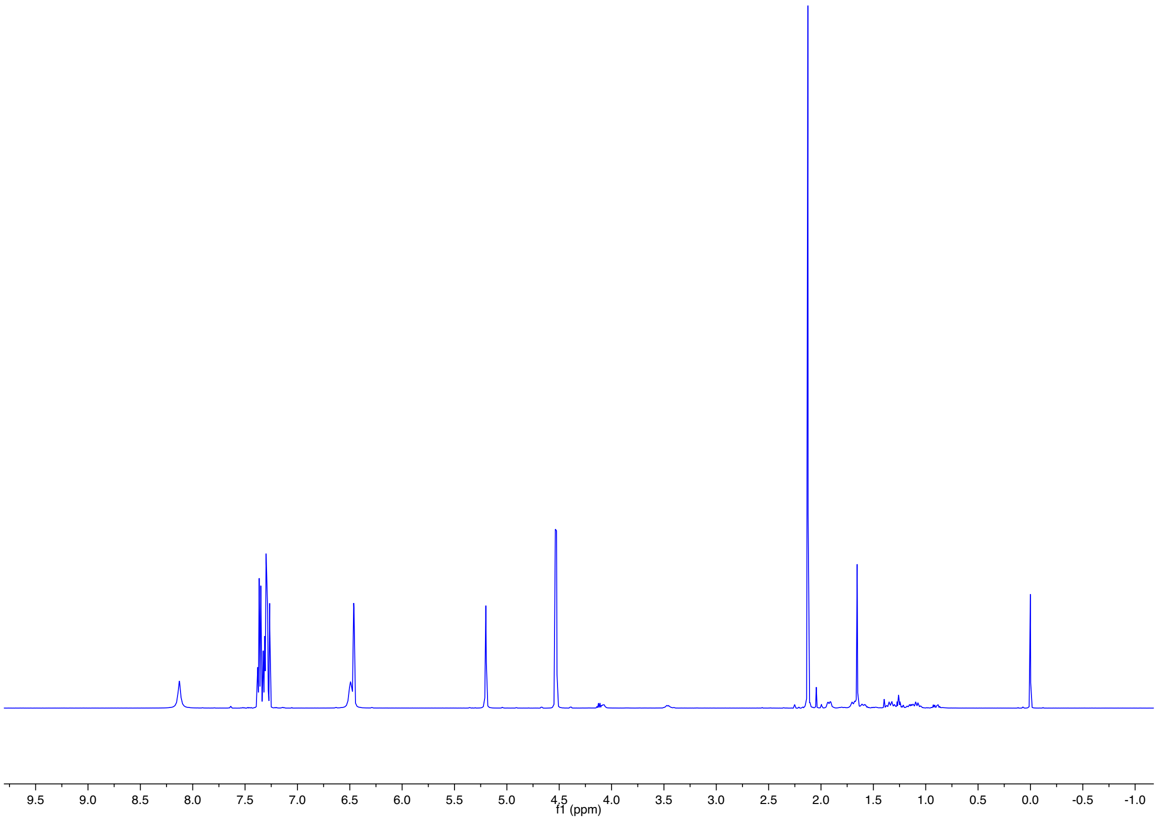

Fig. 1.3.S34. ^{1}H NMR spectrum of **2-acetamido-*N*-benzylacrylamide** in $CDCl_3$ (500 MHz).

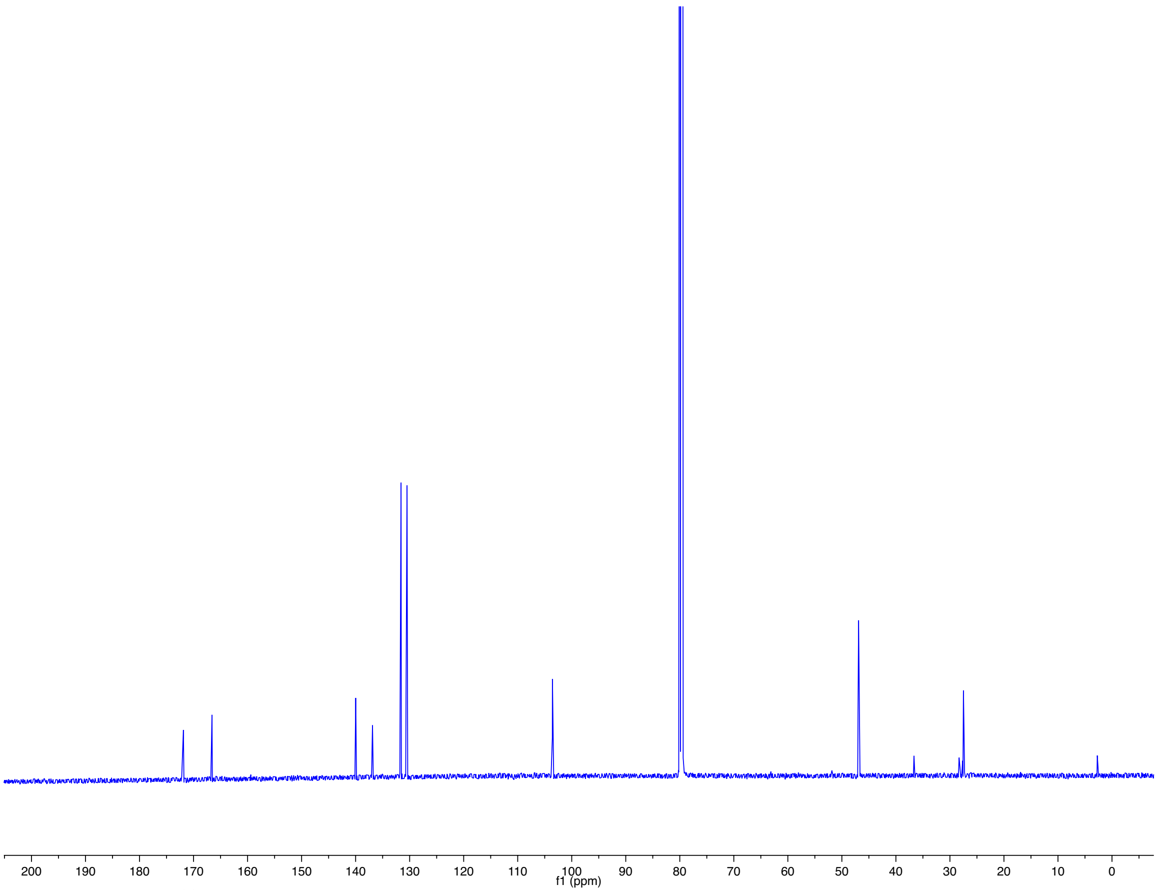

Fig. 1.3.S35. ^{13}C NMR spectrum of **2-acetamido-*N*-benzylacrylamide** in $CDCl_3$ (126 MHz).

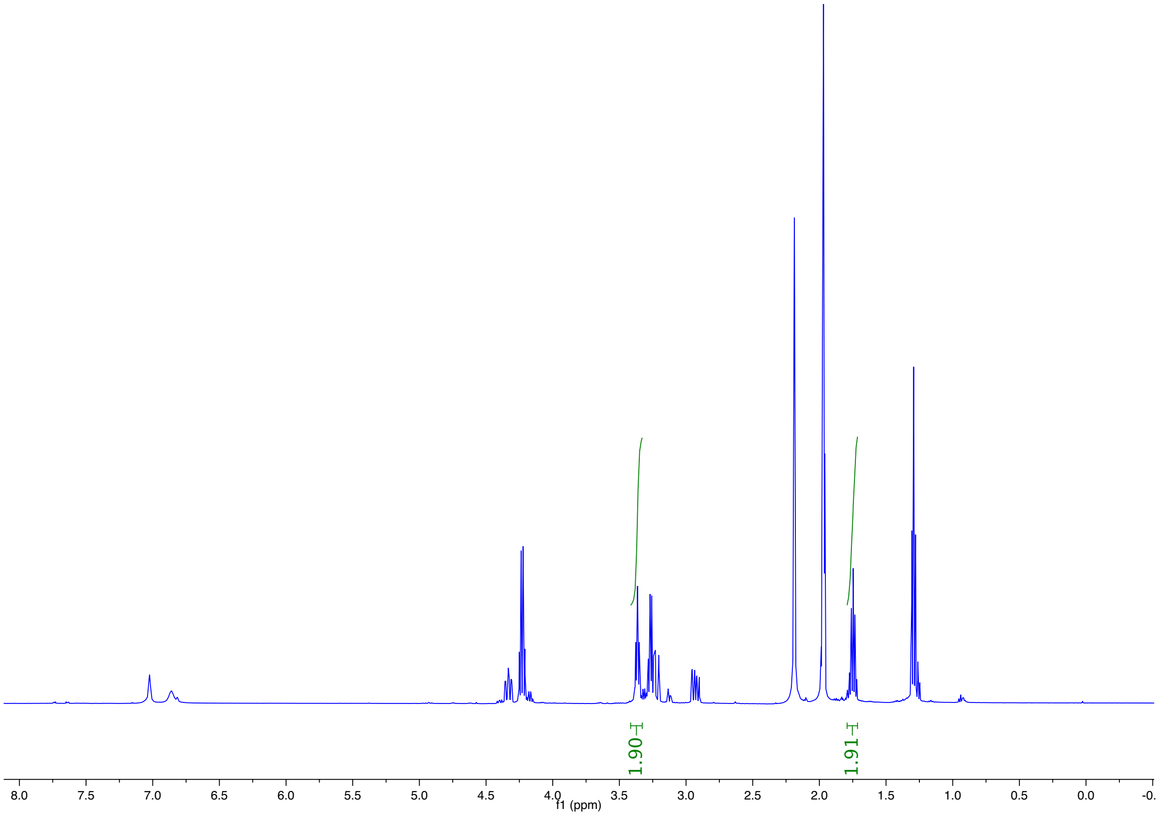

Figure 1.3.S36. ^{1}H NMR spectrum of ***N*-(3-azidopropyl)-2-diazoacetamide** competition reaction with ethylacrylate (**i**) in CD_3CN (500 MHz).

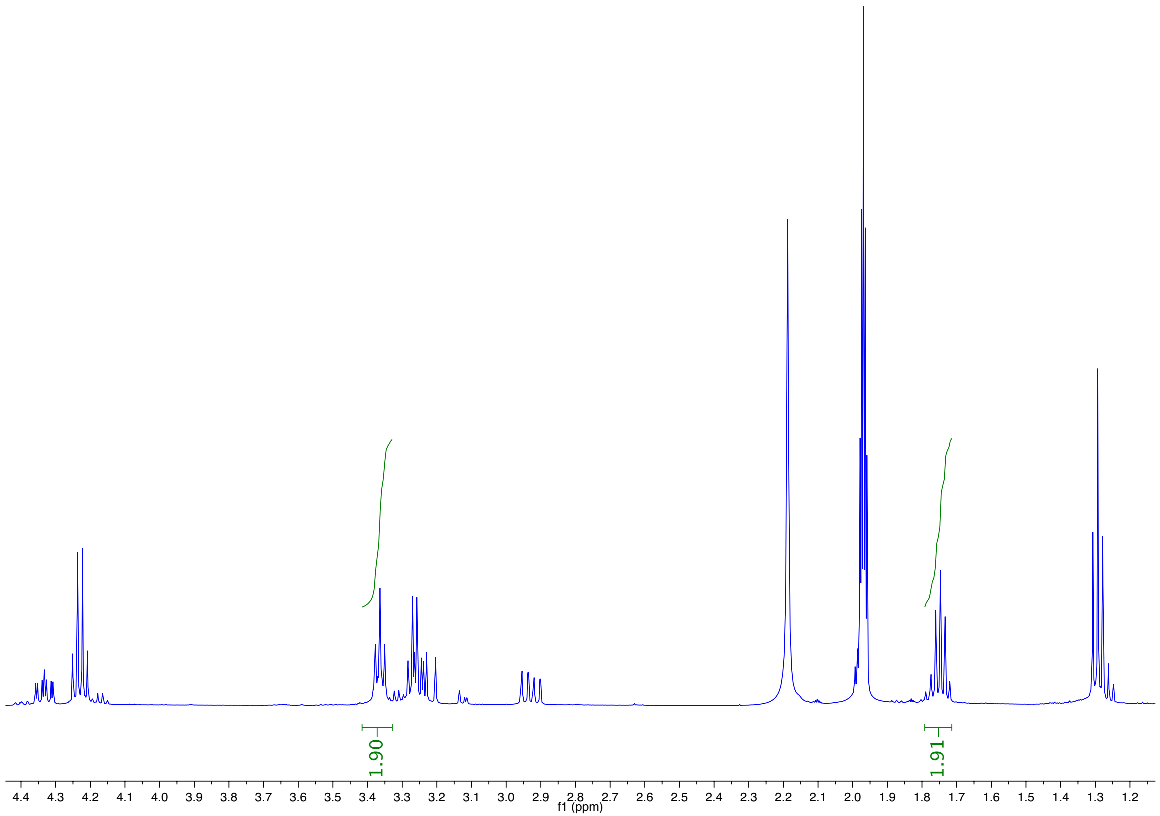

Figure 1.3.S37. (Inset of 1.3.S36) ^{1}H NMR spectrum of ***N*-(3-azidopropyl)-2-diazoacetamide** competition reaction with ethylacrylate (**i**) in CD_3CN (500 MHz).

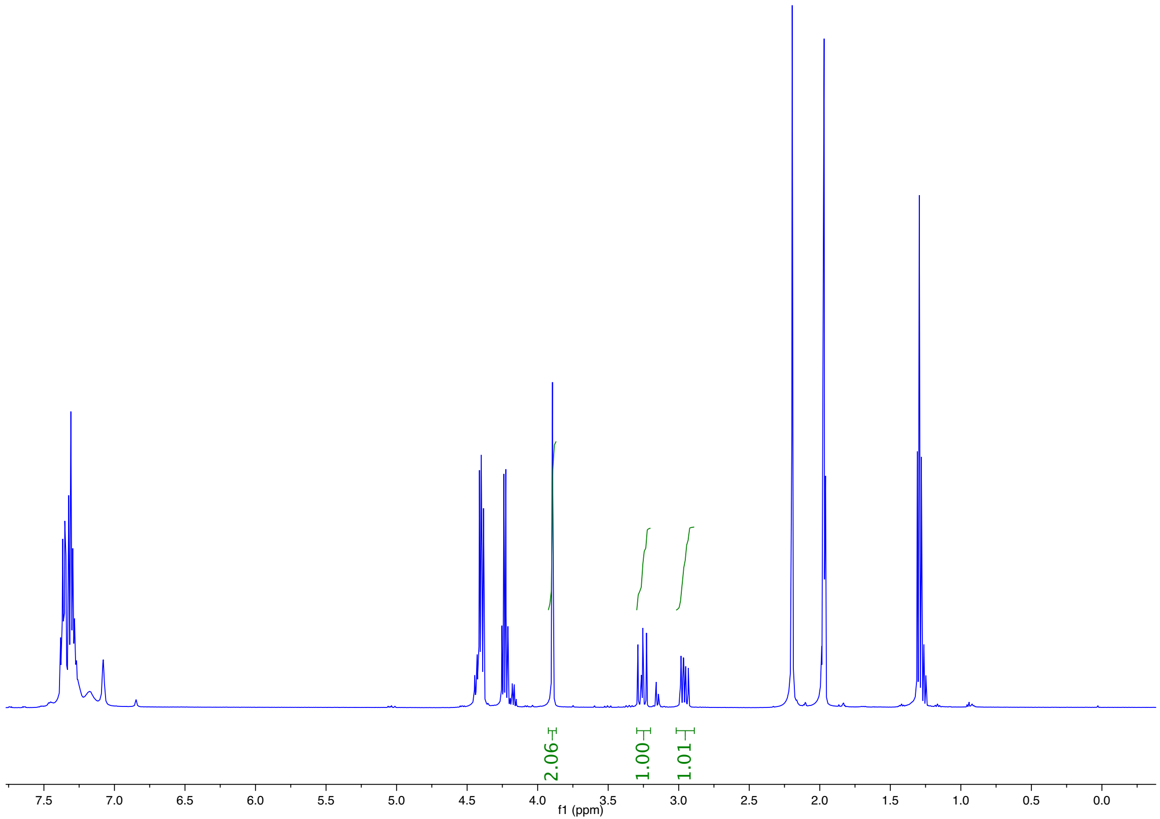

Figure 1.3.S38. ^{1}H-NMR of (**1**) (1 eq) and (**2**) (1 eq) with ethyl acrylate (**i**) (5 eq) after 24 h in CD_3CN (500 MHz).

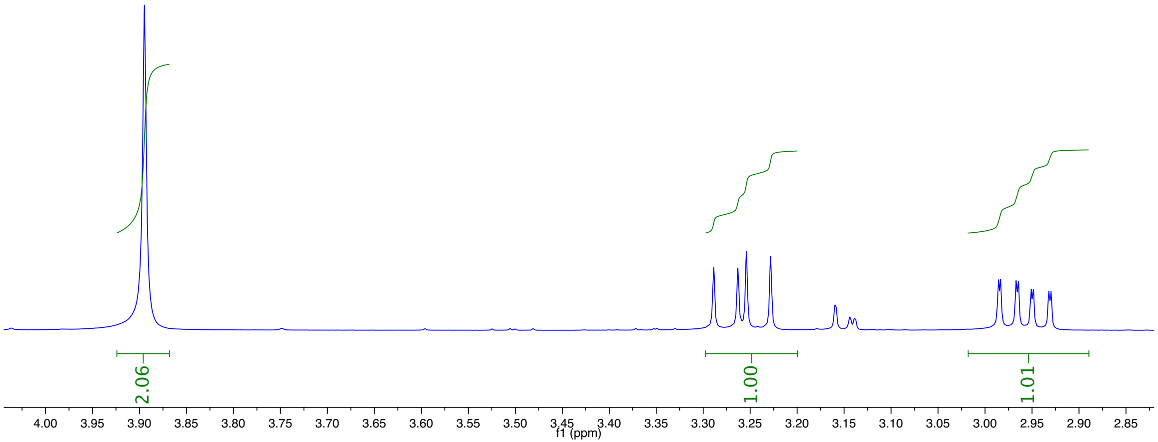

Figure 1.3.S39. ZOOM of **1.3.S38** ^{1}H-NMR of (**1**) (1 eq) and (**2**) (1 eq) with ethylacrylate (**i**) (5eq) after 24 h in CD_3CN (500 MHz).

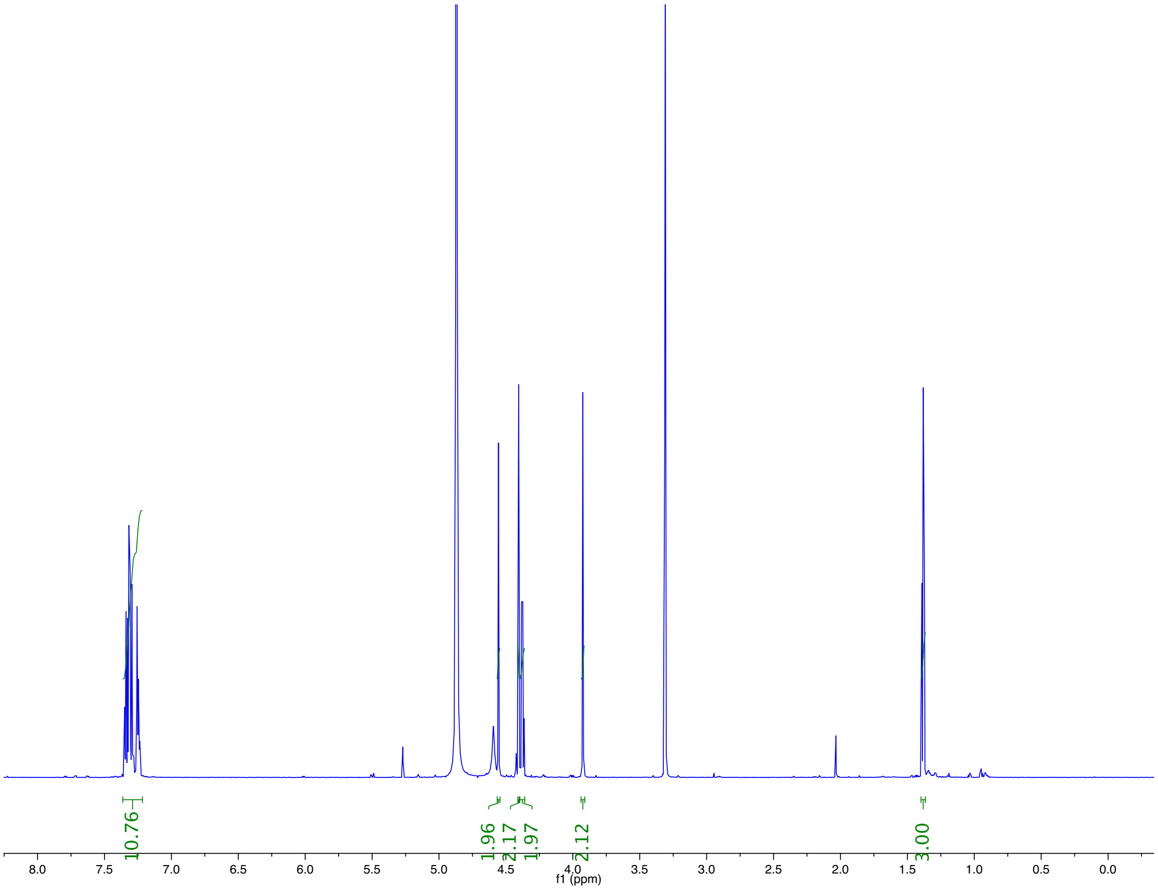

Figure 1.3.S40. ^{1}H-NMR of (**1**) (1eq) and (**2**) (1eq) with ethyl propiolate (**j**) (5eq) after 24 h in MeOD (500 MHz).

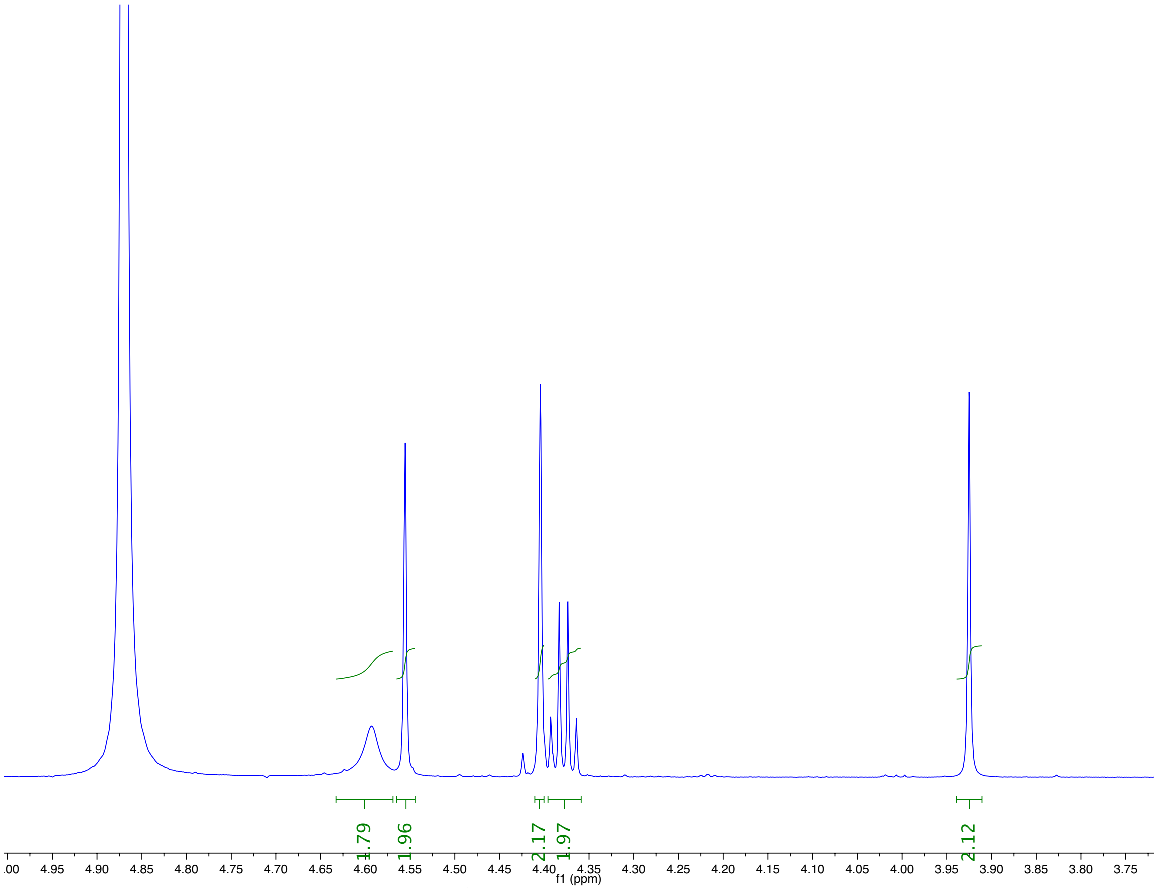

Figure 1.3.S41. ZOOM of **1.3.S40**. ^{1}H-NMR of (**1**) (1 eq) and (**2**) (1 eq) with ethyl propiolate (**2**) (5 eq) after 24 h in MeOD (500 MHz).

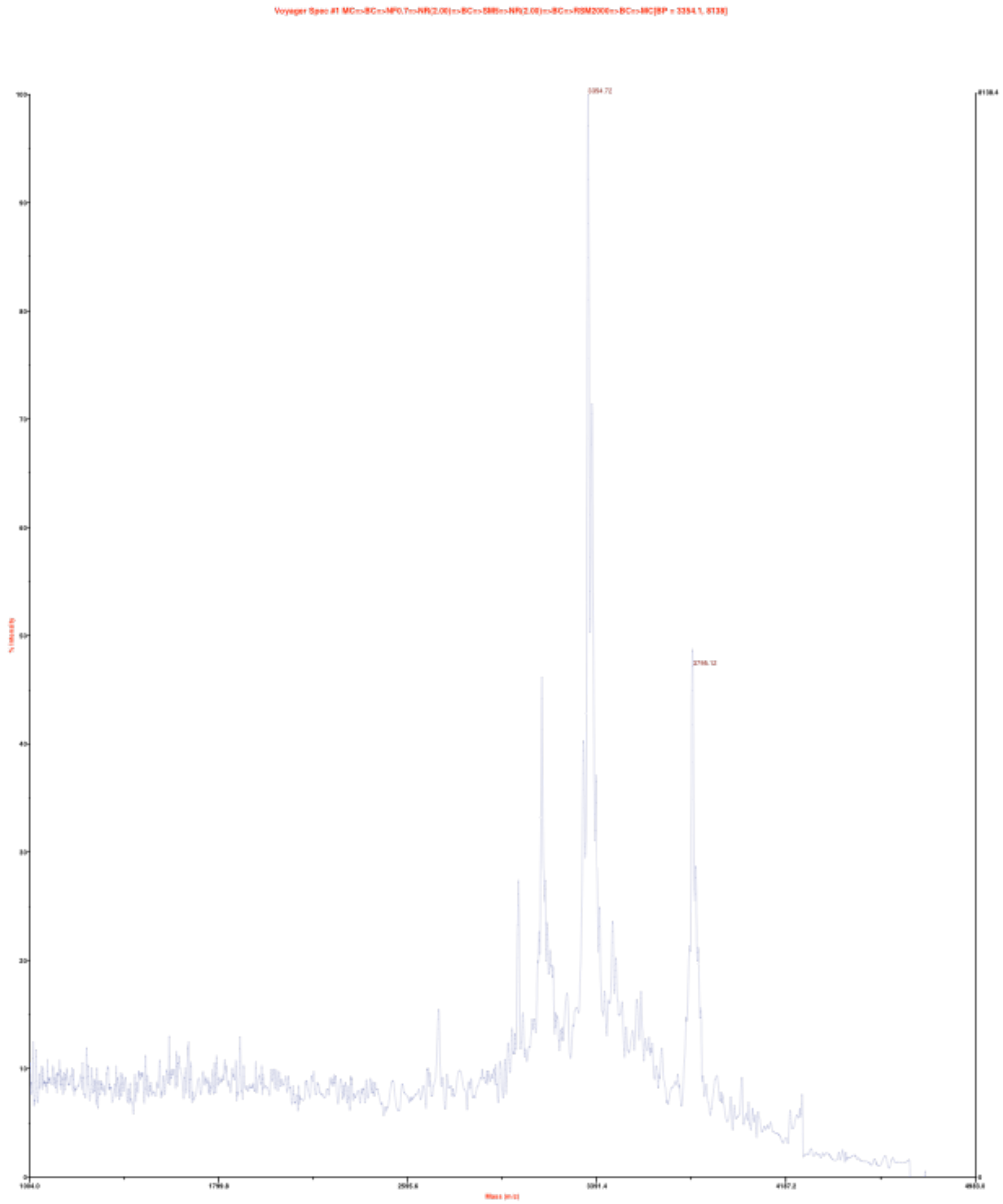

C:\...\first dialysis_0005.dat
Acquired: 14:43:00, May 14, 2015

Figure 1.3.S42. MALDI-TOF trace of Nisin following treatment with diazoacetamide-PEG$_2$-biotin.

PART 1

CHAPTER 4

Uncharged Phosphinothiols for the Traceless Staudinger-Ligation in Aqueous Conditions

This chapter was originally prepared as: Andersen, K.A.,* Aronoff, M.R.,* Martin, L.J., Raines, R.T. A semisynthetic route to authentic ubiquitin chains. *In preparation.*

Contributions: I designed the uncharged water-soluble phosphinothiols, performed all chemical synthesis, and all small molecule ligation studies. Kristen Andersen produced the proteins used in this study and performed experiments involving proteins. The ubiquitin-intein construct was cloned by Langdon J. Martin.

Note: The general method detailed in this chapter was published as: Creating site-specific isopeptide linkages between proteins with the traceless Staudinger ligation. Kristen A. Andersen and Ronald T. Raines (2015). *Methods in Molecular Biology 1248,* 55–65.

Abstract

The traceless Staudinger ligation is a powerful chemoselective tool to form an amide bond without residual atoms or racemization. Here, we increase the compatibility of this reaction with biological systems by improving upon the water solubility and efficiency of the phosphinothiol component of the Staudinger ligation. Then, we utilize the Staudinger ligation to form an authentic isopeptide bond between ubiquitin monomers. The method developed here provides the basis for producing ubiquitin polymers of precise length and connectivity in a semisynthetic manner. This technology allows for the synthesis of chains containing any linkage—including mixed and branched linkages—in a highly controlled manner.

1.4.1 Introduction

The Staudinger ligation, based on the Staudinger reaction, is a powerful chemoselective reaction that is compatible with biological systems. The Staudinger reaction occurs between an azide and a phosphine, wherein a phosphine reduces the azide to an amine via an iminophosphorane intermediate. Acylation of this iminophosphorane intermediate results in an amide, rather than an amine, in what is known as the Staudinger ligation. Importantly, this reaction has the potential to mediate the ligation of peptides at virtually any residue, without installing any additional atoms or causing racemization.[66,69,208]

Previously, the Raines group developed (diphenylphosphino)methanethiol as the most efficient known phosphinothiol that will facilitate this ligation.[60,209] Various functional groups, including tertiary amines and carboxylic acids, were added to the phenyl rings of this scaffold to improve water solubility. Ulimately, bis(*m*-*N*,*N*-dimethylaminomethylphenyl)-phosphinothiomethanethiol (**1**) was determined to the best of the tested reagents for the aqueous Staudinger ligation.[210] The use of this reaction in a completely aqueous environment is critical for its implementation in biomacromolecule ligations that are not able to withstand the presence of organic solvents. Yet, phosphinothiol **1** is challenging to synthesize, and the choice and placement of the *N*,*N*-dimethylamino groups could impart undesirable steric or electronic effects that are heretofore unappreciated, and could hinder the success of the ligation. We sought to investigate this hypothesis further by comparing the established phosphinothiol **1**, against bis(*p*-*N*,*N*-dimethylaminomethylphenyl)phosphinothiomethanethiol (**2**), which would mitigate steric hindrance, and an analogue utilizing the 2-methoxyethoxymethyl ether

(MEM) group at the *meta* position (**3**), which would provide water solubility without introducing a charge to the molecule (Figure 1.4.1).

We explore these three phosphinothiols, and their use in the Staudinger ligation at multiple levels. First, we examine the efficacy of these phosphinothiols to facilitate the Staudinger ligation at the small-molecule level. Next, we append these phosphinothiols to the C terminus of a protein as a phosphinothioester through expressed protein ligation (EPL), and examine the efficacy of the Staudinger ligation with a small-molecule azide. Ultimately, we seek to define the optimal phosphinothiol for protein–protein ligation, and with the isopeptide-linked ubiquitin–ubiquitin dimer as the goal.

The synthesis of ubiquitin chains is an ideal system in which to apply the Staudinger ligation. Ubiquitin is a small, globular protein that serves as an important post-translational modifier in the eukaryotic cell, operating as a signal in the form of both mono- and polyubiquitin chains. Ubiquitin is typically attached to a target protein through an isopeptide bond between the C-terminal glycine residue of ubiquitin and the ε-nitrogen of a lysine on the substrate protein. *In vivo*, the formation of the isopeptide bond is accomplished enzymatically.[211,212] Ubiquitin contains lysine residues at positions 6, 11, 27, 29, 33, 48, and 63 which are all known to serve as sites of attachment for additional ubiquitin molecules.[213] Attachment of ubiquitin, either as a monomer or in a chain connected through any of the seven lysine residues of ubiquitin, designates substrates for a variety of fates including endocytosis, proteasomal degradation, and participation in other signal transduction pathways.[211,214] Recent studies of ubiquitin polymers have found a diverse set of ubiquitin linkages to be present naturally, including all seven homopolymeric ubiquitin chains, branching at the proximal ubiquitin and mixed linkage chains.[215-218]

The current understanding of the complexity of ubiquitin signaling pathways is incomplete due to the limitations of existing techniques used to study ubiquitin signaling, and a lack of facile methods to synthesize ubiquitin chains. Previously, ubiquitin signaling has been studied either through genetic modification, or mass spectrometry; however, these techniques have limitations, particularly in delineating the roles of less abundant linkages (6, 27, 29, 33) and mixed or branched chains.

A convenient and efficient method to assess specific ubiquitin chains *in vitro*—both in isolation and while attached to protein substrates—has become critical to the advancement of the ubiquitin-signaling field. This task has proven to be challenging due to the difficulty of creating the isopeptide bond between proteins with a high degree of specificity. Several groups have recently published syntheses of diubiquitin, as reviewed by Martin and Raines.[219] Unfortunately, while innovative, these methods of native chain production remain mostly unrealistic for mainstream use in the biological community due to highly specialized techniques, harsh conditions, and low overall yields.

Here, the Staudinger ligation will be used to ligate two ubiquitin molecules, produced recombinantly in *Escherichia coli*, via an amide linkage without any residual atoms or racemization (Figure 1.4.2).[65,209] This traceless reaction will produce an isopeptide bond between an azide-labeled proximal ubiquitin and a distal ubiquitin labeled with a C-terminal phosphinothioester. The distal ubiquitin contains a C-terminal phosphinothioester, generated via expressed protein ligation, while the proximal ubiquitin contains an azide on the ε-nitrogen of the lysine to be modified, incorporated as azidonorleucine (ANL) with non-natural amino acid incorporation. This method is an improvement over current technologies because it creates an authentic isopeptide bond between recombinant proteins with highly selective chemistry that operates under mild aqueous conditions, allowing application to a wide variety of substrate proteins.

1.4.2 Results and Discussion

1.4.2.1 Small molecule ligations

Phosphinothiol **2** was synthesized via the route reported previously for phosphinothiol **1**, and with similar synthetic challenges. Phosphinothiol **3** was also synthesized analogously via the Grignard method, but the MEM groups facilitated a one-step reduction and protection of the phosphorous,[220] which is the most challenging step in the *N*,*N*-dimethylamino synthetic route.[221] As a net result, phosphinothiol **3** was obtained in dramatically higher overall yield than phosphinothiol **1** or **2**.

Phosphinothiol **3** was significantly more soluble than phosphinothiol **1** or **2**, dissolving readily in buffer at 5 mg/mL, while **1** and **2** required extended stirring to dissolve. Phosphinothiol **3** also outperformed phosphinothiol **1** or **2** in a small molecule Staudinger ligation test in buffer (Table 1.4.1).

1.4.2.2 Protein Production

The ubiquitin that was to serve as the substrate protein for ubiquitination required an azido group at the N_ε of the lysine side chain at the point to be modified. To accomplish this modification, the non-natural amino acid incorporation system developed by the Tirrell group was utilized to incorporate ANL.[222] This technique hijacks the methionyl t-RNA synthetase by modifying the amino acid-binding pocket, allowing for incorporation of ANL at the AUG codon in the absence of methionine. Ubiquitin does not contain any other methionine residues other than at the start codon. The ubiquitin construct was designed with a His_6 tag and TEV protease recognition site inserted between the N-terminal AUG start codon, and the second codon. This tag enables purification with metal ion-affinity chromatography, and cleavage at the N terminus, which could contain an additional ANL at position 1 (Figure 1.4.3A). The construct was expressed in methionine-auxotrophic *E. coli* cells with induction under conditions of methionine starvation and ANL supplementation. The incorporation of ANL was assessed by copper-catalyzed cycloaddition using an Alexa Fluor® 488 alkyne dye, with a fluorescent signal denoting a protein containing ANL (Figure 1.4.3B). The purified protein was also characterized via MALDI–TOF mass spectrometry, with a mass of 10344 Da representing a protein containing two ANL substitutions (positions 1 and the canonical 63 site) (Figure 1.4.3C). Subsequent cleavage of the tag with TEV Protease and purification resulted in the final protein of 8418 Da.

The pendant ubiquitin to be attached to the substrate above requires a C-terminal phosphinothioester, which was accomplished by EPL (Figure 1.4.4A). The ubiquitin was expressed as a C-terminal intein fusion protein with a chitin-binding domain. During the subsequent purification over chitin resin a pH shift facilitated an *N*→*S* acyl transfer, and incubation with the small-molecule thiol 2-mercaptoethanesulfonate (MESNa) resulted in the elution of the ubiquitin from the resin with a C-terminal thioester (Figure 1.4.4B). A transthioesterification with an excess of the phosphinothiols resulted in the decoration of the ubiquitin with the final C-terminal phosphinothioester (Figure 1.4.4C). This phosphinothioester protein was highly sensitive to oxygen, with oxidation of the phosphine and hydrolysis of the phosphinothioester occurring within hours of air exposure. Due to this sensitivity, the phosphinothioester protein was kept under N_2(g) whenever possible, and used for the ligation immediately.

1.4.2.3 Protein Ligations

A reaction between the ubiquitin C-terminal phosphinothioester proteins and an azido-biotin provided a simple system in which to observe the efficacy of the phosphinothiol in isolation, before transitioning into the protein–protein reaction in which the size of both reactants can introduce complications, including issues of diffusion rates and sterics. In a direct comparison between the ubiquitin phosphinothioesters with phosphinothiols **1** and **2**, phosphinothioester **2** provided a higher ligation yield, which was found to be optimal at pH 8.5. These preliminary data would suggest that the *meta* ligands might have had a deleterious effect on the ligation reaction that is relieved when the substituents are moved to the *para* position.

1.4.2.4 Protein–Protein Ligation

The ubiquitin phosphinothioesters with phosphinothiols **1** and **2** were reacted with the K63M ANL-containing ubiquitin (Figure 1.4.6A). The products of the reaction were quantified from silver-stained SDS–PAGE, and showed a slightly higher yield with phosphinothiol **2**, reinforcing the findings of the protein–small molecule ligation experiments. The products were characterized subsequently by MALDI–TOF mass spectrometry, which showed the formation of a ubiquitin–ubiquitin dimer at 18921 Da (Figure 1.4.6B, C). A lower product yield, in comparison to small-molecule studies is expected, due to the lower reactant concentrations and larger sizes of the reactants. The MALDI–TOF data, however, suggests that the major issue contributing to the lower yields is the oxidation and subsequent hydrolysis of the phosphinothiol from the C terminus. Once this process has occurred, this protein is no longer able to participate in the ligation reaction. Based on the relative sizes of ligation product peaks and oxidized/hydrolyzed pendant ubiquitin, this side reaction appears to occur much more rapidly than does the desired ligation reaction.

1.4.3 Future Directions

The phosphinothioester is highly sensitive to oxygen. The phosphine reacts readily with oxygen to form a phosphine oxide, rendering the phosphine unable to participate in the Staudinger ligation and promoting subsequent hydrolysis of the thioester. This oxidation reaction is in direct competition with the Staudinger ligation, and occurs quickly, particularly at the elevated temperatures used to promote the ligation reaction. At the small-molecule level, the Staudinger ligation has classically been performed under inert gas to limit this side reaction. Excluding oxygen is, however, far more challenging with proteins. In particular, once the distal ubiquitin has been adorned with the phosphinothioester, it must undergo further purification steps while in its highly oxygen-sensitive state. To limit this oxidation, future experiments with the phosphinothioester may be undertaken in an oxygen-free environment. Due to the extensive handling involved, a glove box would allow for the purification of the ubiquitin-phosphinothioester, and subsequent Staudinger ligation with minimal oxidation issues.

Additionally, phosphinothiol **3** will be utilized for protein ligation assays for comparison with phosphinothiols **1** and **2**. Phosphinothiol **3** utilizes MEM groups to promote water solubility, but has no charged side groups. This phosphinothiol is newly synthesized and characterized at the time of writing. In preliminary studies, this phosphine appears to be more water-soluble than phosphinothiols **1** and **2**, which take several minutes to dissolve in buffer. This phosphinothiol will be appended to the pendant ubiquitin, and characterized and analyzed for its ability to facilitate the Staudinger ligation between two ubiquitin molecules.

Upon adaptation of the protocol described here to the glove box, and addition of phosphinothiol **3**, the following experiments should be performed at the protein–protein ligation level:

1. Characterization of ubiquitin–phosphinothioester with phosphinothiol **3**.
2. SDS–PAGE of Staudinger ligation experiments with all three phosphines (**1**, **2**, **3**), at pH 7.0, 7.5, 8.0, and 8.5 to determine optimal phosphine-stability and ligation-yield conditions.
3. Immunoblot of Staudinger ligation products with a general ubiquitin antibody, as well as K48 and K63 specific antibodies. K48 and K63 dimers purchased from Boston Biochem will be used as controls.
4. Digestion of the Staudinger ligation product with Isopeptidase T (USP5), examined by SDS–PAGE (Sypro Ruby or silver stain).
5. Characterization of final dimer via MALDI–TOF mass spectrometry.
6. Trypsin Digest, LC/MS/MS of final dimer to verify that the specific linkage was formed, with the correct fingerprint of an isopeptide bond.

1.4.4 Materials & Methods

1.4.4.1 Materials

Chemicals

Silica gel (40 μm) was from SiliCycle (Québec City, Canada). All reagent-grade materials were from Sigma–Aldrich (St. Louis, MO) and were used without further purification. Ultrapure water with a resistivity of ≥18 MV cm^{-1} was generated with an Arium Pro water purification system from Sartorius (Bohemia, NY). The cDNA encoding *Saccharomyces cerevisiae* ubiquitin was codon-optimized for expression in *Escherichia coli* and synthesized by Bio Basic (Toronto, Canada). The vector pTXB, and *NdeI* and *SapI* restriction enzymes were from New England BioLabs (Ipswich, MA).

Instrumentation

^{1}H, ^{13}C, and ^{31}P NMR spectra for all compounds were acquired at ambient temperature on Bruker spectrometers in the National Magnetic Resonance Facility at Madison (NMRFAM) at the University of Wisconsin–Madison operating at 400, 500, or 750 MHz for ^{1}H and 126 or 189 MHz for ^{13}C, and 162 MHz for ^{31}P NMR. Chemical shift data are reported in units of δ (ppm) relative to residual solvent or TMS. Electrospray ionization (ESI) mass spectrometry was performed with a Micromass LCT at the Mass Spectrometry Facility in the Department of Chemistry at the University of Wisconsin–Madison. The mass of each ubiquitin variant and dimer was confirmed by matrix-assisted laser desorption/ionization time-of-flight (MALDI–TOF) mass spectrometry with a Voyager-DE-PRO Biospectrometry Workstation from Applied Biosystems (Foster City, CA). Absorbance measurements were made with an infinite M1000 plate reader from Tecan (Männedorf, Switzerland).

1.4.4.2 Synthesis

The phrase "concentrated under reduced pressure" refers to the removal of solvents and other volatile materials using a rotary evaporator at water aspirator pressure (<20 torr) while maintaining the water-bath temperature below 40 °C. Residual solvent was removed from samples at high vacuum (<0.1 torr). All reactions were performed at ambient temperature unless indicated otherwise.

$HSCH_2P(C_6H_4\text{-}m\text{-}CH_2NMe_2)_2$ (**1**) was synthesized as reported previously.[210]

Synthesis of $HSCH_2P(C_6H_4\text{-}p\text{-}CH_2NMe_2)_2$ (**2**):

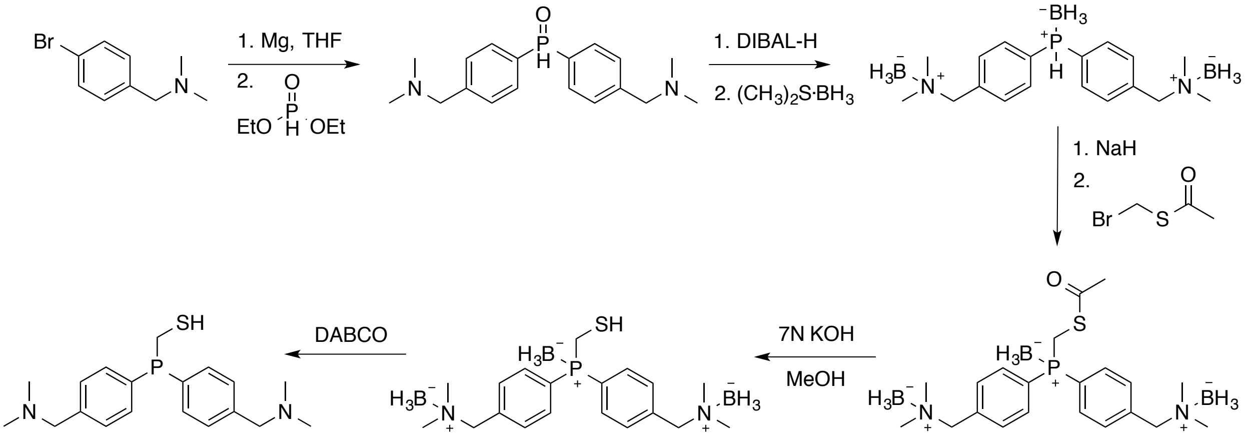

Br
1. Mg, THF
2. EtO P(O)H OEt
1. DIBAL-H
2. (CH3)2S·BH3
1. NaH
2. Br S(O)
7N KOH
MeOH
DABCO

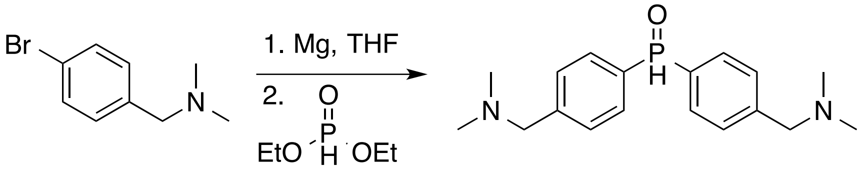

1,1'-(4,4'-phosphorylbis(4,1-phenylene))bis(*N*,*N*-dimethylmethanamine): Freshly ground Mg turnings (0.354 g, 14.56 mmol) and I_2 (cat) were added to a 2-neck 100-mL round-bottom flask that was fitted with a reflux condenser and sealed with a septum. The flask was purged by vacuum and filled with $N_{2(g)}$ (3 cycles) ending with a positive pressure of $N_{2(g)}$. Anhydrous THF (5 mL) was added to cover the Mg, and the resulting suspension was stirred. 1-(4-bromophenyl)-*N*,*N*-dimethylmethanamine (3.1 g, 14.48 mmol) was dissolved in anhydrous THF (25 mL). The resulting solution was added through the septum, and the reaction was heated at reflux for 4 h. The reaction progress was observed by the near complete consumption of the Mg turnings. The reaction mixture was then cooled to room temperature, and placed in an ice bath. Diethyl phosphite (0.465 mL, 3.62 mmol) was added dropwise, and the reaction mixture was allowed to warm to room temperature overnight. The yellow mixture was then quenched with dH_2O and the concentrated under reduced pressure, leaving a white slurry. This slurry was dissolved in MeOH (100 mL) and filtered through a shallow pad of Celite® to remove undissolved solids. The residual solids were washed further with MeOH (100 mL), and the filtrate was concentrated. The residue was purified by chromatography on silica gel (10–20% v/v gradient of MeOH in DCM containing 0.5% v/v TEA) to produce 1,1'-(4,4'-phosphorylbis(4,1-phenylene))bis(*N*,*N*-dimethylmethanamine) as a light yellow solid (1.1 g, 96%). ^{1}H NMR (500 MHz, $CDCl_3$) δ 8.08 (d, J = 480.1 Hz, 1H), 7.67 (dd, J

= 13.5, 7.8 Hz, 4H), 7.48 (dd, *J* = 8.0, 2.6 Hz, 4H), 3.51 (s, 4H), 2.27 (s, 11H). ^{13}C NMR (101 MHz, CDCl$_3$) *δ* 144.05, z131.04, 130.93, 129.75, 129.62, 63.98, 45.46. ^{31}P NMR (162 MHz, CDCl$_3$) *δ* 20.09. HRMS (ESI) *m/z* calc'd for $[C_{18}H_{25}N_2OP+H]^+$ 317.1778, found 317.1781.

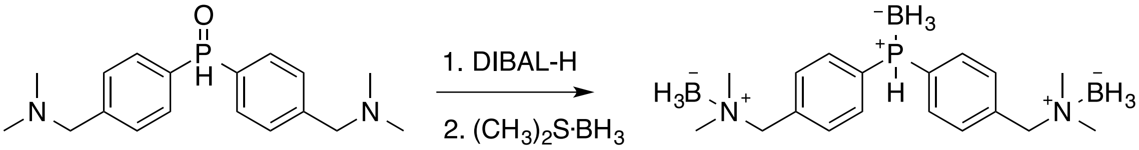

Borane bis{4-[(dimethylamino)methyl]phenyl}phosphine complex: 1,1'-(4,4'-phosphorylbis(4,1-phenylene))bis(*N*,*N*-dimethylmethanamine) (0.509 g, 1.61 mmol) was dissolved in anhydrous THF (8 mL) and the resulting solution was sparged and purged (3x) with $N_{2(g)}$. DIBAL-H as a 1.0 M solution in THF (10 mL, 10 mmol) was added dropwise, producing immediate gas evolution. The reaction mixture was stirred overnight. The reaction mixture was then cooled in an ice bath, and excess DIBAL-H was quenched with water (0.4 mL), 10% w/v NaOH (0.6 mL), and water (1 mL). The reaction mixture was removed from the ice bath, and stirred for 30 min. The resulting slurry was dried over $MgSO_{4(s)}$ and filtered, and the filtrate was concentrated under reduced pressure. The residue was dissolved in anhydrous DCM (20 mL), and the resulting solution was washed with brine (20 mL), dried over $MgSO_{4(s)}$, and filtered. The filtrate was concentrated to approximately half the volume. The solution was cooled in an ice bath, borane dimethylsulfide (0.52 mL, 5.15 mmol) was added dropwise, and the resulting solution was allowed to warm to ambient temperature and stir overnight. The reaction mixture was concentrated under reduced pressure, and the residue was purified by chromatography on silica gel (CH_2Cl_2) to yield a pure white solid (0.17 g, 30% overall from two steps) ^{1}H NMR (500 MHz, $CDCl_3$) δ 7.79 – 7.66 (m, 4H), 7.48 (dd, J = 8.0, 2.1 Hz, 4H), 6.37 (dq, J = 381.6, 7.0 Hz, 1H), 3.98 (s, 4H), 2.55 (s, 12H). ^{13}C NMR (126 MHz, $CDCl_3$) δ 135.34, 135.31, 133.20, 133.11, 133.03, 127.30, 126.85, 67.21, 50.49, 50.46.^{31}P NMR (400MHz, $CDCl_3$) δ -0.269. HRMS (ESI) *m/z* calculated for $[C_{18}H_{34}B_3N_2P+NH_4]^+$ 358.3151, found 358.3155.

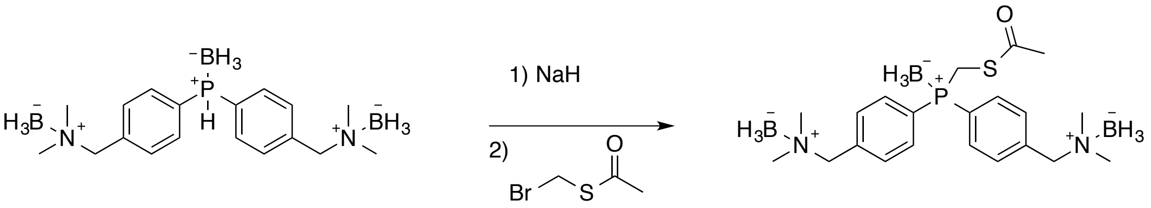

Borane bis{4-[(dimethylamino)methyl]phenyl}phosphine ethanethioate complex: Borane bis{4-[(dimethylamino)methyl]phenyl}phosphine (0.170 g, 0.5 mmol) was dissolved in DMF (2.5 mL) and the solution was cooled to 0 °C. NaH (0.02 g, 0.5 mmol) was added portionwise, and the reaction mixture was stirred until the evolution of gas was no longer observed. The bromothioester (0.17 g, 1 mmol) was added slowly, and the reaction mixture was removed from the ice bath and stirred overnight. The reaction mixture was concentrated by rotary evaporation and purified by chromatography on silica get (2% EtOAc, 28% Hexane, 70% DCM v/v/v) to yield the borane bis{4-

[(dimethylamino)methyl]phenyl}phosphine ethanethioate complex as a white solid (0.1 g, 50%). ^{1}H NMR (500 MHz, $CDCl_3$) δ 7.74 (dd, J = 10.5, 7.9 Hz, 4H), 7.48 (dd, J = 8.1, 2.2 Hz, 4H), 3.98 (s, 4H), 3.73 (d, J = 6.7 Hz, 2H), 2.55 (d, J = 2.5 Hz, 13H), 2.27 (s, 3H), 1.74 (bs, 6H). ^{13}C NMR (126 MHz, $CDCl_3$) δ 193.04, 193.02, 135.40, 135.38, 132.95, 132.87, 132.61, 132.53, 128.75, 128.32, 67.22, 50.54, 50.52, 30.22, 23.75, 23.47. ^{31}P NMR (202 MHz, $CDCl_3$) δ 19.29. HRMS (ESI) *m/z* calc'd for $[C_{21}H_{38}B_3OPS+NH_4]^+$ 446.3134, found 446.3136.

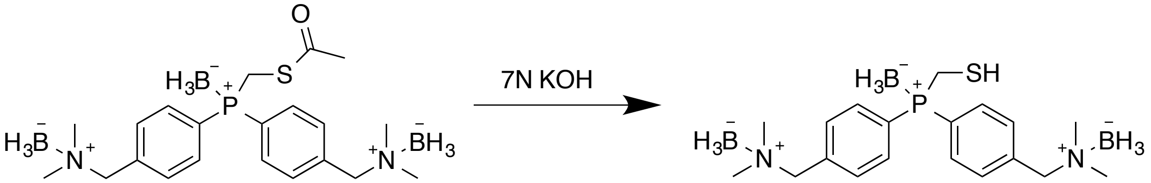

Borane bis{4-[(dimethylamino)methyl]phenyl}phosphine methanethiol complex: Borane bis{4-[(dimethylamino)methyl]phenyl}phosphine thioester (0.01 g, 0.023 mmol) was dissolved in MeOH (1 mL) with stirring. To the resulting solution, an aqueous solution of 7 N KOH (0.05 mL, 0.35 mmol) was added, and the reaction mixture was stirred overnight. The reaction mixture was quenched with saturated NH_4Cl (10 mL) and the solution was concentrated by rotary evaporation. The resulting slurry was extracted with DCM (4 x 10 mL), and the combined organics were dried over $Na_2SO_{4(s)}$, and the solution concentrated under reduced pressure to yield the borane bis{4-

[(dimethylamino)methyl] phenyl}phosphine ethanethiol complex as a yellowish solid (0.01 g, quant). ^{1}H NMR (500 MHz, CDCl$_3$) *δ* 7.74 (dd, *J* = 10.5, 7.9 Hz, 4H), 7.48 (dd, *J* = 8.1, 2.2 Hz, 4H), 3.98 (s, 4H), 3.73 (d, *J* = 6.7 Hz, 2H), 2.55 (d, *J* = 2.5 Hz, 13H), 1.74 (s, 6H). ^{13}C NMR (126 MHz, CDCl$_3$) *δ* 156.87, 135.35, 133.07, 132.99, 132.78, 132.67, 132.60, 132.23, 128.97, 128.54, 67.26, 50.59, 50.53, 34.07, 29.85, 25.73, 25.07. ^{31}P NMR (202 MHz, CDCl$_3$) *δ* 21.11.

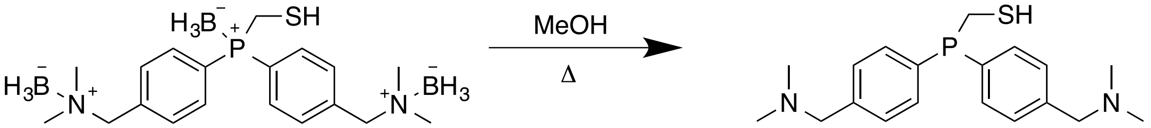

(Bis(3-[(2-methoxyethoxy)-methoxymethyl]phenyl)phosphino)methanethiol: Borane bis(3-[(2-methoxyethoxy)-methoxymethyl]phenyl)phosphine thiol complex (0.01 g, 0.02 mmol) was dissolved in anhydrous MeOH (10 mL) in a sealed vial and heated to 70 °C with stirring for 12 h. The reaction mixture was then concentrated by rotary evaporation and used directly (0.01 g, quant.). ^{1}H NMR (500 MHz, CDCl$_3$) δ 7.74 (dd, *J* = 10.5, 7.9 Hz, 4H), 7.48 (dd, *J* = 8.1, 2.2 Hz, 4H), 3.98 (s, 4H), 3.73 (d, *J* = 6.7 Hz, 2H), 2.55 (d, *J* = 2.5 Hz, 13H). ^{13}C NMR (P-coupled,126 MHz, CDCl$_3$) δ 193.04, 193.02, 135.40, 135.38, 132.95, 132.87, 132.61, 132.53, 128.75, 128.32, 67.22, 50.54, 50.52, 30.22, 23.75, 23.47. ^{31}P NMR (162 MHz, CDCl$_3$) δ -10.02.

Synthesis of $HSCH_2P(C_6H_4$-*m*-$CH_2OCH_2OCH_2CH_2OCH_3)_2$ (**3**):

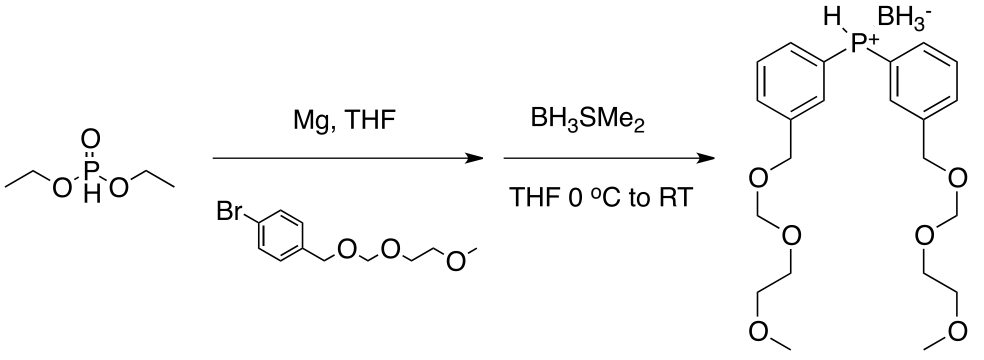

Borane bis(3-[(2-methoxyethoxy)-methoxymethyl]phenyl)phosphine complex: Synthesized as reported previously.[25]

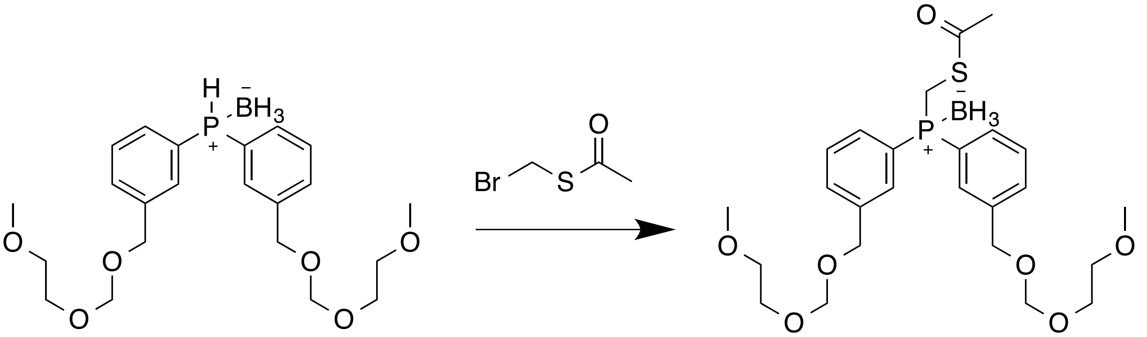

Borane bis(3-[(2-methoxyethoxy)-methoxymethyl]phenyl)phosphine thioester complex: Borane bis(3-[(2-methoxyethoxy)-methoxymethyl]phenyl)phosphine (0.52 g, 1.2 mmol) was dissolved in DMF (5 mL) and the resulting solution was cooled to 0 °C. To this solution NaH (0.048 g, 1.2 mmol) was added portionwise until the cessation of gas evolution was observed. The bromothioester (0.2 g, 3 mmol) was then added to the reaction mixture, and the resulting solution was allowed to warm to room temperature and was stirred overnight. The reaction mixture was concentrated by rotary evaporation and purified by chromatography on silica gel to yield the borane bis(3-[(2-methoxyethoxy)-methoxymethyl]phenyl)phosphine thioester complex as a clear oil (0.234 g, 37%). ^{1}H NMR (400 MHz, CDCl$_3$) δ 7.68 (d, J = 11.2 Hz, 2H), 7.59 (t, 2H), 7.51 (d, J = 7.6 Hz, 2H), 7.43 (td, J = 7.6, 2.5 Hz, 2H), 4.80 (s, 4H), 4.63 (s, 4H), 3.77 – 3.68 (m, 6H), 3.56 (dd, J = 5.8, 3.5 Hz, 4H), 3.39 (s, 6H), 2.26 (s, 3H). ^{13}C NMR (126 MHz, CDCl$_3$) δ 193.29, 193.27, 139.11, 139.03, 131.70, 131.65, 131.63, 131.57, 131.21, 131.19, 129.08, 129.00, 128.00, 127.57, 95.12, 71.80, 68.80, 67.12, 59.15, 30.16, 23.88, 23.59. ^{31}P NMR (162 MHz, CDCl$_3$) δ 18.24. HRMS (ESI) m/z calc'd for [$C_{25}H_{38}BO_7PS$+Na]$^+$ 546.2098, found 546.2097.

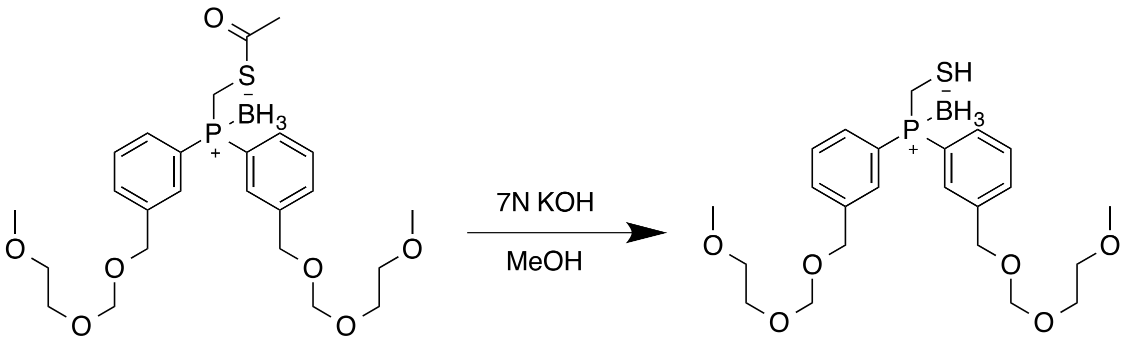

Borane (bis(3-[(2-methoxyethoxy)-methoxymethyl]phenyl)phosphine)methanethiol complex: Borane bis(3-[(2-methoxyethoxy)-methoxymethyl]phenyl)phosphine thioester complex (0.015 g, 0.03 mmol) was dissolved in MeOH (1 mL). To the resulting solution, an aqueous solution of 7 N KOH (0.05 mL, 0.35 mmol) was added, and the reaction mixture was stirred overnight. The reaction mixture was quenched with saturated NH_4Cl

(10 mL) and the organics were removed by rotary evaporation. The suspension was then extracted into DCM (4 x 10 mL), dried over Na_2SO_4, and concentrated to yield the borane bis(3-[(2-methoxyethoxy)-methoxymethyl]phenyl)phosphine thiol complex as a lightly colored oil (0.015 g, quant.). ^{1}H NMR (500 MHz, $CDCl_3$) δ 7.67 (dd, J = 10.4, 8.1 Hz, 4H), 7.46 (dd, J = 8.1, 2.3 Hz, 5H), 4.82 (s, 4H), 4.66 (s, 4H), 3.79 – 3.69 (m, 6H), 3.60 – 3.52 (m, 6H), 3.40 (d, J = 1.7 Hz, 6H). ^{13}C NMR (126 MHz, $CDCl_3$) δ 142.22, 142.20, 132.81, 132.73, 128.16, 128.08, 127.22, 127.17, 126.73, 95.21, 71.85, 68.73, 67.19, 59.22, 59.20. ^{31}P NMR (162 MHz, $CDCl_3$) δ 20.53. HRMS (ESI) *m/z* calc'd for $[C_{23}H_{36}BO_6PS+NH_4]^+$ 499.2438, found 499.2436.

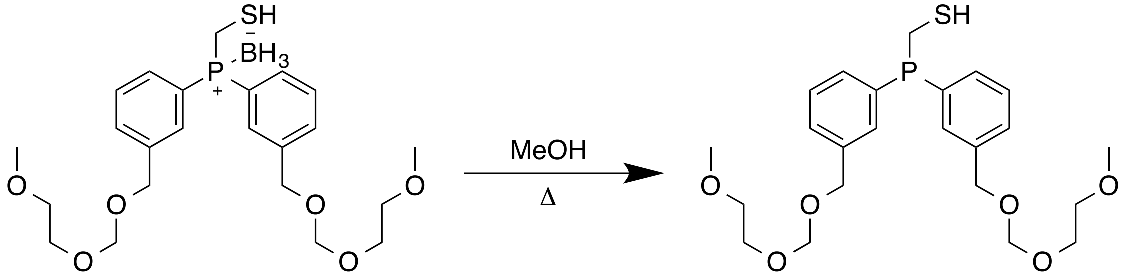

(Bis(3-[(2-methoxyethoxy)-methoxymethyl]phenyl)phosphino)methanethiol: The borane bis{3-[(2-methoxyethoxy)-methoxymethyl]phenyl}phosphine thiol complex (0.015 g, 0.03 mmol) was dissolved in anhydrous MeOH (10 mL) in a sealed vial and the solution was heated to 70°C for 12 h. The reaction mixture was then concentrated by rotary evaporation and used directly (0.015 g, quant.). ^{1}H NMR (500 MHz, $CDCl_3$) δ 7.90 – 7.64 (m, 2H), 7.53 – 7.40 (m, 3H), 7.36 (s, 0H), 4.84 – 4.78 (m, 4H), 4.69 – 4.63 (m, 3H), 3.74 (dd, J = 5.7, 3.6 Hz, 4H), 3.56 (dd, J = 5.8, 3.4 Hz, 4H), 3.40 (s, 4H). ^{13}C

NMR (126 MHz, $CDCl_3$) δ 143.04, 132.25, 132.16, 132.09, 132.02, 131.95, 131.79, 131.71, 131.09, 131.01, 128.52, 128.19, 128.15, 128.09, 128.05, 127.94, 127.45, 95.47, 95.45, 95.43, 72.10, 69.00, 68.89, 67.45, 67.44, 59.46. ^{31}P NMR (162 MHz, $CDCl_3$) δ 28.49.

1.4.4.3 Small Molecule Staudinger Ligation Testing

The phosphinothioester (0.01 mmol) was combined with DABCO (0.01 mmol, or 0.03 mmol), and the vessel was evacuated, and purged with $N_{2(g)}$ for three cycles, ending with positive pressure of $N_{2(g)}$. Anhydrous toluene (1 mL) was added, and the reaction mixture was heated to 40 ^{o}C for 4 h. The reaction mixture was returned to high vacuum and concentrated to dryness. 2-azido-*N*-benzylacetamide[25] was added to the deprotected phosphinothioester as a solution in 1 mL of either DMF or buffer (50 mM Tris, pH 8.0). The reaction mixture was then again evacuated, and purged with $N_{2(g)}$ for three cycles, ending with positive pressure of $N_{2(g)}$ and sealed. The reaction mixture was stirred for 20 h at 40 ^{o}C, and then analyzed by LCMS. The percent conversions were determined by monitoring peak absorbance at 254 nm to provide the integration of the glycine amide-product and the integration of the unreacted 2-azido-*N*-benzylacetamide.

Phosphinothioester reduction *in situ* was performed according to a previously reported procedure.[223] The phosphinothioester (0.01 mmol) was combined with DABCO (0.01 mmol, or 0.03 mmol) and 2-azido-*N*-benzylacetamide[25] and the vessel was evacuated and purged with $N_{2(g)}$ for three cycles, ending with positive pressure of $N_{2(g)}$. Anhydrous DMF (1 mL) was added to the reagents, and the reaction mixture was stirred for 20 h at 40 ^{o}C, and analyzed by LCMS.

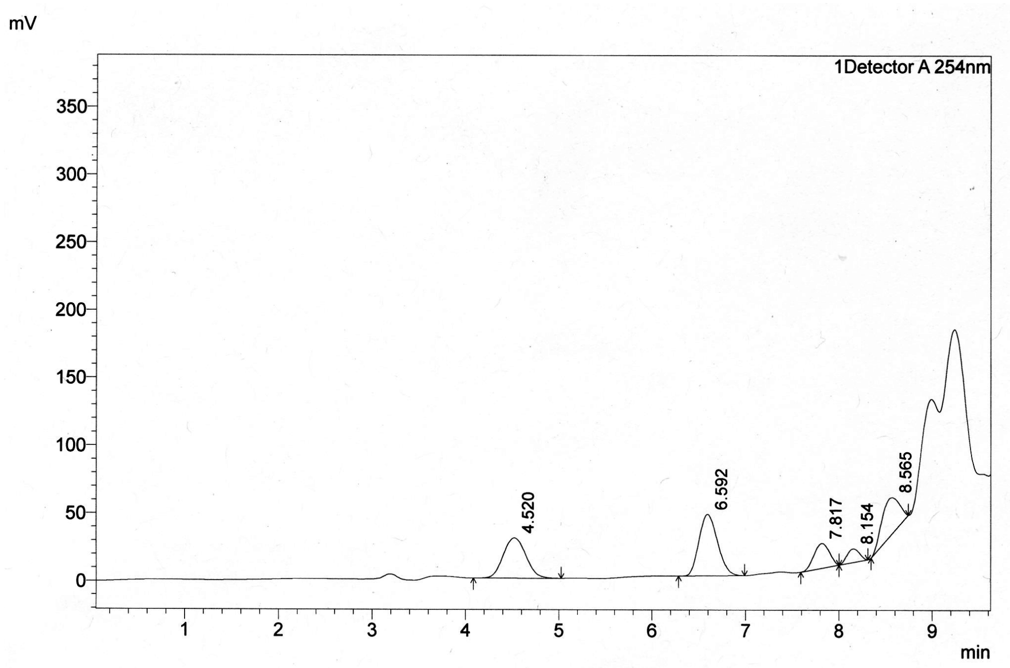

1.4.4.3.1 LCMS Chromatogram of glycine-coupling assay. Amide product is visible at 6.592 min., unreacted azide is observed at 7.817 min.

1.4.4.4 Protein Production

Site-directed mutagenesis with the QuickChange kit from Agilent Technologies (Santa Clara, CA) was used to generate all ubiquitin variants. Constructs were verified by Sanger sequencing at the University of Wisconsin–Madison Biotechnology Center Sequencing Facility.

1.4.4.4.1 Distal Ubiquitin

cDNA encoding *S. cerevisiae* ubiquitin was inserted into the pTXB expression vector between the *NdeI* and *SapI* sites. The ubiquitin protein was expressed as an intein fusion protein with a chitin binding domain in BL21(DE3) *E. coli* cells. The cells were grown and induced at 37°C in autoinduction media for 20 h. The cells were harvested by centrifugation at 5000g for 20 min. The cell pellet was resuspended in lysis buffer (30 mM HEPES–NaOH buffer, pH 8.0, containing 0.30 M NaCl and 1.0 mM EDTA) and lysed at 22 kPSI in a T Series Cell Disrupter 2.2 kW from Constant Systems Limited (Northants, UK). The debris was cleared by centrifugation at 15000g for 45 min at 4 °C. The supernatant was incubated for 4 h at 4 °C with chitin resin equilibrated in lysis buffer (10 mL resin/L liquid growth). The flow through was discarded and the resin was washed with 5 column volumes of wash buffer (30 mM HEPES–NaOH buffer, pH 8.0, containing 0.50 M NaCl and 1.0 mM EDTA). The protein was eluted from the resin as a thioester with MESNa by incubation in elution buffer (30 mM potassium phosphate buffer, pH 6.0, containing 0.20 M NaCl, 1.0 mM EDTA, and 0.10 M MESNa) for 48 h on a nutator at 4 °C. The ubiquitin-MESNa thioester solution was concentrated and purified further by gel filtration chromatography on a Superdex G75 26/60 column, in 50 mM NaOAc pH 5.0, 0.1 M NaCl, 0.05% NaN_3). The protein solution was sparged with nitrogen for 10 min, before adding 100x molar excess of the phosphinothiol. The solution was sparged with nitrogen for a further 10 min, before being stirred at 4 °C for 48 h to induce transthioesterification. The protein was then purified by PD10 column with 50 mM HEPES-NaOH, pH 7.5. The final ubiquitin phosphinothioester was characterized by MALDI-TOF and SDS-PAGE.

1.4.4.4.2 Proximal Ubiquitin

The ubiquitin gene was ligated into the pQE60 vector (Qiagen), with an N-terminal His_6 tag and TEV protease recognition sequence inserted between the start codon and the second amino acid in the protein. Site-directed mutagenesis was used to install a K→M mutation at the desired site of azidonorleucine incorporation. This plasmid was transformed into M15MA cells (Met auxotroph), also containing pREP4, to limit leaky expression. The cells were grown in 1 L Terrific Broth at 37 °C, shaking until OD_{600} reached 1.2 – 1.4. The cells were centrifuged at 5000g for 7 min, and resuspended gently in 1 L M9 media (M9 salts, 0.2% glucose, 1mM $MgSO_4$, 25 mg/L thiamine) containing 19 amino acids (40 mg/L, excluding methionine). The culture was further grown at 37 °C, shaking for 20 minutes, and the centrifugation was repeated. The cells were again taken up in 1 L M9 media, containing 19 amino acids (excluding methionine) with 1 mM azidonorleucine. The cells were grown at 37 °C with shaking for a further 20 minutes before IPTG was added to 1 mM to induce protein expression for 12 h. The cells were harvested at 5000g for 20 minutes, and resuspended in lysis buffer (30 mM phosphate buffer, pH 8.0, containing 0.50 M NaCl and 20 mM imidazole). Cells were lysed at 22 kPSI in a T Series Cell Disrupter 2.2 kW, and the supernatant was clarified by centrifugation at 15000g for 45 minutes. The supernatant was filtered through a 0.45 µm filter, before purification by immobilized metal ion affinity chromatography (IMAC) using a HisTrap SP HP column and an AKTA system from GE Healthcare (Piscataway, NJ) with a linear gradient of imidazole (0.02–0.5 M) in 30 mM phosphate buffer, pH 8.0, with 0.5 M NaCl. The purified protein was dialyzed into 50 mM HEPES-NaOH, pH 7.5 and concentrated to 100-200 µM. If the N-terminal tag needed to be removed, TEV Protease (Promega, Madison, WI), was utilized to cleave off the tag, and a further round of IMAC purified the ubiquitin variant from the enzyme and tag. Incorporation of azidonorleucine was verified by MALDI-TOF and by reaction of the azido group with Alexa Fluor® 488-alkyne.

1.4.4.5 Ubiquitin-Biotin Staudinger Ligations

50 µl of ubiquitin-phosphinothioester **1** or **2** (200 µM, 1 nmol) was combined with 100

fold molar excess of azide-PEG3-biotin (Sigma Aldrich). The pH was adjusted with HEPES-NaOH to 7.0, 7.5, 8.0 or 8.5. A control ubiquitin with no C-terminal modification was also prepared at pH 8.0. The reactions were mixed and reacted at 40 °C for 12 h. The reactions were quenched with the addition of SDS-PAGE sample buffer, and boiled for 5 minutes. The samples were run on a 12% SDS-PAGE gel, and transferred to PVDF for 1.5 h at 100 V. The PVDF was blocked with 5% non-fat milk in 1X TBST for 1 h at room temperature. The blot was washed 3 x 5 min in 1X TBST, and incubated in anti-biotin-HRP antibody (Cell Signaling Technology) for 1 h at room temperature. The blot was washed 3 x 5 min in 1X TBST, and HRP was detected by chemiluminescence, imaging using an ImageQuant LAS 4000 (GE Healthcare).

1.4.4.6 Ubiquitin-Ubiquitin Staudinger Ligations

100 μl of ubiquitin-phosphinothioester **1** or **2** (200 μM, 2 nmol) was combined with 0.5 equivalents of the K63 azidonorleucine protein. The pH was adjusted with HEPES-NaOH to 6.5, 7.0, 7.5, 8.0 or 8.5. A control ubiquitin with no C-terminal modification was also prepared at pH 7.0 and 8.0. The reactions were mixed and reacted at 40 °C for 18 h. A portion of the reaction was removed at 18 h, and spotted on a MALDI-TOF plate with sinapinic acid matrix, for mass spectrometry analysis. The remainder of the reaction was quenched with the addition of SDS-PAGE sample buffer, and boiled for 5 minutes. The samples were run on a 12% SDS-PAGE gel, and then silver stained.

Table 1.4.1 Small-molecule Staudinger ligation testing

Small-molecule Staudinger ligation testing (reported as % amide conversion)

Phosphinothiol	**DMF (Reduced *in situ*)**	**DMF**	**50 mM Tris pH 8.0**
1	n/a	n/a	56
2	64	56	62
3	88	76	91

Figure 1.4.1 Phosphinothiols compared directly in the aqueous Staudinger ligation.

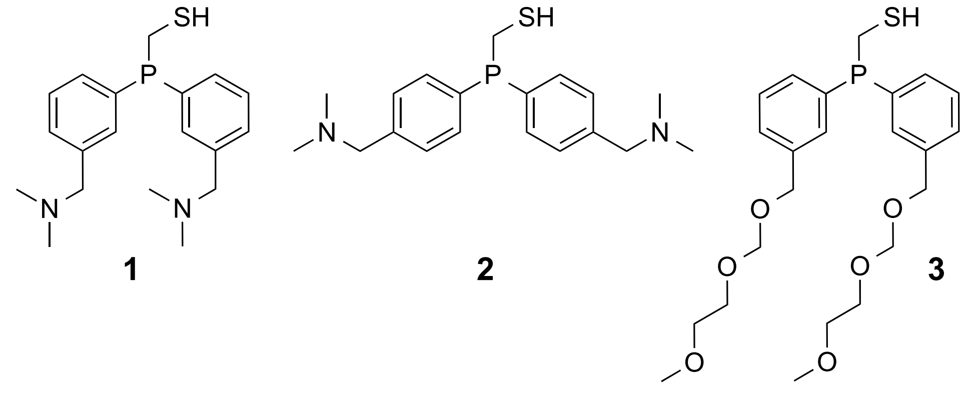

Figure 1.4.1 Phosphinothiols compared directly in the aqueous Staudinger ligation. (**1**) bis(*m*-*N*,*N*-dimethylaminomethylphenyl)-phosphinothiomethanethiol, (**2**) *N*,*N*-dimethylaminomethyl-phenyl)phosphinothiomethanethiol and (**3**) (Bis(3-[(2-methoxyethoxy)-methoxymethyl]-phenyl)phosphino)methanethiol.

Figure 1.4.2 Retrosynthetic scheme for the production of ubiquitin chains.

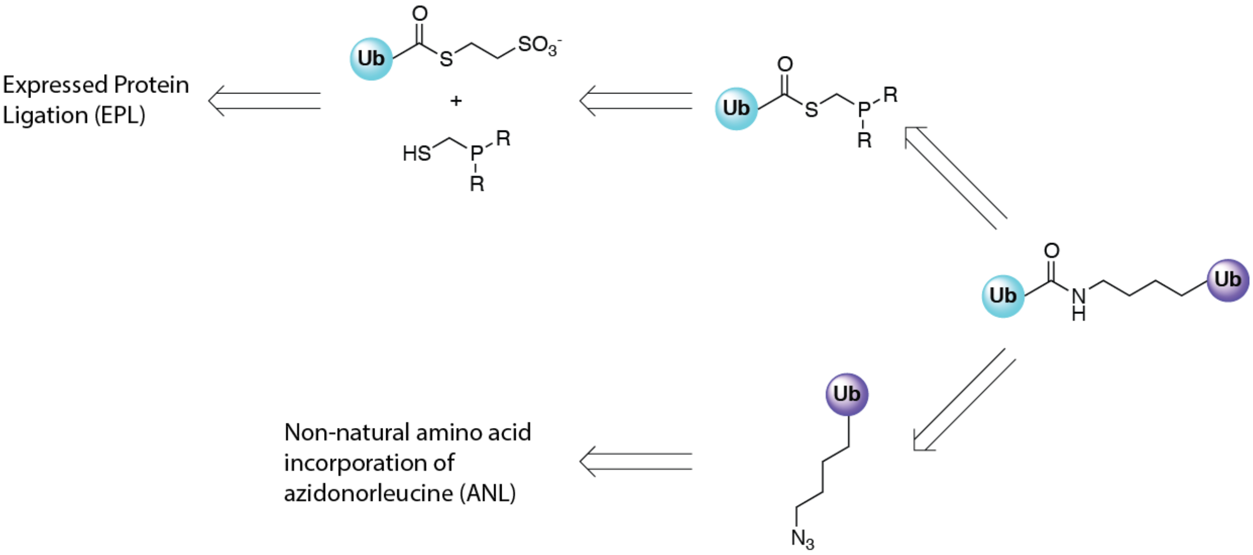
Expressed Protein
Ligation (EPL)
Ub
O
S
SO3-
+
HS
P
R
R
Ub
O
S
P
R
R
Ub
O
N
H
Ub
Ub
N3
Non-natural amino acid
incorporation of
azidonorleucine (ANL)

Figure 1.4.2 Retrosynthetic scheme for the production of ubiquitin chains. The distal ubiquitin (blue) is produced by Expressed Protein Ligation and decorated with a phosphinothiol (R= C_6H_4-*m*-CH_2NMe_2 or C_6H_4-*p*-CH_2NMe_2 or (C_6H_4-*p*-$CH_2OCH_2OCH_2CH_2OCH_3$)). The proximal ubiquitin contains an azide installed through non-native amino acid incorporation. The final dimer is linked through an isopeptide bond formed by the Staudinger ligation.

Figure 1.4.3 Preparation of the proximal ubiquitin.

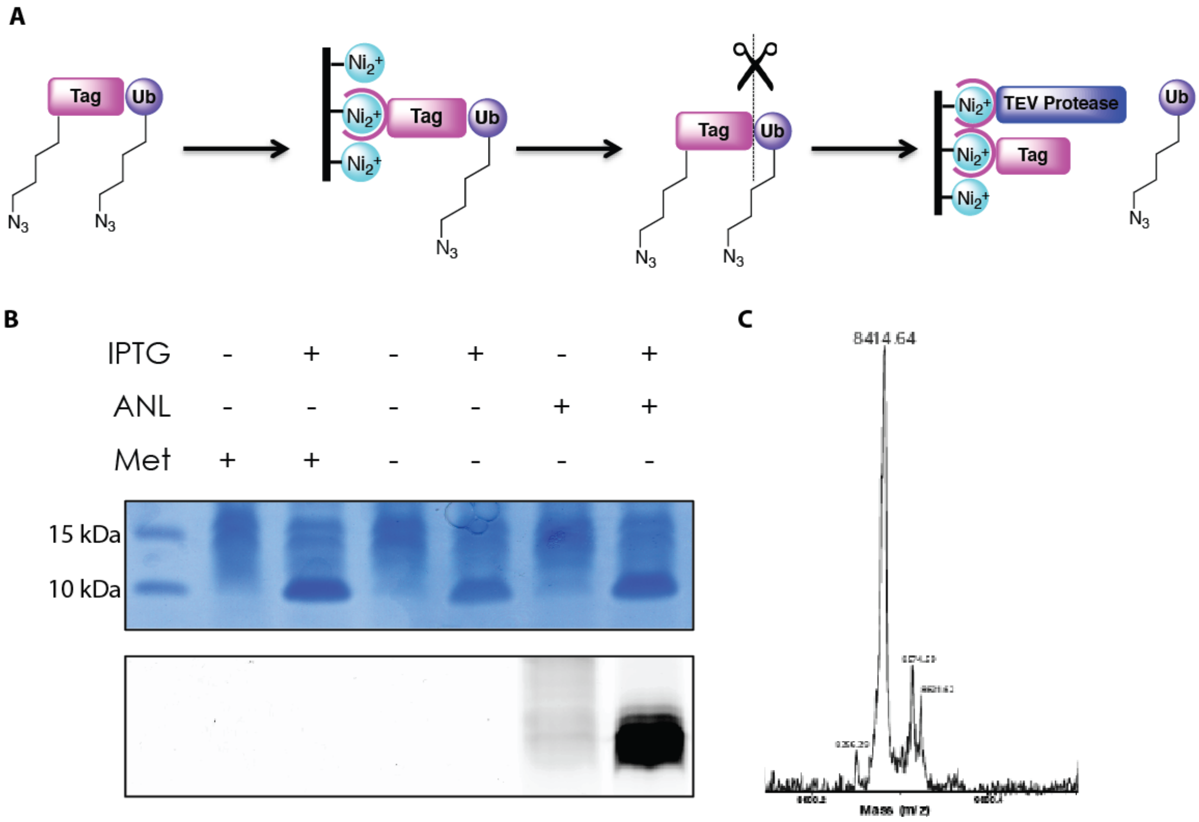

Figure 1.4.3 Preparation of the proximal ubiquitin. (A) The proximal ubiquitin along with a polyhistidine tag and TEV protease recognition sequence is expressed in methionine auxotrophic cells, with a methionyl t-RNA synthetase variant that enables the incorporation of azidonorleucine at methionine codons. The protein is subsequently purified by metal ion affinity chromatography (IMAC). The tag, including the azidonorleucine incorporated at the start codon, is removed with TEV protease. Both the TEV protease and the affinity tag are removed by a second round of IMAC. (B) SDS-PAGE of varying protein expression conditions of the K63M variant, stained with coomassie (top) and scanned for 488 nm fluorescent signal after reaction with an Alexa Fluor® 488 alkyne and Cu(I). (C) MALDI-TOF of the purified K63M variant, after removal of the purification tag.

Figure 1.4.4 Preparation of the distal ubiquitin.

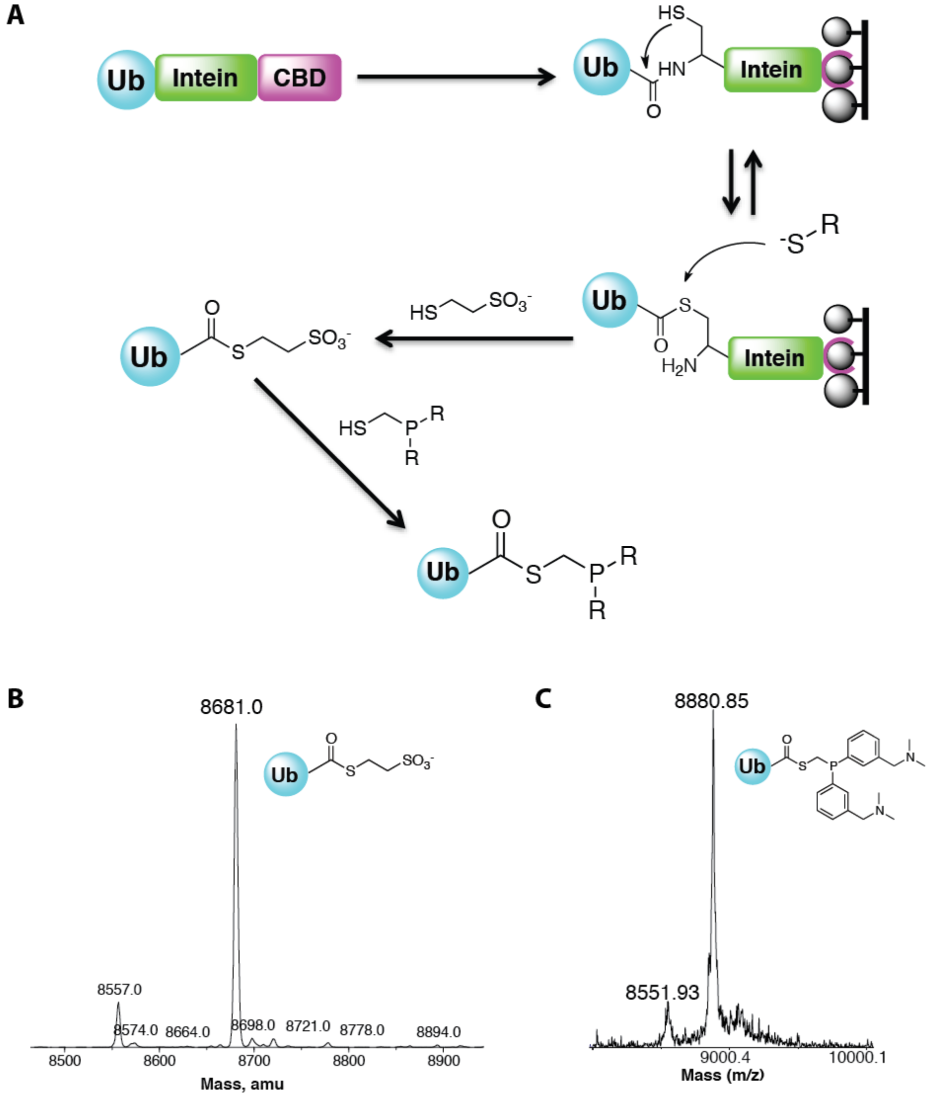
A
Ub
Intein
CBD
HS
HN
O
Intein
-S-R
Ub
S
O
H2N
Intein
HS
SO3-
Ub
O
S
SO3-
HS
P
R
R
O
Ub
S
P
R
R
B
8681.0
Ub
O
S
SO3-
8557.0
8574.0
8664.0
8698.0
8721.0
8778.0
8894.0
8500
8600
8700
8800
8900
Mass, amu
C
8880.85
Ub
O
S
P
N
N
8551.93
9000.4
10000.1
Mass (m/z)

Figure 1.4.4 Preparation of the distal ubiquitin. (A) The distal ubiquitin is expressed recombinantly as an intein fusion protein with a chitin binding protein. The protein is then bound to chitin resin, and a drop in pH facilitates an *N*→*S* acyl rearrangement. The protein is eluted from resin by cleavage with a thiol (typically MESNa). A transthioesterification results in generation of the final ubiquitin phosphinothioester that will be used in the Staudinger ligation. (B) Ubiquitin with a C-terminal MESNa thioester. (C) Ubiquitin with a C-terminal phosphinothioester.

Figure 1.4.5 Protein-small molecule ligations.

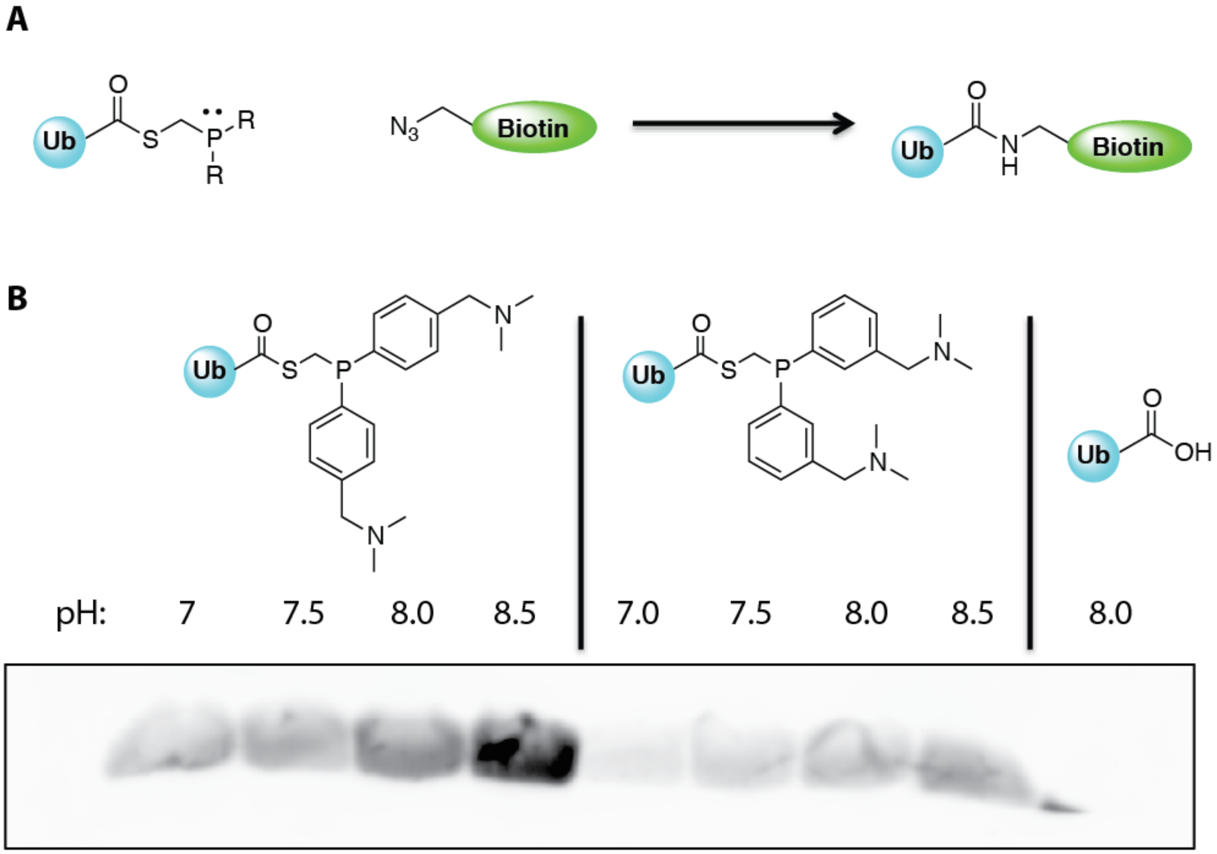
A
Ub
O
S
P
R
R
N3
Biotin
Ub
O
N
H
Biotin
B
Ub
O
S
P
N
N
Ub
O
S
P
N
N
Ub
O
OH
pH:
7
7.5
8.0
8.5
7.0
7.5
8.0
8.5
8.0

Figure 1.4.5 Protein-small molecule ligations. (A) Reaction scheme of ubiquitin C-terminal phosphinothioester with an azido-biotin. (B) Immunoblot of Staudinger ligations with phosphinothiols **1** or **2** at varying pH's (α-biotin).

Figure 1.4.6 Ubiquitin-ubiquitin dimer formation via the Staudinger ligation.

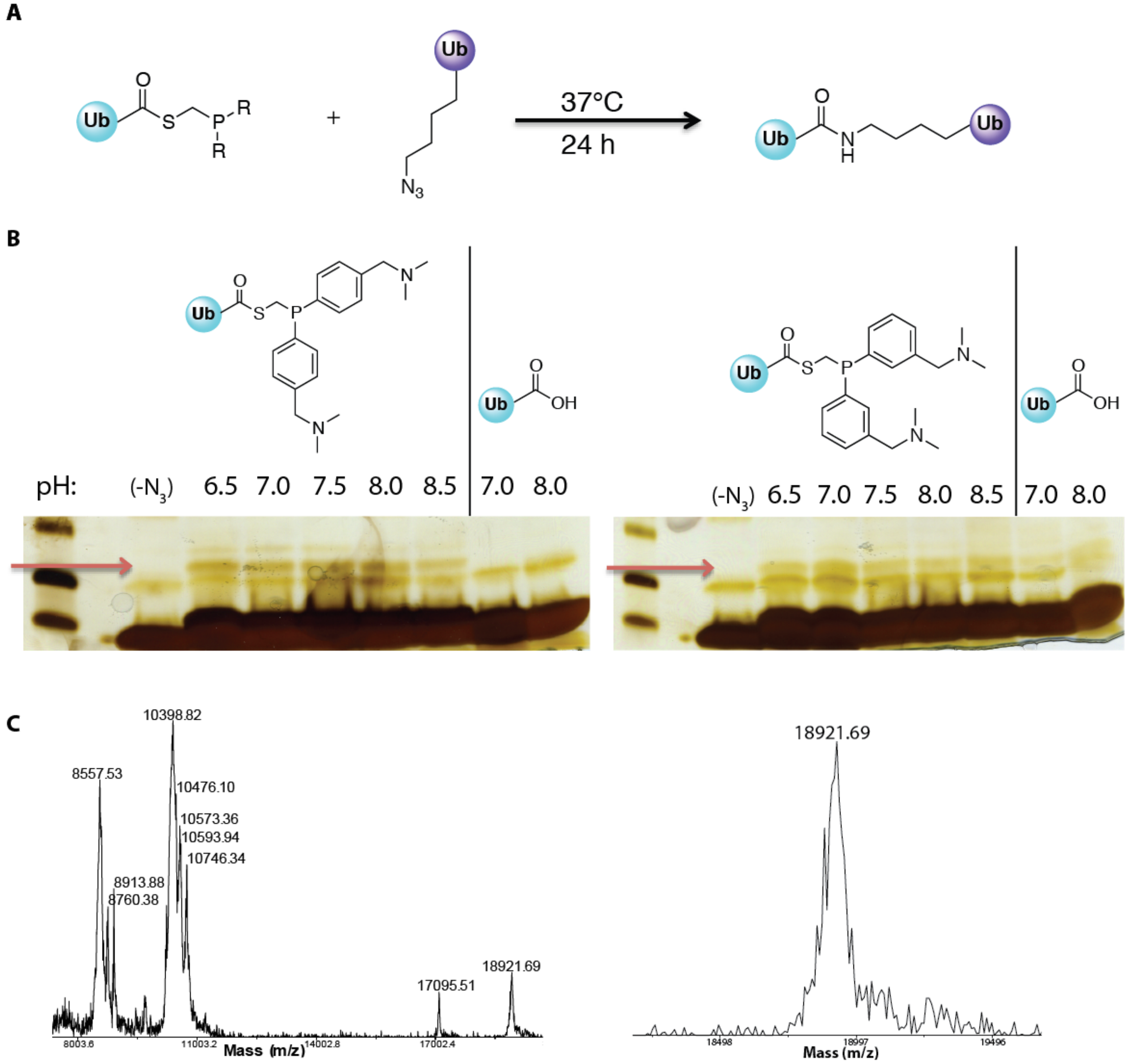
A
Ub
O
S
P
R
R
+
Ub
N3
37°C
24 h
Ub
O
N
H
Ub
B
Ub
O
S
P
N
N
Ub
O
OH
pH:
(-N3)
6.5
7.0
7.5
8.0
8.5
7.0
8.0
Ub
O
S
P
N
N
Ub
O
OH
(-N3)
6.5
7.0
7.5
8.0
8.5
7.0
8.0
C
10398.82
8557.53
10476.10
10573.36
10593.94
10746.34
8913.88
8760.38
18921.69
17095.51
8003.6
11003.2
Mass (m/z)
14002.8
17002.4
18921.69
18498
18997
Mass (m/z)
19496

Figure 1.4.6 Ubiquitin-ubiquitin dimer formation via the Staudinger ligation. (A) Reaction scheme for the formation of the ubiquitin-ubiquitin dimer. (B) Silver-stained SDS-PAGE of Staudinger ligations with the K63M variant at varying pH's, with phosphinothioesters of phosphinothiols **1**, or **2**, or no C-terminal phosphinothioester on the proximal ubiquitin. Red arrows represent the expected position of the ubiquitin-ubiquitin dimer product band. (C) MALDI-TOF data of a Staudinger ligation of the K63M variant with phosphinothioester **2** at pH 8.0.

1.4.5 NMR

^{1}H NMR (500 MHz, $CDCl_3$)

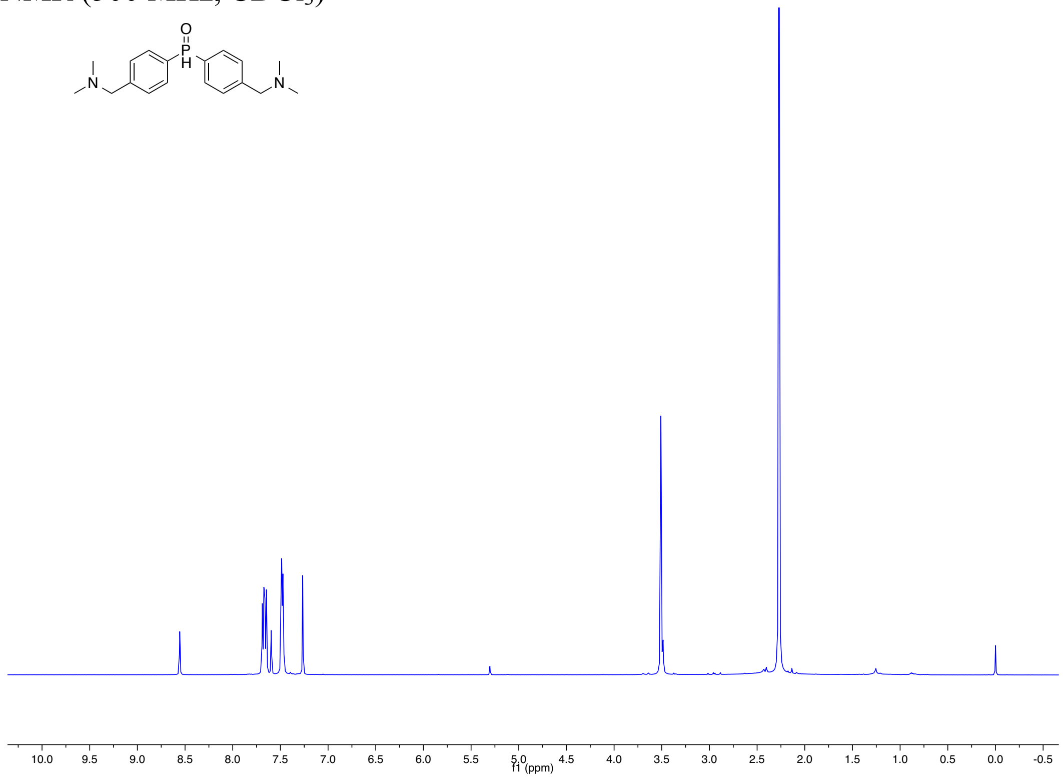

^{13}C NMR (126 MHz, $CDCl_3$)

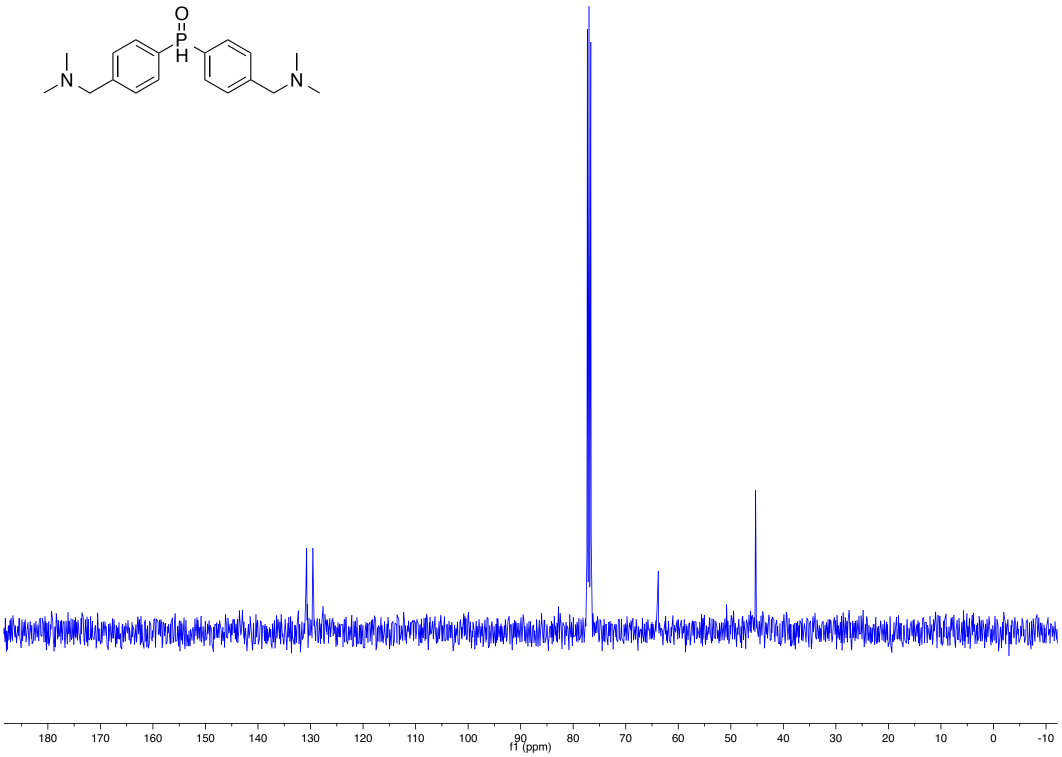

^{31}P NMR (400MHz, CDCl$_3$)

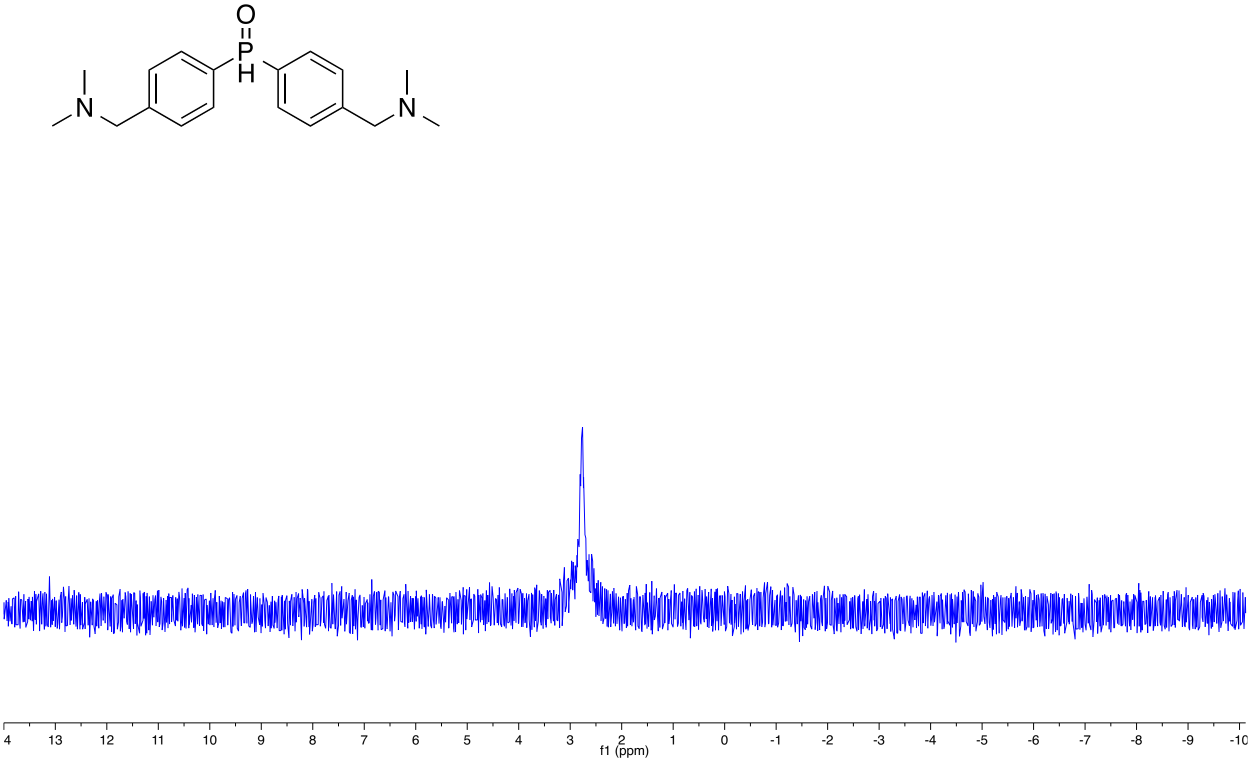

^{1}H NMR (500 MHz, CDCl$_3$)

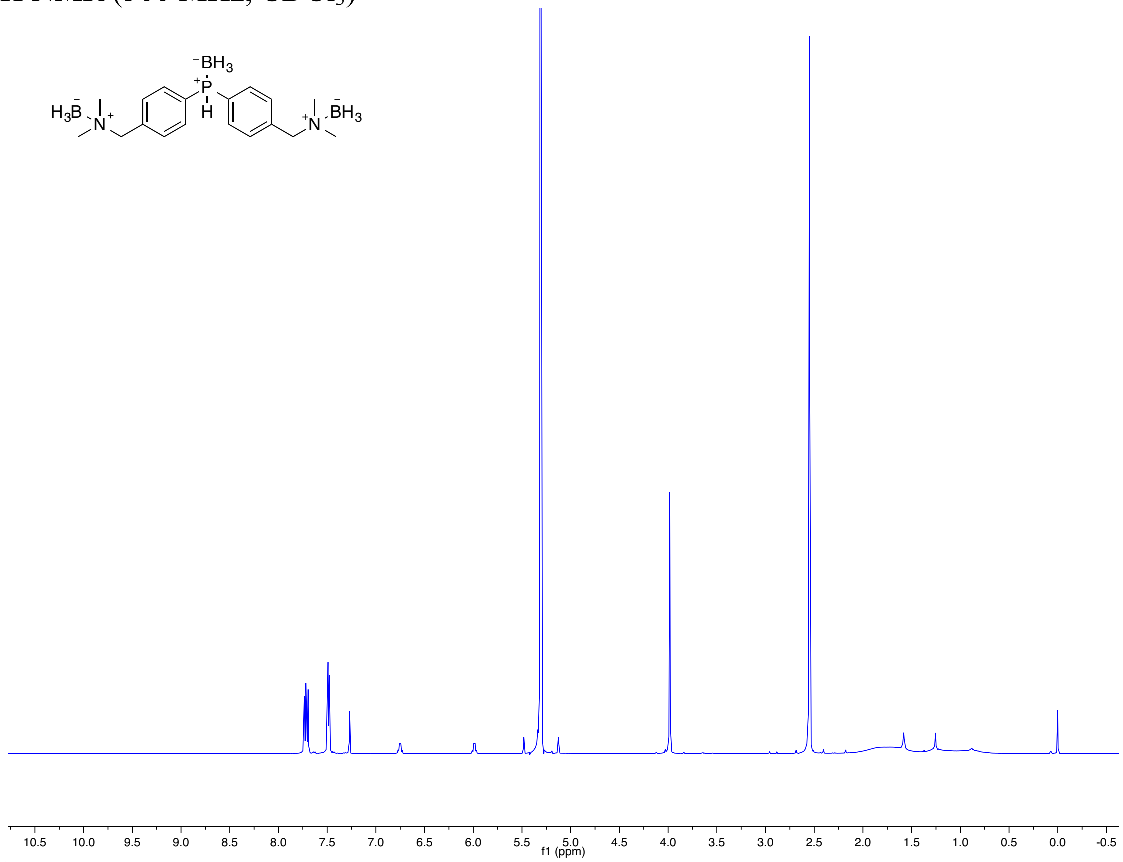

^{13}C NMR (126 MHz, CDCl$_3$)

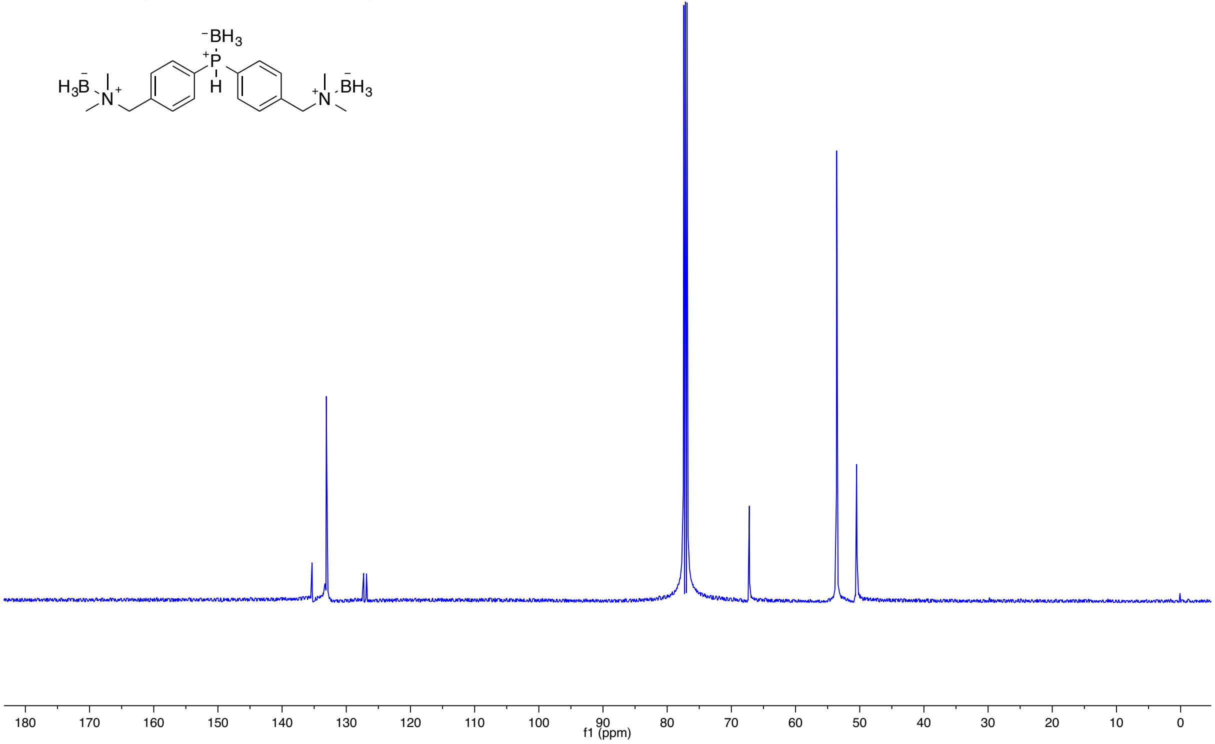

^{31}P NMR (400MHz, CDCl$_3$)

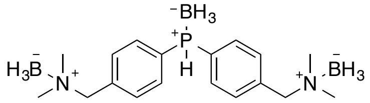

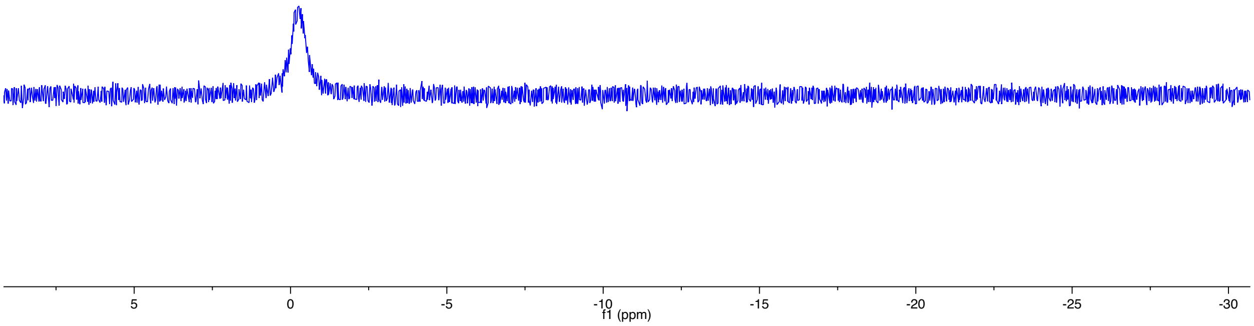

^{1}H NMR (500 MHz, $CDCl_3$)

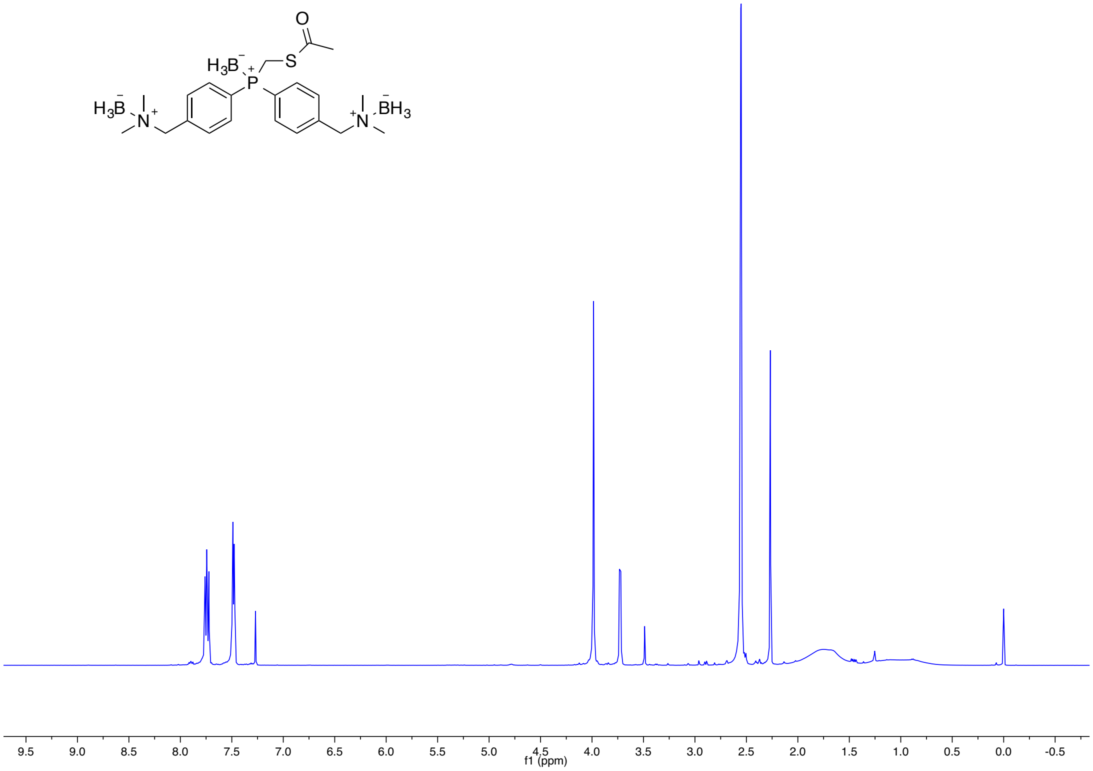

^{13}C NMR (126 MHz, $CDCl_3$)

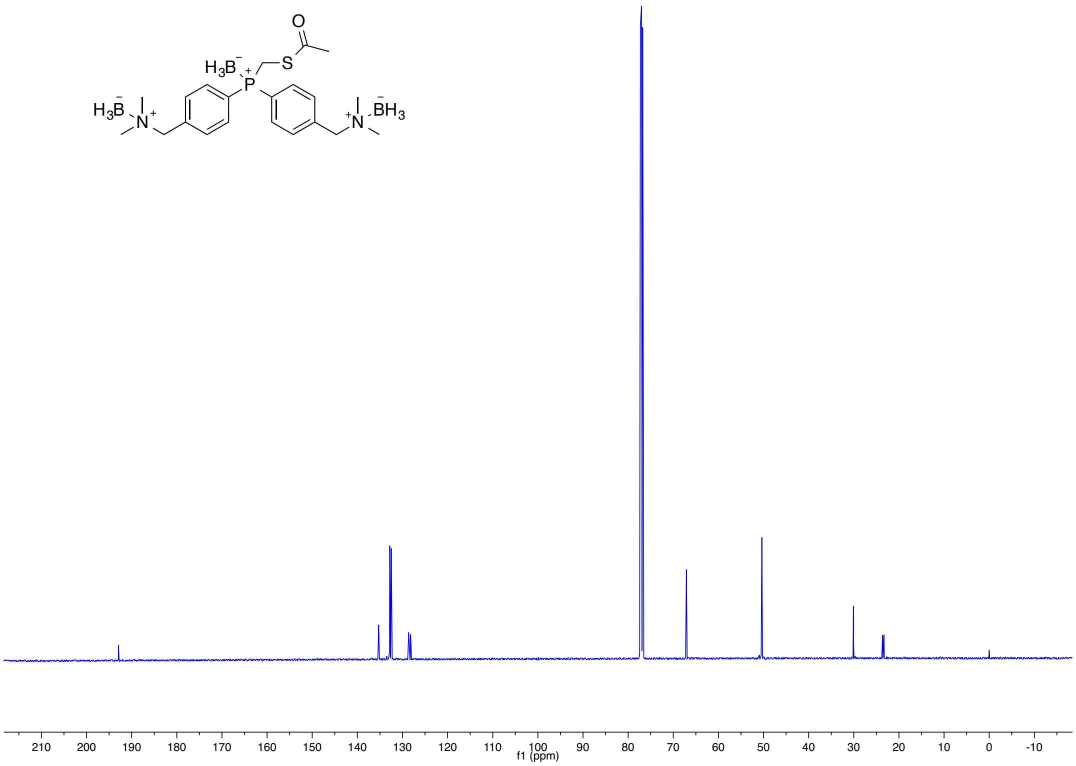

^{31}P NMR (202 MHz, CDCl$_3$)

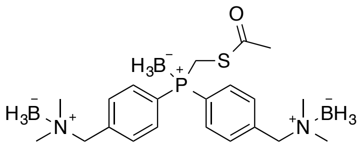
O
S
H3B
P
H3B
N
BH3
N

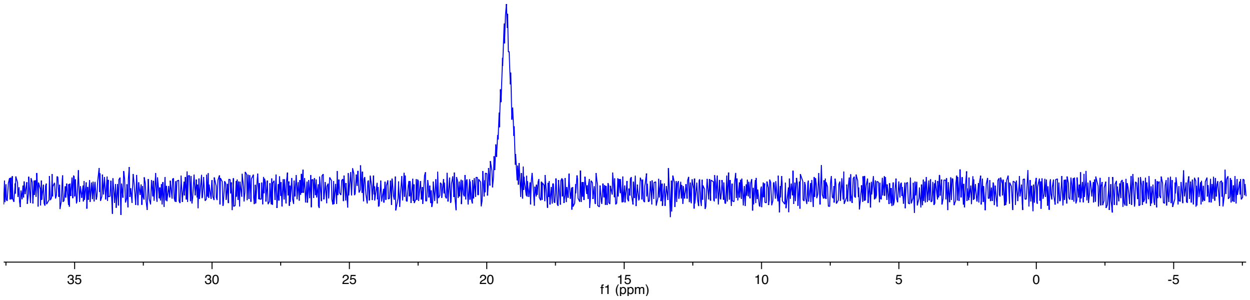

^{1}H NMR (500 MHz, CDCl$_3$)

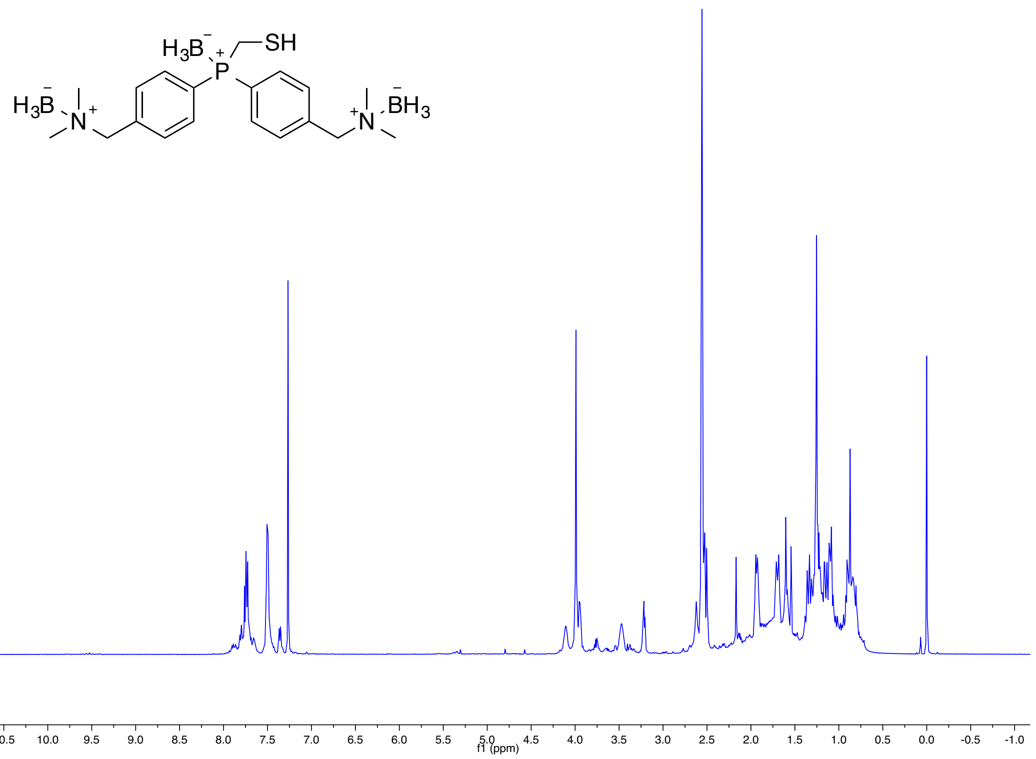

^{13}C NMR (126 MHz CDCl$_3$)

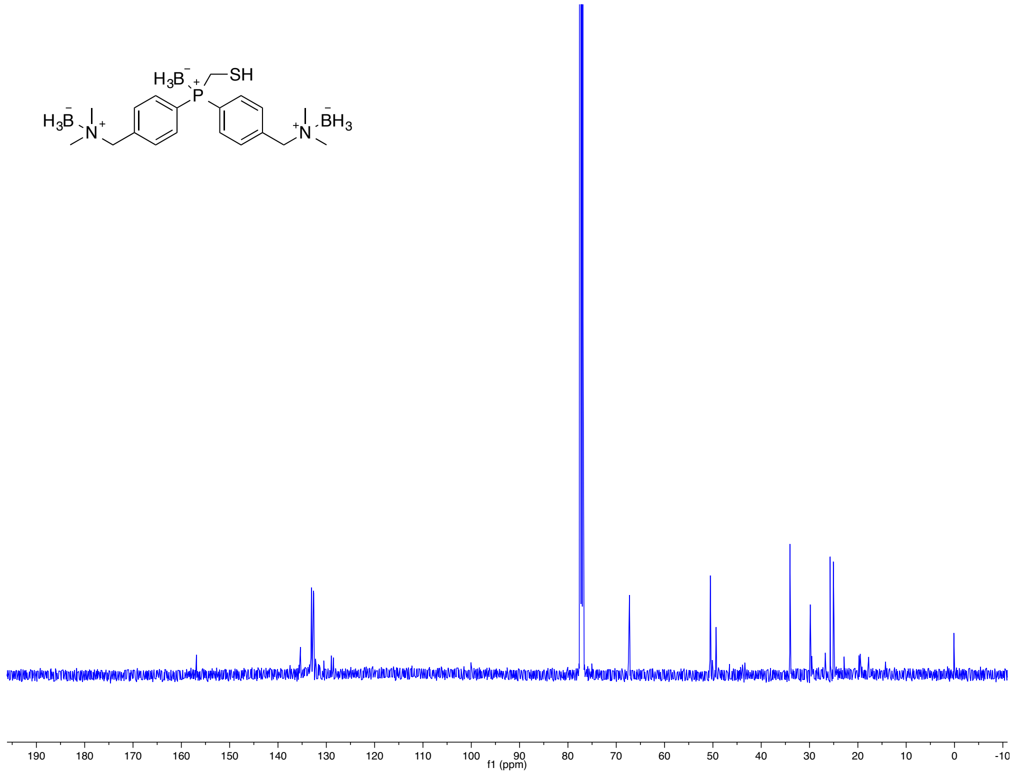

^{31}P NMR (162 MHz, $CDCl_3$)

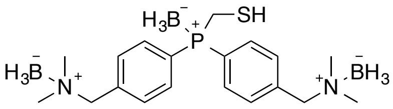

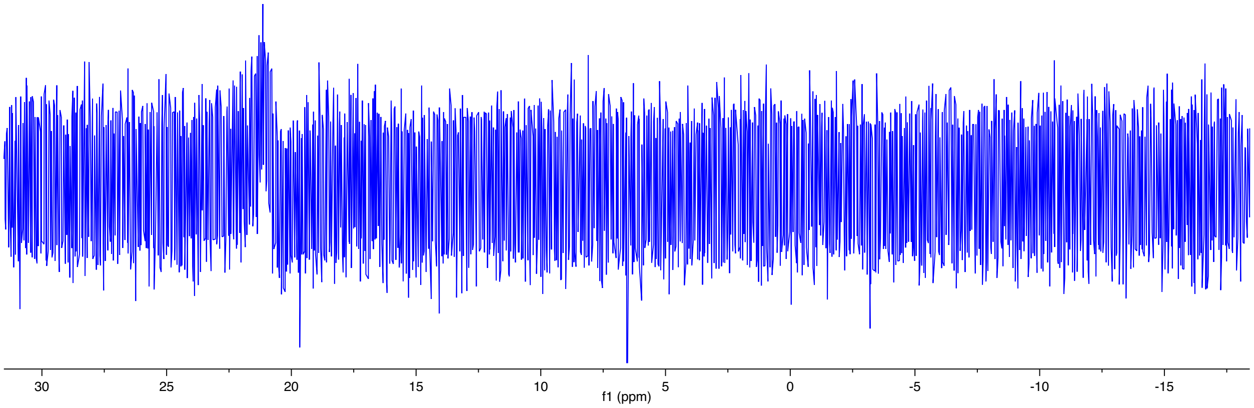

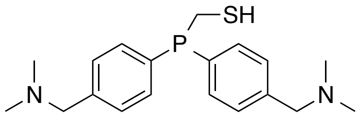

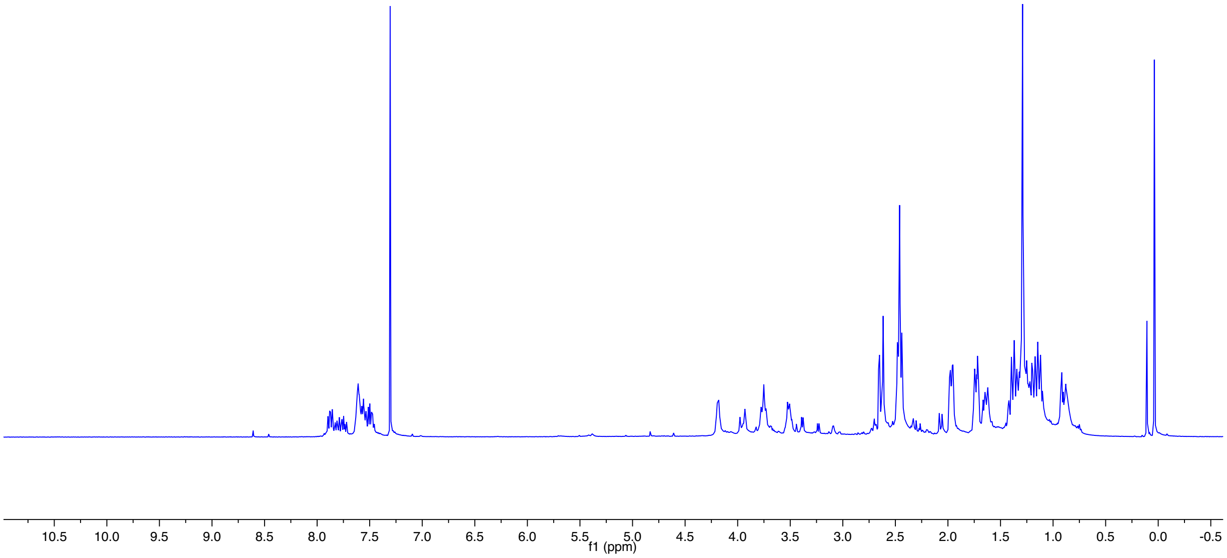

^{13}C NMR (126 MHz, CDCl$_3$)

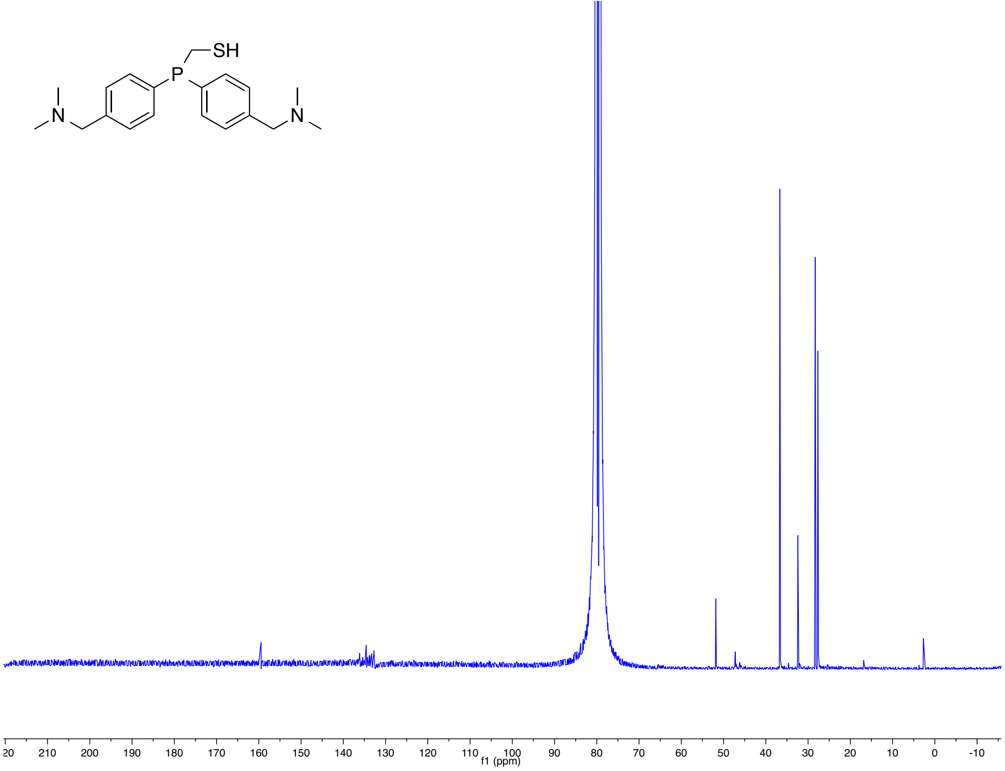

^{31}P NMR (162 MHz, CDCl$_3$)

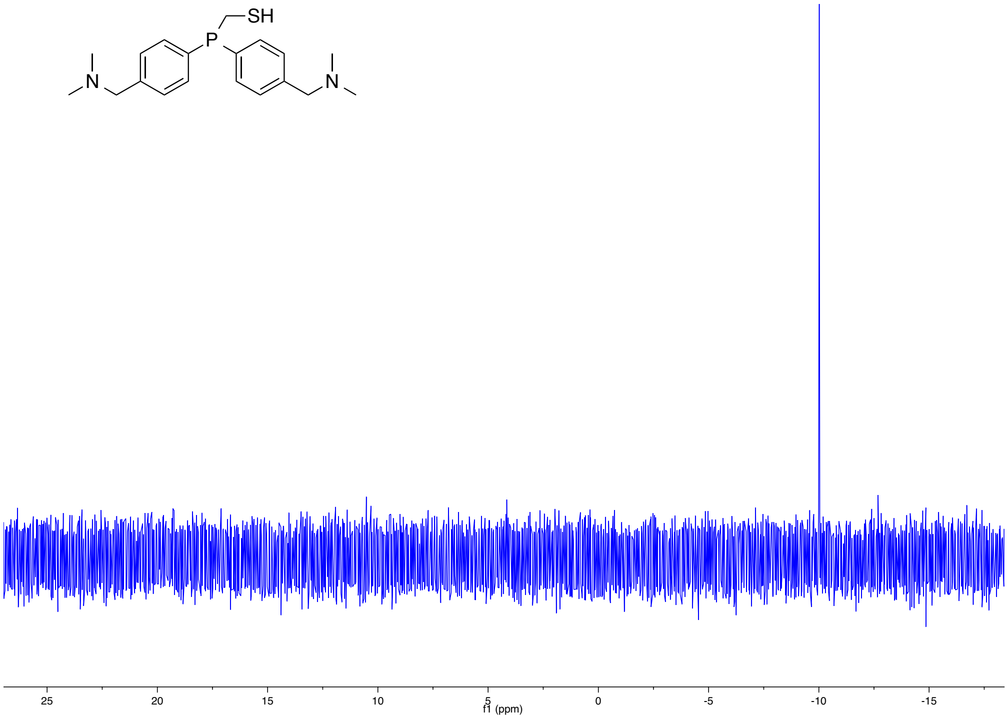

^{1}H NMR (400 MHz, CDCl$_3$)

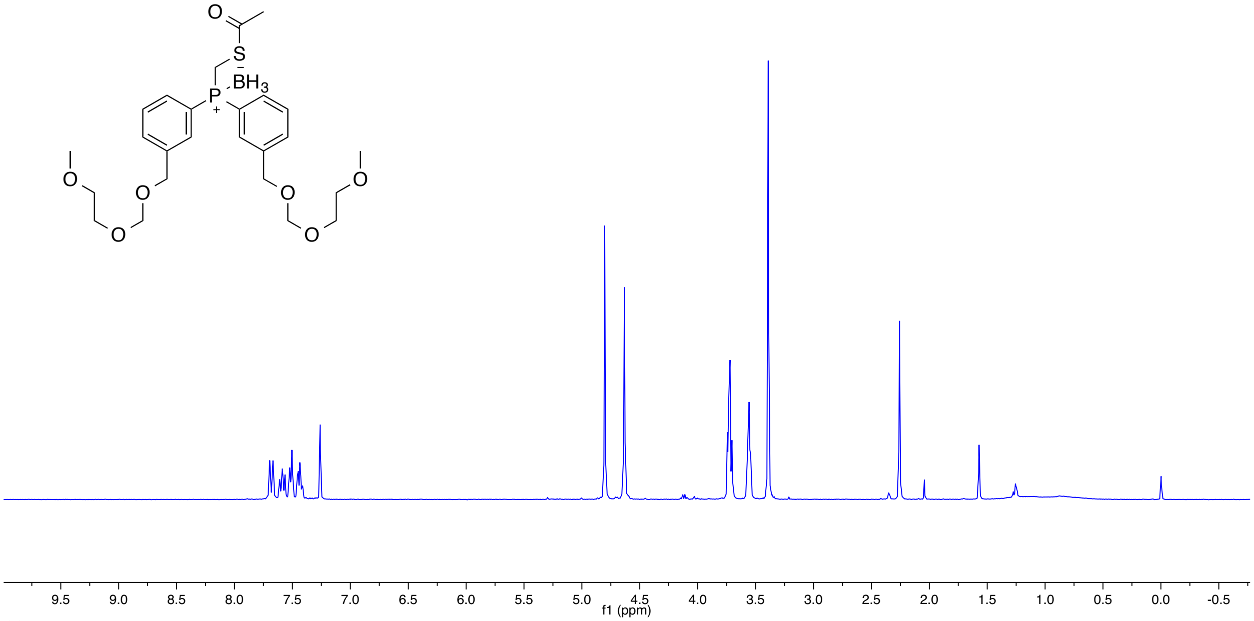

^{13}C NMR (126 MHz, CDCl$_3$)

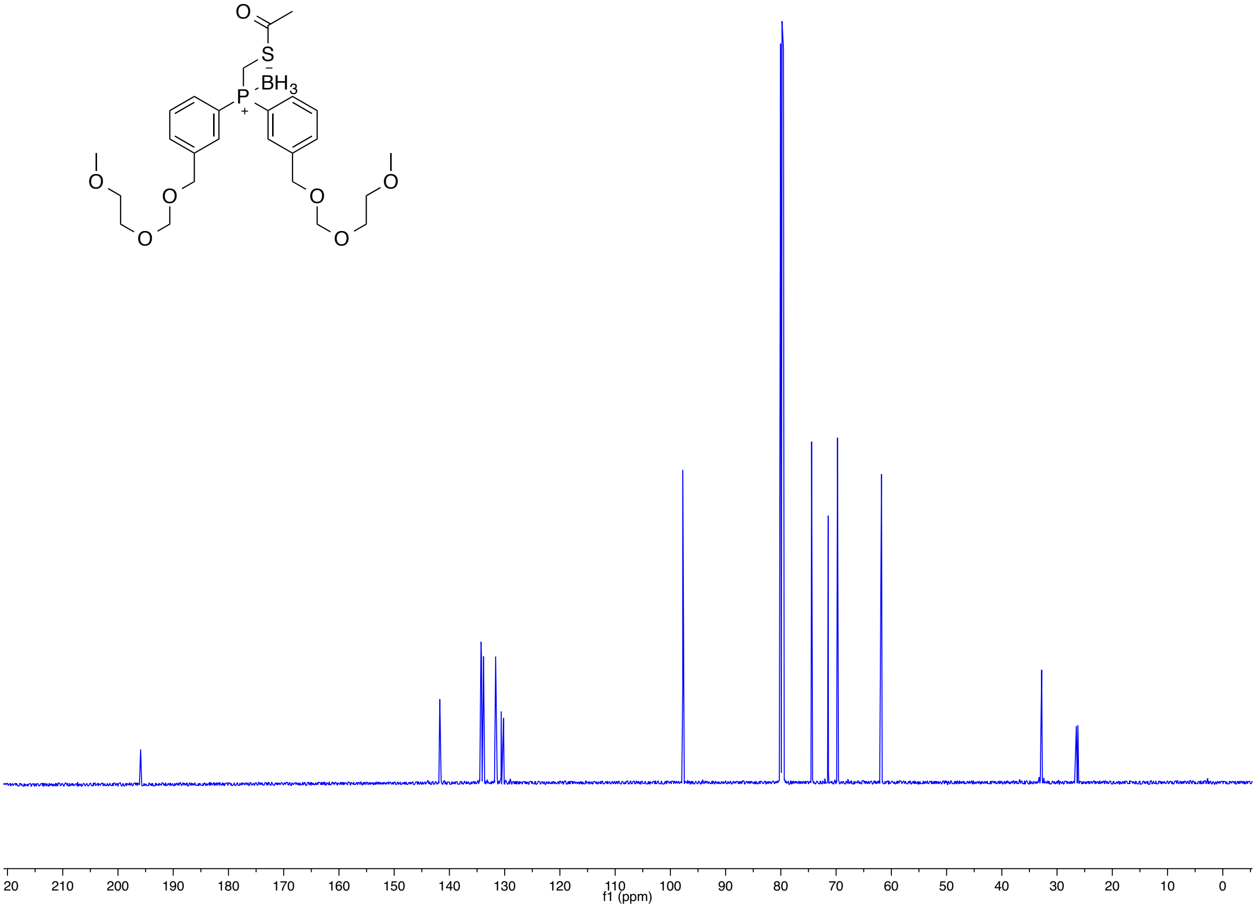

^{31}P NMR (162 MHz, CDCl$_3$)

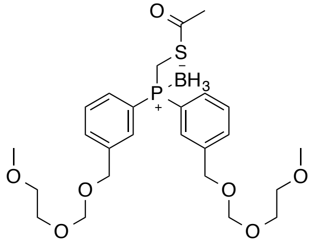
O
S
BH3
P
+
O
O
O
O
O
O

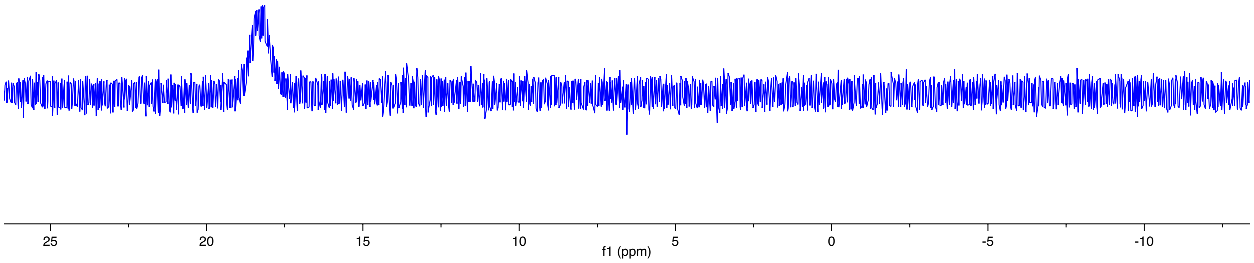

^{1}H NMR (400 MHz, CDCl$_3$)

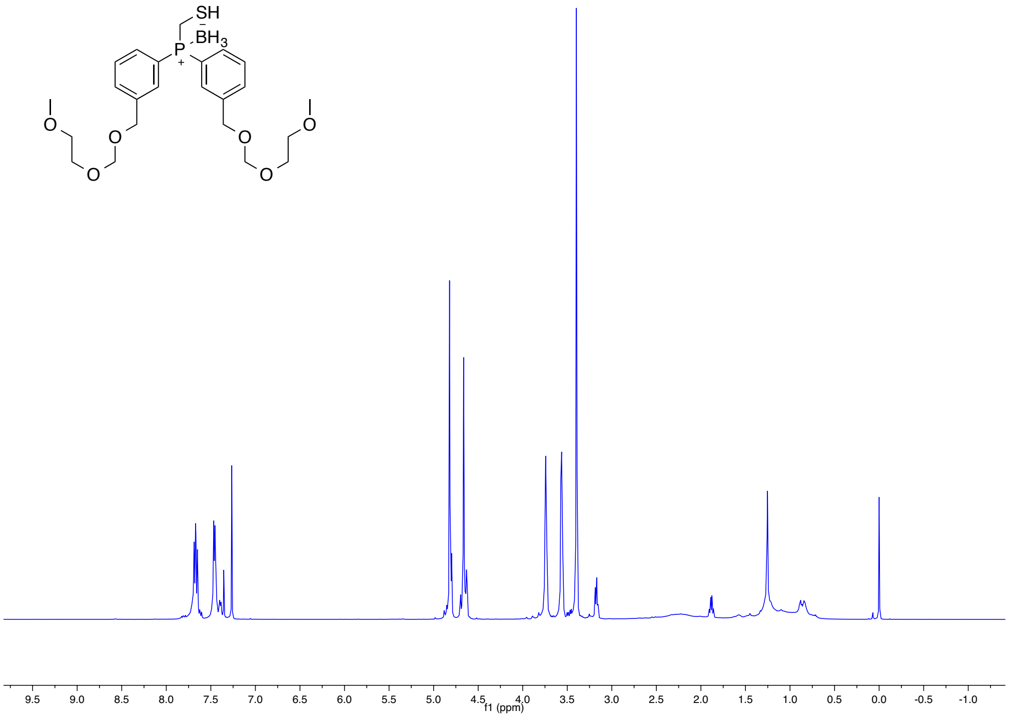

^{13}C NMR (126 MHz, CDCl$_3$)

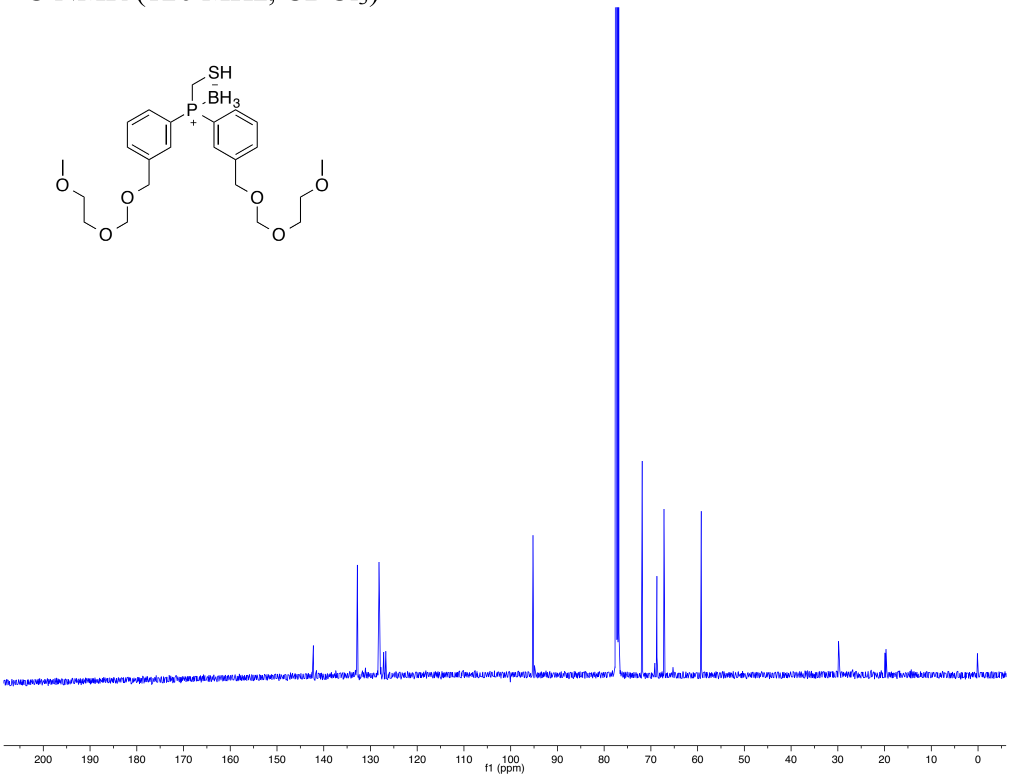

^{31}P NMR (162 MHz, $CDCl_3$)

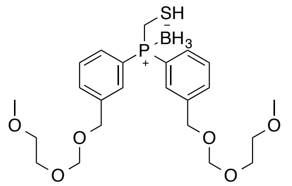
SH
BH3
P
+
O
O
O
O
O
O

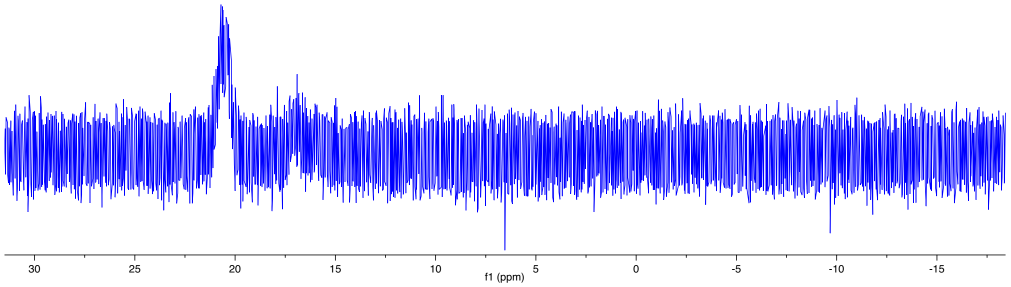

^{1}H NMR (400 MHz, CDCl$_3$)

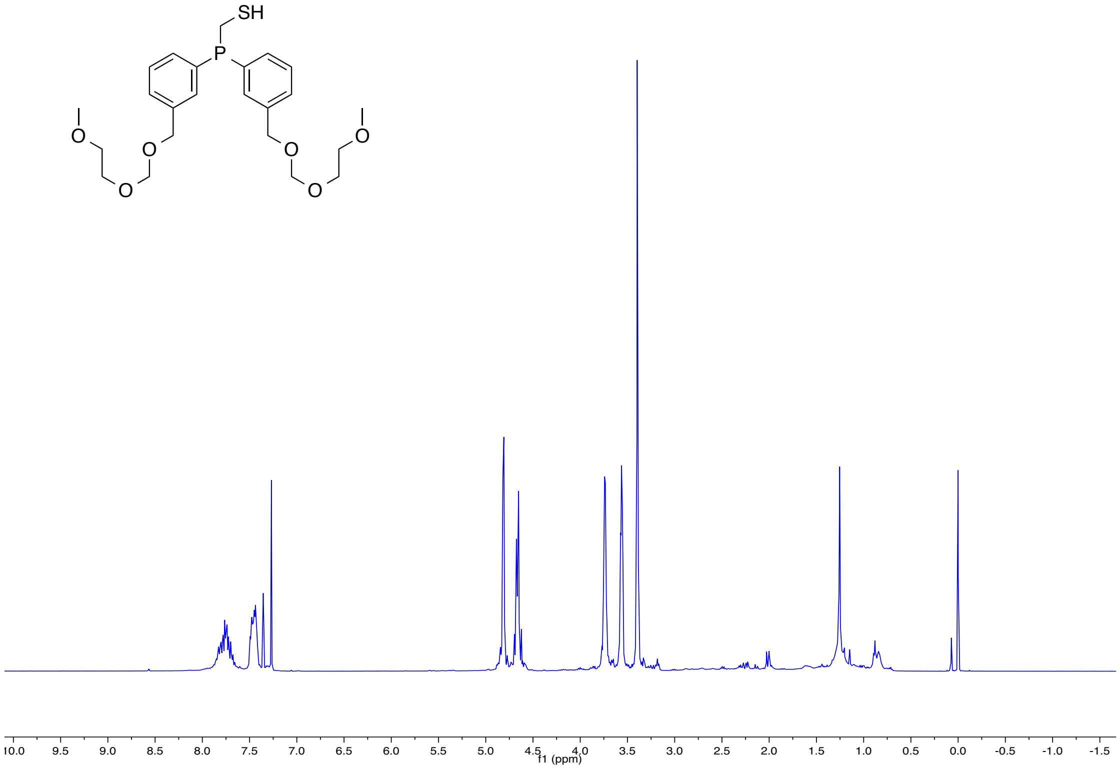

^{13}C NMR (126 MHz, CDCl$_3$)

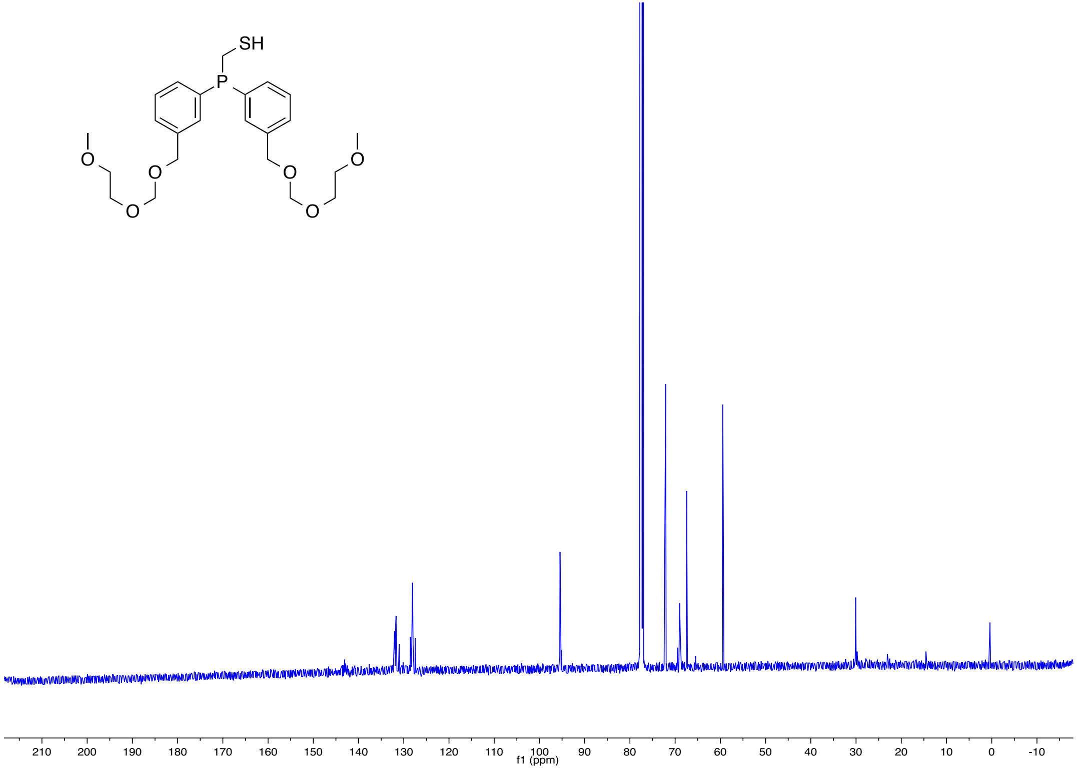

^{31}P NMR (162 MHz, CDCl$_3$)

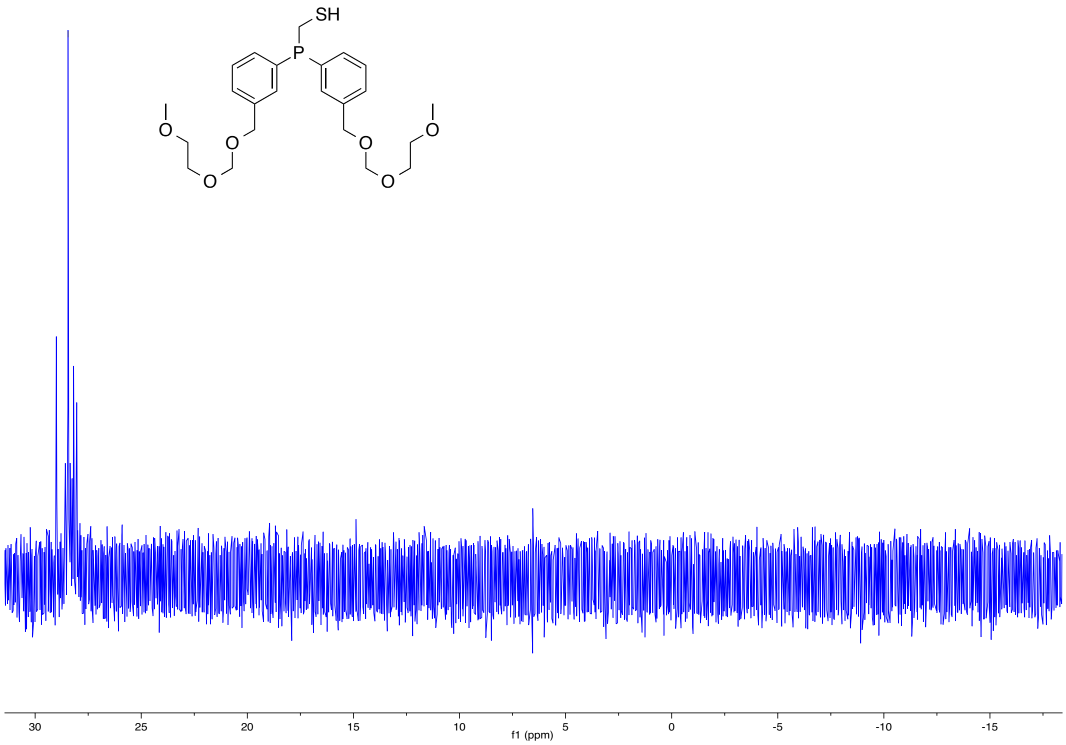

PART 2

CHAPTER 1

Introduction:

Protection and Detection of Boronic Acids

2.1.1 Introduction to Boronic Acids

The unique chemical characteristics of boronic acids provide chemical opportunities not available with other functional groups. Boronic acids are trivalent boron-containing compounds with two hydroxyl groups and a single carbon substituent. Structurally, the boronic acid is the boron-containing variation of a carboxylic acid; but unlike the carbon equivalent, it is not found in nature. Favorable characteristics stem from the unique electronic structure of boron. Because boron has six valence electrons, a vacant *p*-orbital remains on boron that is orthogonal to the three substituents, generating a trigonal planar geometry. The empty orbital on the Lewis acidic boron is of low energy. This empty orbital can accept electrons from another group such as a hydroxide ion. As a result, boronic acids exist in an equilibrium state between the neutral sp^2 and the anionic sp^3 hybridization when bound to another ligand. It is in large part due to this unique Lewis-acidity that boronic acids make such valuable reagents.

Boronic acids have significant chemical value because many derivatives are useful synthetic intermediates. Although the first isolation of a boronic acid was performed by Frankland in 1860 with the oxidation of ethylborane to ethylboronic acid,[224,225] synthetic chemistry did not fully recognize the value of these groups until the development and widespread adoption of the palladium-catalyzed Suzuki–Miyaura cross-coupling reaction for C–C bond formations[226]—work that shared the 2010 Nobel Prize for Chemistry.[227] Major synthetic transformations that apply boronic acids as reactants include the Suzuki–Miyaura cross-coupling reaction,[228] the Rh-catalyzed asymmetric conjugate addition to α,β-unsaturated carbonyl groups,[229] and the Chan–Lam Cu-mediated *N*-arylation reaction.[230] Boronic acids are generally considered to be green chemicals as they oxidize and degrade into boric acid, a boron derivative with the approximate toxicity of NaCl (Merck Index CAS 10043-35-3). The appeal of the boronic acid functional group for biologically-associated applications is due in part to the negligible toxicity of these compounds. This safety has resulted in the implementation of boronic acids as therapeutics, chemical biology tools and sensors, and drug-delivery vehicles.[231]

2.1.2 Synthetic Transformations of Boronic Acid Derivatives

The implementation of boronic acids into chemical biology and medicinal chemistry has created a need for methodological requirements that facilitate handling of these functional groups. Because early interest in boronic acids was for their intermediate value, less focus has been given to utilization of this valuable group when it is carried through synthetic transformations. When the boronic acid functional group is needed as part of the final synthetic target, one frequent strategy is to install the boronic functionality either very late or as the final step in the synthesis. The available methods for installation of an aryl or alkyl boronic acid generally create a carbon nucleophile and as a result require harsh conditions and/or metal catalysts that are incompatible with many common functional groups found on compounds intended for biological use, such as amines or hydroxyl groups. This lack of compatibility requires installing additional protecting groups, adding synthetic steps that lengthen syntheses and present additional compatibility considerations. Additionally, the polarity and potential charge of boronic acids can confound the isolation and purification of these molecules. Consequently, most of these endeavors progress through lengthy and difficult synthetic routes with characteristically poor recovery of intermediates and disappointing yields.

2.1.3 Protection of Boronic Acids with the Pinacol Group

Pinacol, or 2,3-dimethyl-2,3-butanediol, was the first molecule used commonly to protect boronic acids. The condensation of a boronic acid with pinacol produces a boronic pinacol ester with a relatively stable 5-membered ring centered at boron (Figure 2.1.2). The pinacol protection of a boronic acid provides multiple benefits. The boronic ester moiety facilitates handling and isolation of the boron-derivative as it eliminates hydrogen bonds, reducing polarity and increasing solubility in organic solvents. The pinacol ester provides another benefit by mitigating the reactivity of the Lewis-acidic boron through two effects. First, the four methyl groups on pinacol sterically shield the empty orbital on boron from the approach of nucleophiles. Secondly, the oxygen atoms of the pinacol ester provide electronic stability for the boron as the lone pairs of oxygen in boronic esters are more readily conjugated into the electron-deficient boron in part due to the σ-donating ability of carbon (Figure 2.1.2).[232] Ultimately, the pinacol ester serves as a protecting group because it diminishes the Lewis-acidity of the boron, making boronic esters less reactive than boronic acids.

2.1.4 Organotrifluoroborates as Surrogates for Boronic Acids

Although potassium organotrifluorborate salts ($R\text{-}BF_3^{-}K^{+}$) are not technically boronic acids, these compounds provide another approach to the facile usage and handling of boronic acids. These salts avoid much of the inherent instability of tricoordinate boron species. Although they were characterized first in 1960,[233] their general utility was not recognized until the widespread incorporation of boronic acid cross-coupling reactions into synthetic chemistry three decades later. Organotrifluoroborates have three fluorine substituents and are tetrahedral in geometry (Figure 2.1.3). As a result of the additional fluorine ligand bonded to boron, they are not Lewis-acidic like the parent boronic acid. Potassium organotrifluoroborate salts can be prepared easily from boronic acids by treatment with KHF_2. Following the reaction, it is easy to isolate the trifluoroborate salt by precipitation or crystallization from an organic solvent such as acetone after the insoluble KF salts are removed by filtration or Soxhlet extraction.[234] Typically, as the salts of potassium, most organotrifluoroborates are crystalline solids or powders. This crystallinity simplifies handling and storage. These compounds can be effectively analyzed for purity through multinuclear ^{19}F- and ^{11}B-NMR experiments, in addition to ^{1}H- and ^{13}C-NMR experiments.

Trifluoroborate derivatives have been applied for a surprising and impressive number of various chemical transformations without loss of the functional group.[235] Some examples include substitution reactions,[236] reductive aminations,[237] oxidations,[238,239] and 1,3-dipolar cycloadditions.[240] These derivatives also perform well as substrates in the Suzuki coupling reaction.[235,241] Organotrifluoroborates cannot be used for some applications as they are sensitive to hydrolysis or solvolysis, especially in the presence of fluorophiles such as silicon. Stirring the trifluoroborate salt in silica does, however, provide a simple and somewhat economical method for the deprotection and regeneration of the boronic acid. This deprotection method highlights the incompatibility of this protecting group with silica-gel chromatography and ultimately limits any purification to alternative methods.[242]

2.1.5 Diaminonaphthalene-Enabled Iterative Cross-Couplings of Boronic Acids

The first compound employed as a formal protecting group for boronic acids was diaminonaphthalene. Diaminonapthlalene (dan) is a napthalene derivative possessing two flagpole nitrogens in the 1 and 8 positions on the napthalene ring (Figure 2.1.3). Oddly, the complex of diaminonaphthalene with phenylboronic acid as well as an iteration with anthranillamide[243] were first reported as potential chemosterilants for the common housefly.[244] The ligand is installed by refluxing diaminonaphthalene with a boronic acid under conditions for the azeotropic removal of water. This installation involves refluxing toluene with a connected Dean–Stark apparatus to remove the two equivalents of water formed (Figure 2.1.4). The boron–diaminonaphthalene [B(dan)] complex uses the "flagpole" nitrogens of the naphthalene to form a six-membered ring centered on boron. This protecting group complex is more stable than pinacol boranes, in part due to the inherent strength of the boron–nitrogen bond. Additionally, the free lone-pair electrons on nitrogen can delocalize into the vacant orbital on the boron center with enough effect to shield the otherwise Lewis-acidic boron from nucleophilic attack. Lastly, the relatively high pK_a of the N-bound protons makes this complex stable to most bases.

Dan-protected boronic acids can survive some synthetic transformations but were primarily developed for iterative cross-coupling reactions. In this method, one coupling reaction can be performed at another location on the B(dan) protected compound; then, the diaminonaphthalene can be removed and the deprotected boronic acid can participate in a second cross-coupling sequence.[245-248] The increased stability of the B(dan) complex over the pinacol boron has been demonstrated by the selective Suzuki reaction of the pinacol borane on a differentially protected diboron compound presenting both functionalities.[249] The –B(dan) complex can be deprotected to unmask the boronic acid through an extended reaction of 24–48 h with aqueous acid that cleaves the group through protonation of the nitrogens and subsequent hydrolysis.[245]

2.1.6 Multistep Transformations with MIDA Boronic Acids

The most recently developed protecting group for boronic acids employs multiple effects to mitigate the reactivity of boron. This strategy utilizes the commercially available trivalent ligand methyliminodiacetic acid (MIDA) to create a tetracoordinate boron species from two bonds to carboxylate oxygens and a single bond to a tertiary nitrogen (Figure 2.1.5). The two carboxylate oxygens on MIDA replace the hydroxyls of the boronic acid, and the tertiary amine occupies the site of the *p*-orbital, otherwise vacant in tricoordinate boron species. The dative N–B bond is atypically long and permits the otherwise strained bicyclic arrangement. Because the nitrogen is tertiary, the formation of this fourth bond with both atoms creates a charge-neutral complex between the two opposing formal charges on boron and nitrogen (Figure 2.1.5). The MIDA-protected boronate is typically a crystalline solid that is air and temperature-stable, and can be purified through silica-gel chromatography.[250]

The stability conferred by MIDA-boronates allows for a significant number of synthetic transformations on distal functional groups without disruption or degradation of the boron functionality. Although originally developed to create a bench- and air-stable boron reagent that could be applied for iterative cross-couplings, MIDA-boronates are resistant to anhydrous base but can be very rapidly deprotected with mildly basic aqueous conditions, likely through a saponification process.[251] MIDA-boronates require specialized conditions for the Suzuki reaction such as a phosphate base and anhydrous solvent, but because of the speed and efficiency of deprotection, they are more amenable to iterative cross-coupling reactions which can be performed by "slow-release" of the unmasked boronic acid.[250] These features of MIDA allow for boron-containing products to be carried through a number of different transformations, including several oxidations, reductive aminations, and Horner-Wadsworth-Emmons and Takai olefinations, in addition to cross-coupling chemistry.[252] The strategy of MIDA protection was extended to effect stereochemical control—the *N*-methyl group on MIDA was substituted to a chiral ligand to form PIDA, a pinene-iminodiacetic acid derivative for stereoselective synthesis and subsequent iterative cross coupling.[253] Although MIDA-boronates allow for a significant improvement in the handling and versatility of boronic acids, they are incompatible with DIBAL, TBAF, $LiAlH_4$, and metal alkoxides.[252]

2.1.7 Benzoxaborole

Among all boronic acids, the Raines laboratory has been interested principally in the benzoxoaborole derivative. This special boronic acid was first synthesized by Torssell in 1957[254] but the widely accepted value of this compound occurred with the discovery by Hall and coworkers that benzoxaborole binds strongly to diols—in particular those found on carbohydrates.[255] This sugar-binding affinity is much higher than that of other boronic acids because of the strain imparted through the annulated 5-memberd oxaborole ring.[256] Under physiological conditions this effect results in a notable pK_a difference; phenylboronic acid has a pK_a of 8.7 whereas benzoxaborole has a pK_a of 7.3.[257] Although new benzoxaboroles have been reported only in the last few years, this functional group has been used for a tremendous number of biologically-relevant applications that take advantage of its high water solubility and very low toxicity. This work has been outlined thoroughly in recent reviews.[258,259] Some examples of benzoxaborole versatility include applications as β-lactamase inhibitors,[260] antibacterial agents,[261] antivirals specifically for hepatitis C,[262-264] and even anti-inflammatory therapeutics.[265,266] The Raines group has also shown benzoxaborole to be a useful drug-delivery agent for protein internalization owing to interactions between the boronic acid and cell-surface glycans.[267] Additionally, one benzoxaborole, Tavaborole®, is a recently FDA-approved treatment as a topical solution for onychomycosis.[268]

2.1.8 A Protecting Group for Benzoxaborole

While the described protecting group strategies have all contributed greatly to the advancement of chemical pursuits employing boronic acids, none of these approaches can be applied for the most potent boron-containing pharmacophore, benzoxaborole. The biologically directed pursuits of the Raines laboratory involve applications of this unusual boronic acid, but there remains a lack of developed methodology for the synthetic manipulation of this scaffold. For benzoxaborole, the annulated 5-membered oxaborole ring and internal boronic ester is remarkably stable. This makes this group incompatible with trivalent ligands that protect other boronic acids.

Taking inspiration from the approaches applied successfully for boronic acids, I prepared and developed a divalent protecting group for benzoxaborole (Figure 2.1.4). This work is the focus of Chapter 2 of Part 2. The compound is derived from Proton Sponge® and combines the divalent coordination of diaminonaphthalene with the charge neutrality of MIDA in the form of the tertiary amine of 1-dimethylamino-8-methylaminonaphthalene. Following coordination with benzoxaborole, the protected complex is fluorescent. This fluorescence aids in tracking products through synthetic transformations during thin-layer TLC as well as silica-gel chromatography. The new protecting group is highly stable under extremely basic conditions as it lacks any acidic protons, and the occupancy of the otherwise empty *p*-orbital on the benzoxaborole boron atom upon quaternization shields the boron from nucleophilic attack. I applied this novel protection strategy to a variety of benzoxaboroles that include other pendant functional groups such as amines, benzyl ethers, hydroxyl groups, and esters (Figure 2.1.4). Following protection of the benzoxaborole moiety, these compounds were subjected to a number of synthetic transformations that would not be possible without the protecting group on boron. I performed reactions on distal functional groups including amide couplings, protections and deprotections, Suzuki–Miyaura cross-couplings, and Buchwald-aminations. The boron-protecting group is removed by aqueous acid, but is stable to anhydrous acid. This strategy expands the chemical scope of benzoxaboroles, as very few derivatives are known and even fewer are available commercially. With this new technology, future advancements are enabled for this special boronic acid.

2.1.9 Boron-Specific Sensing and Recognition

Fluorescent indicators, imaging, and spectroscopy are arguably the most critical tools for the translation of chemical information, such as the presence and concentration of some compound of interest into a measurable analytical output. Boron and boronic acids have played a substantial role in the development of many fluorescent sensors. Boron sensing first originated for the analysis of boron levels in soil and water samples,[269-271] but widespread application of boron in sensing and sensors arose only after the development of boron-based fluorophores and the recognition of boronic-acid based assays for saccharide detection.[272]

2.1.10 Boron-Based Fluorophores

The dipyrrole-based boron fluorophores represent a successful and widely used class of fluorescent dyes for biological labeling. Those based on 4,4-difluoro-4-bora-3*a*,4*a*-diaza-*s*-indacene, commonly known as BODIPY,[273] possess many desirable attributes, including photo- and chemical stability, high molar absorption coefficients (ε) and fluorescence quantum yields (Φ), narrow emission bands with good intensity, excellent solubility, and excitation and emission frequencies within the visible spectrum.[274] Due to its high hydrophobicity and neutral charge, BODIPY can diffuse through the cellular membrane, and modifications to the dipyrrole scaffold have afforded derivatives that can be targeted intracellularly to various organelles, the cytosol, and mitochondria. Additionally, many derivatives exist for tagging of biomolecules such as proteins. As a result, various types of BODIPY dyes have been developed for fluorescence imaging within living systems, and several are commercially available.[275]

2.1.11 Boron-Sensing Chromophores

Boron-based sensors and indicators have gained popularity as a result of applications that apply competitive binding assays with boron to determine concentration of an analyte. The most common type of assay involves the 1,2-diol containing alizarin red-S (ARS) and a boronic acid with which reversible conjugate formation can occur. In complexation with a boronic acid, a notable red to orange hypsochromic shift is observed as compared to free ARS.[272] Upon exposure to an analyte that can bind the boronic acid, such as a saccharide, the ARS is displaced and the color change can be used to determine saccharide concentration.[276]

Curcumin, the principle curcuminoid found in the spice turmeric, also functions as a colorimetric indicator for boron. Curcumin possesses a 1,3-diketone moiety in the center of an extended, conjugated π-system. The 1,3-diketone undergoes keto–enol tautomerization and as a result, curcumin effectively chelates boron to generate a bathochromic spectral shift from the turmeric orange to red. A 2:1 complex of two curcumin molecules with one boric acid is known as rosocyanine, and the red absorbance maximum at 540 nm is used for quantification of boron.

2.1.12 Boron-Sensing Fluorophores

The widespread utilization of boronic acids through synthetic chemistry has necessitated techniques that facilitate their application. The *in situ* observation and monitoring of boronic acids by fluorescence represents a newer use for boron-sensors. Buchwald and coworkers demonstrated that a fluorescent sensor can be used as a means to assess the state of boronic acids readily in a given reaction. Their method employs a dihydroxy coumarin fluorophore that can bind to boronic acids without interfering with the cross-coupling reaction.[277] The complex created upon binding a boronic acid initiates a visible increase in fluorescence intensity when illuminated with a common long-wavelength handheld UV lamp (365 nm) relative to the unbound coumarin. This visible change upon complex formation allows for the qualitative determination of reaction progress through the consumption of the boronic acid reactant.

2.1.13 Determination of Boron with ESIPT Fluorescence

To ameliorate the challenges presented in assessing and monitoring boronic acids during synthetic transformations, I pursued a simple strategy for the detection of boron and boronic acids. The results of this work comprise Chapter 3 of Part 2. A method that facilitates the detection of boronic acids needs to be very sensitive, but must also apply simple and rapid techniques common to the organic chemistry laboratory. In organic chemistry, the simplest and most frequently applied method to monitor reaction progress and reagent purity is thin-layer chromatography. The divalent protecting group of Chapter 2 of Part 2 forms a fluorescent complex with a protected benzoxaborole. During synthetic transformations of the protected benzoxaborole compounds, its bright fluorescence confers a significant advantage. The development of a boron-specific TLC-stain provides this same advantage to all boronic acids.

10-Hydroxybenzo[*h*]quinolone (HBQ) is a molecule that rapidly forms a complex with the benzoxaborole moiety to produce a very bright fluorescent adduct. I applied HBQ as a boron-specific indicator for TLC and materials applications as outlined in Chapter 3 of Part 2. HBQ is a known excited-state intramolecular proton transfer fluorophore (ESIPT) that is excited at 365 nm but has an emission wavelength ~600 nm (Figure 2.1.5). In complexation with a boronic acid, ESIPT is interrupted for HBQ, and the shorter, brighter emission is observed.

2.1.14 Conclusions

Part 2 of this thesis details the establishment of two novel tools to facilitate the application and development of boronic acids for chemical biology. The second chapter includes a robust protecting group for benzoxaborole—the most widely employed oxaborole in medicinal chemistry and a valuable functional derivative of boronic acid with great potential in drug delivery. The third chapter in this second part also includes the establishment of a novel method for the detection of boron and boron-containing compounds based on interruption of the ESIPT photophysical process. This method is readily applicable with TLC methods, and can also provide quantitative information regarding boron concentration. My hope is that these advances become utilized widely and enable future endeavors for this field.

Figure 2.1.1 Boron-variations utilized in organic chemistry are sorted by oxidation state.

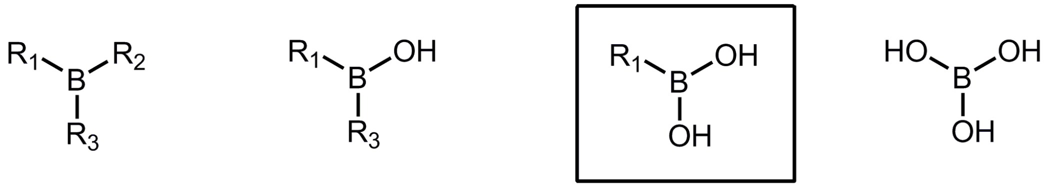
R1
R2
B
R3
R1
OH
B
R3
R1
OH
B
OH
HO
OH
B
OH

borane borinic acid boronic acid boric acid

Figure 2.1.1 Boron-variations utilized in organic chemistry are sorted by oxidation state.

2.1.2 Protection of a boronic acid with pinacol generates a boronic ester.

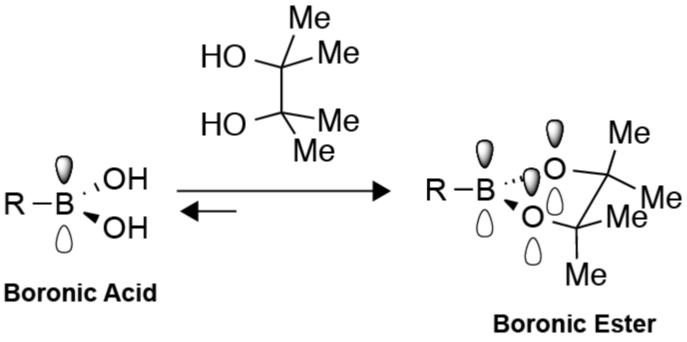
Me
HO
Me
HO
Me
Me
R
B
OH
OH
Boronic Acid
R
B
O
O
Me
Me
Me
Me
Boronic Ester

Figure 2.1.2 Protection of a boronic acid with pinacol generates a boronic ester.

Figure 2.1.3 Common protecting group strategies for boronic acids

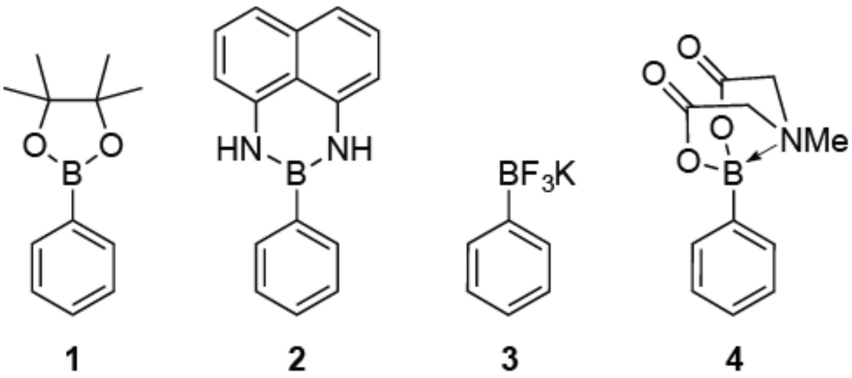
O
B
O
HN
B
NH
BF3K
O
O
O
O
B
NMe
1
2
3
4

Figure 2.1.3 Common protecting group strategies for boronic acids: (**1**) pinacol-borane, (**2**) borane-diaminonaphthalene complex B(dan), (**3**) potassium trifluoroborate salt, (**4**) MIDA boronate.

Figure 2.1.4 Applications of benzoxaborole in medicinal chemistry and chemical biology.

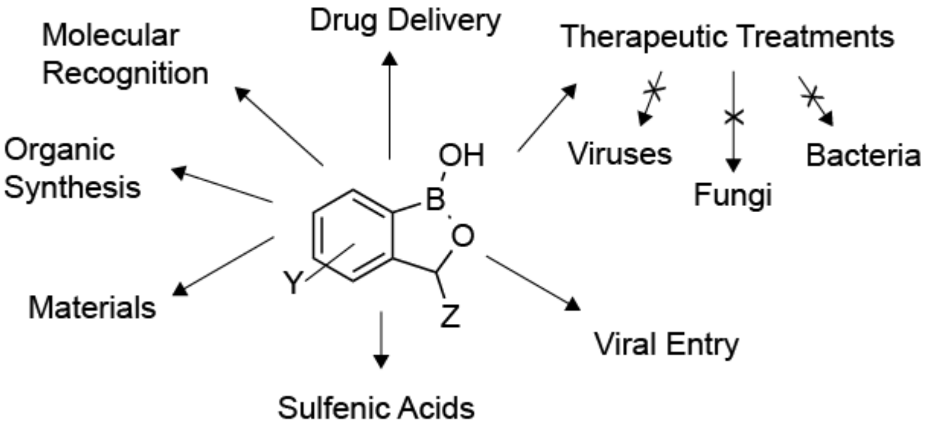
Molecular Recognition
Drug Delivery
Therapeutic Treatments
Organic Synthesis
OH
B
O
Y
Z
Viruses
Fungi
Bacteria
Materials
Viral Entry
Sulfenic Acids

Figure 2.1.4 Applications of benzoxaborole in medicinal chemistry and chemical biology. Adapted from ref. [258].

Figure 2.1.5 The protecting group derived from Proton Sponge® facilitates synthetic manipulation of compounds containing the benzoxaborole moiety.

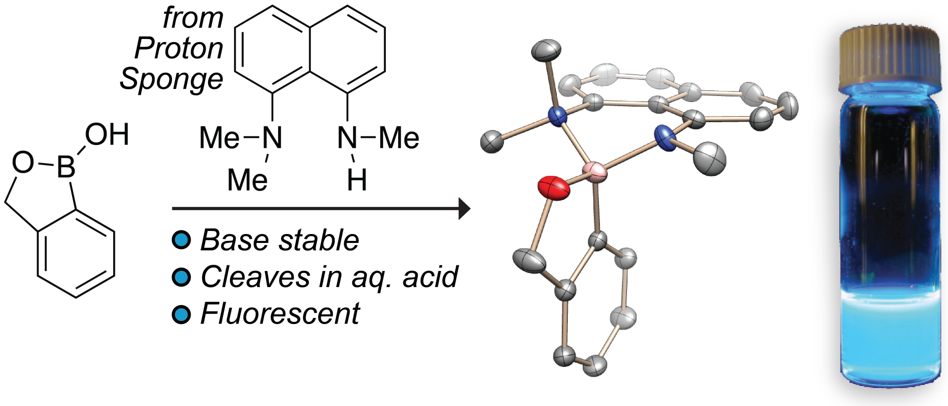
from
Proton
Sponge
OH
O–B
Me–N
Me
N–Me
H
Base stable
Cleaves in aq. acid
Fluorescent

Figure 2.1.5 The protecting group derived from Proton Sponge® facilitates synthetic manipulation of compounds containing the benzoxaborole moiety.

Figure 2.1.6 The boron-interrupted emission of HBQ is ~200 nm shorter than the typically predominating ESIPT emission.

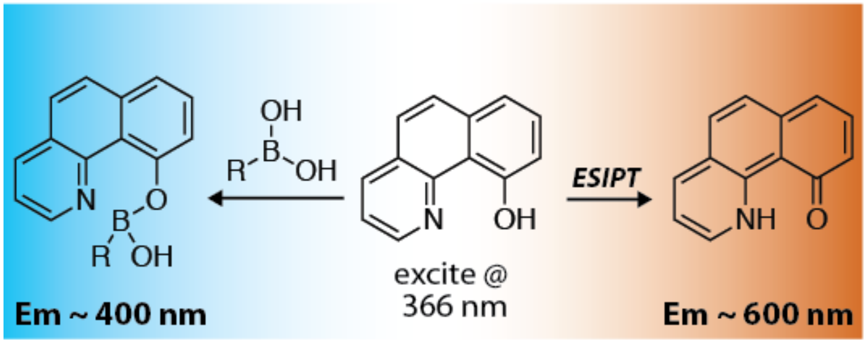
OH
R
B
OH
N
O
B
R
OH
Em ~ 400 nm
N
OH
excite @
366 nm
ESIPT
NH
O
Em ~ 600 nm

Figure 2.1.6 The boron-interrupted emission of HBQ is ~200 nm shorter than the typically predominating ESIPT emission. This shift generates a clearly visible color change that indicates the presence of boron-containing compounds.

PART 2

CHAPTER 2

A Divalent Protecting Group for Benzoxaboroles

Contributions: I synthesized the Proton Sponge derived protecting group, benzoxaborole derivatives, performed the base-stability and acidic deprotection assays, and the synthetic transformations. Brett VanVeller and I cowrote the manuscript.

Note: The following chapter was published in part as Brett VanVeller, Matthew R. Aronoff, and Ronald T. Raines (2013). *RSC Advances 3*, 21331–21333.

This work also appears in the following patent: Protecting Groups for Boronic Acids P130142US01 Raines, R. T.; VanVeller, B.; Aronoff, M. R.

Abstract

1-Dimethylamino-8-methylaminonaphthalene is put forth as a protecting group for benzoxaboroles. The ensuing complex is fluorescent, charge-neutral, highly stable under basic conditions, stable to anhydrous acid, and readily cleavable in aqueous acid to return the free benzoxaborole.

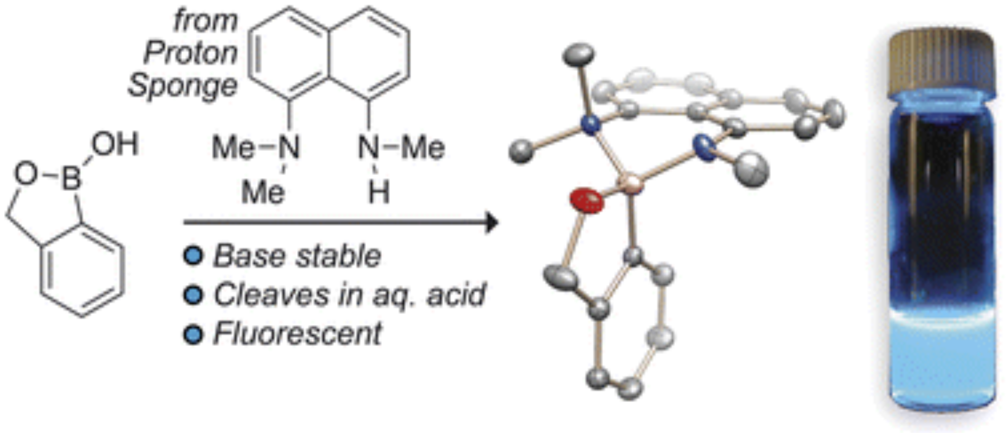
from Proton Sponge
OH
O–B
Me–N
Me
N–Me
H
● Base stable
● Cleaves in aq. acid
● Fluorescent

2.2.1 Introduction

Benzoxaborole is an annulated boronic acid that—in the last five years—has become a privileged structure in drug discovery and biotechnology. Well beyond its role as "just another" reacting partner in Suzuki–Miyaura reactions, the benzoxaborole scaffold can serve as a potent pharmacophore in medicinal chemistry and possesses desirable properties for carbohydrate recognition. Its empty boron *p*-orbital, however, complicates its reactivity and isolation. Classical boron-protecting groups are ineffective for protection of benzoxaborole. Here, in Chapter 2 I report a novel protecting group designed to resolve current limitations. The resulting protected complexes are easily formed and readily compatible with extractive and chromatographic separations, as well as synthetic reagents commonly employed in multistep syntheses. The protecting group is stable to basic and anhydrous acidic conditions, but cleaves readily to return intact benzoxaborole with aqueous acid.

Oxaborole heterocycles are boronic acids that are receiving much attention for applications in drug discovery,[278-287] synthetic methodology,[288] molecular recognition,[255,289-293] and biotechnology.[267,294-297] Benzoxaborole (**1**; Figure 2.1.2),[298] which is characterized by a phenyl ring fused to a five-membered oxaborole, is the most widely employed oxaborole pharmacophore in medicinal chemistry.[278-287] Compared to phenylboronic acid, the annulated benzylic alcohol in **1** confers high stability,[299] low pK_a,[300] and superior polyol-binding (**1**→**2**) under physiological conditions (*i.e.*, water near neutral pH),[255,289,293,301] favorable attributes for applications that entail binding to carbohydrates. [255,267,289-297]

The vacant *p*-orbital on boron—essential for complexation with polyols—can confound multistep synthetic routes and the purification/isolation of derivatives. This issue is compounded further by the commerical availability of countless elaborately functionalized boronic acids but only a small number of simple benzoxaboroles. Our interest in benzoxaboroles for the cellular delivery of chemotherapeutic agents[267] and other pharmacological applications drove us to develop a protecting group for **1** that would enhance its synthetic utility.

A variety of successful protecting group strategies have been developed to modulate the undesired reactivity of boronic acids. A common example is a pinacol ester (**3**), which sterically shields the *p*-orbital from reaction. Similarly, Suginome and coworkers demonstrated the reduced reactivity of boronic acids in a complex with 1,8-diaminonaphthalene (**4**).[302,303] An often-employed strategy developed by Molander and coworkers capitalizes on the fluoro-affinity of boron to form a trifluoroboronate salt (**5**).[234,304] While highly stable, these salts are incompatible with chromatography, limiting their utility in multistep synthetic routes. Burke and coworkers have popularized a trivalent *N*-methyliminodiacetic acid (MIDA)[305] ligand for boronic acids that coordinates the vacant *p*-orbital with a trialkylamine through a dative bond to give a charge-neutral complex (**6**).[251,306] This complex is broadly compatible with synthetic reagents and chromatographic purification.[252] The trivalent MIDA group is not, however, suitable for protecting **1**, which can coordinate to only two ligands. Divalent protecting groups like **3** and **4** are also not appropriate for **1** because they would lead to anionic complexes (**7** and **8**). Likewise, fluoride protection would yield an anionic difluoroborate salt (**9**).

2.2.2 Results and Discussion

We sought to apply the principle of charge neutrality, as demonstrated by the efficacious MIDA protecting group, to the divalent protection of benzoxaboroles. Inspired by the strong complexes that simple boronic acids form with 1,8-diaminonaphthalene (**4**),[302,303] we devised a protecting group based on 1,8-bis(dimethylamino)naphthalene[307] (Proton-sponge®) to generate charge-neutral complexes with **1** that maintain a Lewis basic site to promote acid-mediated cleavage (Figure 2.2.3). We found that complexes **11a**–**e** were fluorescent, stable to basic conditions, moderately stable to anhydrous acid, and readily deprotected under aqueous acidic conditions.

Following a previous report,[308] 1,8-bis(dimethylamino)naphthalene was mono-demethylated to give 1-dimethylamino-8-methylaminonaphthalene (**10**) in one step of >90% yield without chromatography. After azeotropic removal of water, **1a**–**e** and **10** readily formed complexes **11a**–**e** (Figure 2.2.3). Excess **10** was necessary for high yields, but unreacted **10** was re-isolated quantitatively by chromatography (Figure 2.2.4 B, inset). Formation of the complex generated a tetrahedral boron center (**1c**→**11c** ^{11}B NMR δ 33.2 sp^2 → δ 9.1 sp^3)[305] that was stereogenic—the benzylic protons of **1** became nonequivalent (Figure 2.2.4 A) and served as signature of complex formation. The complex was characterized with x-ray crystallography (Figure 2.2.4 C).

Next, we investigated the generality of our protecting group design. First, we investigated a small library of compounds similar to **10** for protection of **1a** (see section **2.2.5**). Only **10**, however, led to complexes that were stable during chromatography. α-Amino acids (which resemble divalent versions of MIDA) are known to form stable complexes with dialkyl boranes (*i.e.*, borinic acids).[309] We found these complexes to be too fragile for effective protection of **1**. From these data, we conclude that the stability of complexes **11a**–**e** stems from both the rigid structure imposed by the diaminonaphthalene ring and the strongly donating nitrogen ligands. The ease of purification also relies on coordinating the vacant *p*-orbital through a dative bond supplied by the dimethyl amino ligand to create a charge-neutral complex. Finally, we note that **11a**–**e** are highly fluorescent (**11a**, Φ_F = 0.45, Fig. 2.2.2B and inset) allowing for easy tracking of product derivatives (**11**–**18**) during multi-step synthesis and purification using a standard long-wave (365 nm) bench-top lamp.[310] Complex **11a** was subjected to a screen of conditions to determine its stability (Table 2.2.5, representative time points, see section 2.2.7 for kinetic traces and further discussion). In general, **11a** is deprotected readily under aqueous acidic conditions (entries 1–3), but exhibits modest (*i.e.*, kinetic) stability under anhydrous acid (entries 4–6) (Table 2.2.5). This sensitivity to acid affirms an aspect of our design—protonation of the methylamino group leads to weaker binding and allows for hydrolytic cleavage. In contrast, **11a** is highly stable under basic conditions (entries 7–10). This reactivity indicates that protecting group **10** is well suited for solid-phase peptide synthesis,[290] in which amino acids are coupled under basic conditions and subsequently cleaved from a solid-support using acid. Finally, the complex tolerated strong reducing reagents, such as $LiAlH_4$ (entry 11). We do note that oxidative conditions were not compatible with **11b** and lead to complex mixtures. This sensitivity is not surprising due to the electron-rich nature of the diaminonaphthalene moiety, which is prone to oxidation.[311,312]

To explore further the stability of the protecting group, we evaluated **11b**, **11d**, and **11e** under a series of synthetic transformations (Figure 2.2.6, see section 2.2.8 for **11b**). As expected, the complex was able to tolerate reducing conditions such as H_2/Pd (**11e**→**12**). Conversion of **12** to triflate **13** and subsequent Suzuki–Miyaura coupling using an XPhos palladacyclic precatalyst,[313] provided **14** in high yield. Notably, **10** prevented reaction at the benzoxaborole center.[314,315] Recent data suggest that Suzuki–Miyaura reactions necessitate a vacant boron *p*-orbital,[316] validating our protecting group design.[317]

The base stability of the complex allowed for Buchwald–Hartwig C–N cross-coupling of the protected boron center to give **15** from **11d**.[318,319] As noted above, protecting group **10** is compatible with organic amine bases associated with peptide bond formation reagents to provide **16** in high yield (94%). In comparison, a similar peptide coupling reaction attempted with unprotected **1d** provided only a 23% yield of the amide **18**. Notably, in both the Pd-catalyzed and peptide-coupling reactions, the methylamino groups in **11d** are unreactive. Finally, evincing the utility of the protecting group under anhydrous acid, selective deprotection of the amino group in **16** with HCl in dioxane gave **17** in good yield (78%), while the benzoxaborole moiety could be deprotected selectively with aqueous acetic acid to return **18**.

2.2.3 Future Directions and Conclusions

In conclusion, benzoxaborole **1** has become a privileged entity in medicinal chemistry and for carbohydrate recognition. Its continued development will rely on the efficiency of its derivitization. We have demonstrated the stability and utility of **1** and other benzoxaboroles when protected with **10**. Protecting group **10** occupies the vacant *p*-orbital on boron while creating charge neutrality in the final product. Its complexes are formed readily and are compatible with synthetic reagents and separation/purification techniques employed commonly in multistep syntheses to enable or improve the efficiency of manipulating benzoxoborole.

2.2.4 Acknowledgements

We are grateful to Dr. Ilia Guzei for X-ray diffraction analysis of complex **11a**. B.V. was supported by postdoctoral fellowship 289613 (CIHR). This work was supported by grant R01 GM044783 (NIH), and made use of the National Magnetic Resonance Facility at Madison, which is supported by grants P41 RR002301 and P41 GM066326 (NIH).

Figure 2.2.2 Structure of free benzoxaborole (1), its complexation with a polyol (2), and other general structures of protected boronic acids (3–6) and their unsuitable complexes (7–9) with 1.

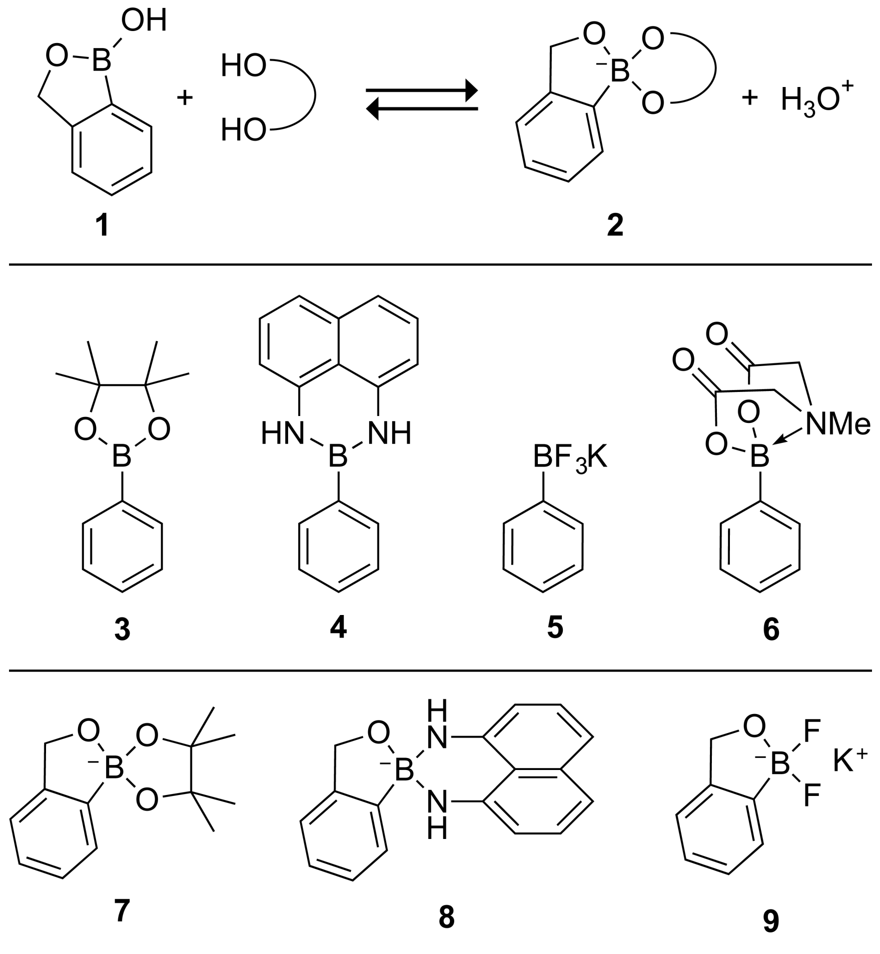
OH
O–B
HO
HO
+
O
B
O
O
+ H3O+
1
2
O
B
O
HN
B
NH
BF3K
O
O
O
O
NMe
O–B
3
4
5
6
O
O
B
O
O
B
H
N
N
H
O
F
B
F
K+
7
8
9

Figure 2.2.2 Structure of free benzoxaborole (**1**), its complexation with a polyol (**2**), and other general structures of protected boronic acids (**3–6**) and their unsuitable complexes (**7–9**) with **1**.

Figure 2.2.3 Protection of benzoxaborole derivatives

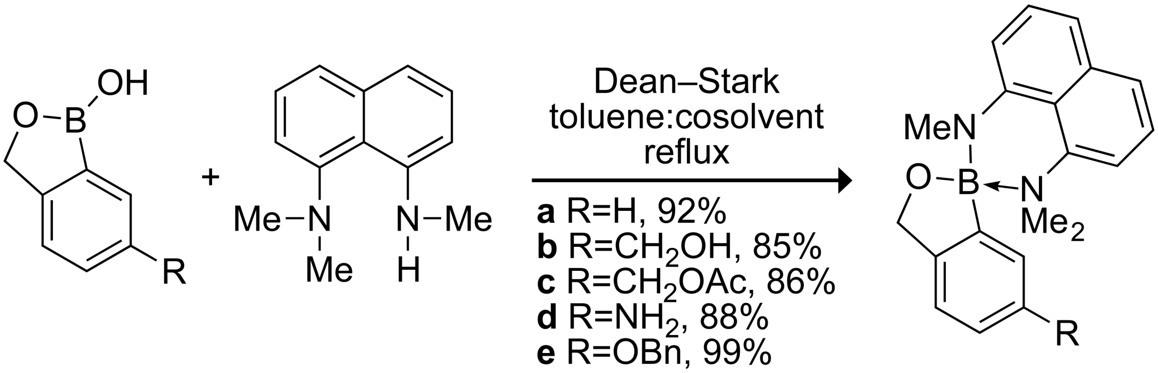
OH
O
B
R
+
Me–N
Me
N–Me
H
Dean–Stark
toluene:cosolvent
reflux
a R=H, 92%
b R=CH2OH, 85%
c R=CH2OAc, 86%
d R=NH2, 88%
e R=OBn, 99%
MeN
O–B
N
Me2
R

1a–e **10** **11a–e**

Figure 2.2.3 Protection of benzoxaborole derivatives

Figure 2.2.4 Characterization of complex 11a

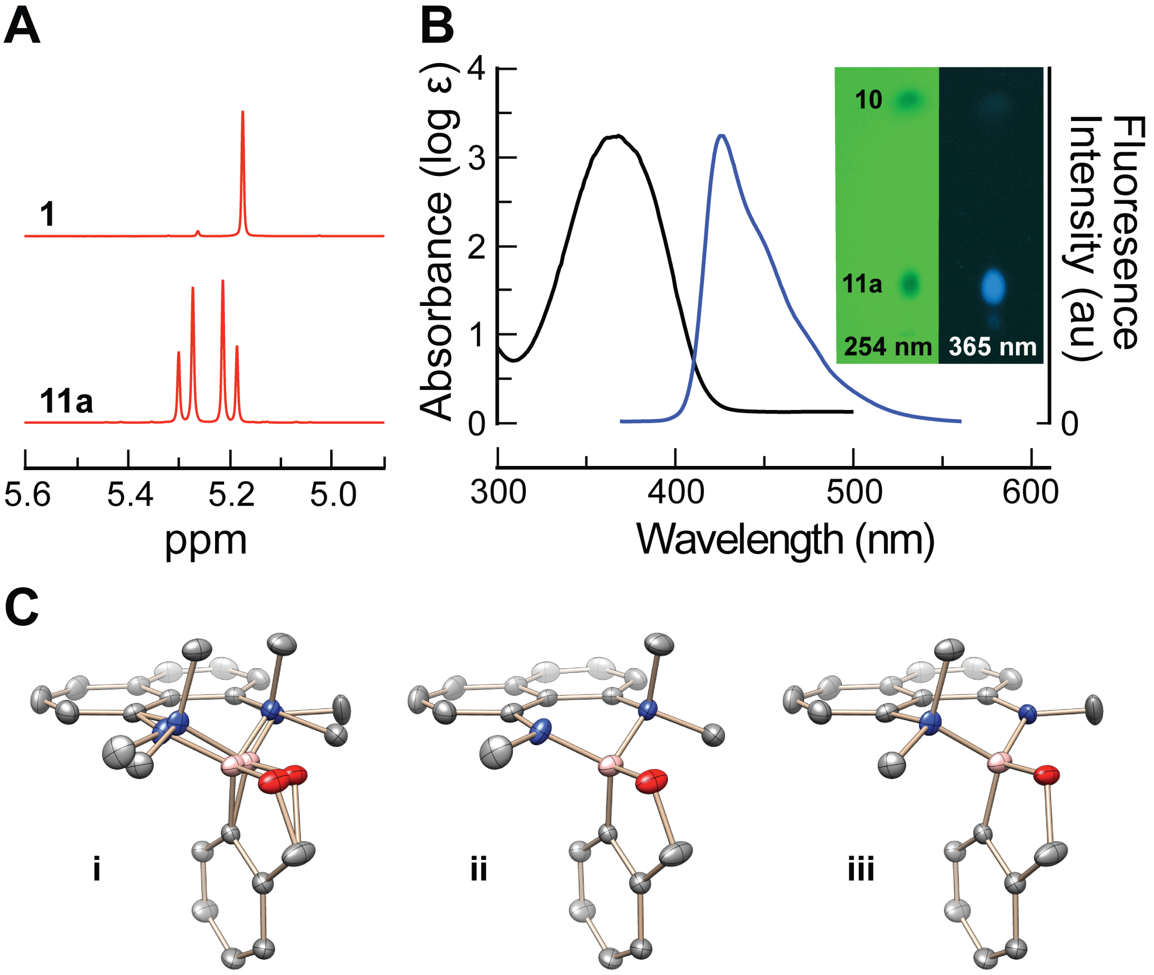

Figure. 2.2.4 Characterization of complex **11a**. (A) ^{1}H NMR spectra of **1a** and **11a** showing the splitting of benzylic proton signals in **1** into two diasteriotopic doublets. (B) Absorbance (black) and fluorescence (blue) spectra of **11a** in $CHCl_3$. Inset: silica gel thin-layer chromatography plate (0.5% v/v MeOH in DCM, $R_f = 0.7$ separation between **10** and **11a**) illuminated under short (254 nm) and long (365 nm) wavelength light. (C) X-ray crystal structure of racemic **11a** with anisotropic thermal ellipsoids set at 50% probability and hydrogen atoms omitted. (i) **11a** showing both components of positional disorder. (ii) and (iii) Disorder components (enantiomers) separated for clarity.

Table 2.2.5 Screening of the stability of 11a under various conditions

Screening of the stability of **11a** under various conditions [a]

Entry	Conditions	% Cleaved	Time (h)
1	0.5 M HCl in (THF/H_2O, 1:1) [b]	94	4
2	0.5 M TFA in (THF/H_2O, 1:1) [b]	99	4
3	0.5 M AcOH in (THF/H_2O, 1:1) [b]	90	4
4	0.5 M TFA in DCM [b]	82	4
5	0.5 M BF_3OEt_2 in DCM [b]	43	4
6	4 M HCl in dioxane [b]	30	4
7	0.1 M pH = 7 PBS in THF (1:1) [c]	0	36
8	0.5 M NaOH in (THF/H_2O, 1:1) [c]	0	72
9	20% v/v piperidine in CH_2Cl_2 [c]	0	72
10	20% v/v DIEA in CH_2Cl_2 [c]	0	72
11	0.5 M $LiAlH_4$ in THF [b,c]	0	2

Table 2.2.5 [a]Average of two experiments at 0.1 M **11a** with 4-bromo-2,6-dimethylaniline as an internal standard. [b]Analyzed with LC-MS. [c]Analyzed with ^{1}H NMR spectroscopy.

Figure 2.2.6 Synthetic evaluation of protected benzoxaborole derivatives

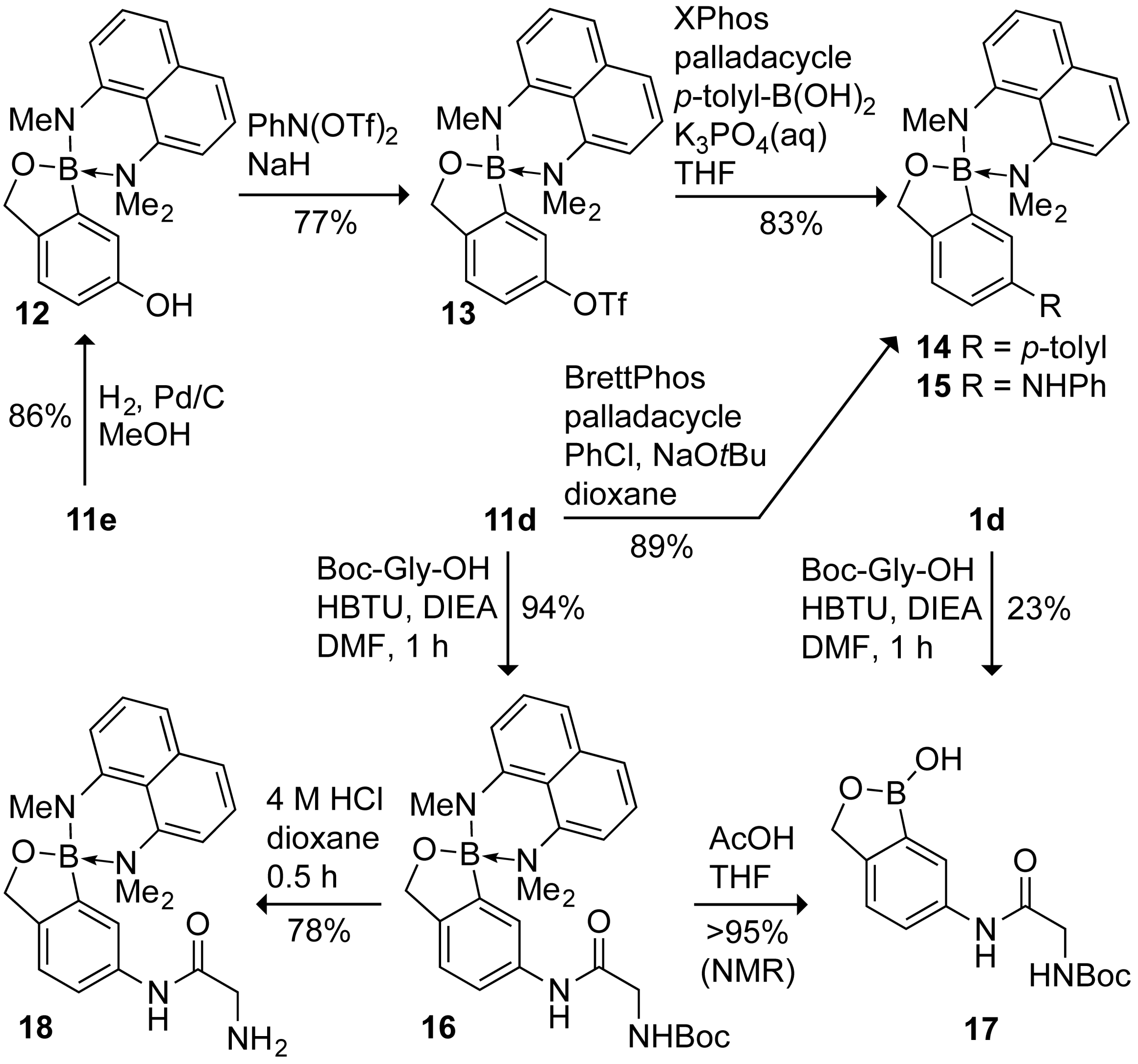
MeN
O–B←N
Me₂
OH
12
PhN(OTf)₂
NaH
77%
13
OTf
XPhos
palladacycle
p-tolyl-B(OH)₂
K₃PO₄(aq)
THF
83%
R
14 R = p-tolyl
15 R = NHPh
86%
H₂, Pd/C
MeOH
11e
BrettPhos
palladacycle
PhCl, NaOtBu
dioxane
89%
11d
1d
Boc-Gly-OH
HBTU, DIEA
DMF, 1 h
94%
Boc-Gly-OH
HBTU, DIEA
DMF, 1 h
23%
18
NH₂
4 M HCl
dioxane
0.5 h
78%
16
NHBoc
AcOH
THF
>95%
(NMR)
OH
O–B
HNBoc
17

Figure 2.2.6 Synthetic evaluation of protected benzoxaborole derivatives; yields are isolated but not optimized.

2.2.5 Materials & Methods

Materials

Silica gel (40 µm) was from SiliCycle. All reagent-grade materials were from Sigma–Aldrich (St. Louis, MO) and were used without further purification, except for 2 hydroxymethylphenylboronic acid and 5-amino-2-hydroxymethylphenylboronic acid, which were from Combi-Blocks (San Diego, CA).

Solvent removal

The phrase "concentrated under reduced pressure" refers to the removal of solvents and other volatile materials using a rotary evaporator at water aspirator pressure (<20 torr) while maintaining the water-bath temperature below 40 °C. Residual solvent was removed from samples at high vacuum (<0.1 torr). The term "high vacuum" refers to vacuum achieved by mechanical belt-drive oil pump.

NMR Spectroscopy

^{1}H, ^{13}C, and ^{11}B NMR spectra for all compounds were acquired on Bruker Spectrometers in the NMRFAM at the University of Wisconsin–Madison operating at 500 and 125 MHz. The chemical shift data are reported in units of δ (ppm) relative to residual solvent and to 20% v/v BF_3-etherate in $CDCl_3$ as an external standard for ^{11}B NMR spectroscopy.

Absorption and Emission Spectroscopy

Fluorescence spectra were measured with a Photon Technology International 810 fluorometer using right-angle detection. Ultraviolet–visible absorption spectra were measured with a Varian Cary 300 Bio diode array spectrophotometer and corrected for background signal with a solvent-filled cuvette. Fluorescence quantum yields in $CHCl_3$ were determined relative to quinine sulfate in 1 N H_2SO_4, and were corrected for solvent refractive index and absorption differences at the excitation wavelength.

Analyses of Deprotection

Deprotection reactions were run with 4-bromo-2,6-dimethylaniline as an internal standard. Samples were taken from the deprotection reaction mixtures at known times and diluted with methanol, and the extent of cleavage was analyzed with an LCMS-2020 single quadrupole liquid chromatograph mass spectrometer from Shimadzu (Kyoto, Japan) using an H_2O/MeCN (0.1% v/v formic acid) gradient suitable for baseline separation of starting material and the internal standard.

2.2.6 Evaluation of Other Protecting Groups

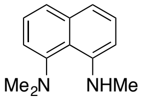

10

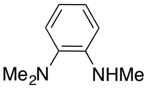

20

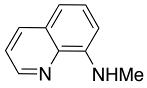

23

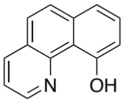

26

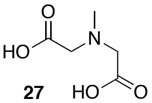

27
MIDA

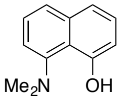

19

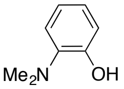

21

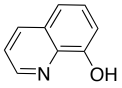

24

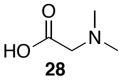

28

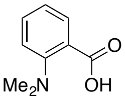

22

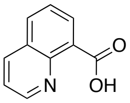

25

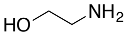

29

The above compounds were tested for complexation of **1a** by refluxing in ethanol or toluene. (Dean–Stark conditions applied in the case of toluene.) The potential protecting groups were selected because they possess a donor nitrogen ligand that would lead to a charge neutral complex (i.e., a tertiary or pyridine nitrogen). Except for **10**, all of the protecting groups above did not form complexes with **1a** that were stable to chromatographic and/or extractive purification. Notably, **19**, **26** and **28** formed complexes that were stable enough for characterization (see table of contents), but were too fragile for further manipulation. Compounds **28** and **29** have been described to form complexes with borinic acids, but were not effective for benzoxaborole.[309,320] Of particular note is the failure of **20**—a 5-membered variant of **10**—as a protecting group. Potential protecting groups with oxygen ligands (-OH, -CO_2H) would often form protected products that were distinguishable by TLC, but would decompose during subsequent extractive or chromatographic purification. Finally, protecting groups that were able to form 6-membered ring complexes with **1a** were formed more readily.

2.2.7 Deprotection Analyses

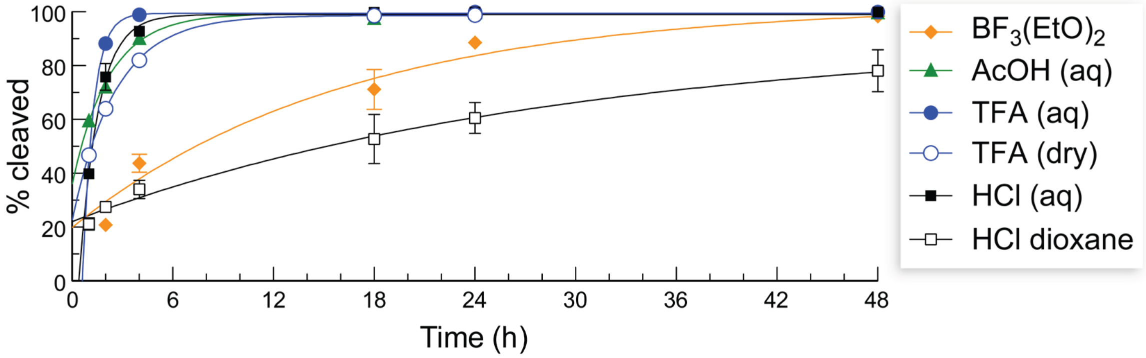

Kinetic traces for the deprotection of compound **11a**. Percent cleavage was determined through comparison of integrations against the internal standard from the LCMS trace and averaged from replicates. Data were fitted to an exponential decay curve with the program Prism 5.0 from GraphPad Software (La Jolla, CA).

Discussion. The complex shows modest kinetic stability in the presence of certain anhydrous acids such as $BF_3(EtO)_2$ and 4 M HCl in dioxane. The initial cleavage rates for these two acids began at 20% due to contaminating water. The synthesis of **17** and **18** confirms the complexes kinetic stability to anhydrous acid and susceptibility to aqueous acid (see Scheme 3 in the main text). Finally, extent of cleavage was made based on disappearance of **11a** because boronic acids have poor detection thresholds under LCMS. The cleaved product was confirmed to be the expected benzoxaborole as shown in NMR spectra comparing compound **18**, **10**, and the reaction of compound **16**.

2.2.8 Synthesis

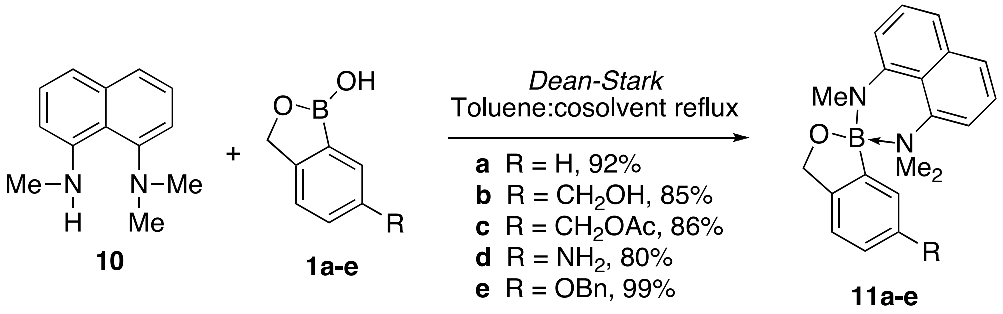

Synthesis of 1c. 2,5-Bis(hydroxymethyl)phenylboronic acid (0.41 g, 2.5 mmol) was dissolved in DCM (25 mL). Triethylamine (0.35 mL, 2.5 mmol), dimethylaminopyridine (0.015 g, 0.125 mmol), and acetic anhydride (0.473 mL, 5 mmol) were added, and the resulting mixture was stirred for 12 h. The reaction mixture was concentrated under reduced pressure, dissolved in EtOAc (15 mL), and washed with 1 M sodium citrate (3 × 10 mL), dried over Na_2SO_4(s), and concentrated under reduced pressure to yield **1c** (80%). ^{1}H NMR (400 MHz, $CDCl_3$) δ 7.63 (s, 1H), 7.47 (d, J=7.8 Hz, 1H), 7.37 (d, J=7.8 Hz, 1H), 5.13 (s, 2H), 5.06 (s, 2H), 2.07 (s, 3H). ^{13}C NMR (125 MHz, MeOD) δ 172.37, 136.30, 132.00, 130.99, 129.22, 122.27, 67.14, 66.76, 20.85. ^{11}B NMR ($CDCl_3$, 96 MHz) δ 33.20. HRMS (ESI) calcd. for $C_{11}H_{13}BO_4$ $[M+NH_4]^+$ 237.1282, found 237.1288.

Synthesis of 1e: 6-Benzyloxy-1,3-dihydro-1-hydroxy-2,1-benzoxaborole was prepared following the reported method of Qiao and coworkers,[287] with the following changes. 5-(Benzyloxy)-2-formylphenylboronic acid (0.5 g, 1.95 mmol) was dissolved in THF (15 mL), and the resulting solution was cooled to 0 °C. To this solution under stirring, $NaBH_4$ (0.094 g, 2.5 mmol) was added. After stirring for 2 h, 1 M HCl (6 mL) was added, and the resulting mixture was concentrated under reduced pressure, extracted with EtOAc

(3 × 10 mL), and dried over Na_2SO_4(s). The resulting white solid was recrystallized from water to give **1e (**6-benzyloxy-1,3-dihydro-1-hydroxy-2,1-benzoxaborole) (94%).

Synthesis of 11a. 1-Dimethylamino-8-methylaminonaphthalene (**10**)[308] (0.540 g, 2.7 mmol), and (2-hydroxymethyl)phenylboronic acid (0.120 g, 0.9 mmol) were dissolved in 20 mL of dry toluene. The reaction mixture was fitted with a Dean–Stark trap (filled with 5 mL of dry toluene) and condenser, then heated at 125 °C for 24 h. The reaction mixture was cooled to room temperature, concentrated under reduced pressure, dissolved in DCM (5 mL), washed with 2.5 M NaOH (3 × 10 mL), dried over Na_2SO_4(s), and concentrated under reduced pressure to a brown oil. The residue was purified by silica gel chromatography (1% MeOH in DCM) to provide **11a** (92%) and quantitative re-isolation of **10**. ^{1}H NMR (500 MHz, $CDCl_3$) δ 7.76 (d, *J*=8.3Hz, 1H), 7.45 (t, *J*=7.9 Hz, 1H), 7.35 (t, *J*=7.9 Hz, 1H), 7.18 (d, *J*=8.3 Hz, 1H), 7.11 (m, 2H), 6.77 (m, 1H), 6.59 (d, *J*=7.8 Hz, 1H), 6.14 (bs, 1H), 5.22 (d, *J*=13.9 Hz, 2H), 5.13 (d, *J*=13.9 Hz, 2H), 2.88 (s, 3H), 2.86 (s, 3H), 2.71 (s, 3H). ^{13}C NMR (125 MHz, $CDCl_3$) δ 149.17, 146.75, 143.66, 135.87, 129.00, 128.87, 128.58, 127.20, 126.13, 124.79, 120.14, 117.49, 113.32, 112.61, 105.43, 72.80, 46.29, 32.17. ^{11}B NMR ($CDCl_3$, 96 MHz) δ 9.25. HRMS (ESI) calcd. for $C_{20}H_{21}BN_2O$ [M+] 316.1857, found 316.1841.

Synthesis of 11b from 1b. 2,5-Bis(hydroxymethyl)phenylboronic acid (0.164 g, 1 mmol) was dissolved in 1 mL of dry DMSO. To this solution was added compound **10** (1-dimethylamino-8-methylaminonaphthalene) (0.6 g, 3 mmol), and 20 mL of dry toluene. The reaction mixture was fitted with a Dean–Stark trap (filled with 5 mL of dry toluene) and condenser, then heated at 130 °C for 24 h. The reaction mixture was cooled to room temperature, concentrated under reduced pressure, dissolved in chloroform (5 mL), washed with 2.5 M NaOH (3 × 10 mL), dried over Na_2SO_4(s), and concentrated under reduced pressure to a brown oil. The residue was purified by silica gel chromatography (2.5% v/v MeOH in DCM) to provide **11b** (85%) and quantitative re-isolation of **10**. ^{1}H-NMR (500 MHz, $CDCl_3$): *d* 7.78 (d 1H), 7.45 (t 1H), 7.37 (t 1H), 7.22 (d 1H), 7.17 (bd 1H), 7.13 (d 2H), 6.09 (d 1H), 5.21 (d 1H), 5.13 (d 1H), 4.29 (s 2H), 2.91 (bs 3H), 2.87 (s 3H), 2.75 (s 3H). ^{13}C NMR (125 MHz, $CDCl_3$): *d* 149.00, 146.55, 143.50, 138.57, 135.87, 128.99, 128.67, 127.72, 126.82, 124.81, 120.40, 117.33, 113.43, 112.62, 105.37, 72.55, 65.78, 50.11, 44.60, 32.18. ^{11}B NMR (DMSO-d_6, 96 MHz): δ 8.53. HRMS (ESI) calcd. for $C_{21}H_{24}BN_2O_2$ [M+] 346.1962, found 346.1972.

Synthesis of 11c. Compound **1c** (0.368 g, 1.91 mmol) and **10** (1-dimethylamino-8-methylaminonaphthalene) (0.6 g, 3 mmol), were dissolved in 35 mL of dry toluene. The reaction mixture was fitted with a Dean–Stark trap (filled with 5 mL of dry toluene), and condenser, then heated at 125 °C for 15 h. The reaction mixture was cooled to room temperature, concentrated under reduced pressure, dissolved in chloroform (5 mL), washed with 2.5 M NaOH (3 × 10 mL), dried over Na_2SO_4(s), and concentrated under reduced pressure to a brown oil. The residue was purified by silica gel chromatography (97.5:2.5 DCM:MeOH) to provide **11c** (86%) and quantitative re-isolation of **10**. ^{1}H-NMR (500 MHz, $CDCl_3$): *d* 7.78 (d 1H), 7.46 (t 1H), 7.38 (t 1H), 7.22 (d 1H), 7.12 (m 3H), 6.61 (d 1H), 6.04 (bs 1H), 5.20 (d 1H), 5.13 (d 1H), 4.73 (m 2H), 2.90 (s 3H), 2.87 (s 3H), 2.74 (s 3H), 1.93 (s 3H). ^{13}C NMR (125 MHz, $CDCl_3$): *d* 170.98, 149.44, 146.56, 143.48, 135.86, 133.42, 128.98, 128.65, 128.48, 127.25, 124.74, 120.31, 117.37, 113.46, 112.60, 105.43, 72.59, 66.73, 32.13, 21.08. ^{11}B NMR ($CDCl_3$, 96 MHz) *d* 9.13. HRMS (ESI) calcd. for $C_{23}H_{25}BN_2O_3$ $[M+]^+$ 388.2067, found 388.2080.

Synthesis of 11d. 5-Amino-2-hydroxymethylphenylboronic acid (0.4 g, 2.7 mmol) was dissolved in 3 mL of MeOH and added to **10**[308] (0.8 g, 4 mmol) in 3 mL of toluene. The mixture was then evaporated to dryness to give an oil. The residue was dissolved in 20 mL of toluene and heated to reflux under Dean–Stark conditions for 12 h under N_2(g). The solution was concentrated under reduced pressure, and the residue was purified by silica gel chromatography (95:5, DCM:MeOH) to give **11d** (88%) and quantitative re-isolation of **10**. ^{1}H NMR ($CDCl_3$, 500 MHz) δ 7.76 (d, *J*=8.5 Hz, 1H), 7.46 (dd, app t, *J*=8, 8 Hz, 1H), 7.37 (dd, app t, *J*=8, 8 Hz, 1H), 7.22 (d, *J*=7.5 Hz, 1H), 7.11 (d, *J*=8 Hz, 1H), 6.91 (d, *J*=8 Hz, 1H), 6.60 (d, *J*=8 Hz, 1H), 6.49 (dd, *J*=8, 2 Hz, 1H), 5.49 (br s, 1H, **H′**), 5.14 (d, *J*=13 Hz, 1H), 5.06 (d, *J*=13 Hz, 1H), 2.89 (s, 3H), 2.87 (s, 3H), 2.76 (s, 3H). ^{13}C NMR ($CDCl_3$, 125 MHz) δ 146.6, 144.2, 143.6, 139.7, 135.8, 128.9, 128.4, 124.8, 120.6, 117.3, 115.3, 115.1, 113.1, 112.6, 105.2, 72.4, 50.1, 44.3, 32.1. ^{11}B NMR ($CDCl_3$, 96 MHz) δ 9.01. HRMS (ESI) calcd. for $C_{20}H_{22}BN_3O$ $[M+H]^+$ 331.1966, found 331.1967.

Assignment of **H′** based on 2D NMR data (Fig. S11 and S12), which showed that, despite its upfield position and broad appearance, **H′** was attached to an aromatic carbon and coupled to the aromatic protons on the ring and the benzylic methylene protons. Further, **H′** was not exchangeable with D_2O.

Synthesis of 11e from 1e. Compound **1e** (6-Benzyloxy-1,3-dihydro-1-hydroxy-2,1-benzoxaborole) (0.4 g, 1.61 mmol) and 1-dimethylamino-8-methylaminonaphthalene (0.96 g 4.8 mmol) was dissolved in DMSO (5 mL), to which was added toluene (20 mL). The reaction mixture was heated at reflux under Dean–Stark conditions for 12 h under N_2(g). The solution was concentration under reduced pressure, and the residue was purified by silica gel chromatography (98:1:1, DCM:MeOH:TEA) to give **11e** (99.5%) and quantitative re-isolation of **10**. ^{1}H NMR ($CDCl_3$, 500 MHz) δ 7.74 (d, *J*=8 Hz, 1H), 7.43 (t, *J*=7 Hz, 1H), 7.34 (t, *J*=7 Hz, 1H), 7.22 (m, 3H), 7.18 (d, *J*=8 Hz, 1H), 7.11 (m, 3H), 7.01 (d, *J*=8 Hz, 1H), 6.72 (dd, *J*=8, 2.5 Hz, 1H), 6.57 (d, *J*=8 Hz, 1H), 5.75 (bs, 1H), 5.15 (d, *J*=13 Hz, 1H), 5.06 (d, *J*=13 Hz, 1H), 4.59 (s, 2H), 2.85 (s, 3H), 2.84 (s 3H), 2.70 (s 3H). ^{13}C NMR ($CDCl_3$, 125 MHz) δ 157.04, 146.31, 143.25, 141.35, 136.95, 135.53, 128.68, 128.27, 128.21, 127.53, 127.51, 124.60, 120.63, 117.04, 114.09, 113.17, 112.46, 105.07, 72.03, 69.42, 49.68, 44.27, 31.92. ^{11}B NMR ($CDCl_3$, 96 MHz) δ 8.83. HRMS (ESI) calcd. for $C_{27}H_{27}BN_2O_2$ $[M+H]^+$ 422.2275, found 422.2261.

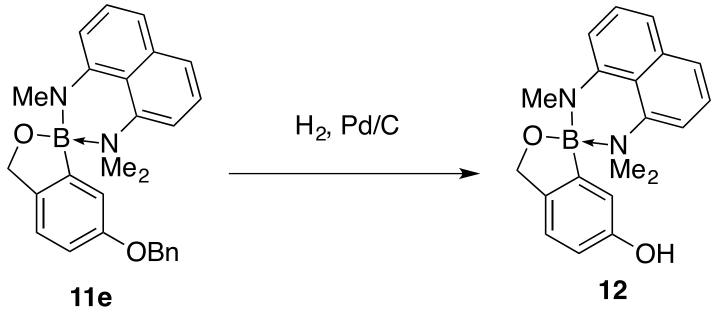

Synthesis of 12 from 11e. Compound **11e** (0.21 g, 0.5 mmol) was dissolved in 10 mL of 6:4 MeOH/EtOAc. To this solution under N_2(g) was added 10% Pd/C (0.1 g, 0.1 mmol

Pd). The reaction mixture was purged with H_2(g) via a balloon, and the resulting slurry was stirred for 1 h. The reaction mixture was filtered through a sintered glass funnel, and concentrated under reduced pressure. The residue was then purified by silica gel chromatography (98:1:1 DCM:MeOH:TEA) to give **12** (86% based on re-isolated starting material). ^{1}H NMR (600 MHz, CD_2Cl_2) δ 7.77 (d, *J*=8.2 Hz, 1H), 7.46–7.39 (m, 2H), 7.27 (d, *J*=7.6 Hz, 1H), 7.11 (d, *J*=7.9 Hz, 1H), 6.97 (d, *J*=8.1 Hz, 1H), 6.58 (t, *J*=7.7 Hz, 2H), 5.53–5.44 (bs, 1H), 5.08 (d, *J*=13.3 Hz, 1H), 5.01 (d, *J*=13.3 Hz, 1H), 2.86 (s, 3H), 2.82 (s, 3H), 2.73 (s, 3H). ^{13}C NMR (126 MHz, CD_2Cl_2) δ 153.75, 146.23, 143.21, 140.97, 135.37, 128.38, 127.88, 124.41, 120.55, 116.92, 113.98, 112.70, 112.42, 104.61, 71.66, 49.48, 43.77, 31.29. ^{11}B NMR ($CDCl_3$, 96 MHz) δ 8.76. HRMS (ESI) calcd. for $C_{20}H_{21}BN_2O_2$ $[M+H]^+$ 332.1806, found 332.1818.

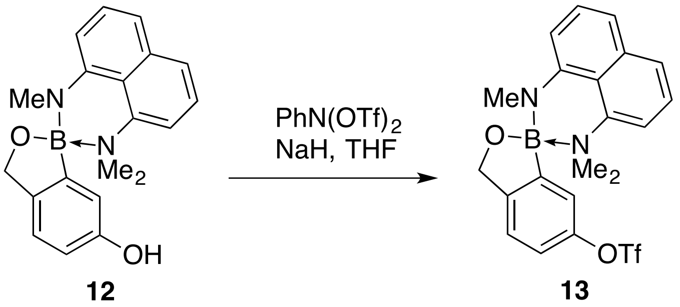

Synthesis of 13. To a solution of **12** (0.1 g, 0.3 mmol) and $PhN(OTf)_2$ (0.22 g, 0.6 mmol) in 10 mL of THF was added NaH as a 60% dispersion in mineral oil (0.120 g, 3.0 mmol). The reaction mixture was stirred for 1 h, diluted with DCM, and washed with sat. $NaHCO_3$(aq). The organic layer was dried over $MgSO_4$(s), concentrated under reduced pressure, and purified by silica gel chromatography (6:4 hexanes/EtOAc) to give **13**

(77%) that was deemed of sufficient purity for the subsequent step. ^{1}H NMR (CDCl$_3$, 500 MHz) δ 7.80 (d, *J*=8.5 Hz, 1H), 7.47 (m, 1H), 7.39 (m, 1H), 7.21 (d, *J*=7.5 Hz, 1H), 7.16 (d, *J*=8 Hz, 1H), 7.14 (d, *J*=8 Hz, 1H), 6.97 (dd, *J*=8.5, 2 Hz, 1H), 6.62 (d, *J*=7.5 Hz, 1H), 5.80 (br s, 1H), 5.21 (d, *J*=14.5 Hz, 1H), 5.12 (d, *J*=14.5 Hz, 1H), 2.90 (s, 3H), 2.86 (s, 3H), 2.71 (s, 3H). ^{13}C NMR (CDCl$_3$, 125 MHz) δ 163.6, 149.9, 148.9, 148.8, 146.2, 142.9, 138.4, 137.4, 135.9, 129.1, 128.9, 128.7, 128.5, 127.9, 127.8, 126.5, 125.5, 124.8, 124.6, 123.9, 123.0, 121.8, 121.3, 119.9, 117.4, 117.2, 116.7, 114.1, 112.9, 105.8, 72.3, 50.1, 45.6, 44.3, 34.6, 31.9. ^{11}B NMR (CDCl$_3$, 96 MHz) δ 8.63. HRMS (ESI) calcd. for $C_{21}H_{20}BF_3N_2O_4S$ $[M+H]^+$ 464.1284, found 464.1299.

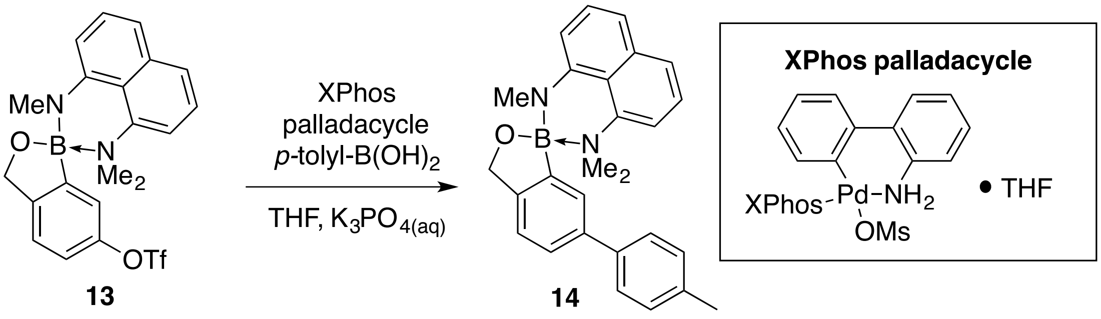

Synthesis of 14. To a solution of **13** (60 mg, 0.13 mmol), XPhos palladacycle (2.35 mg, 0.013 mmol), and *p*-tolylboronic acid (70 mg, 0.52 mmol) in 1 mL of degassed THF under N_2(g) was added 2 mL of degassed 0.5 M K_3PO_4. The reaction mixture was stirred overnight, and then partitioned between DCM and water. The organic layer was dried over $MgSO_4$(s), concentrated under reduced pressure, and purified by silica gel chromatography (7:3 hexanes/EtOAc) to give **14** (83%).^{1}H NMR (CDCl$_3$, 500 MHz) δ 7.77 (d, *J*=8.5 Hz, 1H), 7.45 (m, 1H), 7.36 (m, 2H), 7.24 (m, 2H), 7.18 (d, *J*=8 Hz, 1H), 7.11 (d, *J*=8 Hz, 1H), 7.06 (br s, 3H), 6.61 (d, *J*=8 Hz, 1H), 6.39 (br s, 1H), 5.25 (d, *J*=14

Hz, 1H), 5.17 (d, *J*=14 Hz, 1H), 2.92 (s, 3H), 2.90 (s, 3H), 2.79 (s, 3H), 2.29 (s, 3H). ^{13}C NMR (CDCl$_3$, 125 MHz) δ 148.3, 146.5, 143.5, 139.0, 138.7, 136.2, 135.8, 129.2, 128.9, 128.5, 128.4, 127.7, 127.2, 126.8, 126.8, 126.3, 124.6, 120.3, 117.3, 113.4, 112.5, 105.4, 72.5, 49.7, 44.7, 32.2, 14.2. ^{11}B NMR (CDCl$_3$, 96 MHz) δ 8.72. HRMS (ESI) calcd. for $C_{27}H_{27}BN_2O$ [M+H] 406.2336, found 406.2326.

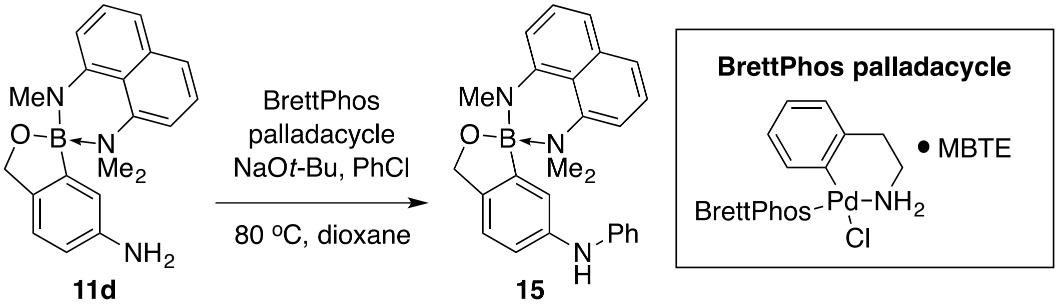
MeN
O–B←N
Me2
NH2
11d
BrettPhos
palladacycle
NaOt-Bu, PhCl
80 °C, dioxane
MeN
O–B←N
Me2
N
H
Ph
15
BrettPhos palladacycle
• MBTE
BrettPhos-Pd-NH2
Cl

Synthesis of 15. Compound **11d** (0.1 g, 0.3 mmol), BrettPhos Palladacycle (2.4 mg, 3 μmol), and NaO*t*-Bu (58 mg, 0.6 mmol) were dissolved in 2 mL of dry, degassed dioxane under N_2(g). Chlorobenzene (35 mg, 0.31 mmol) was added, and the reaction mixture was sealed and heated at 80 °C for 3 h. The solution was concentrated under reduced pressure, and the residue was purified by silica gel chromatography (60:39:1 hexanes/EtOAc/NEt$_3$) to give **15** (89%). ^{1}H NMR (CDCl$_3$, 750 MHz) δ 7.78 (d, *J*=8 Hz, 1H), 7.48 (dd, app t, *J*=8, 8 Hz, 1H), 7.41 (dd, app t, *J*=8, 8 Hz, 1H), 7.28 (dd, *J*=7.5 Hz, 1H), 7.13 (d, *J*=7.5 Hz, 1H), 7.10 (dd, app t, *J*=7.5, 7.5 Hz, 2H), 7.05 (d, *J*=8 Hz, 1H), 6.95 (d, *J*=7.5 Hz, 1H), 6.78 (dd, app t, *J*=7.5 Hz, 1H), 6.72 (d, *J*=8 Hz, 2H), 6.64 (d, *J*=8 Hz, 1H), 5.84 (br s, 1H), 5.33 (br s, 1H), 5.23 (d, *J*=13 Hz, 1H), 5.14 (d, *J*=13 Hz, 1H), 2.95 (s, 3H), 2.92 (s, 3H), 2.82 (s, 3H). ^{13}C NMR (CDCl$_3$, 125 MHz) δ 146.7, 143.9, 143.6, 142.3, 140.5, 135.8, 129.1, 129.0, 128.6, 124.8, 120.6, 119.5, 118.9, 118.1, 115.9, 113.4, 112.6, 105.4, 72.5, 50.1, 44.3, 32.2. ^{11}B NMR (CDCl$_3$, 96 MHz) δ 9.07. HRMS (ESI) calcd. for $C_{26}H_{26}BN_3O$ [M+H]$^+$ 407.2279, found 407.2264.

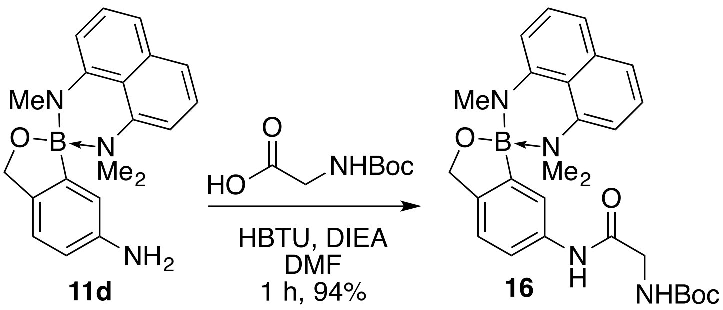

Synthesis of 16. Compound **11d** (0.1 g, 0.3 mmol), Boc-glycine (0.069 g, 0.39 mmol), and HBTU (0.15 g, 0.39 mmol) were dissolved in 4 mL of DMF. DIEA (0.16 g, 1.2 mmol) was added, and the reaction mixture was stirred for 1 h. The solution was concentrated under reduced pressure, and the residue was dissolved in DCM and extracted with sat. NaHCO$_3$(aq) (2×) and water (2×). The organic layer was dried over Na$_2$SO$_4$(s) and concentrated under reduced pressure. The residue was purified by silica gel chromatography (96:4, DCM:MeOH) to give **16** (94%). ^{1}H NMR (CDCl$_3$, 500 MHz) δ 7.77 (d, *J*=8 Hz, 1H), 7.66 (dd, *J*=8, 1 Hz, 1H), 7.47 (dd, app t, *J*=8, 8 Hz, 1H), 7.39 (dd, app t, *J*=8, 8 Hz, 1H), 7.23 (d, *J*=7.5 Hz, 1H), 7.11 (dd, *J*=11.5, 8 Hz, 2H), 6.60 (d, *J*=7.5 Hz, 1H), 5.81 (br s, 1H), 5.18 (d, *J*=14 Hz, 1H), 5.10 (d, *J*=14 Hz, 1H), 3.72 (m, 2H), 2.89-2.75 (isomeric Me, 9H), 1.40 (br s, 9H). ^{13}C NMR (CDCl$_3$, 125 MHz) δ 167.2, 155.4, 146.5, 145.7 143.4, 135.9, 135.1, 129.1, 128.7, 125.0, 120.8, 120.2, 119.9, 117.3, 113.5, 112.8, 105.4, 80.5, 72.5, 50.2, 45.1, 44.5, 38.8, 32.2, 28.4. ^{11}B NMR (CDCl$_3$, 96 MHz) δ 8.95. HRMS (ESI) calcd. for $C_{27}H_{33}BN_4O_4$ [M+H] 488.2704, found 488.2721.

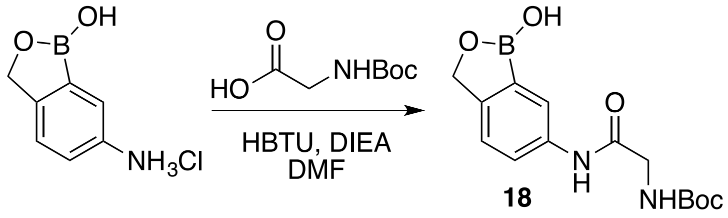
OH
O–B
NH3Cl
O
HO
NHBoc
HBTU, DIEA
DMF
OH
O–B
O
N
H
NHBoc
18

Synthesis of 18. 5-Amino-2-hydroxymethylphenylboronic acid HCl salt (0.056 g, 0.3 mmol), Boc-glycine (0.069 g, 0.39 mmol), and HBTU (0.15 g, 0.39 mmol) were dissolved in 4 mL of DMF. DIEA (0.16 g, 1.2 mmol) was added, and the reaction mixture was stirred for 1 h. The solution was concentrated under reduced pressure, and the residue was dissolved in DCM and extracted with 0.05 M HCl (2×). The organic layer was dried over Na_2SO_4(s) and concentrated under reduced pressure. The residue was purified by silica gel chromatography (93:6:1, DCM:MeOH:HCO_2H) to give **16-unprotected** (23%). ^{1}H NMR (CD_3OD, 500 MHz) δ 7.80 (d, J=1.5 Hz, 1H), 7.67 (dd, J=8.5, 2 Hz, 1H), 7.34 (d, J=8 Hz, 1H), 5.04 (s, 2H), 3.86 (s, 2H), 1.47 (s, 9H). ^{13}C NMR (CD_3OD, 125 MHz) δ 170.7, 158.8, 151.1, 138.8, 124.7, 122.8, 122.7, 80.9, 72.3, 45.1, 28.9. ^{11}B NMR (MeOD-d_4, 96 MHz) δ 31.13. HRMS (ESI) calcd. for $C_9H_9BN_4O_3$ [M–H] 304.1350, found 304.1363.

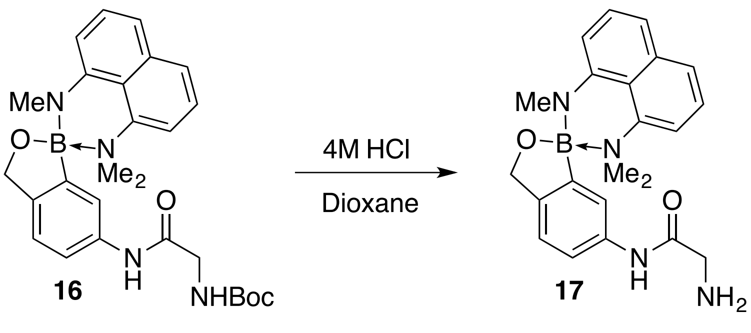
MeN
O–B
N
Me2
O
N
H
NHBoc
16
4M HCl
Dioxane
MeN
O–B
N
Me2
O
N
H
NH2
17

Synthesis of 17. Compound **16** (0.120 g, 0.25 mmol) was dissolved in 3 mL of 4 M HCl in anhydrous dioxane, and the reaction mixture was stirred for 30 min. The solution was concentrated under reduced pressure, and the residue was suspended in 30 mL of DCM, washed with 10% NaOH (2×), dried over Na_2SO_4(s), and evaporated to dryness. The residue was purified by silica gel chromatography (85:14:1, DCM:MeOH:NEt_3) to give **17** (78%). ^{1}H NMR ($CDCl_3$, 500 MHz) δ 8.77 (br s, 1H), 7.78 (d, *J*=8.5 Hz, 1H), 7.72 (dd, *J*=8.5, 2 Hz, 1H), 7.47 (dd, app t, *J*=8, 8 Hz, 1H), 7.39 (dd, app t, *J*=8, 8 Hz, 1H), 7.24 (d, *J*=7.5 Hz, 1H), 7.13 (dd, *J*=7.5, 2.5 Hz, 2H), 6.62 (d, *J*=8 Hz, 1H), 6.04 (br s, 1H), 5.20 (d, *J*=13.5 Hz, 1H), 5.11 (d, *J*=13.5 Hz, 1H), 3.26 (s, 2H), 2.90 (s, 3H), 2.88 (s, 3H), 2.78 (s, 2H), 1.65 (br s, 2H). ^{13}C NMR ($CDCl_3$, 125 MHz) δ 170.5, 146.4, 145.3, 143.4, 135.8, 135.6, 128.9, 128.5, 124.8, 120.6, 119.8, 119.6, 117.1, 113.3, 112.7, 105.2, 72.4, 49.8, 45.8, 45.1, 44.8, 32.3. ^{11}B NMR ($CDCl_3$, 96 MHz) δ 9.13. HRMS (ESI) calcd. for $C_{22}H_{25}BN_4O_2$ [M+H] 388.2180, found 388.2198.

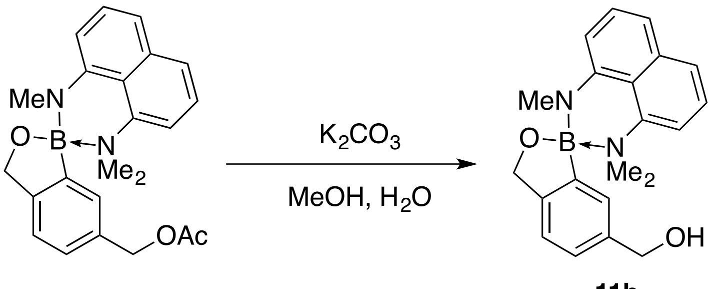

11c **11b**

Synthesis of 11b from 11c. Compound **11c** (0.730 g, 1.88 mmol) was dissolved in 18 mL of MeOH, and 18 mL of sat. K_2CO_3(aq) was added. The resulting slurry was stirred overnight. The solution was concentrated under reduced pressure, and the residue was extracted with DCM (3×), dried over Na_2SO_4(s), and concentrated under reduced pressure. The residue was purified by silica gel chromatography (95:5 DCM/MeOH) to give **11b** (80%).

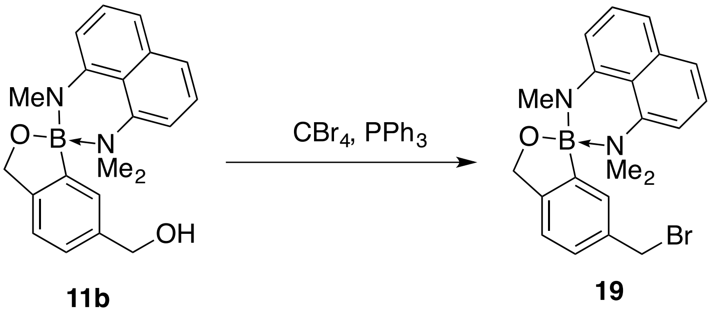

Synthesis of 19. Compound **11b** (0.02 mg, 0.058 mmol) was dissolved in DCM (0.6 mL), and the resulting solution was cooled to 0 °C. Triphenylphospine (0.023 mg, 0.088 mmol) and CBr_4 (0.029 mg, 0.088 mmol) were added, and the reaction mixture was allowed to warm to room temperature and stirred for 12 h. The solution was concentrated under reduced pressure, and the residue was purified by silica gel chromatography (96.5:2.5:1 DCM/MeOH/NEt_3) to give **18** (91%). ^{1}H-NMR (400 MHz, $CDCl_3$): *d* 7.78 (d 1H), 7.47 (t 1H), 7.39 (t 1H), 7.22 (d 1H), 7.17 (bd 1H), 7.14 (d 2H), 7.10 (d 2H), 6.60 (d 2H), 6.11 (d 1H), 5.19 (d 1H), 5.10 (d 1H), 4.16 (s 2H), 2.89 (bs 3H), 2.86 (s 3H), 2.73 (s 3H). ^{13}C NMR (125 MHz, $CDCl_3$): *d* 146.46, 143.39, 135.87, 135.52, 129.31, 129.02, 128.73, 128.58, 127.48, 124.89, 120.66, 119.37, 117.28, 113.53, 112.70, 105.44, 72.57, 50.11, 44.60, 35.01. ^{11}B NMR ($CDCl_3$, 96 MHz) *d* 8.91. HRMS (ESI) calcd. for $C_{21}H_{22}BBrN_2O$ $[M+H]^+$ 408.1118, found 408.1126.

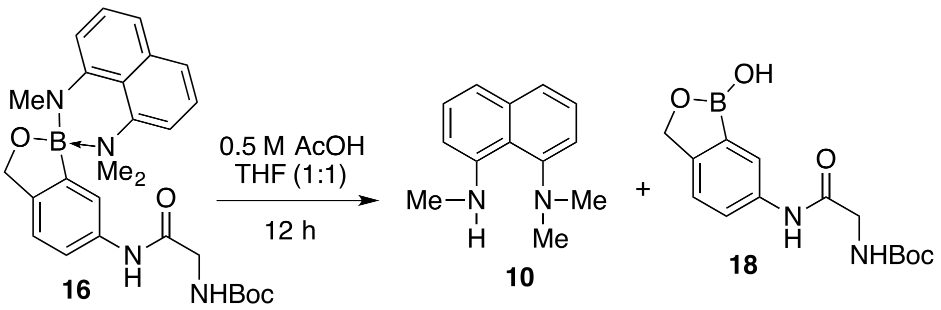

Synthesis of 18 from 16. Compound **16** (10 mg, 20 µmol) was dissolved in 2 mL of 0.5 1:1 AcOH/THF, and the resulting solution was stirred for 12 h. The solution was concentrated under reduced pressure, and the residue was dissolved in methanol-d_4 for analysis by ^{1}H NMR spectroscopy (see: Fig. S32). Compounds **10** and **18** were subjected to the same conditions as was compound **16**, for comparison.

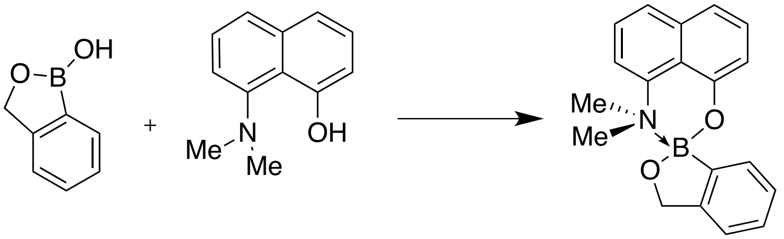

Protection of 1a with 19: 8-(dimethylamino)naphthalen-1-ol (0.427 mmol, 80 mg) and benzoboroxole (0.5127 mmol, 69 mg) were dissolved in toluene (20 mL) and heated at reflux with azeotropic removal of water overnight. The reaction mixture was then concentrated *in vacuo*, and the solid was dissolved in chloroform and washed with aqueous base (10% NaOH) to yield MRA 086 as a white precipitate (72%). ^{1}H NMR (500 MHz, $CDCl_3$) δ 7.90–7.85 (m, 1H), 7.53–7.44 (m, 2H), 7.36–7.32 (m, 2H), 7.10 (dd, J = 7.5, 1.2 Hz, 1H), 6.85 (dd, J = 7.6, 1.2 Hz, 1H), 6.12 (bs, 1H), 5.28 (d, J = 14.0 Hz, 1H), 5.11 (d, J = 14.1 Hz, 1H), 3.03 (s, 3H), 2.84 (s, 3H). ^{13}C NMR (125 MHz, $CDCl_3$) δ

156.87, 150.04, 143.06, 135.42, 129.00, 127.84, 126.79, 126.26, 125.69, 125.20, 120.67, 118.64, 116.90, 113.97, 110.02, 72.55, 49.35, 46.47. HRMS (ESI) calcd. for $C_{19}H_{18}BNO_2$ $[M+Na]^+$ 325.1360, found 325.1367.

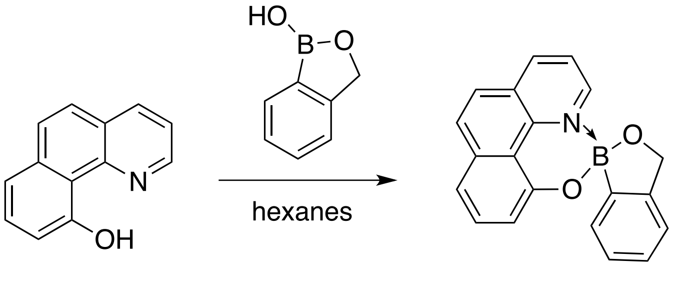

Protection of 1a with 26: Following a previous literature procedure,[321] benzoxaborole (1 mmol, 134 mg) and 10-hydroxybenzo[h]quinoline (1 mmol, 195 mg) were stirred in dry hexanes for 2 h. The resulting precipitate was filtered, and rinsed with hexanes. ^{1}H NMR (500 MHz, $CDCl_3$) δ 8.49–8.42 (m, 2H), 7.99 (d, *J* = 8.9 Hz, 1H), 7.78 (t, *J* = 7.9 Hz, 1H), 7.74 (d, *J* = 9.0 Hz, 1H), 7.64 (dd, *J* = 7.9, 5.6 Hz, 1H), 7.52–7.48 (m, 1H), 7.38 (dd, *J* = 8.0, 0.9 Hz, 1H), 7.31–7.28 (m, 2H), 7.19 (d, *J* = 7.2 Hz, 1H), 7.13–7.09 (m, 1H), 5.35 (d, *J* = 14.0 Hz, 1H), 5.18 (d, *J* = 13.9 Hz, 1H). ^{13}C NMR (125 MHz, $CDCl_3$): δ 159, 155.9, 148.8, 142.3, 139.6, 134.5, 132.8, 130.6, 128.4, 127.8, 126.5, 123.4, 121.5, 120.8, 117.9, 116.9, 72.3. HRMS (ESI) calcd. for $C_{20}H_{14}BNO_2$ $[M+Na]^+$ 333.1047, found 333.1031.

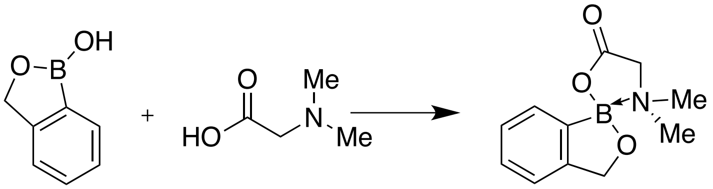

Protection of 1a with 28: Benzoxaborole (1.25 mmole, 167 mg) and N,N-dimethylglycine (1.25 mmole, 129 mg) were dissolved in methanol (5 mL) in a sealed vial, heated at reflux for 1.5 h, and then concentrated. The viscous solid was then dissolved in THF (5 mL), heated at reflux for 1 h, and concentrated under reduce pressure to a white solid (quant.). ^{1}H NMR (500 MHz, $CDCl_3$) δ 7.48 (d, J = 7.2 Hz, 1H), 7.37–7.32 (t, J = 7.2, 1H), 7.29–7.22 (m, 2H), 5.07 (d, J = 14.0 Hz, 1H), 5.01 (d, J = 14.0 Hz, 1H), 3.83 (d, J = 15.2 Hz, 1H), 3.50 (d, J = 15.1 Hz, 1H), 2.74 (s, 3H), 2.63 (s, 3H). ^{13}C NMR (125 MHz, $CDCl_3$) δ 169.54, 150.52, 130.03, 128.55, 126.45, 120.88, 71.74, 60.95, 47.57, 44.82.

2.2.9 NMR Spectra

NMR SPECTRA

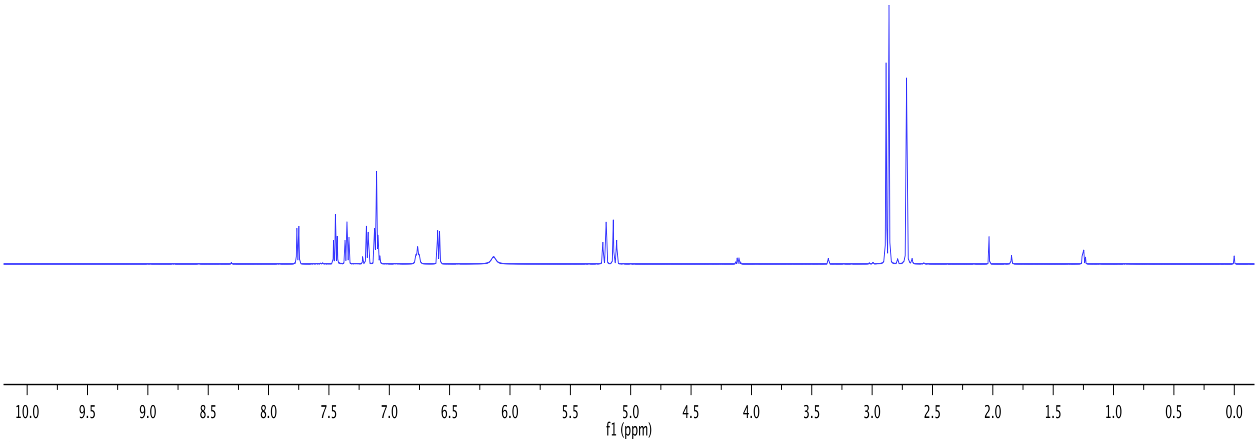

^{1}H NMR spectrum of **11a** in $CDCl_3$ (500 MHz)

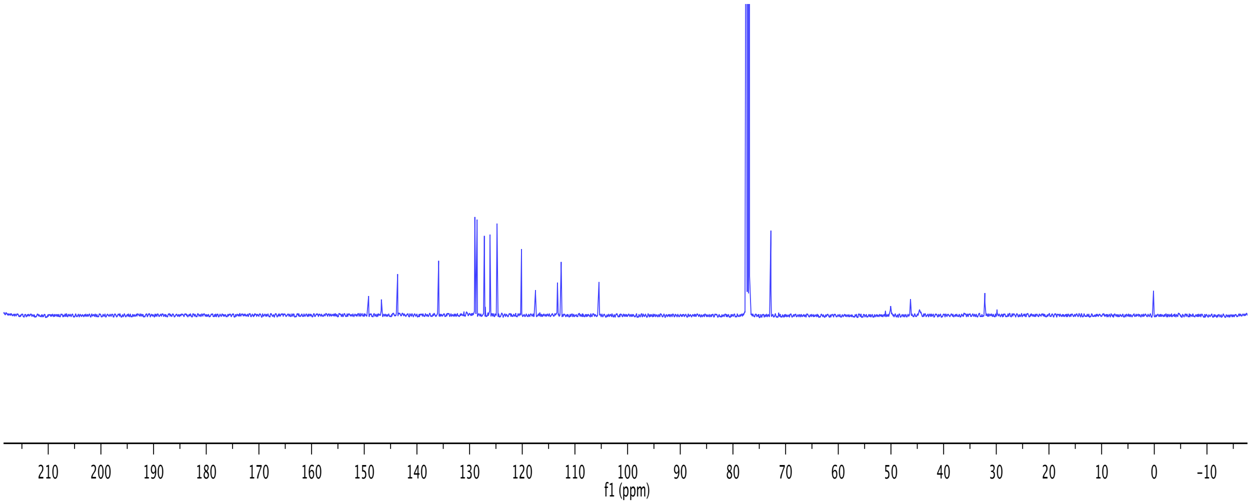

^{13}C NMR spectrum of **11a** in $CDCl_3$ (125 MHz)

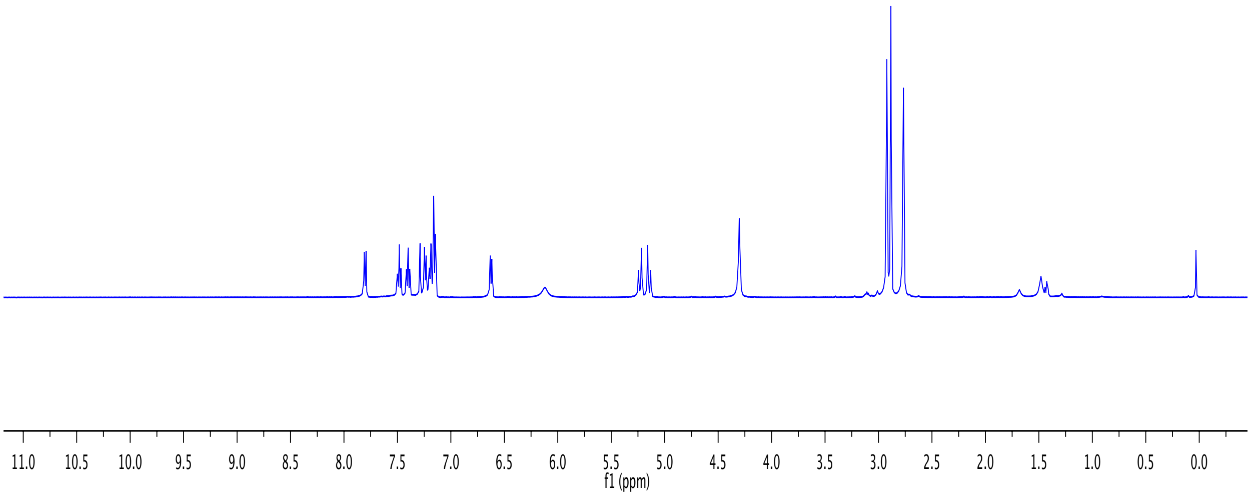

^{1}H NMR spectrum of **11b** in $CDCl_3$ (500 MHz).

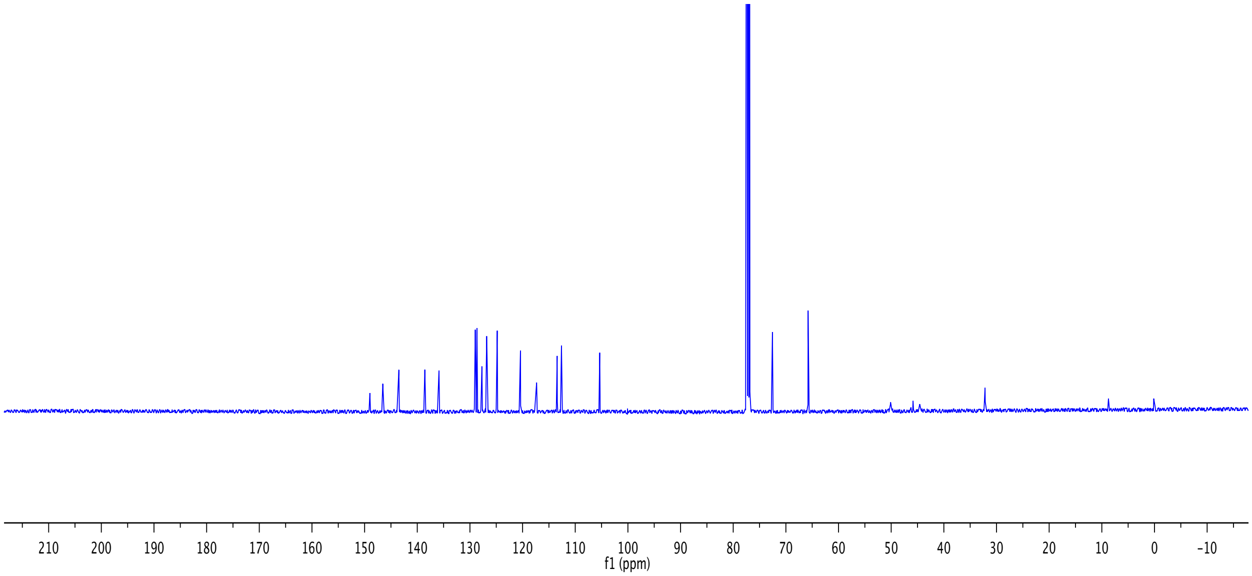

^{13}C NMR spectrum of **11b** in $CDCl_3$ (125 MHz).

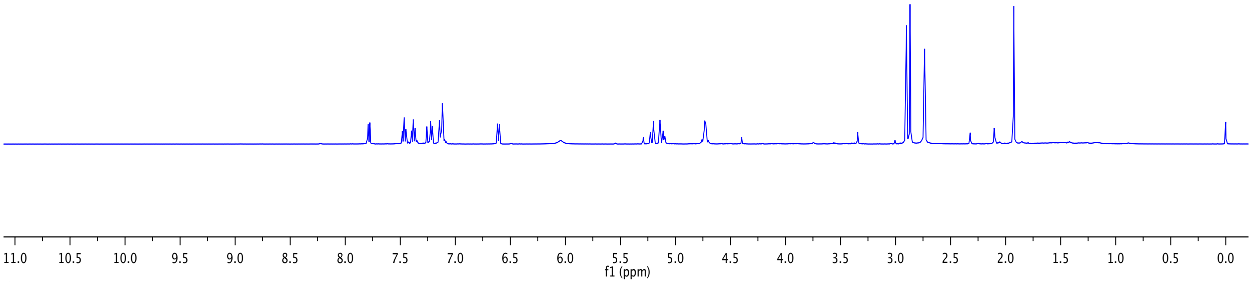

^{1}H NMR spectrum of **11c** in $CDCl_3$ (500 MHz).

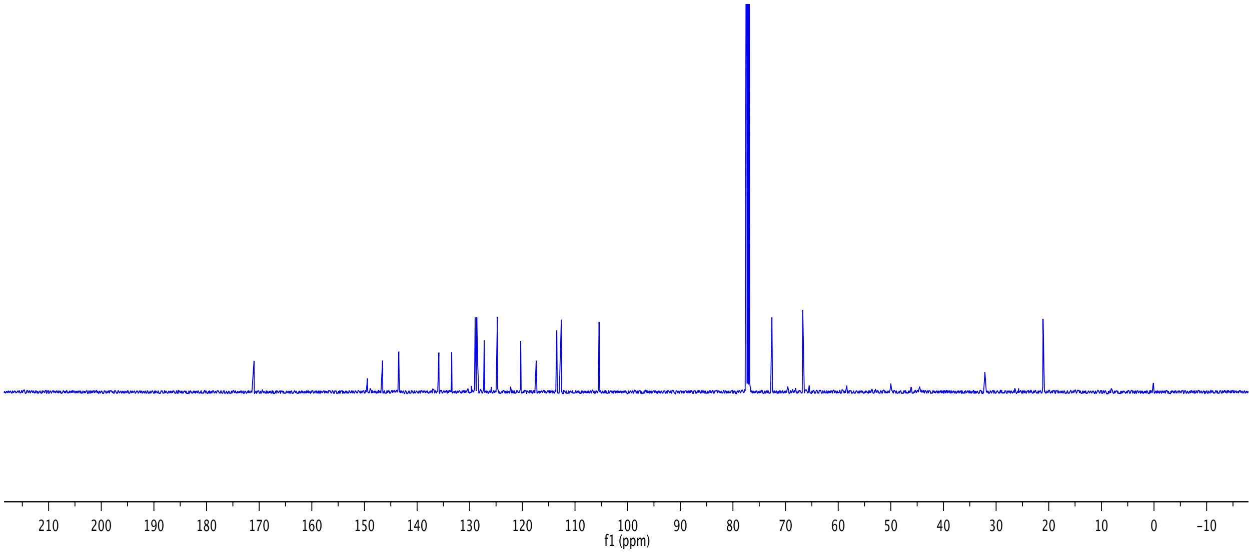

^{13}C NMR spectrum of **11c** in $CDCl_3$ (125 MHz).

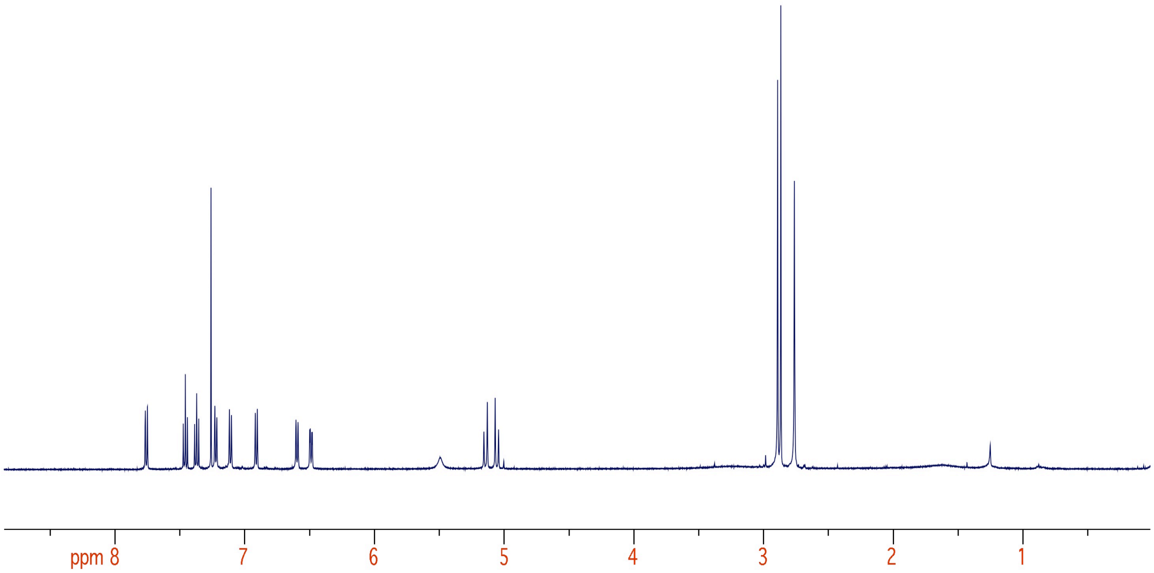

^{1}H NMR spectrum of **11d** in $CDCl_3$ (500 MHz).

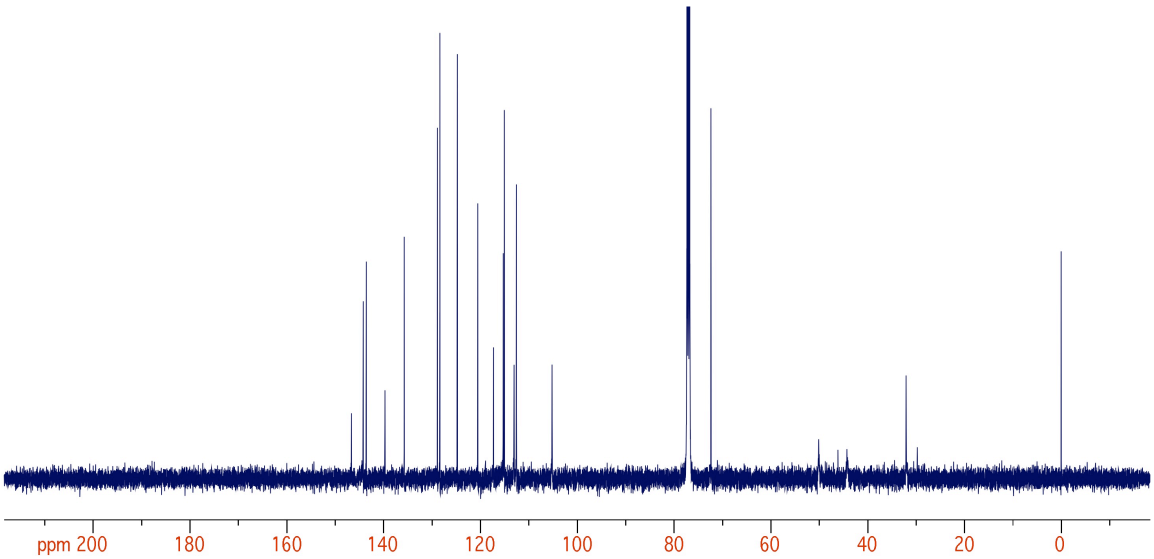

^{13}C NMR spectrum of **11d** in $CDCl_3$ (125 MHz).

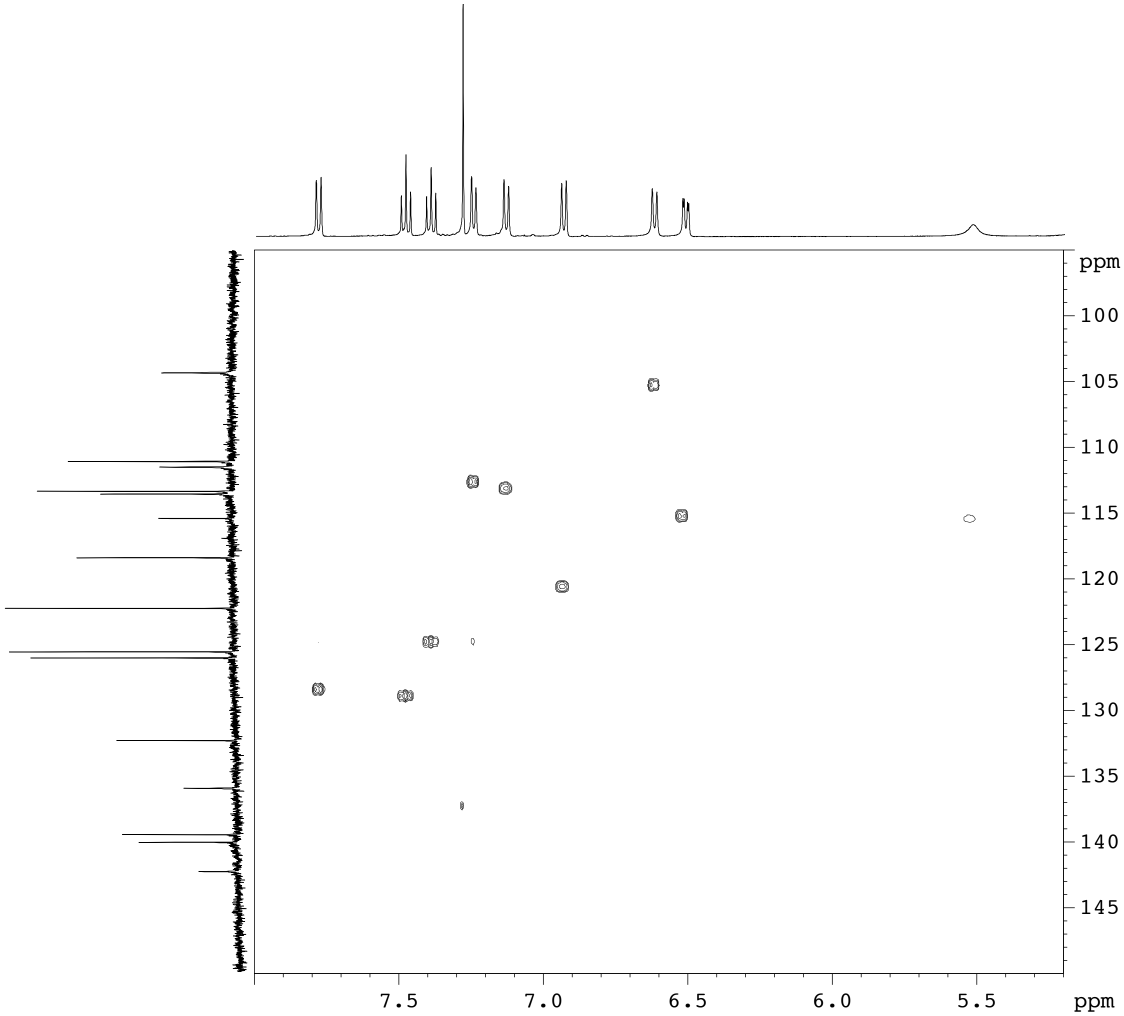

^{1}H-^{13}C HSQC 2D NMR spectrum of **11d** in $CDCl_3$ (500 MHz).

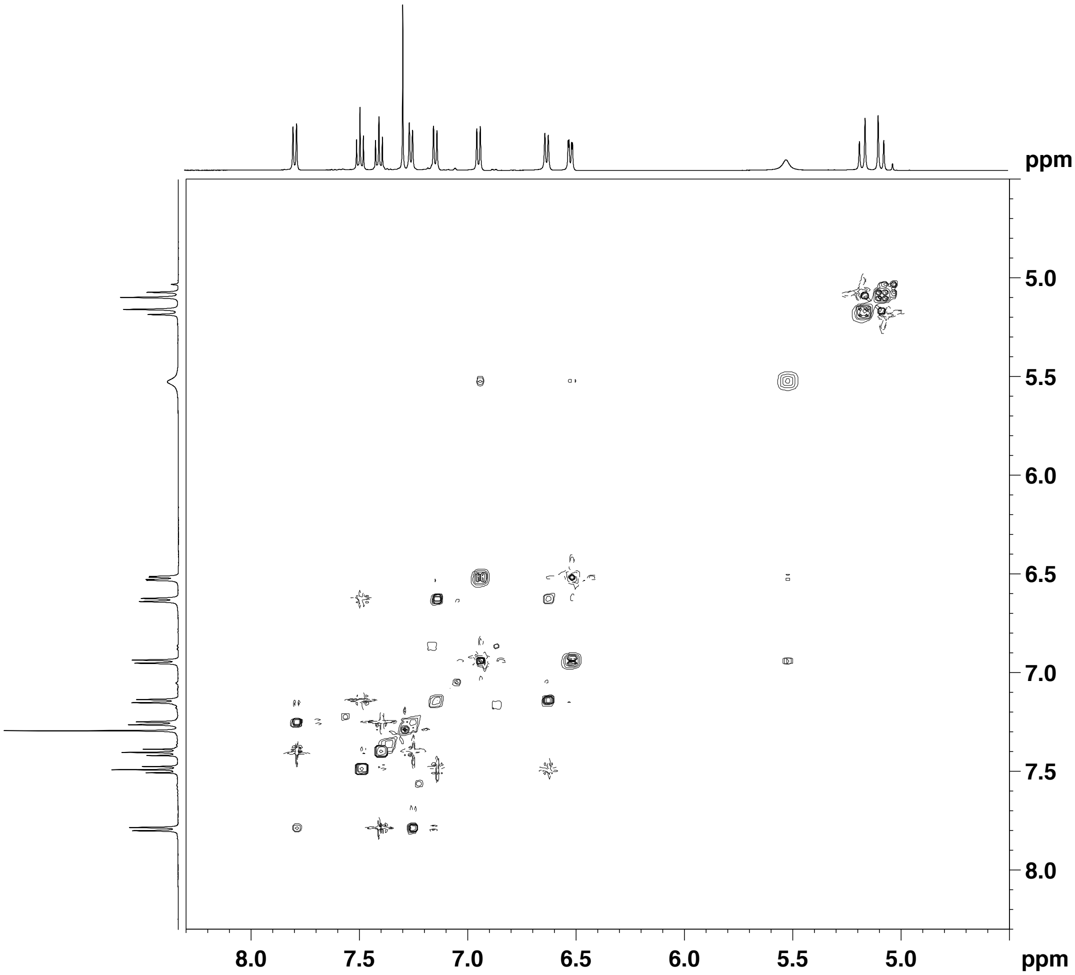

^{1}H-^{1}H TOCSY 2D NMR spectrum of **11d** in CDCl$_3$ (500 MHz)

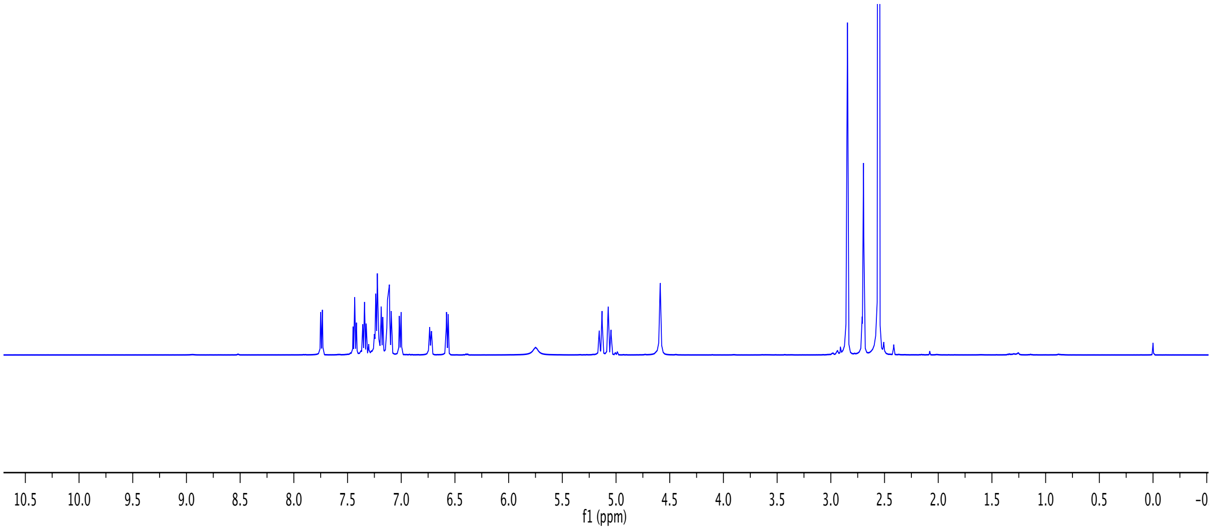

^{1}H NMR spectrum of **11e** in $CDCl_3$ (500 MHz).

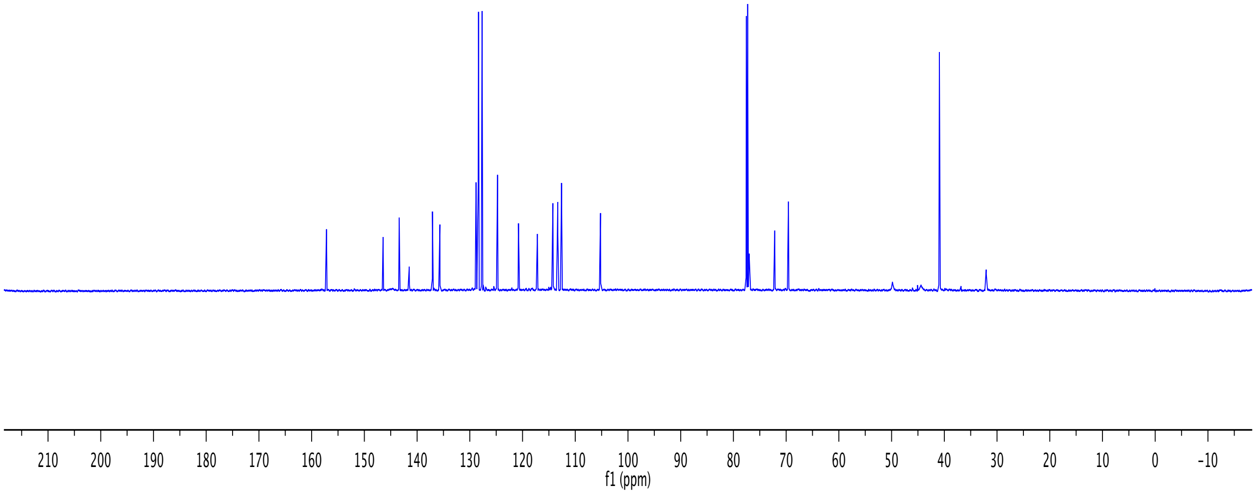

^{13}C NMR spectrum of **11e** in $CDCl_3$ (125 MHz).

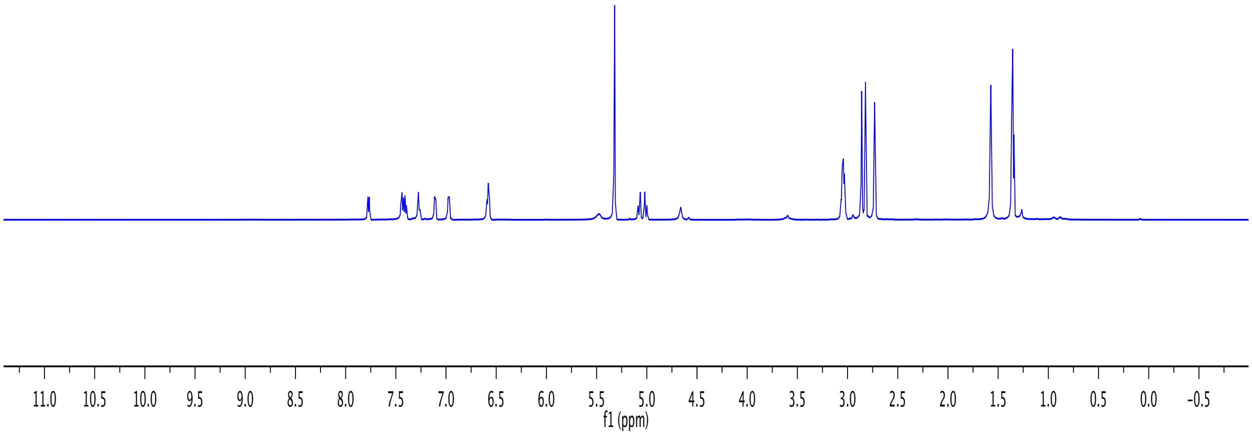

^{1}H NMR spectrum of **12** in CD_2Cl_2 (600 MHz).

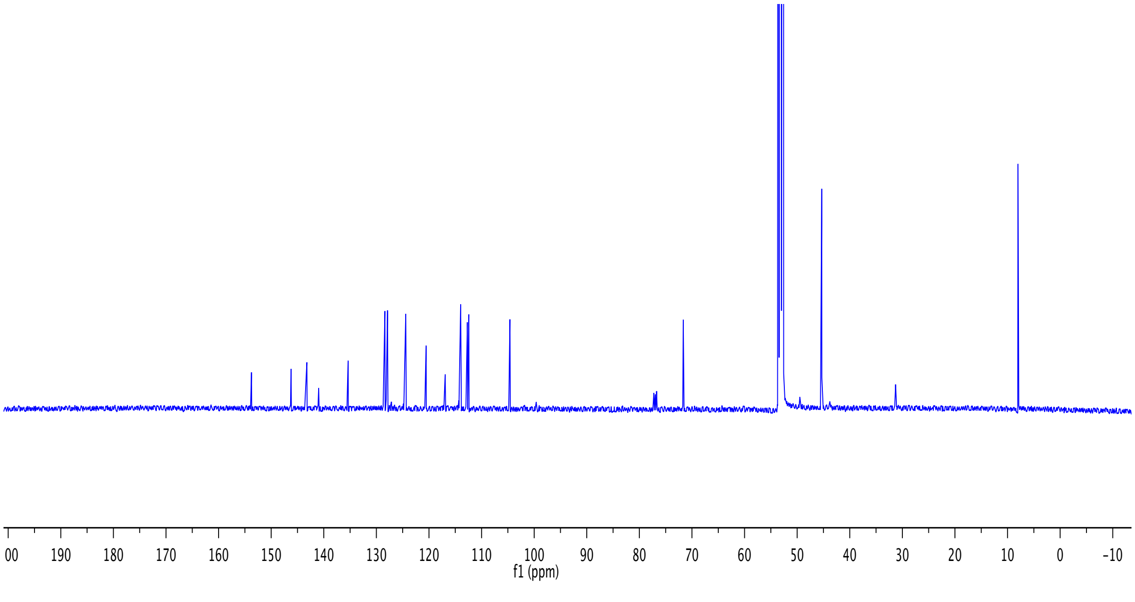

^{13}C NMR spectrum of **12** in CD_2Cl_2 (125 MHz).

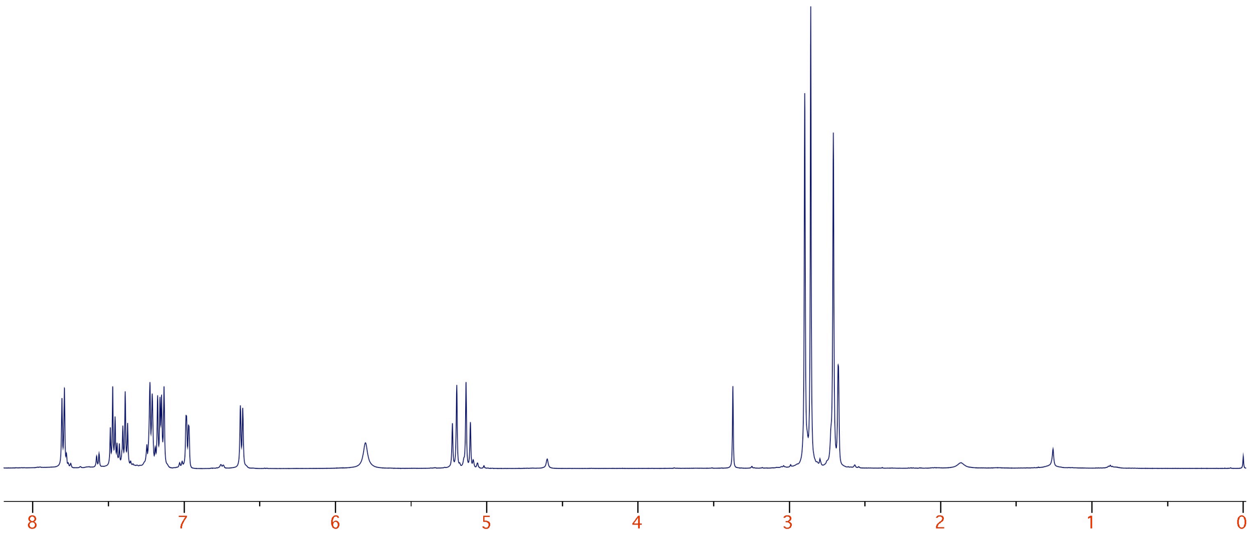

^{1}H NMR spectrum of **13** in $CDCl_3$ (750 MHz).

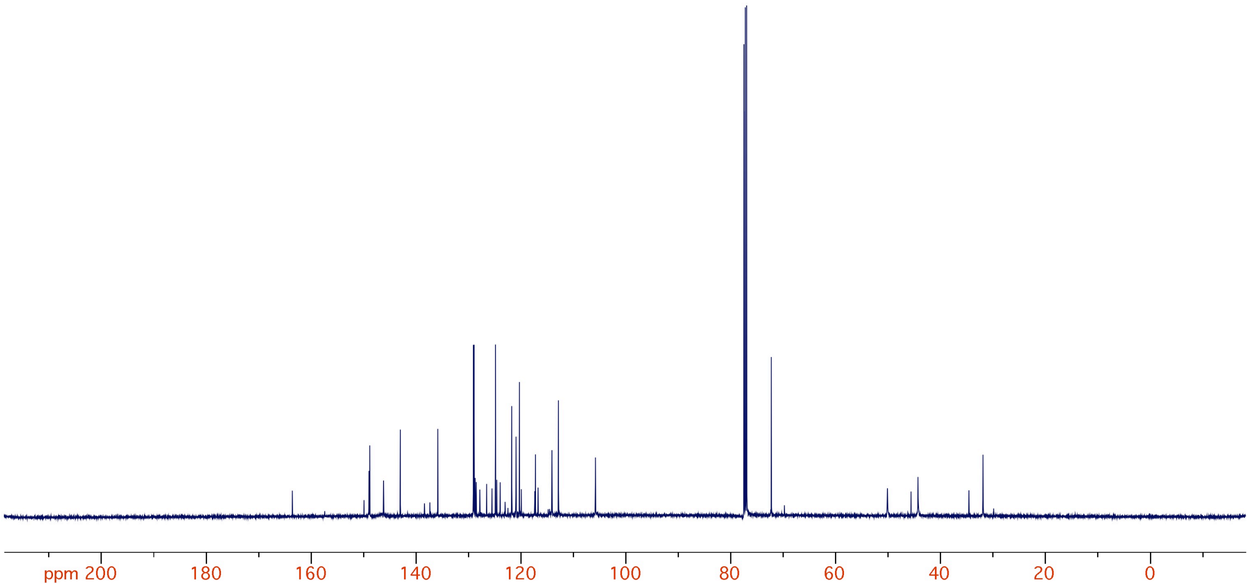

^{13}C NMR spectrum of **13** in $CDCl_3$ (125 MHz).

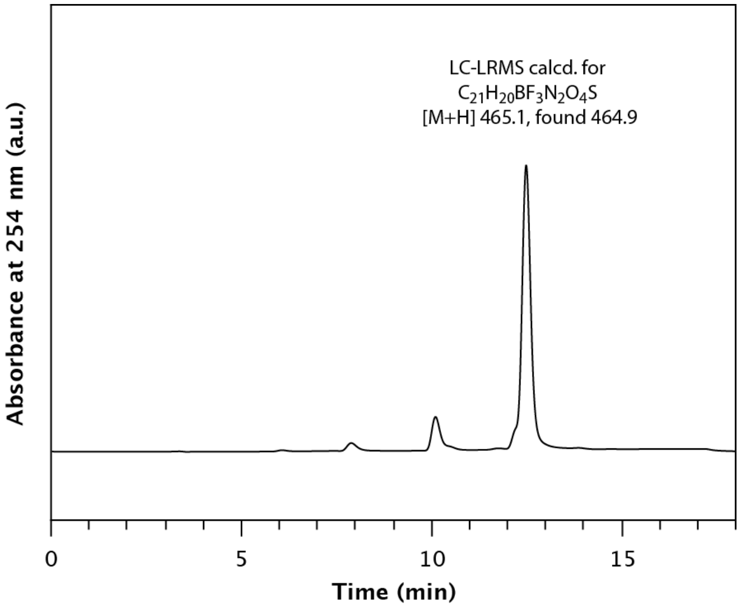

LC-LRMS trace of **13**.

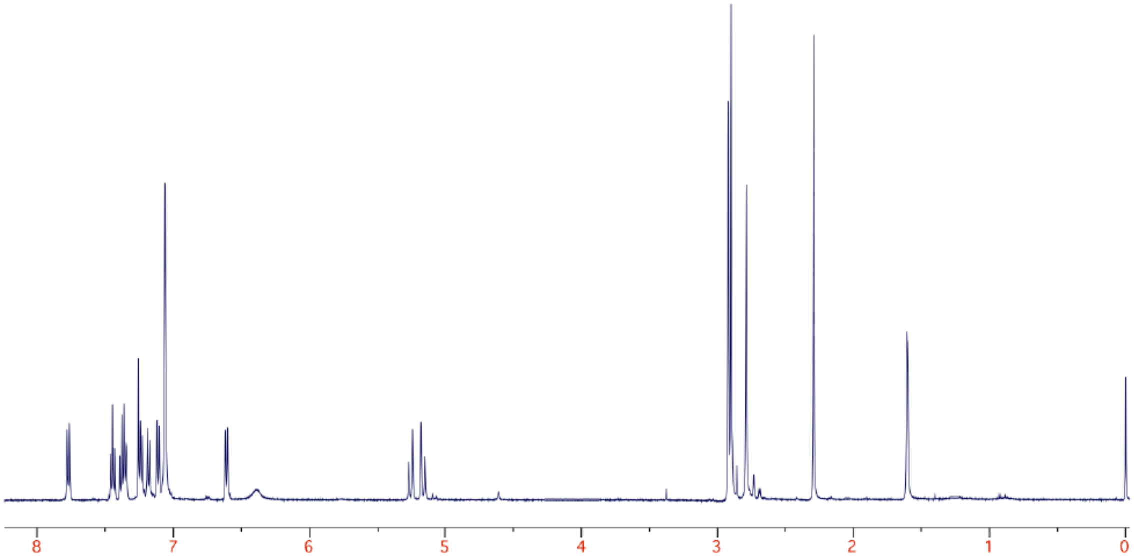

^{1}H NMR spectrum of **14** in $CDCl_3$ (750 MHz).

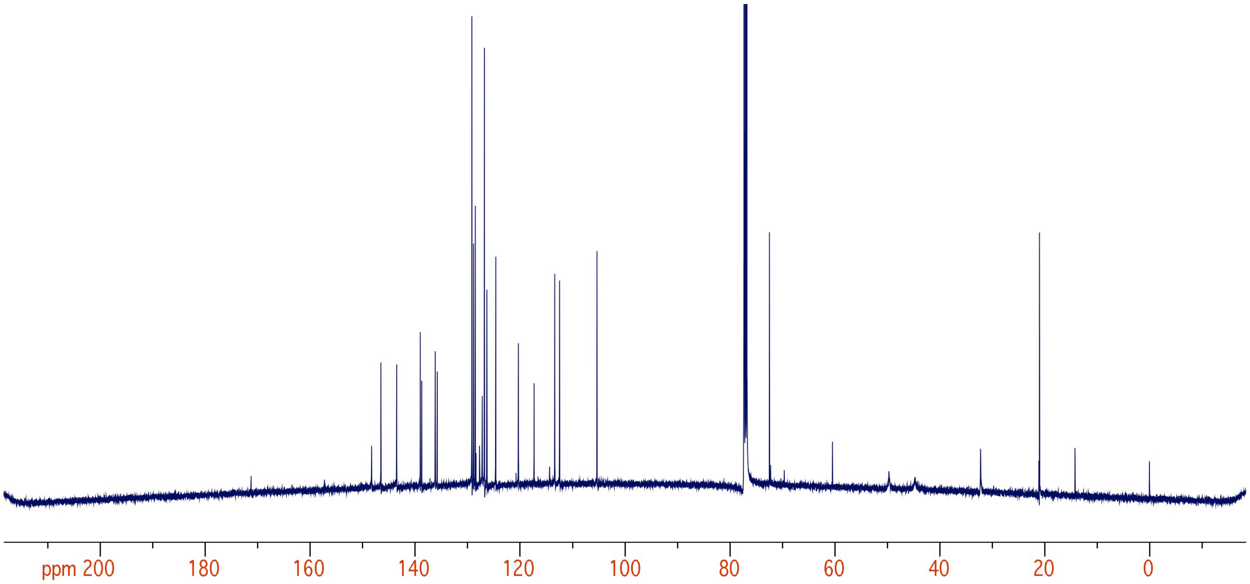

^{13}C NMR spectrum of **14** in $CDCl_3$ (125 MHz).

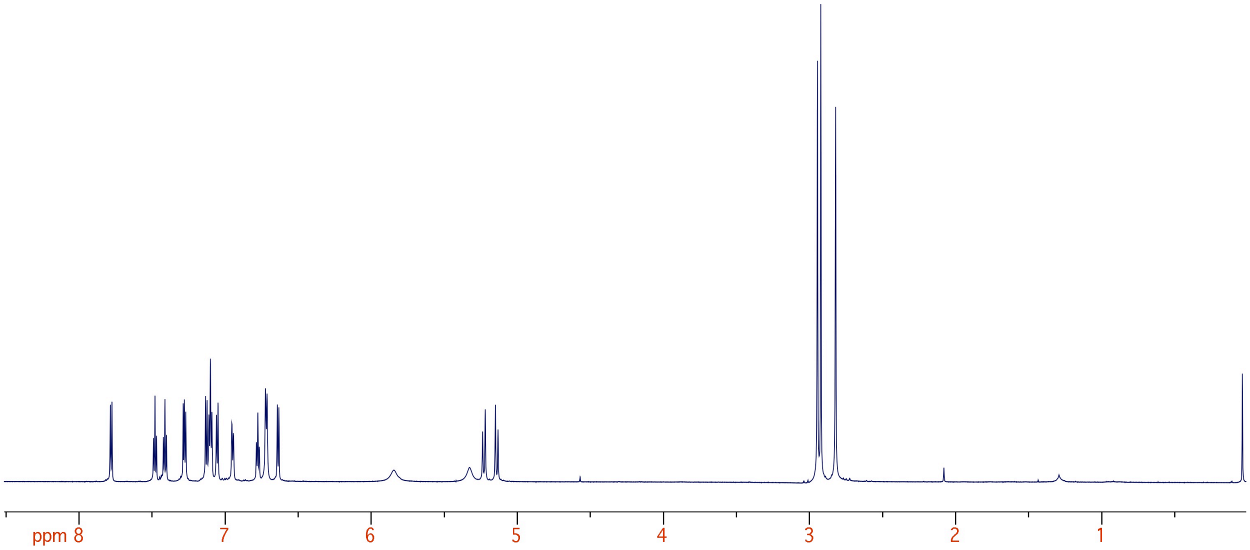

^{1}H NMR spectrum of **15** in $CDCl_3$ (750 MHz).

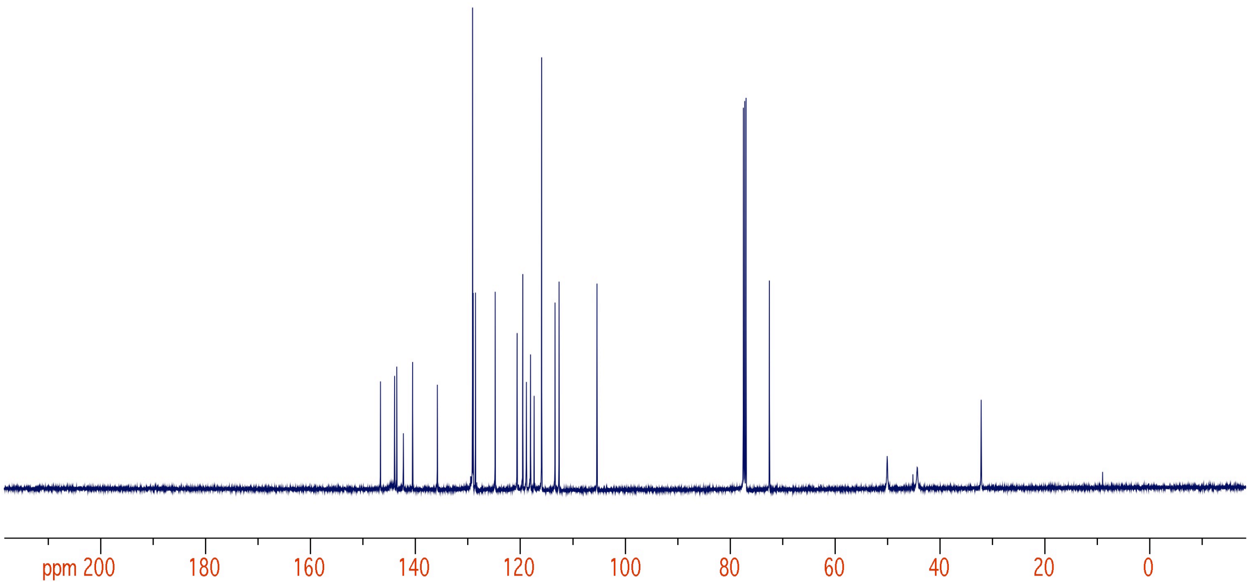

^{13}C NMR spectrum of **15** in $CDCl_3$ (125 MHz).

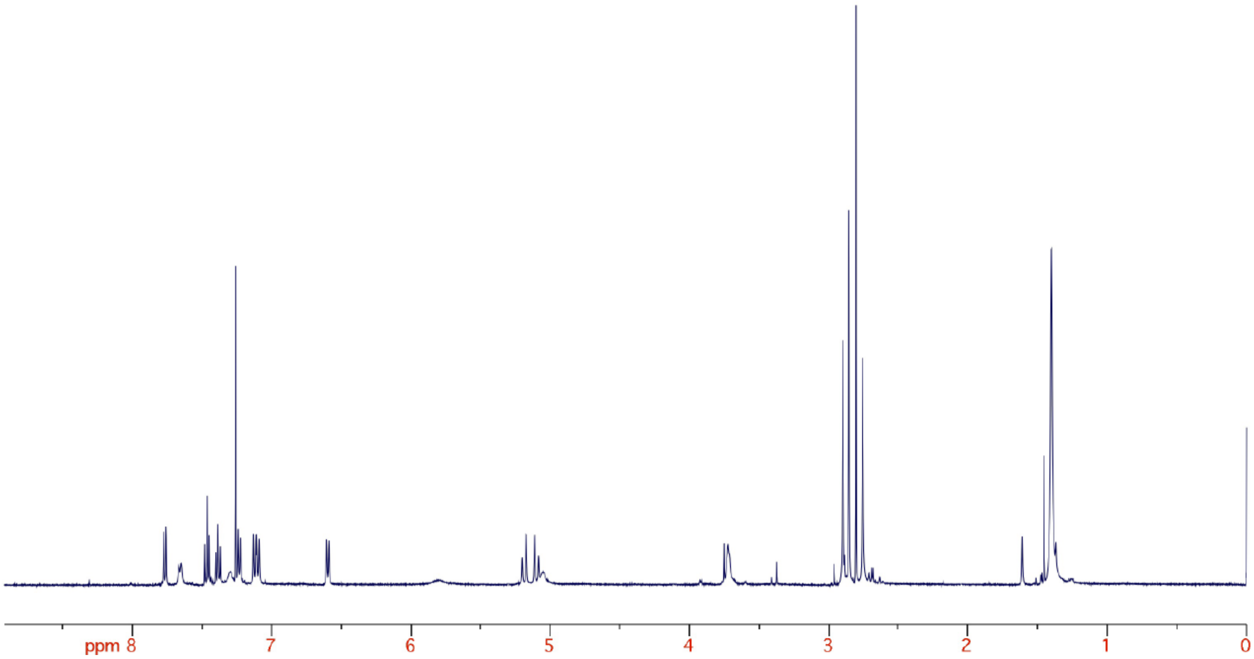

^{1}H NMR spectrum of **16** in $CDCl_3$ (500 MHz).

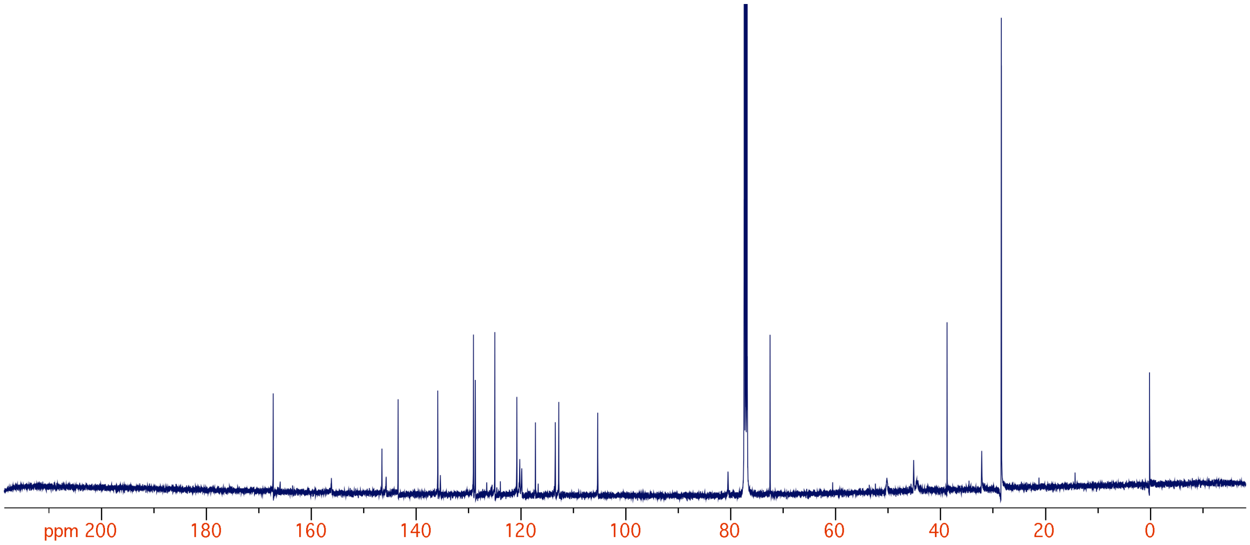

^{13}C NMR spectrum of **16** in $CDCl_3$ (125 MHz).

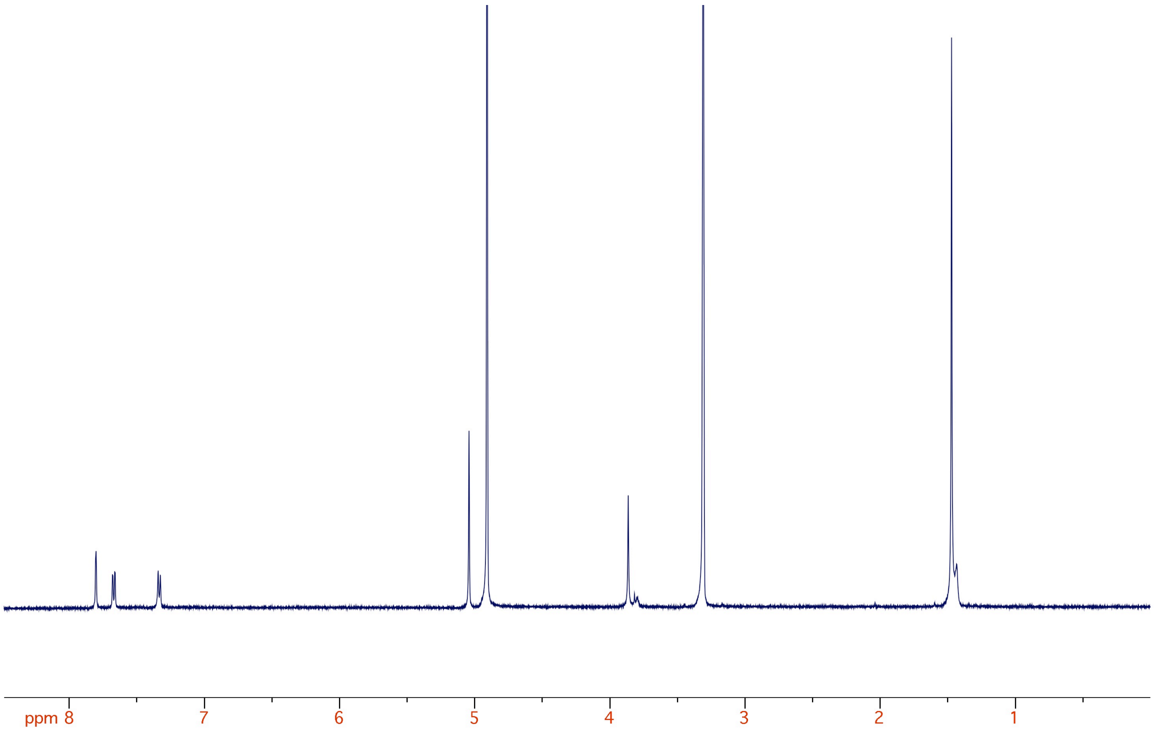

^{1}H NMR spectrum of **18** in $CDCl_3$ (500 MHz).

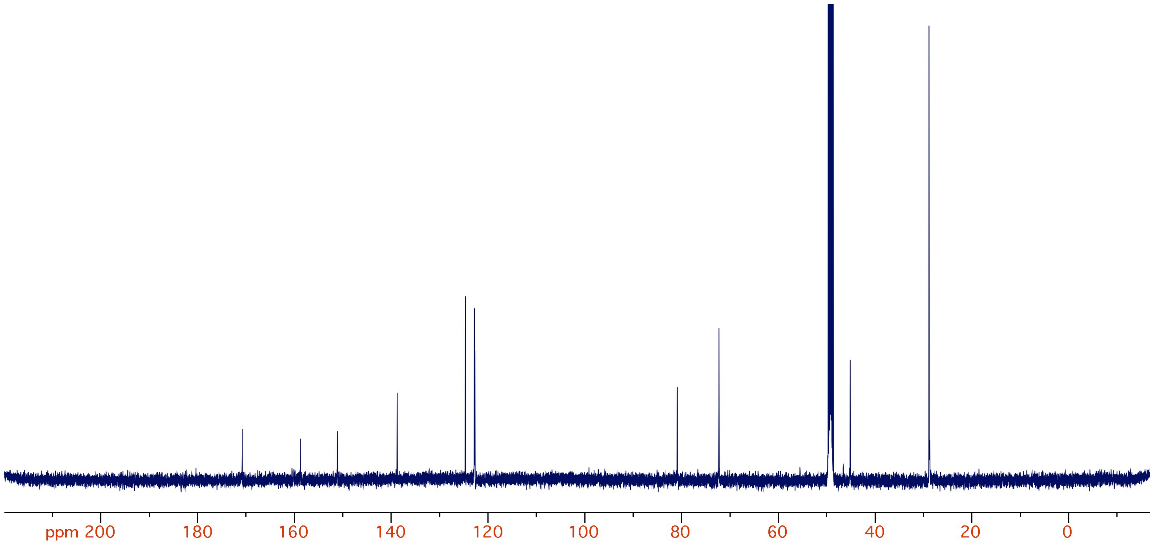

^{13}C NMR spectrum of **18** in $CDCl_3$ (125 MHz).

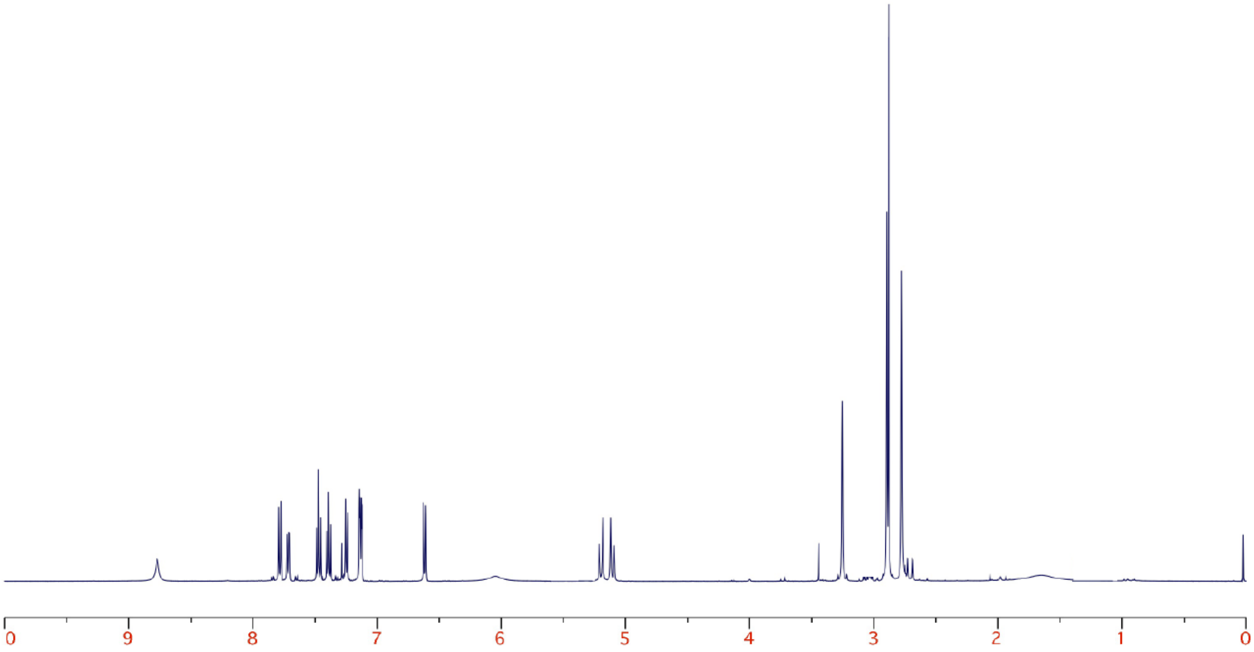

^{1}H NMR spectrum of **17** in $CDCl_3$ (500 MHz).

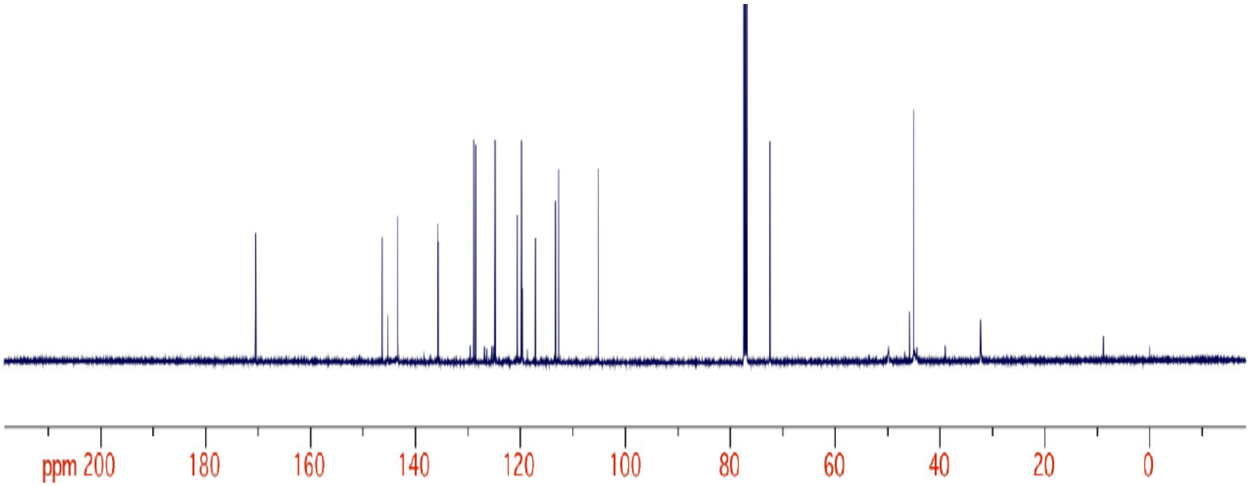

^{13}C NMR spectrum of **17** in $CDCl_3$ (125 MHz).

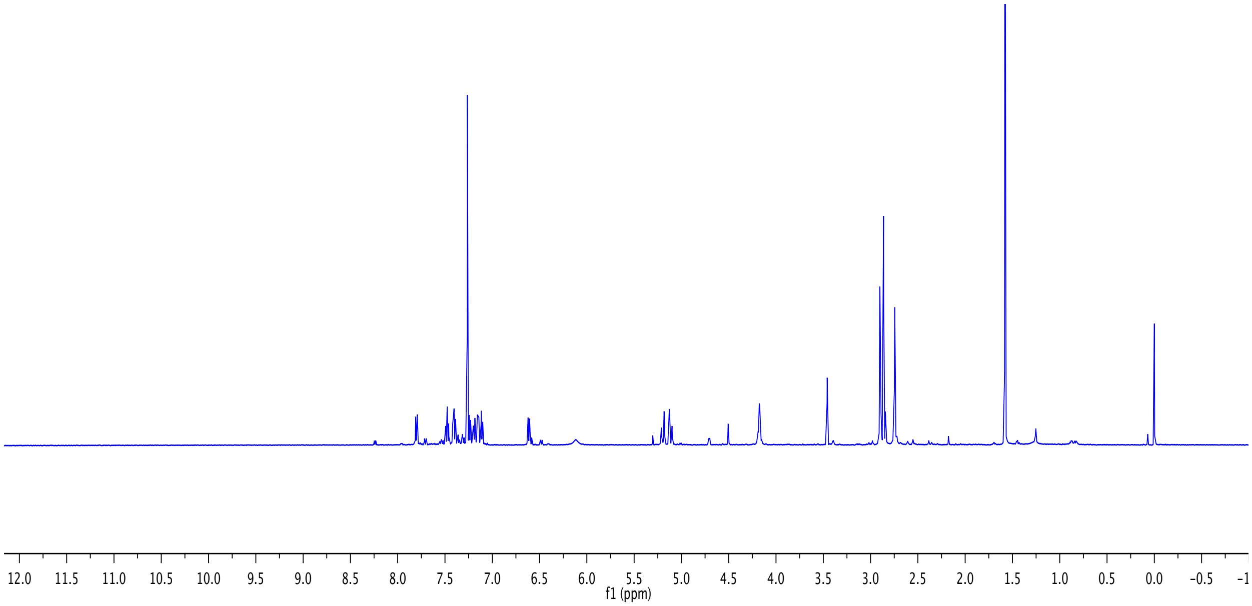

^{1}H NMR spectrum of **19** in $CDCl_3$ (500 MHz).

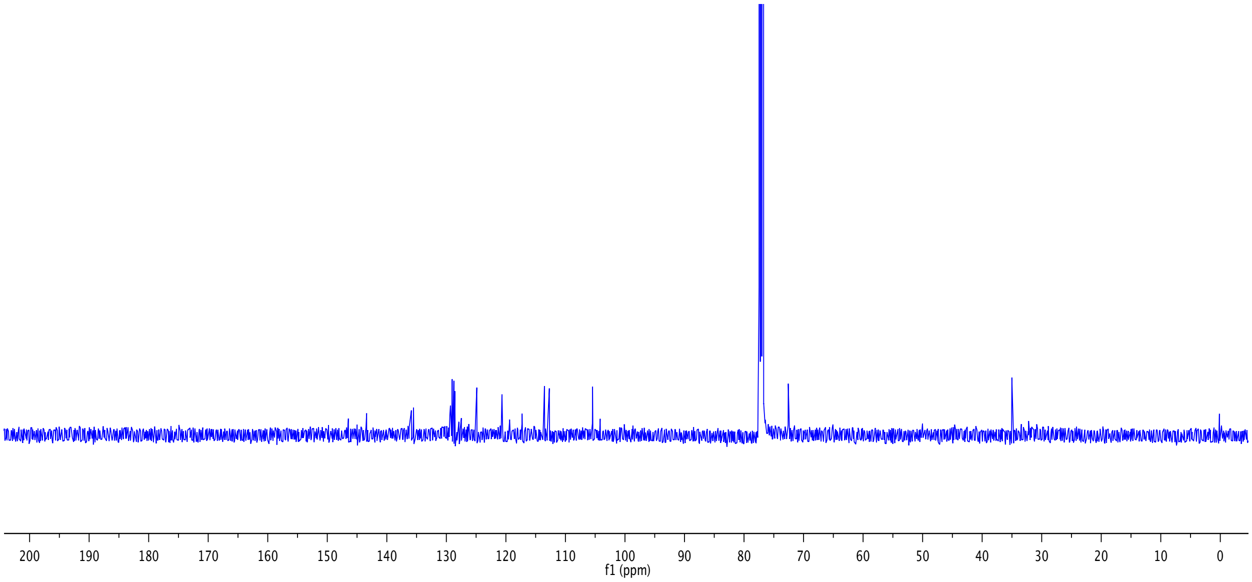

^{13}C NMR spectrum of **19** in $CDCl_3$ (125 MHz).

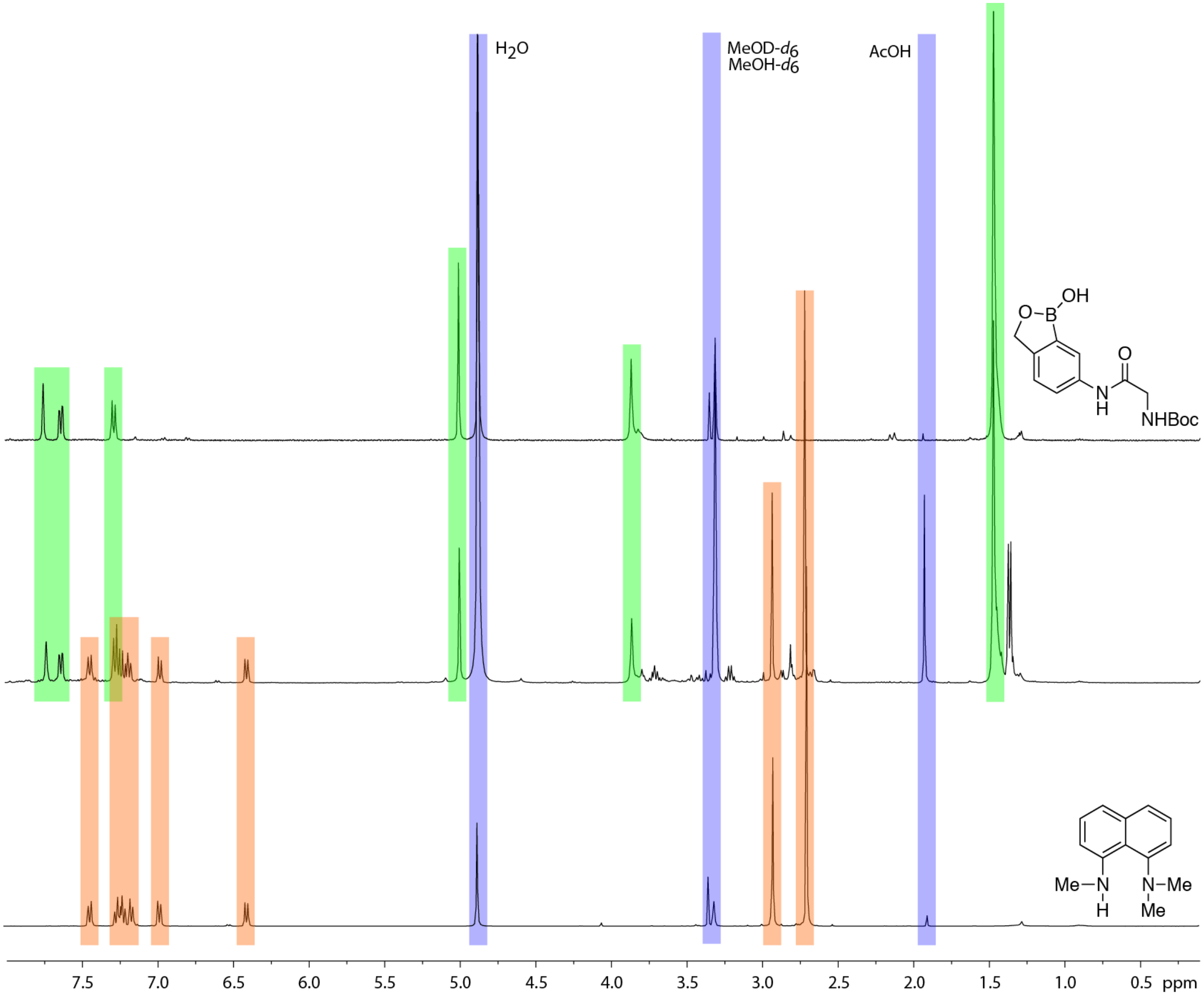

^{1}H NMR spectra (MeOD-d_6, 400 MHz) comparing compound **18** (top), compound **10** (bottom), and the reaction products from compound **16** (middle; for experimental details, see: **Synthesis** section). Colored bars (**18**, green; **10**, orange; solvent, blue) are used to indicate that the expected products are indeed present.

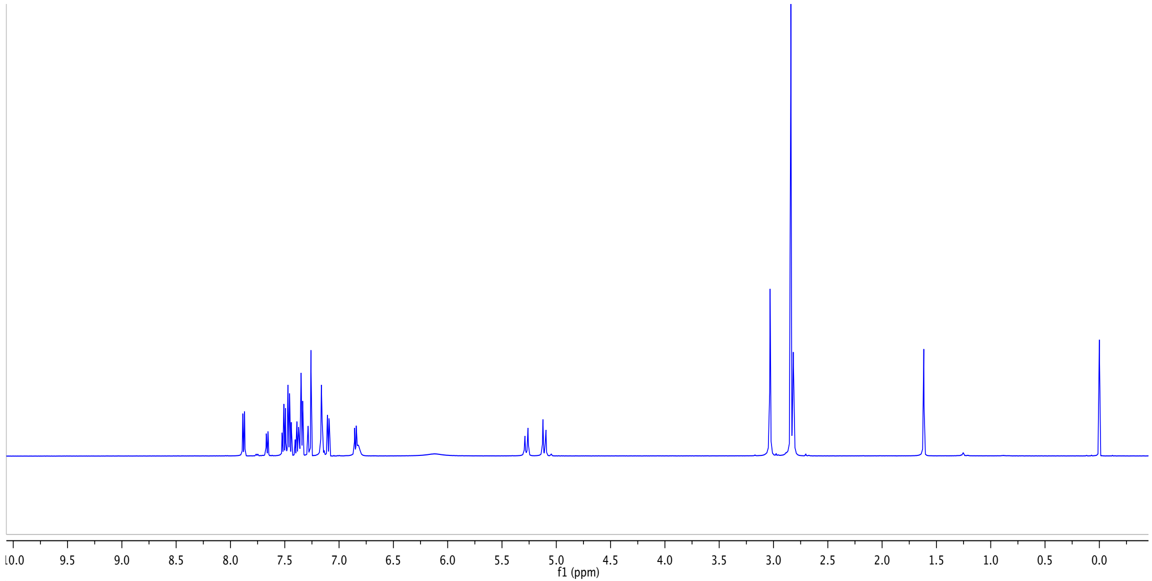

^{1}H NMR spectrum of the complex of **1a** and **19** in $CDCl_3$ (500 MHz).

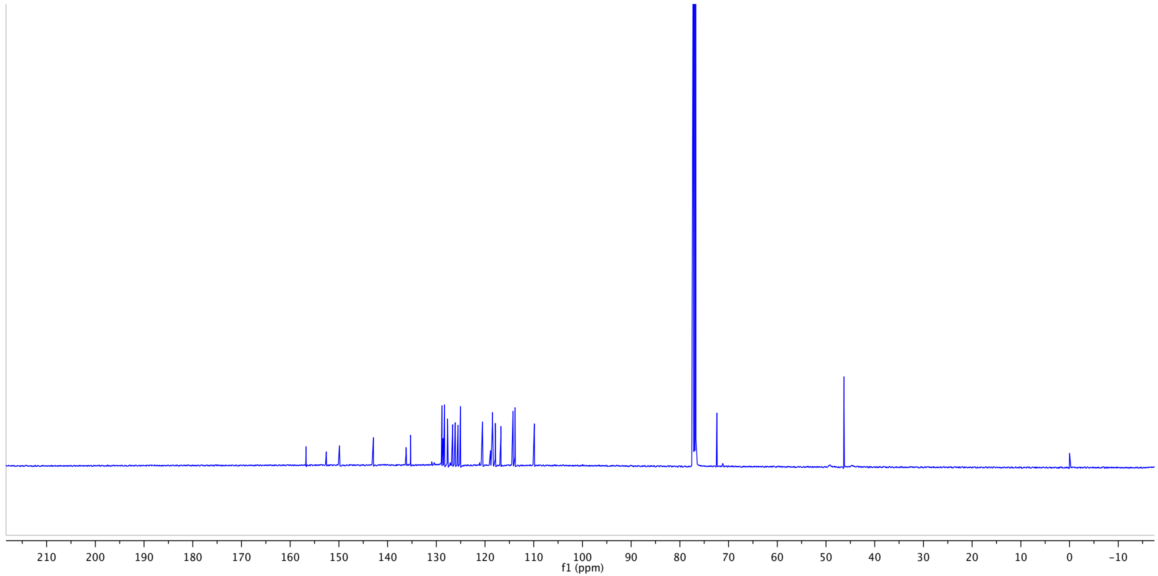

^{13}C NMR spectrum of the complex of **1a** and **26** in $CDCl_3$ (125 MHz).

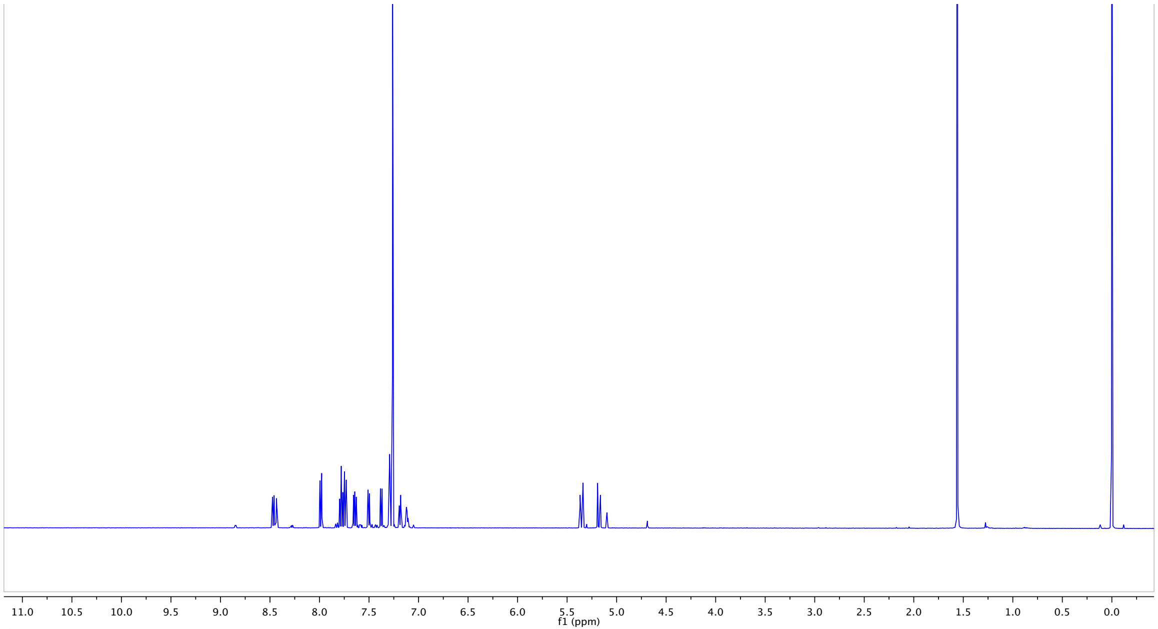

^{1}H NMR spectrum of the complex of **1a** and **26** in $CDCl_3$ (500 MHz).

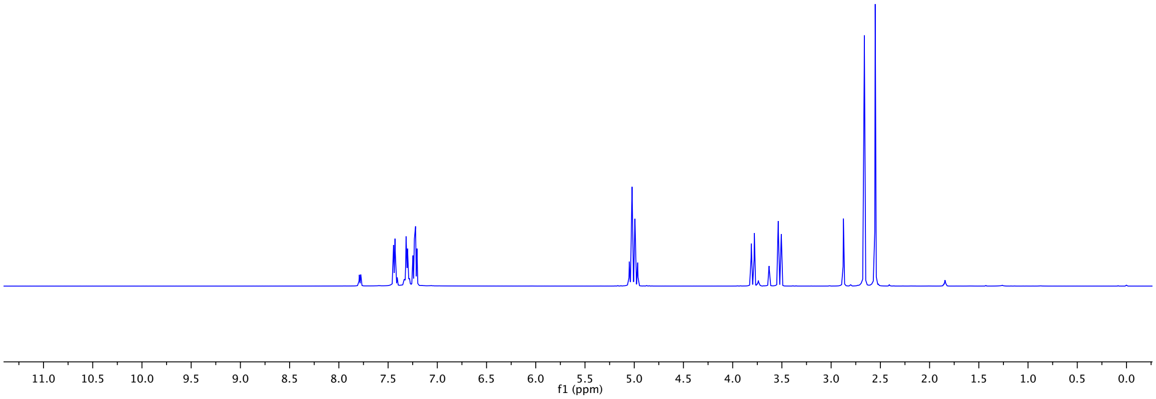

^{1}H NMR spectrum of the complex of **1a** and **28** in $CDCl_3$ (500 MHz).

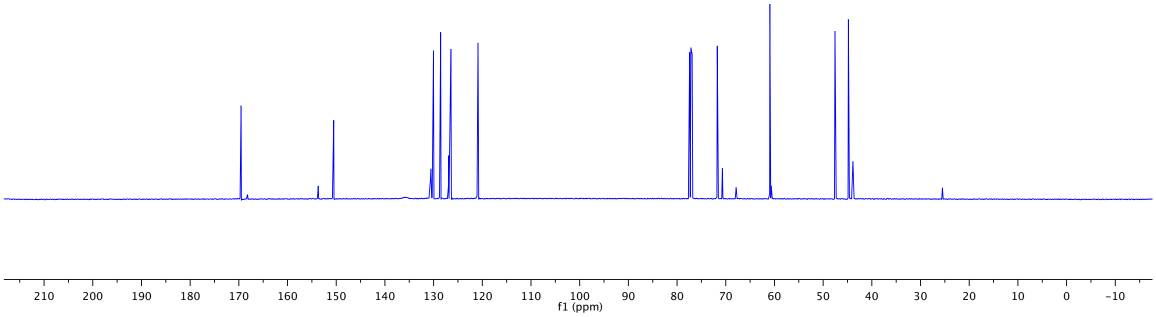

^{13}C NMR spectrum of the complex of **1a** and **28** in CDCl$_3$ (125 MHz).

Photophysical Data for Compound **11a**

abs λ_{max} (nm)^a	em λ_{max} (nm)^a	log ε	Φ_F
366	424	3.24	0.45

^{a} In CHCl$_3$.

PART 2

CHAPTER 3

Detection of Boronic Acids through Excited-State Intramolecular Proton-Transfer Fluorescence

Prepared as: Matthew R. Aronoff, Brett VanVeller, and Ronald T. Raines (2013). *Org. Lett.*, *15*, 5382–5385

Contributions: I made the initial discovery of the fluorescent complexes formed by HBQ with boronic acids, developed the conditions of the assay, and performed various testing and analysis. B.V. investigated materials applications and physical characteristics, and I wrote the manuscript with assistance from B.V.

Note: This chapter was published in part as Matthew R. Aronoff, Brett VanVeller, and Ronald T. Raines (2013). *Org. Lett.*, *15*, 5382–5385

This work also appears in the following patent: Protecting Groups for Boronic Acids P130142US01 Raines, R. T.; VanVeller, B.; Aronoff, M. R.

Abstract

Boronic acids are versatile reagents for the chemical synthesis of organic molecules. They and other boron-containing compounds can be detected readily by the interruption of the excited-state intramolecular proton transfer (ESIPT) of 10-hydroxybenzo[*h*]quinolone. This method is highly sensitive and selective, and useful for monitoring synthetic reactions and detecting boron-containing compounds on a solid support.

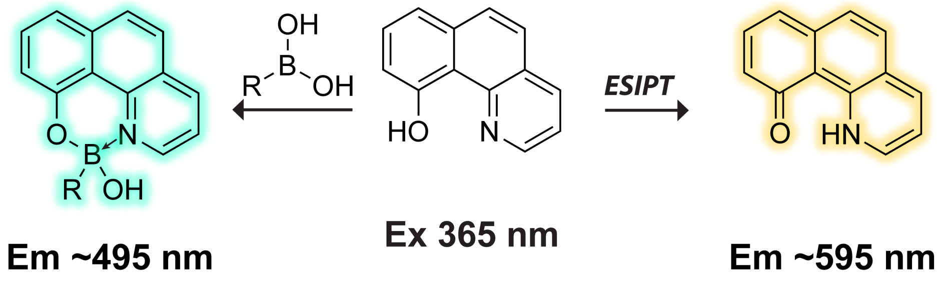
O
B
N
R
OH
OH
R
B
OH
HO
N
ESIPT
O
HN
Em ~495 nm
Ex 365 nm
Em ~595 nm

2.3.1 Introduction

Boronic acids are among the most useful reagents in modern synthetic organic chemistry.[322] Boronic acids also have notable utility in carbohydrate sensing[231] and medicinal chemistry.[323] These applications and underlying synthetic transformations could benefit from facile means to detect boronic acid moieties, a task that is now problematic.[324-326] Neither UV absorption nor common staining reagents (*e.g.*, $KMnO_4$, ceric ammonium molybdate, or vanillin) identify boronic acid-containing synthetic targets selectively. [323,327,328] Buchwald and coworkers reported the *in situ* detection of boronic acid consumption using dihydroxycoumarins.[324] This method does not, however, extend to the detection of boronic acids during thin-layer chromatography (TLC). Alizarin (ARS) has also been put forth as a boron-selective TLC stain,[269-271] but is not especially senstitive (*vide infra*). Here, we present a new approach for the selective and sensitive detection of boronic acids based on the photophysical process known as excited-state intramolecular proton transfer (ESIPT).[329]

We were aware that the absorbance of phenols can be modulated by their complexation to boronic acids.[276,330-332] We also knew that protic solvents interrupt the ESIPT of 10-hydroxybenzo[*h*]quinolone (HBQ)[333] by disrupting the intramolecular hydrogen bond.[334] Accordingly, we envisioned that boronic acids could disrupt the ESIPT of HBQ through complexation with its phenolic oxygen and nitrogen.[321,335336]

In its ground state, the HBQ chromophore exists as an enol with an intramolecular hydrogen bond (**A**; Figure 2.3.1). At its absorbance maximum (365 nm), singlet-excitation of HBQ occurs without geometry relaxation, in accord with the Franck–Condon principle (**B**). There are two fates for this excited state: (i) relaxation back to the ground state (**A**) through fluorescence (~400 nm), or (ii) ultrafast ESIPT (~100 fs) to the keto tautomer in its singlet excited state (**C**). The geometry-relaxed keto form **C** is distinct from the enol form **B**, leading to a large Stokes shift upon emissive relaxation (~600 nm) to **D**, where ground-state reverse proton transfer returns the enol form **A**. ESIPT (**B→C**) is typically faster than fluorescence relaxation (**B→A**), and the emission from ESIPT tends to dominate.

2.3.2 Results and Discussion

In initial experiments, we compared the sensitivity of HBQ and ARS as a TLC-stain for phenylboronic acid. We found that the 365-nm absorbance maximum of HBQ (which, conveniently, is the output wavelength of most common bench lamps) and the large Stokes shift provided by ESIPT lead HBQ to have ~10^3-fold greater sensitivity than ARS (Figure 2.3.2).

Encouraged by the high sensitivity of HBQ, we sought to explore the generality of the HBQ stain by testing a series of structurally diverse boronic acids. High concentrations of aliphatic boronic acids were not visible under a standard short-wave UV handheld lamp (Figure 2.3.3). Nonetheless, by immersing the TLC plate in a 1 mM solution of HBQ and drying, all spots became brightly fluorescent, with differences in emission wavelength related to the substituents on the boronic acid.[337] The spots appear as bright blue-green (emission from **B**) against a yellow-orange background (emission from **C**). Both pinacol- and diaminonaphthalene-protected boronic acids possess a vacant *p*-orbital, allowing efficient staining with HBQ according to our proposed mechanism. Even a boronic acid protected with *N*-methyliminodiacetic acid (MIDA) is detectable by the (presumably) small amount of boron with a vacant *p*-orbital. Trifluoroborates likely suffer hydrolysis on the TLC plate[338] to form a detectable boronic acid.

Next, we assessed the selectivity of HBQ for boronic acids. Compounds with a wide variety of functional groups (but not a boronic acid) were spotted onto silica plates at concentrations visible with a standard short-wave UV handheld lamp, and treated with HBQ stain. In general, there was no fluorescence with the functional groups (Figure 2.3.4). Notably, the dark spots remained visible upon illumination at 254 nm following treatment with the HBQ stain. Thus, information from short-wave illumination is retained after the stain develops, in marked contrast to other staining methods. Whereas sensitive functional groups (*e.g.*, aldehydes, diazos, anhydrides, and epoxides) resisted staining, highly electrophilic functional groups (*e.g.*, acyl chlorides and sulfonyl chlorides) gave false-positive results, producing a blue fluorescence upon illumination at 365 nm that is similar to that observed from boronic acids. These data validate our mechanism, as these electrophilic functional groups can react with the phenolic hydroxyl group of HBQ and interrupt the ESIPT cycle. Moreover, these false-positive results do not compromise selectivity in practice, as TLC is used only rarely to monitor such reactive functional groups.

We reasoned that the detection method could apply to boronic acids bound to a solid support. Immobilized boronic acids have found application in glycan-affinity chromatography because of their ability to bind to diols.[331,339,340] Similarly, boronated solid supports are used widely for the immobilization of biomolecules,[341-344] lithography,[345] and various glycan-sensing schemes.[276,346-348] Using a boronated agarose as a model, we observed ESIPT-off fluorescence upon treatment with 10 mM HBQ in

EtOH. In contrast, only ESIPT-on fluorescence was observed for unconjugated agarose, and no native fluorescence was ascribed to conjugated agarose in the absence of HBQ (Figure 2.3.5). Such facile detection could be used to assess boron functionalization qualitatively during solid-support device fabrication.

Lastly, we investigated the potential of HBQ for the quantitative detection of boron-containing compounds. A simple plate-reader enabled the detection of nanomoles of phenylboronic acid (Figure 2.3.7). Notably, fluorescence intensity correlated linearly with the amount of boron.

2.3.3 Conclusions

In summary, we present a novel method for the sensitive and selective detection of boronic acids and other boron-containing compounds. The method, which is based on the ability to turn off the ESIPT of HBQ, provides much greater sensitivity than extant methods. Moreover, the resultant HBQ–boron complexes remain fluorescent in the solid state. Accordingly, this method could be beneficial to synthetic chemistry and materials science.

2.3.4 Acknowledgements

The authors are gratefull to Dr. M.J. Palte for contributive discussions, R. Davies of the MediaLab for assistance with photography, and T. Santos for assistance with microscopy. This work was supported by grant R01 GM044783 (NIH). B.V. was supported by postdoctoral fellowship 289613 (CIHR).

2.3.5 Materials & Methods

Materials

Silica-coated thin layer chromatography plates were obtained from Macherey Nagel (Duren, Germany). All reagent-grade materials were from Sigma–Aldrich (St. Louis, MO) and were used without further purification, except for phenylboronic acid, benzoxaborole, and 3-nitrophenylboronic acid, which were from Combi-Blocks (San Diego, CA).

Image Capture

The images in Figures 2.3.2 and 2.3.3 were acquired with a Nikon digital SLR camera under identical exposure times. Technical details are provided in the Camera Settings section. Bright-field and epifluorescent microscopy images of agarose beads were performed on an upright microscope equipped with a CCD camera with 4× magnification. Epifluorescence images were taken by illuminating at ~365 nm using a handheld UV lamp.

Experimental Methods

Spotting for Figure 2.3.2. Alizarin Red Stain was prepared and applied according to the previous report of Duval and coworkers.[325] A 1.0 mM solution was prepared by adding 0.10 mmol of Alizarin to 0.10 L of anhydrous acetone. Optimal visualization was accomplished by slow immersion of silica-coated glass TLC plates in the alizarin solution, removal, and then allowing the stain to dry completely at room temperature.

Plates were then viewed by illuminating the beads at ~365 nm using a handheld UV lamp.

A 1.0 mM solution of HBQ stain was prepared by adding 0.10 mmol of 10-hydroxybenzo[*h*]quinoline to 0.10 L of absolute ethanol. Optimal visualization was accomplished by immersion of silica-coated glass TLC plates in the HBQ solution, and then allowing the stain to dry completely by applying a standard laboratory heat gun. Plates were then viewed by illuminating at ~365 nm using a handheld UV lamp.

A 10 mM solution of phenylboronic acid was prepared by addition to methanol. Subsequent dilutions were prepared in methanol from the original 10 mM stock.

Spotting for Figures 2.3.3 and 2.3.4. All positive controls were prepared as solutions at 10 mM concentrations in methanol. All compounds tested were applied as 2-μL samples to a glass backed TLC plate and allowed to air-dry at room temperature. Negative control samples were prepared in methanol at concentrations required for sufficient visualization following absorbance at 254 nm, prior to dye treatment, and allowed to air-dry at room temperature.

A 1.0 mM solution of Alizarin in acetone was prepared. Visualization was accomplished by slow immersion of silica-coated glass TLC plates in the alizarin solution, removal, and then allowing the stain to dry completely at room temperature. Plates were then viewed by illuminating at ~365 nm using a handheld UV lamp

HBQ stain was prepared by adding 0.10 mmol of 10-hydroxybenzo[*h*]quinoline to 0.10 L of absolute ethanol. Detection was performed by briefly immersing the TLC plate in solution, then drying the plate using a standard laboratory heat gun. Plates were viewed by illuminating at ~365 nm using a handheld UV lamp.

Detection of Boronic Acids on Agarose Support. The following preparation was performed on Agarose beads (6% cross-linking) with and without bound *m*-aminophenylboronic acid. Agarose beads (50 mg) were suspended in methanol and filtered. The beads were resuspended in 1.0 mL of HBQ stain solution for 1 min and filtered and washed with 5 mL EtOH. The beads were dried and imaged using microscopy.

HBQ fluorescence relationship with phenylboronic acid (Figure 2.3.7). Fluorescence intensity was measured with an Infinite M1000 Pro microplate reader (Tecan Group, Mannedorf, Switzerland). Phenylboronic acid (PBA) was prepared from a 20 mM stock in methanol, as described previously. PBA solution (20 μL) was applied to cover the bottom of each well of a sterile 96-well plate (Costar black plate, clear bottom with lid from Corning, Tewksbury, MA). To ensure that HBQ stain was in excess, to each sample was added 50 μL of a 10 mM HBQ solution in ethanol for 20, 10, and 5 mM PBA, and 20 μL of a 1 mM HBQ solution in ethanol for other dilutions of PBA. The resulting solutions were allowed to dry completely before analysis.

Bottom-up fluorescence was measured in triplicate for each dilution. Excitation was applied at 365 nm with a 5.0-nm bandwidth. Emission was detected at 500 nm with a 5.0-nm bandwidth to minimize oversaturation of the detector. Multiple reads per well were measured in a 4 × 4 filled circle with a 100-μm border, and then averaged for each sample well. Average values of fluorescence intensity were plotted with the program Prism from GraphPad (La Jolla, CA). Error bars were determined based on standard deviation from average values.

Figure 2.3.1 Excited-State Intramolecular Proton Transfer (ESIPT) cycle of 10-hydroxybenzo[*h*]quinoline (HBQ).

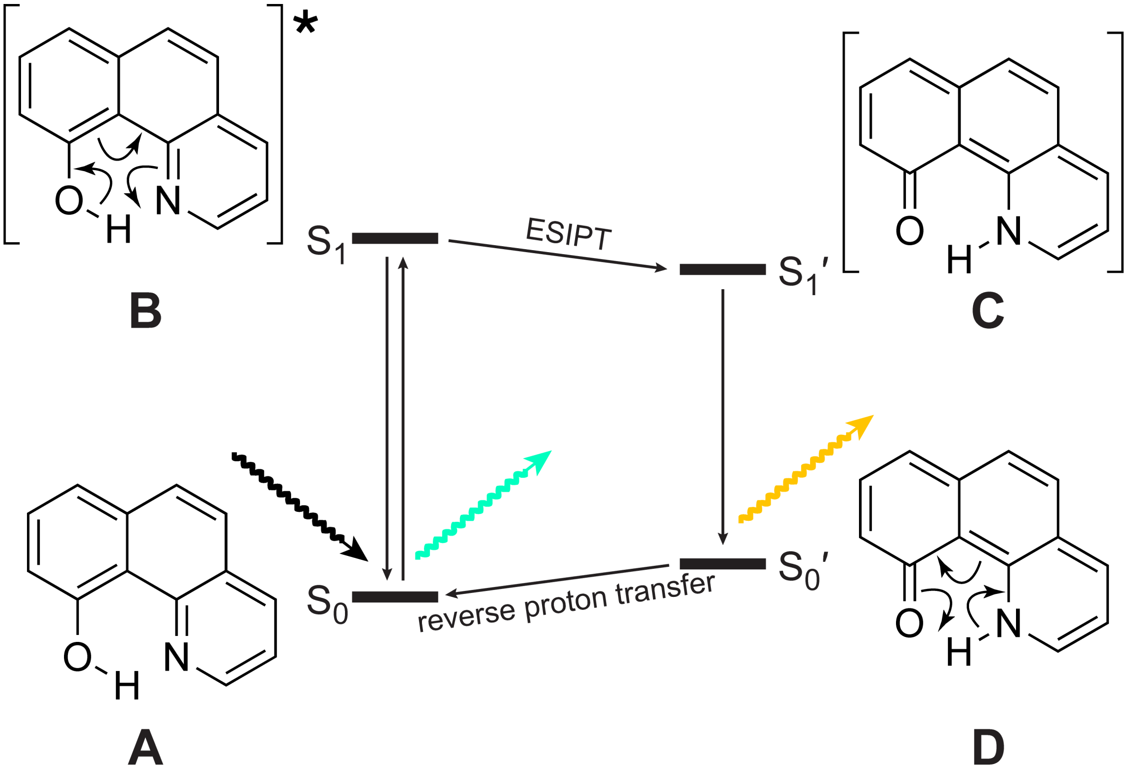

B
C
A
D
S1
S1′
S0
S0′
ESIPT
reverse proton transfer

Figure 2.3.1 Excited-State Intramolecular Proton Transfer (ESIPT) cycle of 10-hydroxybenzo[*h*]quinoline (HBQ). A Lewis acidic boronic acid or other boron-containing compound can coordinate to **A** and **B**, which interrupts the cycle by shutting down long wavelength emission ($S_1' \rightarrow S_0'$) and activating short wavelength emission ($S_1 \rightarrow S_0$).

Figure 2.3.2 Comparison of the sensitivity of HBQ and ARS for the detection of a boronic acid.

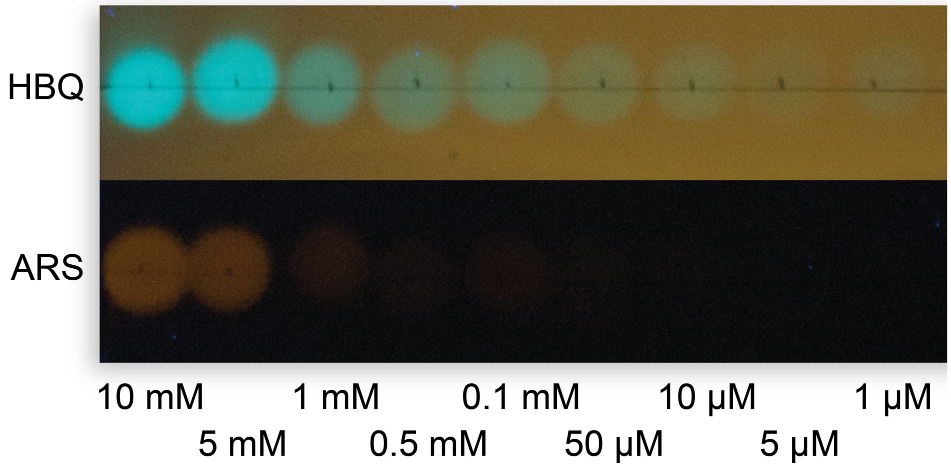
HBQ
ARS
10 mM
5 mM
1 mM
0.5 mM
0.1 mM
50 µM
10 µM
5 µM
1 µM

Figure 2.3.2 Comparison of the sensitivity of HBQ and ARS for the detection of a boronic acid. Serial dilutions of phenylboronic acid (PBA) were spotted on a silica gel thin-layer chromatography plate, stained with HBQ or ARS, and illuminated at 365 nm with a standard handheld lamp.

Figure 2.3.3 Detection of boronic acids and other boron-containing compounds with HBQ.

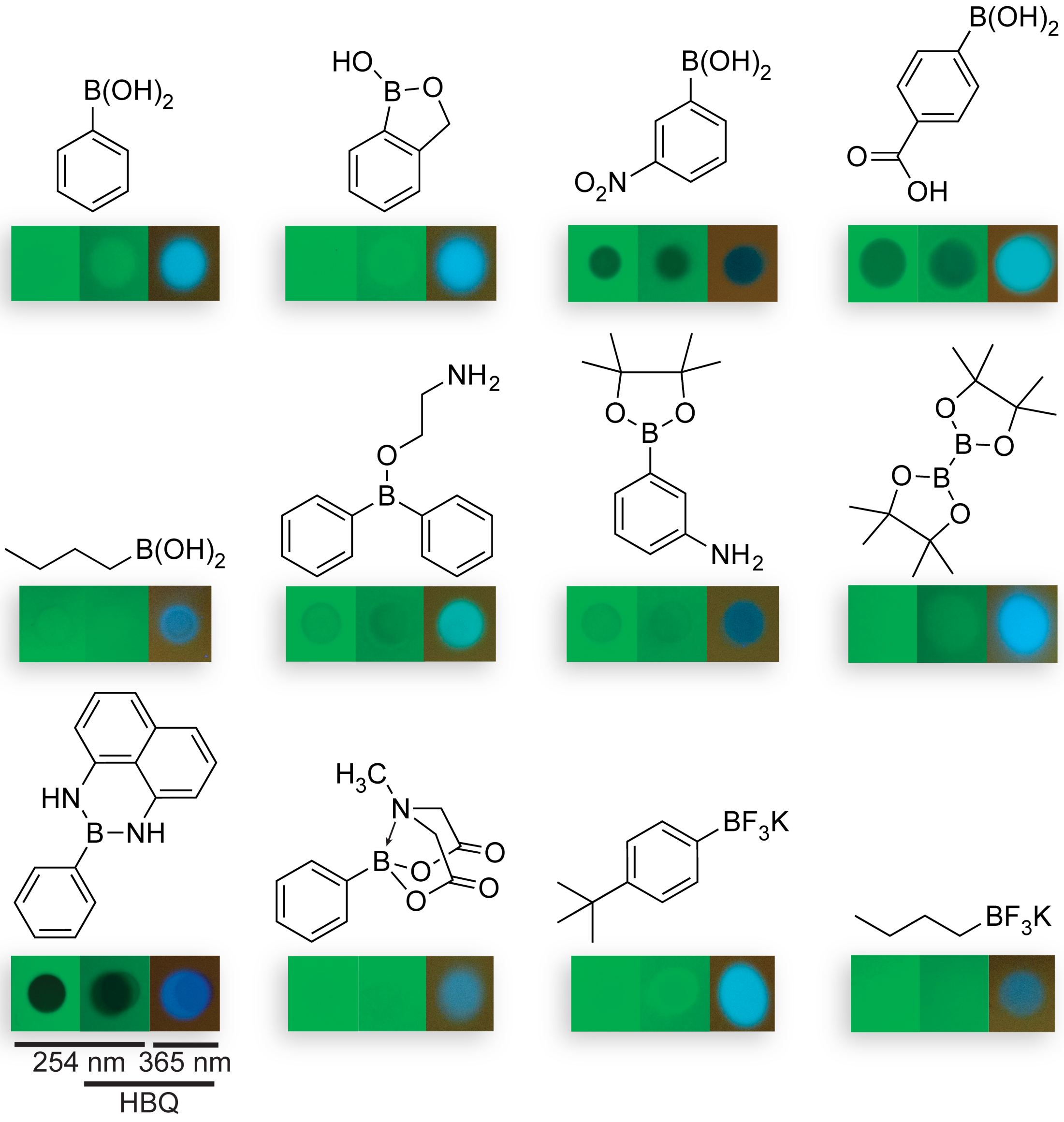
B(OH)$_2$
HO
B–O
B(OH)$_2$
O$_2$N
B(OH)$_2$
O
OH
B(OH)$_2$
NH$_2$
O
B
O
B
O
NH$_2$
O
B–O
O–B
O
HN
B–NH
H$_3$C
N
B
O
O
O
O
BF$_3$K
BF$_3$K
254 nm
365 nm
HBQ

Figure 2.3.3 Detection of boronic acids and other boron-containing compounds with HBQ. Whereas most compounds at 10 mM concentrations were not visible upon illumination at 254 nm, all produced a brilliant blue ESIPT-off fluorescence after staining with HBQ.

Figure 2.3.4 Selectivity of HBQ for functional groups.

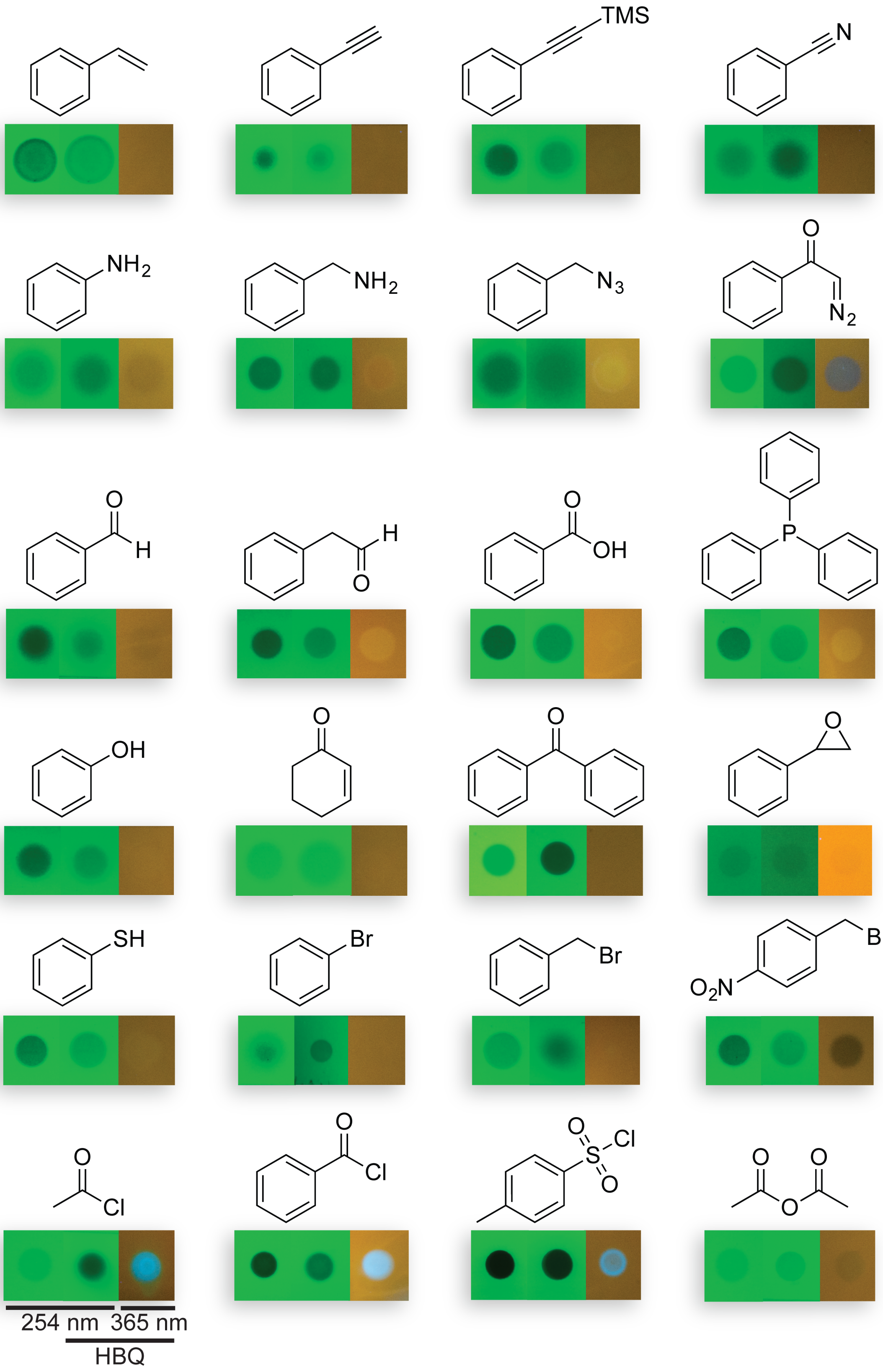
TMS
N
NH_2
NH_2
N_3
O
N_2
O
H
H
O
O
OH
P
OH
O
O
O
SH
Br
Br
Br
O_2N
O
Cl
O
Cl
O
S
Cl
O
O
O
O
254 nm
365 nm
HBQ

Figure 2.3.4 Selectivity of HBQ for functional groups. Compounds visible upon illumination at 254 nm retained this quality following staining with HBQ.

Figure 2.3.5 Detection of a boronic acid on a solid support.

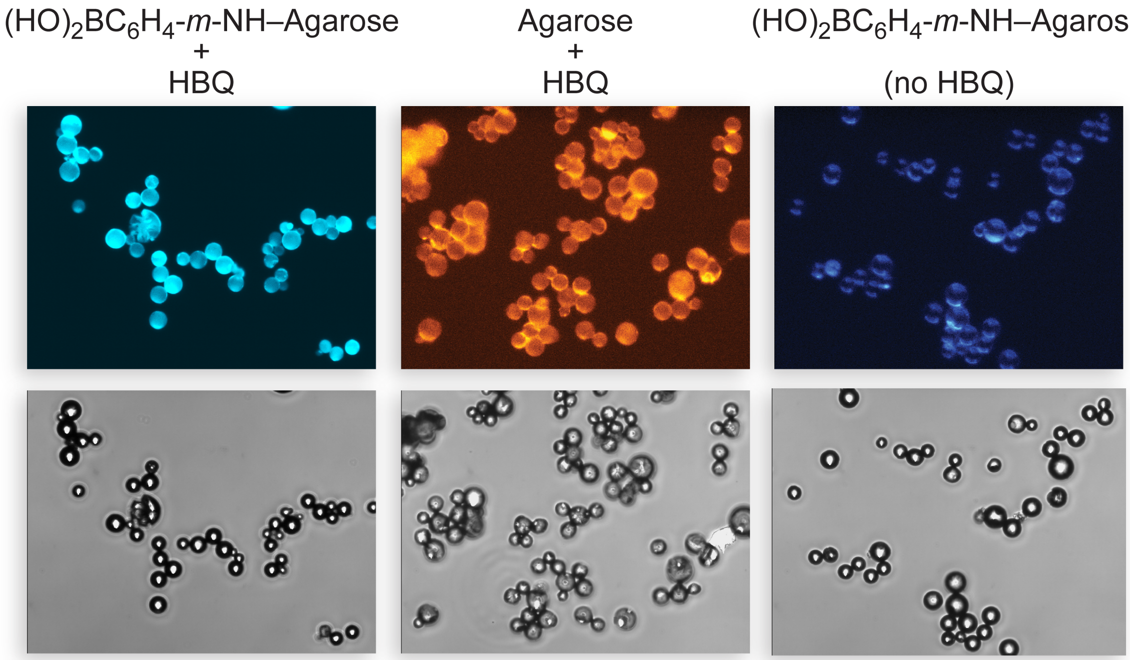

$(HO)_2BC_6H_4$-*m*-NH–Agarose + HBQ

Agarose + HBQ

$(HO)_2BC_6H_4$-*m*-NH–Agarose (no HBQ)

Figure 2.3.5 Detection of a boronic acid on a solid support. Agarose beads (6% cross-linking) were modified covalently with *m*-aminophenylboronic acid and visualized under a microscope upon excitation at 365 nm (top) and in a bright field (bottom).

Figure 2.3.6 Agarose beads viewed "in vial" by illuminating at ~365 nm using a handheld UV lamp without (left image) supplemental lights, and with (right image) overhead lighting.

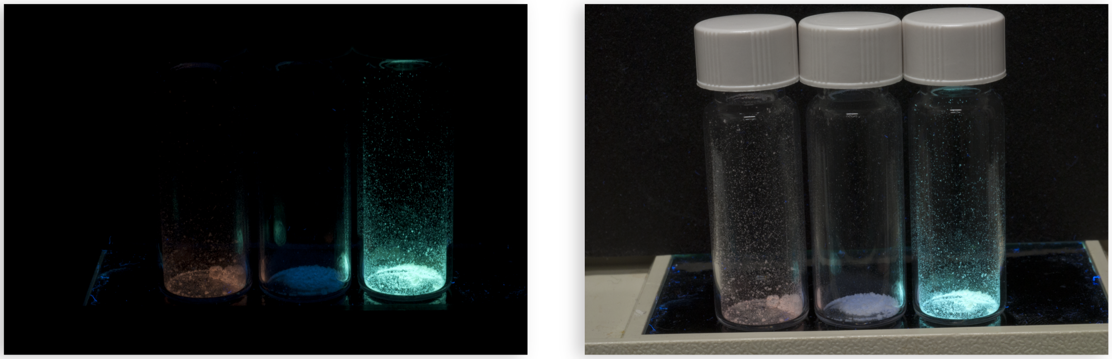

UV lamp only

UV lamp + overhead lighting

Figure 2.3.6 Agarose beads viewed “in vial” by illuminating at ~365 nm using a handheld UV lamp without (left image) supplemental lights, and with (right image) overhead lighting. Non-functionalized agarose treated with HBQ (left, “orange”), 5-amino phenylboronic acid crosslinked agarose, untreated (center), and 5-amino phenylboronic acid functionalized agarose following treatment with HBQ (right, “blue-green fluorescent”).

Figure 2.3.7 Relationship between phenylboronic acid concentration and emitted fluorescence following staining with HBQ.

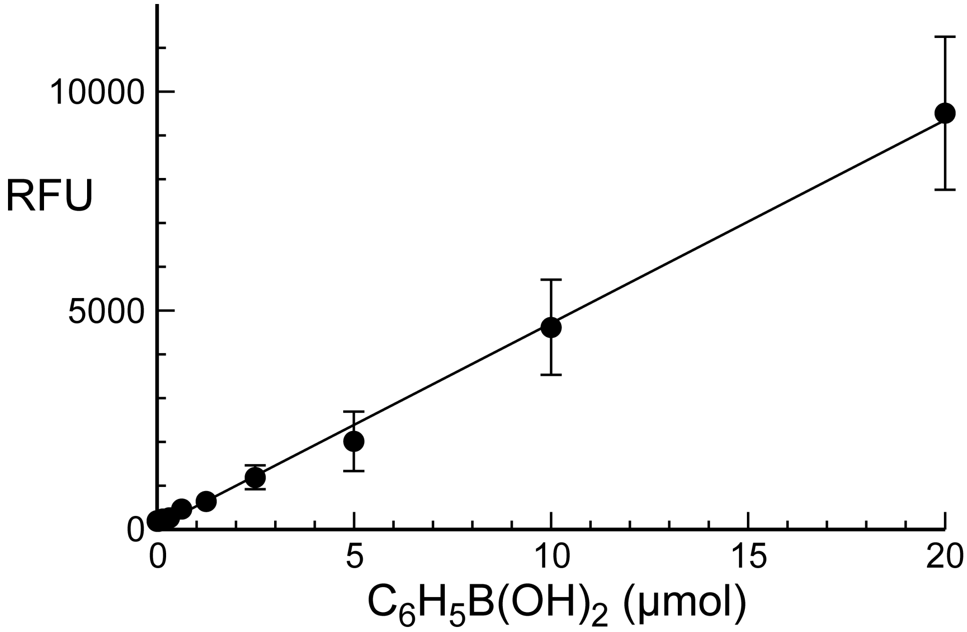

Figure 2.3.7 Relationship between phenylboronic acid concentration and emitted fluorescence following staining with HBQ. Fluorescence was detected using a standard plate-reader and expressed as relative fluorescence units (RFU). Slope = (462 ± 7) RFU/µmol by linear regression analysis ($R^2 = 0.9973$).

Figure 2.3.8 Comparison of 10-hydroxybenzo[*h*]quinolone (HBQ) to 2-(2′-hydroxyphenyl)benzimidazole.

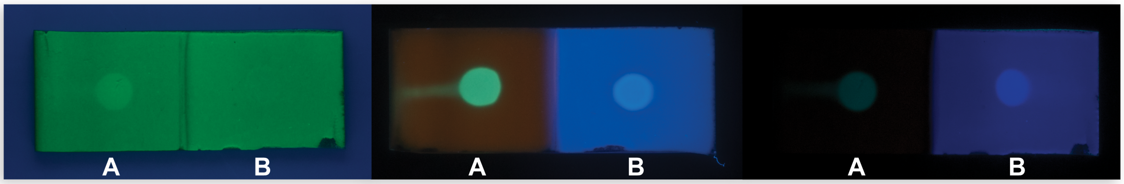

254 nm, 1 s exposure   365 nm, 1 s exposure   365 nm, 0.5 s exposure

Figure 2.3.8 Comparison of 10-hydroxybenzo[*h*]quinolone (HBQ) to 2-(2′-hydroxyphenyl)benzimidazole.[335] Phenylboronic acid in methanol (2 μL of a 10 mM solution) was spotted onto two halves of a glass-backed TLC silica plate and air-dried. The plate was dipped on one side into a 1 mM solution of HBQ in ethanol (A), or a 1 mM solution of 2-(2′-hydroxyphenyl)benzimidazole in ethanol (B). The plate was then dried using a heating gun, and visualized by illuminating at a short (~254 nm) or long (~365 nm) wavelength using a handheld UV lamp. 2-(2′-Hydroxyphenyl)benzimidazole was judged to be inferior as a stain due to the mildly discernable small stokes shift between the ESIPT-on and ESIPT-off emissions compared to those of HBQ.

Figure 2.3.9 Absorption and emission spectra of HBQ and its complex with benzoxaborole.

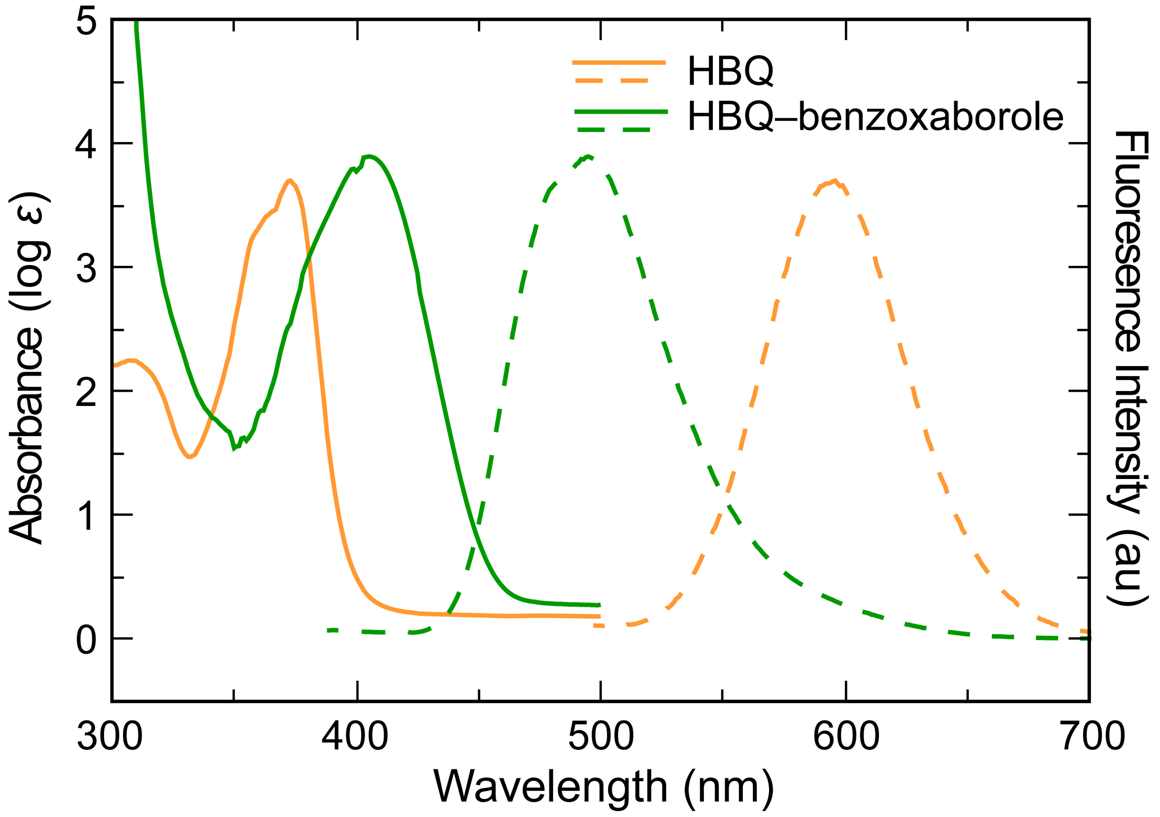

Figure 2.3.9 Absorption and emission spectra of HBQ and its complex with benzoxaborole. Fluorescence spectra were recorded in $CHCl_3$ with a Photon Technology International 810 fluorometer using right-angle detection. Ultraviolet–visible absorption spectra were measured with a Varian Cary 300 Bio diode array spectrophotometer and corrected for background signal with a solvent-filled cuvette. The instability of the HBQ–benzoxaborole precluded determination of its quantum yield.[321,349]

PART 3

FUTURE DIRECTIONS

Part 1 Chapter 2: Diazo Groups as Chemical Reporters

The diazo group has tremendous potential as a chemoselective group in the field of chemical biology. In Part 1 Chapter 2, I discuss the first application of a diazo group as a chemical reporter. The newness of this field opens many avenues of exploration, especially as we have proven that a stabilized diazo group can survive cellular metabolism and undergo a chemoselective reaction with a cyclooctyne. It is unusual that the diazo group allows for multiple component labeling with CuAAC, unlike its azido equivalent. This selectivity is possible through the use of a strong ligand for Cu(I) that reacts with the azido group but does not react the diazo group. As the origin for chemoselectivity with the diazo group, this compelling discovery begs exploration. The metabolic transformations of the diazo reporter also require further investigation. We assume that due to inherent similarities the mannosamine appended with a diazo group will undergo the same enzymatic transformations as the parent azido derivative,[106] but we did not explore this reactivity in detail.

A multicomponent, three-color cellular glycan labeling experiment that includes alkynyl, azido, and diazo group chemical reporters can be accomplished using current chemical technology.[97,350] This labeling necessitates the use of CuAAC to label the alkyne derivative and SPAAC to label the diazo group, and will require a phosphine to perform a Staudinger ligation with the azido group reporter.[54,115] This type of experiment has never been performed on three different types of glycans in the glycocalyx. The diazo group can also be utilized with reporters of other posttranslational modifications, building on previous investigations with the azido group.[75,98] One possible application is to incorporate a stabilized diazo group as a non-natural amino acid. This approach has been explored in detail for other chemoselective functional groups, including the azido group.[222]

Part 1 Chapter 3: Diazo Specific Dipolar Cycloadditions

The ability to perform a diazo group-selective 1,3-dipolar cycloaddition in the presence of other 1,3-dipoles will be valuable for the development of the diazo group in chemical biology. As an extension of Part 1 Chapter 2, this chemistry adds a further degree of chemoselectivity to existing reactions when the diazo group is applied as a chemical reporter. Insights provided suggest that an optimal balance of strain and electronic activation can provide both the reactivity and selectivity required for biological applications that are not yet possible. Still, some applications exist using currently known dipolarophiles that are specific to the diazo group. Nonnatural amino acid-bearing proteins have been reported that display an acrylamide sidechain.[198,199] The diazo group is a good reactant for this functionality (*vide infra*), and can be used for conjugation with an acrylamide derivative for a number of appendages, including possible heterodimerization with a diazo-bearing protein.

The diazo-specific dipolar cycloaddition reactions explored in this thesis have potential for *in vitro* applications in their current form. Installation of a diazo group onto a protein surface would allow for site-selective functionalization. This installation is possible, albeit without selectivity, using the *N*-hydroxysuccinimide ester of the diazo group.[351,352] In contrast, using the water soluble azide deimidogenation reagent developed in the Raines laboratory,[25] a stabilized diazo group could be generated selectively on the protein from an azido group at the N-terminus. Azido groups could be installed nongenetically by a Regitz diazo-transfer reaction, but this reaction would occur on all amines including lysine residues.[353] Some selectivity might be afforded through the deimidogenation process, but an excess of the phosphine would lead to reaction with the diazo group.[24] If some azido groups remain, the diazo group-selective cycloaddition reaction described in this chapter would provide differential labeling between the protein N-terminus and other sites on the protein.

Part 1 Chapter 4: Uncharged Water-Soluble Phosphinothioesters for the Traceless Staudinger Ligation

Two major goals for this project require completion before ubiquitin dimerization can be performed. First, the effect of electronics on phosphorous must be interrogated to determine the optimal reagent to perform the traceless Staudinger ligation. This interrogation requires completion of the synthesis of an isomer of the *para*-CH_2OMEM that is instead conjugated to the aryl ring (Figure 3.1.2). This phenolic derivative will be prepared by a route similar to the one used to access its non-conjugated isomer. Once prepared, these reagents will need to be tested for amide-bond formation in aqueous buffer in comparison to that from known phosphinothioesters. The optimal reagent would then be applied in the formation of ubiquitin dimers via isopeptide linkages, as described in Part 1 Chapter 4.

Part 2 Chapter 2: A Divalent Protecting Group for Benzoxaboroles

In the future, it will be possible to use the benzoxaborole protecting group for a number of synthetic transformations. This method for benzoxaborole protection is also compatible with the reagents involved in Fmoc-mediated solid-phase peptide synthesis. This use allows for the preparation of a peptide that bears benzoxaborole functionalities for applications in carbohydrate recognition and protein delivery.[354] It was shown recently that a phenylboronic acid-appended peptide demonstrates a strong affinity for sugars in aqueous conditions.[355] Benzoxaborole has a higher affinity than phenylboronic acid for many saccharides present at the cellular surface,[354] and a peptide with pendant benzoxaborole functionalities should be prepared and tested in relevant assays.

Part 2 Chapter 3: Detection of Boronic Acids through ESIPT

The detection of boronic acids through ESIPT-off fluorescence is more sensitive than by other methods. In chemical biology studies, this high sensitivity permits detection of boron at lower concentrations. Still, in order to perform these experiments, the ESIPT sensor must have an efficient ESIPT fluorescence in water, and the fluorophore requires aqueous solubility. HBQ is unique among ESIPT fluorophores because solvation interactions will not inhibit the ESIPT process. Most ESIPT fluorophores are benzoxazole-based and possess a freely rotating bond that connects the two aromatic systems (Figure 3.1.3 A1). These fluorophores must remain mostly planar to optimize both conjugation and hydrogen bonding. In a polar protic solvent like water, these interactions are disrupted significantly.[356,357] The lack of any rotation with HBQ produces a stable bond, and an ESIPT fluorescence that is not diminished in polar protic solvents (Figure 3.1.3 A2).

HBQ has very poor solubility in water. Its solubility can, however, be enhanced through sulfonylation of the backbone. The preparation of a sulfonated HBQ, HBQ-S, is shown in Figure 3.1.3 B. The sulfonyl group should not interfere with boron detection, and will facilitate the use of the HBQ in aqueous conditions (Figure 3.1.3 C). HBQ was sensitive to picomolar concentrations of boron in ethanol. HBQ-S should retain this sensitivity, allowing for the detection of trace quantities of boron in aqueous conditions. In particular, HBQ-S can be used to detect boronic acids within biological applications for carbohydrate recognition using a dye-displacement assay. This includes the interactions of boron-appended peptides and proteins with various carbohydrates. This process should be sensitive to both monomeric carbohydrates in solution, as well as those present on biomolecules such as proteins or the cellular glycocalyx.[358]

Figure 3.1.2 Phosphinothioesters investigated for efficiency during the traceless Staudinger ligation

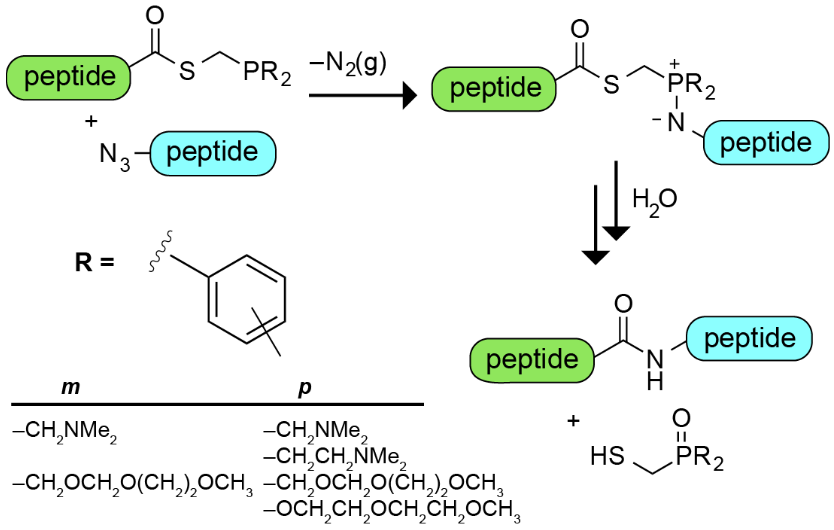
peptide
PR2
+
N3
peptide
−N2(g)
peptide
S
PR2
N
peptide
H2O
R =
peptide
N
H
peptide
+
HS
PR2
m
p
–CH2NMe2
–CH2OCH2O(CH2)2OCH3
–CH2NMe2
–CH2CH2NMe2
–CH2OCH2O(CH2)2OCH3
–OCH2CH2OCH2CH2OCH3

Figure 3.1.2 Phosphinothioesters investigated for efficiency during the traceless Staudinger ligation bearing different substitutions at the *meta* and *para* positions on the aryl rings.

Figure 3.1.3 Water soluble HBQ-S for the ESIPT detection of boronic acids

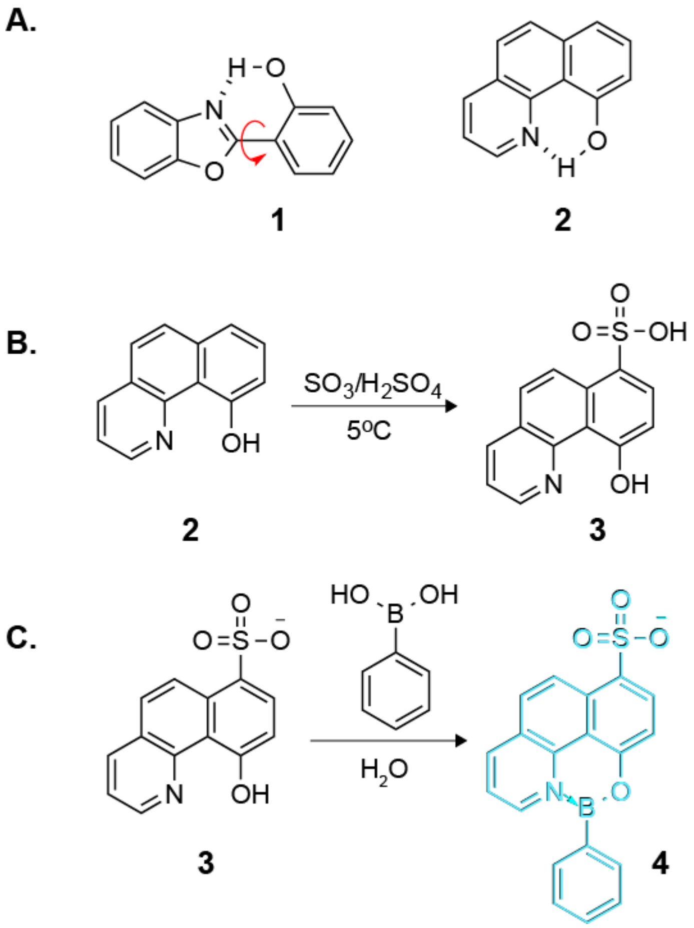
A.
H-O
N
O
1
N
H
O
2
B.
N
OH
2
SO3/H2SO4
5ºC
O=S-OH
O
N
OH
3
C.
O=S-O
O
N
OH
3
HO B OH
H2O
O=S-O
O
N
B
O
4

Figure 3.1.3 Water soluble HBQ-S for the ESIPT detection of boronic acids: **A.** ESIPT emission is problematic with benzoxazole fluorophores such as (**1**) in polar protic solutions from intermolecular hydrogen bonds with solvent resulting in decreased fluorescence. HBQ (**2**) has a very strong intramolecular hydrogen bond due to the rigidity of the backbone and is unaffected by solvation. **B.** Sulfonylation conditions for the conversion of HBQ (**2**) into the water-soluble derivative HBQ-S (**3**). **C.** Coordination of HBQ-S to phenylboronic acid in aqueous conditions produces a similar fluorescent ESIPT-off emission for detection of boron.

APPENDIX

Investigations Toward Orthogonal Reactivity Between the Azido and Diazo Groups

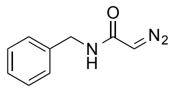

1

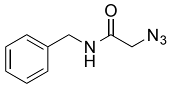

2

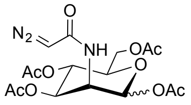

3

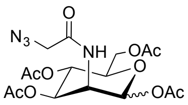

4

Compound	Diazo/Azide	Conditions	General Comments
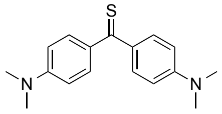	**3,4**	PBS pH 7.3 37 C	Very slow, and mixed products with only some trace Barton Kellogg product observed by LCMS
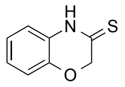	**3,4**	1:1 PBS:ACN pH 7.3 37 C	Very slow, trace product by TLC and LCMS
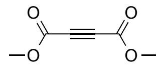	**1,2**	ACN or MeOH r.t.	Rapid reaction, but also reacts with azide
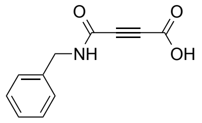	**3,4**	1:1 PBS:ACN pH 7.3 r.t.	Reacts selectively with the diazo through cycloaddition without an ester product at this pH
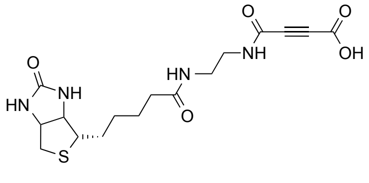	**3,4**	PBS pH 7.3 37 C	Tested on cells incubated with diazo-mannosamine and azido-mannosamine. The reaction did not produce effective labeling of the cells.
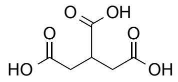	**1,2,3,4**	PBS pH 7.3 r.t.	The product mass from a single esterification was observed by LCMS
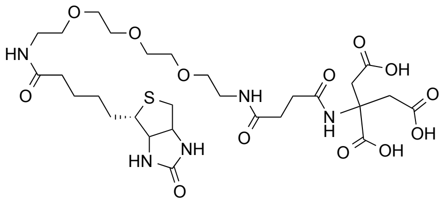	**3,4**	PBS pH 7.3 37 C	Tested on cells incubated with diazo-mannosamine and azido-mannosamine. The reaction did not produce effective labeling of the cells. It is hypothesized that the negative charge on the cellular surface repelled the label.
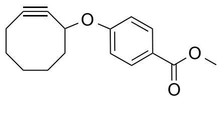	**1,2**	1:1 PBS:ACN pH 7.3 r.t.	Rapid reaction with both azides and diazo groups, and is not preferential for the diazo group.
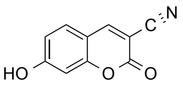	**1,2**	PBS pH 7.3 r.t.	Reacts selectively and rapidly with the diazo group, but the rate was not determined.

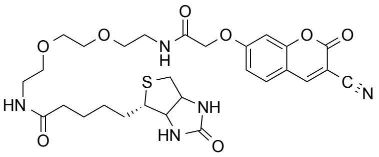	**1,2,3,4**	PBS pH 7.3 37 C	Tested on cells incubated with diazo-mannosamine and azido-mannosamine. The reaction did not produce effective labeling of the cells, but small amounts of fluorescence were observed by confocal microscopy that corresponded to the coumarin.
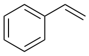 $Rh_2(OAc)_4$	**1,2**	DCM r.t.	Rapid carbene generation provides the cyclopropanation product or the dimerization of two diazo-group generated carbenes. Rh(II) is selective for the diazo group and does not react with the azide.
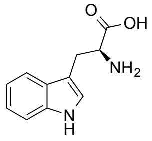 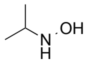 75mM	**1,2**	$Rh_2(OAc)_4$ 90:10 PBS:THF r.t.	The diazo group was completely converted to the below product: 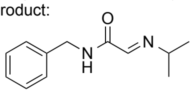
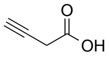	**1**	$CuSO_4$ sodium ascorbate TBTA THF:H_2O r.t.	No copper-mediated click reaction was observed, and some hydrolysis to the diazo group from carbene generation occurred. The presence of a stronger ligand such as THTPA will hinder any reaction with the diazo group, but can still facilitate a click reaction with the azide. This reaction should be selective in a biological context with higher loading of the ligand.
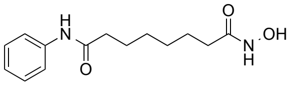	**1**	CH_3CN or PBS pH 6.3, r.t.	No reaction
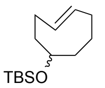	**1**	MeOH r.t.	Reaction is very slow.
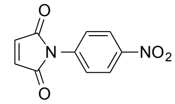	**1**	1:1 CH_3CN:H_2O r.t.	Very rapid cycloaddition. The maleimide was not tested for selectivity with the azido group.
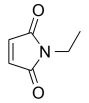	**1**	1:1 CH_3CN:H_2O r.t.	Very rapid cycloaddition. The maleimide was not tested for selectivity with the azido group.
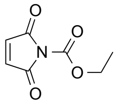	**1**	1:1 CH_3CN:H_2O r.t.	Very rapid cycloaddition. Diazo was consumed within the first minute of the reaction. The maleimide was not tested for selectivity with the azido group.
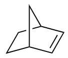	**1,2**	1:1 CH_3CN:H_2O r.t.	No reaction
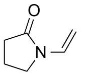	**1,2**	1:1 CH_3CN:H_2O r.t.	No reaction

References

1. Staudinger, H., and Meyer, J. Über neue organische Phosphorverbindungen III. Phosphinmethylenderivate und Phosphinimine, *Helv. Chim. Acta* **2**, 635-646 (1919).

2. Pawlak, J. B., Gential, G. P. P., Ruckwardt, T. J., Bremmers, J. S., Meeuwenoord, N. J., Ossendorp, F. A., Overkleeft, H. S., Filippov, D. V., and van Kasteren, S. I. Bioorthogonal deprotection on the dendritic cell surface for chemical control of antigen cross-presentation, *Angew. Chem. Int. Ed.* **54**, 5628-5631 (2015).

3. Gololobov, Y. G., Zhmurova, I. N., and Kasukhin, L. F. Sixty years of Staudinger reaction, *Tetrahedron* **37**, 437-472 (1981).

4. Gololobov, Y. G., and Kasukhin, L. F. Recent advances in the Staudinger reaction, *Tetrahedron* **48**, 1353-1406 (1992).

5. Regitz, M., and Maas, G. (1986) Chapter 3 - Reactivity toward Acids, In *Diazo Compounds* (Maas, M. R., Ed.), pp 96-165, Academic Press.

6. Regitz, M., and Maas, G. (1986) Chapter 4 - Photochemistry of Aliphatic Diazo Compounds, In *Diazo Compounds* (Maas, M. R., Ed.), pp 166-198, Academic Press, London.

7. Padwa, A., and Krumpe, K. E. Application of intramolecular carbenoid reactions in organic synthesis, *Tetrahedron* **48**, 5385-5453 (1992).

8. Doyle, M. P., and Forbes, D. C. Recent advances in asymmetric catalytic metal carbene transformations, *Chem. Rev.* **98**, 911-936 (1998).

9. Davies, H. M. L., and Beckwith, R. E. J. Catalytic enantioselective C−H activation by means of metal−carbenoid-induced C−H insertion, *Chem. Rev.* **103**, 2861-2904 (2003).

10. Padwa, A. (1984) *1,3-dipolar cycloaddition chemistry*, John Wiley & Sons, Inc.

11. Maas, G. (2003) Diazoalkanes, In *Synthetic Applications of 1,3-Dipolar Cycloaddition Chemistry Toward Heterocycles and Natural Products*, pp 539-621, John Wiley & Sons, New York.

12. Curtius, T. Ueber Stickstoffwasserstoffsäure (Azoimid) N3H, *Ber. Dtsch. Chem. Ges.* **23**, 3023-3033 (1890).

13. Curtius, T. 20. Hydrazide und Azide organischer Säuren I. Abhandlung, *J. Prakt. Chem.* **50**, 275-294 (1894).

14. Pechmann, H. V. Ueber Diazomethan, *Ber. Dtsch. Chem. Ges.* **27**, 1888-1891 (1894).

15. v. Pechmann, H. Ueber Diazomethan, *Ber. Dtsch. Chem. Ges.* **28**, 855-861 (1895).

16. Regitz, M. New methods of preparative organic chemistry. Transfer of diazo groups, *Angew. Chem. Int. Ed. Engl.* **6**, 733-749 (1967).

17. Baum, J. S., Shook, D. A., Davies, H. M. L., and Smith, H. D. Diazotransfer reactions with *p*-acetamidobenzenesulfonyl azide, *Synth. Commun.* **17**, 1709-1716 (1987).

18. Curtius, T. Ueber die Einwirkung von salpetriger Säure auf salzsauren Glycocolläther, *Ber. Dtsch. Chem. Ges.* **16**, 2230-2231 (1883).

19. Bamford, W. R., and Stevens, T. S. 924. The decomposition of toluene-*p*-sulphonylhydrazones by alkali, *J. Chem. Soc.* **0**, 4735-4740 (1952).

20. Holton, T. L., and Schechter, H. Advantageous syntheses of diazo compounds by oxidation of hydrazones with lead tetraacetate in basic environments, *J. Org. Chem.* **60**, 4725-4729 (1995).

21. Furrow, M. E., and Myers, A. G. A general procedure for the esterification of carboxylic acids with diazoalkanes generated in situ by the oxidation of *N*-tert-butyldimethylsilylhydrazones with (difluoroiodo)benzene, *J. Am. Chem. Soc.* **126**, 12222-12223 (2004).

22. Baumgarten, R. J. Preparation of ethyl diazoacetate via a triazene intermediate, *J. Org. Chem.* **32**, 484-485 (1967).

23. Schroen, M., and Bräse, S. Polymer-bound diazonium salts for the synthesis of diazoacetic esters, *Tetrahedron* **61**, 12186-12192 (2005).

24. Myers, E. L., and Raines, R. T. A phosphine-mediated conversion of azides into diazo compounds, *Angew. Chem. Int. Ed.* **48**, 2359-2363 (2009).

25. Chou, H.-H., and Raines, R. T. Conversion of azides into diazo compounds in water, *J. Am. Chem. Soc.* **135**, 14936-14939 (2013).

26. Rostovtsev, V. V., Green, L. G., Fokin, V. V., and Sharpless, K. B. A stepwise Huisgen cycloaddition process: copper(I)-catalyzed regioselective "ligation" of azides and terminal alkynes, *Angew. Chem. Int. Ed.* **41**, 2596-2599 (2002).

27. Tornøe, C. W., Christensen, C., and Meldal, M. Peptidotriazoles on solid phase: [1,2,3]-triazoles by regiospecific copper(I)-catalyzed 1,3-dipolar cycloadditions of terminal alkynes to azides, *J. Org. Chem.* **67**, 3057-3064 (2002).

28. Kolb, H. C., Finn, M. G., and Sharpless, K. B. Click chemistry: Diverse chemical function from a few good reactions, *Angew. Chem. Int. Ed.* **40**, 2004-2021 (2001).

29. Wittig, G., and Krebs, A. Zur Existenz niedergliedriger Cycloalkine, I, *Chem. Ber.* **94**, 3260-3275 (1961).

30. Baskin, J. M., Prescher, J. A., Laughlin, S. T., Agard, N. J., Chang, P. V., Miller, I. A., Lo, A., Codelli, J. A., and Bertozzi, C. R. Copper-free click chemistry for dynamic in vivo imaging, *Proc. Nat. Acad. Sci.* **104**, 16793-16797 (2007).

31. Agard, N. J., Prescher, J. A., and Bertozzi, C. R. A strain-promoted [3 + 2] azide−alkyne cycloaddition for covalent modification of biomolecules in living systems, *J. Am. Chem. Soc.* **126**, 15046-15047 (2004).

32. Sletten, E. M., and Bertozzi, C. R. From mechanism to mouse: a tale of two bioorthogonal reactions, *Acc. Chem. Res.* **44**, 666-676 (2011).

33. Patterson, D. M., Nazarova, L. A., and Prescher, J. A. Finding the right (bioorthogonal) chemistry, *ACS Chem. Biol.* **9**, 592-605 (2014).

34. Tishinov, K., Schmidt, K., Häussinger, D., and Gillingham, D. G. Structure-selective catalytic alkylation of DNA and RNA, *Angew. Chem. Int. Ed.* **51**, 12000-12004 (2012).

35. Fei, N., Haussinger, D., Blumli, S., Laventie, B.-J., Bizzini, L. D., Zimmermann, K., Jenal, U., and Gillingham, D. Catalytic carbene transfer allows the direct customization of cyclic purine dinucleotides, *Chem. Commun.* **50**, 8499-8502 (2014).

36. Gillingham, D., and Fei, N. Catalytic X-H insertion reactions based on carbenoids, *Chem. Soc. Rev.* **42**, 4918-4931 (2013).

37. Tishinov, K., Fei, N., and Gillingham, D. Cu(I)-catalysed N-H insertion in water: a new tool for chemical biology, *Chem. Sci.* **4**, 4401-4406 (2013).

38. Chen, Z., Vohidov, F., Coughlin, J.M., Stagg, L.J., Arnold, S.T., Ladbury, J.E., Ball, Z.T. Catalytic protein modification with dirhodium metallopeptides: specificity in designed and natural systems, *J. Am. Chem. Soc.* **134** (2012).

39. Ball, Z. T. Molecular recognition in protein modification with rhodium metallopeptides, *Curr. Opin. Chem. Biol.* **25**, 98-102 (2015).

40. Antos, J. M., and Francis, M. B. Selective tryptophan modification with rhodium carbenoids in aqueous solution, *J. Am. Chem. Soc.* **126**, 10256-10257 (2004).

41. Antos, J. M., McFarland, J. M., Iavarone, A. T., and Francis, M. B. Chemoselective tryptophan labeling with rhodium carbenoids at mild pH, *J. Am. Chem. Soc.* **131**, 6301-6308 (2009).

42. Riehm, J. P., and Scheraga, H. A. Structural studies of ribonuclease. XVII. A reactive carboxyl group in ribonuclease, *Biochemistry* **4**, 772-782 (1965).

43. McGrath, N. A., Andersen, K. A., Davis, A. K. F., Lomax, J. E., and Raines, R. T. Diazo compounds for the bioreversible esterification of proteins, *Chem. Sci.* **6**, 752–755 (2014).

44. Mix, K. A., and Raines, R. T. Optimized diazo scaffold for protein esterification, *Org. Lett.* **17**, 2358-2361 (2015).

45. McGrath, N. A., and Raines, R. T. Diazo compounds as highly tunable reactants in 1,3-dipolar cycloaddition reactions with cycloalkynes, *Chem. Sci.* **3**, 3237-3240 (2012).

46. Huisgen, R. 1.3-Dipolare Cycloadditionen Rückschau und Ausblick, *Angew. Chem.* **75**, 604-637 (1963).

47. Moran, J., McKay, C.S., Pezacki, J.P. Strain-promoted 1,3-dipolar cycloadditions of diazo compounds with cyclooctynes, *Can. J. Chem.* **89**, 148-151 (2011).

48. Sanders, B. C., Friscourt, F., Ledin, P. A., Mbua, N. E., Arumugam, S., Guo, J., Boltje, T. J., Popik, V. V., and Boons, G.-J. Metal-free sequential [3 + 2]-dipolar cycloadditions using cyclooctynes and 1,3-dipoles of different reactivity, *J. Am. Chem. Soc.* **133**, 949-957 (2011).

49. Friscourt, F., Fahrni, C. J., and Boons, G.-J. Fluorogenic strain-promoted alkyne–diazo cycloadditions, *Chem. Eur. J.* **21**, 13996-14001 (2015).

50. Moran, J., McKay, C. S., and Pezacki, J. P. Strain-promoted 1,3-dipolar cycloadditions of diazo compounds with cyclooctynes, *Can. J. Chem.* **89**, 148-151 (2011).

51. Neunhoeffer, H., Cuny, G., and Franke, W. K. Diazoessigsäureazid, *Justus Liebigs Ann. Chem.* **713**, 96-100 (1968).

52. Dommerholt, J., van Rooijen, O., Borrmann, A., Guerra, C. F., Bickelhaupt, F. M., and van Delft, F. L. Highly accelerated inverse electron-demand cycloaddition of electron-deficient azides with aliphatic cyclooctynes, *Nat. Commun.* **5** (2014).

53. Staudinger, H., and Hauser, E. Über neue organische Phosphorverbindungen IV Phosphinimine, *Helv. Chim. Acta* **4**, 861-886 (1921).

54. Saxon, E., and Bertozzi, C. R. Cell surface engineering by a modified Staudinger reaction, *Science* **287**, 2007-2010 (2000).

55. Schilling, C. I., Jung, N., Biskup, M., Schepers, U., and Brase, S. Bioconjugation via azide-Staudinger ligation: an overview, *Chem. Soc. Rev.* **40**, 4840-4871 (2011).

56. Kalia, J., and Raines, R. T. Advances in bioconjugation, *Curr. Org. Chem.* **14**, 138-147 (2010).

57. Nilsson, B. L., Kiessling, L. L., and Raines, R. T. Staudinger ligation: a peptide from a thioester and azide, *Org. Lett.* **2**, 1939-1941 (2000).

58. Saxon, E., Armstrong, J. I., and Bertozzi, C. R. A "traceless" Staudinger ligation for the chemoselective synthesis of amide bonds, *Org. Lett.* **2**, 2141-2143 (2000).

59. Nilsson, B. L., Kiessling, L. L., and Raines, R. T. High-yielding Staudinger ligation of a phosphinothioester and azide to form a peptide, *Org. Lett.* **3**, 9-12 (2001).

60. Soellner, M. B., Nilsson, B. L., and Raines, R. T. Reaction mechanism and kinetics of the traceless Staudinger ligation, *J. Am. Chem. Soc.* **128**, 8820-8828 (2006).

61. Lin, F. L., Hoyt, H. M., van Halbeek, H., Bergman, R. G., and Bertozzi, C. R. Mechanistic investigation of the Staudinger ligation, *J. Am. Chem. Soc.* **127**, 2686-2695 (2005).

62. Tam, A., Soellner, M. B., and Raines, R. T. Electronic and steric effects on the rate of the traceless Staudinger ligation, *Org. Biomol. Chem.* **6**, 1173-1175 (2008).

63. Soellner, M. B., Dickson, K. A., Nilsson, B. L., and Raines, R. T. Site-specific protein immobilization by Staudinger ligation, *J. Am. Chem. Soc.* **125**, 11790-11791 (2003).

64. He, Y., Hinklin, R. J., Chang, J., and Kiessling, L. L. Stereoselective *N*-glycosylation by Staudinger ligation, *Org. Lett.* **6**, 4479-4482 (2004).

65. Nilsson, B. L., Hondal, R. J., Soellner, M. B., and Raines, R. T. Protein assembly by orthogonal chemical ligation methods, *J. Am. Chem. Soc.* **125**, 5268-5269 (2003).

66. Nilsson, B. L., Soellner, M. B., and Raines, R. T. Chemical synthesis of proteins, *Annu. Rev. Biophys. Biomol. Struct.* **34**, 91-118 (2005).

67. Dawson, P. E., Muir, T. W., Clark-Lewis, I., and Kent, S. B. Synthesis of proteins by native chemical ligation, *Science* **266**, 776-779 (1994).

68. Tam, A., Soellner, M. B., and Raines, R. T. Water-soluble phosphinothiols for traceless Staudinger ligation and integration with expressed protein ligation, *J. Am. Chem. Soc.* **129**, 11421-11430 (2007).

69. Soellner, M. B., Tam, A., and Raines, R. T. Staudinger ligation of peptides at non-glycyl residues, *J. Org. Chem.* **71**, 9824-9830 (2006).

70. Kolb, H. C., Finn, M. G., and Sharpless, K. B. Click chemistry: Diverse chemical function from a few good reactions, *Angew. Chem. Int. Ed.* **40**, 2004-2021 (2001).

71. Rostovtsev, V. V., Green, L. G., Fokin, V. V., and Sharpless, K. B. A stepwise Huisgen cycloaddition process: copper(I)-catalyzed regioselective “ligation” of azides and terminal alkynes, *Angew. Chem. Int. Ed.* **41**, 2596-2599 (2002).

72. Tornøe, C. W., Christensen, C., and Meldal, M. Peptidotriazoles on solid phase: [1,2,3]-Triazoles by regiospecific copper(I)-catalyzed 1,3-dipolar cycloadditions of terminal alkynes to azides, *J. Org. Chem.* **67**, 3057-3064 (2002).

73. Huisgen, R., Szeimies, G., and Möbius, L. 1.3-dipolare cycloadditionen, XXXII. kinetik der additionen organischer azide an CC-mehrfachbindungen, *Chem. Ber.* **100**, 2494-2507 (1967).

74. Bräse, S., Gil, C., Knepper, K., and Zimmermann, V. Organic azides: An exploding diversity of a unique class of compounds, *Angew. Chem. Int. Ed.* **44**, 5188-5240 (2005).

75. Sletten, E. M., and Bertozzi, C. R. Bioorthogonal chemistry: Fishing for selectivity in a sea of functionality, *Angew. Chem. Int. Ed.* **48**, 6974-6998 (2009).

76. Patterson, D. M., Nazarova, L. A., and Prescher, J. A. Finding the right (bioorthogonal) chemistry, *ACS Chem. Biol.* **9**, 592-605 (2014).

77. Lang, K., and Chin, J. W. Cellular incorporation of unnatural amino acids and bioorthogonal labeling of proteins, *Chem. Rev.* **114**, 4764-4806 (2014).

78. McGrath, N. A., and Raines, R. T. Diazo compounds as highly tunable reactants in 1,3-dipolar cycloaddition reactions with cycloalkynes, *Chem. Sci.* **3**, 3237-3240 (2012).

79. McGrath, N. A., Andersen, K. A., Davis, A. K. F., Lomax, J. E., and Raines, R. T. Diazo compounds for the bioreversible esterification of proteins, *Chem. Sci.* **6**, 752-755 (2015).

80. Pechmann, H. V. Ueber diazomethan, *Berichte der deutschen chemischen Gesellschaft* **27**, 1888-1891 (1894).

81. Wolff, L. Ueber diazoanhydride, *Justus Liebigs Ann. Chem.* **325**, 129-195 (1902).

82. Kirmse, W. 100 years of the Wolff rearrangement, *Eur. J. Org. Chem.* **2002**, 2193-2256 (2002).

83. Morandi, B., and Carreira, E. M. Iron-catalyzed cyclopropanation in 6 M KOH with *in situ* generation of diazomethane, *Science* **335**, 1471-1474 (2012).

84. Regitz, M. (1986) *Diazo compounds: Properties and synthesis*, Academic Press, London.

85. Padwa, A., and Weingarten, M. D. Cascade processes of metallo carbenoids, *Chem. Rev.* **96**, 223-270 (1996).

86. Doyle, M. P., McKervey, M. A., and Ye, T. (1998) *Modern catalytic methods for organic synthesis with diazo compounds: From cyclopropanes to ylides*, Wiley, New York.

87. Davies, H. M. L., and Beckwith, R. E. J. Catalytic enantioselective C−H activation by means of metal−carbenoid-induced C−H insertion, *Chem. Rev.* **103**, 2861-2904 (2003).

88. Zhang, Z., and Wang, J. Recent studies on the reactions of α-diazocarbonyl compounds, *Tetrahedron* **64**, 6577-6605 (2008).

89. Maas, G. New syntheses of diazo compounds, *Angew. Chem. Int. Ed.* **48**, 8186-8195 (2009).

90. LeWinn, E. B. Diazomethane poisoning: Report of a fatal case with autopsy, *Am. J. Med. Sci.* **218**, 556–562 (1949).

91. Schoental, R. Carcinogenic action of diazomethane and of nitroso-*N*-methyl urethane, *Nature* **188**, 420-421 (1960).

92. Lewis, C. E. Diazomethane poisoning. Report of a case suggesting sensitization reaction., *J. Occup. Environ. Med.* **6**, 91–92 (1964).

93. Myers, E. L., and Raines, R. T. A phosphine-mediated conversion of azides into diazo compounds, *Angew. Chem. Int. Ed.* **48**, 2359-2363 (2009).

94. Chou, H.-H., and Raines, R. T. Conversion of azides into diazo compounds in water, *J. Am. Chem. Soc.* **135**, 14936-14939 (2013).

95. Chang, P. V., Prescher, J. A., Hangauer, M. J., and Bertozzi, C. R. Imaging cell surface glycans with bioorthogonal chemical reporters, *J. Am. Chem. Soc.* **129**, 8400-8401 (2007).

96. Laughlin, S. T., Baskin, J. M., Amacher, S. L., and Bertozzi, C. R. *In vivo* imaging of membrane-associated glycans in developing zebrafish, *Science* **320**, 664-667 (2008).

97. Ning, X., Guo, J., Wolfert, M. A., and Boons, G.-J. Visualizing metabolically-labeled glycoconjugates of living cells by copper-free and fast Huisgen cycloadditions, *Angew. Chem. Int. Ed.* **47**, 2253-2255 (2008).

98. Friscourt, F., and Boons, G.-J. (2013) Bioorthogonal reactions for labeling glycoconjugates, In *Click Chemistry in Glycoscience*, pp 211-233, John Wiley & Sons, New York.

99. Laughlin, S. T., and Bertozzi, C. R. Imaging the glycome, *Proc. Natl. Acad. Sci. U. S. A.* **106**, 12-17 (2009).

100. Kayser, H., Zeitler, R., Kannicht, C., Grunow, D., Nuck, R., and Reutter, W. Biosynthesis of a nonphysiological sialic acid in different rat organs, using *N*-propanoyl-D-hexosamines as precursors, *J. Biol. Chem.* **267**, 16934-16938 (1992).

101. Mahal, L. K., Yarema, K. J., and Bertozzi, C. R. Engineering chemical reactivity on cell surfaces through oligosaccharide biosynthesis, *Science* **276**, 1125-1128 (1997).

102. Ess, D. H., Jones, G. O., and Houk, K. N. Conceptual, qualitative, and quantitative theories of 1,3-dipolar and Diels–Alder cycloadditions used in synthesis, *Adv. Synth. Catal.* **348**, 2337-2361 (2006).

103. Breslow, R. Hydrophobic effects on simple organic reactions in water, *Acc. Chem. Res.* **24**, 159-164 (1991).

104. Sarkar, A. K., Fritz, T. A., Taylor, W. H., and Esko, J. D. Disaccharide uptake and priming in animal cells: Inhibition of sialyl lewis X by acetylated gal beta 1-4Glc*N*Ac beta-*O*-naphthalenemethanol, *Proc. Natl. Acad. Sci. U. S. A.* **92**, 3323-3327 (1995).

105. Galloway, C. J., Dean, G. E., Marsh, M., Rudnick, G., and Mellman, I. Acidification of macrophage and fibroblast endocytic vesicles *in vitro*, *Proc. Natl. Acad. Sci. U. S. A.* **80**, 3334-3338 (1983).

106. Möller, H., Böhrsch, V., Bentrop, J., Bender, J., Hinderlich, S., and Hackenberger, C. P. R. Glycan-specific metabolic oligosaccharide engineering of C7-substituted sialic acids, *Angew. Chem. Int. Ed.* **51**, 5986-5990 (2012).

107. Rashidian, M., Kumarapperuma, S. C., Gabrielse, K., Fegan, A., Wagner, C. R., and Distefano, M. D. Simultaneous dual protein labeling using a triorthogonal reagent, *J. Am. Chem. Soc.* **135**, 16388-16396 (2013).

108. Schoch, J., Staudt, M., Samanta, A., Wiessler, M., and Jäschke, A. Site-specific one-pot dual labeling of DNA by orthogonal cycloaddition chemistry, *Bioconjugate Chem.* **23**, 1382-1386 (2012).

109. Yang, Y., Lin, S., Lin, W., and Chen, P. R. Ligand-assisted dual-site click labeling of EGFR on living cells, *ChemBioChem* **15**, 1738-1743 (2014).

110. Sachdeva, A., Wang, K., Elliott, T., and Chin, J. W. Concerted, rapid, quantitative, and site-specific dual labeling of proteins, *J. Am. Chem. Soc.* **136**, 7785-7788 (2014).

111. Hong, V., Presolski, S. I., Ma, C., and Finn, M. G. Analysis and optimization of copper-catalyzed azide–alkyne cycloaddition for bioconjugation, *Angew. Chem. Int. Ed.* **48**, 9879-9883 (2009).

112. Uttamapinant, C., Tangpeerachaikul, A., Grecian, S., Clarke, S., Singh, U., Slade, P., Gee, K. R., and Ting, A. Y. Fast, cell-compatible click chemistry with copper-chelating azides for biomolecular labeling, *Angew. Chem. Int. Ed.* **51**, 5852-5856 (2012).

113. Hang, H. C., Yu, C., Kato, D. L., and Bertozzi, C. R. A metabolic labeling approach toward proteomic analysis of mucin-type *O*-linked glycosylation, *Proc. Natl. Acad. Sci. U. S. A.* **100**, 14846-14851 (2003).

114. Goddard-Borger, E. D., and Stick, R. V. An efficient, inexpensive, and shelf-stable diazotransfer reagent: Imidazole-1-sulfonyl azide hydrochloride, *Org. Lett.* **9**, 3797-3800 (2007).

115. Laughlin, S. T., and Bertozzi, C. R. Metabolic labeling of glycans with azido sugars and subsequent glycan-profiling and visualization via Staudinger ligation, *Nat. Protoc.* **2**, 2930-2944 (2007).

116. Hsu, T.-L., Hanson, S. R., Kishikawa, K., Wang, S.-K., Sawa, M., and Wong, C.-H. Alkynyl sugar analogs for the labeling and visualization of glycoconjugates in cells, *Proc. Natl. Acad. Sci. U. S. A.* **104**, 2614-2619 (2007).

117. Rodrigues, D. C., Bader, R. A., and Hasenwinkel, J. M. Grafting of nanospherical PMMA brushes on cross-linked PMMA nanospheres for addition in two-solution bone cements, *Polymer* **52**, 2505-2513 (2011).

118. Mukherjee, M., Gupta, A. K., Lu, Z., Zhang, Y., and Wulff, W. D. Seeking passe-partout in the catalytic asymmetric aziridination of imines: Evolving toward substrate generality for a single chemzyme, *J. Org. Chem.* **75**, 5643-5660 (2010).

119. Ouihia, A., Rene, L., Guilhem, J., Pascard, C., and Badet, B. A new diazoacylating reagent: Preparation, structure, and use of succinimidyl diazoacetate, *J. Org. Chem.* **58**, 1641-1642 (1993).

120. Huisgen, R. Proceedings of the Chemical Society. October 1961, *Proc. Chem. Soc.*, 357-396 (1961).

121. Baskin, J. M., Prescher, J. A., Laughlin, S. T., Agard, N. J., Chang, P. V., Miller, I. A., Lo, A., Codelli, J. A., and Bertozzi, C. R. Copper-free click chemistry for dynamic in vivo imaging, *Proc. Natl. Acad. Sci. U. S. A.* **104**, 16793-16797 (2007).

122. Ning, X., Guo, J., Wolfert, M. A., and Boons, G.-J. Visualizing metabolically labeled Glycoconjugates of Living cells by copper-free and fast huisgen cycloadditions, *Angew. Chem. Int. Ed.* **47**, 2253-2255 (2008).

123. Poloukhtine, A. A., Mbua, N. E., Wolfert, M. A., Boons, G.-J., and Popik, V. V. Selective labeling of living cells by a photo-triggered click reaction, *J. Am. Chem. Soc.* **131**, 15769-15776 (2009).

124. Dommerholt, J., Schmidt, S., Temming, R., Hendriks, L. J. A., Rutjes, F. P. J. T., van Hest, J. C. M., Lefeber, D. J., Friedl, P., and van Delft, F. L. Readily accessible bicyclononynes for bioorthogonal labeling and three-dimensional imaging of living cells, *Angew. Chem. Int. Ed.* **49**, 9422-9425 (2010).

125. Varga, B. R., Kállay, M., Hegyi, K., Béni, S., and Kele, P. A non-fluorinated monobenzocyclooctyne for rapid copper-free click reactions, *Chem. Eur. J.* **18**, 822-828 (2012).

126. Debets, M. F., van Berkel, S. S., Schoffelen, S., Rutjes, F. P. J. T., van Hest, J. C. M., and van Delft, F. L. Aza-dibenzocyclooctynes for fast and efficient enzyme PEGylation via copper-free (3+2) cycloaddition, *Chem. Commun.* **46**, 97-99 (2010).

127. Jewett, J. C., Sletten, E. M., and Bertozzi, C. R. Rapid Cu-free click chemistry with readily synthesized biarylazacyclooctynones, *J. Am. Chem. Soc.* **132**, 3688-3690 (2010).

128. Gold, B., Dudley, G. B., and Alabugin, I. V. Moderating strain without sacrificing reactivity: Design of fast and tunable noncatalyzed alkyne–azide cycloadditions via stereoelectronically controlled transition state stabilization, *J. Am. Chem. Soc.* **135**, 1558-1569 (2013).

129. Ni, R., Mitsuda, N., Kashiwagi, T., Igawa, K., and Tomooka, K. Heteroatom-embedded medium-sized cycloalkynes: Concise synthesis, structural analysis, and reactions, *Angew. Chem. Int. Ed.* **54**, 1190-1194 (2015).

130. Cowell, G. W., and Ledwith, A. Developments in the chemistry of diazo-alkanes, *Q. Rev. Chem. Soc.* **24**, 119-167 (1970).

131. Regitz, M. (2012) *Diazo compounds: properties and synthesis*, Elsevier.

132. Maas, G. (1987) Transition-metal catalyzed decomposition of aliphatic diazo compounds—New results and applications in organic synthesis, In *Organic Synthesis, Reactions and Mechanisms*, pp 75-253, Springer.

133. v. Pechmann, H. Pyrazol aus Acetylen und Diazomethan, *Ber. Dtsch. Chem. Ges.* **31**, 2950-2951 (1898).

134. Andersen, K. A., Aronoff, M. R., McGrath, N. A., and Raines, R. T. Diazo groups endure metabolism and enable chemoselectivity in cellulo, *J. Am. Chem. Soc.* **137**, 2412-2415 (2015).

135. Ball, Z. T. Designing enzyme-like catalysts: A rhodium(II) metallopeptide case study, *Acc. Chem. Res.* **46**, 560-570 (2013).

136. McGrath, N. A., Andersen, K. A., Davis, A. K. F., Lomax, J. E., and Raines, R. T. Diazo compounds for the bioreversible esterification of proteins, *Chem. Sci.* **6**, 752-755 (2015).

137. Zhang, Y., and Wang, J. Recent development of reactions with [small alpha]-diazocarbonyl compounds as nucleophiles, *Chem. Commun.* **.** , 5350-5361 (2009).

138. Gold, B., Shevchenko, N. E., Bonus, N., Dudley, G. B., and Alabugin, I. V. Selective transition state stabilization via hyperconjugative and conjugative assistance: Stereoelectronic concept for copper-free click chemistry, *J. Org. Chem.* **77**, 75-89 (2012).

139. Gold, B., Batsomboon, P., Dudley, G. B., and Alabugin, I. V. Alkynyl crown ethers as a scaffold for hyperconjugative assistance in noncatalyzed azide–alkyne click reactions: Ion sensing through enhanced transition-state stabilization, *J. Org. Chem.* **79**, 6221-6232 (2014).

140. Schoenebeck, F., Ess, D. H., Jones, G. O., and Houk, K. N. Reactivity and regioselectivity in 1,3-dipolar cycloadditions of azides to strained alkynes and alkenes: A computational study, *J. Am. Chem. Soc.* **131**, 8121-8133 (2009).

141. Chenoweth, K., Chenoweth, D., and Goddard Iii, W. A. Cyclooctyne-based reagents for uncatalyzed click chemistry: A computational survey, *Org. Biomol. Chem.* **7**, 5255-5258 (2009).

142. Garcia-Hartjes, J., Dommerholt, J., Wennekes, T., van Delft, F. L., and Zuilhof, H. Electronic effects versus distortion energies during strain-promoted alkyne-azide cycloadditions: A theoretical tool to predict reaction kinetics, *Eur. J. Org. Chem.* **2013**, 3712-3720 (2013).

143. Jones, G. O., and Houk, K. N. Predictions of substituent effects in thermal azide 1,3-dipolar cycloadditions: Implications for dynamic combinatorial (reversible) and click (irreversible) chemistry, *J. Org. Chem.* **73**, 1333-1342 (2008).

144. Xie, S., Lopez, S. A., Ramström, O., Yan, M., and Houk, K. N. 1,3-dipolar cycloaddition reactivities of perfluorinated aryl azides with enamines and strained dipolarophiles, *J. Am. Chem. Soc.* **137**, 2958-2966 (2015).

145. Sanders, B. C., Friscourt, F., Ledin, P. A., Mbua, N. E., Arumugam, S., Guo, J., Boltje, T. J., Popik, V. V., and Boons, G.-J. Metal-free sequential [3 + 2]-dipolar cycloadditions using cyclooctynes and 1,3-dipoles of different reactivity, *J. Am. Chem. Soc.* **133**, 949-957 (2010).

146. Yoshida, S., Shiraishi, A., Kanno, K., Matsushita, T., Johmoto, K., Uekusa, H., and Hosoya, T. Enhanced clickability of doubly sterically-hindered aryl azides, *Sci. Rep.* **1**, 82 (2011).

147. Zimmerman, E. S., Heibeck, T. H., Gill, A., Li, X., Murray, C. J., Madlansacay, M. R., Tran, C., Uter, N. T., Yin, G., Rivers, P. J., Yam, A. Y., Wang, W. D., Steiner, A. R., Bajad, S. U., Penta, K., Yang, W., Hallam, T. J., Thanos, C. D., and Sato, A. K. Production of site-specific antibody–drug conjugates using optimized non-natural amino acids in a cell-free expression system, *Bioconjugate Chem.* **25**, 351-361 (2014).

148. There are, of course, examples of alternate reactions, such as tetrazine/TCO: (a) Selvaraj, R.; Giglio, B.; Liu, S.; Wang, H.; Wang, M.; Yuan, H.; Chintala, S. R.; Yap, L.-P.; Conti, P. S.; Fox, J. M.; Li, Z. Bioconj. Chem. 2015, 26, 435. (b) Darko, A.; Wallace, S.; Dmitrenko, O.; Machovina, M. M.; Mehl, R. A.; Chin, J. W.; Fox, J. M. Chem. Sci. 2014, 5, 3770. (c) Blackman, M. L.; Royzen, M.; Fox, J. M. J. Am. Chem. Soc. 2008, 130, 13518. tetrazine/cyclopropene: (d) Kamber, D. N.; Nazarova, L. A.; Liang, Y.; Lopez, S. A.; Patterson, D. M.; Shih, H.-W.; Houk, K. N.; Prescher, J. A. J. Am. Chem. Soc. 2013, 135, 13680. (e) Patterson, D. M.; Nazarova, L. A.; Xie, B.; Kamber, D. N.; Prescher, J. A. J. Am. Chem. Soc. 2012, 134, 18638. (f) Sachdeva, A.; Wang, K.; Elliott, T.; Chin, J. W. J. Am. Chem. Soc. 2014, 136, 7785. (g) Yang, J.; Liang, Y.; Šečkutė, J.; Houk, K. N.; Devaraj, N. K. Chem. Eur. J. 2014, 20, 3365. (h) Yang, J.; Šečkutė, J.; Cole, C. M.; Devaraj, N. K. Angew. Chem. Int. Ed. 2012, 51, 7476. triazine/cyclopropene: (i) Kamber, D. N.; Liang, Y.; Blizzard, R. J.; Liu, F.; Mehl, R. A.; Houk, K. N.; Prescher, J. A. J. Am. Chem. Soc. 2015. in press and nitrile imine cyclopropene: (j) Wang, Y.; Song, W.; Hu, W. J.; Lin, Q. Angew. Chem. Int. Ed. 2009, 48, 5330.

149. Ess, D. H., and Houk, K. N. Theory of 1,3-dipolar cycloadditions: Distortion/interaction and frontier molecular orbital models, *J. Am. Chem. Soc.* **130**, 10187-10198 (2008).

150. MacKenzie, D. A., and Pezacki, J. P. Kinetics studies of rapid strain-promoted [3+2] cycloadditions of nitrones with bicyclo[6.1.0]nonyne, *Can. J. Chem.* **92**, 337-340 (2014).

151. While nitrile imine photoclick reactions provide faster rates, the nitrile imine is an ephemeral dipole.

152. Frisch, M. J., Trucks, G. W., Schlegel, H. B., Scuseria, G. E., Robb, M. A., Cheeseman, J. R., Scalmani, G., Barone, V., Mennucci, B., Petersson, G. A., Nakatsuji, H., Caricato, M., Li, X., Hratchian, H. P., Izmaylov, A. F., Bloino, J., Zheng, G., Sonnenberg, J. L., Hada, M., Ehara, M., Toyota, K., Fukuda, R., Hasegawa, J., Ishida, M., Nakajima, T., Honda, Y., Kitao, O., Nakai, H., Vreven, T., Montgomery Jr., J. A., Peralta, J. E., Ogliaro, F., Bearpark, M. J., Heyd, J., Brothers, E. N., Kudin, K. N., Staroverov, V. N., Kobayashi, R., Normand, J., Raghavachari, K., Rendell, A. P., Burant, J. C., Iyengar, S. S., Tomasi, J., Cossi, M., Rega, N., Millam, N. J., Klene, M., Knox, J. E., Cross, J. B., Bakken, V., Adamo, C., Jaramillo, J., Gomperts, R., Stratmann, R. E., Yazyev, O., Austin, A. J., Cammi, R., Pomelli, C., Ochterski, J. W., Martin, R. L., Morokuma, K., Zakrzewski, V. G., Voth, G. A., Salvador, P., Dannenberg, J. J., Dapprich, S., Daniels, A. D., Farkas, Ö., Foresman, J. B., Ortiz, J. V., Cioslowski, J., and Fox, D. J. (2009) Gaussian 09, Gaussian, Inc., Wallingford, CT, USA.

153. Zhao, Y., and Truhlar, D. The M06 suite of density functionals for main group thermochemistry, thermochemical kinetics, noncovalent interactions, excited states, and transition elements: two new functionals and systematic testing of four M06-class functionals and 12 other functionals, *Theor. Chem. Acc.* **120**, 215-241 (2008).

154. Zhao, Y., and Truhlar, D. G. Density functionals with broad applicability in chemistry, *Acc. Chem. Res.* **41**, 157-167 (2008).

155. Lan, Y., Zou, L., Cao, Y., and Houk, K. N. Computational methods to calculate accurate activation and reaction energies of 1,3-dipolar cycloadditions of 24 1,3-Dipoles, *J. Phys. Chem. A* **115**, 13906-13920 (2011).

156. Jung, M. E., Min, S.-J., Houk, K. N., and Ess, D. Synthesis and relative stability of 3,5-diacyl-4,5-dihydro-1H-pyrazoles prepared by dipolar cycloaddition of enones and α-diazoketones, *J. Org. Chem.* **69**, 9085-9089 (2004).

157. Liu, F., Liang, Y., and Houk, K. N. Theoretical elucidation of the origins of substituent and strain effects on the rates of Diels–Alder reactions of 1,2,4,5-tetrazines, *J. Am. Chem. Soc.* **136**, 11483-11493 (2014).

158. This is also why we focus on alkene dipolarophiles in Figure 1.

159. Sletten, E. M., de Almeida, G., and Bertozzi, C. R. A homologation approach to the dynthesis of difluorinated cycloalkynes, *Org. Lett.* **16**, 1634-1637 (2014).

160. This statement downplays the importance of electronics, however, as the necessary substrates to maximize stereoelectronic stabilization had not yet been reported Ni, R.; Mitsuda, N.; Kashiwagi, T.; Igawa, K.; Tomooka, K. Angewandte Chemie International Edition 2015, 54, 1190.

161. Mayr, H., and Ofial, A. R. The reactivity–selectivity principle: An imperishable myth in organic chemistry, *Angew. Chem. Int. Ed.* **45**, 1844-1854 (2006).

162. Houk, K. N., Sims, J., Duke, R. E., Strozier, R. W., and George, J. K. Frontier molecular orbitals of 1,3 dipoles and dipolarophiles, *J. Am. Chem. Soc.* **95**, 7287-7301 (1973).

163. Epiotis, N. D. Electrocyclic reactions. I. Importance of donor-acceptor interactions in thermal intermolecular cycloaddition reactions, *J. Am. Chem. Soc.* **94**, 1924-1934 (1972).

164. Sustmann, R. A simple model for substituent effects in cycloaddition reactions. I. 1,3-dipolar cycloadditions, *Tetrahedron Lett.* **12**, 2717-2720 (1971).

165. Sustmann, R., and Trill, H. Substituent effects in 1,3-dipolar cycloadditions of phenyl azide, *Angew. Chem. Int. Ed. (English)* **11**, 838-840 (1972).

166. Houk, K. N. Regioselectivity and reactivity in the 1,3-dipolar cycloadditions of diazonium betaines (diazoalkanes, azides, and nitrous oxide), *J. Am. Chem. Soc.* **94**, 8953-8955 (1972).

167. Ess, D. H., and Houk, K. N. Distortion/interaction energy control of 1,3-dipolar cycloaddition reactivity, *J. Am. Chem. Soc.* **129**, 10646-10647 (2007).

168. Fernandez, I., and Bickelhaupt, F. M. The activation strain model and molecular orbital theory: understanding and designing chemical reactions, *Chem. Soc. Rev.* **43**, 4953-4967 (2014).

169. Ess, D. H., Jones, G. O., and Houk, K. N. Transition states of strain-promoted metal-free click chemistry: 1,3-Dipolar cycloadditions of phenyl azide and cyclooctynes, *Org. Lett.* **10**, 1633-1636 (2008).

170. Lopez, S. A., and Houk, K. N. Alkene distortion energies and torsional effects control reactivities, and stereoselectivities of azide cycloadditions to norbornene and substituted norbornenes, *J. Org. Chem.* **78**, 1778-1783 (2013).

171. It is surprising that this is the approach commonly utilized to accelerate cycloadditon reactions, as the dipole displays a much more product-like geometry, while the dipolarohpile remains relatively linear. Ess, D. H.; Houk, K. N. J. Am. Chem. Soc. 2008, 130, 10187.

172. Additionally, the present study utilizes the M06-2X level of theory, shown to be better suited for asynchronous cycloadditions: Linder, M.; Brinck, T. Phys. Chem. Chem. Phys. 2013, 15, 5108.

173. It has been shown that FMO interaction energies differentiate reactivity when distortion energies are nearly constant. Ess, D. H.; Houk, K. N. J. Am. Chem. Soc. 2008, 130, 10187.

174. Distortion of dipolarophiles also decreases the FMO gaps of reacting partners, indirectly decreasing dipole distortion.

175. A strategy of "HOMO lifting" has been reported for nitrile-imine cycloadditions, but the efficiency relative to LUMO lowering via strain was not examined. Wang, Y.; Song, W.; Hu, W. J.; Lin, Q. Angew. Chem. Int. Ed. 2009, 48, 5330.

176. Marcus, R. A. On the theory of oxidation - reduction reactions involving electron transfer. I, *J. Chem. Phys* **24**, 966-978 (1956).

177. Marcus, R. A. Chemical and electrochemical electron-transfer theory, *Annu. Rev. Phys. Chem.* **15**, 155-196 (1964).

178. Marcus, R. A. Theoretical relations among rate constants, barriers, and Broensted slopes of chemical reactions, *J. Phys. Chem.* **72**, 891-899 (1968).

179. Koeppl, G. W., and Kresge, A. J. Marcus rate theory and the relationship between Bronsted exponents and energy of reaction, *J. Chem. Soc., Chem. Commun.*, 371-373 (1973).

180. Alabugin, I. V., Gilmore, K., and Manoharan, M. Rules for anionic and radical ring closure of alkynes, *J. Am. Chem. Soc.* **133**, 12608-12623 (2011).

181. Mondal, S., Gold, B., Mohamed, R. K., and Alabugin, I. V. Design of leaving groups in radical C–C fragmentations: Through-bond 2c–3e interactions in self-terminating radical cascades, *Chem. Eur. J.* **20**, 8664-8669 (2014).

182. Mayr, H., Breugst, M., and Ofial, A. R. Farewell to the HSAB treatment of ambident reactivity, *Angew. Chem. Int. Ed.* **50**, 6470-6505 (2011).

183. Evans, M. G., and Polanyi, M. Inertia and driving force of chemical reactions, *Trans. Faraday Soc.* **34**, 11-24 (1938).

184. Bell, R. P. The theory of reactions involving proton transfers, *Proc. R. Soc. A* **154**, 414-429 (1936).

185. Nicolaides, A., and Borden, W. T. Ab initio calculations of the relative strengths of the .pi. bonds in acetylene and ethylene and of their effect on the relative energies of .pi.-bond addition reactions, *J. Am. Chem. Soc.* **113**, 6750-6755 (1991).

186. Alabugin, I. V., and Gold, B. "Two functional groups in one package": Using both alkyne π-bonds in cascade transformations, *J. Org. Chem.* **78**, 7777-7784 (2013).

187. Osuna, S., and Houk, K. N. Cycloaddition reactions of butadiene and 1,3-dipoles to curved arenes, fullerenes, and nanotubes: Theoretical evaluation of the role of distortion energies on activation barriers, *Chem. Eur. J.* **15**, 13219-13231 (2009).

188. Anastas, P. T.; Warner, J. C. Green Chemistry: Theory and Practice, Oxford University Press: New York, 1998, p.30

189. Huisgen, R. Cycloaddition mechanism and the solvent dependence of rate, *Pure Appl. Chem.* **52**, 2283-2302 (1980).

190. Sauer, J., and Sustmann, R. Mechanistic aspects of Diels-Alder reactions: A critical survey, *Angew. Chem. Int. Ed. (English)* **19**, 779-807 (1980).

191. Narayan, S., Muldoon, J., Finn, M. G., Fokin, V. V., Kolb, H. C., and Sharpless, K. B. "On water": Unique reactivity of organic compounds in aqueous suspension, *Angew. Chem. Int. Ed.* **44**, 3275-3279 (2005).

192. Meijer, A., Otto, S., and Engberts, J. B. F. N. Effects of the hydrophobicity of the reactants on Diels−Alder reactions in water, *J. Org. Chem.* **63**, 8989-8994 (1998).

193. Jung, Y., and Marcus, R. A. On the theory of organic catalysis "on water", *J. Am. Chem. Soc.* **129**, 5492-5502 (2007).

194. Chandrasekhar, J., Shariffskul, S., and Jorgensen, W. L. QM/MM simulations for Diels−Alder reactions in water: Contribution of enhanced hydrogen bonding at the transition state to the solvent effect, *J. Phys. Chem. B* **106**, 8078-8085 (2002).

195. Miertuš, S., Scrocco, E., and Tomasi, J. Electrostatic interaction of a solute with a continuum. A direct utilizaion of AB initio molecular potentials for the prevision of solvent effects, *Chem. Phys.* **55**, 117-129 (1981).

196. Tomasi, J., Mennucci, B., and Cancès, E. The IEF version of the PCM solvation method: an overview of a new method addressed to study molecular solutes at the QM ab initio level, *J. Mol. Struc.-THEOCHEM* **464**, 211-226 (1999).

197. Tomasi, J., Mennucci, B., and Cammi, R. Quantum mechanical continuum solvation models, *Chem. Rev.* **105**, 2999-3094 (2005).

198. Lee, Y.-J., Wu, B., Raymond, J. E., Zeng, Y., Fang, X., Wooley, K. L., and Liu, W. R. A genetically encoded acrylamide functionality, *ACS Chem. Biol.* **8**, 1664-1670 (2013).

199. Wang, X. S., Lee, Y.-J., and Liu, W. R. The nitrilimine-alkene cycloaddition is an ultra rapid click reaction, *Chem. Commun.* **50**, 3176-3179 (2014).

200. Bernardes, G. J. L., Chalker, J. M., Errey, J. C., and Davis, B. G. Facile conversion of cysteine and alkyl cysteines to dehydroalanine on protein surfaces: Versatile and switchable access to functionalized proteins, *J. Am. Chem. Soc.* **130**, 5052-5053 (2008).

201. Chalker, J. M., Gunnoo, S. B., Boutureira, O., Gerstberger, S. C., Fernandez-Gonzalez, M., Bernardes, G. J. L., Griffin, L., Hailu, H., Schofield, C. J., and Davis, B. G. Methods for converting cysteine to dehydroalanine on peptides and proteins, *Chem. Sci.* **2**, 1666-1676 (2011).

202. Chalker, J. M., Lercher, L., Rose, N. R., Schofield, C. J., and Davis, B. G. Conversion of systeine into dehydroalanine enables access to synthetic histones bearing diverse post-translational modifications, *Angew. Chem. Int. Ed.* **51**, 1835-1839 (2012).

203. Lubelski, J., Rink, R., Khusainov, R., Moll, G. N., and Kuipers, O. P. Biosynthesis, immunity, regulation, mode of action and engineering of the model lantibiotic nisin, *Cell. Mol. Life Sci.* **65**, 455-476 (2008).

204. Gross, E., and Morell, J. L. Structure of nisin, *J. Am. Chem. Soc.* **93**, 4634-4635 (1971).

205. Wiedemann, I., Breukink, E., van Kraaij, C., Kuipers, O. P., Bierbaum, G., de Kruijff, B., and Sahl, H.-G. Specific binding of Nisin to the peptidoglycan precursor Lipid II combines pore formation and inhibition of cell wall biosynthesis for potent antibiotic activity, *J. Biol. Chem.* **276**, 1772-1779 (2001).

206. Ortega, M. A., Hao, Y., Zhang, Q., Walker, M. C., van der Donk, W. A., and Nair, S. K. Structure and mechanism of the tRNA-dependent lantibiotic dehydratase NisB, *Nature* **517**, 509-512 (2015).

207. Bach, R. D. Ring strain energy in the cyclooctyl system. The effect of strain energy on [3 + 2] cycloaddition reactions with azides, *J. Am. Chem. Soc.* **131**, 5233-5243 (2009).

208. Soellner, M. B., Nilsson, B. L., and Raines, R. T. Staudinger ligation of α-azido acids retains stereochemistry, *J. Org. Chem.* **67**, 4993-4996 (2002).

209. Nilsson, B. L., Kiessling, L. L., and Raines, R. T. High-yielding Staudinger ligation of a phosphinothioester and azide to form a peptide, *Org. Lett.* **3**, 9-12 (2000).

210. Tam, A., and Raines, R. T. Coulombic effects on the traceless Staudinger ligation in water, *Bioorg. Med. Chem.* **17**, 1055-1063 (2009).

211. Komander, D. The emerging complexity of protein ubiquitination, *Biochem. Soc. Trans.* **37**, 937-953 (2009).

212. Ciechanover, A., and Iwai, K. The ubiquitin system: From basic mechanisms to the patient bed, *IUBMB Life* **56**, 193-201 (2004).

213. Li, W., and Ye, Y. Polyubiquitin chains: Functions, structures, and mechanisms, *Cell. Mol. Life Sci.* **65**, 2397-2406 (2008).

214. Wickliffe, K., Williamson, A., Jin, L., and Rape, M. The multiple layers of ubiquitin-dependent cell cycle control, *Chem. Rev.* **109**, 1537-1548 (2009).

215. Peng, J., Schwartz, D., Elias, J. E., Thoreen, C. C., Cheng, D., Marsischky, G., Roelofs, J., Finley, D., and Gygi, S. P. A proteomics approach to understanding protein ubiquitination, *Nat. Biotechnol.* **21**, 921-926 (2003).

216. Kirkpatrick, D. S., Denison, C., and Gygi, S. P. Weighing in on ubiquitin: The expanding role of mass-spectrometry-based proteomics, *Nat. Cell Biol.* **7**, 750-757 (2005).

217. Kirkpatrick, D. S., Hathaway, N. A., Hanna, J., Elsasser, S., Rush, J., Finley, D., King, R. W., and Gygi, S. P. Quantitative analysis of *in vitro* ubiquitinated cyclin B1 reveals complex chain topology, *Nat. Cell Biol.* **8**, 700-710 (2006).

218. Xu, P., Duong, D. M., Seyfried, N. T., Cheng, D., Xie, Y., Robert, J., Rush, J., Hochstrasser, M., Finley, D., and Peng, J. Quantitative proteomics reveals the function of unconventional ubiquitin chains in proteasomal degradation, *Cell* **137**, 133-145 (2009).

219. Martin, L. J., and Raines, R. T. Carpe diubiquitin, *Angew. Chem. Int. Ed.* **49**, 9042-9044 (2010).

220. Sowa, S., Stankevič, M., Szmigielska, A., Małuszyńska, H., Kozioł, A. E., and Pietrusiewicz, K. M. Reduction of functionalized tertiary phosphine oxides with BH3, *J. Org. Chem.* **80**, 1672-1688 (2015).

221. Sowa, S., Mühlberg, M., Pietrusiewicz, K. M., and Hackenberger, C. P. R. Traceless Staudinger acetylation of azides in aqueous buffers, *Bioorg. Med. Chem.* **21**, 3465-3472 (2013).

222. Tanrikulu, I. C., Schmitt, E., Mechulam, Y., Goddard, W. A., and Tirrell, D. A. Discovery of *Escherichia coli* methionyl-tRNA synthetase mutants for efficient labeling of proteins with azidonorleucine *in vivo*, *Proc. Natl. Acad. Sci. U.S.A.* **106**, 15285-15290 (2009).

223. Mühlberg, M., Jaradat, D. s. M. M., Kleineweischede, R., Papp, I., Dechtrirat, D., Muth, S., Broncel, M., and Hackenberger, C. P. R. Acidic and basic deprotection strategies of borane-protected phosphinothioesters for the traceless Staudinger ligation, *Bioorg. Med. Chem.* **18**, 3679-3686 (2010).

224. Frankland, E., and Duppa, B. F. Vorläufige Notiz über Boräthyl, *Justus Liebigs Ann. Chem.* **115**, 319-322 (1860).

225. Frankland, E. XLVI. On a new series of organic compounds containing boron, *J. Chem. Soc.* **15**, 363-381 (1862).

226. Miyaura, N., Yamada, K., and Suzuki, A. A new stereospecific cross-coupling by the palladium-catalyzed reaction of 1-alkenylboranes with 1-alkenyl or 1-alkynyl halides, *Tetrahedron Lett.* **20**, 3437-3440 (1979).

227. "The Nobel Prize in Chemistry 2010". Nobelprize.org. Nobel Media AB 2014. Web. 22 Aug 2015. <http://www.nobelprize.org/nobel_prizes/chemistry/laureates/2010/>

228. Kotha, S., Lahiri, K., and Kashinath, D. Recent applications of the Suzuki–Miyaura cross-coupling reaction in organic synthesis, *Tetrahedron* **58**, 9633-9695 (2002).

229. Hayashi, T., and Yamasaki, K. Rhodium-catalyzed asymmetric 1,4-addition and its related asymmetric reactions, *Chem. Rev.* **103**, 2829-2844 (2003).

230. Qiao, J. X., and Lam, P. Y. S. (2011) Recent advances in Chan–Lam coupling reaction: Copper-promoted C–heteroatom bond cross-coupling reactions with boronic acids and derivatives, In *Boronic Acids*, pp 315-361, Wiley-VCH Verlag GmbH & Co. KGaA.

231. Hall, D. G., Ed. (2005) *Structure, Properties, and Preparation Of Boronic Acid Derivatives. Overview of Their Reactions and Applications*, Wiley-VCH, Weinheim, Germany.

232. Lennox, A. J. J., and Lloyd-Jones, G. C. Selection of boron reagents for Suzuki–Miyaura coupling, *Chem. Soc. Rev.* **43**, 412-443 (2014).

233. Chambers, R. D., Clark, H. C., and Willis, C. J. Some salts of trifluoromethylfluoroboric acid, *J. Am. Chem. Soc.* **82**, 5298-5301 (1960).

234. Molander, G. A., and Jean-Gérard, L. (2011) Organotrifluoroborates: Organoboron reagents for the twenty-first century, In *Boronic Acids*, pp 507-550, Wiley-VCH Verlag GmbH & Co. KGaA.

235. Molander, G. A. Organotrifluoroborates: Another branch of the mighty oak, *J. Org. Chem.* 10.1021/acs.joc.5b00981 (2015).

236. Molander, G. A., and Ham, J. Synthesis of functionalized organotrifluoroborates via halomethyltrifluoroborates, *Org. Lett.* **8**, 2031-2034 (2006).

237. Molander, G. A., and Cooper, D. J. Functionalization of organotrifluoroborates: reductive amination, *J. Org. Chem.* **73**, 3885-3891 (2008).

238. Molander, G. A., and Ribagorda, M. Expanding organoboron chemistry: epoxidation of potassium organotrifluoroborates, *J. Am. Chem. Soc.* **125**, 11148-11149 (2003).

239. Molander, G. A., and Cooper, D. J. Ozonolysis of unsaturated organotrifluoroborates, *J. Org. Chem.* **72**, 3558-3560 (2007).

240. Molander, G. A., and Ham, J. Synthesis of functionalized organotrifluoroborates via the 1,3-dipolar cycloaddition of azides, *Org. Lett.* **8**, 2767-2770 (2006).

241. Molander, G. A., and Ellis, N. Organotrifluoroborates: protected boronic acids that expand the versatility of the suzuki coupling reaction, *Acc. Chem. Res.* **40**, 275-286 (2007).

242. Molander, G. A., Cavalcanti, L. N., Canturk, B., Pan, P.-S., and Kennedy, L. E. Efficient hydrolysis of organotrifluoroborates via silica gel and water, *J. Org. Chem.* **74**, 7364-7369 (2009).

243. Ihara, H., Koyanagi, M., and Suginome, M. Anthranilamide: a simple, removable ortho-directing modifier for arylboronic acids serving also as a protecting group in cross-coupling reactions, *Org. Lett.* **13**, 2662-2665 (2011).

244. Settepani, J. A., Stokes, J. B., and Borkovec, A. B. Insect chemosterilants. VIII. Boron compounds, *J. Med. Chem.* **13**, 128-131 (1970).

245. Noguchi, H., Hojo, K., and Suginome, M. Boron-masking strategy for the selective synthesis of oligoarenes via iterative Suzuki−Miyaura coupling, *J. Am. Chem. Soc.* **129**, 758-759 (2007).

246. Noguchi, H., Shioda, T., Chou, C.-M., and Suginome, M. Differentially protected benzenediboronic acids: divalent cross-coupling modules for the efficient synthesis of boron-substituted oligoarenes, *Org. Lett.* **10**, 377-380 (2008).

247. Iwadate, N., and Suginome, M. Synthesis of masked haloareneboronic acids via iridium-catalyzed aromatic C–H borylation with 1,8-naphthalenediaminatoborane (danBH), *J. Organomet. Chem.* **694**, 1713-1717 (2009).

248. Iwadate, N., and Suginome, M. Synthesis of *B*-protected β-styrylboronic acids via iridium-catalyzed hydroboration of alkynes with 1,8-naphthalenediaminatoborane leading to iterative synthesis of oligo(phenylenevinylene)s, *Org. Lett.* **11**, 1899-1902 (2009).

249. Iwadate, N., and Suginome, M. Differentially protected diboron for regioselective diboration of alkynes: internal-selective cross-coupling of 1-alkene-1,2-diboronic acid derivatives, *J. Am. Chem. Soc.* **132**, 2548-2549 (2010).

250. Li, J., Grillo, A. S., and Burke, M. D. From synthesis to function via iterative assembly of N-methyliminodiacetic acid boronate building blocks, *Acc. Chem. Res.* **48**, 2297-2307 (2015).

251. Gillis, E. P., and Burke, M. D. A simple and modular strategy for small molecule synthesis: iterative Suzuki−Miyaura coupling of *B*-protected haloboronic acid building blocks, *J. Am. Chem. Soc.* **129**, 6716-6717 (2007).

252. Gillis, E. P., and Burke, M. D. Multistep synthesis of complex boronic acids from simple MIDA boronates, *J. Am. Chem. Soc.* **130**, 14084-14085 (2008).

253. Li, J., and Burke, M. D. Pinene-derived iminodiacetic acid (PIDA): A powerful ligand for stereoselective synthesis and iterative cross-coupling of C(sp3) boronate building blocks, *J. Am. Chem. Soc.* **133**, 13774-13777 (2011).

254. Torssell, K. Arylboronic acids. III. Bromination of tolylboronic acids according to Wohl-Ziegler. Arkiv Foer Kemi, 10, 507-511 (1957).

255. Dowlut, M., and Hall, D. G. An improved class of sugar-binding boronic acids, soluble and capable of complexing glycosides in neutral water, *J. Am. Chem. Soc.* **128**, 4226-4227 (2006).

256. Zhdankin, V. V., Persichini Iii, P. J., Zhang, L., Fix, S., and Kiprof, P. Synthesis and structure of benzoboroxoles: novel organoboron heterocycles, *Tetrahedron Lett.* **40**, 6705-6708 (1999).

257. Tomsho, J. W., Pal, A., Hall, D. G., and Benkovic, S. J. Ring structure and aromatic substituent effects on the pK_a of the benzoxaborole pharmacophore, *ACS Med. Chem. Lett.* **3**, 48-52 (2012).

258. Liu, C. T., Tomsho, J. W., and Benkovic, S. J. The unique chemistry of benzoxaboroles: current and emerging applications in biotechnology and therapeutic treatments, *Bioorg. Med. Chem.* **22**, 4462-4473 (2014).

259. Adamczyk-Woźniak, A., Borys, K. M., and Sporzyński, A. Recent developments in the chemistry and biological applications of benzoxaboroles, *Chem. Rev.* **115**, 5224-5247 (2015).

260. Smoum, R., Rubinstein, A., Dembitsky, V. M., and Srebnik, M. Boron containing compounds as protease inhibitors, *Chem. Rev.* **112**, 4156-4220 (2012).

261. Hernandez, V., Crépin, T., Palencia, A., Cusack, S., Akama, T., Baker, S. J., Bu, W., Feng, L., Freund, Y. R., Liu, L., Meewan, M., Mohan, M., Mao, W., Rock, F. L., Sexton, H., Sheoran, A., Zhang, Y., Zhang, Y.-K., Zhou, Y., Nieman, J. A., Anugula, M. R., Keramane, E. M., Savariraj, K., Reddy, D. S., Sharma, R., Subedi, R., Singh, R., O'Leary, A., Simon, N. L., De Marsh, P. L., Mushtaq, S., Warner, M., Livermore, D. M., Alley, M. R. K., and Plattner, J. J. Discovery of a novel class of boron-based antibacterials with activity against gram-negative bacteria, *Antimicrob. Agents Chemother.* **57**, 1394-1403 (2013).

262. Li, X., Zhang, Y.-K., Liu, Y., Zhang, S., Ding, C. Z., Zhou, Y., Plattner, J. J., Baker, S. J., Liu, L., Bu, W., Kazmierski, W. M., Wright, L. L., Smith, G. K., Jarvest, R. L., Duan, M., Ji, J.-J., Cooper, J. P., Tallant, M. D., Crosby, R. M., Creech, K., Ni, Z.-J., Zou, W., and Wright, J. Synthesis of new acylsulfamoyl benzoxaboroles as potent inhibitors of HCV NS3 protease, *Bioorg. Med. Chem. Lett.* **20**, 7493-7497 (2010).

263. Li, X., Zhang, S., Zhang, Y.-K., Liu, Y., Ding, C. Z., Zhou, Y., Plattner, J. J., Baker, S. J., Bu, W., Liu, L., Kazmierski, W. M., Duan, M., Grimes, R. M., Wright, L. L., Smith, G. K., Jarvest, R. L., Ji, J.-J., Cooper, J. P., Tallant, M. D., Crosby, R. M., Creech, K., Ni, Z.-J., Zou, W., and Wright, J. Synthesis and SAR of acyclic HCV NS3 protease inhibitors with novel P4-benzoxaborole moieties, *Bioorg. Med. Chem. Lett.* **21**, 2048-2054 (2011).

264. Ding, C. Z., Zhang, Y.-K., Li, X., Liu, Y., Zhang, S., Zhou, Y., Plattner, J. J., Baker, S. J., Liu, L., Duan, M., Jarvest, R. L., Ji, J., Kazmierski, W. M., Tallant, M. D., Wright, L. L., Smith, G. K., Crosby, R. M., Wang, A. A., Ni, Z.-J., Zou, W., and Wright, J. Synthesis

and biological evaluations of P4-benzoxaborole-substituted macrocyclic inhibitors of HCV NS3 protease, *Bioorg. Med. Chem. Lett.* **20**, 7317-7322 (2010).

265. Akama, T., Baker, S. J., Zhang, Y.-K., Hernandez, V., Zhou, H., Sanders, V., Freund, Y., Kimura, R., Maples, K. R., and Plattner, J. J. Discovery and structure–activity study of a novel benzoxaborole anti-inflammatory agent (AN2728) for the potential topical treatment of psoriasis and atopic dermatitis, *Bioorg. Med. Chem. Lett.* **19**, 2129-2132 (2009).

266. Freund, Y. R., Akama, T., Alley, M. R. K., Antunes, J., Dong, C., Jarnagin, K., Kimura, R., Nieman, J. A., Maples, K. R., Plattner, J. J., Rock, F., Sharma, R., Singh, R., Sanders, V., and Zhou, Y. Boron-based phosphodiesterase inhibitors show novel binding of boron to PDE4 bimetal center, *FEBS Lett.* **586**, 3410-3414 (2012).

267. Ellis, G. A., Palte, M. J., and Raines, R. T. Boronate-mediated biologic delivery, *J. Am. Chem. Soc.* **134**, 3631-3634 (2012).

268. Anacor Pharmaceuticals. FDA Approves Anacor Pharmaceuticals' KERYDINTM (Tavaborole) Topical Solution, 5% for the Treatment of Onychomycosis of the Toenails. Press release, July 8, 2014; http://investor.anacor.com/.

269. Szebellédy, L., and Tanay, S. Beiträge zum Nachweis der Borsäure mit Alizarin, *Z. Anal. Chem.* **107**, 26-30 (1936).

270. Campaña, A. M. G., Barrero, F. A., and Ceba, M. R. Spectrofluorometric determination of boron in soils, plants and natural-waters with alizarin red-S, *Analyst* **117**, 1189-1191 (1992).

271. Chimpalee, N., Chimpalee, D., Boonyanitchayakul, B., and Burns, D. T. Flow-injection spectrofluorometric determination of boron using alizarin-red-s in aqueous solution, *Anal. Chim. Acta* **282**, 643-646 (1993).

272. Bull, S. D., Davidson, M. G., van den Elsen, J. M. H., Fossey, J. S., Jenkins, A. T. A., Jiang, Y.-B., Kubo, Y., Marken, F., Sakurai, K., Zhao, J., and James, T. D. Exploiting the reversible covalent bonding of boronic acids: recognition, sensing, and assembly, *Acc. Chem. Res.* **46**, 312-326 (2013).

273. Ulrich, G., Ziessel, R., and Harriman, A. The chemistry of fluorescent BODIPY dyes: versatility unsurpassed, *Angew. Chem. Int. Ed. Engl.* **47**, 1184-1201 (2008).

274. Boens, N., Leen, V., and Dehaen, W. Fluorescent indicators based on BODIPY, *Chem. Soc. Rev.* **41**, 1130-1172 (2012).

275. Kowada, T., Maeda, H., and Kikuchi, K. BODIPY-based probes for the fluorescence imaging of biomolecules in living cells, *Chem. Soc. Rev.* **44**, 4953-4972 (2015).

276. Ma, W. M. J., Pereira Morais, M. P., D'Hooge, F., van den Elsen, J. M. H., Cox, J. P. L., James, T. D., and Fossey, J. S. Dye displacement assay for saccharide detection with boronate hydrogels, *Chem. Commun.*, 532-534 (2009).

277. Barder, T. E., and Buchwald, S. L. Benchtop monitoring of reaction progress via visual recognition with a handheld UV lamp: in situ monitoring of boronic acids in the Suzuki−Miyaura reaction, *Org. Lett.* **9**, 137-139 (2007).

278. Rock, F. L., Mao, W., Yaremchuk, A., Tukalo, M., Crepin, T., Zhou, H., Zhang, Y. K., Hernandez, V., Akama, T., Baker, S. J., Plattner, J. J., Shapiro, L., Martinis, S. A., Benkovic, S. J., Cusack, S., and Alley, M. R. An antifungal agent inhibits an aminoacyl-tRNA synthetase by trapping tRNA in the editing site, *Science* **316**, 1759-1761 (2007).

279. Baker, S. J., Ding, C. Z., Akama, T., Zhang, Y. K., Hernandez, V., and Xia, Y. Therapeutic potential of boron-containing compounds, *Future Med. Chem.* **1**, 1275-1288 (2009).

280. Akama, T., Baker, S. J., Zhang, Y. K., Hernandez, V., Zhou, H., Sanders, V., Freund, Y., Kimura, R., Maples, K. R., and Plattner, J. J. Discovery and structure-activity study of a novel benzoxaborole anti-inflammatory agent (AN2728) for the potential topical treatment of psoriasis and atopic dermatitis, *Bioorg. Med. Chem. Lett.* **19**, 2129-2132 (2009).

281. Ding, D., Zhao, Y., Meng, Q., Xie, D., Nare, B., Chen, D., Bacchi, C. J., Yarlett, N., Zhang, Y.-K., Hernandez, V., Xia, Y., Freund, Y., Abdulla, M., Ang, K.-H., Ratnam, J., McKerrow, J. H., Jacobs, R. T., Zhou, H., and Plattner, J. J. Discovery of Novel Benzoxaborole-Based Potent Antitrypanosomal Agents, *ACS Med. Chem. Lett.* **1**, 165-169 (2010).

282. Li, X., Zhang, Y. K., Liu, Y., Ding, C. Z., Li, Q., Zhou, Y., Plattner, J. J., Baker, S. J., Qian, X., Fan, D., Liao, L., Ni, Z. J., White, G. V., Mordaunt, J. E., Lazarides, L. X., Slater, M. J., Jarvest, R. L., Thommes, P., Ellis, M., Edge, C. M., Hubbard, J. A., Somers, D., Rowland, P., Nassau, P., McDowell, B., Skarzynski, T. J., Kazmierski, W. M., Grimes, R. M., Wright, L. L., Smith, G. K., Zou, W., Wright, J., and Pennicott, L. E. Synthesis and evaluation of novel alpha-amino cyclic boronates as inhibitors of HCV NS3 protease, *Bioorg. Med. Chem. Lett.* **20**, 3550-3556 (2010).

283. Obrecht, D., Bernardini, F., Dale, G., and Dembowsky, K. (2011) Chapter 15 - Emerging New Therapeutics Against Key Gram-Negative Pathogens, In *Annual Reports in Medicinal Chemistry* (John, E. M., Ed.), pp 245-262, Academic Press.

284. Ding, D., Meng, Q., Gao, G., Zhao, Y., Wang, Q., Nare, B., Jacobs, R., Rock, F., Alley, M. R., Plattner, J. J., Chen, G., Li, D., and Zhou, H. Design, synthesis, and structure-activity relationship of Trypanosoma brucei leucyl-tRNA synthetase inhibitors as antitrypanosomal agents, *J. Med. Chem.* **54**, 1276-1287 (2011).

285. Xia, Y., Cao, K., Zhou, Y., Alley, M. R., Rock, F., Mohan, M., Meewan, M., Baker, S. J., Lux, S., Ding, C. Z., Jia, G., Kully, M., and Plattner, J. J. Synthesis and SAR of novel

benzoxaboroles as a new class of beta-lactamase inhibitors, *Bioorg. Med. Chem. Lett.* **21**, 2533-2536 (2011).

286. Baker, S. J., Tomsho, J. W., and Benkovic, S. J. Boron-containing inhibitors of synthetases, *Chem. Soc. Rev.* **40**, 4279-4285 (2011).

287. Qiao, Z., Wang, Q., Zhang, F., Wang, Z., Bowling, T., Nare, B., Jacobs, R. T., Zhang, J., Ding, D., Liu, Y., and Zhou, H. Chalcone-benzoxaborole hybrid molecules as potent antitrypanosomal agents, *J. Med. Chem.* **55**, 3553-3557 (2012).

288. Dixon, D. D., Lockner, J. W., Zhou, Q., and Baran, P. S. Scalable, divergent synthesis of meroterpenoids via "borono-sclareolide", *J. Am. Chem. Soc.* **134**, 8432-8435 (2012).

289. Berube, M., Dowlut, M., and Hall, D. G. Benzoboroxoles as efficient glycopyranoside-binding agents in physiological conditions: structure and selectivity of complex formation, *J. Org. Chem.* **73**, 6471-6479 (2008).

290. Pal, A., Berube, M., and Hall, D. G. Design, synthesis, and screening of a library of peptidyl bis(boroxoles) as oligosaccharide receptors in water: identification of a receptor for the tumor marker TF-antigen disaccharide, *Angew. Chem. Int. Ed.* **49**, 1492-1495 (2010).

291. Schumacher, S., Katterle, M., Hettrich, C., Paulke, B.-R., Pal, A., Hall, D. G., Scheller, F. W., and Gajovic-Eichelmann, N. Benzoboroxole-modified nanoparticles for the recognition of glucose at neutral pH, *Chem. Sens.* **1**, 1-7 (2011).

292. Schumacher, S., Katterle, M., Hettrich, C., Paulke, B.-R., Hall, D. G., Scheller, F. W., and Gajovic-Eichelmann, N. Label-free detection of enhanced saccharide binding at pH 7.4 to nanoparticulate benzoboroxole based receptor units, *J. Mol. Recognit.* **24**, 953-959 (2011).

293. Adamczyk-Wozniak, A., Borys, K. M., Madura, I. D., Pawelko, A., Tomecka, E., and Zukowski, K. Lewis acidity and sugar receptor activity of 3-amino-substituted benzoxaboroles and their ortho-aminomethylphenylboronic acid analogues, *New J. Chem.* **37**, 188-194 (2013).

294. Kim, H., Kang, Y. J., Kang, S., and Kim, K. T. Monosaccharide-responsive release of insulin from polymersomes of polyboroxole block copolymers at neutral pH, *J. Am. Chem. Soc.* **134**, 4030-4033 (2012).

295. Li, H., Wang, H., Liu, Y., and Liu, Z. A benzoboroxole-functionalized monolithic column for the selective enrichment and separation of cis-diol containing biomolecules, *Chem. Commun.* **48**, 4115-4117 (2012).

296. Kotsuchibashi, Y., Agustin, R. V. C., Lu, J. Y., Hall, D. G., and Narain, R. Temperature, pH, and glucose responsive gels via simple mixing of boroxole- and glyco-based polymers, *ACS Macro. Lett.* **2**, 260-264 (2013).

297. Biswas, S., Kinbara, K., Niwa, T., Taguchi, H., Ishii, N., Watanabe, S., Miyata, K., Kataoka, K., and Aida, T. Biomolecular robotics for chemomechanically driven guest delivery fuelled by intracellular ATP, *Nat. Chem.* **5**, 613-620 (2013).

298. Adamczyk-Wozniak, A., Cyranski, M. K., Zubrowska, A., and Sporzynski, A. Benzoxaboroles - old compounds with new applications, *J. Organomet. Chem.* **694**, 3533-3541 (2009).

299. Snyder, H. R., Reedy, A. J., and Lennarz, W. J. Synthesis of aromatic boronic acids. Aldehydo boronic acids and a boronic acid analog of tyrosine, *J. Am. Chem. Soc.* **80**, 835-838 (1958).

300. Tomsho, J. W., Pal, A., Hall, D. G., and Benkovic, S. J. Ring structure and aromatic substituent effects on the pKa of the benzoxaborole pharmacophore, *ACS Med. Chem. Lett.* **3**, 48-52 (2011).

301. Tomsho, J. W., and Benkovic, S. J. Examination of the reactivity of benzoxaboroles and related compounds with a cis-diol, *J. Org. Chem.* **77**, 11200-11209 (2012).

302. Noguchi, H., Hojo, K., and Suginome, M. Boron-masking strategy for the selective synthesis of oligoarenes via iterative Suzuki-Miyaura coupling, *J. Am. Chem. Soc.* **129**, 758-759 (2007).

303. Noguchi, H., Shioda, T., Chou, C. M., and Suginome, M. Differentially protected benzenediboronic acids: divalent cross-coupling modules for the efficient synthesis of boron-substituted oligoarenes, *Org. Lett.* **10**, 377-380 (2008).

304. Molander, G. A., and Ellis, N. Organotrifluoroborates: protected boronic acids that expand the versatility of the Suzuki coupling reaction, *Acc. Chem. Res.* **40**, 275-286 (2007).

305. Mancilla, T., Contreras, R., and Wrackmeyer, B. New bicyclic organylboronic esters derived from iminodiacetic acids, *J. Organomet. Chem.* **307**, 1-6 (1986).

306. Knapp, D. M., Gillis, E. P., and Burke, M. D. A general solution for unstable boronic acids: slow-release cross-coupling from air-stable MIDA boronates, *J. Am. Chem. Soc.* **131**, 6961-6963 (2009).

307. Alder, R. W., Bowman, P. S., Steele, W. R. S., and Winterma, D. R. Remarkable basicity of 1,8-bis(dimethylamino)naphthalene, *Chem. Commun.*, 723 (1968).

308. Ozeryanskii, V. A., Pozharskii, A. F., Koroleva, M. G., Shevchuk, D. A., Kazheva, O. N., Chekhlov, A. N., Shilov, G. V., and Dyachenko, O. A. *N,N,N'*-trialkyl-1,8-diaminonaphthalenes: convenient method of preparation from protonated proton sponges and the first X-ray information, *Tetrahedron* **61**, 4221-4232 (2005).

309. Dent, W. H., III, Erickson, W. R., Fields, S. C., Parker, M. H., and Tromiczak, E. G. 9-BBN: An amino acid protecting group for functionalization of amino acid side chains in organic solvents, *Org. Lett.* **4**, 1249-1251 (2002).

310. Protonated proton sponge is known to be highly fluorescent, See: Szemik-Hojniak, A. Rettig, W., Deperasinka, I., The forbidden emission of protonated proton sponge, Chem. Phys. Lett. 343, 404-412, and references therein.

311. Li, X. G., Huang, M. R., and Li, S. X. Facile synthesis of poly(1,8-diaminonaphthalene) microparticles with a very high silver-ion adsorbability by a chemical oxidative polymerization, *Acta Mater.* **52**, 5363-5374 (2004).

312. Davis, R., and Tamaoki, N. Novel photochromic spiroheterocyclic molecules via oxidation of 1,8-diaminonaphthalene, *Org. Lett.* **7**, 1461-1464 (2005).

313. Kinzel, T., Zhang, Y., and Buchwald, S. L. A new palladium precatalyst allows for the fast Suzuki-Miyaura coupling reactions of unstable polyfluorophenyl and 2-heteroaryl boronic acids, *J. Am. Chem. Soc.* **132**, 14073-14075 (2010).

314. Yamamoto, Y., Ishii, J., Nishiyama, H., and Itoh, K. Cp(*)RuCl-catalyzed formal intermolecular cyclotrimerization of three unsymmetrical alkynes through a boron temporary tether: regioselective four-component coupling synthesis of phthalides, *J. Am. Chem. Soc.* **127**, 9625-9631 (2005).

315. Gunasekera, D. S., Gerold, D. J., Aalderks, N. S., Chandra, J. S., Maanu, C. A., Kiprof, P., Zhdankin, V. V., and Reddy, M. V. R. Practical synthesis and application of benzoboroxoles, *Tetrahedron* **63**, 9401-9405 (2007).

316. Carrow, B. P., and Hartwig, J. F. Distinguishing between pathways for transmetalation in Suzuki-Miyaura reactions, *J. Am. Chem. Soc.* **133**, 2116-2119 (2011).

317. Attenuating the reactivity of boronic acids by rehybridization of the boron center from sp2 to sp3 using a dative nitrogen ligand was demonstrated initially by Burke and coworkers.

318. Biscoe, M. R., Fors, B. P., and Buchwald, S. L. A new class of easily activated palladium precatalysts for facile C−N cross-coupling reactions and the low temperature oxidative addition of aryl chlorides, *J. Am. Chem. Soc.* **130**, 6686-6687 (2008).

319. Fors, B. P., Watson, D. A., Biscoe, M. R., and Buchwald, S. L. A highly active catalyst for Pd-catalyzed amination reactions: cross-coupling reactions using aryl mesylates and the highly selective monoarylation of primary amines using aryl chlorides, *J. Am. Chem. Soc.* **130**, 13552-13554 (2008).

320. Letsinger, R. L., Skoog, I., and Remes, N. Aminoethyl diarylborinates; isolation of a stable unsymmetrical organoboron compound, *J. Am. Chem. Soc.* **76**, 4047-4048 (1954).

321. Robin, B., Buell, G., Kiprof, P., and Nemykin, V. N. 3H-1,2-Benzoxaborole-1-spiro-4'-(5-oxa-3a-aza-4-borapyrene), *Acta Crystallogr., Sect. E* **64**, o314-o315 (2008).

322. Bull, S. D., Davidson, M. G., van den Elsen, J. M., Fossey, J. S., Jenkins, A. T., Jiang, Y. B., Kubo, Y., Marken, F., Sakurai, K., Zhao, J., and James, T. D. Exploiting the reversible covalent bonding of boronic acids: recognition, sensing, and assembly, *Acc. Chem. Res.* **46**, 312-326 (2013).

323. Baker, S. J., Ding, C. Z., Akama, T., Zhang, Y.-K., Hernandez, V., and Xia, Y. Therapeutic potential of boron-containing compounds, *Future Med. Chem.* **1**, 1275-1288 (2009).

324. Barder, T. E., and Buchwald, S. L. Benchtop monitoring of reaction progress via visual recognition with a handheld UV lamp: In situ monitoring of boronic acids in the Suzuki-Miyaura reaction, *Org. Lett.* **9**, 137-139 (2007).

325. Duval, F., van Beek, T. A., and Zuilhof, H. Sensitive thin-layer chromatography detection of boronic acids using alizarin, *Synlett* **1**, 1751-1754 (2012).

326. Lawrence, K., Flower, S. E., Kociok-Kohn, G., Frost, C. G., and James, T. D. A simple and effective colorimetric technique for the detection of boronic acids and their derivatives, *Anal. Methods* **4**, 2215-2217 (2012).

327. Ciani, L. R., S. Boron as a platform for new drug design, *Expert Opin. Drug Discovery* **7**, 1017-1027 (2012).

328. Das, B. C., Thapa, P., Karki, R., Schinke, C., Das, S., Kambhampati, S., Banerjee, S. K., Van Veldhuizen, P., Verma, A., Weiss, L. M., and Evans, T. Boron chemicals in diagnosis and therapeutics, *Future Med. Chem.* **5**, 653-676 (2013).

329. Zhao, J. Z., Ji, S. M., Chen, Y. H., Guo, H. M., and Yang, P. Excited state intramolecular proton transfer (ESIPT): from principal photophysics to the development of new chromophores and applications in fluorescent molecular probes and luminescent materials, *Phys. Chem. Chem. Phys.* **14**, 8803-8817 (2012).

330. Wiskur, S. L., Lavigne, J. J., Ait-Haddou, H., Lynch, V., Chiu, Y. H., Canary, J. W., and Anslyn, E. V. pK_a values and geometries of secondary and tertiary amines complexed to boronic acids - Implications for sensor design, *Org. Lett.* **3**, 1311-1314 (2001).

331. Springsteen, G., and Wang, B. H. A detailed examination of boronic acid-diol complexation, *Tetrahedron* **58**, 5291-5300 (2002).

332. Kubo, Y., Kobayashi, A., Ishida, T., Misawa, Y., and James, T. D. Detection of anions using a fluorescent alizarin-phenylboronic acid ensemble, *Chem. Commun.*, 2846-2848 (2005).

333. Schenkel-Rudin, H., and Schenkel-Rudin, M. Zur Bildung schwerlöslicher Metallsalze bei Oxyverbindungen von Stickstoff-Heterocyclen, *Helv. Chim. Acta* **27**, 1456-1463 (1944).

334. Kenfack, C. A., Klymchenko, A. S., Duportail, G., Burger, A., and Mely, Y. Ab initio study of the solvent H-bonding effect on ESIPT reaction and electronic transitions of 3-hydroxychromone derivatives, *Phys. Chem. Chem. Phys.* **14**, 8910-8918 (2012).

335. Benelhadj, K., Massue, J., Retailleau, P., Ulrich, G., and Ziessel, R. 2-(2′ -Hydroxyphenyl)benzimidazole and 9,10-phenanthroimidazole chelates and borate complexes: Solution- and solid-state emitters, *Org. Lett.* **15**, 2918-2921 (2013).

336. We attempted to use the ESIPT chromophore 2-(2'-hydroxyphenyl)benzimidazole as a stain, but its low contrast and visible brightness on TLC made it ineffective. See Figure 2.2.11

337. Lim, J., Nam, D., and Miljanic, O. S. Identification of carboxylic and organoboronic acids and phenols with a single benzobisoxazole fluorophore, *Chem. Sci.* **3**, 559-563 (2012).

338. Molander, G. A., Cavalcanti, L. N., Canturk, B., Pan, P.-S., and Kennedy, L. E. Efficient hydrolysis of organotrifluoroborates via silica gel and water, *J. Org. Chem.* **74**, 7364-7369 (2009).

339. James, T. D., Sandanayake, K., Iguchi, R., and Shinkai, S. Novel saccharide-photoinduced electron-transfer sensors based on the interaction of boronic acid and amine, *J. Am. Chem. Soc.* **117**, 8982-8987 (1995).

340. Arimori, S., Ward, C. J., and James, T. D. A D-glucose selective fluorescent assay, *Tetrahedron Lett.* **43**, 303-305 (2002).

341. Liang, L., and Liu, Z. A self-assembled molecular team of boronic acids at the gold surface for specific capture of cis-diol biomolecules at neutral pH, *Chem. Commun.* **47**, 2255-2257 (2011).

342. Liu, Y. C., Ren, L. B., and Liu, Z. A unique boronic acid functionalized monolithic capillary for specific capture, separation and immobilization of cis-diol biomolecules, *Chem. Commun.* **47**, 5067-5069 (2011).

343. Lin, Z., Pang, J., Yang, H., Cai, Z., Zhang, L., and Chen, G. One-pot synthesis of an organic-inorganic hybrid affinity monolithic column for specific capture of glycoproteins, *Chem. Commun.* **47**, 9675-9677 (2011).

344. Li, H. Y., Wang, H. Y., Liu, Y. C., and Liu, Z. A benzoboroxole-functionalized monolithic column for the selective enrichment and separation of cis-diol containing biomolecules, *Chem. Commun.* **48**, 4115-4117 (2012).

345. Li, L., Lu, Y., Bie, Z., Chen, H.-Y., and Liu, Z. Photolithographic boronate affinity molecular imprinting: A general and facile approach for glycoprotein imprinting, *Angew. Chem., Int. Ed.* **52**, 7451-7454 (2013).

346. Lavigne, J. J., and Anslyn, E. V. Teaching old indicators new tricks: A colorimetric chemosensing ensemble for tartrate/malate in beverages, *Angew. Chem., Int. Ed.* **38**, 3666-3669 (1999).

347. Cabell, L. A., Monahan, M. K., and Anslyn, E. V. A competition assay for determining glucose-6-phosphate concentration with a tris-boronic acid receptor, *Tetrahedron Lett.* **40**, 7753-7756 (1999).

348. Nishiyabu, R., Kubo, Y., James, T. D., and Fossey, J. S. Boronic acid building blocks: tools for self assembly, *Chem. Commun.* **47**, 1124-1150 (2011).

349. Chou, P.-T., Chen, Y.-C., Yu, W.-S., Chou, Y.-H., Wei, C.-Y., and Cheng, Y.-M. Excited-state intramolecular proton transfer in 10-hydroxybenzo[h]quinoline, *J. Phys. Chem. A* **105**, 1731-1740 (2001).

350. Laughlin, S. T., and Bertozzi, C. R. Imaging the glycome, *Proc. Natl. Acad. Sci. U.S.A.* **106**, 12-17 (2009).

351. Josa-Cullere, L., Wainman, Y. A., Brindle, K. M., and Leeper, F. J. Diazo group as a new chemical reporter for bioorthogonal labelling of biomolecules, *RSC Adv.* **4**, 52241-52244 (2014).

352. Friscourt, F., Fahrni, C. J., and Boons, G.-J. Fluorogenic strain-promoted alkyne–diazo cycloadditions, *Chem. Eur. J.* **21**, 13996-14001 (2015).

353. van Dongen, S. F. M., Teeuwen, R. L. M., Nallani, M., van Berkel, S. S., Cornelissen, J. J. L. M., Nolte, R. J. M., and van Hest, J. C. M. Single-step azide introduction in proteins via an aqueous diazo transfer, *Bioconjugate Chem.* **20**, 20-23 (2009).

354. Ellis, G. A., Palte, M. J., and Raines, R. T. Boronate-mediated biologic delivery, *J. Am. Chem. Soc.* **134**, 3631-3634 (2012).

355. Melicher, M. S., Walker, A. S., Shen, J., Miller, S. J., and Schepartz, A. Improved carbohydrate recognition in water with an electrostatically enhanced β-peptide bundle, *Org. Lett.* 10.1021/acs.orglett.5b02187 (2015).

356. Seo, J., Kim, S., and Park, S. Y. Strong solvatochromic fluorescence from the intramolecular charge-transfer state created by excited-state intramolecular proton transfer, *J. Am. Chem. Soc.* **126**, 11154-11155 (2004).

357. Zhao, J., Ji, S., Chen, Y., Guo, H., and Yang, P. Excited state intramolecular proton transfer (ESIPT): From principal photophysics to the development of new chromophores and applications in fluorescent molecular probes and luminescent materials, *Phys. Chem. Chem. Phys.* **14**, 8803-8817 (2012).

358. Jin, S., Cheng, Y., Reid, S., Li, M., and Wang, B. Carbohydrate recognition by boronolectins, small molecules, and lectins, *Med. Res. Rev.* **30**, 171-257 (2010).